Development and Mechanistic Investigations into Metal-Catalysed Cycloisomerisation of Enynamides

A thesis submitted to the

Board of the Faculty of Physical Sciences

in partial fulfilment of the requirements for the degree of

Doctor of Philosophy

Aroonroj Mekareeya

Wolfson College, University of Oxford

Under the supervision of

Prof Edward Anderson



Development and Mechanistic Investigations into Metal-Catalysed Cycloisomerisation of Enynamides

Aroonroj Mekareeya **Doctor of Philosophy**

Wolfson College **Michaelmas Term 2017**

This thesis reports the work on investigations into the mechanism of palladium-catalysed enynamide cycloisomerisations (with $Pd(OAc)_2$ / bis(benzylidene)ethylenediamine (bbeda) catalyst system in particular). Herein, it has been shown that the mechanism of this catalyst system is likely to proceed *via* a hydropalladation mechanism. In the course of study, we have uncovered the crucial influences of water, the pre-catalyst, and the ligand (bbeda) in this reaction. One of the key highlights is bbeda itself serves as a source of palladium(II) hydride during the reaction. In addition, kinetic isotope effects obtained from theoretical analysis are consistent with the experimental data. The computational studies also offer enhanced understanding in the stereoselectivity of the reaction.

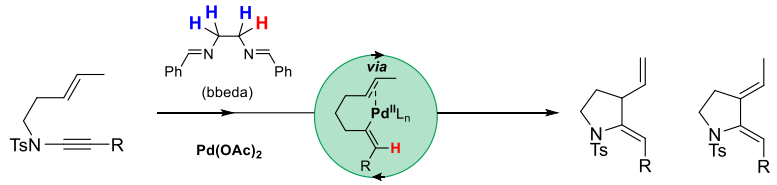

Apart from the mechanistic study work, we have developed a new bench stable rhodium pre-catalyst from commercially available sources, which is much easier to handle compared to typical catalyst systems. Using this new rhodium complex, various array of alkene substituents has been surveyed, and observed that enynamides with (*Z*)-alkene geometry give excellent yields and enantioselectivities.

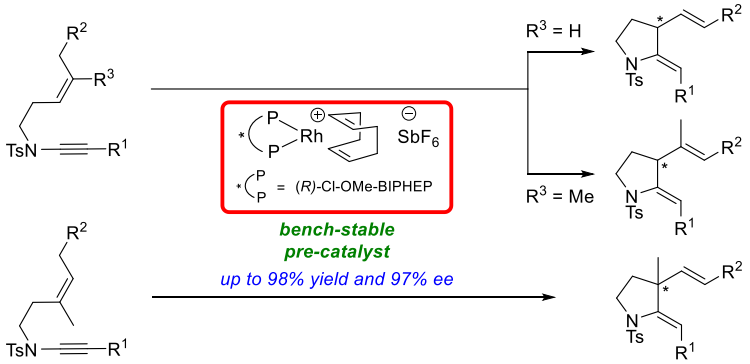

Acknowledgments

There have been several people throughout my DPhil journey whom I would very much like to express my deep gratitude and appreciation to:

Firstly, I thank Prof Edward Anderson for granting me such a great opportunity to work within his group, and for all his continual help, support, time and plenty of invaluable advice that he has generously provided. Indeed, although I still have to improve myself in many aspects, it is unarguably that I have learned a lot from you during my time in the group.

To all the members of the Anderson group past and present – Shermin, Steve, Guilhem, Carlos, Muji, Glenn, Minh, Kai, Felix, Dimitri, Venky, Rob, Halli, Marie, Marius, Clare, Christian, Eddy, Craig, Bryony, Ross, and our Part IIs, for support, advice and joy during working in the lab. Shermin – thank you for introducing me to badminton, it's now my best hobby which I cannot live without; also valuable advice and help. Steve, Guilhem, Carlos, Craig and Halli for all their academic advice and discussions. Steve, Minh and Glenn for very good moments outside the lab, especially films and pizzas.

To the members of staff of the CRL for their expertise and assistance, in particular, those of the NMR department.

To my friends in the badminton group: Steve, Lok, Brian, Lee, Mike, Wilson, Tim, Daniel, Arron. For making my wonderful badminton time in Oxford, and making me don't want to leave Oxford.

To my dearest girlfriend, Mean, for metal support, always being along my side, and making my life meaningful and wonderful; and also Nong Mee for being beside me all the time.

To my mum, dad, and my beloved brother for always being supportive and always to understand. I would not be able to come this far without your support and love.

Abbreviations

Ac	acetyl
APC	allyl palladium chloride dimer
Ar	generic aryl group
Ar^F	3,5-bis(trifluoromethyl)benzene
aq.	aqueous
bbeda	*N*,*N*′-dibenzylideneethane-1,2-diamine
BINAP	2,2′-bis(diphenylphosphino)-1,1′-binaphthyl
Bn	benzyl
Boc	*tert*-butoxycarbonyl
cod	cyclooctadiene
conc.	concentrated
COSY	correlation spectroscopy
Cp*	pentamethylcyclopentadiene
dba	dibenzylideneacetone
1,2-DCE	1,2-dichloroethane
DEPT	distortionless enhancement by polarisation transfer
DFT	density functional theory
DIAD	diisopropyl azodicarboxylate
DIBALH	diisobutylaluminium hydride
DMAP	4-dimethylaminopyridine
DMF	*N*,*N*-dimethylformamide
DPPA	diphenylphosphoryl azide
d.r.	diastereomeric ratio
ee	enantiomeric excess
equiv.	equivalent(s)

ESI	electrospray ionisation
EWG	electron-withdrawing group
Fc	ferrocenyl
Fmoc	fluorenylmethyloxycarbonyl
H	hour(s)
HMBC	heteronuclear multiple-bond correlation
HMQC	heteronuclear multiple-quantum correlation
HPLC	high performance liquid chromatography
HRMS	high resolution mass spectrometry
HSQC	heteronuclear single-quantum correlation
Hz	Hertz
IPA	propan-2-ol
J	coupling constant
KHMDS	potassium bis(trimethylsilyl)amide
LDA	lithium diisopropylamide
LiHMDS	lithium bis(trimethylsilyl)amide
M	molar
m-	meta
m.p.	melting point
m/z	mass to charge ratio
min	minute(s)
mol	mole(s)
Ms	mesyl, methanesulfonyl
n.a.	not applicable
NBS	*N*-bromosuccinimide
NMR	nuclear magnetic resonance
nOe	nuclear Overhauser effect
NOESY	nuclear Overhauser effect spectroscopy

Ns	*p*-nitrobenzenesulfonyl
o-	ortho
p-	para
Ph	Phenyl
PG	protecting group
py	pyridine
ppm	parts per million
R	generic organic group
R_f	retention factor
RDS	rate determining step
Red-Al®	sodium bis(2-methoxyethoxy)aluminiumhydride
sat.	saturated
t_R	retention time
tert	tertiary
TBAF	tetrabutylammonium fluoride
TBS	*tert*-butyldimethylsilyl
TFA	trifluoroacetic acid
THF	tetrahydrofuran
TLC	thin layer chromatography
TMS	trimethylsilyl
Tol	toluyl
Ts	*p*-toluenesulfonyl
Wilkinson's catalyst	$RhCl(PPh_3)_3$
wt%	weight percent

Table of Contents

Chapter 1: Introduction:

Mechanistic Studies on Enyne Cycloisomerisation.....1

1.1 History of Enyne Cycloisomerisation……1

1.2 Mechanistic Investigations on Enyne Cycloisomerisation……3

1.2.1 Palladium……...4

1.2.2 Ruthenium……14

1.2.3 Other Metals…….21

1.2.3.1 Gold…….21

1.2.3.2 Rhodium……...23

1.2.3.2 Titanium……...24

Chapter 2: Mechanistic Insights into Palladium-catalysed Cycloisomerisation—Isotopic Labelling Study and Kinetic Profiling…….....26

2.1 Deuterium Crossover Experiments……..28

2.2 Timecourse ^{1}H NMR Spectroscopic Experiments……..32

2.2.1 Kinetic Profile Comparison…….32

2.2.2 The Role of Water……41

2.2.3 The Role of Bbeda……...44

2.3 Palladium Sources……52

2.4 Conclusions……..54

Chapter 3: Mechanistic Insights into Palladium-catalysed Cycloisomerisation—Computational Analysis and Kinetic Isotope Effects……..56

3.1 Computational Analysis……...56

3.1.1 Reaction Pathway…….56

3.1.2 Stereoselectivity Explanation……...61

3.2 Experiments on Kinetic Isotope Effects……...66

3.3 Conclusions……..72

Chapter 4: Introduction:

Asymmetric Transition Metal-Catalysed 1,6- and 1,7-Enyne Cycloisomerisations……..73

4.1 Palladium…….73

4.2 Rhodium……...79

4.3 Other Related Metal-Catalysed Processes……...88

4.4 Conclusions……..89

Chapter 5: Asymmetric Rhodium-Catalysed Cycloisomerisation of Enynamides…….....90

5.1 Preliminary Study on Asymmetric Cycloisomerisation of Enynamides…….90

5.1.1 Test substrate synthesis……90

5.1.2 Palladium Catalysis……..91

5.1.2 Rhodium Catalysis……...98

5.2 Catalysis System Development……99

5.2.1 Catalyst System Optimisation……..99

5.2.2 The 2nd Generation Catalyst System…….104

5.3 Scope of the Asymmetric Rhodium-Catalysed Cycloisomerisation……..109

5.3.1 Substrate Synthesis……109

5.3.2 Substrate Scope……..114

5.4 Conclusions……117

Chapter 6: Conclusions and Future Work…….....118

6.1 Conclusions……118

6.2 Future Work: Double Stereodifferentiation in Enynamide Cycloisomerisation……120

6.3 Future Work: Kinetic Resolution in Enynamide Cycloisomerisation……...122

Chapter 7: Experimental……...123

7.1 General Experimental……123

7.2 General Experimental Procedures……..124

7.3 Characterisation of Compounds……..128

7.4 X-Ray Crystallographic Data…….203

Chapter 8: References……...205

Chapter 9: Appendix……...…..212

9.1 Publications during DPhil research……212

Chapter 1: Introduction: Mechanistic Studies on Enyne Cycloisomerisation

Enyne cycloisomerisation – a process whereby 1,*n*-enynes undergo an intramolecular Alder-ene reaction to give carbocyclic compounds – is a valuable and fully atom-economic method for ring construction.[1] Since cyclic organic frameworks are common in natural products and biologically active compounds, this method of skeletal reorganisation is a powerful tool for chemists to synthesise such complex molecules.

1.1 History of Enyne Cycloisomerisation

Although the uncatalysed thermal pericyclic cycloisomerisation of enynes has been known for over a century,[2–4] the high temperatures required (often over 300 °C) severely limited its scope. As a result, it was used relatively little in organic synthesis.[5]

In 1985, Trost and co-workers reported the first metal-catalysed cycloisomerisation of 1,6-enynes through palladium catalysis (Scheme 1.1).[6]

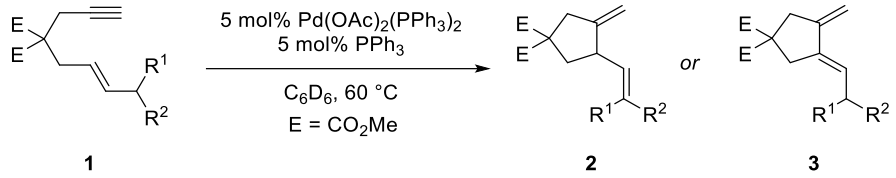

Scheme 1.1

Since then many other transition metals (*e.g.* Rh, Ru, Pt, Au) have been shown to facilitate the cycloisomerisation of 1,*n*-enynes (*n* = 4, 5, 6, 7, *etc*.). In comparison to the thermal cycloisomerisation, the metal-catalysed transformation can provide 1,3- and/or 1,4-dienes as the products with decent selectivity, while only 1,4-dienes can be obtained from the thermal uncatalysed reactions (Scheme 1.2).[7]

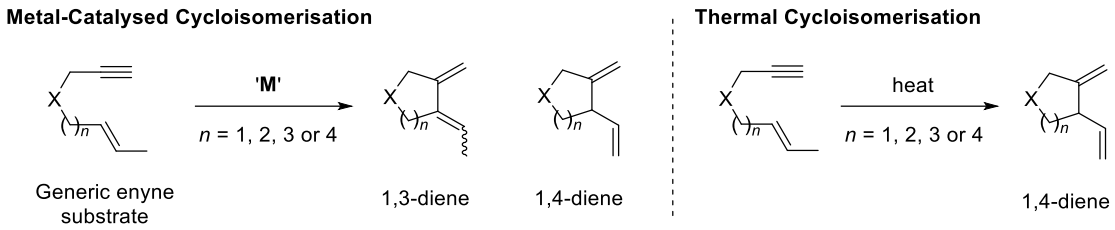

Scheme 1.2

In addition, the metal-catalysed cycloisomerisation usually offers better regiochemical and stereochemical controls compared to the thermal process. As a consequence, cycloisomerisation has become one of the most effective approaches for rapid construction of complex organic cyclic molecules.

The mechanism of a transition metal-catalysed cycloisomerisation depends on the catalyst system and reaction conditions. The following represents some of the possible routes for the cyclisation process to proceed:

Metal hydride species mediated pathway

The alkyne undergoes hydrometallation to give a vinyl metal complex **4** (Scheme 1.3). This vinyl species subsequently undergoes carbometallation, and eliminates the β-hydrogen to yield the cyclic dienes.

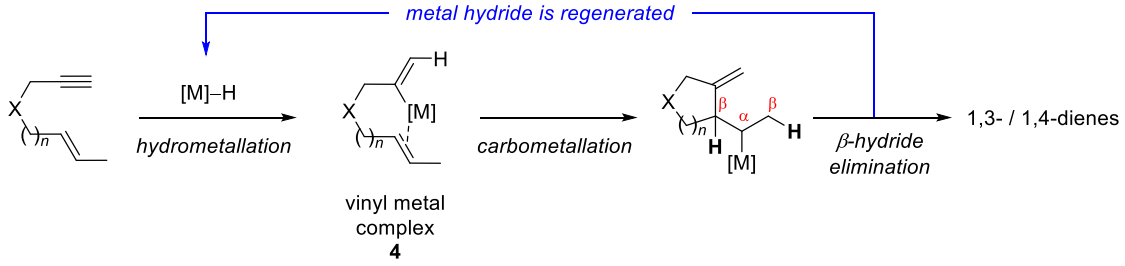

Scheme 1.3

Activated η^2*-metal species mediated pathway*

The metal can complex the alkyne unit to give an electrophilic η^2-metal-alkyne intermediate **5**, which is prone to nucleophilic cyclisation *via* either 5-*exo*-dig or 6-*endo*-dig pathways with the alkene to form the corresponding cyclopropyl metal carbenes **6**, which can participate in further reactions (*e.g.* skeletal reorganisation) to give the products (Scheme 1.4).

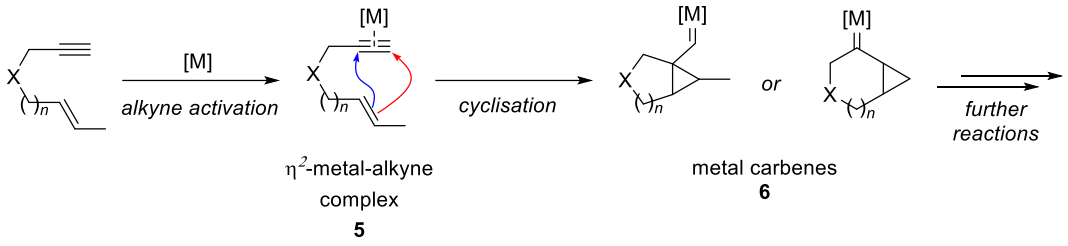

Scheme 1.4

Metallacyclopentene mediated pathway

In this mechanism, the metal simultaneously complexes to both alkene and alkyne units, forming a metallacycle intermediate **7** *via* an oxidative coupling process (Scheme 1.5). This cyclic metal complex can undergo β-hydride elimination to relieve the ring strain. The cyclic olefin product is obtained by the reductive elimination of metal hydride complex **8**.

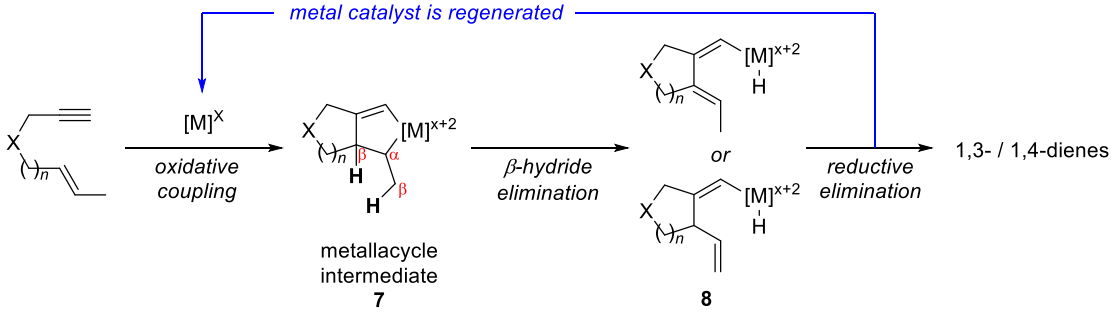

Scheme 1.5

1.2 Mechanistic Investigations on Enyne Cycloisomerisation

Despite its versatility in organic synthesis, this methodology can still be improved in many aspects, for example, efficiency and robustness of catalysts, scope and selectivity of the reaction, *etc*. It is challenging to address such issues as the transition metal complex used in most metal-catalysed cycloisomerisation processes is usually in the form of a pre-catalyst, which will subsequently generate the active species.[8] This active catalyst can facilitate undesired pathways, leading to the formation of many unwanted products. Indeed, gaining more mechanistic understanding on the metal-catalysed cycloisomerisation will allow chemists not only to suppress side reactions, but also to enhance the catalyst efficiency, and improve selectivity of the reaction.

Herein we focus on the mechanistic studies on the metal-catalysed (mainly palladium and ruthenium) cycloisomerisation of 1,*n*-enynes that only involves migrations of hydrogen and associated bond

reorganisation with no carbon–carbon bond cleavage. That is, the processes where no carbon skeletal rearrangement takes place (Scheme 1.6).

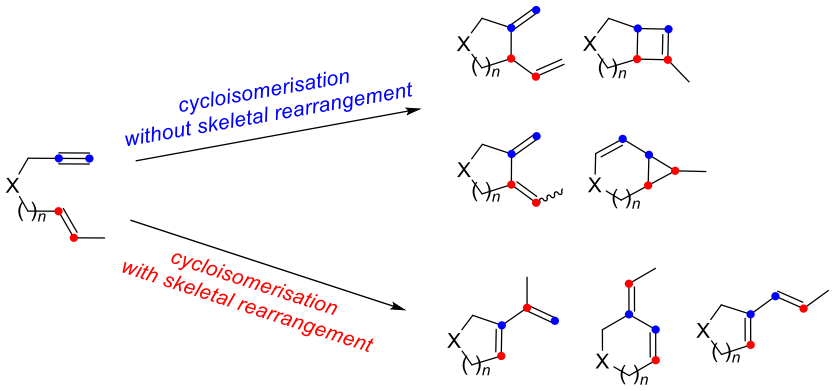

Scheme 1.6

1.2.1 Palladium

As noted above, the exploration in palladium-catalysed cycloisomerisation of 1,*n*-enynes was initiated by Trost and Lautens,[6] who performed carbocyclisation of 1,6-enynes **1** using $Pd(OAc)_2(PPh_3)_2$ as catalyst; 1,3-dienes **3** were exclusively obtained when the allylic carbon was disubstituted (R^1 and $R^2 \neq$ H, Scheme 1.7, left), while (*E*)-1,4-dienes (*E*)-**2a** were formed with high selectivity when the allylic carbon was monosubstituted (R^1 = H, Scheme 1.7, right).

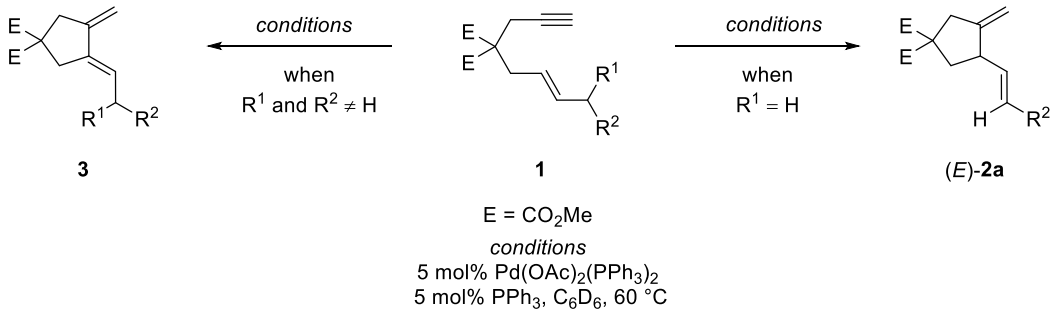

Scheme 1.7

In this early work, Trost *et al.* considered two mechanisms for this palladium-catalysed cyclisation: 1) allylic C–H insertion, and 2) oxidative cyclopalladation (Scheme 1.8). Since the cycloisomerisation of enyne **1** with a disubstituted allylic group provided 1,3-dienes **3** as sole product, the mechanism for this process cannot proceed *via* the allylic C–H insertion route. In addition, this mechanism cannot explain some cases where both 1,3- and 1,4 dienes were observed in the reaction, because such a mechanism can only account for the formation of 1,4-dienes.

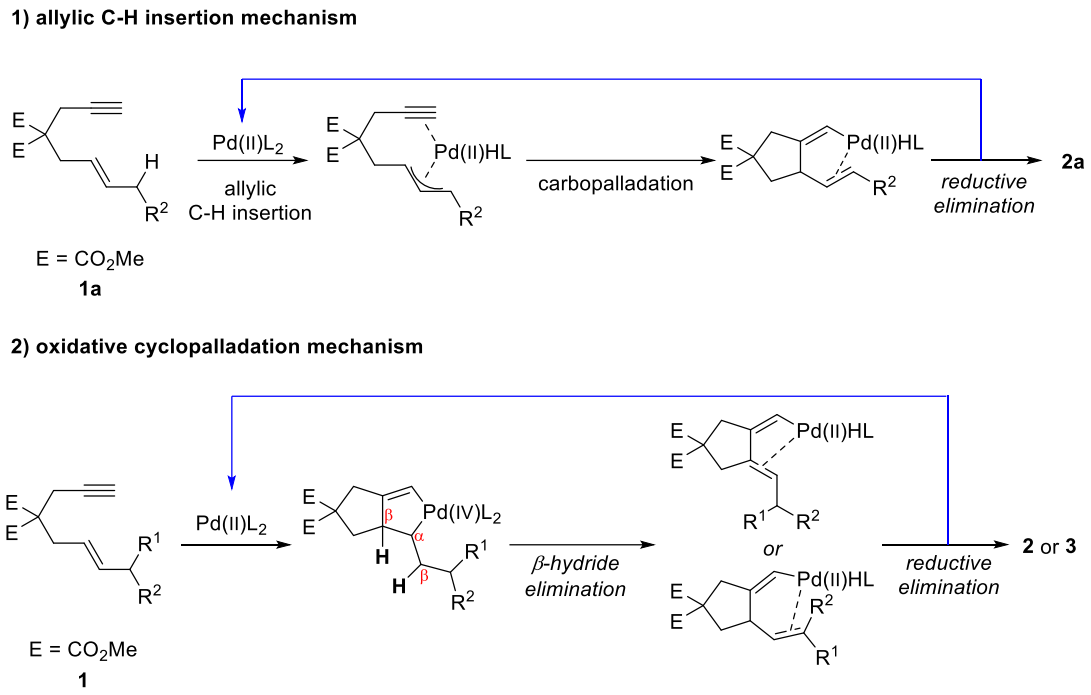

Scheme 1.8

Interestingly, Trost *et al*. discovered that when a Pd(0) species such as $Pd(PPh_3)_4$ was used as catalyst, no reaction was observed after 12 h at reflux in THF (Table 1.1, Entry 1). This suggested that the active species of palladium complex ought to be in the Pd(II) oxidation sate. They also found that the effectiveness of the Pd(II) species was connected to the Lewis acidity of the metal centre. For instance, the cyclisation of enyne **9** to give diene **10** in the presence of $Pd(CH_3CN)_2Cl_2$ was sluggish (16% conversion after 6.5 h at reflux in THF, Entry 2); while $Pd(OAc)_2L_2$ (L = PPh_3 or P(*o*-MePh)$_3$) could effect complete conversion at room temperature or reflux depending on the ligand (Entries 4 and 5).

Table 1.1 Cycloisomerisation of enyne **9** with various palladium sources.

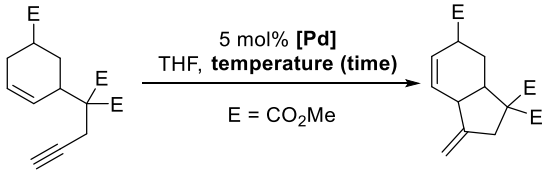

Entry	[Pd]	Temperature (time)	Conversion
1	$Pd(PPh_3)_4$	reflux (12 h)	no conversion
2	$Pd(MeCN)_2Cl$	relux (6.5 h)	16%
3	$Pd(OAc)_2$	r.t. (n/a)	50%
4	$Pd(OAc)_2(PPh_3)_2$	r.t. (12 h)	>99%
5	$Pd(OAc)_2[(o\text{-}MePh)_3P]_2$	60 °C (1.5 h)	>99%

This suggested that the mechanistic pathway for 1,*n*-enyne cycloisomerisation with the Pd(II) catalysts could be the palladacycle pathway (Scheme 1.8, bottom).

In 1991, Trost and co-workers revised their earlier conclusion on the mechanism of palladium-catalysed enyne cycloisomerisation after more detailed investigations.[9] It was discovered that during the process of preparing enyne **9** using Pd(0)-catalysed alkylation of cyclohexene **11** with alkyne **12**, a small amount of 1,4-diene **10** (about 35%) was observed (Scheme 1.9). This unexpected product could have been obtained from a palladium-catalysed cycloisomerisation of enyne **9**.

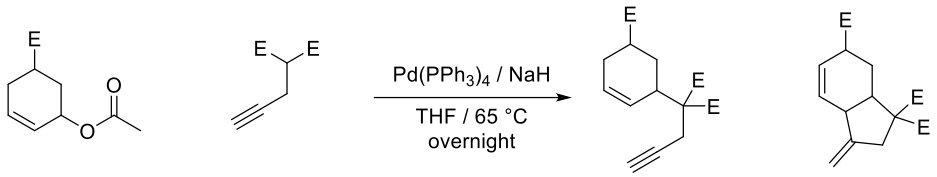

11 **12** **9** **10** (35%)

Scheme 1.9

It was proposed that the Pd(0) catalyst from the coupling reaction could be oxidised by oxygen present in air to give some Pd(II) species, which catalysed the cyclisation of the enyne. The hypothesis was tested by performing the cycloisomerisation of enyne **9** with 5 mol% of $Pd(OAc)_2$, which indeed gave product **10** with moderate yield at room temperature (Table 1.1, Entry 3). Furthermore, an isotopic labelling study with by cyclohexenyl malonate d_1-**9** (>95% D) was conducted (Scheme 1.10); this experiment showed that 1,4 diene (*E*)-d_1-**10** was formed as the major kinetic product at the early stages of the reaction (after 30 min). Later, this product (*E*)-d_1-**10** slowly converted to thermodynamic product (*Z*)-d_1-**10** until an equilibrium was reached. Neither deuterium loss in the substrate and products, nor double bond migration was observed.

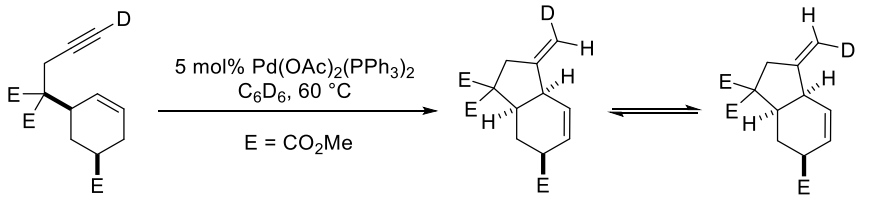

d_1-**9** (*E*)-d_1-**10** *kinetic product* (*Z*)-d_1-**10** *formed over time*

Scheme 1.10

Although H/D exchange of the acetylenic proton is possible, the corresponding protiated substrate **9** was not observed over time. Moreover, NMR spectroscopy showed no signs of products d_2-**10** and **10**. Hence, the presence of (*Z*)-d_1-**10** in the product mixture was proposed to arise from a side reaction that

was unrelated to the cycloisomerisation. This result is consistent with both the *syn*-hydropalladation of alkyne pathway (Scheme 1.11), which was at first overlooked, and the oxidative cyclopalladation mechanism.

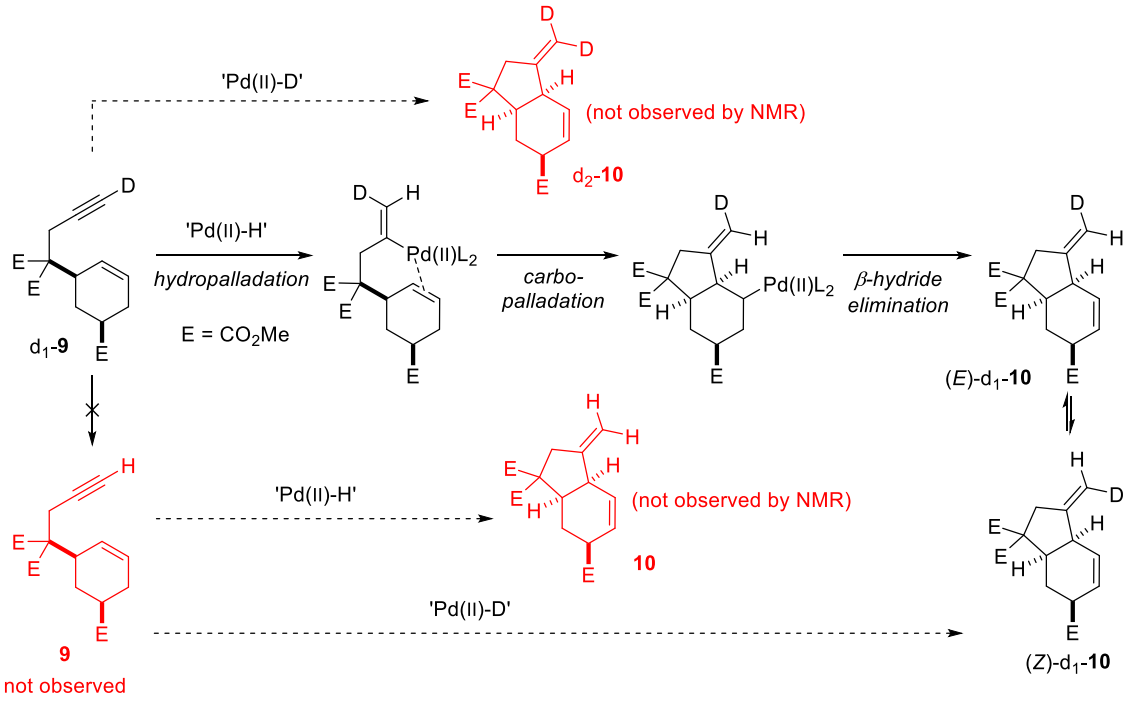

Scheme 1.11

The Lewis acidity of the Pd(II) source was found to affect the yields, rate of the reaction, and product purity; addition of a Lewis basic nitrogen ligand, for example, *N*,*N*-bis(benzylidene)ethylenediamine (bbeda), together with $Pd(OAc)_2$ to the reaction substantially improved the yields. Trost proposed that bbeda could not only lead to suitable π-acidity of the Pd(II) complex, but the ligand could also stabilise the putative Pd(IV) palladacyclopentene intermediate (Scheme 1.12).[10]

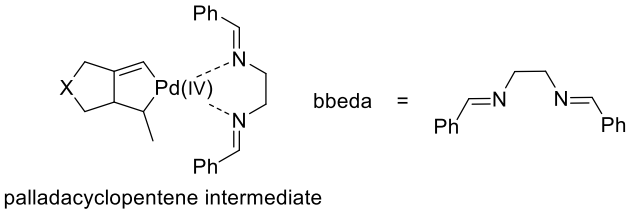

Scheme 1.12

Therefore, it was suggested that the $Pd(OAc)_2$ / bbeda catalyst system could promote the Pd(II) / Pd(IV) cycle. However, this alone did not rule out the hydropalladation mechanism; to strengthen the feasibility of the oxidative metallacycle mechanism, Trost and Tanoury employed a palladacyclopentene **13** / tri-

o-tolyl phosphine catalyst system to cycloisomerise enyne **14**.[11] Pleasingly, this reaction indeed proceeded to give dienes **15** and **16** (Scheme 1.13). This reaction was the first example for the 1,6-enyne cycloisomerisation with a skeletal rearrangement.

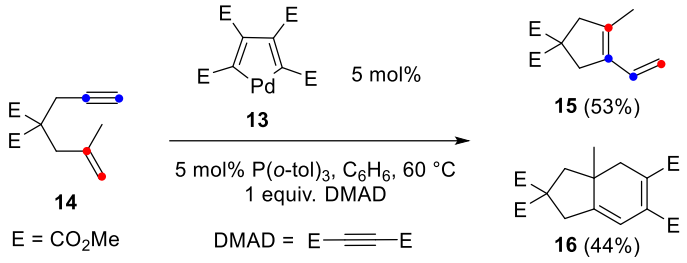

Scheme 1.13

Not long after the first introduction of this palladacycle pre-catalyst, the Trost group reported a new catalyst system: $Pd_2(dba)_3{\cdot}CHCl_3$ / AcOH.[12] Trost proposed that this system could generate a Pd(II)–H species *in situ* from oxidative addition, *i.e.* insertion of Pd(0) into the H–O bond of the acid (Scheme 1.14),[13] although, this species was not observed by ^{1}H NMR spectroscopy when mixing AcOH and $Pd_2(dba)_3$ in $CDCl_3$.

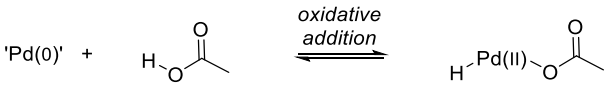

Scheme 1.14

Intriguingly, the cycloisomerisation of electron deficient enyne **17** with $Pd(OAc)_2$ proceeded smoothly, whereas under $Pd_2(dba)_3{\cdot}CHCl_3$ / AcOH conditions, the substrate failed to cyclise to give **18** (Scheme 1.15).[14] This seemed to imply that the two catalyst systems operate *via* different mechanisms: $Pd_2(dba)_3{\cdot}CHCl_3$ / AcOH system *via* a Pd(II)–H mediated mechanism, while $Pd(OAc)_2$ *via* a palladacyclopentene mediated pathway.

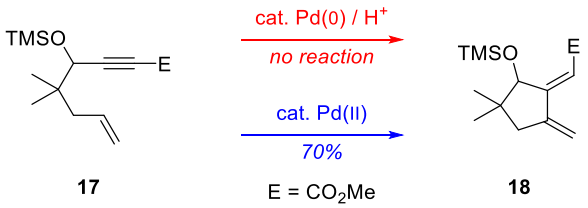

Scheme 1.15

Trost *et al*. revealed evidence that supported the hydropalladation mechanism for 1,6-enyne cycloisomerisation using Pd(0) / AcOH. When enyne **19** was cycloisomerised using $Pd_2(dba)_3{\cdot}CHCl_3$

as Pd(0) source in the presence of 1 equiv. AcOD, 1,3-diene **20** was obtained with a high level of deuterium scrambling in the products: d_0-**20** (54%), d_1-**20** (39%),1:5 *E*/*Z* ratio, and d_2-**20** (7%) were all formed.[15] H/D exchange at the terminal alkyne hydrogen of **19**, forming d_1-**19**, was also detected. The small amount of d_2-**20** produced was proposed to arise from deuteriopalladation of the alkyne in starting material d_1-**19** (Scheme 1.16). The 5:1 *Z*/*E* ratio of d_1-**20** could be explained by the *syn*-addition of Pd(II)–D to alkyne **19**, and the *syn*-addition of Pd(II)–H to alkyne d_1-**19**, respectively.

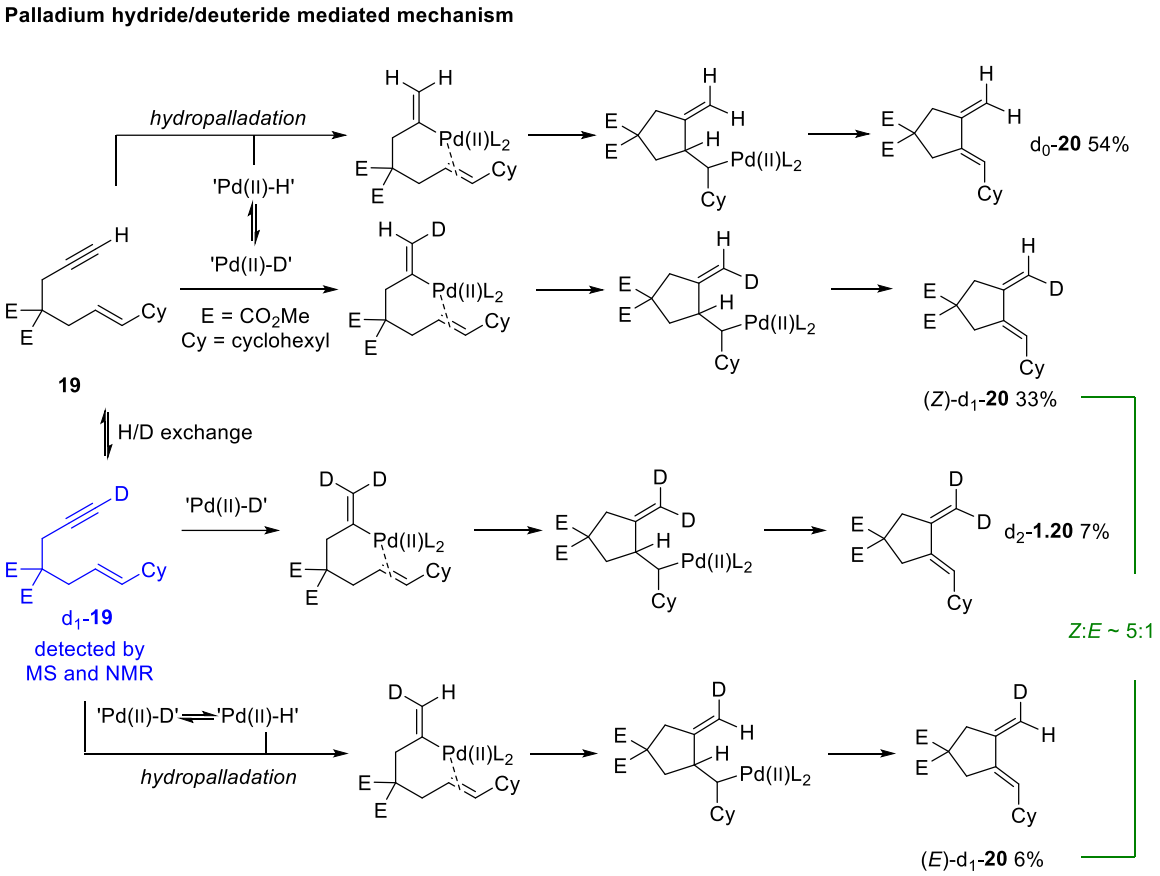

Scheme 1.16

While, the hydrometallation mechanism can provide a satisfactory rationale for deuterium scrambling in the products, the Pd(II) / Pd(IV) cycle pathway can also rationalise this. Vinylpalladium hydride species d_0-**21**, formed after β-H elimination, can undergo H/D exchange with AcOD to give corresponding deuteride intermediate d_1-**21**. Reductive elimination of such an intermediate leads to monodeuterated product (*Z*)-d_1-**20** (Scheme 1.17). H/D exchange to deuterated substrate d_1-**19**, followed by the same reaction pathway, results in products d_2-**20** and (*E*)-d_1-**20**.

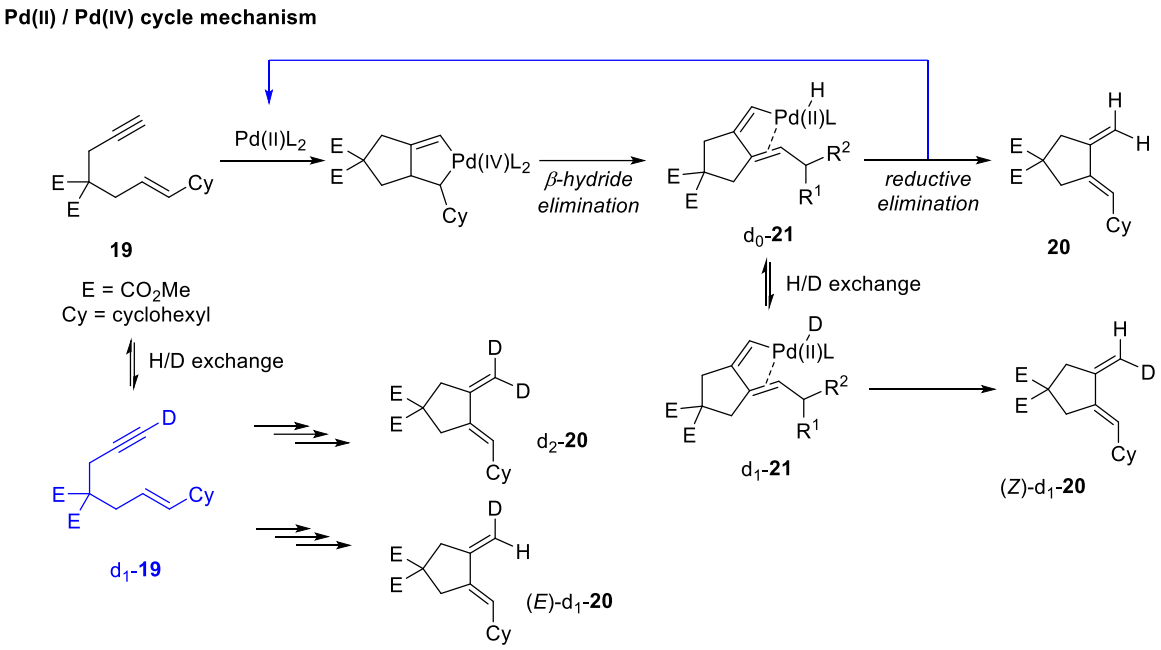

Scheme 1.17

A key indication that the hydropalladation mechanism is operative for the $Pd_2(dba)_3{\cdot}CHCl_3$ / AcOH was found through interception of the alkylpalladium intermediate. If β-hydride elimination cannot proceed due to no β-hydrogen atom, and the molecule contains another alkene unit, a further *syn*-carbopalladation can take place to generate additional ring frameworks. To illustrate, dienyne **22** can be cycloisomerised to generate [4.3.3] and [3.3.3] propellanes **24**. Such tricyclic propellanes can be then converted into propellenones **25** (Scheme 1.18).[16]

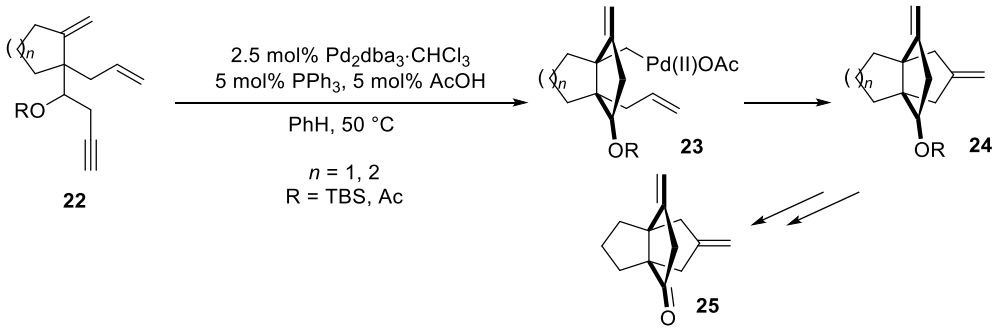

Scheme 1.18

Mikami and co-workers investigated the mechanism of palladium-catalysed asymmetric cycloisomerisations, and have reported that deuterium incorporation in the product (74% D) was observed during the cycloisomerisation of enyne **26** using $Pd(CF_3CO_2)$ or $Pd(MeCN)_4(BF_4)_2$ and (*R*)-BINAP, in the presence of 6 equiv. D_2O (Scheme 1.19).[17]

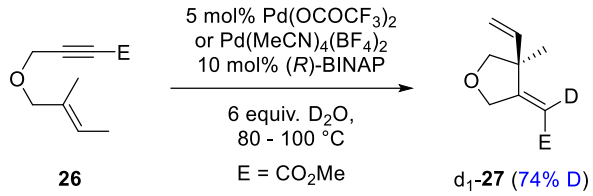

Scheme 1.19

Mikami proposed that Pd(II)–H species could undergo hydride exchange with D_2O to produce Pd(II)–D intermediates, which enter a deuteriometallation cycle. However, a rationale for how Pd(II)–H species was generated in the first place was not given.

Mikami and Hotano later carried out a detailed mechanistic investigation on oxygen-tethered asymmetric 1,6-enyne cycloisomerisation with a Pd(II) metal precursor and chiral bisphosphine ligand.[18] Mikami *et al*. first considered three possible pathways for this cyclisation to take place: the η^2-metal activated alkyne species mediated pathway, the oxidative enyne coupling *via* metallacycle intermediate mechanism, and the alkyne hydrometallation route. The study started with the Pd(II)-catalysed cycloisomerisation of enyne **28a** to give 1,3-dienes **29a** and 1,4-dienes **30a** (Scheme 1.20). Since the formation of cyclic *exo*-diene **31a** was not observed, which could have been generated if the π-acid activation mechanism was operating, this mechanism was proposed to be unlikely to be the case.

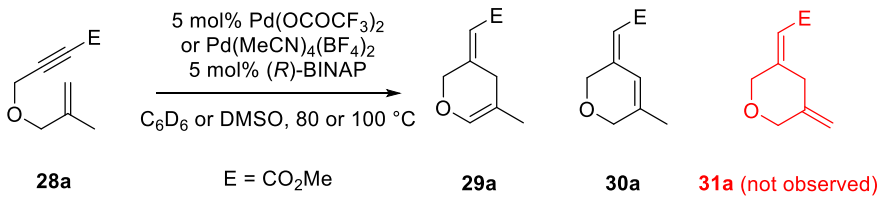

Scheme 1.20

Next, Mikami *et al.* aimed to isolate palladacyclopentene **32** from the cyclisation of β-phenyl enyne **28b**, as this enyne substrate should lead to a palladacycle species that has no β-hydrogen atom. This was unsuccessful with the reaction instead giving a mixture of dienes **29b** (26%) and **30b** (55%) (Scheme 1.21). Thus, palladacycle pathway was rejected.

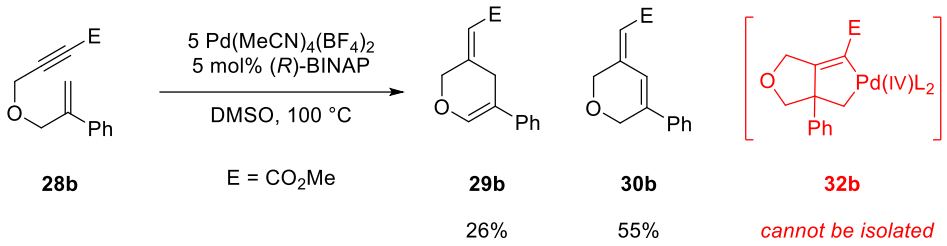

Scheme 1.21

This led to an examination of a hydrometallation mechanism: once again, Pd(II)-catalysed cycloisomerisation of enyne **28a** was performed, but this time in presence of 6 equiv. D_2O (Scheme 1.22). A high percentage of deuterium incorporation was observed in the products at the exocyclic olefin, α-position to the ester unit.

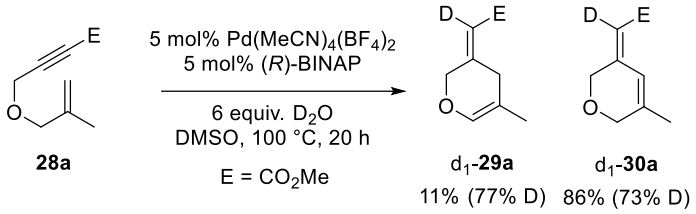

Scheme 1.22

This suggested a *syn*-addition of Pd(II)–D across the alkyne, then *syn*-carbopalladation by the vinylpalladium complex with the alkene to give d_1-**33a**. Since this species lacks β-hydrogens, it can then undergo *syn*-addition / elimination *via* the cyclopropane intermediate d_1-**34a** to give 6-membered cyclic *exo*-olefin d_1-**35a**. Elimination of one of the β-hydrogens produces d_1-**29a** or d_1-**30a** as products (Scheme 1.23). Although hydropalladation could thus provide a highly satisfactory explanation for the product distribution and deuterium incorporation, the generation of the active Pd(II)–H species from the Pd(II) precursor was mysterious.

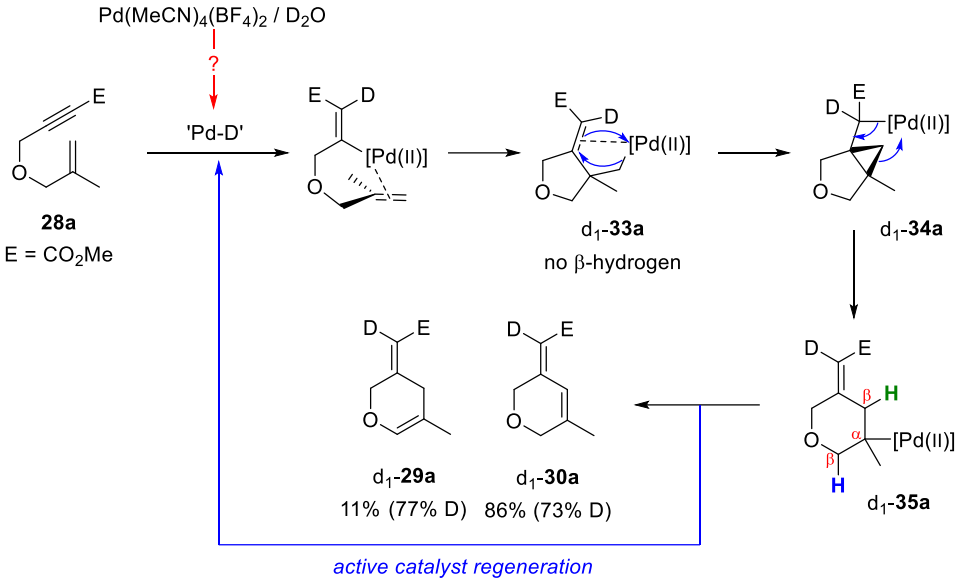

Scheme 1.23

Trost and co-workers also used the $Pd_2(dba)_3{\cdot}CHCl_3$ / AcOH catalyst system to isomerise enyne **36** to yield bicyclic dienes **37**.[19] Trost discovered that in the absence of acetonitrile, diene isomers **38** and **39** were obtained together with the major product **37**. However, in the presence of acetonitrile, the olefin isomerisation was completely suppressed (Scheme 1.24).

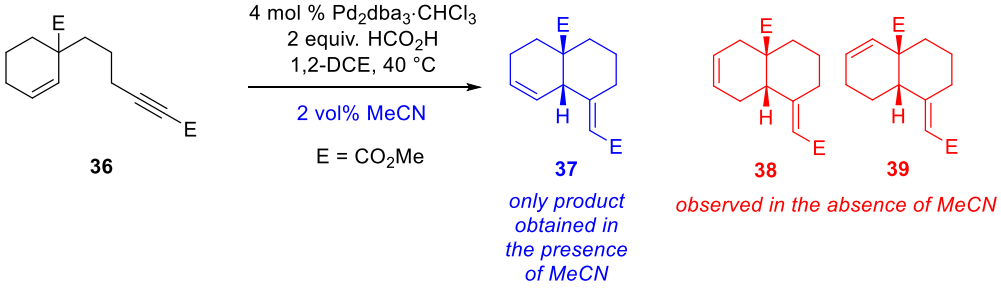

Scheme 1.24

This may indicate that decomplexation of the product from the active Pd(II)–H species is promoted by the presence of acetonitrile *via* a ligand exchange process. On the other hand, without acetonitrile, the 1,4-diene product can still be bound to the Pd(II)–H species, allowing the hydride re-insertion / elimination to take place, resulting in double isomerisation to give products **38** and **39** (Scheme 1.25).

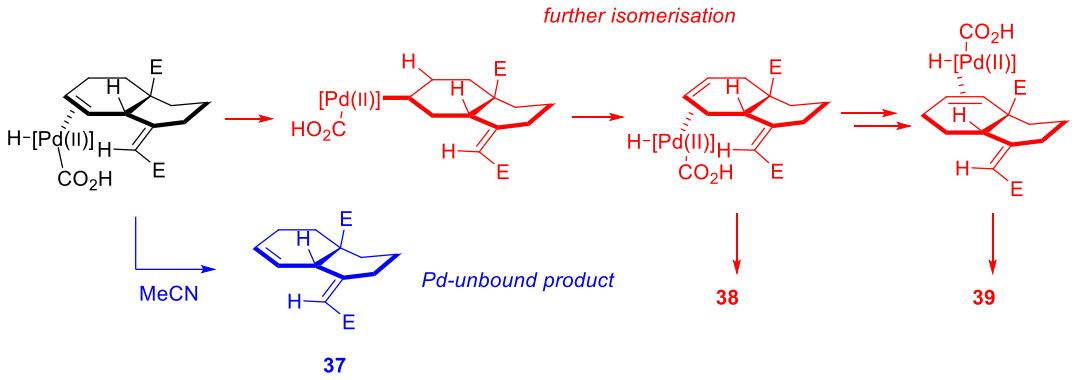

Scheme 1.25

Our group recently reported the use of 1,6-enynamides to investigate the mechanism of cycloisomerisation when using $Pd(OAc)_2$ / bbeda catalyst system.[20] We found that the reaction pathway is unlikely to proceed *via* the Pd(II) / Pd(IV) catalytic cycle. We reported that the mechanism by which this catalyst system operates is a Pd (II)–H mediated pathway with supporting evidence from ^{1}H NMR spectroscopic kinetic profile studies, kinetic isotope effects, and computational analysis. Moreover, we discovered a ground-breaking role of bbeda, which was believed to only act as a ligand. Bbeda in fact is very crucial for the generation of Pd(II)–H species, as it serves as a hydride source for such a process. Equally importantly, we proved that this process also occurs in the enyne cycloisomerisation. The details of this work will be discussed in the later chapters of this thesis.

1.2.2 Ruthenium

The first ruthenium-catalysed 1,5- and 1,6-enyne cycloisomerisation (without carbon backbone rearrangement) was reported by Mori and co-workers, who used $RuHCl(CO)(PPh_3)_3$ as the ruthenium pre-catalyst for the cycloisomerisation of enyne **40** to give cyclic 1,3-dienes **41** and **42** respectively (Scheme 1.26).[21–22]

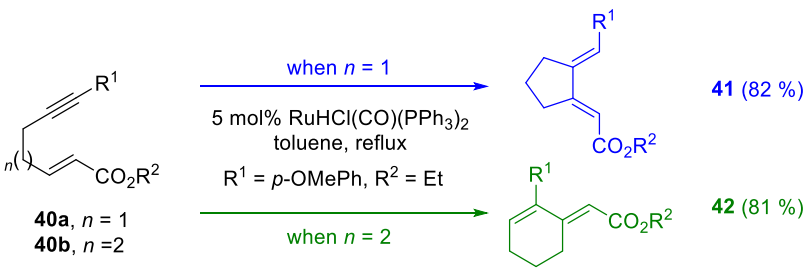

Scheme 1.26

Not long after this work, the Trost[23–26] and Dixneuf[27] groups reported another two catalyst systems for enyne cycloisomerisation: $CpRu(MeCN)_3PF_6$ and Cp*Ru(cod)Cl / AcOH, respectively. Both Mori and Dixneuf suggested that this reaction proceeds *via* a hydroruthenation mechanism (Dixneuf proposed that the required Ru–H intermediate could be generated from ruthenium insertion into the O–H bond of acetic acid). This was supported by complete stereospecific deuterium incorporation in product **44** when an excess of AcOD was used instead of AcOH (Scheme 1.27).[27]

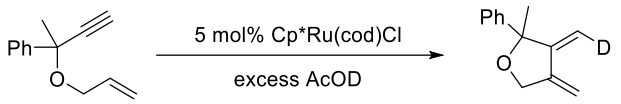

43 d_1-**44** (100%D),

Scheme 1.27

In addition, the cycloisomerisation of 1,6-enyne substrates with either the Mori or Dixneuf catalyst systems gives exocylic 1,3-dienes **46**, where R^1 and R^2 are in *trans*-relationships to the new C–C bond (Scheme 1.28).[21,27] This again supports the proposed hydrometallation mechanism due to the stereoelectronic requirement for β-hydride elimination.

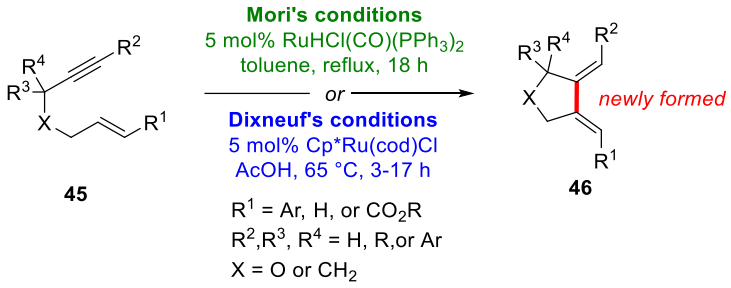

Scheme 1.28

On the other hand, the Trost group proposed two different modes of operation for the catalyst system $[CpRu(MeCN)_3]PF_6$, depending on the substrate: 1) ruthenacycle and 2) allylic C–H insertion mechanisms (Scheme 1.29).[24, 25] The first pathway leads to the formation of 5-membered cyclic 1,4-dienes, while the latter results in 7-membered cyclic 1,4-dienes as the products. When simple enyne **47a** was subjected to the ruthenium catalyst in acetone at room temperature, 1,4-diene **48** (3:1 *cis*:*trans* ratio) was obtained in 46% yield with no formation of the 1,3-diene that is prevalent with the equivalent palladium-catalysed process. This reaction can proceed *via* a normal ruthenacycle pathway. In contrast,

when similar enyne **47b** was reacted under the same conditions, the 7-membered ring product **49** was generated, which was proposed to proceed *via* a allylic C–H insertion mechanism.

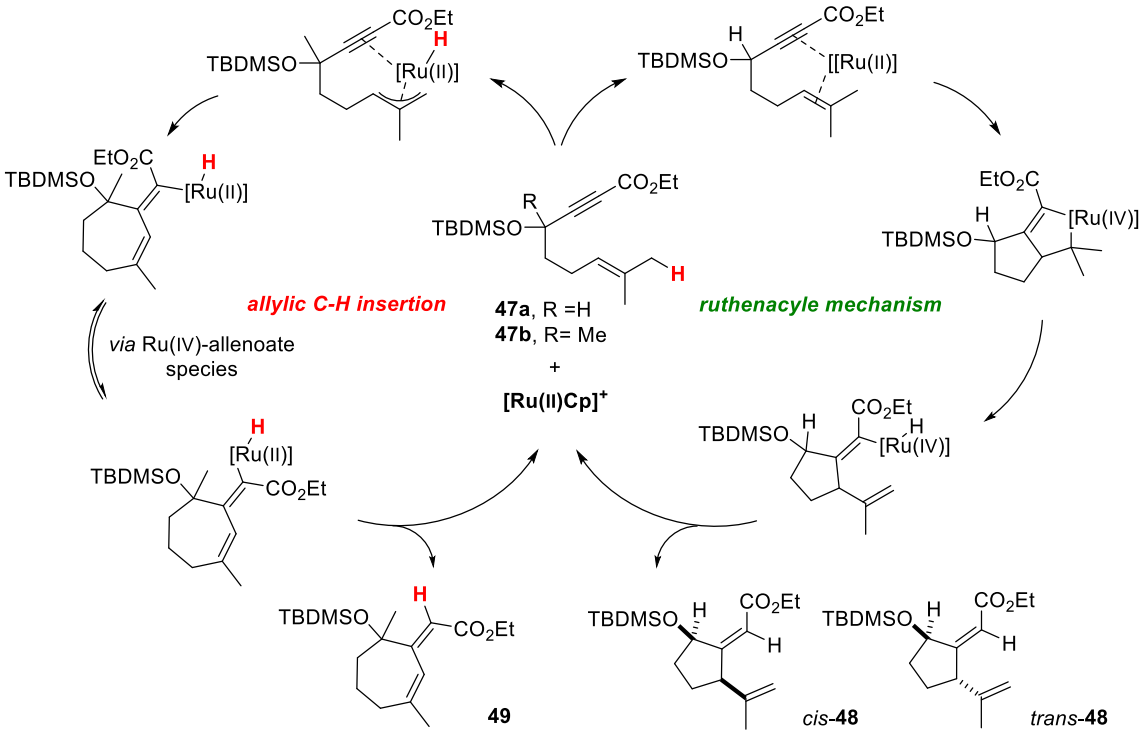

Scheme 1.29

The reason for this dramatic difference in the reaction mechanism could be attributed to steric hindrance in hypothetical enyne-ruthenium complex **51a**. When R^1 is OTBDMS and R^3 is Me, disfavoured $A_{1,3}$-strain between R^3 at the quaternary centre and the ester group (R^4) would be very pronounced. Together with severe 1,4 -diaxial steric clash between R^1 and R^2 (Me) groups, these steric interactions are likely present the formation of **51a** (Scheme 1.30).

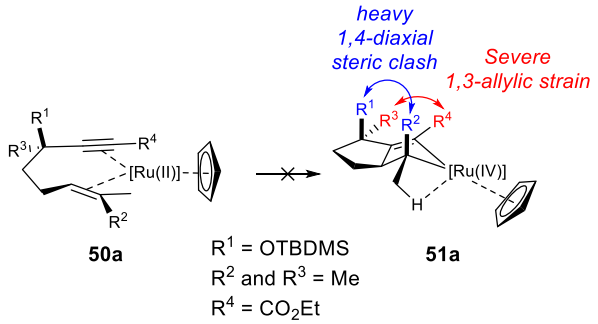

Scheme 1.30

The normal ruthenacycle mechanism in which the ruthenacyclopentene complex could adopt two different conformations: **51b′** and **51b″**. For the first possible conformation, **51b′**, the silyl ether group

(R^3) is placed in a pseudoequatorial position which leads to severe 1,3-allylic strain with the ester group (R^4). Another possibility is **51b″**, the OTBDMS unit (R^3) is in a pseudoaxial position, resulting in a decrease in 1,3 -allylic strain. However, R^4 group can still create a 1,4-diaxial steric repulsion with the pseudoaxial methyl group (R^2). These steric factors lead to the observed diastereoselectivity of the reaction (Scheme 1.31).

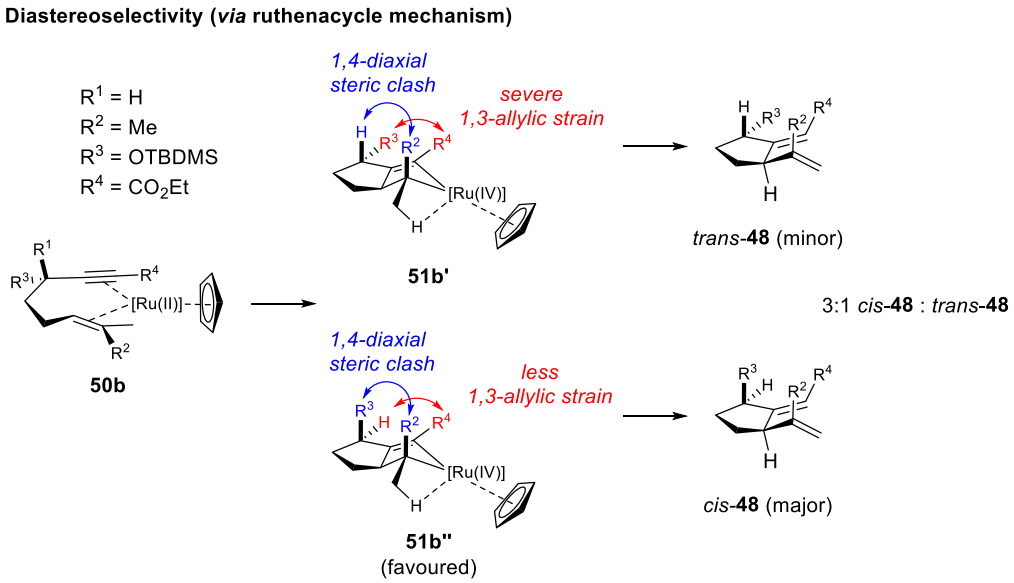

Scheme 1.31

For enyne **47b**, the generation of a 7-membered ring product (**49**) was observed (*via* allyl-ruthenation of the alkyne). The proposed mechanism was strongly supported by the reaction of deuterated substrate (*Z*)-d_3-**47b**, which smoothly produced d_3-**49** (with >95%D) as a single regioisotopomer (Scheme 1.32).

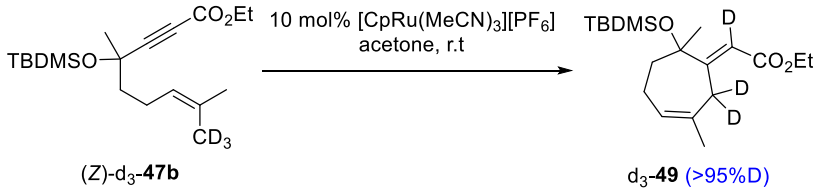

Scheme 1.32

In 2004, Trost and co-workers reported the effect of an allylic silyl ether on the stereoselectivity of the ruthenium-catalysed 1,6- and 1,7-enyne cycloisomerisations.[28] The reaction diastereoselectivity is dependent on the geometry of substrate **52** (*E*- or *Z*-isomer). The ruthenacycle mechanism can be used to account for the observed stereoselectivity of the enol silane formation: starting from enyne (*E*)-**52**, ruthenacyclopentene **53″** places the silyl ether group in a favourable pseudoequatorial position.

Conformer **53″** (leading to silane (*E*)-**54**) is slightly preferred over conformer **53′** (leading to silane (*Z*)-**54**), as a result the products are obtained with a 2.4:1 *E*:*Z* ratio (Scheme 1.33).

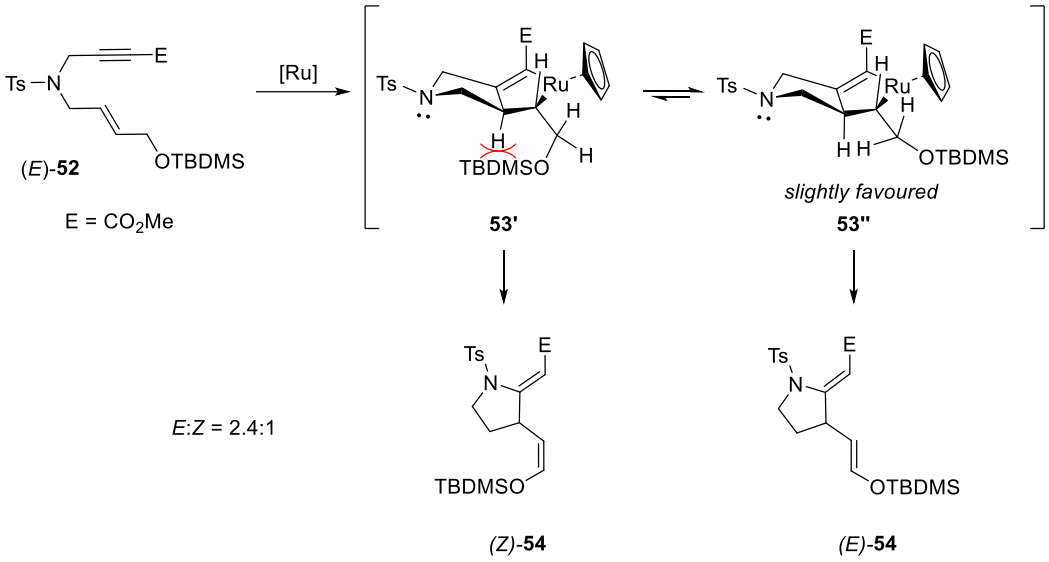

Scheme 1.33

Interestingly, when the Cp group on the ruthenium catalyst is changed to Cp*, the selectivity is reversed, *i.e.* (*Z*)-**54** is the major product (*E*:*Z* ratio = 1:5). This is because the difference of steric congestion (with the Cp* ligand) between conformer **55′** and **55″** is markedly increased; ruthenium complex **55′** is now much more favourable (Scheme 1.34).

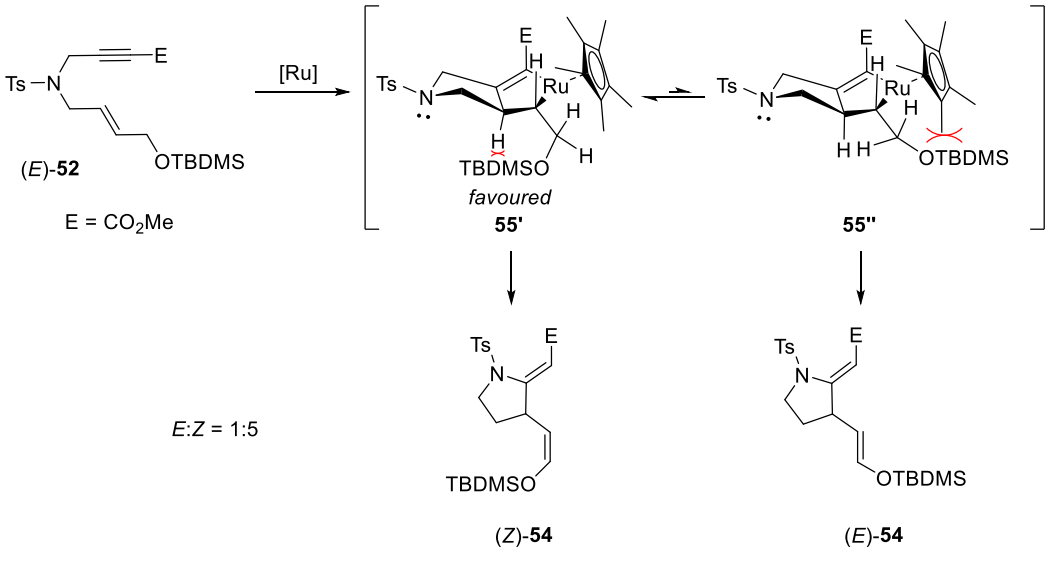

Scheme 1.34

In case of the cycloisomerisation of enyne (*Z*)-**52**, the silyl ether group is now forced to orient in a pseudoaxial position in intermediate **56′**. This time, conformer **56″** is much more sterically stable

compared to **56′** (Scheme 1.35), and a dramatic increase in *E*:*Z* selectivity is observed (from 2.4:1 to 25:1).

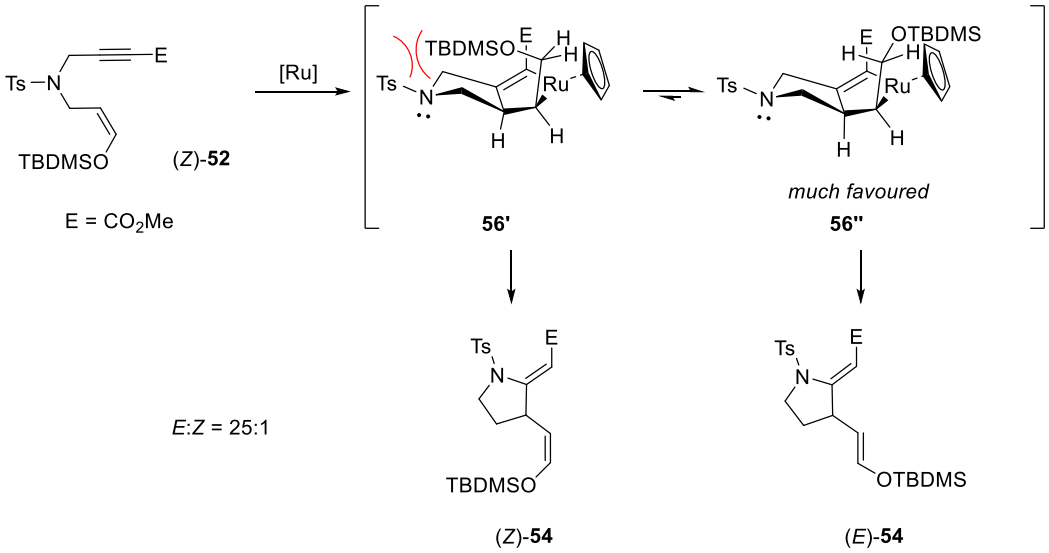

Scheme 1.35

In 2008, The Trost group reported that ruthenium-catalysed enyne cycloisomerisation could also facilitate the stereoselective formation of bicyclic structures.[29] At the beginning, their attempt to cyclise enyne **57a** was unsuccessful (Scheme 1.36).

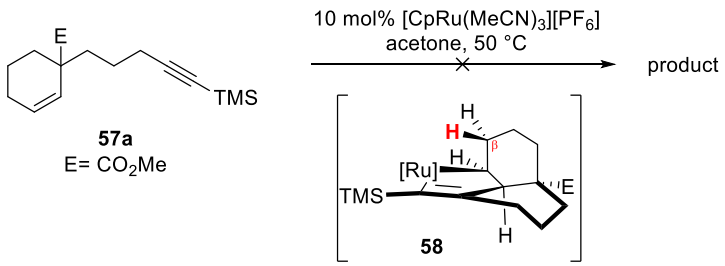

Scheme 1.36

Trost rationalised that the reaction was initiated by ruthenacyclopentene formation between the alkyne, alkene, and the ruthenium catalyst to form intermediate **58**. Possibly due to the high activation energy for β-elimination of the hydrogen at the pseudoaxial position in **58**, β-elimination does not occur, and hence no product was formed.

Using enynes with an electron-deficient alkyne unit, such as **57b**, the reaction proceeds cleanly to afford 1,4 enyne *trans*-**59** in a single diastereomer with excellent yield (Scheme 1.37).

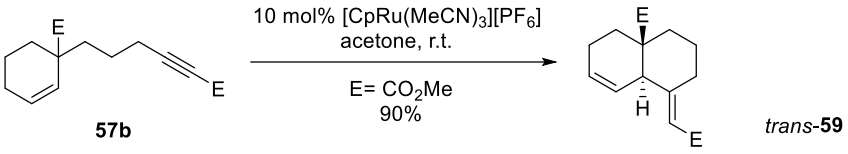

Scheme 1.37

This outcome was proposed to arise from an allylic C–H insertion mechanism, which explains the diastreroselectivity of the reaction. The carbonyl group of the ester was proposed to direct the formation of η^3-allyl complex **60**, then ligand exchange between the carbonyl and the alkyne groups takes place to form intermediate **61**. Carboruthenation, followed by reductive elimination subsequently occur to produce product *trans*-**59** (Scheme 1.38).

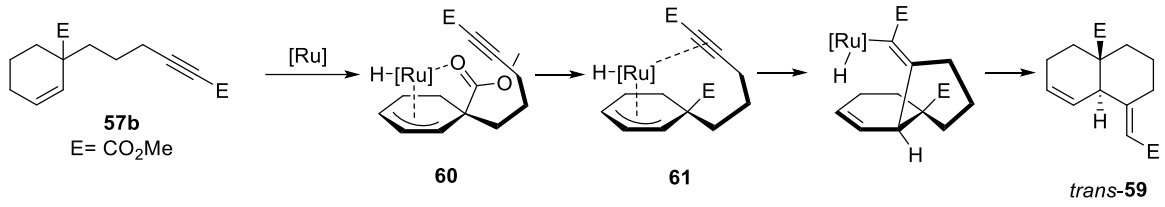

Scheme 1.38

Arisawa and co-workers showed that ruthenium hydride complex **62** derived from the second-generation Grubbs catalyst (Grubbs II) could catalyse the cycloisomerisation of silyl enol ether with alkynyl silane **63** to produce indoline **64** (Scheme 1.39).[30]

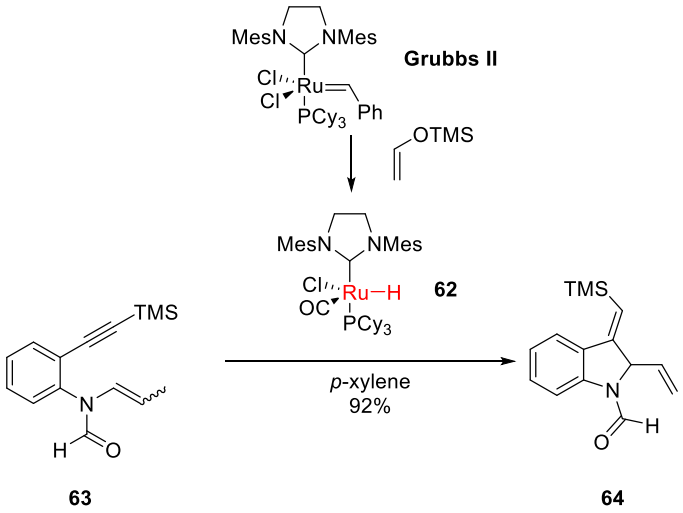

Scheme 1.39

The cycloisomerisation reactions were performed with Grubbs II catalyst and rhodium hydride complex **62** in *p*-xylene separately. Timecourse (^{1}H and ^{31}P) NMR experiments supported the mechanism of

hydroruthenation of the alkyne. Ruthenium hydride complex **62** coordinates to enyne **63**, hydroruthenation at the alkyne subsequently takes place to give the vinylruthenium species. The intermediate then undergoes carbometallation and β-hydride elimination respectively to give product **64** (Scheme 1.40).

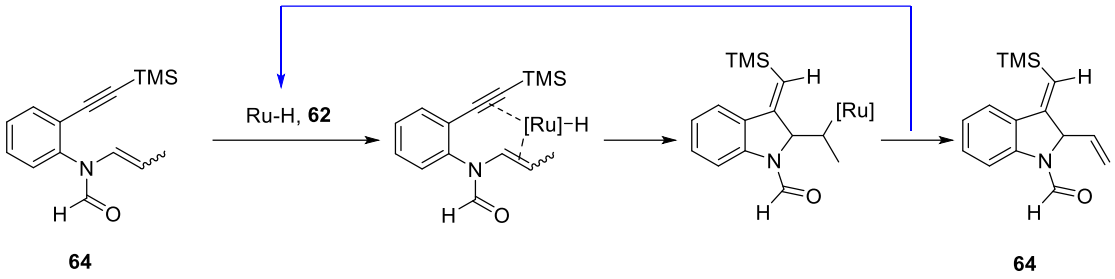

Scheme 1.40

1.2.3 Other Metals

1.2.3.1 Gold

Gold (I) complexes are powerful catalysts for the electrophilic activation of alkyne towards nucleophilic attack by various species, including alkenes. Since the $[AuL]^+$ complex is isolobal to H^+, it is unlikely to coordinate to the alkene and the alkyne simultaneously. Consequently, unlike Pd(II) or Ru(II) catalysis, the mechanism for Au(I)-catalysed enyne cycloisomerisations usually initiates *via* the activated η^2-metal alkyne complex mediated pathway (Scheme 1.41).[31, 32]

Gold-catalysed enyne cycloisomerisations can proceed through a number of different mechanisms. For instance, the enyne substrate can be transformed *via* 5-*exo*-dig cyclisation into cyclopropylcarbenes **66**, which then rearrange to form dienes **67** (single cleavage) and/or **68** (double cleavage); such skeletal rearrangements are well known in gold catalysis. On the other hand, 6-*endo*-dig cyclisation can take place to give alternative carbenes **69** that can lead to non-skeletal rearrangement products **70** *via* deprotonation / protodeauration. Alternatively, these cyclopropylcarbenes can undergo cyclopropane ring expansion isomerisation to give η^2-cyclobutene-gold(I) complexes **71**. This intermediate was detected by NMR spectroscopy and has been characterised by X-ray diffraction.[33] Isomerisation and decomplexation subsequently takes place to give cyclobutene products **72**. Apart from isomerisation,

complex **71** can also undergo gold-catalysed 4π-electrocyclic ring opening, which leads to **67** (Scheme 1.41).

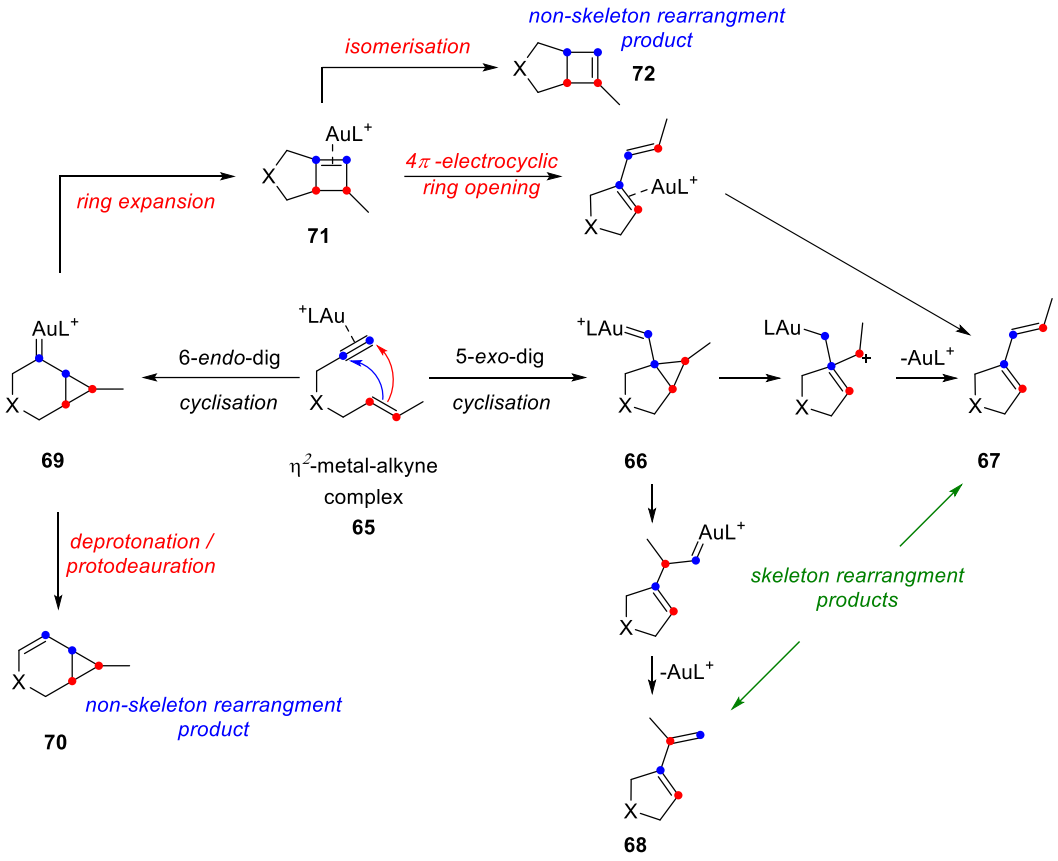

Scheme 1.41

The Echavarren group has conducted mechanistic investigations of gold-catalysed 1,6-enyne cycloisomerisation. 1,6-enyne **73** was cyclised using gold complex **74** to give a mixture of dienes **75** and **76** (Scheme 1.42).[34]

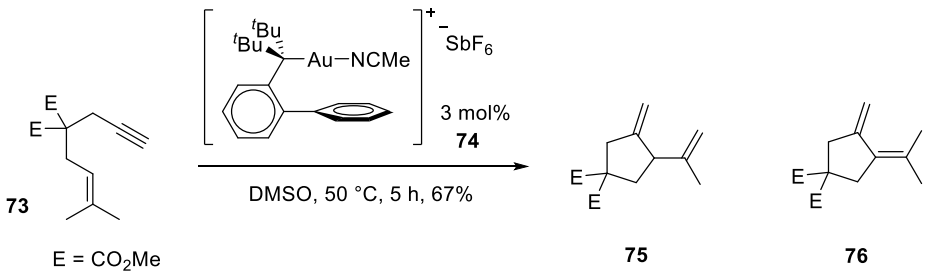

Scheme 1.42

Although diene product **75** appears to be the product from traditional Alder-ene isomerisation, the cyclisation of deuterated enyne d_1-**73** with the same catalyst provided dienes d_1-**75** and d_1-**76** in a 1:0.6 ratio. This deuteration pattern is not that expected from the Alder-ene cycloisomerisation, as the classic

cycloisomerisation would lead to d_1-**77**. The formation of products **75** and **76** can instead be explained by ring opening of cyclopropylcarbene **79** to afford cationic vinylgold complex **80**, then deprotonation and protodeauration to give the products (Scheme 1.43).

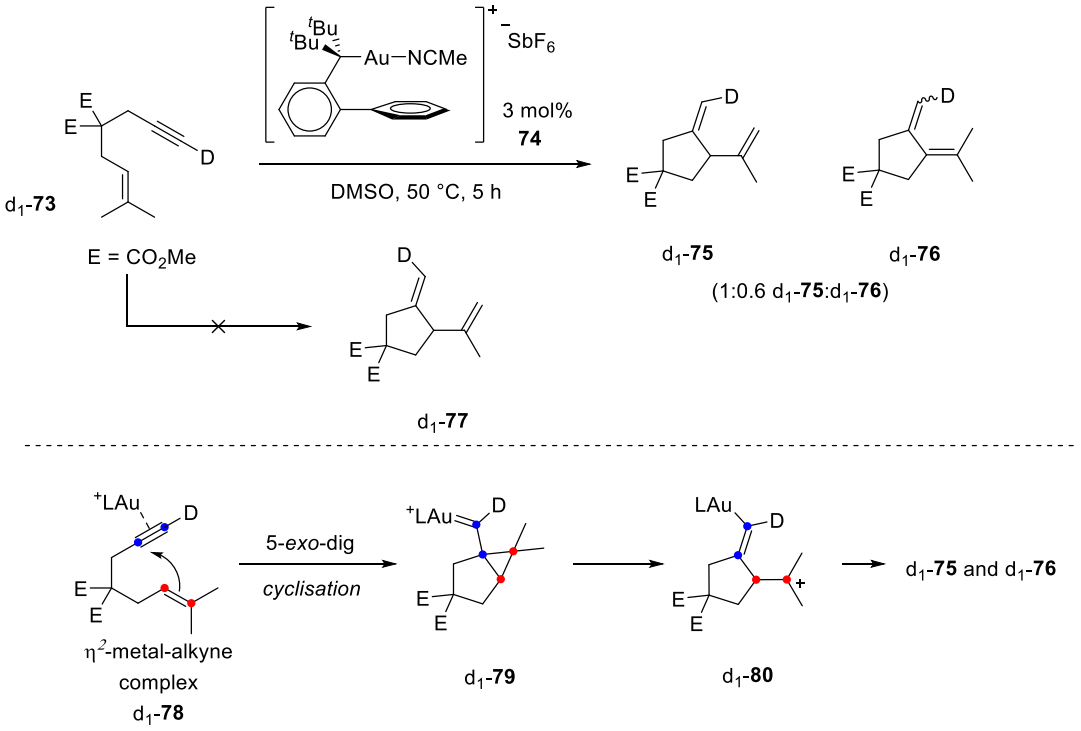

Scheme 1.43

1.2.3.2 Rhodium

The first rhodium catalysed 1,6-enyne cycloisomerisation was achieved by Grigg using Wilkinson's catalyst, whereby enyne **81** was reacted to give cycloisomer **82** (Scheme 1.44).[35]

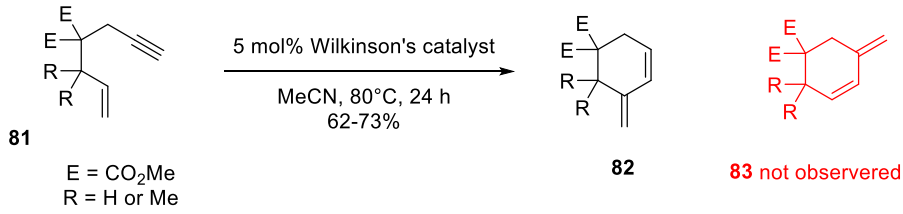

Scheme 1.44

However, this reaction was restricted the use of a terminal alkyne, which is indicative of the insertion of the metal into the C–H bond of the alkyne to generate a Rh(III) hydride intermediate **84**. Given that only product **82a** was observed (not product **83a**), an usual *trans*-hydrorhodation of the alkyne was

proposed, followed by 6-*exo*-trig carboruthenation to afford cyclohexene **85** β-hydride elimination subsequently occurs to give product **82a** (Scheme 1.45).

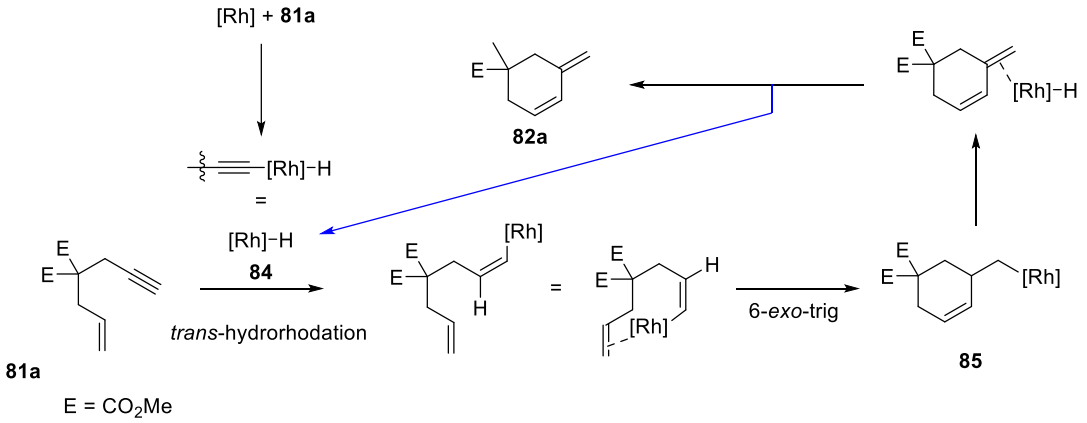

Scheme 1.45

It is worth noting that prior to the Grigg's work Trost and Tour had attempted to use a Ni-Cr-based catalyst to facilitate the cyclisation of similar enynes, but the reaction yield is poor.[36] The Zhang group later demonstrated the use of cationic rhodium catalysts with a chiral ligand, such as (*R*,*R*)-Me-DuPhos, to perform a highly enantioselective cycloisomerisation of 1,6-oxygen tethered enyne **86** to give **87** (Scheme 1.46).[37] This is the first example of asymmetric rhodium-catalysed cycloisomerisation. The mechanism of this rhodium catalysis will be later discussed (*see* Chapter 4).

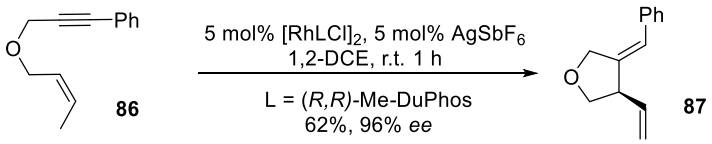

Scheme 1.46

1.2.3.2 Titanium

Buchwald reported a rare example of using early transition state metal to catalyse the enyne cycloisomerisation, which involved a highly regioselective cycloisomerisation of enyne **89** to obtain only 1,4-dienes **90** in presence of titanocene catalyst **88** (Scheme 1.47).[38]

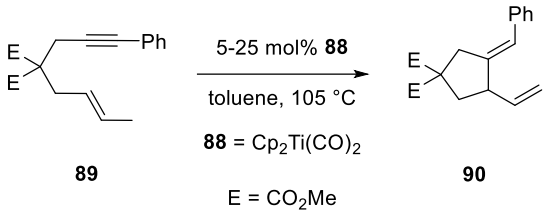

Scheme 1.47

The mechanism was proposed to operate *via* oxidative coupling, β-H elimination, and then CO-driven reductive elimination (Scheme 1.48). This proposed pathway was validated by the preparation of titanocycle **91**, which is a key intermediate involved in this mechanism. At high temperature, metalacycle *trans*-**91** decomposes to give the product **90**. Interestingly, it was found that this thermal decomposition of the complex can be enhanced by introducing a high pressure of CO.

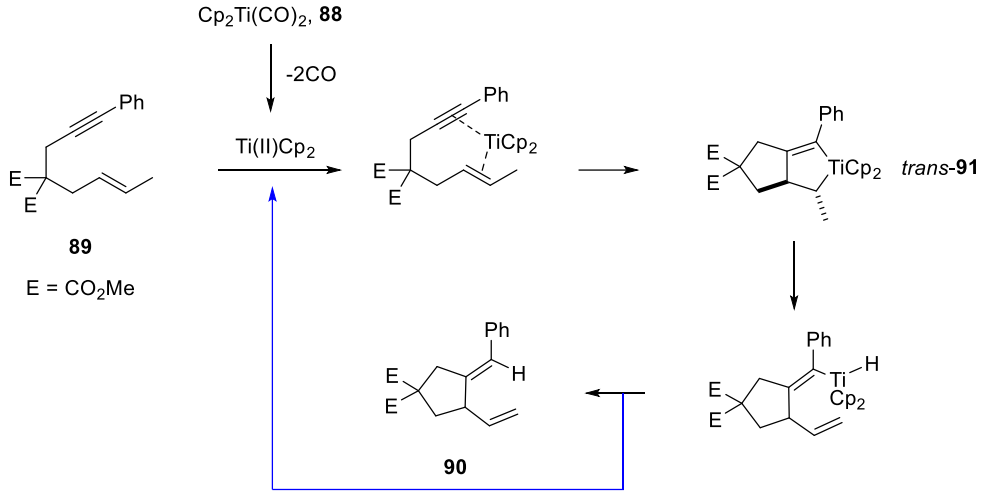

Scheme 1.48

In addition, *cis*-**91** was prepared and proved to be inactive towards the thermal decomposition, as β-hydride elimination is geometrically unfeasible (Scheme 1.49).

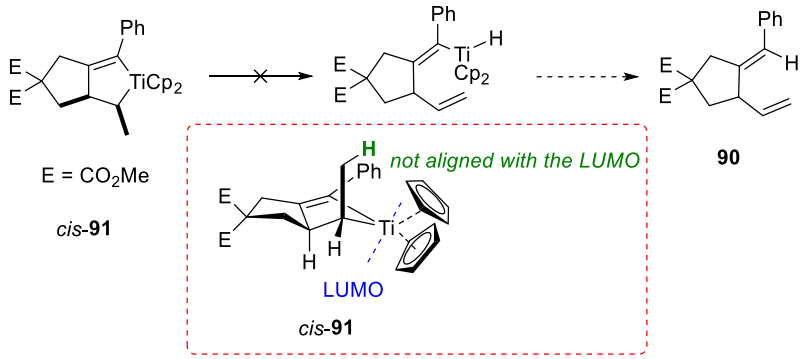

Scheme 1.49

Chapter 2: Mechanistic Insights into Palladium-catalysed Cycloisomerisation—Isotopic Labelling Study and Kinetic Profiling

The remarkable benefits of palladium-catalysed cycloisomerisation in building organic cyclic frameworks have long been long recognised by chemists, especially with the palladium-based catalyst systems developed by the Trost group: $Pd(OAc)_2$ / PAr_3, $Pd(OAc)_2$ / bbeda, and $Pd_2dba_3 \cdot CHCl_3$ / AcOH (with or without phosphine ligand or bbeda) (Scheme 2.1).[9, 14, 39, 40]

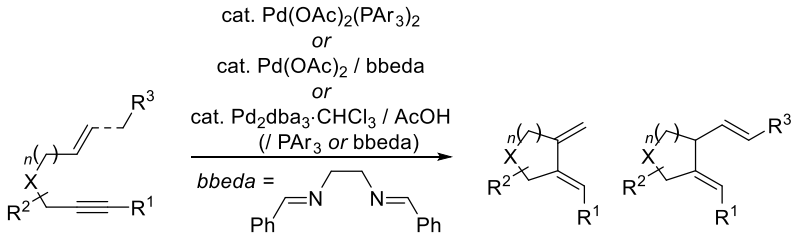

Scheme 2.1

In 2013, our group demonstrated the palladium-catalysed cycloisomerisations of enynamides to form pyrrolidine and piperidine enamides (Scheme 2.2).[20] Such nitrogen heterocyclic compounds are of importance in many fields, such as pharmaceutical and agrochemical industries. In addition, we found that the reaction conditions and time required for enynamide cycloisomerisation are usually milder and shorter compared to that of the regular palladium-catalysed enyne cyclisation.

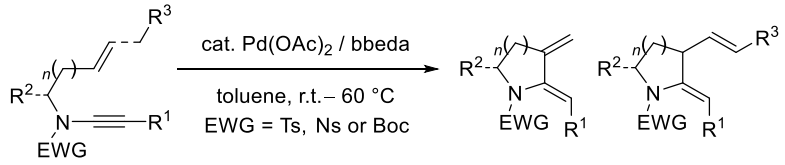

Scheme 2.2

As discussed in the earlier chapter, some mechanistic studies have been carried out for such catalyst systems. This led to strong support for the system of $Pd_2dba_3 \cdot CHCl_3$ / AcOH to operate *via* the mediation of palladium hydride intermediacy. On the other hand, it is still unclear how the $Pd(OAc)_2$ / bbeda catalyst system works during the cycloisomerisation. Trost suggested two possible pathways for

the latter system to proceed: either palladium hydride mediated or palladacycle mediated mechanisms (Scheme 2.3).

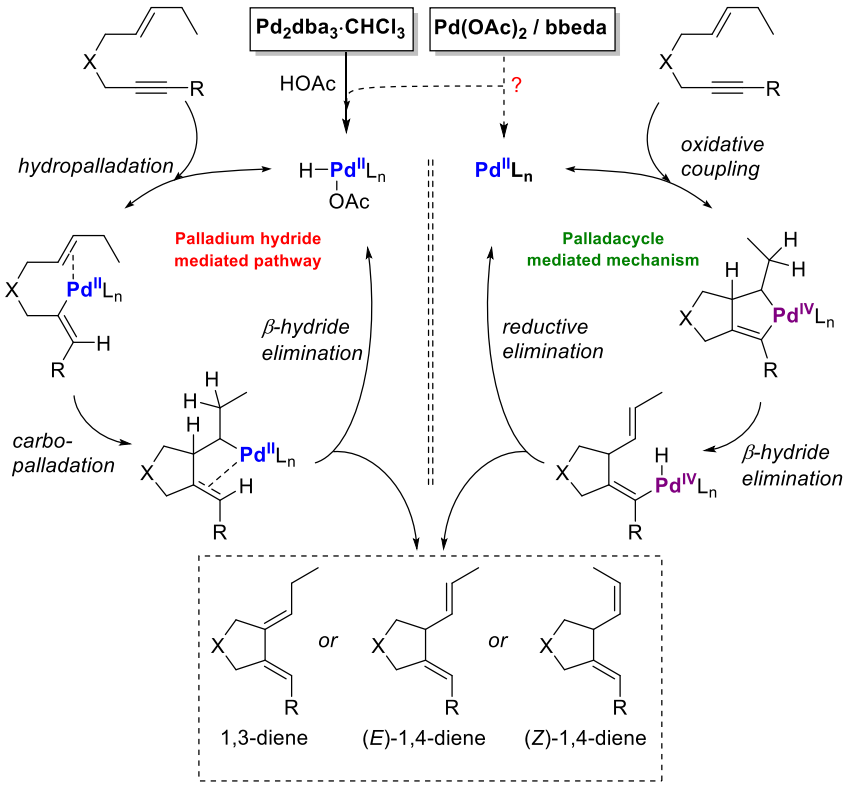

Scheme 2.3

For the former (left), the alkyne undergoes *syn*-hydropalladation resulting in a vinyl palladium complex. This species subsequently undergoes carbopalladation and β-hydride elimination, producing the cyclic dienes. For the latter (right), palladium simultaneously coordinates to both alkene and alkyne units, forming a palladacyclopentene *via* oxidative coupling. This cyclic metal complex then undergoes β-hydride elimination. The cyclic olefin products are obtained by reductive elimination of vinyl palladium hydride complex.

Although both mechanisms can account for the formation of 1,3- and 1,4-diene products. The latter route was favoured by Trost, as bbeda was thought to have a capability to stabilise the Pd(IV) intermediate.[10] However, there is no clear evidence for this. As enynamides had been shown to be rapidly cyclised under mild conditions, we elected to use them as substrates for investigating the mechanism of 1,6-enyne cycloisomerisation with the highly effective catalyst system of $Pd(OAc)_2$ / bbeda.

In our previous work, we reported that the optimised reaction conditions for $Pd(OAc)_2$ / bbeda catalyst system involved the use of 5 mol% of $Pd(OAc)_2$ and 5 mol% of bbeda in toluene (Scheme 2.4). It is also worth noting that the cycloisomerisation of enynamides can also be facilitated by the $Pd_2dba_3{\cdot}CHCl_3$ / AcOH / bbeda system, as well as the ruthenium-based catalyst system: Cp*Ru(cod)Cl in MeCN at 60 °C.

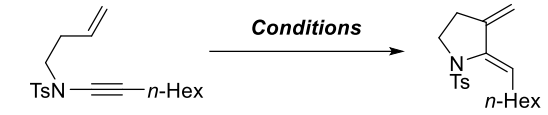

92 **102**

Conditions:

$Pd(OAc)_2$ / bbeda (2.5 mol%), toluene, r.t., 20 min, 85%

or

$Pd_2dba_3{\cdot}CHCl_3$ / AcOH / bbeda (5 mol%), toluene, 60 °C, 10 min, 53%

or

Cp*Ru(cod)Cl (5 mol%), MeCN, 60 °C, 1.5 h, 80%

Scheme 2.4

2.1 Deuterium Crossover Experiments

One apparent difference between the two proposed mechanisms in Scheme 2.3 is the way in which the hydride is transferred during the reaction. An intermolecular hydride transfer is involved in the mechanism operating *via* a palladium hydride species, whilst an intramolecular transfer of hydride supports the palladacycle mechanism. We began our studies with a series of deuterium crossover experiments. In the experiments, deuterated enynamide d_1-**92** (>98% D) and non-deuterated enynamide **93** were reacted in a 1:1 ratio under the optimised conditions of three different catalyst systems: $Pd_2dba_3{\cdot}CHCl_3$ / AcOH / bbeda, Cp*Ru(cod)Cl, and $Pd(OAc)_2$ / bbeda.

Deuterated substrate d_1-**92** was prepared from β-alanine methyl ester hydrochloride salt (Scheme 2.5). First, the salt was converted to sulfonamide **94**, which was then reduced to alcohol d_2-**95** using $LiAlD_4$. The alcohol was subjected to Dess-Martin oxidation to afford the corresponding deuterated aldehyde d_1-**96**. A Wittig olefination of deuterated aldehyde d_1-**96** gave homoallyl sulfonamide d_1-**97**, which was subsequently converted into deuterated ynamide d_1-**92** using Hsung copper-catalysed ynamide formation.[41]

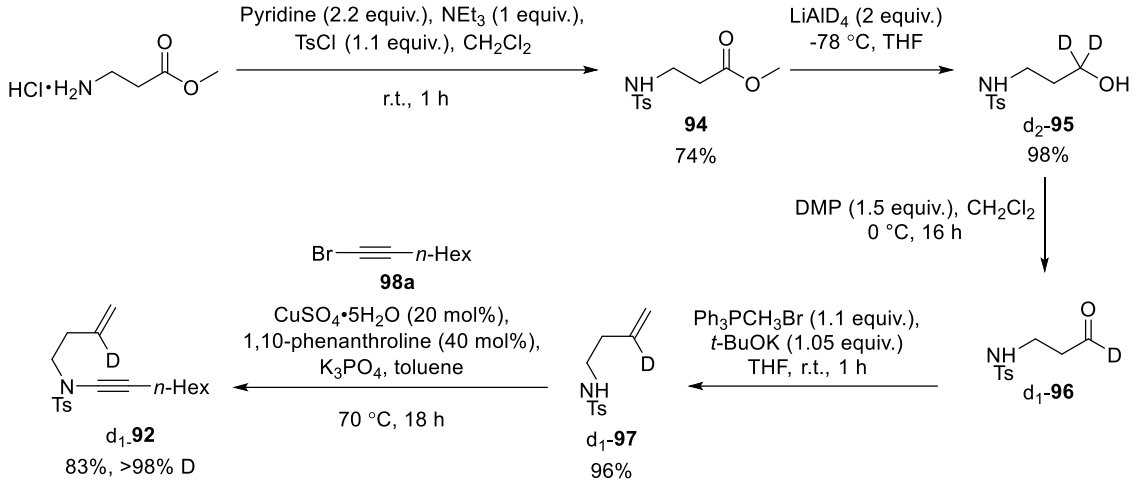

Scheme 2.5

In case of ynamide **93**, A Mitsunobu reaction was employed to facilitate the reaction between commercially available alcohol **99** and $BocNHSO_2C_6H_4NO_2$ to produce Boc-protected *p*-nitrosulfonamide **100** (Scheme 2.6). Removal of the Boc group was performed by using a solution of TFA in CH_2Cl_2, giving sulfonamide **101**. The resulting sulfonamide was converted into ynamide **93** using the same ynamide formation strategy.

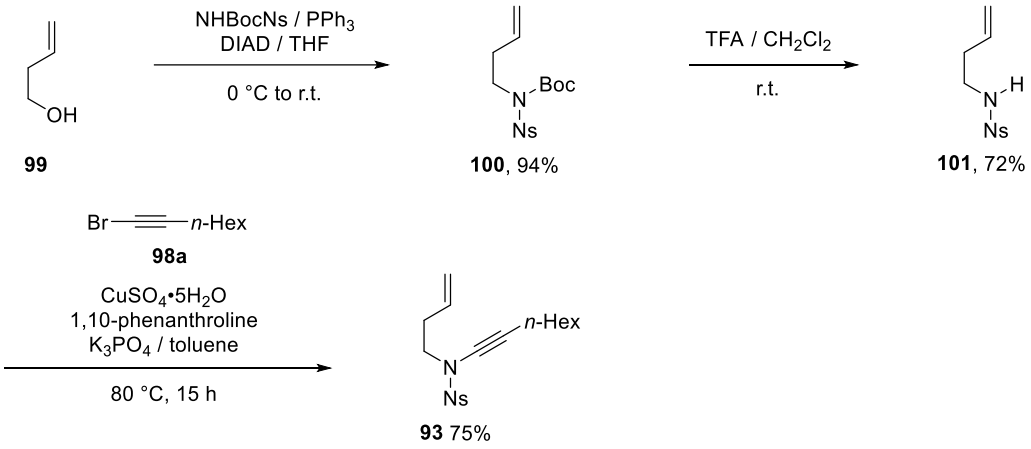

Scheme 2.6

For $Pd_2dba_3{\cdot}CHCl_3$ / AcOH / bbeda, it is believed that an active palladium hydride is generated *in situ*, and subsequently undergoes through a hydropalladation mechanism. Therefore, the result would be expected to observe an intermolecular hydride transfer (Scheme 2.7, left). For the ruthenium system, the catalyst can proceed *via* either allylic C–H insertion or ruthenacycle mechanisms. Since the allylic C–H insertion pathway cannot explain the formation of the 1,3-diene product, the mechanism of this

catalysis is therefore likely to be a ruthenacycle mechanism. Hence, an intramolecular hydride transfer is expected (right).

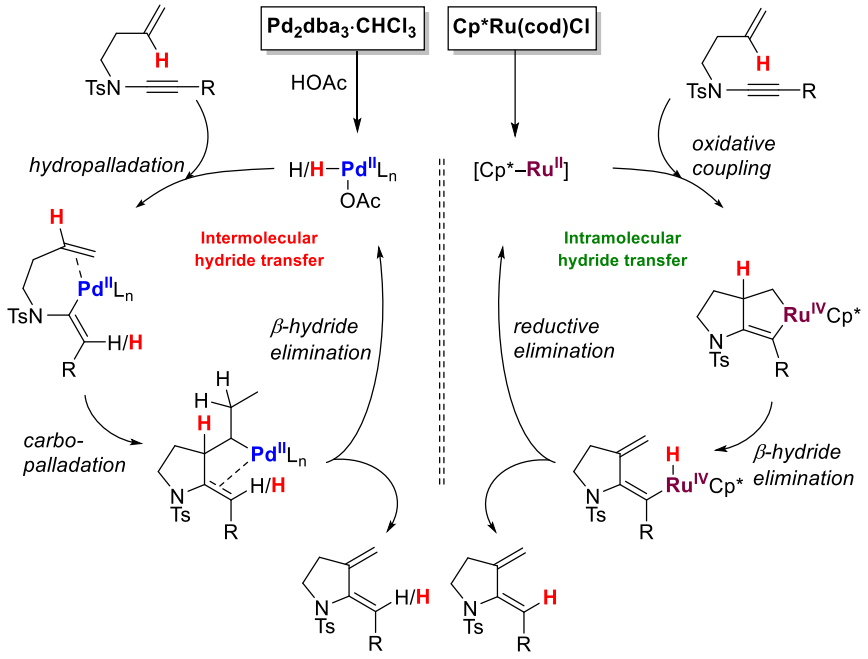

Scheme 2.7

We were pleased to discover that, with $Pd_2(dba)_3{\cdot}CHCl_3$ / AcOH / bbeda, complete crossover of the deuterium label was detected, suggesting that hydride is transferred intermolecularly as we anticipated. In contrast, under ruthenium catalysis, no crossover was observed, and 83% D incorporation was found in product d_1-**102** This indicates that an intramolecular hydride transfer took place during the reaction course (Scheme 2.8).

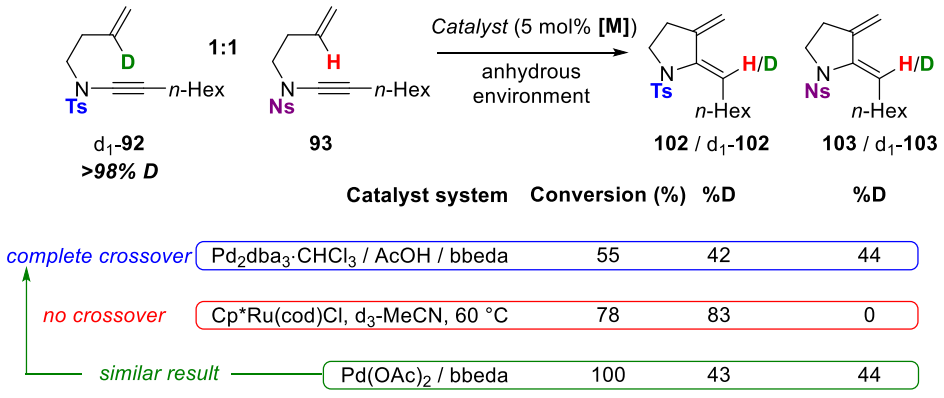

Scheme 2.8

For the system of $Pd(OAc)_2$ / bbeda, which we would like to gain some insight of its mechanism, a similar result to that of the system with $Pd_2dba_3{\cdot}CHCl_3$ / AcOH / bbeda was obtained. That is, products

102 / d_1-**102** and **103** / d_1-**103** featured nearly equivalent amounts of deuterium incorporation (43 and 44% respectively, determined by ^{1}H NMR spectroscopy, Figure 2.1), Hence, the result offers support for an intermolecular transfer of hydride *via* a discrete palladium hydride/deuteride species.

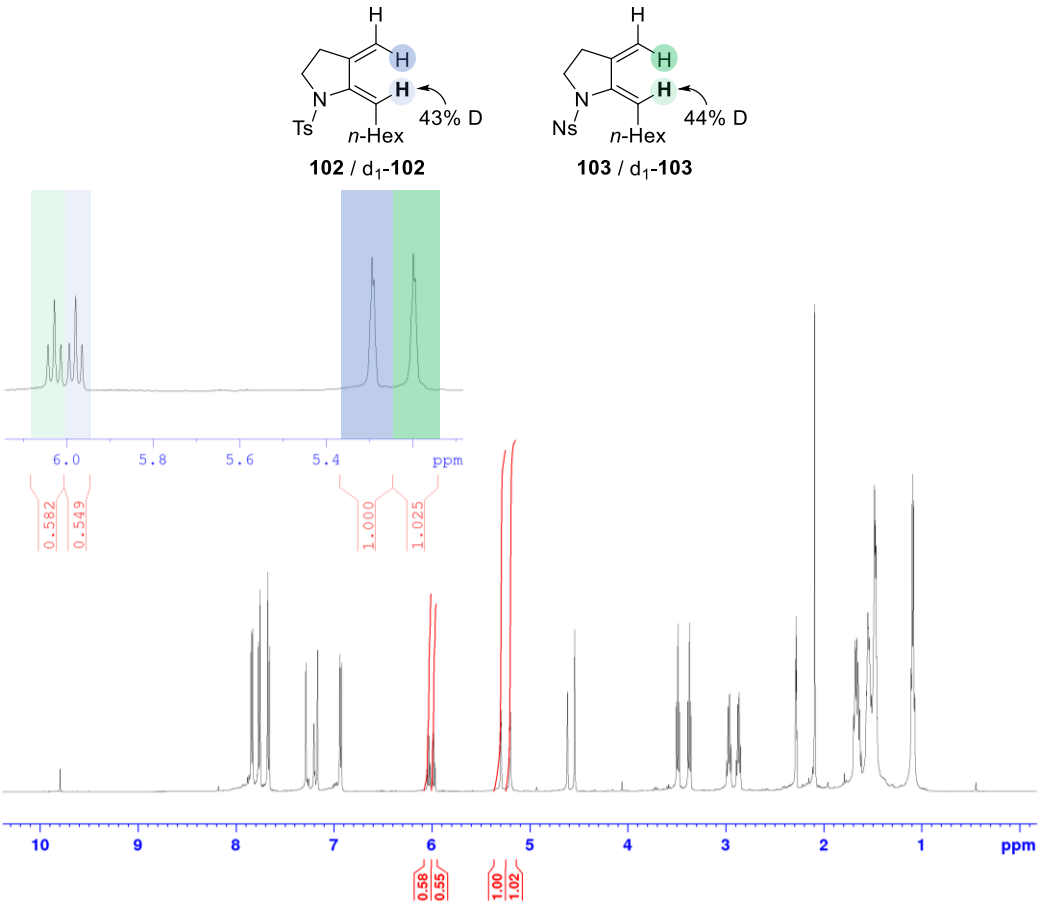

Figure 2.1 ^{1}H NMR spectrum shows product scrambling when using the $Pd(OAc)_2$ / bbeda system.

2.2 Timecourse ^{1}H NMR Spectroscopic Experiments

2.2.1 Kinetic Profile Comparison

We next exploited timecourse ^{1}H NMR spectroscopy, which is a powerful technique to probe reaction mechanisms, to monitor the cycloisomerisation of enynamide **92** under different catalytic conditions. Substrate **92** was obtained in good yield from the similar synthetic strategy to synthesise enynamide **93**, BocNHTs was used to react with alcohol **99** instead of $BocNHSO_2C_6H_4NO_2$ (Scheme 2.9).

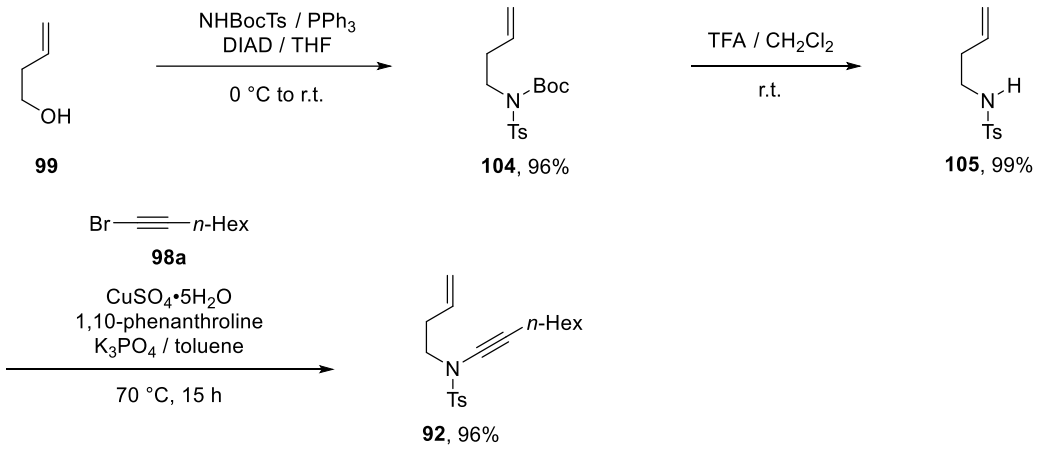

Scheme 2.9

Starting material **92** was submitted to the conditions of $Pd_2dba_3 \cdot CHCl_3$ / AcOH / bbeda. Product **102** was formed immediately after the reaction was initiated (Graph 2.1), indicating that the putative Pd(II)–H species is rapidly generated from the oxidation of $Pd_2dba_3 \cdot CHCl_3$ with AcOH. As a consequence, the formation of product **102** was observed soon after the substrate was mixed with the pre-catalyst. Although the reaction initiated instantaneously, the reaction failed to reach full conversion of starting material. This is perhaps due to the short lifespan of the active palladium species.

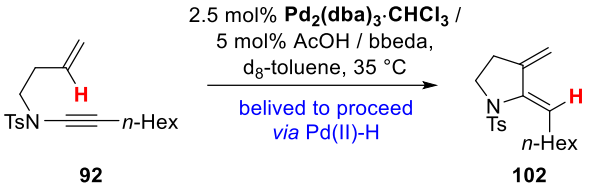

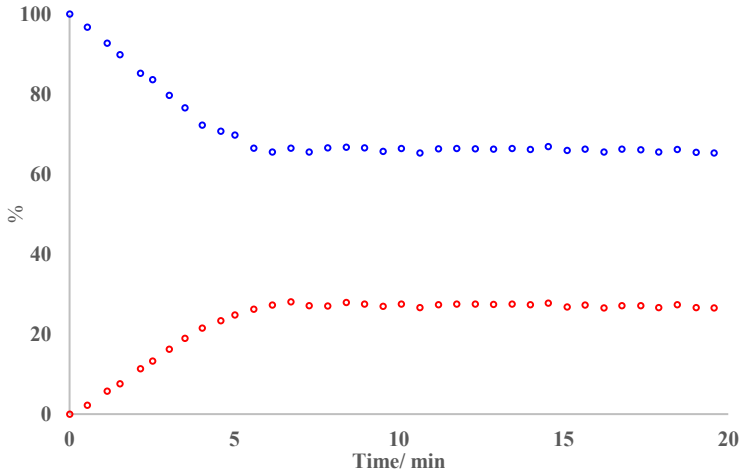

Graph 2.1

Similar instantaneous formation of product was also observed from the ruthenium catalysis with Cp*Ru(cod)Cl (Graph 2.2). This is also indicative of the presence of a catalytically reactive species at early stages of the reaction, which is sensible because substrate **92** can easily bind to the ruthenium centre *via* ligand exchange with the cyclooctadiene (cod) and chloride ion.

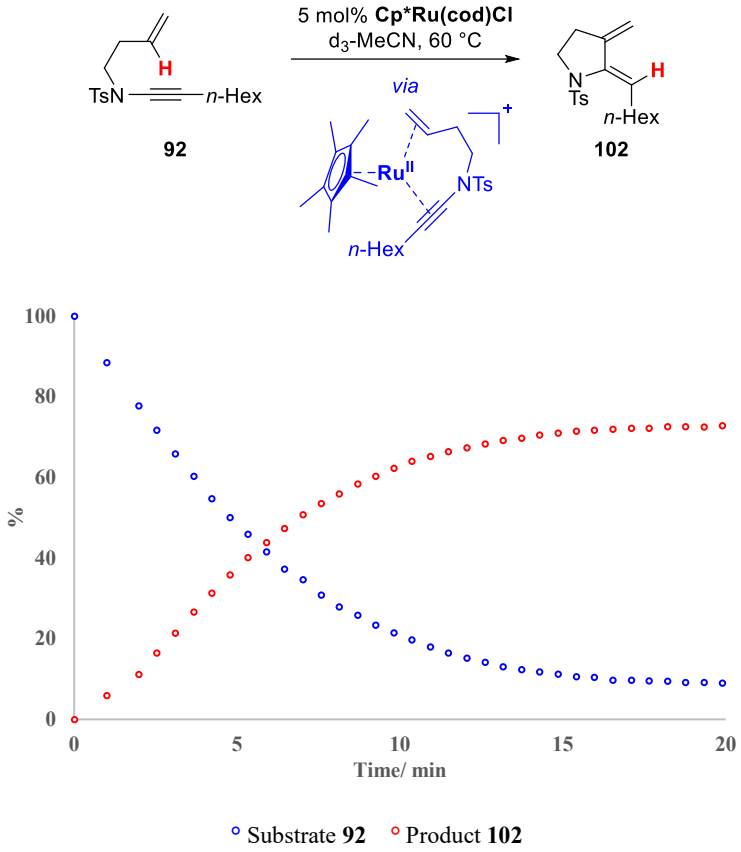

Graph 2.2

Unlike the two previous catalyst systems, the reaction kinetic profile obtained from the system of $Pd(OAc)_2$ / bbeda shows a slight delay in product formation (Graph 2.3), which is suggestive of the generation of an active catalyst species from the $Pd(OAc)_2$ pre-catalyst before cycloisomerisation initiates.

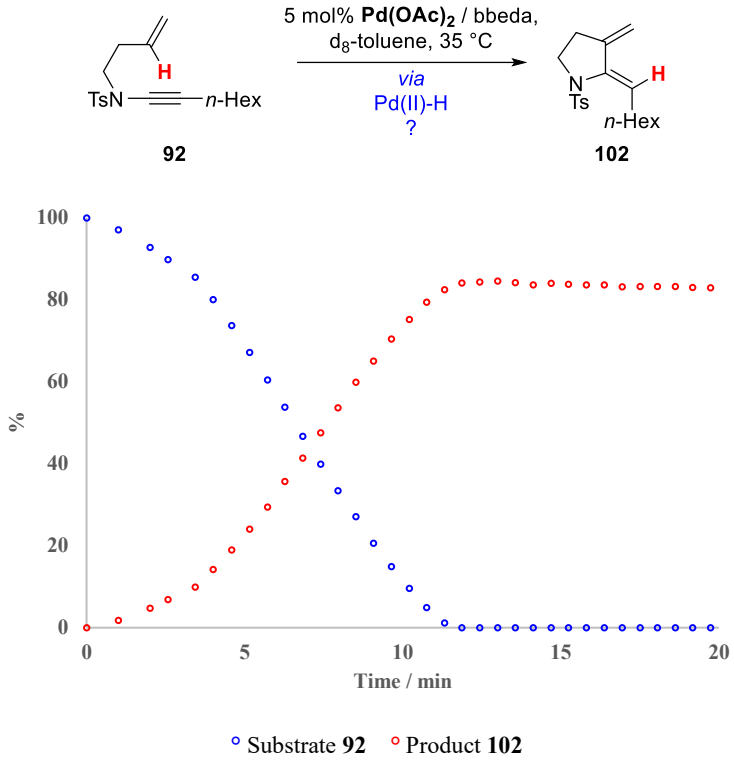

Graph 2.3

Comparison between the product formation profiles of the three catalyst systems illustrates clearly a delay in product formation under $Pd(OAc)_2$ / bbeda conditions (Graph 2.4, green), while the profiles from the other two systems a rapid production formation (red and blue).

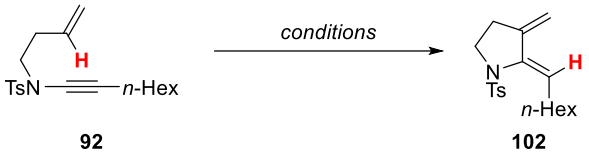

92 **102**

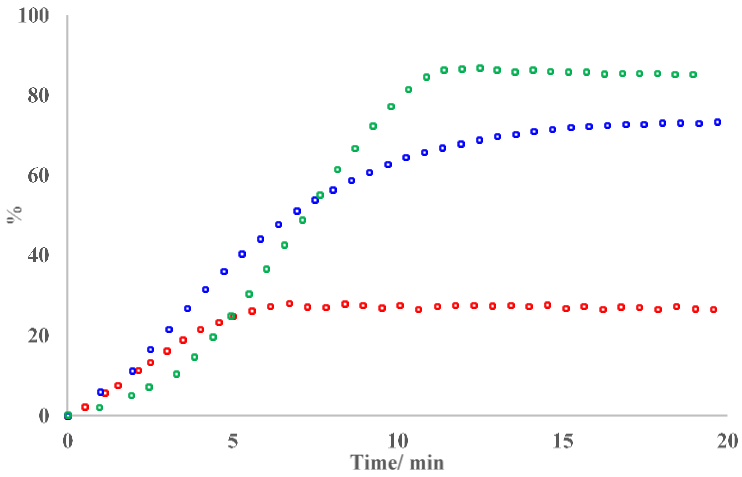

° $Pd_2dba_3 \cdot CHCl_3$ / AcOH / bbeda / d_8-toluene at 35 °C

° Cp*Ru(cod)Cl / d_3-MeCN at 60 °C

° $Pd(OAc)_2$ / bbeda/ d_8-toluene at 35 °C

Graph 2.4

In addition to the difference in the kinetic profiles, when d_1-**92** was cycloisomerised with $Pd(OAc)_2$ / bbeda system to give product d_1-**102** (Graph 2.5), a significant decrease in the rate of reaction was observed compared to that of the cyclisation of substrate **92**. This reflects deuterium isotope effects, which will be discussed in more detail in the next chapter. The kinetic profile of the reaction also shows the extent of product deuteration changed during the reaction. Intriguingly, at the beginning of the reaction (first 5-7 mins), only protiated product **102** was produced (Graph 2.5, red curve), then reaching a plateau after ~ 10 minutes. At later stages of the reaction, deuterated product d_1-**102** was mainly produced (Graph 2.5, green curve) with incremental increase of corresponding protiated product **102**. Thus, deuterium incorporation overall drops from >98% D in the starting material to about 70% in the products.

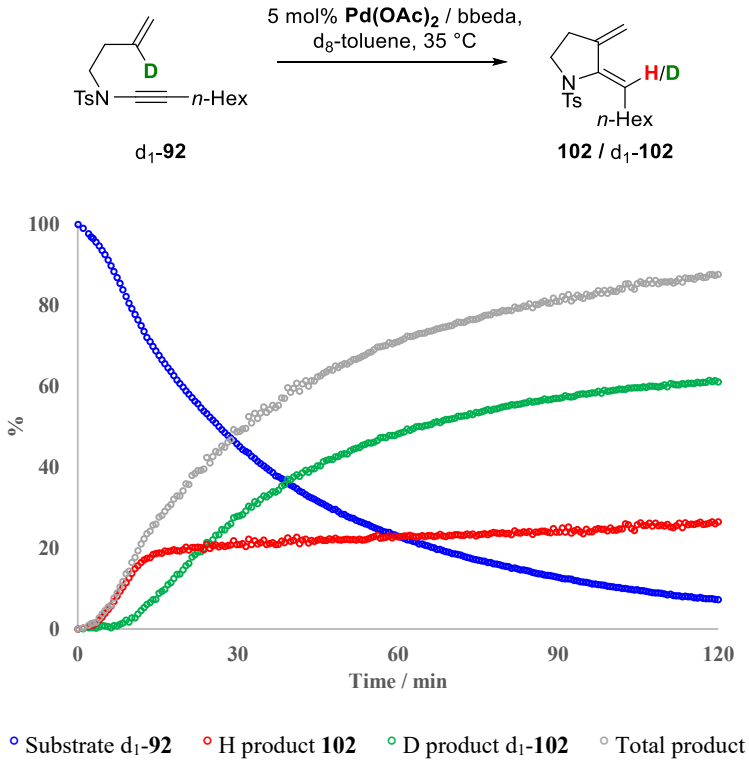

Graph 2.5

Such a diminution in deuterium incorporation could be related to the catalyst activation process, for example, with the hydride source being the substrate itself, or it could imply that water plays a role in the product formation. For instance, the loss of deuterium could arise from an exchange process with water present in the reaction solvent. We therefore studied the effect of water on the reaction by comparing the reaction profiles of the cycloisomerisation of enynamide **92** in d_8-toluene with variation of water concentration (Graph 2.6). In order to obtain different concentrations of water in reaction solvent, the deuterated solvents for the NMR experiments were dried by storing freshly-opened bottle d_8-toluene over 3 Å molecular sieves for at least 24 h.[42] The water contents in the solvent were then determined by Karl-Fischer titration. Applying such a drying method, the water content was reduced to ~ 3 ppm (for d_8-toluene). The concentration of water in freshly-opened bottle d_8-toluene was found to be ~ 82 ppm. The water content of water-saturated d_8-toluene was determined to be ~ 480 ppm.

Longer reaction times were observed when performing the cycloisomerisation of enynamide **92** with sieve-dried d_8-toluene, compared to the reaction run in 'bottle' solvent (Graph 2.6, blue curve). This trend continued to the reaction in water-saturated environment, *i.e.* a shorter reaction time was required to completely convert substrate to product (Graph 2.6, red curve). These results reveal a positive effect of water on the rate of reaction.

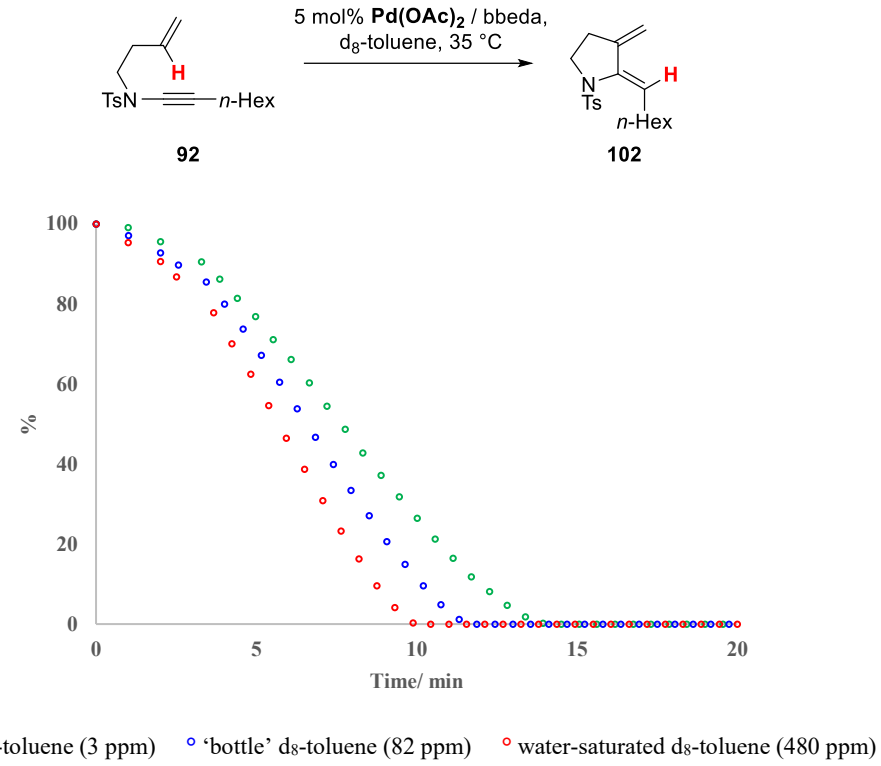

Graph 2.6

Most interestingly, when D_2O was used to saturate the reaction environment instead of H_2O (Graph 2.7), a small level of deuterium incorporation was detected in the product obtained from the reaction of protiated substrate **92** (Graph 2.7, green curve). This indicates that D_2O can serve as a source of deuteride, potentially *via* H/D exchange of a palladium hydride intermediate.

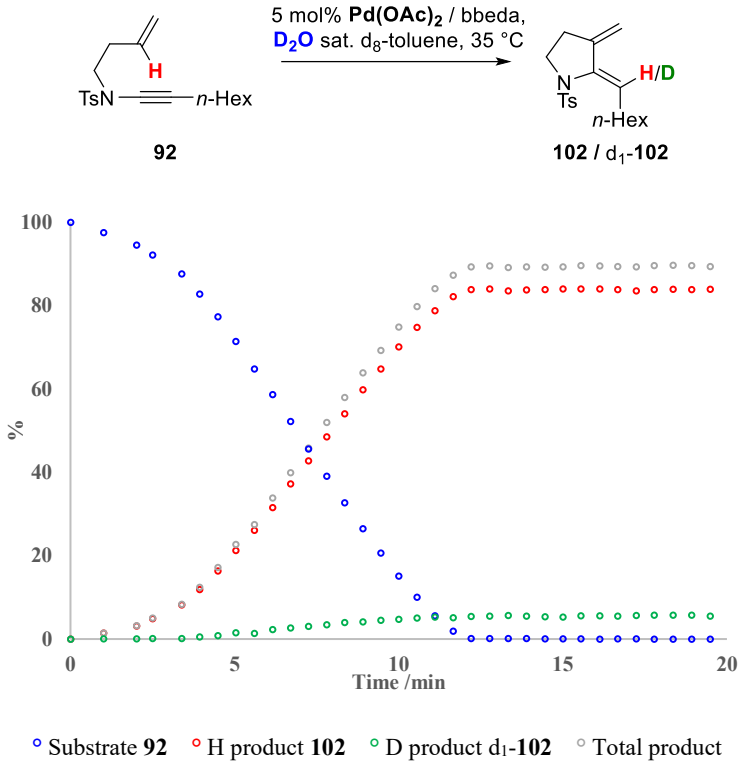

Graph 2.7

Performing equivalent reactions with deuterated substrate d_1-**92**, the formation of protiated product **102** was detected even using sieve-dried solvent, and with no other obvious proton sources (Graph 2.8, top). In addition, a direct correlation between the H_2O content of the reaction solvent and the amount of protiated product **102** was observed; ~ 15% of non-deuterated product **102** was formed in absence of water (Graph 2.8, top left), 26% of product **102** was found when 'bottle' d_8-toluene was used as solvent (Graph 2.8, bottom left), and ~ 44% of **102** was detected under water saturated conditions (Graph 2.8, bottom right). In all cases, protiated product **102** was exclusively produced at the early stages of the reaction.

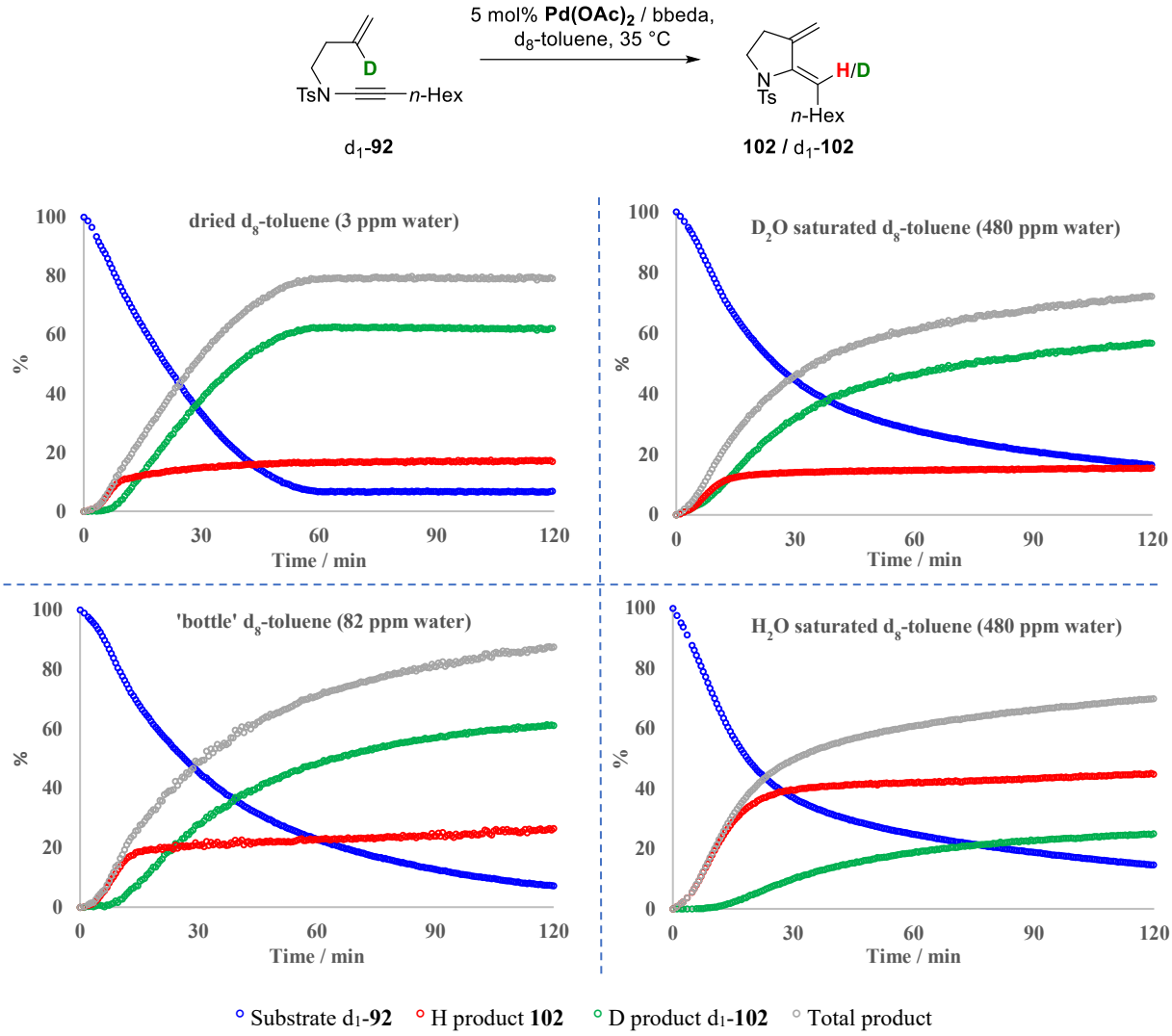

Graph 2.8

2.2.2 The Role of Water

One reason for the observed rate enhancement for substrate **92** with increasing water content could be that water is involved in the initiation process whereby an active (or more reactive) catalyst species is produced. Bedford and co-workers reported that $Pd(OAc)_2$, which is known to exist in a form of trimer **106** in organic solvents, can be hydrolysed by water or alcohols to give complex **107**, $Pd_3(OAc)_5OR$ where R is hydrogen or an alkyl group.[43] The structures of trimeric palladium acetate **106** and the bridging hydroxide complex **107a** possess D_{3h} and C*s* symmetries, respectively, which can clearly seen from the X-ray crystal structures (Figure 2.2).

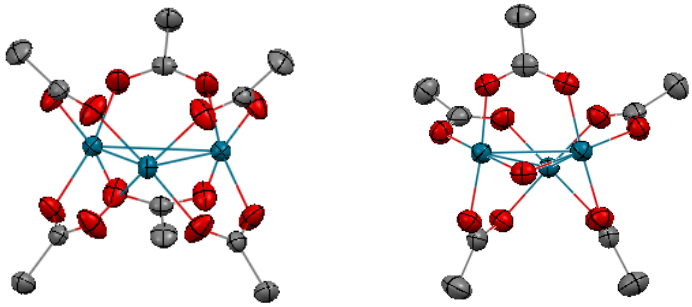

$Pd_3(OAc)_6$, **106** $Pd_3(OAc)_5OH$, **107a**

Figure 2.2 X-ray crystal structures of palladium complexes **106** and **107a**.

These two species are in equilibrium in organic solvents in the presence of water; with increasing water content, a greater proportion of the bridging hydroxide complex **107** is formed (Scheme 2.10).

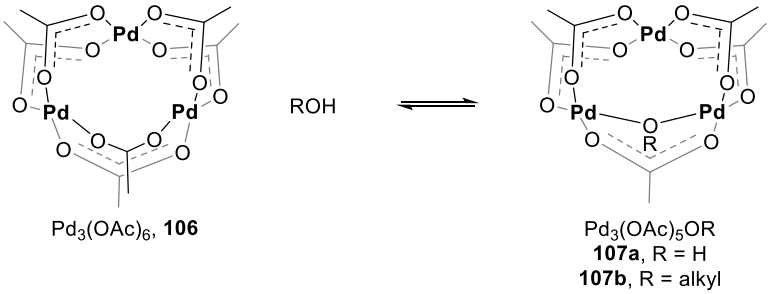

$Pd_3(OAc)_6$, **106**

$Pd_3(OAc)_5OR$
107a, R = H
107b, R = alkyl

Scheme 2.10

It was hypothesised that such a hydroxy bridged complex could serve as a more reactive pre-catalyst. To confirm this hypothesis, complex **107a** was prepared as reported by Bedford *et al*. and used in the cycloisomerisation of enynamide **92** (5 mol% Pd), with an equivalent amount of bbeda (5 mol%) in

sieve-dried d_8-toluene. We were pleased to observe that although an induction period remained, it was diminished compared to $Pd_3(OAc)_6$, **106** / bbeda in H_2O-saturated d_8-toluene (Graph 2.9).

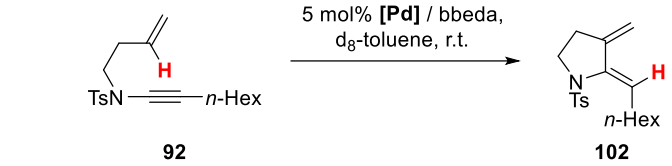

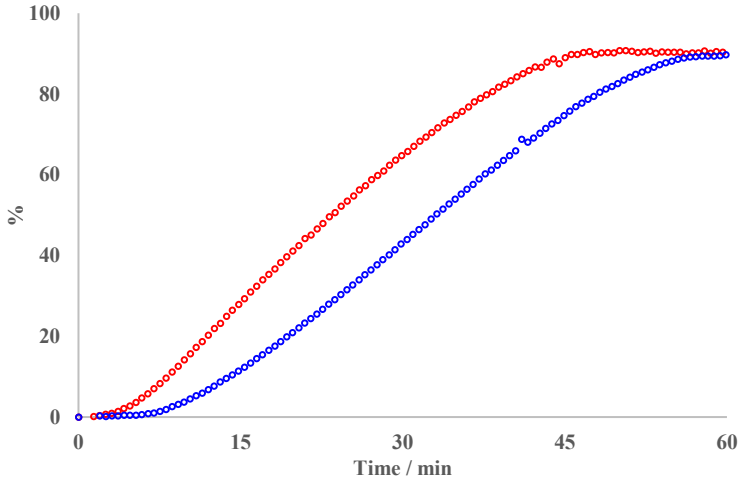

° $Pd_3(OAc)_6$, **106** in water-saturated d_8-toluene ° $Pd_3(OAc)_5OH$, **107a** in anhydrous d_8-toluene

Graph 2.9

This observation on the effect of water on accelerating reaction initiation through the formation of palladium complex **107a** suggested that this hydroxy-bridging species could be an intermediate in the formation of monomeric palladium hydride, meaning that hydrolysis of trimeric complex **106** is crucial for initiating the cycloisomerisation. Interestingly, the kinetic profiles of both reactions are similar in the post-initiation phase, implying that these two catalyst systems proceed through common intermediates.

To our surprise, the equivalent reactions of the deuterated substrate d_1-**92** showed a retardation of reaction rate in H_2O-rich environment, compared to the reaction in D_2O-saturated solvent after ~25 mins (Graph 2.10).

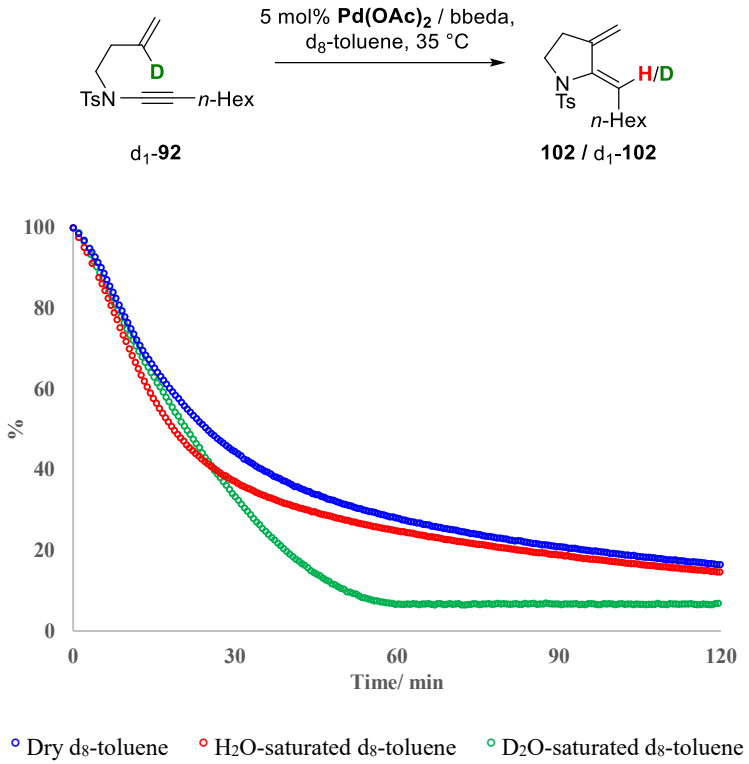

Graph 2.10

This paradoxical role of water was further examined by the reaction of substrate **92** in a solvent more water-miscible than toluene, for which d_8-THF was selected. The cyclisation reaction of **92** in d_8-THF was examined in the presence of increasing amounts of water (from 4Å molecular sieve-dried solvent (~ 23 ppm H_2O) to > ~ 8000 ppm H_2O). Under these conditions, high reactivity was observed until ~ 2300 ppm H_2O; above this point, retardation of the reaction became apparent (Graph 2.11). We suggest that this retardation may result from the off-pathway coordination of water to Pd(II) complexes, which prevents complexation of the alkyne substrate, and thus inhibits the reaction.

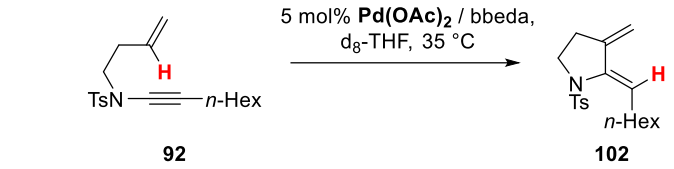

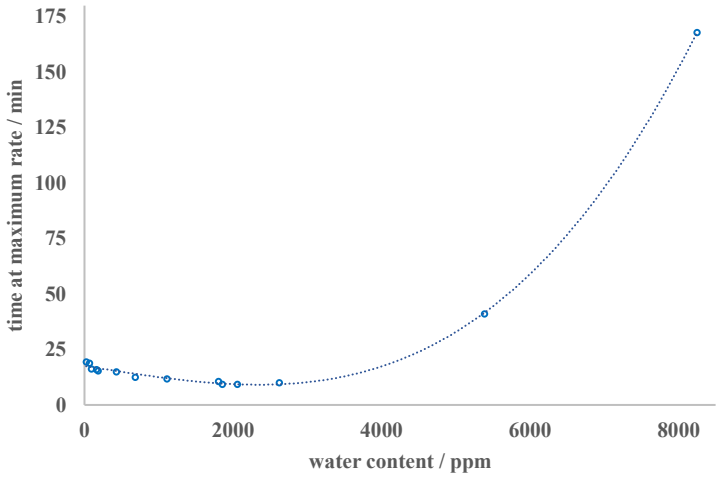

Graph 2.11

2.2.3 The Role of Bbeda

Bbeda has proven to enhance the rate of $Pd(OAc)_2$-catalysed cycloisomerisation.[20] This has also been confirmed by the ^1H NMR spectroscopic reaction profiles for cycloisomerisation of enynamide **92**. The reaction with bbeda could reach completion after ~ 15 minutes (Graph 2.12, blue curve), while the reaction in the absence of bbeda failed to reach completion after 3 h (Graph 2.12, red curve). In addition, a black suspension was observed over time when the reaction was performed in the absence of bbeda. This is markedly different from the cyclisation with bbeda whereby no or little particulate develops during the reaction. As proposed by Trost,[44] bbeda could act as a ligand that accelerates the catalytic cycle, and / or stabilises off-cycle palladium species (as evidence by the different appearance of the reactions). However, it was discovered that addition of bbeda after ~ 20 minutes to a bbeda-free reaction did not lead to a rate acceleration (Graph 2.12, green curve). Instead, the rate of reaction was sustained at a slightly higher level compared to the bbeda-free reaction. This supports the idea that bbeda might prevent the aggregation of palladium catalyst.

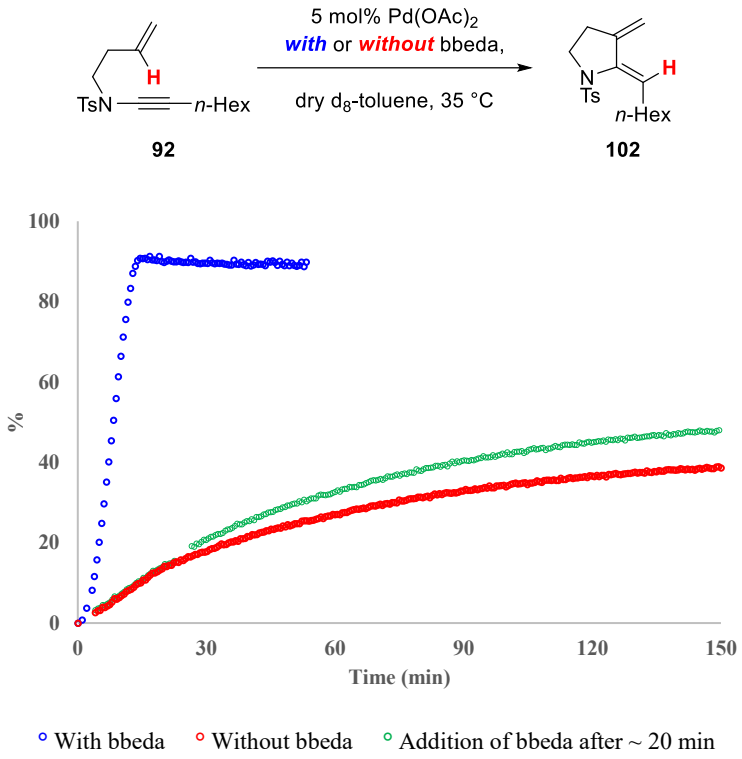

Graph 2.12

For such experimental results, it therefore seemed possible that bbeda could be involved in pre-catalyst deaggregation and / or reaction initiation. To further investigate this, solutions of $Pd_3(OAc)_5(OH)$ and $Pd_3(OAc)_6$ in anhydrous d_8-toluene were titrated with bbeda (Figure 2.3). A marked spectral change was observed after 0.25 equiv. of bbeda was added to a solution of $Pd_3(OAc)_5(OH)$ in $CDCl_3$ (Titration A): the authentic ^1H NMR signals of $Pd_3(OAc)_5(OH)$ at δ_H 1.70, 1.60 and 1.55 ppm shifted to the more deshielded regions (indicated by dash arrows); the signal belonging to trimeric palladium acetate at (+, 1.67 ppm), $Pd_3(OAc)_6$, was also found to have a higher proportion, which reflects an equilibrium between this trimeric species and the hydroxide bridging complex; more interestingly, a new signal showed up at 1.69 ppm (*). When more bbeda was added, the signal of $Pd_3(OAc)_6$ at 1.67 ppm diminished, suggesting that the trimeric palladium complex turns into an unidentified species in presence of bbeda. We thought that this unknown species might be related to deaggregated complex.

On the other hand, when a solution of $Pd_3(OAc)_6$ in $CDCl_3$ was titrated with bbeda (Titration B), a full equivalent of bbeda had to be added to the reaction in order to observe a significant change in the ^1H NMR signals. The heightened reactivity of $Pd_3(OAc)_5OH$ towards bbeda might explain the decrease in

lag time when using $Pd_3(OAc)_5(OH)$ / bbeda catalyst system for the cycloisomerisation, and equally performing the reaction with $Pd(OAc)_2$ / bbeda in a water saturated environment (Graph 2.9).

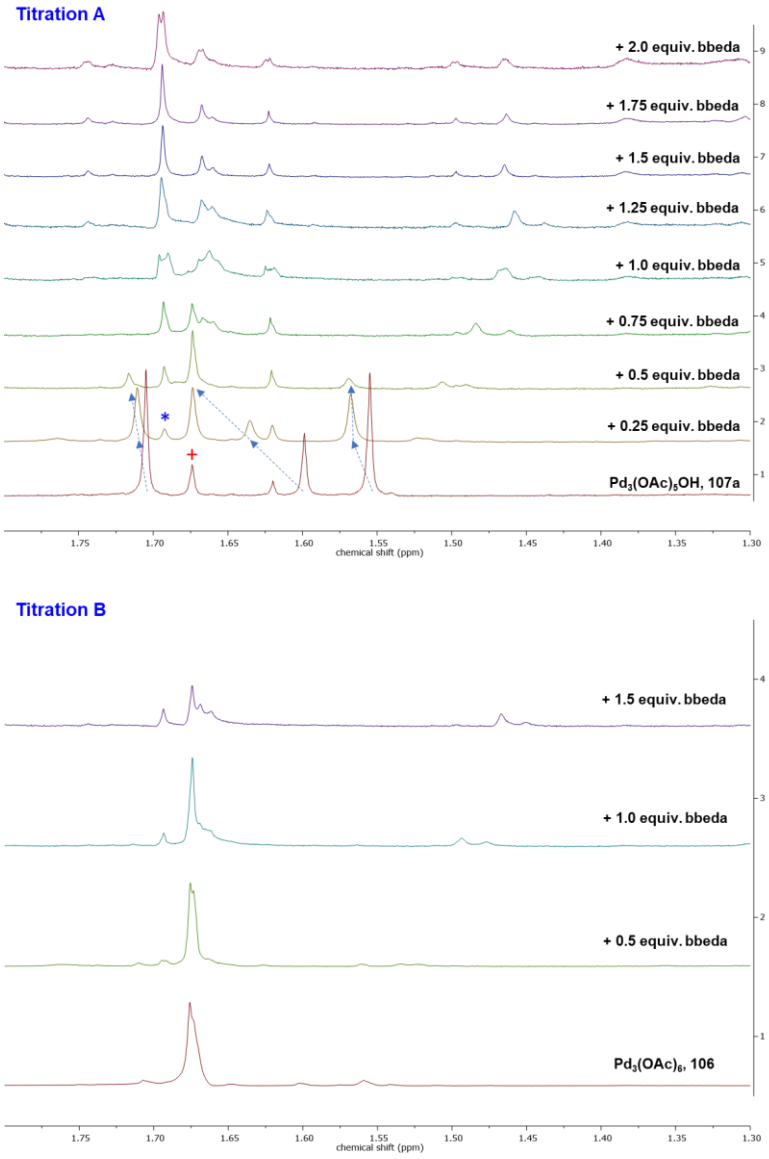

Figure 2.3 Effect of bbeda on (a) $[Pd_3(OAc)_5OH]$ and (b) $[Pd_3(OAc)_6]$. Titrations performed in dry d_8-toluene at room temperature and monitored by ^1H NMR spectroscopy.

Even if reactions were run carefully in an environment devoid of H_2O (or other apparent proton source, *i.e.* >98% deuterated substrate d_1-**92**), a low level of protiated product **102** was consistently observed during the reaction (Graph 2.8, top left and top right, red curve). This perhaps implies that a source of hydride is related to the initiation process, potentially involving the substrate itself. To explore this, various deuterated substrates were prepared.

Deuterated substrate d_2-**108** was synthesised from aldehyde **96**, prepared in the same manner as the corresponding deuterated version (d_1-**96**), but without using deuterated reagents. The aldehyde was reacted with the per-deuterated Wittig salt d_3-**109** (prepared from the procedure reported by Miyashita *et al.*)[45] to obtain deuterated sulfonamide d_2-**110** which was subsequently submitted to Hsung conditions with 1-bromooctyne to afford deuterated enynamide d_2-**108** (Scheme 2.11).

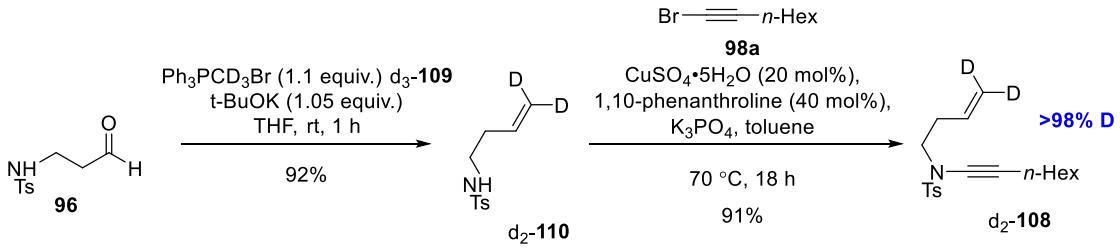

Scheme 2.11

For deuterated ynamide d_2-**111**, *β*-alanine methyl ester hydrochloride salt was tosylated, and the resulting sulfonamide **94** was deuterated at the α-position to the ester using K_2CO_3 in CD_3OD (91% D). Ester d_5-**112** was then reduced with DIBALH, and the resulting aldehyde was converted to an alkene using Tebbe reagent, giving deuterated alkenyl sulfonamide d_2-**113**. Copper-catalysed ynamide formation then provided deuterated enynamide d_2-**111** with 91% D incorporation (Scheme 2.12).

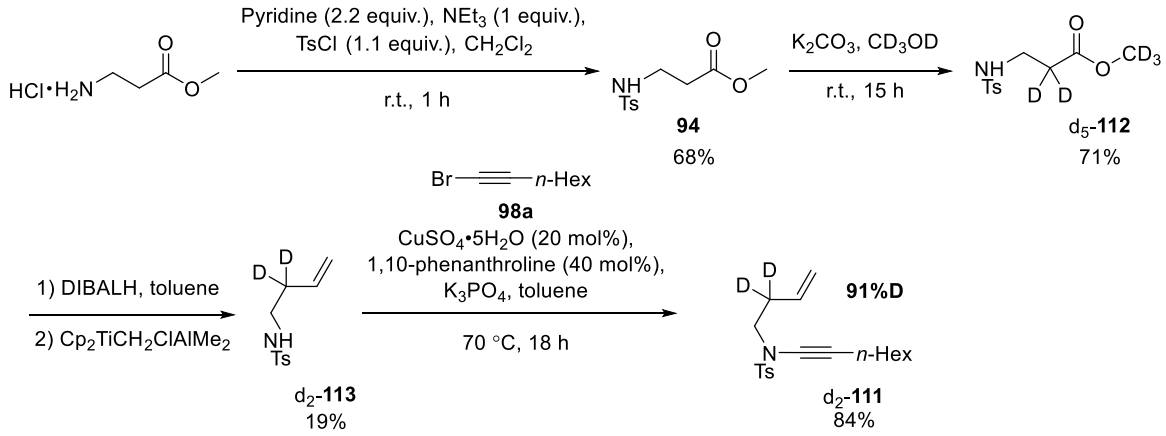

Scheme 2.12

The synthesised deuterated substrates (d_2-**108** and d_2-**111**) were cycloisomerised with $Pd(OAc)_2$ /bbeda, no transfer of deuterium was observed (Scheme 2.13), suggesting the substrate is not the source of hydride.

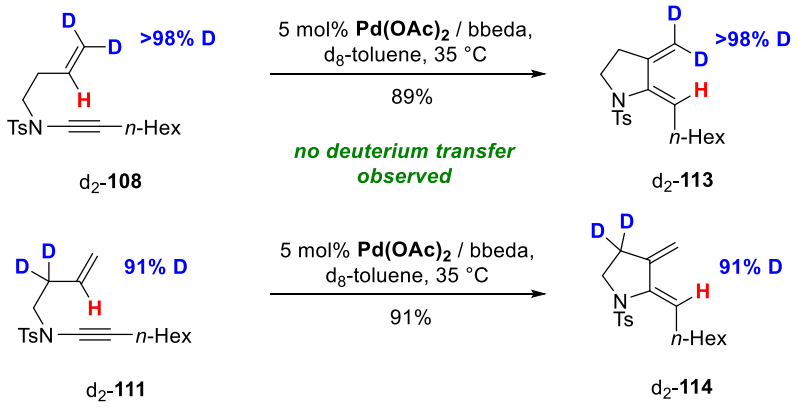

Scheme 2.13

Small amounts of benzaldehyde were consistently observed by ^{1}H NMR spectroscopy at the beginning of the non-anhydrous reactions. This observation led us to suspect whether bbeda could be essential for generation of palladium hydride (Scheme 2.14). Bbeda can chelate to $Pd(OAc)_2$ *via* σ-donation of the nitrogen atoms, making the imine groups of bbeda more susceptible to an adventitious nucleophile, *e.g.* water, acetate. In presence of water, hydrolysis of the imine results in the formation of benzaldehyde and primary amine **115**, which could undergo β-hydride elimination to generate palladium hydride. Tautomerisation of the resulting imine **116** gives the corresponding enamine which can then liberate further hydrogen atoms. Under anhydrous conditions, acetate can act as a nucleophile to attack the activated imine to form aminal **117**. This species can similarly undergo β-elimination to afford active palladium hydride species. Unsurprisingly, very small amounts of benzaldehyde were observed when reactions were performed in absence of water.

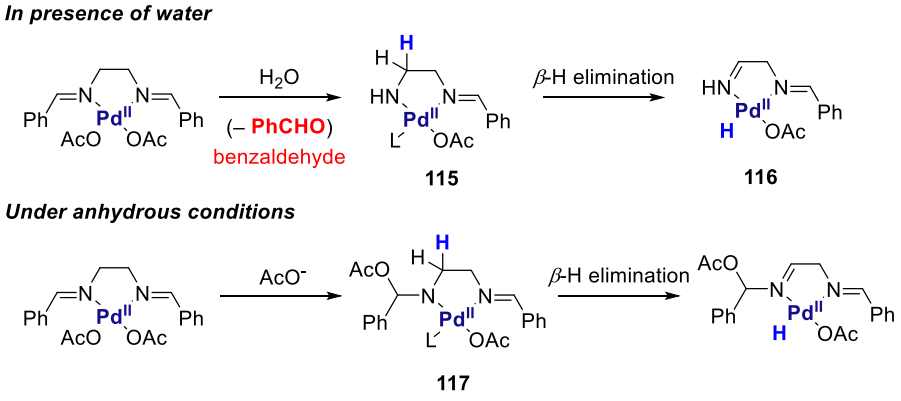

Scheme 2.14

We proved this assumption by preparing d_4-bbeda from the Gabriel amine synthesis of commercially available d_4-dibromoethane, followed by hydrazinolysis deprotection, and imine formation with benzaldehyde (Scheme 2.15).[46]

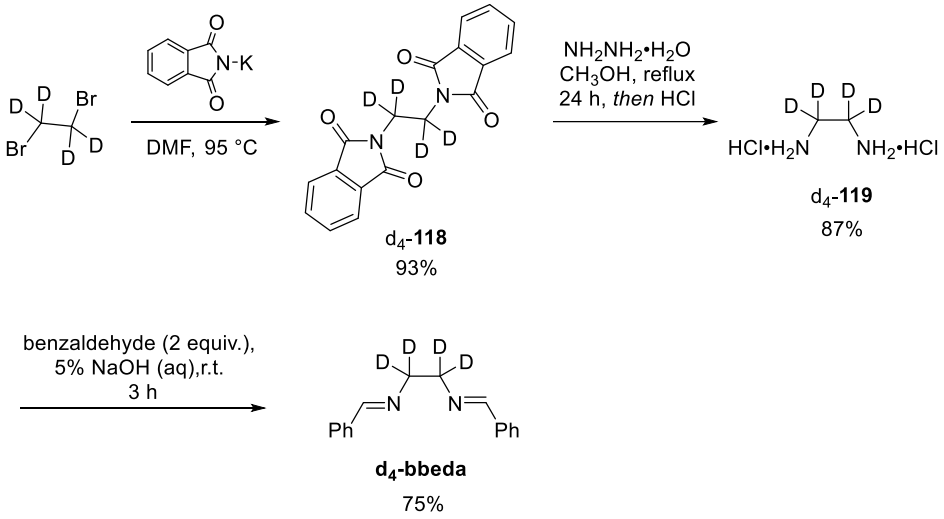

Scheme 2.15

With d_4-bbeda in hand, the cycloisomerisation of d_1-**92** in dry toluene using d_4-bbeda was performed. To our delight, deuterated product d_1-**102** was obtained as a sole product with >98% deuteration, *i.e.* no corresponding protiated product **102** produced (Graph 2.13). This strongly supports the proposal that bbeda itself serves as a source of hydride in the initiation pathway, and explains the formation of protiated product **102** in the reaction using deuterated substrate d_1-**92** with h_4-bbeda.

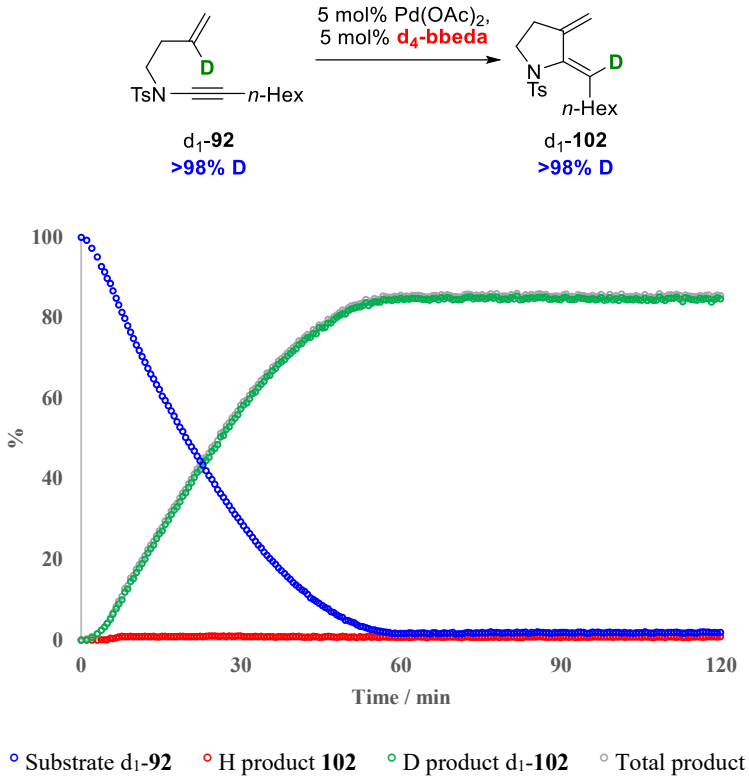

Graph 2.13

The hypothesis was also reinforced by the fact that the reaction of protiated substrate **92** in anhydrous toluene with d_4-bbeda and $Pd(OAc)_2$ (5 mol% each), which also produced about 15% of deuterated product d_1-**102** (Graph 2.14).

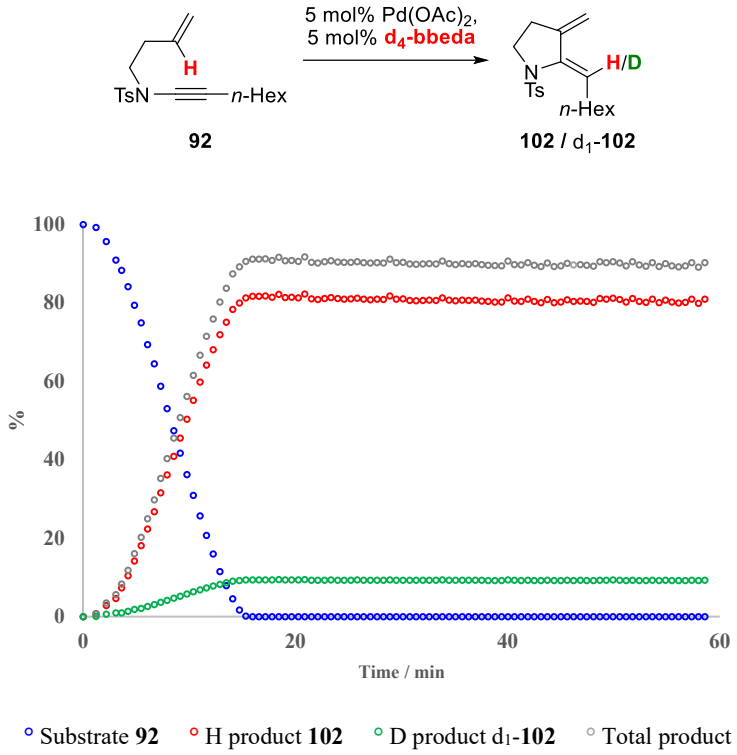

Graph 2.14

In addition, we were pleased to see that the product **121** was obtained with 15% D incorporation when enyne **120** was submitted to a solution of d_4-bbeda and $Pd(OAc)_2$ (5 mol% each) in anhydrous toluene at 60 °C (87% yield). Therefore, this initiation process appears to be a general mechanism for initiation of enyne cycloisomerisation with the $Pd(OAc)_2$ / bbeda catalyst system (Scheme 2.16).

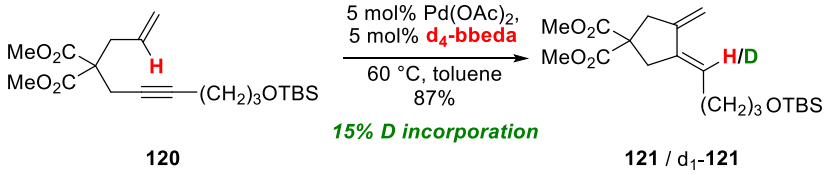

Scheme 2.16

2.3 Palladium Sources

During our investigations, we also discovered that the batch of $Pd(OAc)_2$ employed as catalyst can influence the stereochemical outcome of enynamide cycloisomerisation of enynamides (Table 2.1). To our surprise however, when the reaction was performed with $Pd(OAc)_2$ from a different supplier (Acros), instead of obtaining the usual *Z*:*E* ratio of 97:3 as usual (Entry 1), a ratio of 80:20 was observed (Entry 2). We therefore set about testing various samples of commercially available $Pd(OAc)_2$, with the most extreme being a reversal of stereoselectivity to 38:62 in favour of the (*E*)-isomer (Entry 3).

Table 2.1 Changes in diastereoselectivity with different batches of commercial $Pd(OAc)_2$**.**

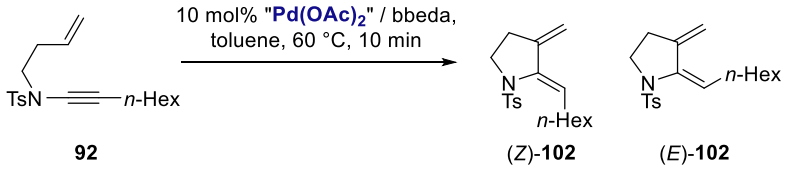

92 (*Z*)-**102** (*E*)-**102**

Entry	Source of $Pd(OAc)_2$	ratio *Z*	*E*
1	Strem Chemicals	97	3
2	Acros	80	20
3	Sigma-Aldrich	38	62

To inspect the discrepancy in diastereoselectivity, a ^1H NMR spectrum of each bottle of $Pd(OAc)_2$ from the different suppliers (Figure 2.4). $Pd(OAc)_2$ from Strem Chemicals gave a singlet at 1.96 ppm (running and calibrated with $CDCl_3$), which is consistent with pure $Pd(OAc)_2$ existing in a trimeric form with D_{3h} symmetry (red spectrum). In addition to the singlet, there are some minor peaks corresponding to the hydroxide bridging complex **107a** (dark blue spectrum). For $Pd(OAc)_2$ from Acros, the ^1H NMR spectrum shows a singlet of $Pd_3(OAc)_6$ and extra peaks arising from neither $Pd_3(OAc)_6$ nor $Pd_3(OAc)_5OH$. The Cotton group reported that $Pd_3(OAc)_5NO_2$, **122** was commonly found as impurity in commercial palladium acetate.[47] This is because $Pd(OAc)_2$ is manufactured by the oxidation of freshly formed palladium powder using a mixture of HNO_3 and AcOH. The structure of $Pd_3(OAc)_5NO_2$ is similar to that of trimeric palladium acetate, but one of the κ^2-acetate groups is replaced by nitrite. As a result, the D_{3h} symmetry is broken, leading to five acetate singlets of equal intensity, instead of one singlet. Once the authentic spectrum of $Pd_3(OAc)_5NO_2$ was overlaid with the spectrum of the Acros

sample, the extra peaks of the impurity were found to match well with $Pd_3(OAc)_5NO_2$. In case of $Pd(OAc)_2$ from Sigma-Aldrich, this sample disappointedly contained solely $Pd_3(OAc)_5NO_2$.

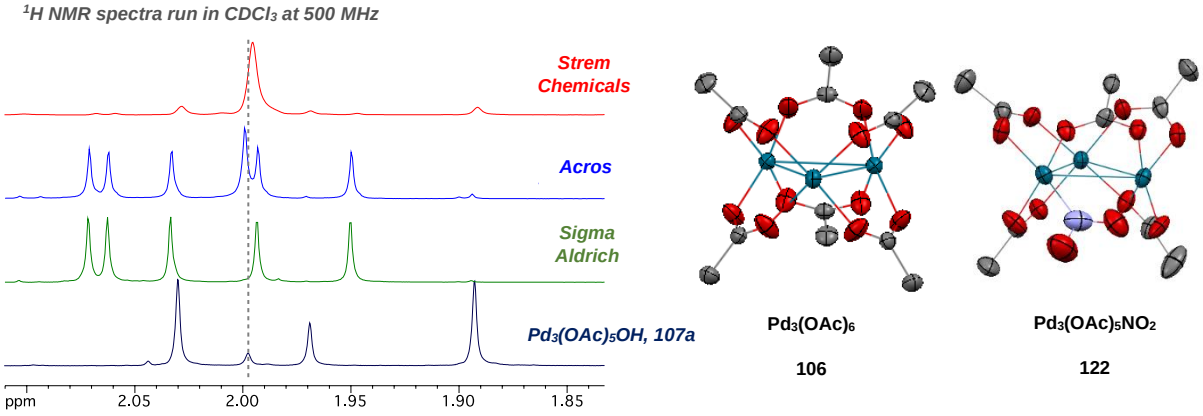

Figure 2.4 ^{1}H NMR spectra of batches of $Pd(OAc)_2$, and batch-dependent product ratio for cycloisomerisation of **92** (left). X-ray crystal structures of palladium complexes **106** and **122** (right).

Although, this contamination of $Pd(OAc)_2$ has been recognised for a long time, many palladium-catalysed reactions are not significantly affected by the nitrite. However, Fairlamb *et al.* reported that using $Pd_3(OAc)_5NO_2$ (instead of $Pd(OAc)_2$) in the synthesis of $Pd(OAc)_2(pip)_2$, (pip = piperidine), led to a complex mixture of products.[48] For enynamide cycloisomerisation, this does not seem to be the case, and such an extensive impact on the reaction outcome is, to our knowledge, unprecedented.

The synthesis of $Pd(OAc)_2$ by heating $Pd_3(OPiv)_6$ in excess acetic acid as reported by Colacot *et al.* offers high purity palladium acetate (Scheme 2.17),[49] which is equivalent to the original supply (from Strem Chemicals). The purity was confirmed by ^{1}H NMR spectroscopic analysis.

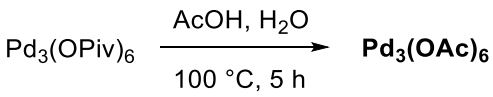

Scheme 2.17

When the reaction of enynamide **92** with $Pd_3(OAc)_5NO_2$ / bbeda was monitored by ^{1}H NMR spectroscopy (Scheme 2.15), a slower reaction rate was observed, compared to that of $Pd_3(OAc)_6$. In addition, the *E*/*Z* isomeric ratio (1:1.8) of enamide products (*Z*)-**102** and (*E*)-**102** remained approximately constant throughout the reaction. Furthermore, no olefin isomerisation was observed on submission of product (*Z*)-**102** to the catalyst, indicating that the formation of these two isomers during the reaction is likely a result of a divergent reaction mechanism, rather than post-cyclisation isomerisation.

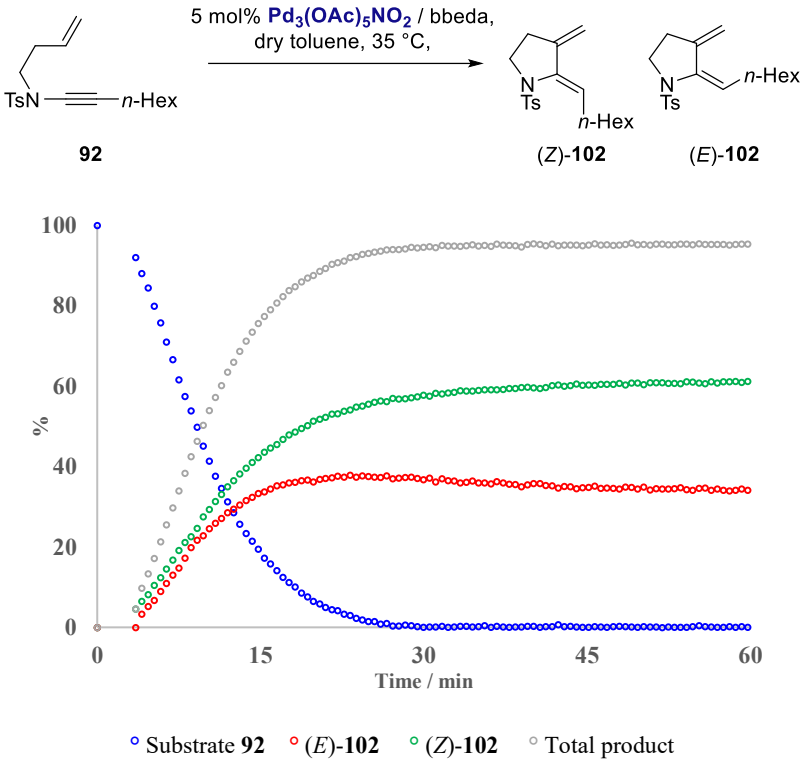

Graph 2.15

2.4 Conclusions

A palladium hydride-mediated pathway is likely to be the mechanism of cycloisomerisation using $Pd(OAc)_2$ / bbeda as pre-catalyst, based on the crossover experiments which support the intramolecular hydride transfer type mechanism. Bbeda has been identified as the source of hydride for the generation of a putative palladium hydride intermediate, through a hydrolysis of the bbeda imine / β-hydride elimination, as demonstrated by the use of d_4-bbeda. This process is found to be a general mechanism of initiation in the cycloisomerisation of enyne substrates. In addition to serving as the source of hydride, bbeda also promotes pre-catalyst deaggregation; and also likely stabilises off-pathway Pd(II) species, which prevents catalyst degradation through aggregate formation.

Moreover, water has been shown to play several roles in the reaction. It promotes the equilibration between $Pd_3(OAc)_6$ and $Pd_3(OAc)_5OH$ (which exhibits a reduced induction period compared to $Pd_3(OAc)_6$). Water also hydrolyses bbeda as discussed earlier, and thereby increases the rate of generation of palladium hydride species. Additionally, it can serve as a source of hydride as evidenced by reactions performed in solvents of various H_2O / D_2O contents. Paradoxically, water can also exhibit

an inhibitory effect on the rate of reactions while running cycloisomerisation of deuterated substrate in water-rich environments. This could imply that water could coordinate to active palladium species and prevent the complexation of the alkyne substrate.

The rate and product diastereoselectivity of the cycloisomerisations of enynamides are sensitive towards the purity of palladium precursor $Pd_3(OAc)_6$. In the presence of $Pd_3(OAc)_5NO_2$, a common contaminant in commercial palladium acetate, cycloisomerisation processes are retarded and the *E*/*Z* ratio of the cyclic enamine product is affected.

Chapter 3: Mechanistic Insights into Palladium-catalysed Cycloisomerisation— Computational Analysis and Kinetic Isotope Effects

With experimental evidence for the intermediacy of palladium hydride species in hand, we also wished to explore the reaction pathway by means of computational modelling to determine whether a hydropalladation reaction mechanism would be energetically feasible. In addition, we hoped to justify the stereoselectivity of the reaction, where substrate control operates in the formation of new stereocentres, and to rationalise the kinetic isotope effects we had observed. This theoretical work was carried out in collaboration with Professor Robert Paton and Dr Almudena Couce-Rios.

3.1 Computational Analysis

3.1.1 Reaction Pathway

A catalytic cycle involving hydropalladation, carbopalladation and β-hydride elimination steps was obtained for a palladium acetate catalyst featuring a single acetate ligand, using model enynamide **123**, (which is similar to substrate **92** with the alkyne substituent represented by a methyl group, Figure 3.1). Hydropalladation was found to proceed from Pd(0) acetic acid complex **A**. The palladium(II) hydride complex **F** was found to be less stable than the complex **A** at all levels of theory, by 21.4–33.1 kcal mol^{-1} (Table 3.1).

During hydropalladation to give complex **B**, the hydrogen atom is transferred to the β-carbon of the ynamide with the aid of an agostic interaction with the metal (**TS_AB**, $\Delta G^{\ddagger}$ = 7.4 kcal mol^{-1}). This suggests that a discrete palladium hydride is unlikely to be generated. Instead, oxidative addition to Pd(0) by acetic acid, and hydropalladation, undergoes as a single concerted irreversible process from the substrate-bound Pd(0)(HOAc) complex **A** (**A → B**). In addition to offering a new pathway for alkyne hydropalladation, acetic acid complex **A** also accounts for the facile exchange of H/D when water is present in the reaction solvent, meaning that the exchange can be mediated by acetic acid rather than requiring a specific isotope exchange process at the metal.

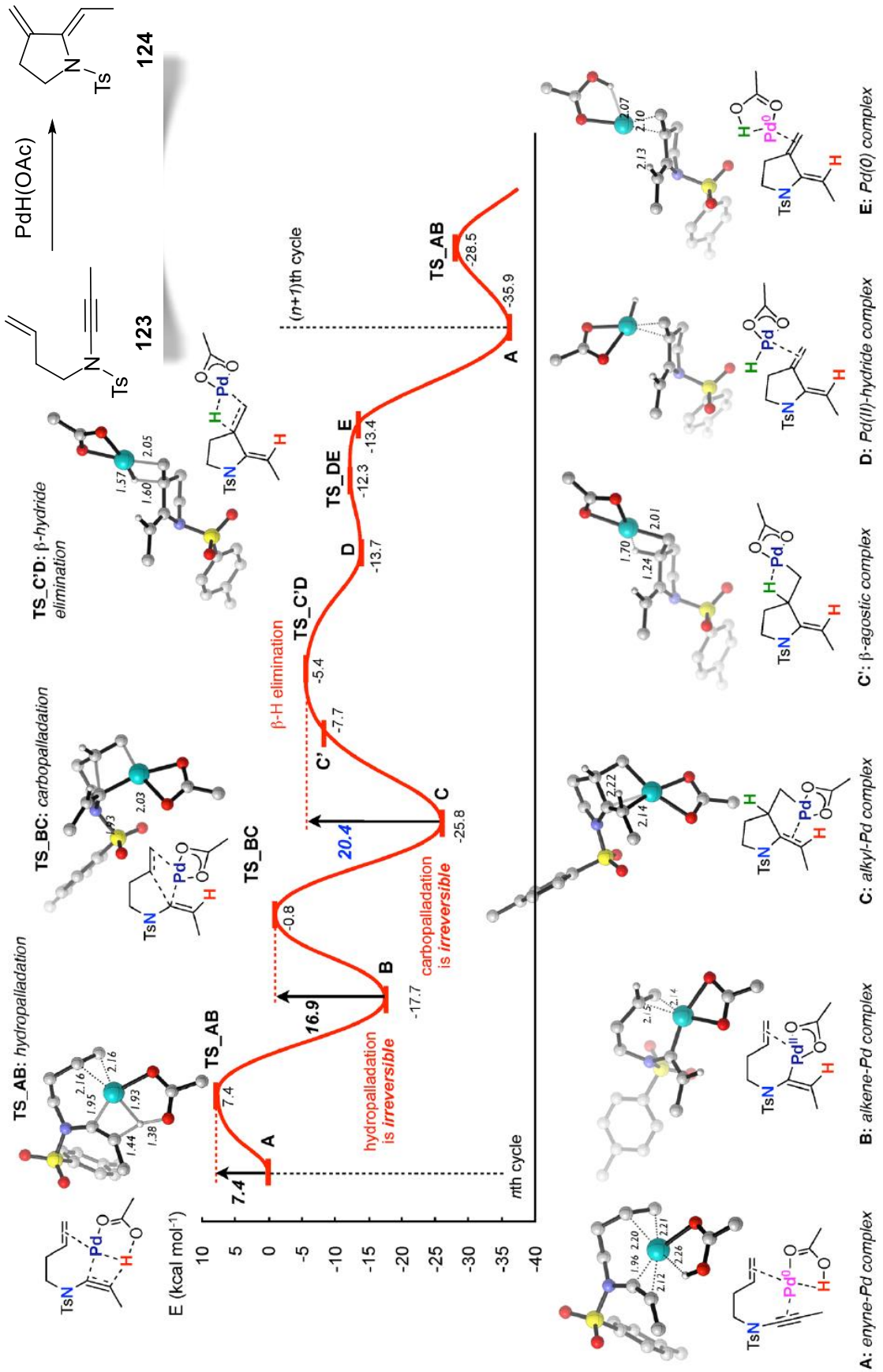

Figure 3.1 Energy Profile for the catalytic cycle of the cycloisomerisation.

Table 3.1 Mechanism of hydropalladation.

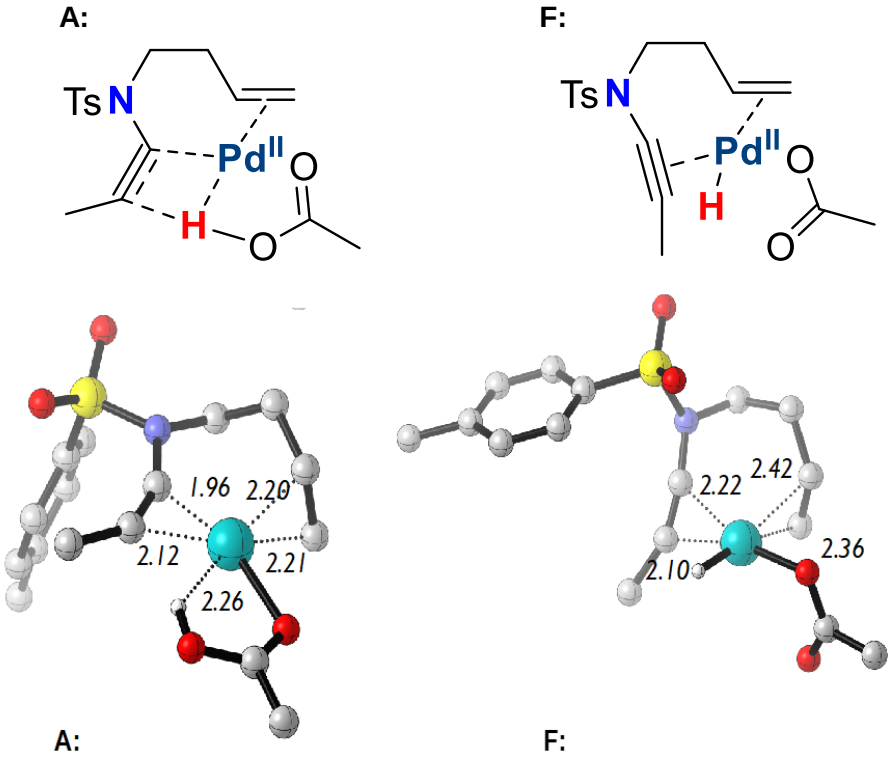

Method	$E_{activation}$ / kcal mol^{-1}	Δ E / kcal mol^{-1}
TPSS	25.1	24.5
M06	27.4	27.3
TPSS-D3	21.6	21.4
PW6B95-D3	26.6	32.4
DLPNO-CCSD(T)	27.2	33.1

This may in part account for the failure to detect discrete palladium hydride species by ^{1}H NMR spectroscopy. Moreover, the fact that oxidative addition of Pd(0) into acetic acid and hydropalladation take place in a concerted fashion supports the idea that the equilibrium of the oxidative addition process is rapid. The vinylpalladium then undergoes carbopalladation with the alkene unit (**TS_BC**, $\Delta G^{\ddagger}$ = 16.9 kcal mol^{-1}), resulting in alkylpalladium species **C**, which remains complexed to the enamide alkene. This step is followed by β-hydride elimination (**TS_C'D**, $\Delta G^{\ddagger}$ = 20.4 kcal mol^{-1}), which is the rate-limiting step. This requires palladium to decomplex from the enamide alkene to enable rotation about the C–C bond in order to align the C–Pd bond *syn*-coplanar with the C–H bond (**C**→**C'**). While, this β-hydride elimination is in theory reversible, the degree of reversibility is likely to be dependent on the facility of product dissociation from the resultant (alkene)Pd(H)(OAc) complex **D** or (alkene)Pd(HOAc) complex **E** (and complexation with the next substrate molecule to initiate the next round of the cycle). Experimentally, this depends on the nature of the products formed, because in some

cases the alkene within the products is indeed found to undergo isomerisation. The energy barrier between the product–palladium(II) hydride complex **D** (form after β-hydride elimination) and the product–Pd(0)(HOAc) complex **E** was calculated to be just 2.1 kcal mol^{-1} by M06 calculation. This magnitude of energy is consistent with that of other computational means (1.7 – 4.2 kcal mol^{-1}) as shown in Table 3.2.

Table 3.2 Mechanism of product decomplexation.

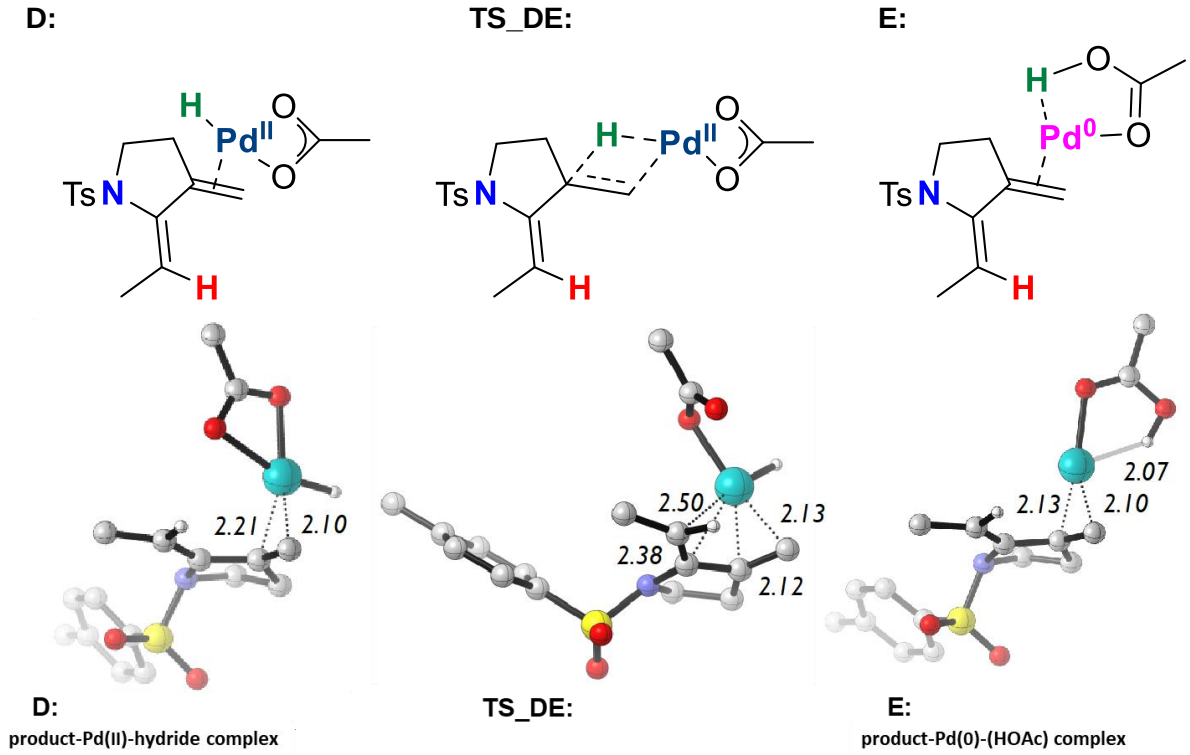

Method	$E_{activation}$ / kcal mol^{-1}	Δ E / kcal mol^{-1}
TPSS	4.2	-0.8
M06	2.1	-14.4
TPSS-D3	1.4	0.3
PW6B95-D3	1.7	-5.8
DLPNO-CCSD(T)	3.4	0.1

We also are able to locate the transition state for the interconversion between such Pd(II) and Pd(0) species (**TS_DE**). At this transition state, the κ^2-acetate (from complex **D**) rotates out of the plane to adopt a κ^1-coordination manner bound *cis*-to the hydride.

In addition to the neutral catalytic cycle with (AcO)Pd(II)–H, we also considered a cationic catalytic cycle involving (bbeda)Pd(II)–H. The reaction pathway was found to be similar to that of the neutral catalytic cycle with (AcO)Pd(II)–H: the three steps (hydropalladation, migratory insertion, and β-

hydride elimination) are feasible, again with β-hydride elimination showing the highest barrier (Figure 3.2).

Furthermore, the calculations predict a primary KIE for β-hydride elimination of 2.221 at 35 °C, an inverse secondary KIE of 0.912 for carbopalladation at 35 °C, and a primary KIE for alkyne hydropalladation of 4.665 at 35 °C (12.604 with a parabolic tunnelling correction). The high magnitude of this later KIE may indicate the unique nature of bonding to the hydrogen atom in the hydropalladation transition state **TS_AB**.

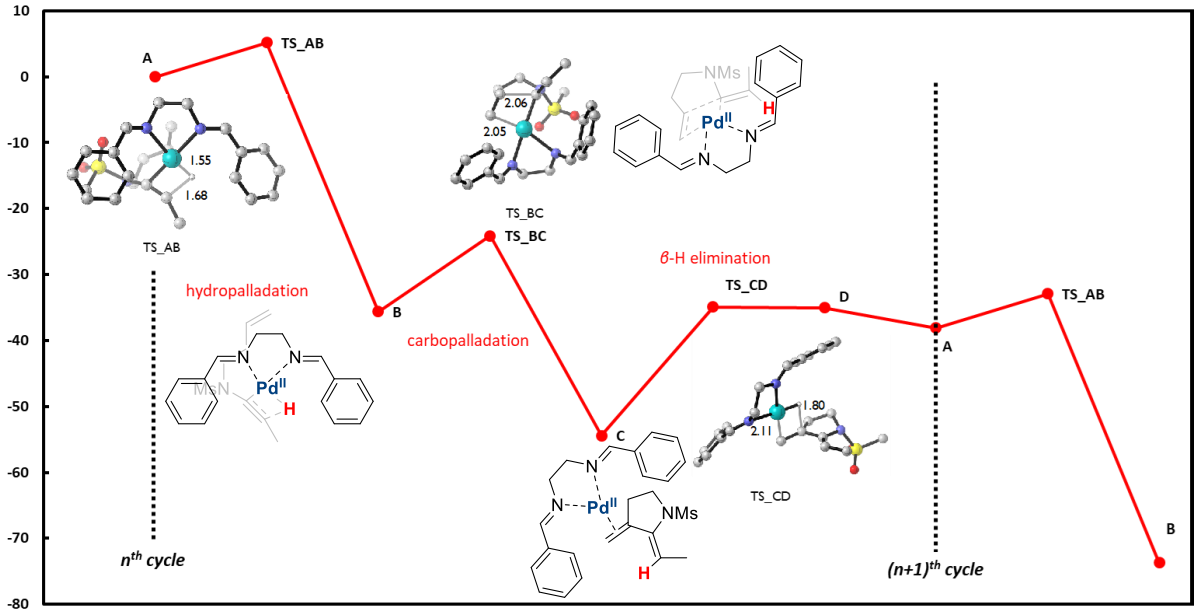

Figure 3.2 Energy Profile for the catalytic cycle with bbeda as a ligand.

3.1.2 Stereoselectivity Explanation

In the course of our investigations into enynamide cycloisomerisations, we observed very high levels of substrate stereocontrol in cycloisomerisations that generate new stereocentres within the product (Table 3.3). Entry 1 reveals the effect of a substituent adjacent to the nitrogen atom of the ynamide, which gave a single regio- and stereoisomer of pyrrolidine enamide **126**. Trisubstituted piperidine enamide **128** was yielded with equivalent stereoselectivity, with slight drop in regioselectivity, *i.e.* small amounts of 1,3- and 1,5-diene produced as side products (Entry 2). The production of the 1,5-diene may be indicative of the reversibility of β-hydride elimination of the catalytic pathway; this scenario is often observed in Heck reactions. A *syn*-α,β-substituted enynamide gave excellent stereoselectivity in the formation of tetrasubstituted pyrrolidine **130** (Entry 3).Trisubstituted enynamides with a phenyl group at α-position provide quaternary stereocentres containing products as single diastereomers (Entries 4 and 5).

Table 3.3 Diastereoselective cycloisomerizations of enynamides with substituted tethers. [a]

Entry	Substrate	Product(s)	Yield (%)[b]	Ratio / comments
1	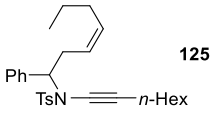 **125**	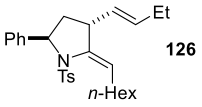 **126**	87	single isomer
2	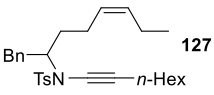 **127**	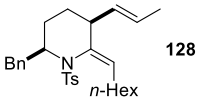 **128**	86	9:77:14[c]
3	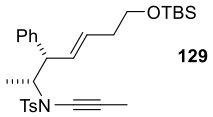 **129**	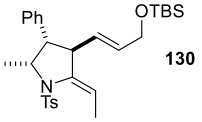 **130**	95	single isomer
4	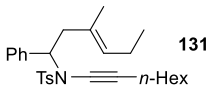 **131**	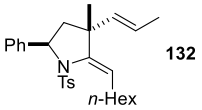 **132**	84	single isomer
5	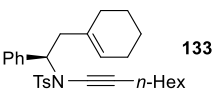 **133**	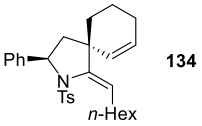 **134**	78	single isomer

[a] Reaction conditions: 5 mol% Pd(OAc)2, 5 mol% bbeda, toluene (0.167 M), 60 °C, 30 min; Entry 2 reaction time = 90 min. [b] Isolated yield. [c] Ratio of 1,3-:1,4-:1,5-dienes as determined by ^{1}H NMR spectroscopic analysis of the crude reaction mixture.

The substrates shown in Table 3.3 were prepared as follows. For **125**, alcohol **136** was prepared using the opening of epoxide **135** with an alkynyl anion (Scheme 3.1). The corresponding Boc-protected

sulfonamide **137** underwent a Lindlar hydrogenation in order to install the (*Z*)-double bond. Boc deprotection and ynamide formation then gave the desired enynamide **125** (the route was pioneered by Dr Ross Walker).

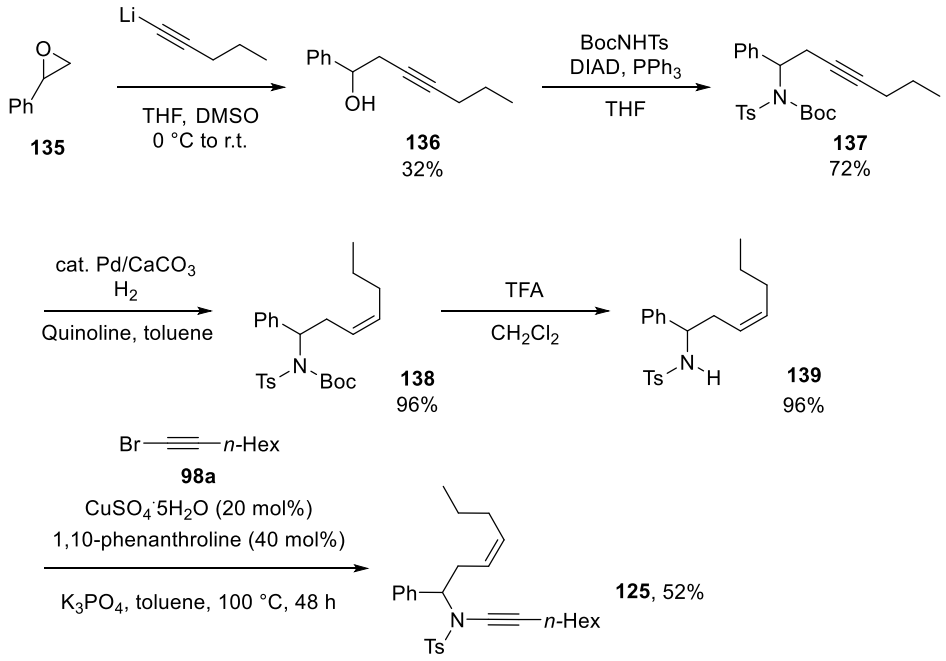

Scheme 3.1

The synthesis of α-benzyl enynamide **127** was implemented by Dr Craig Campbell;[20] and ynamide **129** was synthesised by Dr Venkaiah Chintalapudi.[50]

Substrate **131** was made from sulfonamide **143**, which was synthesised from the Ireland-Claisen rearrangement of ester **140**, followed by the Curtius rearrangement, Boc deprotection, and tosylation of the resulting amine (Scheme 3.2). **143** was converted to ynamide **131** using ynamide formation method developed by the Hsung group.[41] The work was first undertaken by Dr Ross Walker.

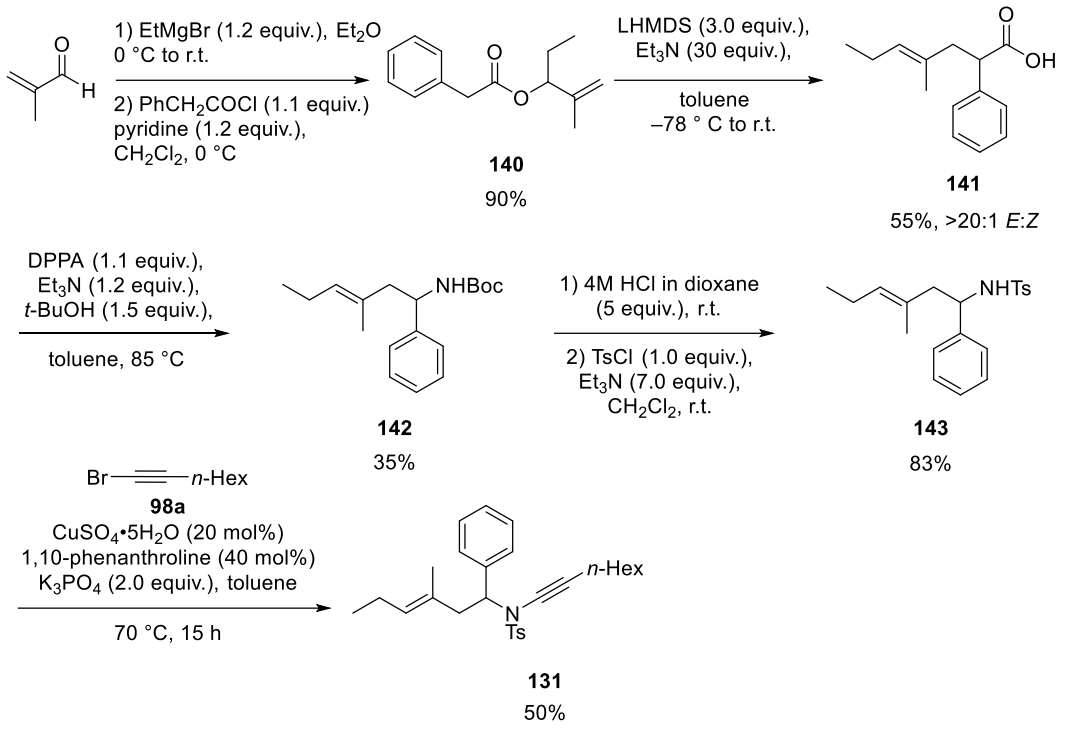

Scheme 3.2

Cyclohexenyl ynamide **133** was prepared from sulfonamide **146** *via* copper-catalysed alkynylation. Sulfonamide **146** was prepared from alcohol **144** by Mitsunobu reaction to produce carbamate **145**, then the Boc group was removed using potassium carbonate in refluxing methanol (Scheme 3.3).

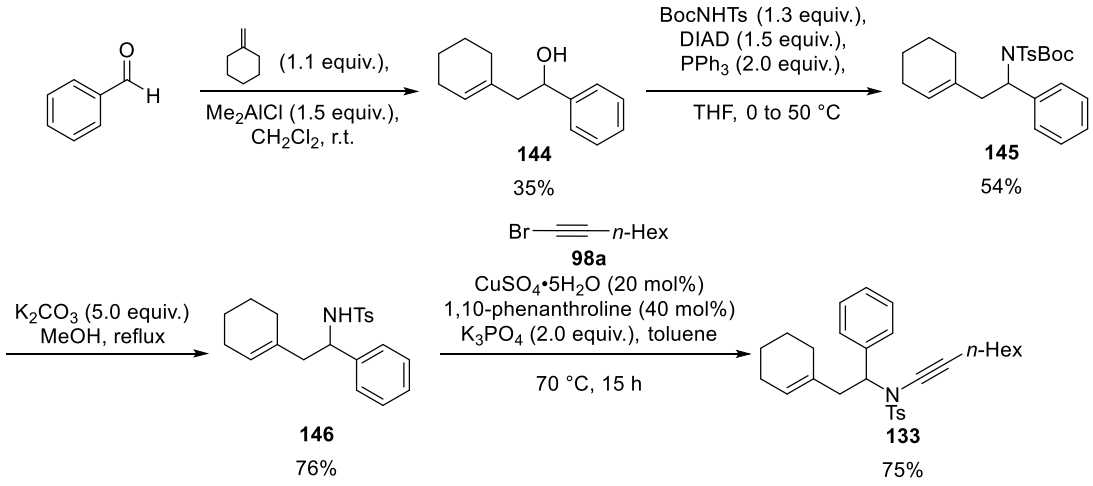

Scheme 3.3

The stereoselectivity of the cyclisation of enynamide **125** (Table 3.3, Entry 1) was modelled using substrate **147** in which the alkyne substituent and the group connected to the alkene are represented by a methyl group (Figure 3.3). The carbopalladation substrate resulting from **148** exists in two similar conformations: **148-*anti*** and **148-*syn***, the transition states (**TS-149-*anti*** and **TS-149-*syn***) from the

conformers lead to products **150-*anti*** (green profile, the observed outcome) and **150-*syn*** (red profile) respectively. A free energy difference between such transition states ($\Delta\Delta G^{\ddagger}$ = 3.4 kcal mol^{-1}) corresponds to a calculated diastereoselectivity of more than 180:1 (assuming that carbopalladation is irreversible and also the diastereodetermining step). This is consistent with the observed reaction stereoselectivity. The energy difference between these transition states can be explained by changes in torsional strain during the carbopalladation step: for **TS-149-*anti***, the strain is relieved as carbopalladation proceeds (from the eclipsed C–H bonds to red and green hydrogens in **148-*anti***). In case of transition state **TS-149-*syn***, eclipsing interactions increase the torsional strain as this step proceeds (from the staggered C–H bonds to red and green hydrogens in **148-*syn***).

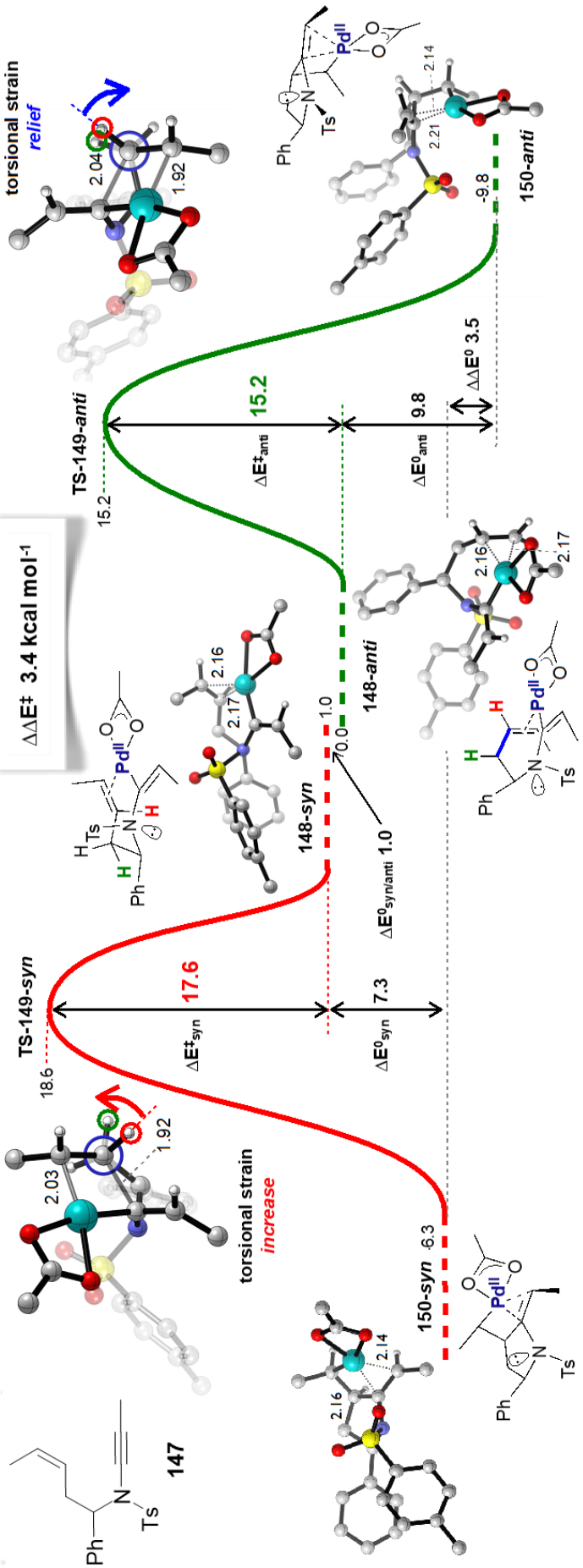

Figure 3.3 DFT calculations rationalize the stereochemical outcome of the anti-diastereoselective cycloisomerization of enynamide **147.**

3.2 Experiments on Kinetic Isotope Effects

The data obtained from the ^{1}H NMR timecourse experiments indicated the occurrence of isotope effects. Such effects cause distinct differences in reaction rate and isotope incorporation during the course of reaction. With the computational prediction of the KIE for the rate-limiting step (β-hydride elimination) in hand, we aimed to measure the magnitude of the KIE experimentally. The determination of this KIE was carried out by comparing the product distribution from disubstituted alkenyl ynamide (*E*)-**151a**[20] with that of its deuterated equivalent (*E*)-d$_1$-**151a** (Scheme 3.4).

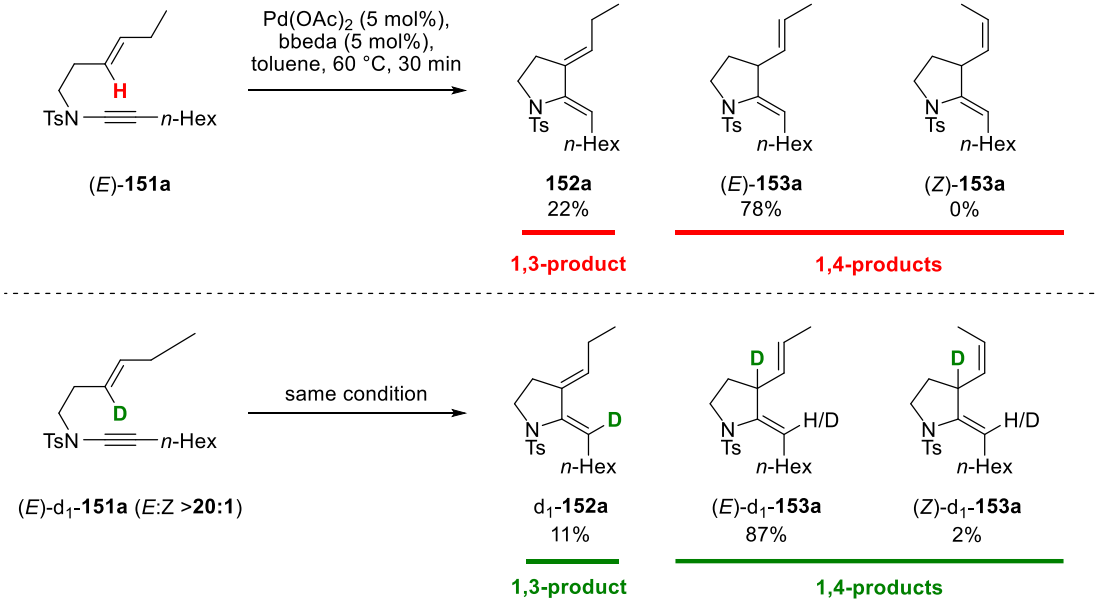

k_H/k_D (*β-hydride elimination*) = ratio of 1,4-:1,3-dienes from (*E*)-d$_1$-**151a** and **151a**

$$= \frac{\text{d}_1\text{-153a / d}_1\text{-152a}}{\text{153a / 152a}} = \frac{89 / 11}{78 / 22} = \frac{8.09}{3.54}$$

$$= 2.29$$

Scheme 3.4

Deuterated substrate (*E*)-d$_1$-**151a** was prepared as shown in Scheme 3.5. β-alanine methyl ester hydrochloride salt was converted to sulfonamide **94**, then reduced to alcohol d$_2$-**95** using $LiAlD_4$. Dess-Martin oxidation gave the corresponding deuterated aldehyde d$_1$-**96**. Enynamide (*E*)-d$_1$-**151a** (*E*:*Z* = <20:1) was synthesised from aldehyde d$_1$-**96** using a Wittig reaction with NaHMDS as base, followed by ynamide formation under Hsung's conditions.[41]

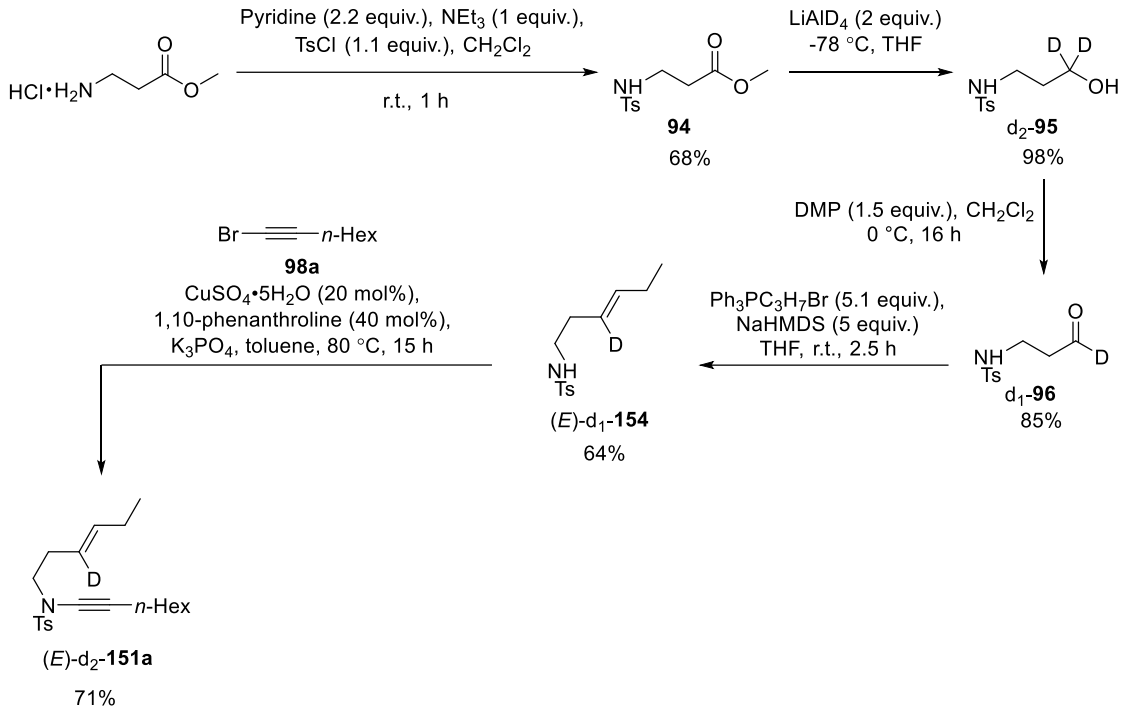

Scheme 3.5

For the reaction with the deuterated substrate, (*E*)-d$_1$-**151a**, β-deuteride elimination is required to generate 1,3-diene products. The ratio of 1,3-:1,4-dienes was determined by ^{1}H NMR spectroscopy, and the KIE for β-hydride elimination was determined to have a value of 2.29. This value is consistent with the theoretical value (2.07 at 60 °C; 2.23 at 35 °C for model substrate **123**), as well as other reports on β-hydride elimination from alkylpalladium complexes.[51–54]

While the KIE associated with β-hydride elimination is consistent with computation and with literature values, the overall difference in reaction rate between substrates **151a** and d$_1$-**151a** at 5 mol% catalyst loading is clearly not solely dependent on the KIE for β-hydride elimination. Although KIEs would be expected from the hydropalladation and carbopalladation steps, it was fortunately that the KIE for β-hydride elimination would not be affected by those of the hydropalladation and carbopalladation steps. As aforementioned, the computation suggested that the reaction pathway with bbeda serving as a ligand for palladium(II) hydride (bbeda·Pd(II)–H) is also feasible. That is, the path from product decomplexation to substrate complexation, and entry to the catalytic cycle *via* irreversible hydropalladation, perhaps involves a number of 'off-pathway' processes, for example, coordination by bbeda (or its hydrolysed species) to Pd(II)H(OAc) or Pd(0)(HOAc). We therefore speculated whether the catalyst concentration could affect the observed reaction rates of substrate **92**, in comparison with

that of deuterated substrate d_1-**92**, such that the concentration of active catalyst species is dependent on the isotope. We were pleased that this was found to be the case as shown by measurement (run in triplicate) of the rates of cycloisomerisation for each substrate at different catalyst loadings (0.5, 1, 2.5, 5 and 10 mol%). The rate constants for both substrates, and their associated errors (one standard deviation) were plotted and tabulated as shown in Graph 3.1. Plateau effects were observed for both substrates at higher catalyst concentrations: for **92**, this occurs above 5 mol%, while for d_1-**92**, at or above 2.5 mol%.

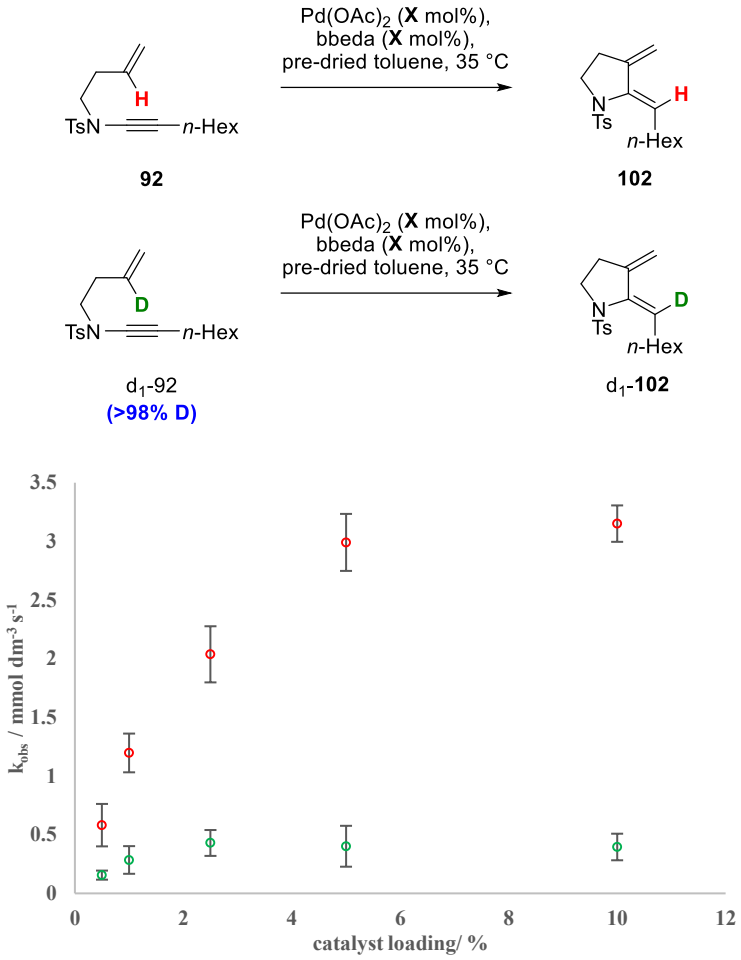

Catalyst loading **X** (mol%)	$\langle k_H(obs)\rangle$ (mmol dm^{-3} s^{-1})	$\langle k_D(obs)\rangle$ (mmol dm^{-3} s^{-1})	$k_H(obs) / k_D(obs)$
0.5	0.58 ± 0.18	0.16 ± 0.039	3.74 ± 0.40
1	1.20 ± 0.17	0.28 ± 0.12	4.20 ± 0.44
2.5	2.04 ± 0.24	0.43 ± 0.11	4.74 ± 0.28
5	2.99 ± 0.24	0.40 ± 0.17	7.45 ± 0.44
10	3.15 ± 0.16	0.40 ± 0.11	7.97 ± 0.29

Graph 3.1

This backs up the idea that the difference in energy barriers for hydro- and deuteriopalladation could have an influence on off-cycle equilibrium processes. That is, hydropalladation is much lower in energy than deuteriopalladation. This suggests the impact of the hydropalladation step on entry to the catalytic cycle, as well as illustrating H/D exchange process that can intercept the released Pd(II)–D species *en route* to complexation of the next molecule of substrate.

Moreover, the order of reaction with respect to the metal catalyst can also be determined by these data. Plotting a relationship between $\ln(k_{obs})$ and $\ln([Pd(OAc)_2])$ reveals straight line graph (Graph 3.2), which supports the proposal of a monomeric palladium species as the active catalyst.[55] Although the linear with the value of gradient less than 1 reflects the equilibrium between monomeric and dimeric forms of palladium species, the slope magnitude of 0.69 (>0.5) indicates the preference of the monomeric form over the dimeric form.

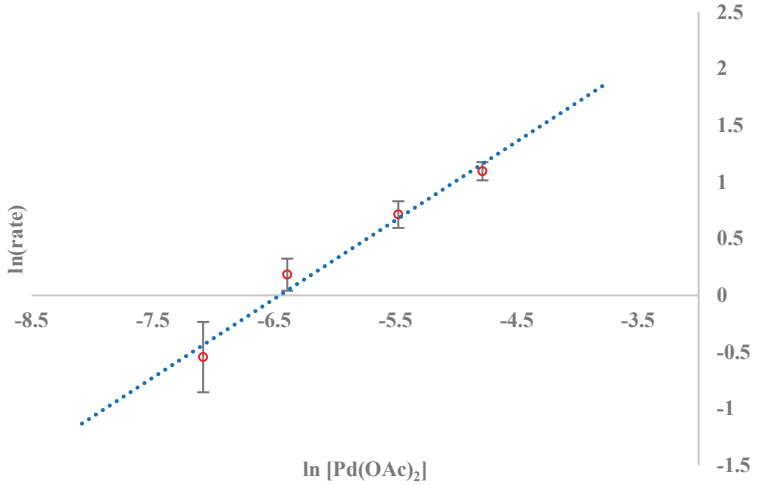

slope = 0.69, R^2 = 0.98

Graph 3.2

In addition, a secondary kinetic isotope effect was observed when comparing the absolute rates of cycloisomerisation of (*Z*)-**151a** and (*Z*)-d_1-**151a**. These substrates gave exclusively 1,4-diene products, *i.e.*, there is no effect β-hydride/deuteride elimination on the rate of reaction.

Deuterated substrate (*Z*)-d_1-**151a** was prepared as shown in Scheme 3.6. Deuterated aldehyde d_1-**96** was reacted with $Ph_3PC_3H_7Br$ under basic conditions, followed by the copper-catalysed alkynylation of the sulfonamide to afford the desired ynamide.

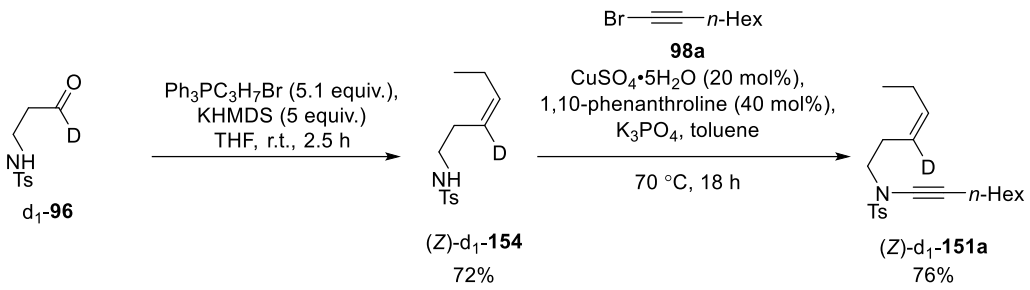

Scheme 3.6

The gradients of the cycloisomerisation kinetic profiles were measured in the pseudo-0th order steady state region of the reaction (6-11 minutes), Graph 3.3. A straight-line fit of these linear regions gives two gradients, the ratio of which corresponds to an inverse secondary kinetic isotope effect of 0.87±0.01. The reason for this being secondary KIE is not clear: with the theoretical pathway indicating carbopalladation to be a non-rate limiting step, we suggest that this effect could relate to differences between the two isotopes in agostic interactions, or hyperconjugation effects during the enamide decomplexation / β-hydride elimination steps, or during product decomplexation.

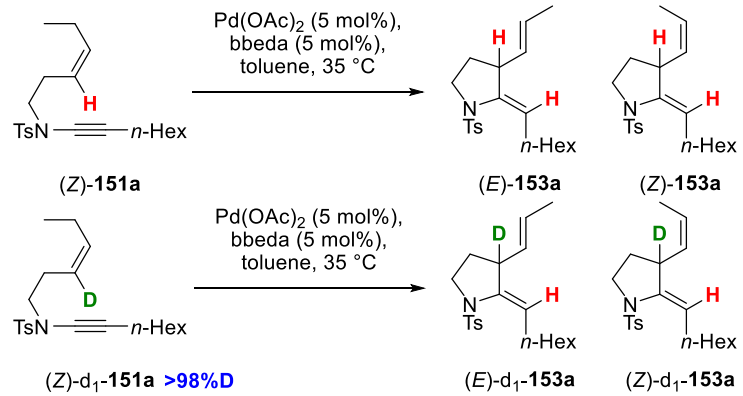

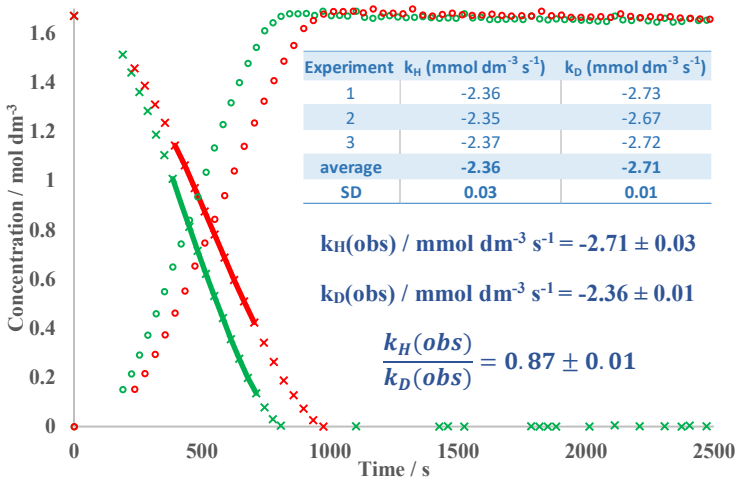

Graph 3.3

3.3 Conclusions

The reaction mechanism is examined computationally to confirm that a Pd(II)–H mediated pathway is feasible. Modelling of $L_2Pd(II)H(OAc)$ and $L_2Pd(0)(HOAc)$ complexes (which are in rapid equilibrium) shows that the latter is the active *pre*-hydropalladation (Pd(0)) complex. Hydropalladation is illustrated to proceed *via* a novel mechanism in which a hydride transfer from Pd(0)-complexed HOAc to the alkyne is stabilised by an agostic interaction with the metal centre – oxidative hydropalladation type process. This mechanism could have wider implications for other hydrometallation reactions. The rate-limiting step of the reaction is found to be β-hydride elimination, with hydropalladation and carbopalladation both being irreversible.

Exploiting computational analysis, the high stereoselectivity observed from cycloisomerisation of chiral enynamides can be explained. From the calculations, we discovered that torsional strain effects play a crucial role in producing excellent level of diastereoselectivity.

Finally, experimental determination of the KIE for β-hydride elimination correlates well with the theoretical prediction. In addition, we also observed the unexpected KIE, which may indicate an influence of the isotope on the rate of enamide decomplexation / β-hydride elimination (to the 1,4-diene), or on product decomplexation. This combination of experiment and theory therefore provides further support for the palladium hydride mechanism.

Chapter 4: Introduction: Asymmetric Transition Metal-Catalysed 1,6- and 1,7-Enyne Cycloisomerisations

In the previous chapter, the benefits of transition metal-catalysed cycloisomerisation of 1,*n*-enyne has been demonstrated in accessing various types of cyclic compounds. We now turn our attention to the process in which stereo-defined cyclic 1,3- and 1,4-dienes are produced. Over the past decades, the development of enantioselective enyne cycloisomerisation has attracted of significant interests; this chapter will focus on progress in this field using various metals as catalysts.[56]

4.1 Palladium

Enantioselective metal-catalysed enyne cycloisomerisation was first reported by the Trost group.[14] In this work, chiral carboxylic acids (*e.g.* Mosher's acid, (*S*)-binapthoic acid) were used in combination with with $Pd_2(dba)_3{\cdot}CHCl_3$ (5 mol%) instead of achiral acid, such as acetic acid (Scheme 4.1). Based on the idea that Pd(0) would undergo oxidative addition across the acid to give H–Pd(II)–O_2CR^* , the chiral moiety (R^*) of the acid should facilitate stereochemical induction during the cycloisomerisation process. The reaction produced chiral 1,4-diene **3a** in moderate yield, but with only modest level of enantioselectivity (up to 33% *ee*).

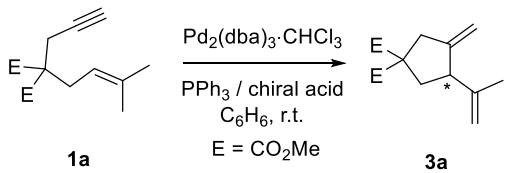

1a **3a**

chiral acid	yield / %	*ee* / %
(*S*)-binapthoic acid	61	33
(*S*)-Mosher's acid	60	8
(+)-camphorcarboxylic acid	64	2-5

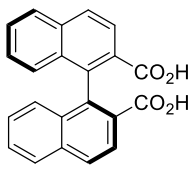

(*S*)-binapthoic acid

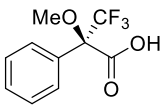

(*S*)-Mosher's acid

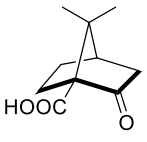

(*S*)-camphorcarboxylic acid

Scheme 4.1

The Trost group later illustrated an improvement in the enantioselectivity by using amidodiphosphane ligand **155** together with a tartrate auxiliary installed on 1,6- and 1,7-enyne substrates **154** (Scheme

4.2).[57] This enabled a double stereodifferentiating cycloisomerisation to take place, again leading to modest stereoselectivity.

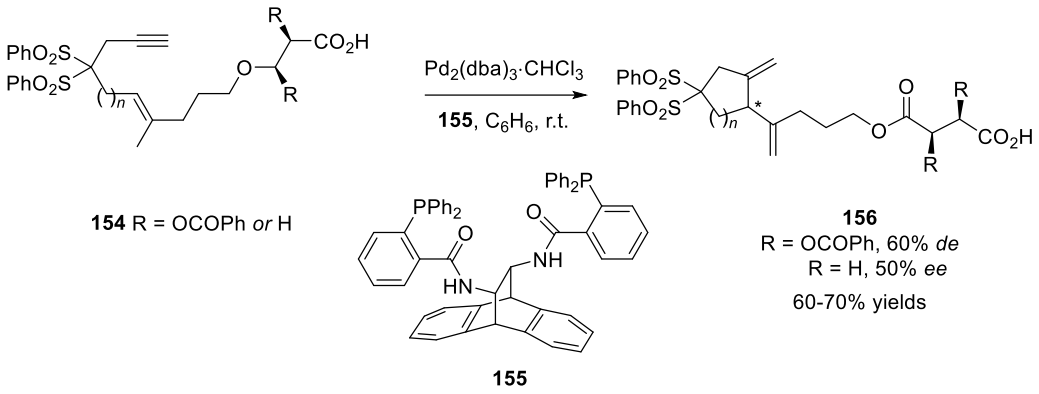

Scheme 4.2

The group discovered that the carboxylic acid group in the substrate is crucial for asymmetric induction, rather than the stereocentres of the tatrate unit. This was supported by the fact that when ethyl and methyl esters, instead of carboxylic acid, were used; poor selectivity (0-6% *de*) was observed.

In 1996, Ito and co-workers introduced a new ferrocene-based bidentate ligand, (*S,S*)-(*R,R*)-Trap, **158**.[58] This ligand enabled palladium-catalysed cycloisomerisation of enynes **157**, producing 1,4-dienes **159** as the major product (3.5:1, **159**:**160**) with excellent enantiopurity (95% *ee*). It is worth noting that the reason for 1,4 dienes being more favoured is that the presence of this ligand reduces the reaction rate; as a result, elimination of H_b (blue) was preferred to the elimination of H_a (green) (Scheme 4.3). Moreover, changing the configuration of the olefin from *E* to *Z* led to a reversal the configuration of the stereogenic centre of the product (*R* to *S*).

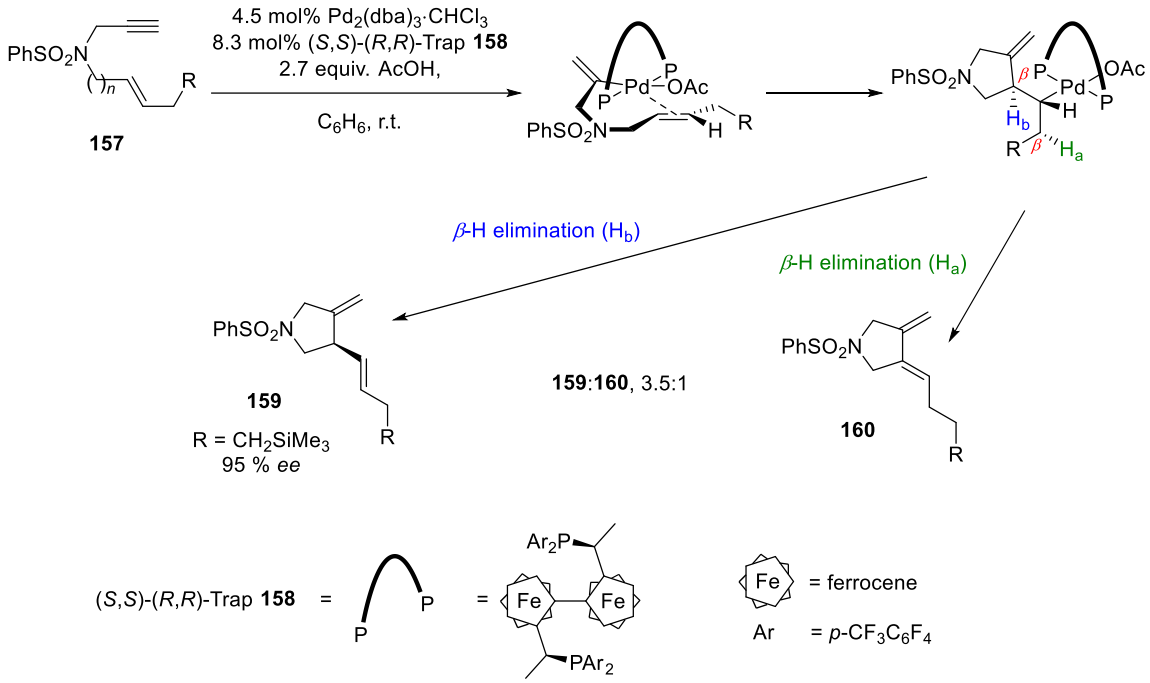

Scheme 4.3

Mikami and co-workers reported that oxygen-tethered enyne **161** could be cycloisomerised using serveral palladium salts in the presence of chiral bidentate phosphine ligands to give product **162** with up to 99% *ee*.[17] Reaction yields were found to be dependent on the palladium salt. $Pd(OCOCF_3)_2$ gave the best yield (Scheme 4.4), while others ($Pd(OAc)_2$ or $Pd_2(dba)_3{\cdot}CHCl_3$ / AcOH) led to poor reaction yields (< 25%). Interestingly, Mikami observed a marked solvent effect on the stereoselectivity and reaction rates. In DMSO, the cationic palladium species **163** is formed as the CF_3COO^- ion can dissociate from Pd, and adopts a square-planar geometry. In non-polar solvents, like benzene, the CF_3COO^- ion remains coordinated to the metal centre. As a consequence, a five-coordinate intermediate **164**, in which the alkene unit is weakly coordinated (out of plane) to the palladium, is formed. This species leads to a high activation energy, hence a sluggish reaction rate.

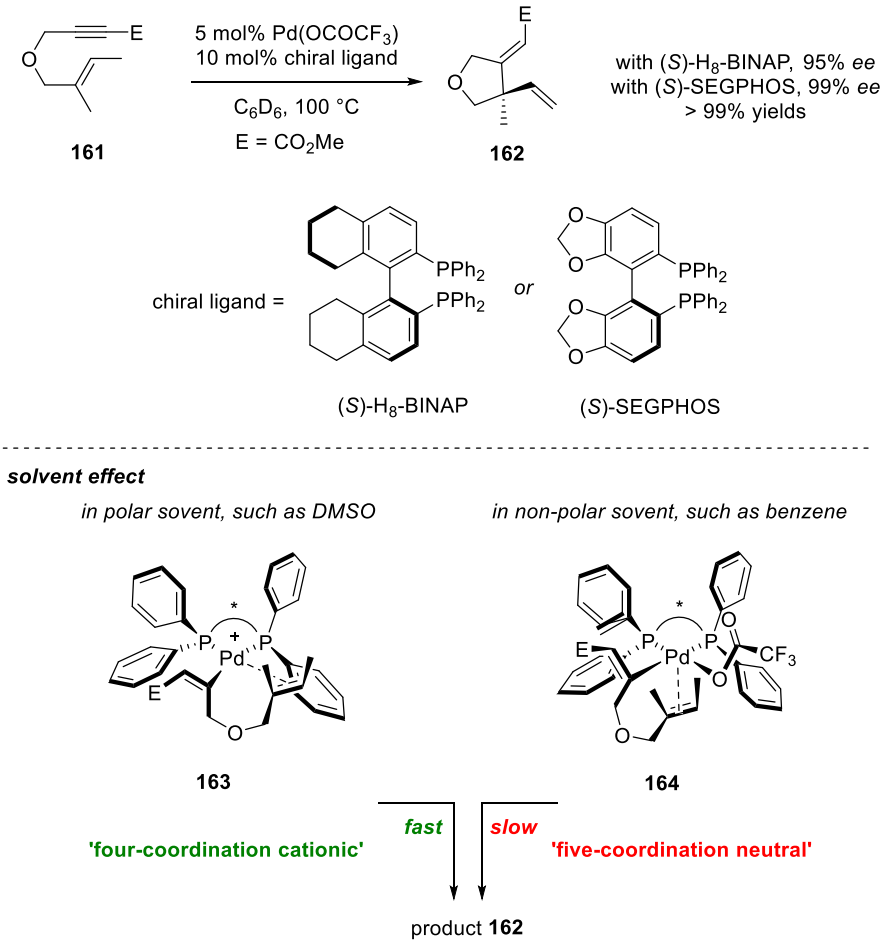

Scheme 4.4

The Mikami group also demonstrated the asymmetric cycloisomerisation of 1,7-enynes (Scheme 4.5).[59] In this work, the cycloisomerisation of enynes **165** and dihydropyranyl alkyne **166** was catalysed by a combination of $[Pd(MeCN)_4](BF_4)_2$, (*S*)-BINAP, and formic acid in DMSO at 100 °C to give quinoline derivatives **167** and spiro products **168**, respectively.

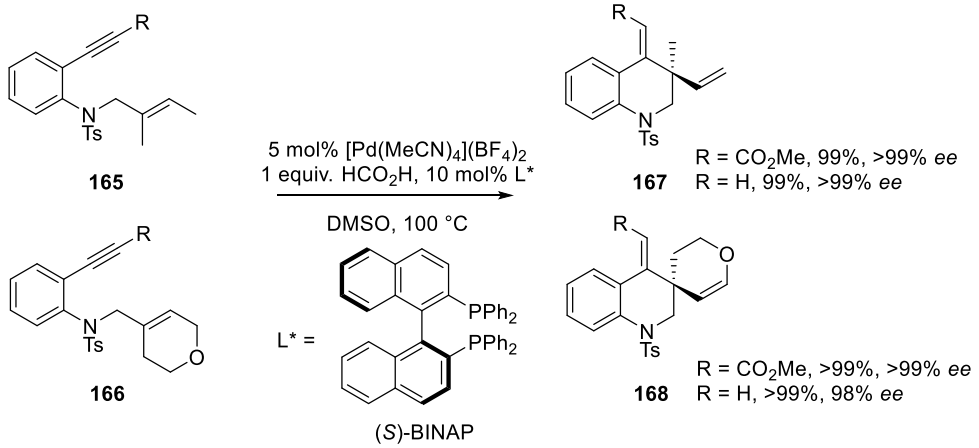

Scheme 4.5

Since Mikami's conditions were introduced, more recent palladium-based catalyst systems for enantioselective cycloisomerisations have been developed based on such conditions. In 2009, Tanaka *et al*. showed that a combination of $[Pd(MeCN)_4](BF_4)_2$ and (*S*)-xyl-SEGPHOS could cyclise *N*-alkenyl arylethynylamides **169** to give axially chiral 4-aryl-2-pyridones **170** with excellent yields and enantiomeric excess (Scheme 4.6).[60]

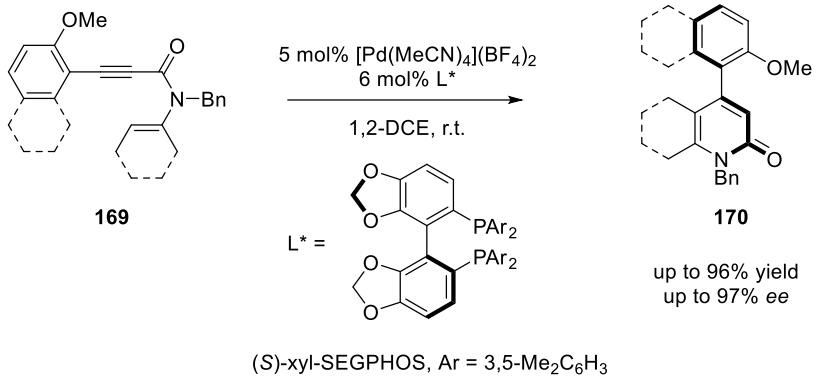

Scheme 4.6

Although the catalyst system used for this cycloisomerisation very much resembles that of Mikami, the mechanisms of catalysis differ. This reaction is proposed to begin with π-activation of the alkyne *via* η^2-coordination of palladium, instead of the usual hydrometallation pathway.

Another example of exploiting palladium-catalysed isomerisation to construct axially chiral biaryl compounds is found in work from Uemura *et al*.[61] This work illustrated that a combination of $[Pd(MeCN)_4](BF_4)_2$ and (*R*)-BINAP could be used to asymmetrically cycloisomerise enynes **171** to give biaryls **172** with decent yields and excellent enantioselectivity (Scheme 4.7).

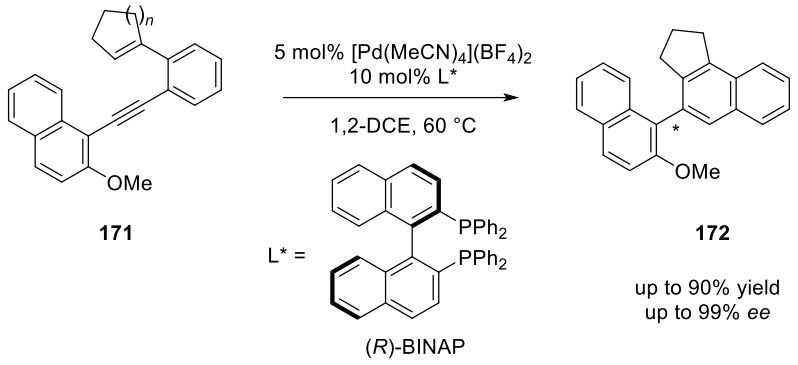

Scheme 4.7

Recently, the Andersson group showed that thiazole, imidazole and oxazoline based *N*,*P*-ligands could be also used to cyclise oxygen-tethered enyne **173** (similar to Mikami's substrates) to afford chiral tetrahydrofurans **174** in up to 84% yield and 81% *ee* (Scheme 4.8).[62]

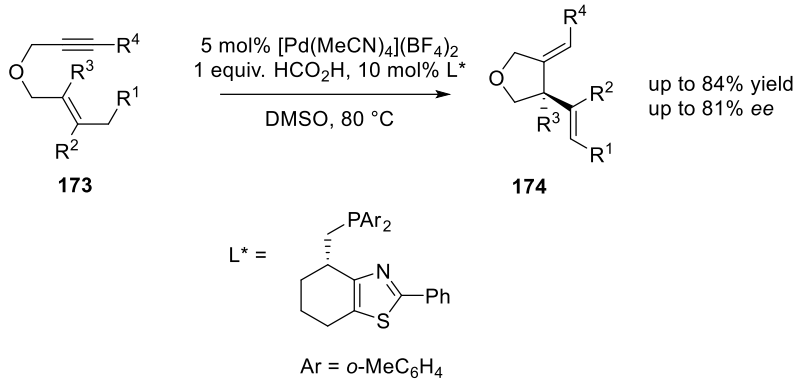

Scheme 4.8

The stereochemical outcome of this reaction can be rationalised by the model illustrated in Scheme 4.9. Using DFT calculations, an optimised structure of palladium-ligand complex **175** was obtained. This structure reveals that quadrant 2 and 4 display strong steric crowding resulting from the chiral ligand. When substrate **173** binds to complex **175**, intermediate **176** is sterically favourable to be formed (compared to intermediate **177**). This species leads to (*S*)-configuration of the product, **174a**.

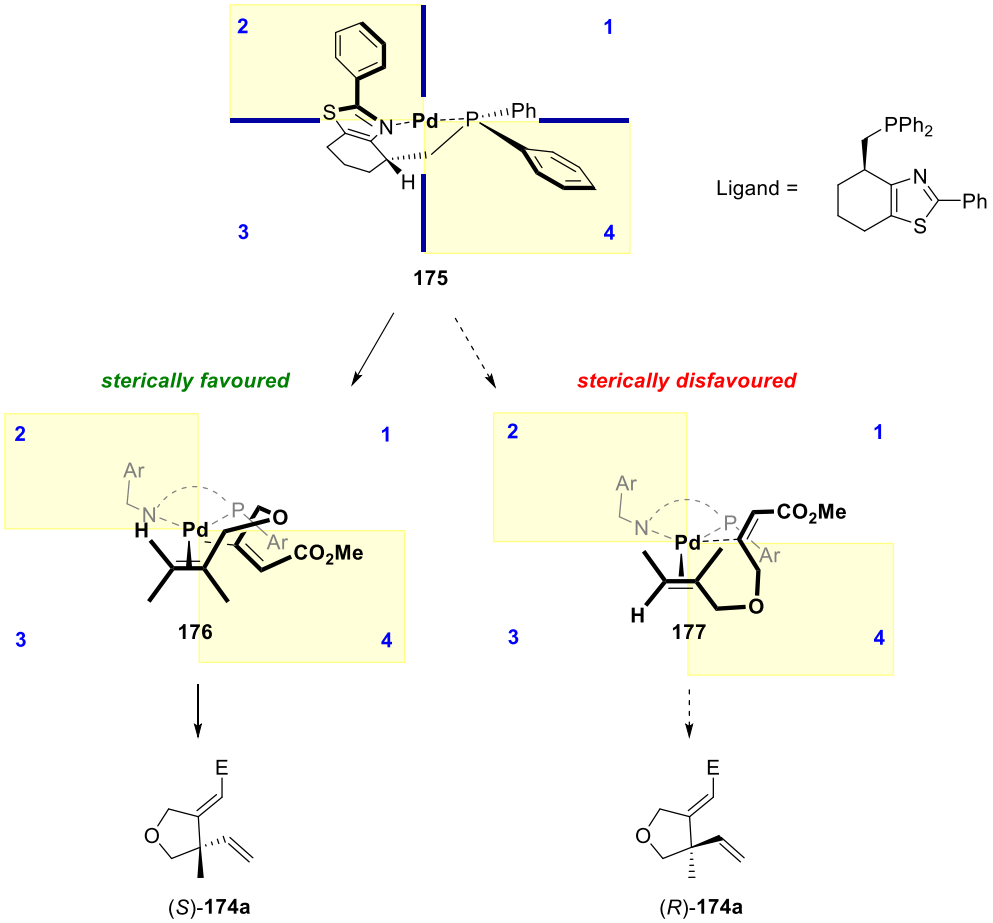

Scheme 4.9

4.2 Rhodium

Zhang *et al*. demonstrated the first asymmetric rhodium-catalysed enyne cycloisomerisation,[37] which employed a cationic rhodium catalyst with chiral diphosphane / diphosphinite ligands in the cyclisation of 1,6-enynes (*Z*)-**178** to give cyclic products (*E*)-**179** (Scheme 4.10).

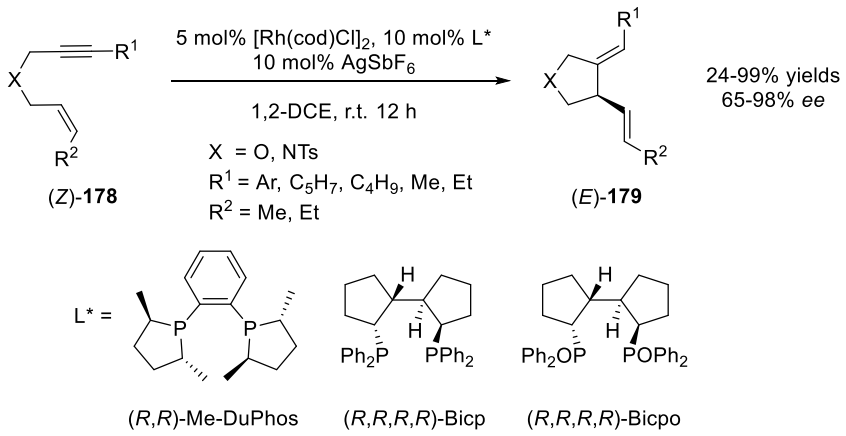

Scheme 4.10

In addition to 1,6-oxygen/nitrogen tethered enynes, many prototypical substrates with heteroatom tether linkages, such as **180**, could also be cycloisomerised with the same catalyst system.[63] It was found that when the ligand was changed to (*S*)-BINAP, the level of enantioselectivity and reaction reactivity were improved (up to 91% yield and > 99% *ee*, Scheme 4.11).

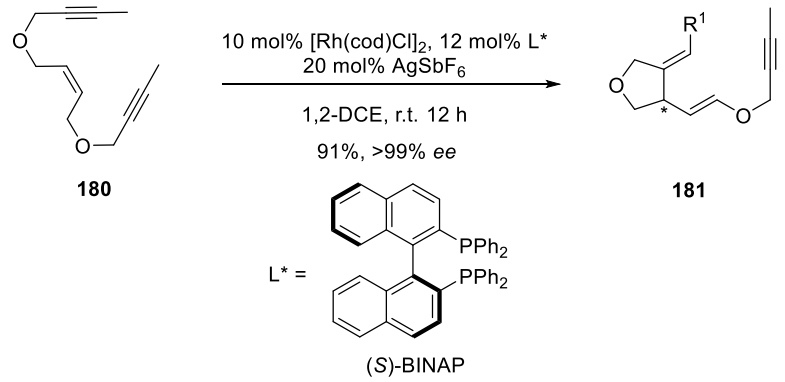

Scheme 4.11

Substrate scope for the catalyst system has been expanded by implementing the new experimental protocol, as a result chiral functionalised lactams **183** were yielded with high enantiopurity (Scheme 4.12, top).[64] Moreover, Zhang *et al.* illustrated the enantioselective synthesis of kainic acid analogues using the same catalyst system (Scheme 4.12, bottom).

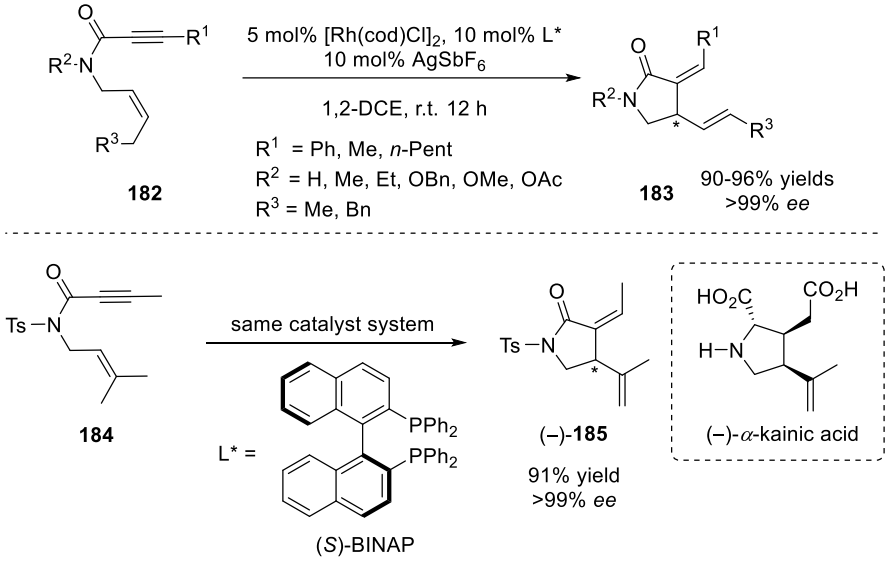

Scheme 4.12

In this work, the authors also suggested the possible mechanism for the operation of this catalyst (Scheme 4.13). First, the cationic rhodium catalyst binds to the alkene and alkyne simultaneously. This complex (**187**) then undergoes oxidative coupling to give rhodacycle **188**. Subsequent β-hydride

elimination gives vinyl rhodium complex **189** which then proceeds reductive elimination to give 1,4-diene product (*E*)-**179**. It is also possible that rhodium complex **188** is in equilibrium with less stable (due to steric clash) complex **192**. β-hydride elimination of this complex, followed by reductive elimination can lead to the formation of a (*Z*)-1,4 diene product, (*Z*)-**179**. Another possibility is that the hydrogen on the cyclic unit undergoes β-hydride elimination, leading to 1,3-product **191**, but this product is not generally observed. However, Zhang *et al*. reported that this reaction was incompatible with (*E*)-alkenyl substrates with poor conversion and enantioselectivity observed. This is perhaps due to weaker coordination of (*E*)-substrate to the rhodium centre.

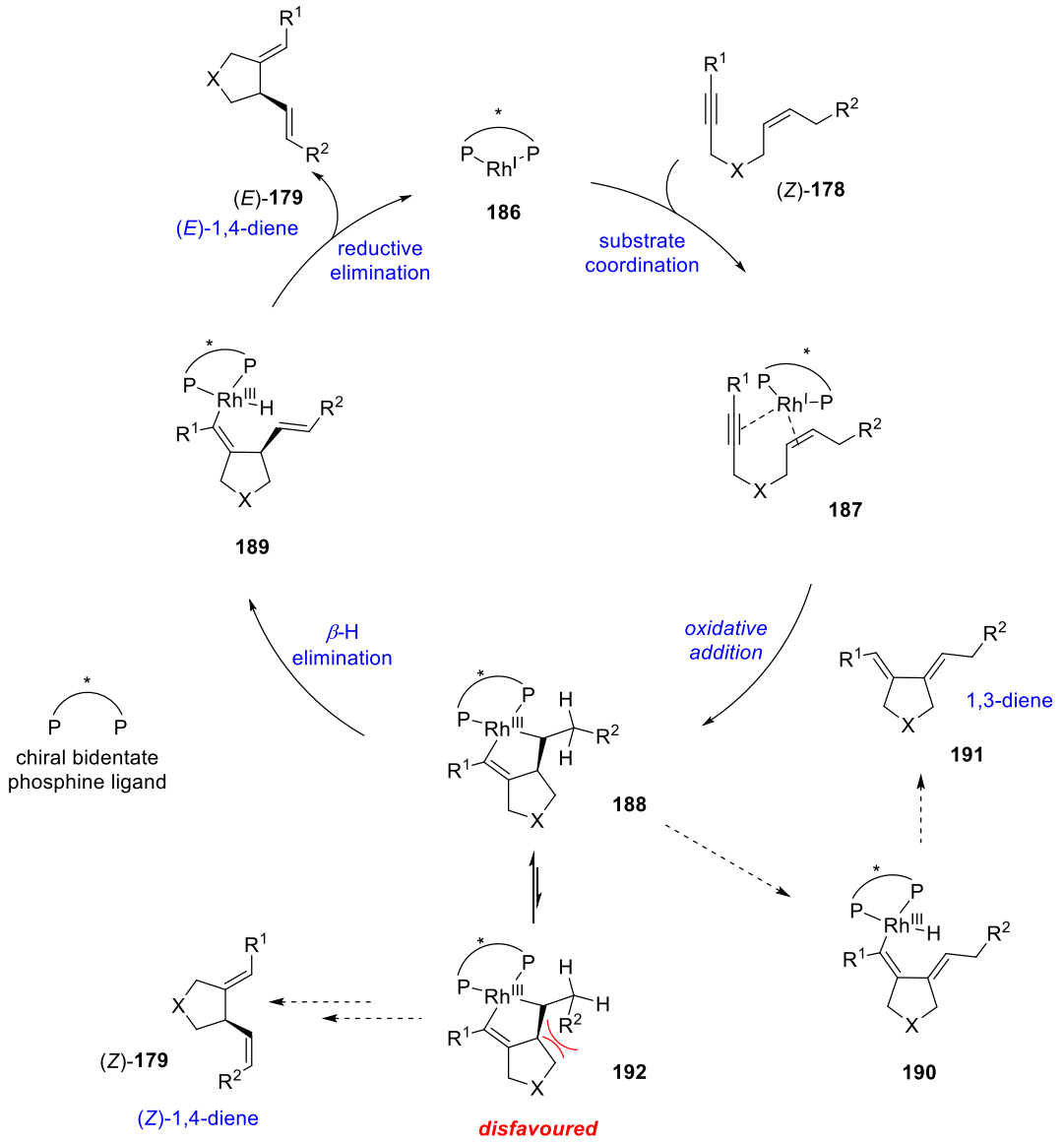

Scheme 4.13

Zhang and co-workers applied this chemistry a formal synthesis of (+)-pilocarpine with rhodium catalysis as the key synthetic step (Scheme 4.14).[65] It was also shown that chiral γ-lactones **194** could be readily prepared with excellent yields and enantioselectivities (less than 5 min of reaction time).

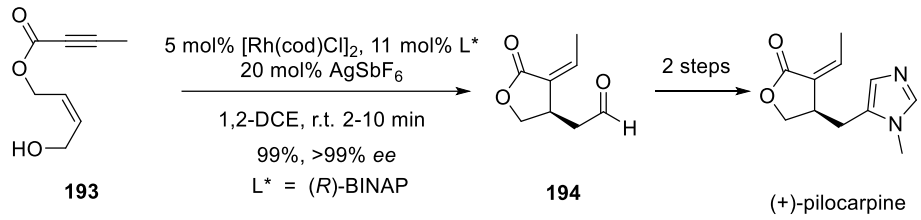

Scheme 4.14

Not long after reporting the synthesis of (+)-pilocarpine, the Zhang group developed the first highly enantioselective kinetic resolution enyne cycloisomerisation.[66] When 1,6-oxygen tethered enyne **195** was submitted to the catalytic reaction with (*S*)-BINAP, *syn*-(±)-**195** led to enantiopure (2*R*, 3*S*)-**196** and *syn*-(+)-**195**, while *anti*-(±)-**195** gave >99% *ee* of (2*R*, 3*S*)-**196** and *anti*-(+)-**195** with the same ligand (Scheme 4.15). The use of (*R*)-BINAP with the same isomers gave the opposite hand of the products also with > 99% *ee*. The limitation of this resolution is that the production of *syn*-products (**196**) could not be achieved by performing the mismatched reaction.

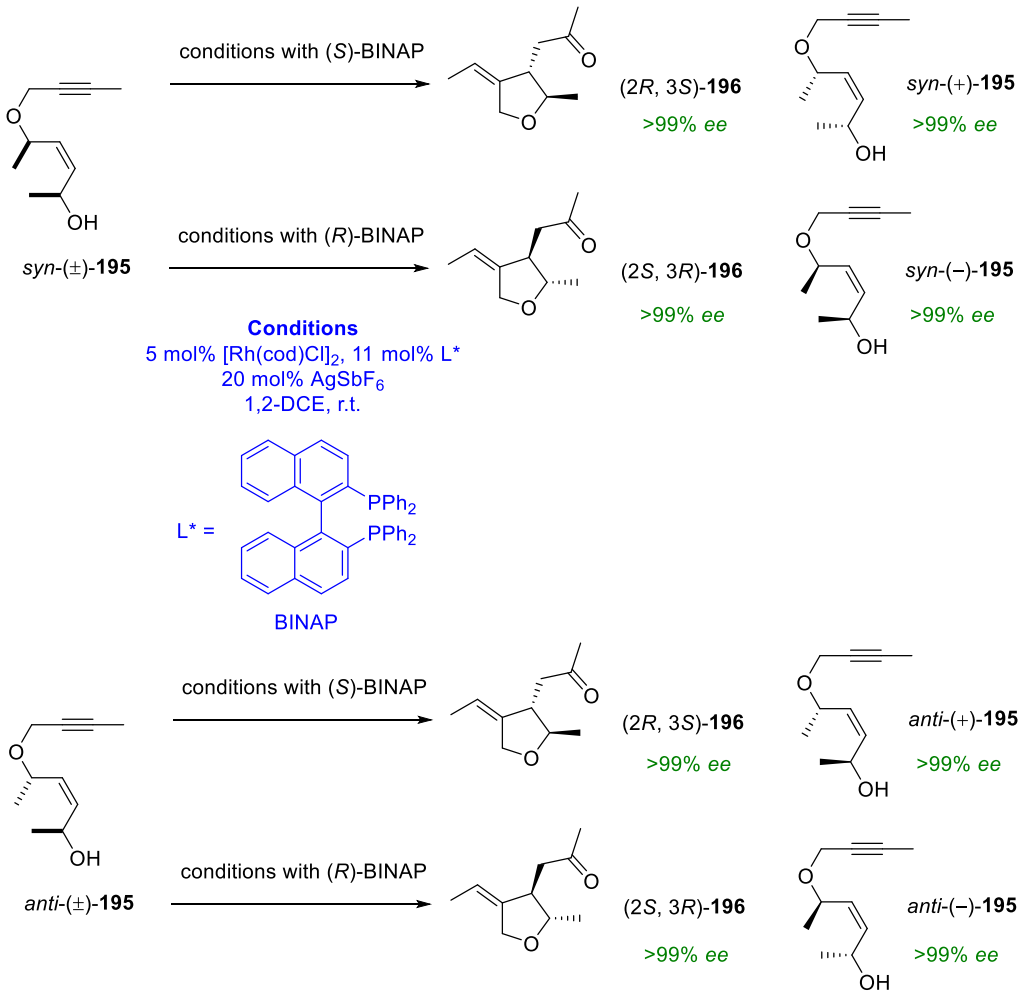

Scheme 4.15

In 2009, Muller *et al*. used Zhang's catalyst to enantioselectively cyclise allyl alcohols **197** to afford chiral ketones.[67] These ketones can be reduced by $NaBH_4$ in one-pot fashion to obtain chiral alcohols **198** (Scheme 4.16) with moderate to high yields (38-95%) and excellent enantiomeric excess (>99% *ee*).

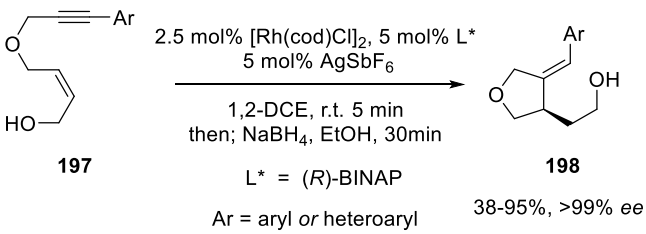

Scheme 4.16

During the study towards the total synthesis of platensimycin, Nicolaou *et al*. reported that the reaction conversion and the level of asymmetric induction improved when [Rh((*S*)-BINAP)]SbF_6 was used as

catalyst instead of Zhang's catalyst system.[68] The model substrate used in the study of this asymmetric cycloisomerisation was allyl alcohol **199**, which gave chiral aldehyde **200** (Scheme 4.17). The yield and enantioselectivity of the reaction were decent. However, this catalyst must be prepared freshly as a solution in order to obtain good results.

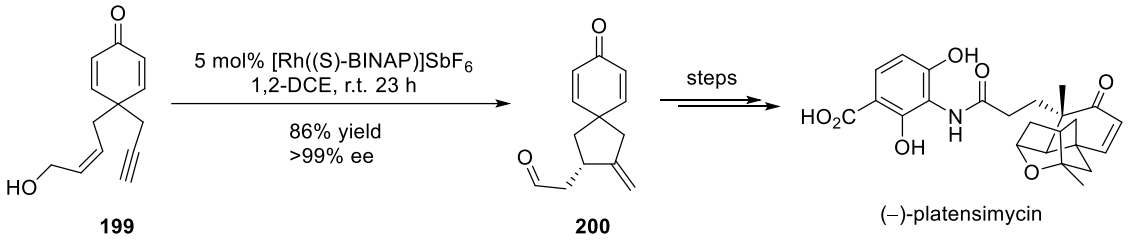

Scheme 4.17

Hayashi reported that chiral diene-phosphine tridentate ligands with rhodium catalyst could facilitate asymmetric cycloisomerisation of 1,6-enynes **201** (Scheme 4.18).[69] In stark contrast, the products obtained from this rhodium catalysis is different from that of Zhang's or Nicolaou's catalyst systems: chiral azabicyclo[4.1.0]heptenes **202** instead of chiral pyrrolidine analogues. The results were excellent, high reaction yields and great enantioselectivities were observed. In addition, the bicyclic product, **202a**, could be further converted to a highly functionalised cyclopropane **203a**.

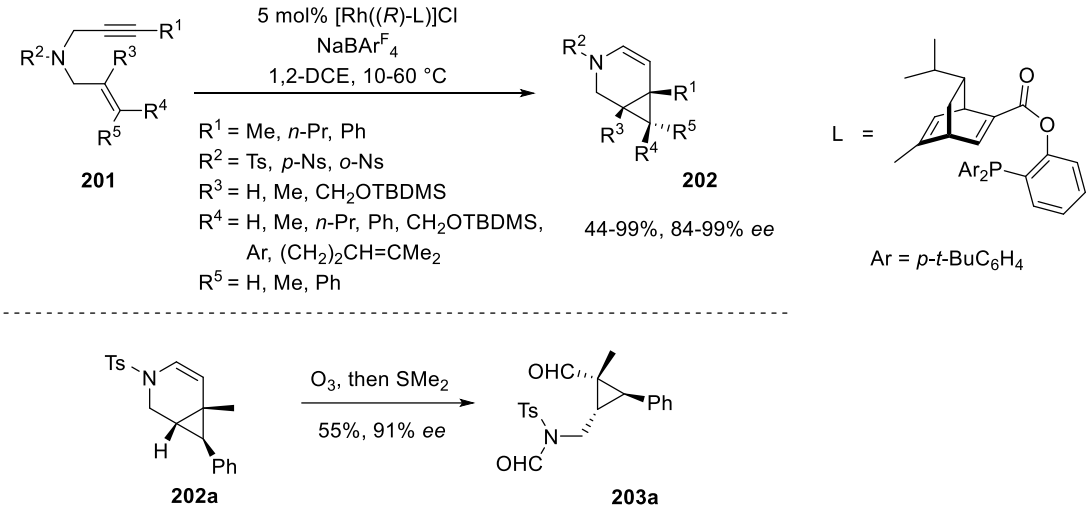

Scheme 4.18

Hayashi *et al*. extended their idea of utilising chiral diene ligands to promote the rhodium-catalysed cycloisomerisation. 1,6-Ene-ynamides **204** were cyclised by their rhodium-based catalyst to give enantioenriched bicyclic products **205**.[70] The reactions showed good reactivity with excellent levels of

enantiomeric excess. This work also revealed that chiral diene ligands offer much higher reactivity compared with chiral bidentate phosphines, *e.g.* BINAP (Scheme 4.19). In addition, this is the first example of asymmetric ynamide cycloisomerisation.

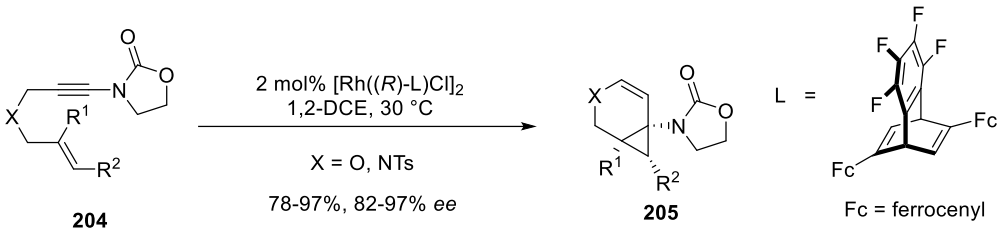

Scheme 4.19

The stereoselectivity of this catalytic reaction is proposed to originate from steric hindrance between the ligand and substrate (Scheme 4.20). The cationic rhodium species is coordinated with the alkyne and a carbonyl oxygen of eneamide to give complex **206**. The preferred conformation of the coordinated ene-ynamide **207**, where the *N*-tosyl group is placed at a less hindered site, was adopted. The more steric conformation is illustrated as **208**. Complex **207** then proceeded *via* 6-*endo-dig* cyclisation to give rhodium-carbenoid **209**, leading to product **205a**.

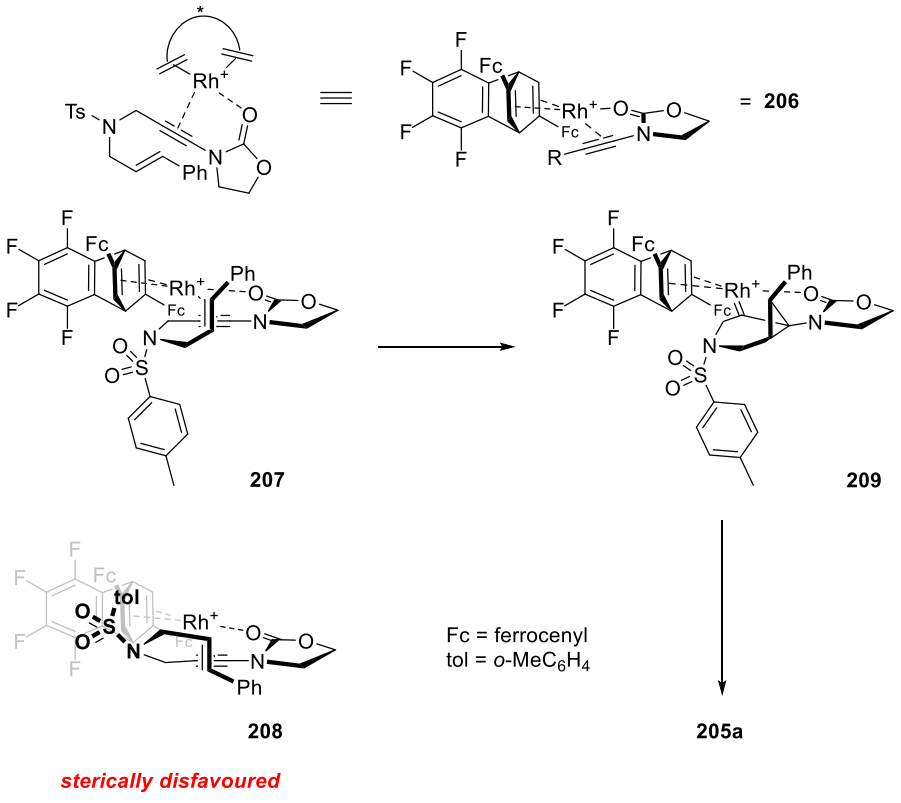

Scheme 4.20

Tanaka and co-workers demonstrated that a rhodium catalyst with chiral bidentate phosphine ligands could cycloisomerise 1,6-enynes **210** in presence of benzoic acid to give bicyclo[3.1.0]hexanes **211** (Scheme 4.21)[71]

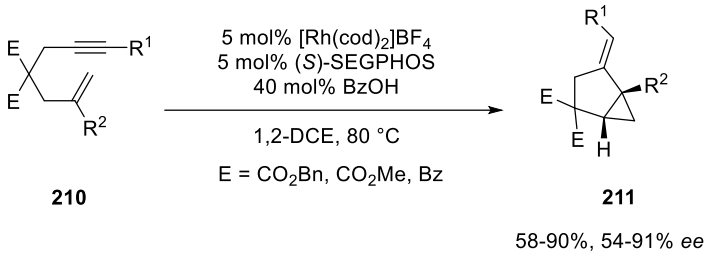

Scheme 4.21

A mechanistic study with deuterium labelling suggested that this reaction proceeds *via* a rhodacycle mediated mechanism (Scheme 4.22), because the reaction of deuterated enyne d_2-**212** possessing a dideuterated allylic methylene group furnished monodeuterated product d_1-**211a**.

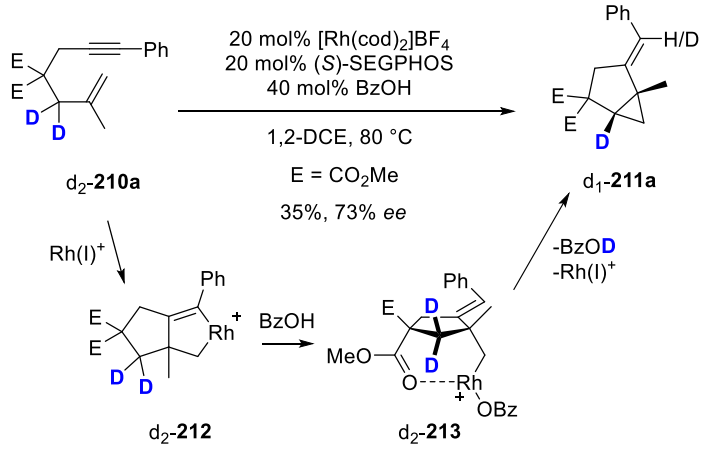

Scheme 4.22

The products from this rhodium-catalysed reaction can undergo acid-promoted lactonisation on treatment with TsOH to give bicyclic lactones **214** (Scheme 4.23). The mechanism of lactonisation with TsOH is illustrated in Scheme 4.23, and initiates with alkene protonation, which promotes cyclopropane ring opening.

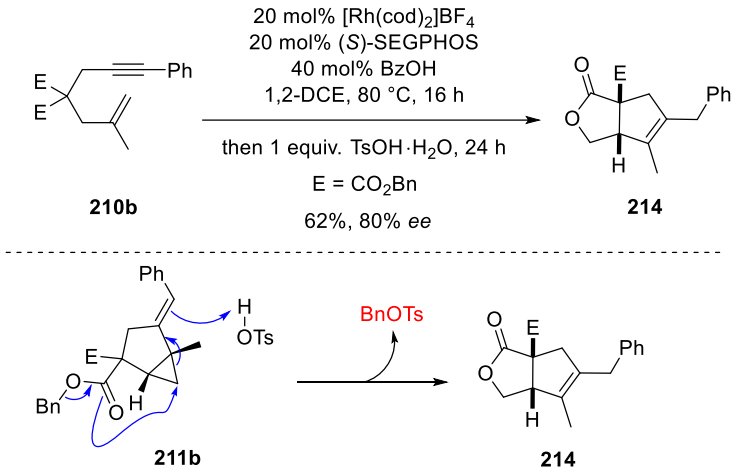

Scheme 4.23

Recently, the Zhang group reported the first asymmetric cycloisomerisation of (*E*)-1,6 enynes (Scheme 4.24).[72] It was found that common chiral diphosphine ligands, such as BINAP, SEGPHOS, or BIPHEP, were unreactive towards the cyclisation of (*E*)-substrates. However, when DuanPhos or TangPhos was used with $[Rh(cod)Cl]_2$, cycloisomerisation of (*E*)-1,6 enynes **215** could proceed to give enantoenriched pyrrolidines **216**. Computational studies suggested that DuanPhos and TangPhos give positive results in cyclising (*E*)-enynes, because such ligands lead to lower energy of activations throughout the catalysis, compared to common ligands, like BINAP.

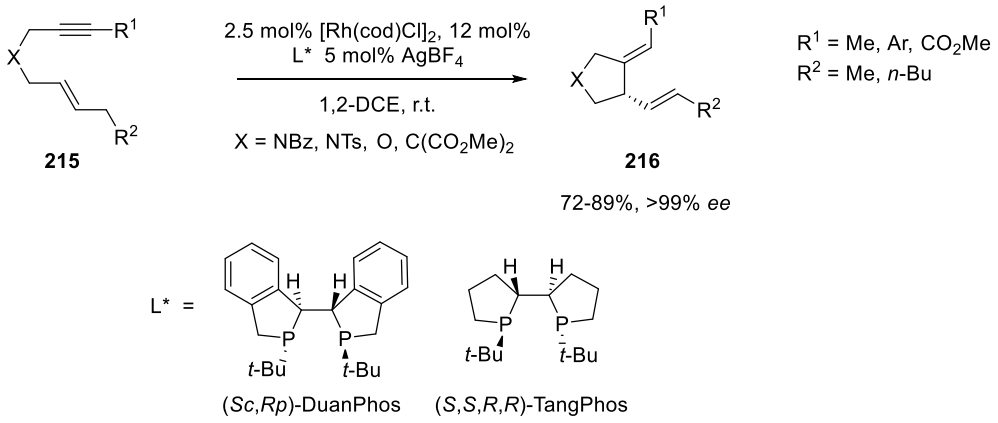

Scheme 4.24

4.3 Other Related Metal-Catalysed Processes

Although palladium and rhodium based catalyst systems can effect cycloisomerisations in excellent yields and enantiomeric excess, some other metals (*e.g.* platinum, iridium, gold) also show good cycloisomerisation reactivity and stereochemical induction.

In 2004, Genêt *et al.* reported that chiral monodentate phosphine ((*R*)-**218**) with platinum(II) chloride could promote the asymmetric alkoxycarbocyclisation (cycloisomerisation in presence of external nucleophile) of enyne **217** to give enantioenriched chiral carbocycle **219** (Scheme 4.25).[73] The results were satisfying (94% yield and 85% *ee*).

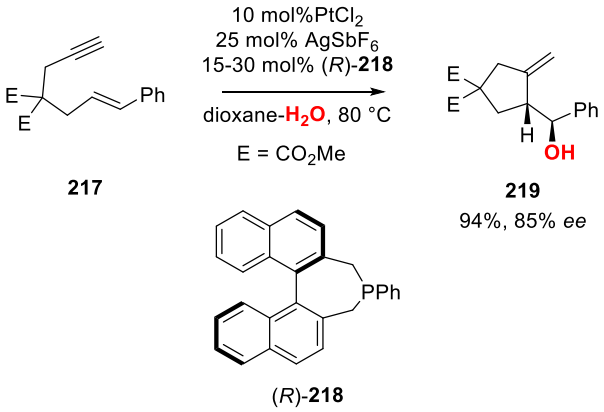

Scheme 4.25

The Echavarren group demonstrated the first enantioselective gold-catalysed alkoxycarbocyclisation. In this work, enyne **220** in methanol (external nucleophile) was cyclised with a combination of AuCl and (*R*)-tol-BINAP in 2:1 ratio to afford cyclic product **221**.[74] The yield was moderate, but the enantioenrichment of the product was excellent (Scheme 4.26).

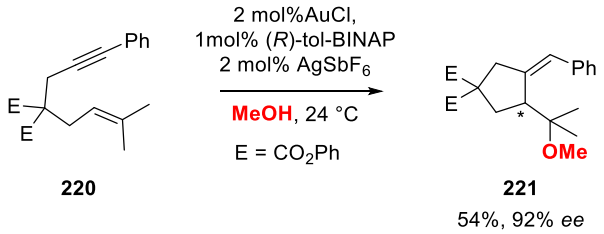

Scheme 4.26

In the same year, the first example of asymmetric iridium-catalysed cycloisomerisation of 1,6-enyne was reported. Azabicyclo[4.1.0]hetenes **223** were made from the cycloisomerisation of nitrogen

tethered enynes **222** with the iridium-chiral diphosphine complex, generated from mixing $[Ir(cod)Cl]_2$ and tol-BINAP in presence of AgOTf under a carbon monoxide atmosphere. (Scheme 4.27).[75]

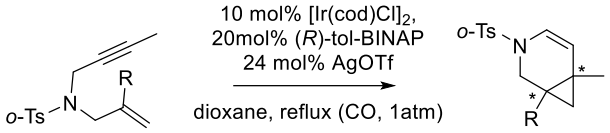

222 **223**

up to 71%, up to 74% *ee*

Scheme 4.27

4.4 Conclusions

During the past decades, there have been marvellous advances in the area of metal-catalysed enantioselective cycloisomerisations. A vast variety of compounds can now be readily cyclised to afford chiral products with high enantiopurity. At present, the power of such methodologies has yet to be widely explore in organic synthesis, as asymmetric cycloisomerisations are occasionally used as critical steps in natural product or complex target syntheses.[76] It is unarguable that such great impacts and applications produced of these cyclisation processes would not reverberate without these pioneering developments.

Chapter 5: Asymmetric Rhodium-Catalysed Cycloisomerisation of Enynamides

In the previous chapter, palladium and rhodium catalyst systems were shown to provide good reactivity and high levels of enantioselectivity in the cycloisomerisations of enynes. In this chapter, we report our investigations to effect asymmetric enynamide cycloisomerisations using palladium and rhodium catalysts.

5.1 Preliminary Study on Asymmetric Cycloisomerisation of Enynamides

5.1.1 Test substrate synthesis

Ynamide (Z)-**151a** was chosen as the test substrate for our investigations. It was readily prepared from the commercially available alcohol (*Z*)-**224** by Mitsunobu reaction with BocNHTs, followed by Boc-deprotection to afford sulfonamide (*Z*)-**153**, and finally coupling with bromoalkyne **98a** to give ynamide (Z)-**151a** in excellent yield (Scheme 5.1).[41]

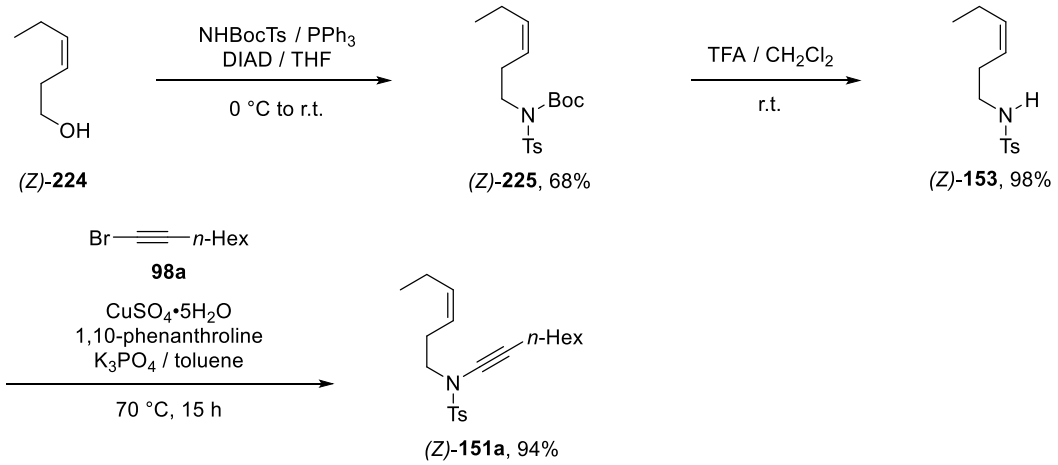

Scheme 5.1

5.1.2 Palladium Catalysis

Inspired by the work from the Trost group (*see* Chapter 4),[14] we attempted to use the system of $Pd_2dba_3{\cdot}CHCl_3$ / PPh_3 in combination with a chiral acid (Table 5.1, Entries 1 and 2). Poor conversions of substrate (*Z*)-**151a** to give 1,4-diene products **153a** were observed (32%) with 85:15 *E*/*Z* ratio. In addition, the ratio between 1,4- and 1,3-dienes (**153a** and **152a**) was found to be 87:13. We next investigated the ability of a variety of chiral ligands to provide stereoselectivity in the reaction using a combination of $Pd_2dba_3{\cdot}CHCl_3$ and chiral ligand with AcOH (Entries 3–7), once again poor cycloisomerisation yields were obtained with 1,4-dienes **153a** as major products. The *E*/*Z* ratio of product **153a** was consistently between 85:15 and 90:10, but disappointingly, all attempts failed to afford any enantioselectivity.

Table 5.1 Catalyst system screening (based on Trost's conditions) for asymmetric enynamide cycloisomerisation.

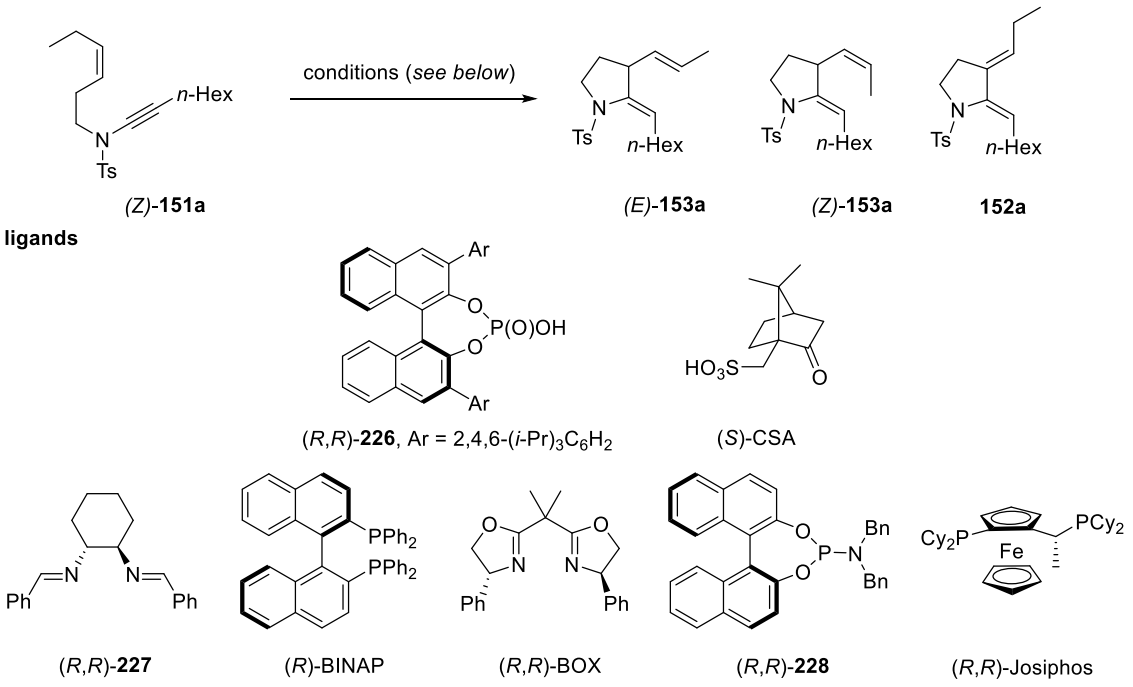

Entry	Catalyst system (mol%)	Solvent	T / °C	(*E*)-**153a**:(*Z*)-**153a**:**152a**[a]	Yield[b] / %
1	$Pd_2dba_3{\cdot}CHCl_3$ (5) / (*R*,*R*)-**226** (120) / PPh_3 (12)	C_6H_6	r.t. to 60	74:13:13	32
2	$Pd_2dba_3{\cdot}CHCl_3$ (5) / (*S*)-CSA (120) / PPh_3 (12)	C_6H_6	r.t. to 60	69:13:18	12
3	$Pd_2dba_3{\cdot}CHCl_3$ (5) / AcOH (110) / (*R*,*R*)-**227** (12)	PhMe	60	77:14:10	24
4	$Pd_2dba_3{\cdot}CHCl_3$ (5) / AcOH (110) / (*R*)-BINAP (12)	PhMe	60	76:17:7	27
5	$Pd_2dba_3{\cdot}CHCl_3$ (5) / AcOH (110) / (*R*,*R*)-BOX (12)	PhMe	60	79:9:12	24
6	$Pd_2dba_3{\cdot}CHCl_3$ (5) / AcOH (110) / (*R*,*R*)-**228** (12)	PhMe	60	n/a	2[c]
7	$Pd_2dba_3{\cdot}CHCl_3$ (5) / AcOH (110) / (*R*,*R*)-Josiphos (12)	PhMe	60	71:15:14	18

[a] Determined by ^{1}H NMR spectroscopy; [b] Isolated yield; [c] NMR yield; n/a = not applicable.

According to Mikami's work,[17] $Pd(OCOCF_3)_2$ or $[Pd(MeCN)_4](BF_4)_2$ / AcOH with chiral ligands are reported as good conditions for asymmetric cycloisomerisation of enynes. Taking (*Z*)-**151a** with $Pd(OCOCF_3)_2$ failed to yield any cycloisomerisation, however, $[Pd(MeCN)_4](BF_4)_2$ / AcOH was found to be effective with **153a**/**152a** isolated in a combined 70% yield (Table 5.2, Entries 1 and 2). Interestingly, the absence of AcOH resulted in an increased yield whilst maintaining isomer ratios. In both cases, though, (*R*)-BINAP did not induce enantioselectivity in the reaction (Entry 3). When the chiral ligand was changed to (*R*,*R*)-BOX or chiral imine (*R*,*R*)-**227** (Entries 4 and 5), yields dropped slightly to 55–65 %; but the product ratio between 1,4-dienes **153a** and 1,3-diene **152a** (~90:10) was better than that of (*R*)-BINAP (72:28). Combinations of $Pd(OAc)_2$ with chiral bidentate phosphine ligand provided moderate to good cycloisomerisation yields. To our surprise, when the ligand was (*R*)-BINAP or (*R*)-SEGPHOS (Entries 6 and 7), 1,3-diene **152a** was formed preferably with 94:6 and 92:8

1,3-:1,4-product ratios, respectively. Once palladium complexes **229** and **230** prepared according to the procedure reported by Buchwald *et al*.[77] were used with AcOH (Entries 9 and 10), cycloisomerisation underwent with decent yields and regioselectivities: ~90:10 (1,4-:1,3-diene ratios) and ~85:15 *E*/*Z* ratios for 1,4-diene products. On the contrary, $PdCl_2$ and either (*R*)-BINAP or (*R*)-SEGPHOS together with $AgSbF_6$ were found to be inactive towards the cycloisomerisation (Entries 11 and 12). None of the catalyst systems gave detectable enantiomeric excess.

Table 5.2 Further Pd-based catalyst screening

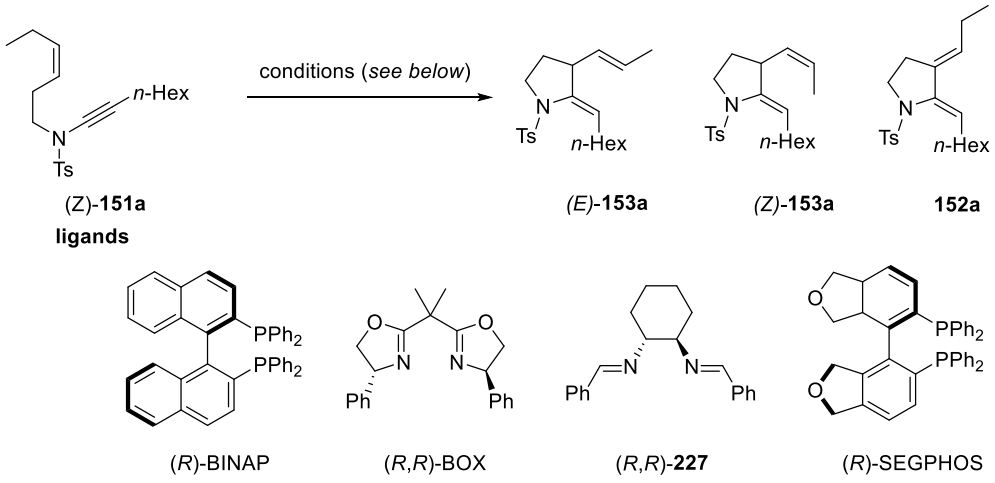

Entry	Catalyst sytem (mol%)	Solvent	T / °C	(*E*)-**153a**:(*Z*)-**153a**:**152a**[a]	Yield[b] / %
1	$Pd(OCOCF_3)_2$ (10) / (*R*)-BINAP (12)	C_6H_6	80	n/a	n.r
2	$[Pd(MeCN)_4](BF_4)_2$ (10) / AcOH (110) / (*R*)-BINAP (12)	DMSO	100	58:14:28	70
3	$[Pd(MeCN)_4](BF_4)_2$ (10) / (*R*)-BINAP (12)	DMSO	100	58:14:28	85
4	$[Pd(MeCN)_4](BF_4)_2$ (10) / AcOH (110) / (*R*,*R*)-BOX (12)	DMSO	100	72:18:10	65
5	$[Pd(MeCN)_4](BF_4)_2$ (10) / (*R*,*R*)-**227** (12)	DMSO	100	69:18:13	55
6	$Pd(OAc)_2$ (10) / (*R*)-BINAP (12)	PhMe	60	5:1:94	67
7	$Pd(OAc)_2$ (10) / (*R*)-SEGPHOS (12)	PhMe	60	7:1:92	89
8	$Pd(OAc)_2$ (10) / (*R*,*R*)-**227** (12)	PhMe	60	75:13:12	90
9	$Pd(OAc)_2$ (10) / (*R*,*R*)-BOX (12)	PhMe	60	76:15:9	71
10	[Pd(*R*)-BINAP](dba) **229** (10) / AcOH (110)	PhMe	r.t. to 60	78:15:7	70
11	[Pd(*R*)-SEGPHOS](dba) **230** (10) / AcOH (110)	PhMe	r.t. to 60	77:13:10	90
12	$PdCl_2$ (10) / (*R*)-BINAP (12) / $AgSbF_6$ (20)	MeCN	40	n/a	n.r.
12	$PdCl_2$ (10) / (*R*)-SEGPHOS (12) / $AgSbF_6$ (20)	MeCN	40	n/a	n.r.

[a] Determined by ^1H NMR spectroscopy; [b] Isolated yield; n/a = not applicable; n.r. = no reaction.

During the course of these studies, we envisaged a Heck-type reaction on (*E*)-α-haloenamides to perform a cyclisation giving cyclic enamides as products (Scheme 5.2).

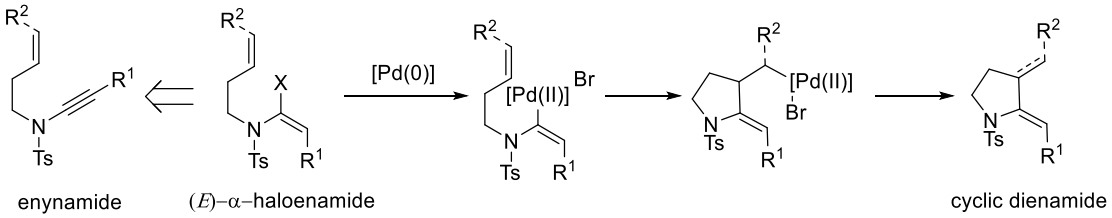

Scheme 5.2

It is worth noting that only (*E*)-isomer of α-haloenamides work for the cyclisation to take place. It is difficult for the (*Z*)-isomer to undergo such a cyclisation, because the carbopalladation step of this isomer is sterically disfavoured (Scheme 5.3).

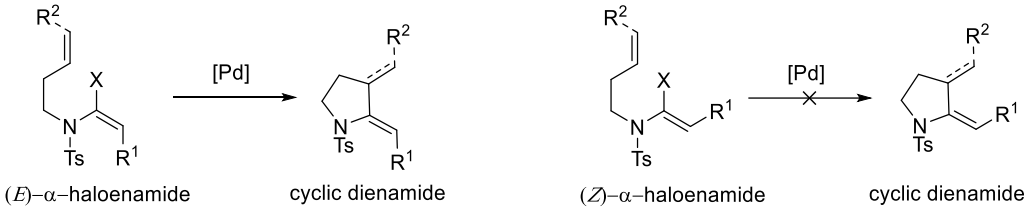

Scheme 5.3

We began the study with making (*E*)-α-haloenamides from our ynamides (Table 5.3). Using Hsung's method of preparing (*E*)-α-haloenamides,[76] the reaction was highly stereoselective, but required overnight stirring at 55 °C (Entries 1–3). In 2013, Iwasawa *et al*. demonstrated the regio- and stereospecific synthesis of (*E*)-α-haloenamide from ynamides in the presence of halotrimethylsilane (TMSX, where X is halide) and H_2O.[77] The procedure relies on the *in situ* generation of hydrogen halide from TMSX. Using this method, (*E*)-α-haloenamides were prepared as the sole product from the parent ynamides in quantitative yields within 1 h (Entries 4–7). It was found that iodoenamides were prone to be more reactive towards moisture in air, compared to bromoenamides, which could be because iodine is a better leaving group than bromide.

Table 5.3 Preparations of (*E*)-α-haloenamides from enynamides

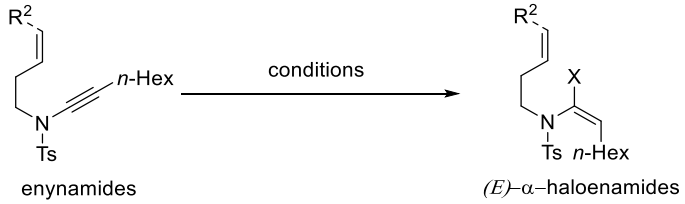

enynamides **92 / 151** — *(E)*–α–haloenamides **231**

Entry	Substrate, R^1	Conditions[a]	time / h	Yield[b] / %	*E*/*Z* ratio[c]
1	(*Z*)-**151a**, (*Z*)-Et	$MgBr_2 \cdot 6H_2O$ (2 equiv.) /55 °C	12	89	95:5
2	(*E*)-**151a**, (*E*)-Et	$MgBr_2 \cdot 6H_2O$ (2 equiv.) /55 °C	12	87	95:5
3	**92**, H	$MgBr_2 \cdot 6H_2O$ (2 equiv.) /55 °C	15	80	95:5
4	(*Z*)-**151a**, (*Z*)-Et	TMSX, X = Br (2 equiv.) / -78 °C *then* H_2O (20 equiv.) / 0 °C to r.t.	1	>98	100:0
5	(*E*)-**151a**, (*E*)-Et	TMSX, X = Br (2 equiv.) / -78 °C *then* H_2O (20 equiv.) / 0 °C to r.t.	1	>98	100:0
6	**92**, H	TMSX, X = Br (2 equiv.) / -78 °C *then* H_2O (20 equiv.) / 0 °C to r.t.	1	>98	100:0
7	**92**, H	TMSX, X = I (2 equiv.) / -78 °C *then* H_2O (20 equiv.) / 0 °C to r.t.	1	>98	100:0

[a] The reactions were conducted in anhydrous CH_2Cl_2; [b] Isolated yield; [c] The *E*/*Z* ratio was determined by ^1H NMR spectroscopy.

With α-haloenamides in hand, asymmetric Heck reactions were performed with the hope to achieve an asymmetric cyclisation of α-haloenamides (Table 5.4). First, the reaction was run under cationic Heck conditions with Ag_2CO_3 as base to accelerate the rate of oxidative addition (Entry 1).[78] This led to moderate reaction yield but promising enantioselectivity (~20% *ee*). When the reaction was carried out under Heck conditions without a silver salt additive, it was clear that the reaction rate was sluggish (Entry 2). Once $Pd(dba)_2$ was used as palladium source, no conversion was detected (Entry 3). Allylpalladiumchloride (APC) dimer with (*R*)-BINAP gave the best reaction yield (80%), as well as good enantiomeric excess of the product (Entry 5). In addition, when enamides **231c** and **231c′**

(monosubstituted olefin) were used as substrate, *endo*-1,3-dieneamide **232** was obtained as minor product. However, when the base was changed from heterogeneous inorganic base (K_2CO_3) to homogeneous organic base (NEt_3), the reaction was failed to proceed. (Entry 6).

Table 5.4 Condition optimisation for Heck cyclisation of α-haloenynamides.

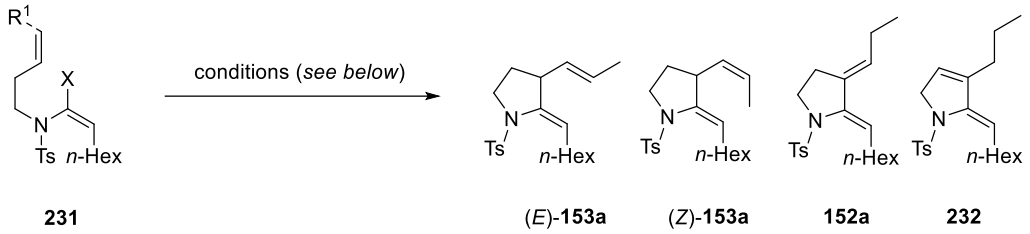

Entry	Substrate, R^1, X	Catalyst system (mol%)[a]	time / h	Yield[b] / %	(*Z*)-**153a**:**152a**:**232**[c]	(*E*)-**153a**: *ee*[d] / %
1	(*Z*)-**231a**, (*Z*)-Et, Br	$Pd(OAc)_2$ (10) / (*R*)-BINAP (15) / Ag_2CO_3 (200)	2	63	56:10:34:0	21
2	**231c′**, H, I	$Pd(OAc)_2$ (10) / (*R*)-BINAP (15) / Ag_2CO_3 (200)	20	60	-:-:81:19	-
3	**231c**, H, Br	$Pd(dba)_2$ (10) / (*R*)-BINAP (15) / Ag_2CO_3 (200)	20	30	n/a	-
4	**231c**, H, Br	APC (5) / (*R*)-BINAP (15) / K_2CO_3 (200)	19	72	-:-:80:20	-
5	(*Z*)-**231a**, (*Z*)-Et, Br	APC (5) / (*R*)-BINAP (15) / K_2CO_3 (200)	18	90	56:12:32:0	80
6	(*Z*)-**231a**, (*Z*)-Et, Br	APC (5) / (*R*)-BINAP (15) / NEt_3 (200)	24	n.r.	n/a	n/a

[a] Run in PhMe at 80 °C; [b] Isolated yield; [c] Determined by ^{1}H NMR spectroscopy; d Enantiomeric excess of (*E*)-**153a**, which determined by chiral HPLC; n.r. = no reaction; n/a = not applicable; APC = allyl palladium chloride dimer.

Unfortunately, attempts to unify the formation of α-haloenamides and the Heck cyclisation to perform ynamide cyclisation in one step were unsuccessful. The key issue arises from the fact that the formation of α-haloenamides from ynamides requires acidic conditions; while the Heck cyclisation must be done under basic conditions, since base is required to regenerate the active palladium(0) catalyst from palladium(II) hydride.

5.1.2 Rhodium Catalysis

As discussed in Chapter 4, many research groups have reported conditions for rhodium-catalysed asymmetric enyne cycloisomerisations.[79] In addition to enyne substrates, our group has developed a rhodium catalyst system for a [5+2] cycloisomerisation of vinyl cyclopropane ynamides.[80] In a preliminary examination, a range of Rh-catalysts were screened with enynamide (*Z*)-**151a**. We began the investigations with Zhang's cationic rhodium catalyst system (Table 5.5, Entry 1).[81] Pleasingly, substrate (*Z*)-**151a** was cyclised to give product in good yield with very high stereoselectivities. Employing the catalytic conditions reported by Nicolaou *et al.* (Entry 2),[82] product (*E*)-**153a** was exclusively afforded in good yield with 95% *ee*. In contrast, the catalyst system developed in our group for the [5+2] enynamide cycloisomerisation gave a mixture of products in low yield (28%) after three days (Entry 3). Although Wilkinson's catalyst has been shown to effect enynamide cycloisomerisation,[83] no conversion was observed with substrate (*Z*)-**151a** (Entry 4).

Table 5.5 Preliminary survey of the rhodium-based catalyst systems for enynamide cycloisomerisation.

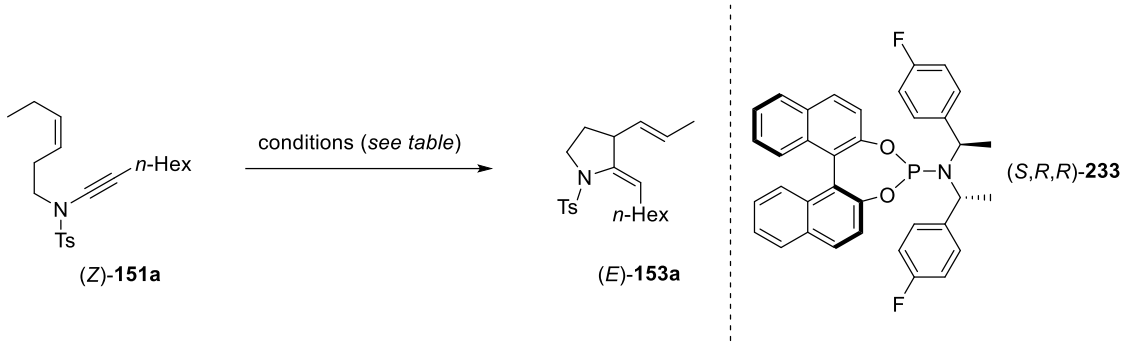

(*Z*)-**151a** (*E*)-**153a** (*S*,*R*,*R*)-**233**

Entry	Catalyst system (mol%)	Time	Yield[a] / %	*ee*[b] / %
1	$[Rh(cod)Cl]_2$ (5) / (*R*)-BINAP (12) / $AgSbF_6$ (10) / 1,2-DCE / r.t.	75 min	85	95
2	[Rh((*R*)-BINAP)][SbF_6] (10) / 1,2-DCE / r.t.	60 min	84	95
3	$[Rh(C_2H_4)_2Cl]_2$ (5) / (*S*,*R*,*R*)-**233** (12) / $NaBAr^F_4$ (12) / r.t. to 40 °C	3 days	~28[c]	n/a
4	$Rh(PPh_3)_3Cl$ (10) / toluene / r.t. to 40 °C	3 h	n.r.	-

[a] Isolated yield; [b] Determined by chiral HPLC; [c] Determined by ^{1}H NMR spectroscopy (unable to be purified by column chromatography); n/a = not applicable; n.r. = no reaction.

5.2 Catalysis System Development

5.2.1 Catalyst System Optimisation

This initial catalyst survey indicated that the Zhang's and Nicolaou's conditions are well-suited for enynamide cycloisomerisation. Whilst the specific conditions reported by Nicolaou *et al*. provided the excellent outcome, we anticipated that tuning of the reaction conditions would be practically difficult to achieve: the catalyst must be prepared freshly each time due to its extreme sensitivity and short life-span. We therefore used Zhang's catalyst system as a starting point to optimise the cycloisomerisation conditions. We began the optimisation by varying the rhodium source in the reaction (Entries 1–3). No significant differences in reaction yields and stereoselectivities were observed. For the further optimisation, $[Rh(cod)Cl]_2$ was then used due to its availability in our lab. Next, we examined the solvent effect on the catalysis. The reaction performed in CH_2Cl_2 gave identical results to the reaction running in 1,2-DCE (Entry 4). During the reaction, CH_2Cl_2 was inclined to evaporate as the reaction

proceeded. When the solvent was chloroform (Entry 5), poor reaction conversion was detected leading to low isolated yield, the enantiomeric excess of the product was not therefore determined. No conversion of starting material to product was observed when toluene was used as solvent (Entry 6). Polar solvents, like DMSO (Entry 7), caused a solubility issue of the salts; as a consequence, the substrate remained intact in a reaction mixture.

During the course of our optimisation, we noticed that silver salts also influenced the outcome of the reaction. When the reaction was conducted without $AgSbF_6$ (Entry 8), the reaction did not proceed to give products. This is likely because the phosphine is unable to break apart the dimer into a monomeric rhodium species (will be discussed later). In presence of 5 mol% $AgSbF_6$ (Entry 9), the reaction required 2 h to reach completion, which was significantly slower than the reaction with 10 mol% $AgSbF_6$. In addition, the level of enantiomeric excess was deteriorated to 89%. With 20 mol% of $AgSbF_6$ (Entry 10), reaction proceeded with the similar rate to the reaction with 10 mol% $AgSbF_6$. Interestingly, product **234** was observed (~10% yield) along with major product **153a**. Once the reaction was loaded with 50 mol% $AgSbF_6$ (Entry 11), the proportion of **234** increased to 20%, and the rate of reaction was significantly retarded. We then questioned if this unexpected product **234** was derived from the isomerisation of product (*E*)-**153a**, whether it was generated from a side pathway. To address this curiosity, the reaction was conducted with the conditions reported in Table 5.6, Entry 1, and allowed to reach completion, then an additional amount of $AgSbF_6$ (10 mol%) was added to the crude reaction mixture, and stirred for another 3 h. The reaction mixture was then examined by ^{1}H NMR spectroscopy. Small amount (~10%) of product isomer **234** was detected. This supports our conclusion that compound **234** results from a subsequent isomerisation of **153a** in the reaction. However, we cannot yet absolutely confirm that the decrease in enantioselectivity is due to the excess amount of $AgSbF_6$. This is because the silver salt might also interrupt the process of asymmetric induction during catalysis. Further studies are required to prove whether the post-isomerisation of the product results in the deterioration of product's enantiopurity. Finally, we altered the additive which facilitates the breakdown of the rhodium dimer (Entries 12 and 13). $NaBAr^F{}_4$ and $AgBF_4$ failed to drive the reaction forward after 3 h. In the latter case, the reaction mixture turned black, but the starting material could be recovered.

Table 5.6 Optimisation of the Rh-catalysed enynamide cycloisomerisation.

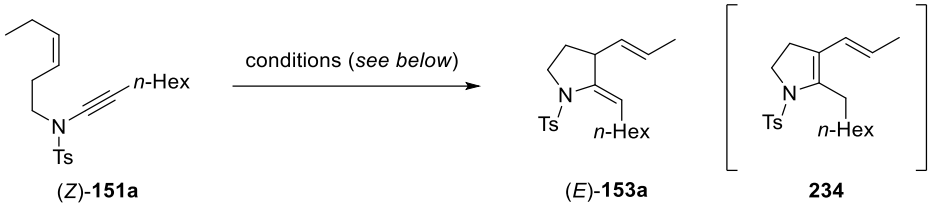

(*Z*)-**151a** (*E*)-**153a** **234**

Entry	Conditions (mol%)[a]	Time	Yield[b] / %	*ee*[c] / %	Note
1	$[Rh(cod)Cl]_2$ (5) / $AgSbF_6$ (10) / 1,2-DCE	75 min	85	95	-
2	$[Rh(C_2H_4)_2Cl]_2$ (5) / $AgSbF_6$ (10) / 1,2-DCE	75 min	84	94	-
3	$[Rh(nbd)Cl]_2$ (5) / $AgSbF_6$ (10) / 1,2-DCE	75 min	84	95	-
4	$[Rh(cod)Cl]_2$ (5) / $AgSbF_6$ (10) / CH_2Cl_2	75 min	85	95	CH_2Cl_2 easily evaporated
5	$[Rh(cod)Cl]_2$ (5) / $AgSbF_6$ (10) / $CHCl_3$	2 h	15	n/a	-
6	$[Rh(cod)Cl]_2$ (5) / $AgSbF_6$ (10) / toluene	60 min	n.r.	n/a	-
7	$[Rh(cod)Cl]_2$ (5) / $AgSbF_6$ (10) / DMSO	3 h	n.r.	n/a	poor solubility of the salts
8	$[Rh(cod)Cl]_2$ (5) / $AgSbF_6$ (0) / 1,2-DCE	2 h	n.r.	n/a	-
9	$[Rh(cod)Cl]_2$ (5) / $AgSbF_6$ (5) / 1,2-DCE	2 h	80	89	-
10	$[Rh(cod)Cl]_2$ (5) / $AgSbF_6$ (20) / 1,2-DCE	75	77	90	product **234** formed, ~10%
11	$[Rh(cod)Cl]_2$ (5) / $AgSbF_6$ (50) / 1,2-DCE	2h	60	90	product **234** formed, ~20%
12	$[Rh(cod)Cl]_2$ (5) / $NaBAr^F{}_4$ (10) / 1,2-DCE	3 h	n.r.	n/a	no precipitation of $AgBAr^F{}_4$
13	$[Rh(cod)Cl]_2$ (5) / $AgBF_4$ (10) / 1,2-DCE	3 h	trace	n/a	reaction turned black after 3 h

[a] With 12 mol% (*R*)-BINAP at room temperature; [b] Isolated yield; [c] Determined by chiral HPLC; n.r. = no reaction; n/a = not applicable.

With these initially optimised conditions in hand (Table 5.7, Entry 1), various chiral ligands were screened to obtain the best enantioselectivity from the reaction. It was found that (*R*)-tol-BINAP also facilitated an asymmetric cycloisomerisation to give sole product (*E*)-**153a** in good yield and *ee* (Entry 2). However, the reaction took more than 3.5 h to get to obtain full conversion. When the ligand was (*R*)-SEGPHOS, product (*E*)-**153a** was obtained in excellent yield and enantioselectivity within 5 min. Interestingly, a ligand with a similar structure, (*R*)-SYNPHOS, gave comparable level of enantiomeric excess in the product (Entry 4), but the reaction required longer time to finish (35 min) and the yield is less than the reaction with (*R*)-SEGPHOS. Moving from chiral binapthyl core to biphenyl core ligands (Entries 5-7), overall reactions were more rapid, with higher yields and enantioselectivities. We found that by far (*R*)-Cl-OMe-BIPHEP and (*R*)-OMe-BIPHEP provided the best results. The reaction was also attempted with (*S*,*S*)-Me-DuPhos (Entry 8) and (*S*)-BINAPINE (Entry 9). Unfortunately, no cycloisomerisations were observed; however, starting material could be fully recovered from both conditions. Next, we tried to adjust the temperature of the reaction to see whether even better results could be achieved. Lowering the temperature did not affect the reaction yield and product's enantiopurity, but the reaction time was slightly prolonged (Entries 10 and 11). In contrast, raising the temperature to 45 °C (Entry 12), the reaction underwent to completion instantaneously, but the enantiomeric excess of the product slightly diminished.

Table 5.7 Ligand and temperature optimisations.

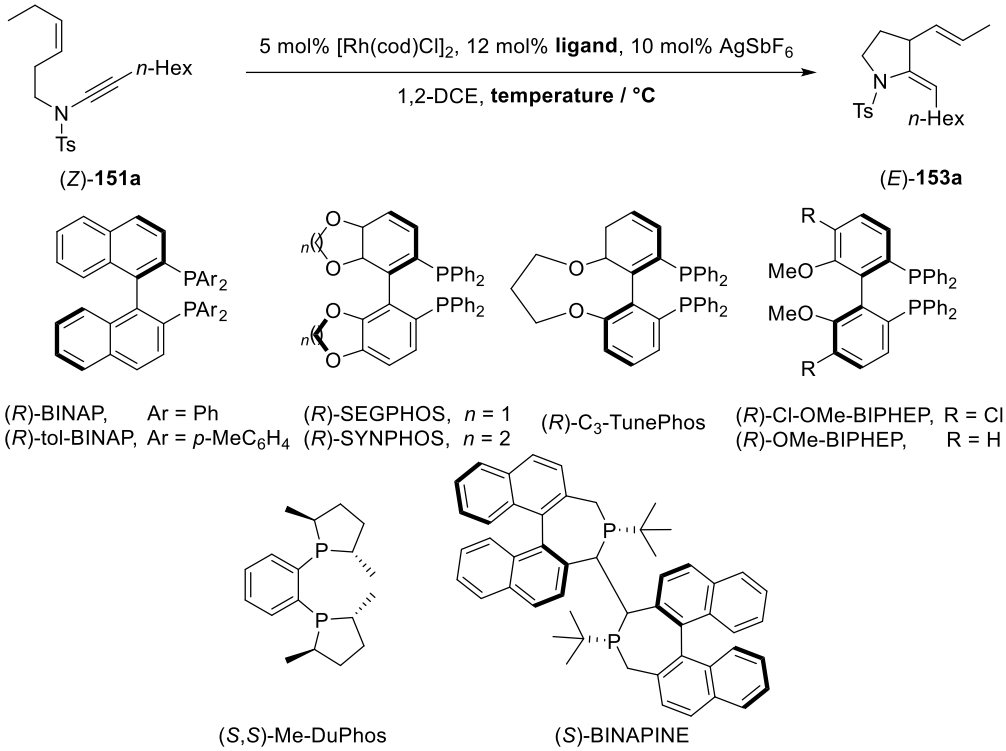

Entry	Ligand / temperature	Time	Yield[a] / %	*ee*[b] / %
1	(*R*)-BINAP / r.t.	75 min	85	95
2	(*R*)-tol-BINAP / r.t.	> 3.5 h	85	93
3	(*R*)-SEGPHOS / r.t.	5 min	96	95
4	(*R*)-SYNPHOS / r.t.	35 min	83	94
5	(*R*)-C_3-TunePhos / r.t.	15 min	94	96
6	(*R*)-Cl-OMe-BIPHEP / r.t.	<5 min	98	97
7	(*R*)-OMe-BIPHEP / r.t.	<5 min	98	97
8	(*S*,*S*)-Me-DuPhos / r.t.	10 h	n.r.	n/a
9	(*S*)-BINAPINE / r.t.	10 h	n.r.	n/a
10	(*R*)-Cl-OMe-BIPHEP / 0 °C	5 min	98	97
11	(*R*)-Cl-OMe-BIPHEP / –10 °C	10 min	98	97
12	(*R*)-Cl-OMe-BIPHEP / 45 °C	<1min	97	93

[b] Isolated yield; [c] Determined by chiral HPLC.

5.2.2 The 2nd Generation Catalyst System

The catalyst system used for the optimisation must be prepared and handled under an inert atmosphere such as nitrogen or argon (not as sensitive as Nicolaou's system). This is due to the fact that the metal centre is exposed to oxidising or nucleophilic species, *e.g.* oxygen, water, during the preparation of catalyst solution. First, the rhodium dimer **235** precursor breaks down in presence of $AgSbF_6$ to give monomeric cationic rhodium species **236** (Scheme 5.4). This process is rapid and thermodynamically driven by the precipitation of AgCl. Rhodium species **236** is reactive, as the rhodium centre has two labile coordinating sites, which can allow ligand exchange to take place. In the next step, a chiral diphosphine ligand was introduced to the reaction mixture, followed by hydrogenation to facilitate the decomplexation of cyclooctadiene from the rhodium species. This allows the bidentate phosphine ligand to chelate to the metal centre, giving the rhodium-phosphine complex **237**. This complex is likely an active catalyst to react with the enynamide substrate.[84] The reactive cationic rhodium species **236** and **237** formed during these steps can readily react with unwanted nucleophilic species, if the reaction environment is not carefully controlled to be free of air and/or moisture.

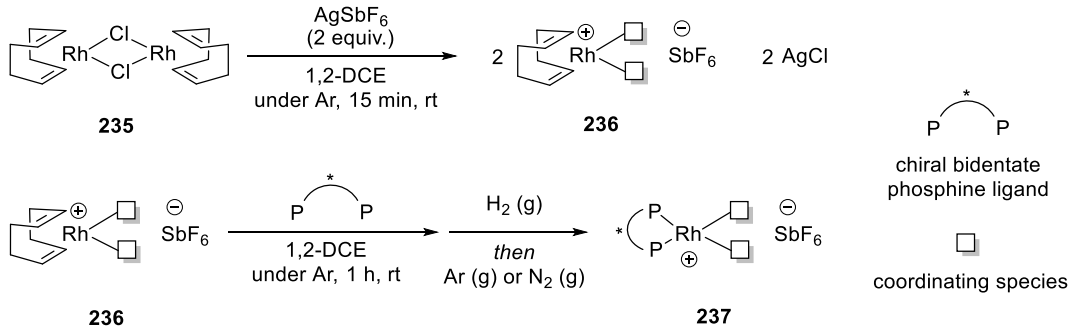

Scheme 5.4

To circumvent this procedural issue, we envisaged the preparation of a bench-stable precursor, such as **239**, for use in these reactions. Various complexes **239** could be prepared from **238**, itself commercially available but more conveniently prepared from **235** by treatment with $AgSbF_6$ and cyclooctadiene. Rhodium complex **238** was submitted to a solution of chiral diphosphine ligand in CH_2Cl_2. One of the cyclooctadienes is substituted by the phosphine ligand, giving a bench stable rhodium complex **239**.

This perhaps results from the fact that the rhodium centre is bound to both cyclooctadiene and bidentate phosphine, protecting the metal from reacting with external nucleophiles.

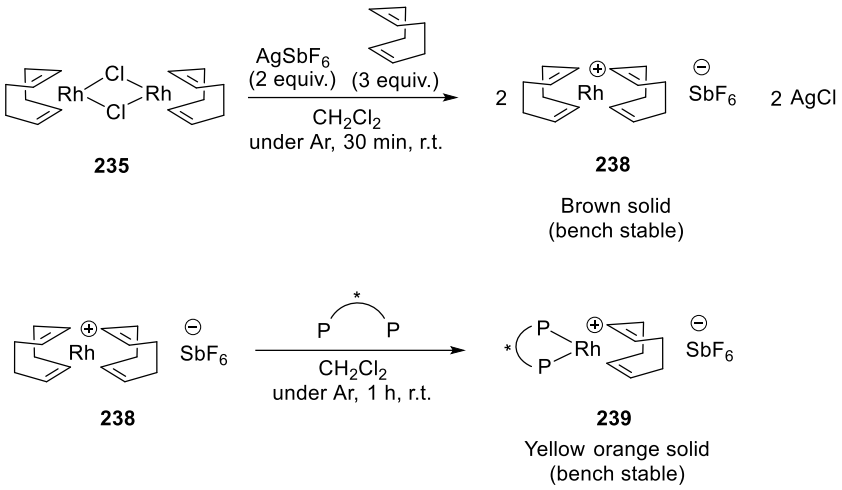

Scheme 5.5

The structure and absolute configuration of complex **239a** was determined by single crystal X-ray analysis (Figure 5.1).

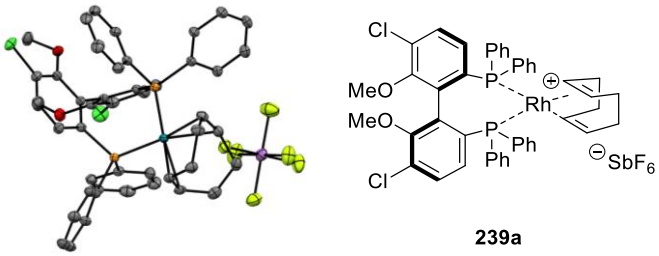

Figure 5.1 Solid state structure of **239a**. Displacement ellipsoid plots are shown at 50% probability. (hydrogen atoms have been omitted for clarity).[1]

With this new pre-catalyst in hand, we set up experiments to compare the performance of this new rhodium complex with the typical catalyst systems (Table 5.8). Gratifyingly, the new pre-catalyst showed that the reactivity and degree of asymmetric induction were comparable to Zhang's and Nicolaou's type systems (Entries 1–3). In addition, we discovered that the catalyst loading could be decreased to 5 mol% with respect to rhodium, and still maintained reactivity and selectivity (Entry 4). However, when we pushed the system further to 2.5 mol% catalyst loading, a clear drop in reaction rate

[1] The X-ray data were collected and processed by Steven J. Mansfield.

was observed as well as the level of enantiomeric excess (Entry 5). This could either result from the fact that the active catalyst is more vulnerable to air and/or moisture as its amount in the reaction mixture decreases, or the catalyst degradation is more pronounced at smaller scale.

Table 5.8 Comparison between the new catalyst system and conventional systems.

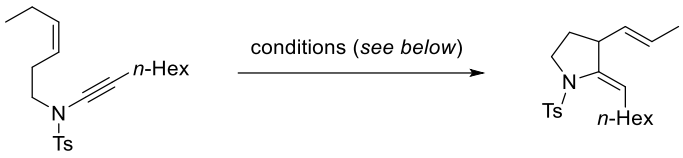

(*Z*)-**151a** (*E*)-**153a**

Entry	Catalyst system (mol%)	Time	Yield[a] / %	*ee*[b] %
1	[Rh((*R*)-Cl-OMe-BIPHEP)(cod)]SbF_6 (10) then H_2 (balloon) for 10 min, followed by N_2 (balloon) for 10 min / 1,2-DCE / r.t.	<5 min	>99	97
2	[Rh(cod)Cl]$_2$ (5) / (*R*)-Cl-OMe-BIPHEP (12) / $AgSbF_6$ (10) / 1,2-DCE / r.t.	<5 min	98	97
3	[Rh((*R*)-Cl-OMe-BIPHEP)]SbF_6 (10) / 1,2-DCE / r.t.	5 min	95	96
4	[Rh((*R*)-Cl-OMe-BIPHEP)(cod)]SbF_6 (5) then H_2 (balloon) for 10 min, followed by N_2 (balloon) for 10 min / 1,2-DCE / r.t.	7 min	>99	97
5	[Rh((*R*)-Cl-OMe-BIPHEP)(cod)]SbF_6 (2.5) then H_2 (balloon) for 10 min, followed by N_2 (balloon) for 10 min / 1,2-DCE / r.t.	25 min	96	91

[a] Isolated yield; [b] Determined by chiral HPLC.

Since this new pre-catalyst requires hydrogenation to activate itself, one could argue that the active catalyst is perhaps in the form of rhodium hydride complex, instead of the cationic rhodium species. To prove this is not the case, hydrogenation of rhodium complex **239a** was conducted and characterised by $^{31}P\{^1H\}$ NMR spectroscopy. It was found that no rhodium hydride species was formed in detectable amounts after hydrogenation (Figure 5.2). Instead, the signals of a rhodium dimer **240** were detected (two signals of double of doublets at 40.9 and 45.2 ppm).

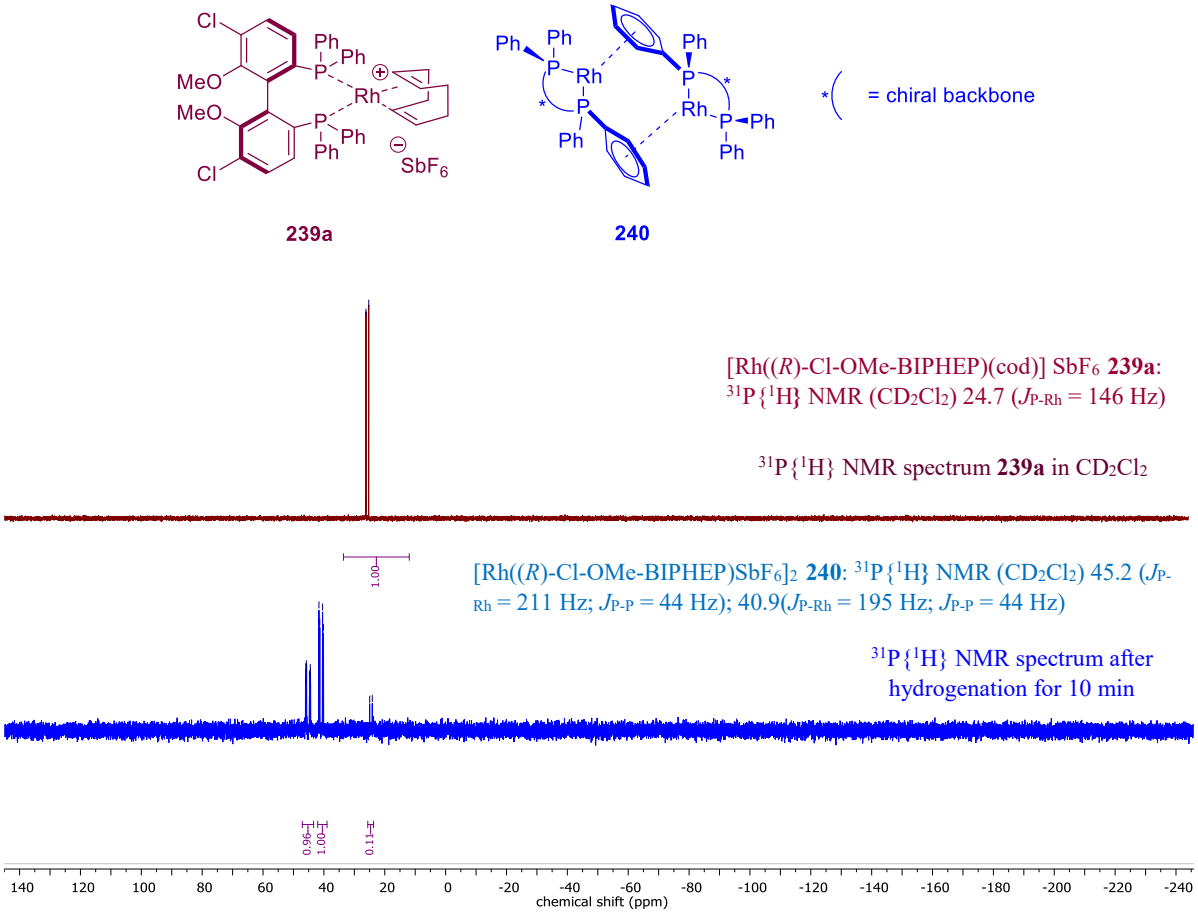

Figure 5.2 $^{31}P\{^{1}H\}$ NMR spectra of complex **239a** in CD_2Cl_2 (maroon) and the solution after 10 min of hydrogenation (blue).

In addition, Imamoto *et al*. have conducted in-depth studies on the mechanism of asymmetric hydrogenation with rhodium complex **241** as pre-catalyst (Scheme 5.6).[85] They discovered that even though rhodium hydride species **243a** and **243b** are in equilibrium with a solvate rhodium complex **242** under a hydrogen atmosphere, to form a fair amount of such hydride species very low temperature (–90 °C) was required (sometimes high pressure of hydrogen is also needed) to facilitate oxidative addition of dihydrogen (H_2). Imamoto *et al*. also suggested that bubbling Ar or N_2 through the reaction mixture after hydrogenation could prevent the formation of rhodium hydrides **243**. This agrees with Le Chatelier's principle – removal of H_2 shifts the equilibrium towards **242**.

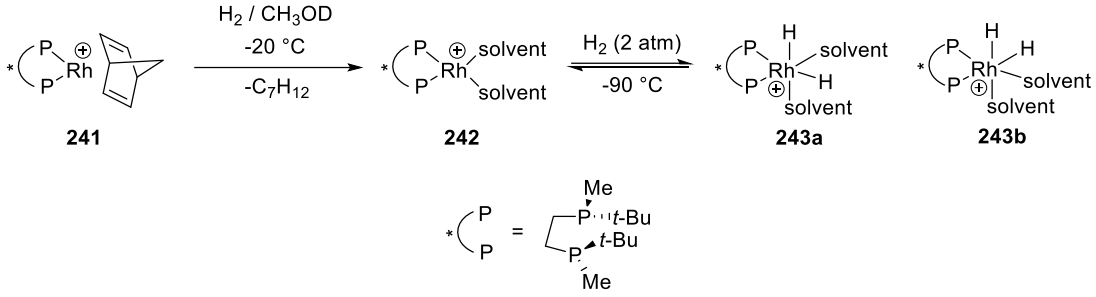

Scheme 5.6

Furthermore, Heller *et al*. showed that hydrogenation of rhodium-BINAP-diolefin complex **244** at –20 °C or room temperature could facilitate the formation of a solvate cationic rhodium complex **245** and its dimeric form **246**, depending on the solvent used in the reaction (Scheme 5.7); and no sign of rhodium hydride species was observed. [86]

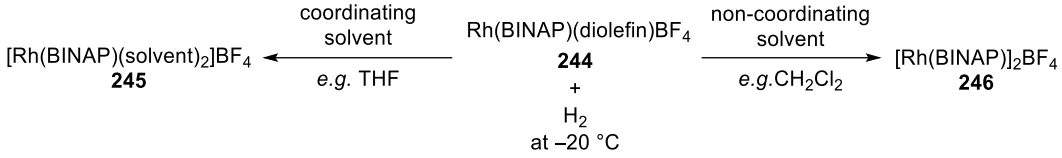

Scheme 5.7

Overall, the experimental evidence we have collected, alongside the observations reported in the literatures, support the involvement of a cationic rhodium species, possibly **247** or **248** (Scheme 5.8), to catalyse the asymmetric enynamide cycloisomerisation. First, the pre-catalyst **239** was activated by hydrogenation leading to an equilibrium between a solvate species **247** and a rhodium dimer **248**; the ratio between these two species is depending on solvent. If the solvent is capable of binding to the rhodium centre (*e.g.* THF), intermediate **247** is produced preferably. If the solvent is a non-coordinating solvent (*e.g.* CH_2Cl_2 or 1,2-DCE), rhodium species **248** is majorly formed. Once the substrate (*e.g.* (*Z*)-**151a**) was introduced to the reaction mixture, ligand exchange can take place at the rhodium centre, as a result, intermediate **249** is formed. This species can undergo oxidative addition to generate rhodacycle **250**, which proceeds *via* β-hydride elimination to give rhodium hydride **251**. The product (*E*)-**153a** is formed by reductive elimination of species **251**, and the active catalyst **247** is regenerated.

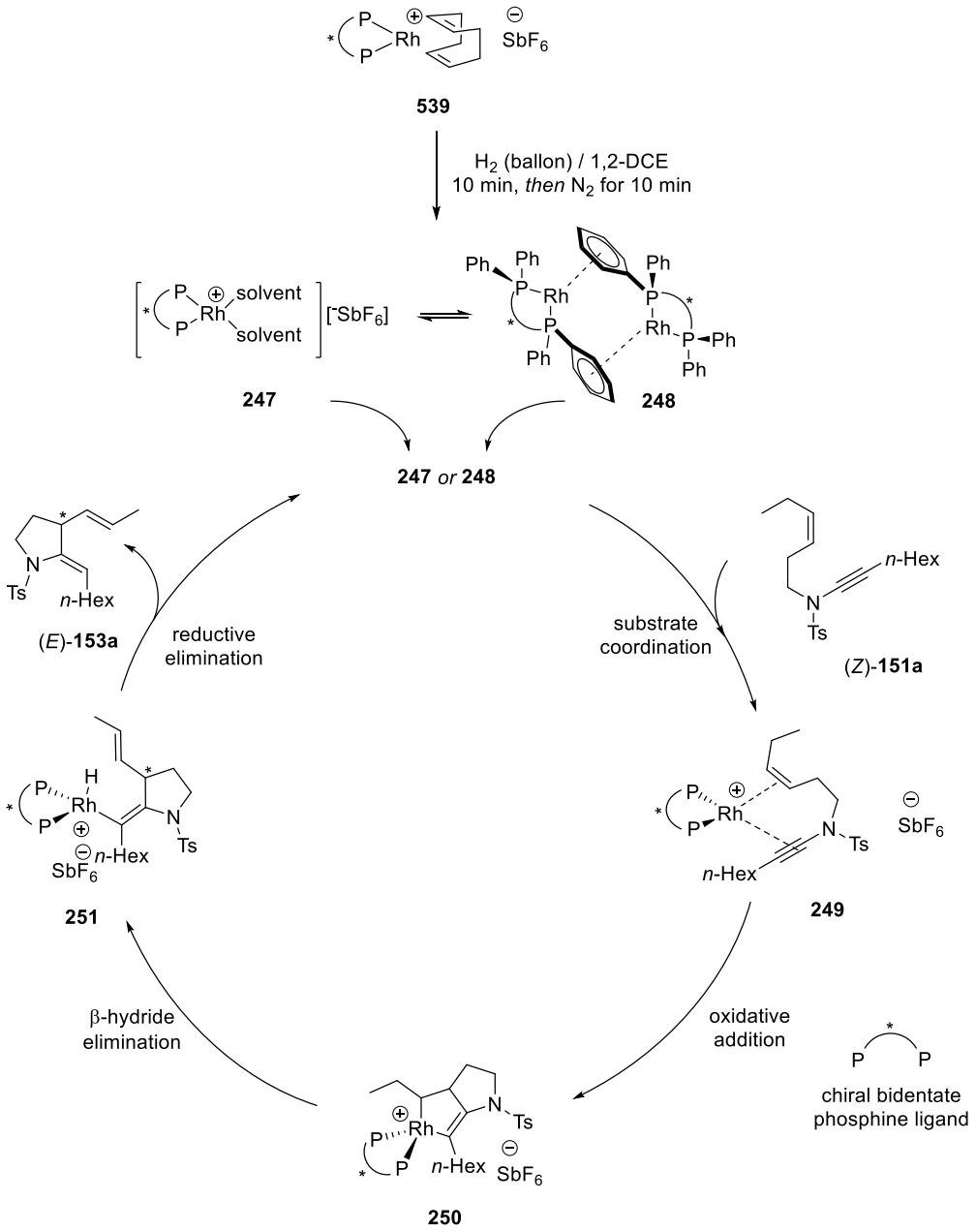

Scheme 5.8

5.3 Scope of the Asymmetric Rhodium-Catalysed Cycloisomerisation

5.3.1 Substrate Synthesis

A range of enynamides were prepared in order to examine the substrate scope and limitations of the rhodium catalyst system. The substrates were classified into three categories: disubstituted alkenyl ynamides, trisubstituted alkenyl ynamides, and cycloalkenyl ynamides.

Disubstituted Alkenyl Ynamides

By analogy to the formation of ynamide (*Z*)-**151a** from alcohol **224** (Scheme 5.1), a range of ynamides **151b-d** were prepared (Scheme 5.9).

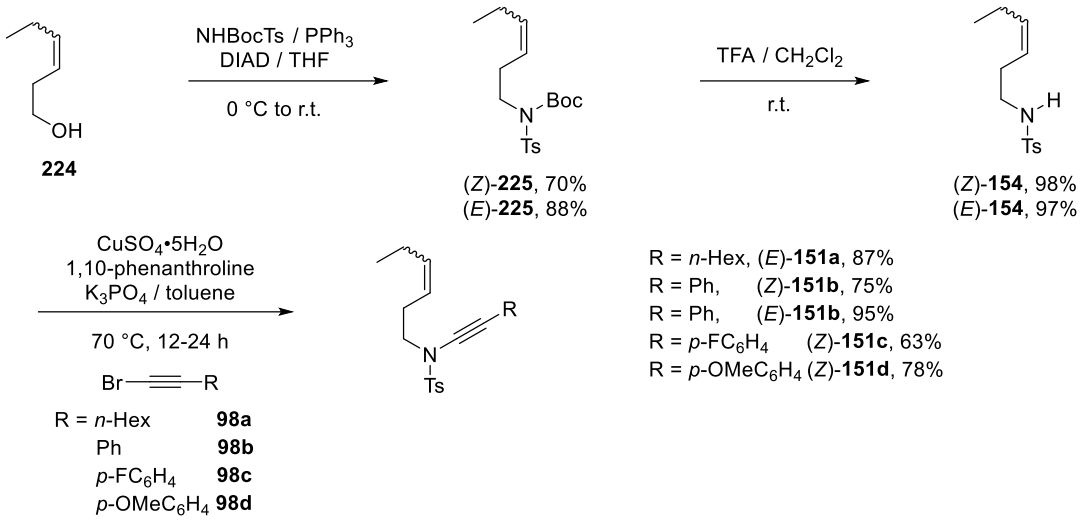

Scheme 5.9

Ynamides (Z)-**151e** were prepared from alcohol **252** in seven steps (Scheme 5.10). After TBS protection, alkyne lithiation and electrophilic trapping with benzyl bromide afforded alkyne **254** in moderate yield. Subsequent Lindlar hydrogenation afforded (*Z*)-**255** in quantitative yield. Upon TBS deprotection and Mitsunobu reaction with $HNTsCO_2Me$, sulfonamide (*Z*)-**257** was isolated in 67% yield. Decarboxylation with K_2CO_3/MeOH afforded the desired sulfonamide, which was coupled with bromoalkynes **98** to give ynamides (*Z*)-**151e** and **f.**

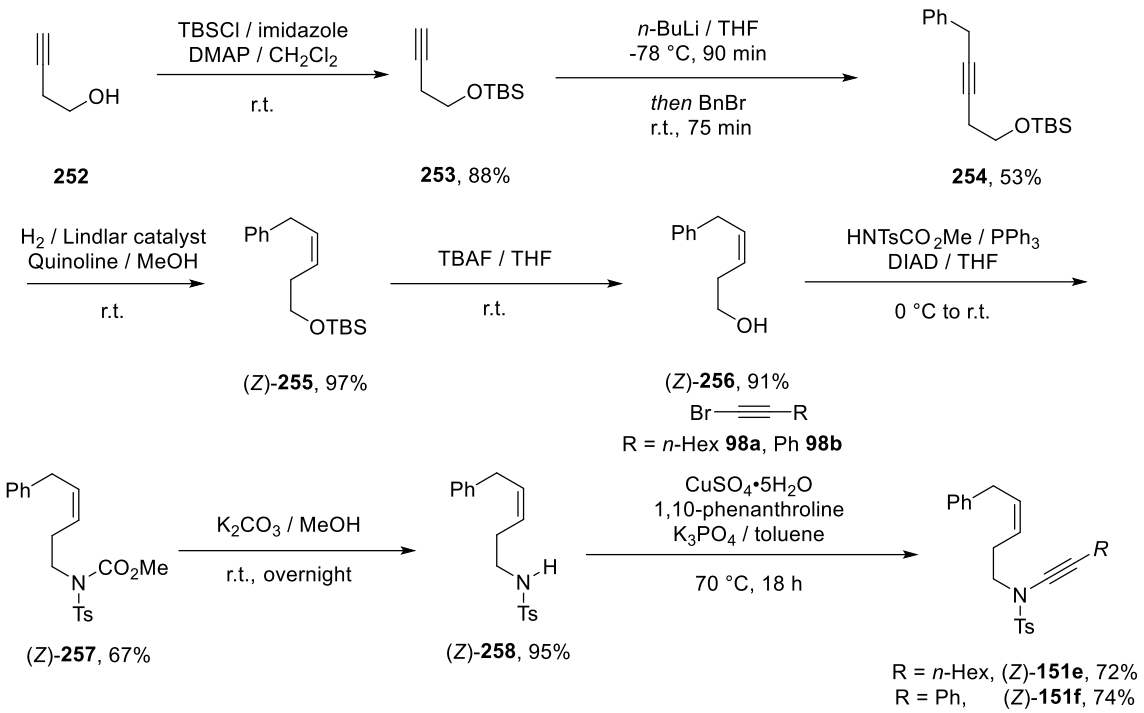

Scheme 5.10

Trisubstituted Alkenyl Ynamides

For ynamides with a methyl group at position 4, (*E*)-**264a** and **b** (Scheme 5.11), commercially available alkynyl alcohol **252** was reacted with trimethylaluminum and Cp_2ZrCl_2, followed by addition of a solution of I_2 in anhydrous THF.[87] The alcohol unit in the resulting vinyl iodide (*E*)-**259** was protected using TBSCl under basic conditions. (*E*)-**260** was coupled with propylmagnesium bromide by Pd-catalysed Kumada reaction to afford alcohol (*E*)-**261** in 75% yield.[88] The same protocol to covert an alcohol to ynamides was used (Mitsunobu reaction with $HNTsCO_2Me$, carbamate deprotection, and Hsung ynamide formation[5.1]), ynamides (*E*)-**264a** and **b** were obtained.

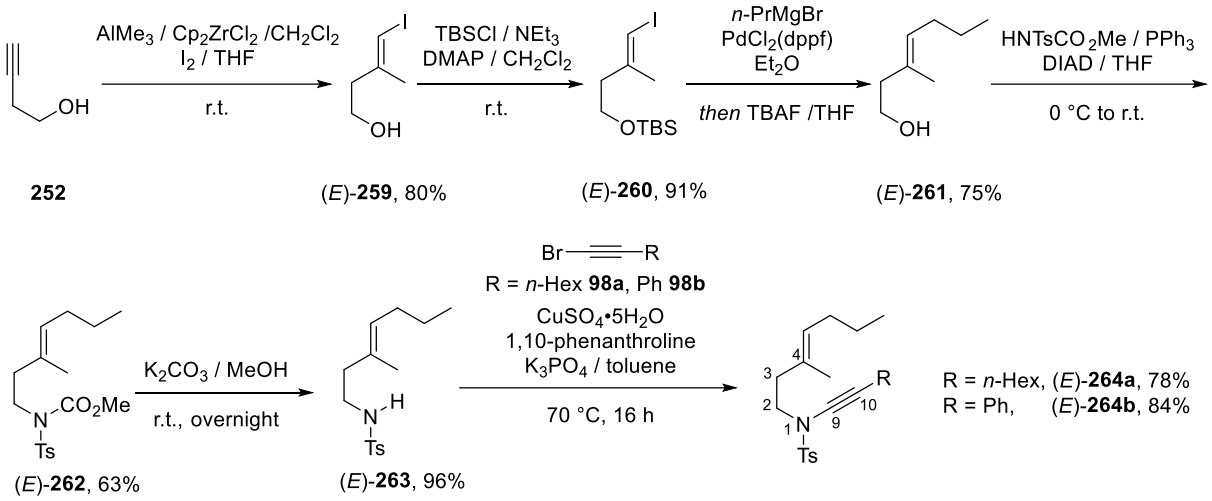

Scheme 5.11

For the preparation of isomeric ynamide (*Z*)-**264a** and **b** (Scheme 5.12), an equivalent synthesis was followed which differed only in the initial step. Reaction of alcohol **252** with trimethylaluminum and Cp_2ZrCl_2 at reflux for 3 days afforded (*Z*)-**259** because of the thermal chelation-controlled isomerisation of the methylalumination product.[89] A solution of I_2 in THF was subsequently added to the reaction mixture to afford vinyl iodide (*Z*)-**259**.

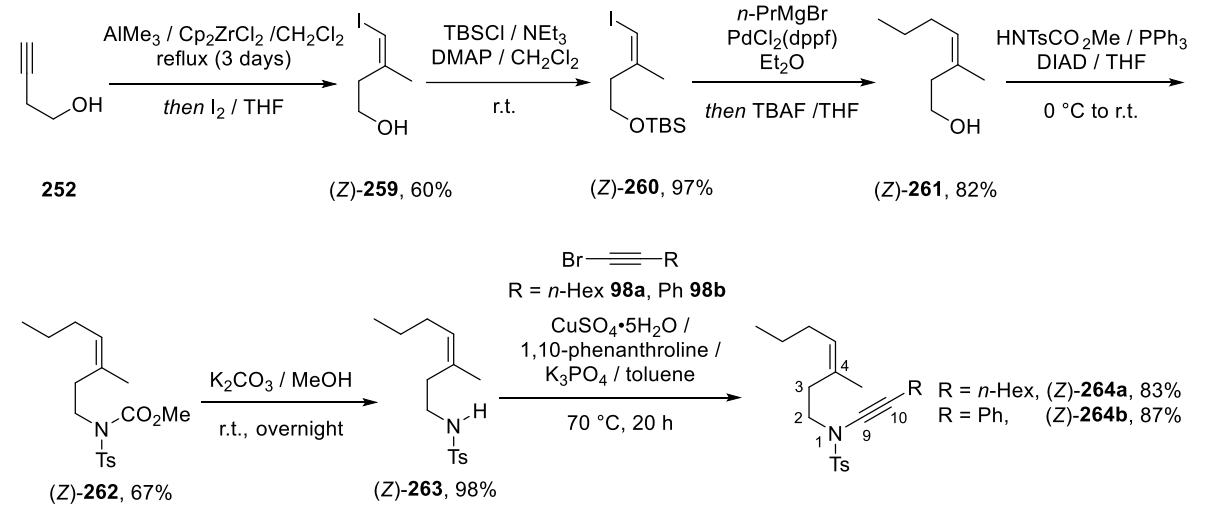

Scheme 5.12

Ynamides (*E*)-**269a** and **b** which processes a methyl group at the position 5 were also prepared (Scheme 5.13). First commercially available dihydrofuran **265** was reacted with *t*-BuLi and 1-iodobutane at –50 °C in anhydrous THF. The functionalised dihydrofuran underwent Kumada cross-coupling with

MeMgBr to give alcohol (*E*)-**266**.[90] This alcohol was subjected to the aforementioned series of reactions to afford ynamides (*E*)-**269a** and **b**.

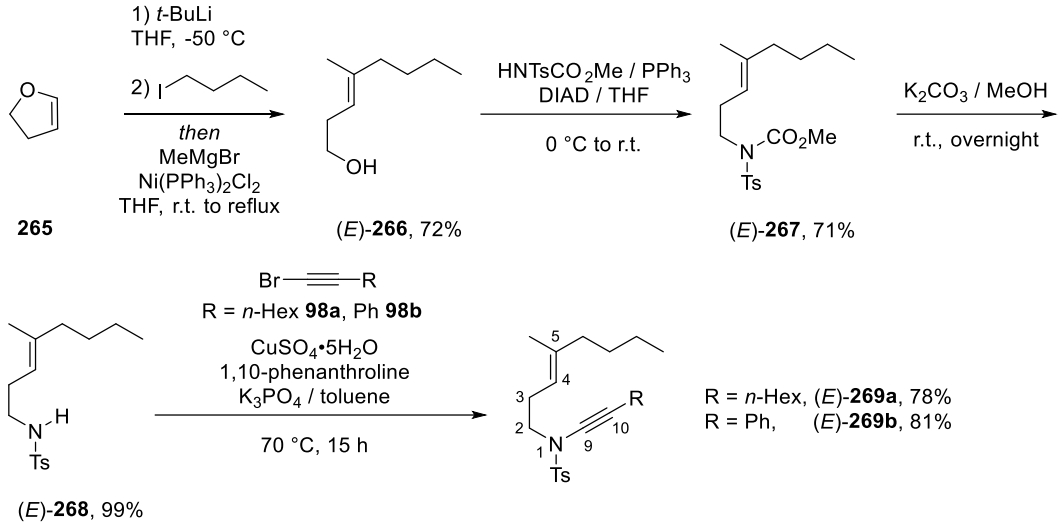

Scheme 5.13

The (*Z*)-isomers of enyneamides **269a** and **b** were prepared from commercially available alcohol **270**. First the alcohol was reacted with trimethylaluminum and titanium(IV) chloride to afford trisubstituted (*E*)-alkenyl alcohol (*Z*)-**266**.[91] The same synthetic steps were then followed to convert alcohol (*Z*)-**266** to the corresponding ynamides.

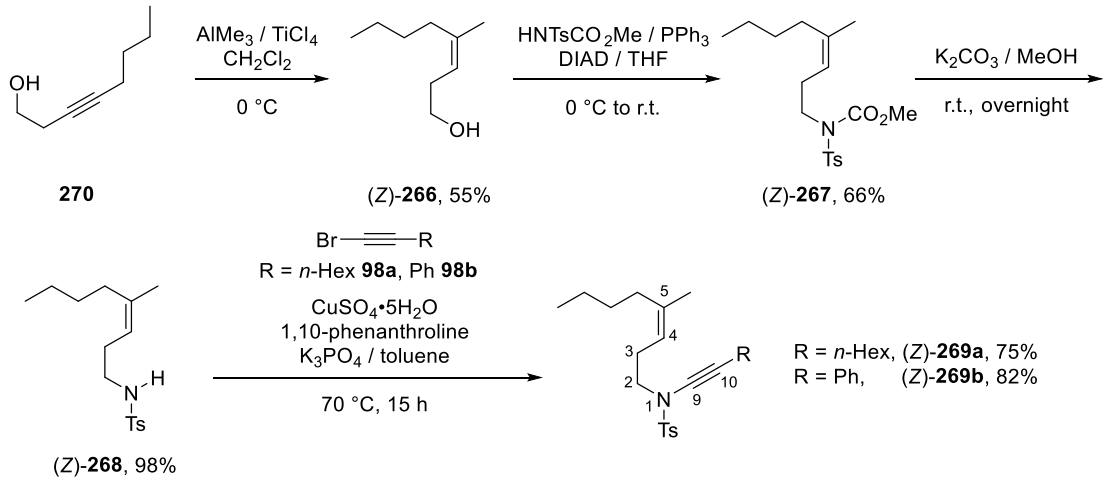

Scheme 5.14

Cycloalkenyl Ynamides

Cycloalkenyl ynamides **275** were prepared from commercially available carboxylic acid **271** (Scheme 5.15). Reduction of such an acid with $LiAlH_4$ gave alcohol **272**. Once again, the alcohol was processed using aforementioned procedures to furnish enynamides **275 a** and **b**.

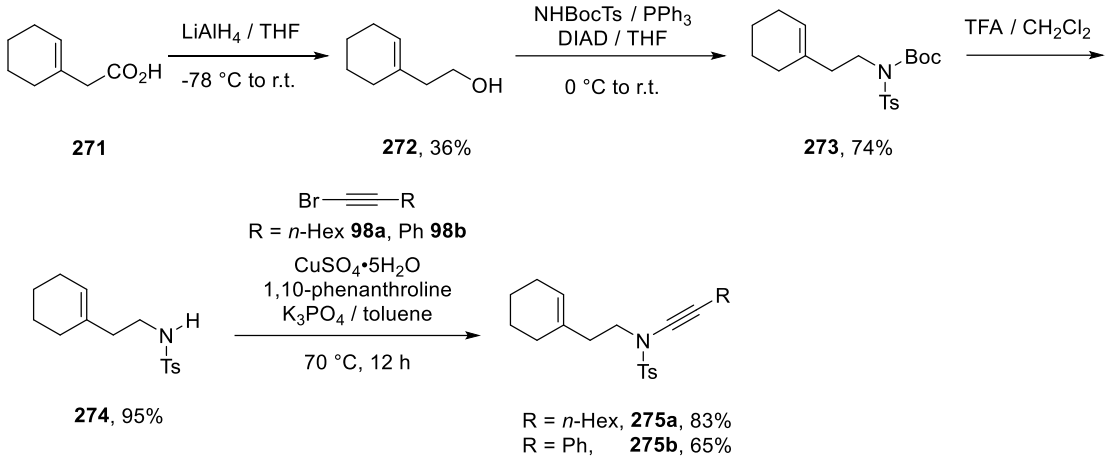

Scheme 5.15

5.3.2 Substrate Scope

With a comprehensive variety of enynamides in hand, we investigated the compatibility of the prepared substrates with the optimised catalyst system for cycloisomerisation.

Di and trisubstituted Alkenyl Ynamides

Disubstituted alkenyl ynamides **151a-f** were submitted to the cycloisomerisation conditions with the hope to produce heterocyclic dienamides (*E*)-**153a-f** (Table 5.9). In general, the reactions with (*Z*)-alkenyl ynamides reached completion within 45 minutes, with the products isolated in good yield and enantioselectivity at room temperature and 5 mol% catalyst loading (Entries 1–4 and 7–8). It was found that variation of the alkynyl substituent did not affect the enantioselectivity of the cycloisomerisation (Entries 1–4), while a slight drop in yield was observed when the group was electron withdrawing. Substrates possessing an (*E*)-alkene were not converted into product (Entries 5 and 6). Once the group attached to the olefin was benzyl instead of alkyl, the reaction still proceeded with a lower rate of reaction, which could be the effect of steric hindrance caused by the benzyl group (Entries 7 and 8).

However, the yield and enantiopurity remained in good levels. It is worth noting that all reactions produced a single product, a 1,4-dienamide with (*E*)-geometry at the non-enamide olefin.

Table 5.10 Cycloisomerisation of disubstituted alkenyl ynamides.

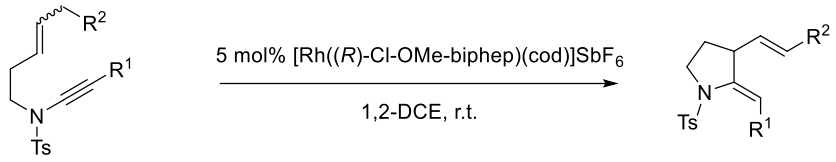

151a-f (*E*)-**153a-f**

Entry	Substrate, Geometry, R^1, R^2	Time	Yield[a] / %	*ee*[b] / %
1	(*Z*)-**151a**, *Z*, *n*-Hex, Me	5 min	98	97
2	(*Z*)-**151b**, *Z*, Ph, Me	10 min	93	96
3	(*Z*)-**151c**, *Z*, *p*-FC_6H_4, Me	30 min	95	94
4	(*Z*)-**151d**, *Z*, *p*-$OMeC_6H_4$, Me	5 min	87	95
5[c]	(*E*)-**151a**, *E*, *n*-Hex, Me	3 h	n.r.[d]	n/a
6[c]	(*E*)-**151b**, *E*, Ph, Me	3 h	n.r.[d]	n/a
7	(*Z*)-**151e**, *Z*, *n*-Hex, Ph	30 min	93	93
8	(*Z*)-**151f**, *Z*, Ph, Ph	45 min	83	94

[a] Isolated yield; [b] Determined by chiral HPLC; [c] The temperature was raised to 40 ° C after 1 h; [d] Starting material was fully recovered; n.r. = no reaction; n/a = not applicable.

The structures of the products were confirmed by the analysis of coupling constants of the alkene signals (J = 15.4 Hz) as well as NOESY experiments, which in all cases showed the relative *exo* position of the substituents (Scheme 5.16).

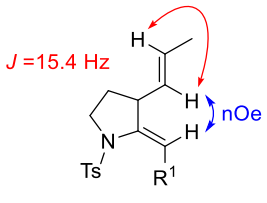

(*E*)-**153**

Scheme 5.16

Next, the catalyst system was tested with trisubstituted alkenyl ynamides **264** and **269** (Table 5.11). Similar results were obtained, only substrates with a (*Z*)-alkene unit underwent cyclisation to give products as (*E*)-1,4-dienamides (*E*)-**276** (Entries 1–2 and 5–6). The yields and enantiomeric excess are at satisfactory levels. In addition, we were pleased to see that enynamides (*Z*)-**264a** and **b** could also be cycloisomerised to give products (*E*)-**269a** and **b** with a quaternary centre in high degrees of enantioselectivity and moderate yields (Entries 1 and 2). However, when substrates (*E*)-**264** and (*E*)-**269** were submitted to the cycloisomerisation conditions, no reaction progress was observed even at higher temperature; the starting material was fully recovered (Entries 3–4 and 7–8).

Table 5.11 Cycloisomerisation of trisubstituted alkenyl ynamides.



264 / **269** (*E*)-**276**

Entry	Substrate, R^1, R^2, R^3, R^4	Time	Yield[a] / %	*ee*[b] / %
1	(*Z*)-**264a**, *n*-Hex, *n*-Pr, H, Me	80 min	61	94
2	(*Z*)-**264b**, Ph, *n*-Pr, H, Me	105 min	52	92
3[c]	(*E*)-**264a**, *n*-Hex, H, *n*-Pr, Me	9 h	n.r.[d]	n/a
4[c]	(*E*)-**264b**, Ph, H, *n*-Pr, Me	13 h	n.r.[d]	n/a
5	(*Z*)-**269a**, *n*-Hex, *n*-Bu, Me, H	45 min	95	93
6	(*Z*)-**269b**, Ph, *n*-Bu, Me, H	55 min	92	94
7[c]	(*E*)-**269a**, *n*-Hex, Me, *n*-Bu, H	10 h	n.r.[d]	n/a
8[c]	(*E*)-**269b**, Ph, Me, *n*-Bu, H	13 h	n.r.[d]	n/a

[a] Isolated yield; [b] Determined by chiral HPLC; [c] The temperature was raised to 40 °C after 3 h; [d] Starting material was fully recovered; n.r. = no reaction; n/a = not applicable.

Cycloalkenyl Ynamides

Since we had observed a successful cycloisomerisation of substrates (*Z*)-**264a** and **b** to furnish products (*E*)-**269a** and **b** with a quaternary carbon centre, we questioned if cyclohexenyl ynamides **275** could be cyclised to give spiro compounds **277**. Disappointingly, when the reactions were performed with such substrates (Scheme 5.16), it turned out that an unknown compound was obtained. Despite many NMR techniques (^{1}H, ^{13}C, COSY, HSQC, HMBC, DEPTs) were used to characterise the product, we could not define the structure of the products.

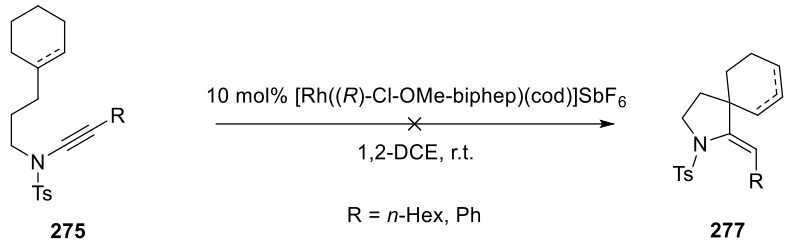

275 **277**

Scheme 5.16

5.4 Conclusions

We have successfully prepared a bench stable rhodium pre-catalyst for enynamide cycloisomerisation. As a result, the procedure for performing the cycloisomerisation is much simplified, compared to previous work. Using NMR spectroscopic experiments, our experimental evidence agrees with previous studies and implies that a rhodium hydride species is unlikely to be the active catalyst in our reaction; instead, a solvate cationic rhodium complex **247** or a dimeric complex **248** is formed. The improved catalyst system showed excellent reactivity and enantiomeric excess. We discovered that this catalysis worked well with enynamides with (*Z*)-geometry olefin, but (*E*)-alkenyl substrates were found to be inactive. Ynamides containing a cycloalkenyl group afforded either a complex mixture of products or an unidentified by-product.

Chapter 6: Conclusions and Future Work

6.1 Conclusions

Using various NMR spectroscopic techniques together with deuterium labelling, we have uncovered the crucial influences of water, the pre-catalyst, and the ligand (bbeda) in this reaction. Our demonstration that bbeda itself serves as a source of palladium(II) hydride, combined with the computational studies of the reaction pathway correlated with experimental isotope effect, offers a new level of understanding of this classic cyclisation process and allows us to rationalise the substrate stereocontrol under this palladium-catalysed conditions. This work was published in the *Journal of the American Chemical Society* (*see* Appendix).[92]

In addition to the mechanistic investigations, we also introduced a more robust rhodium-based catalyst system for enynamide cycloisomerisations. Despite, in comparison with the traditional catalyst systems, this new pre-catalyst provides better results, the substrate scope of this catalysis is still limited to enynamides in which the olefin unit is in *Z*-geometry. Unfortunately, we are still unable to make the catalyst system work with ynamides containing *E*-alkene or cycloalkenyl group. With some preliminary NMR spectroscopic experiments, we are convinced that the cycloisomerisation proceeds *via* mediation of a cationic rhodium active catalyst **237**. This active species is supposedly derived from hydrogenation of pre-catalyst **239**, which subsequently generates either a solvate monomeric rhodium complex **247** or a dimeric rhodium intermediate **248** (Scheme 6.1). We suggest that rhodium hydride species are unlikely to be formed during the hydrogenation, as the complexes could not be detected by ^{31}P NMR spectroscopy, which is in accordance with precedent literatures.[93, 94]

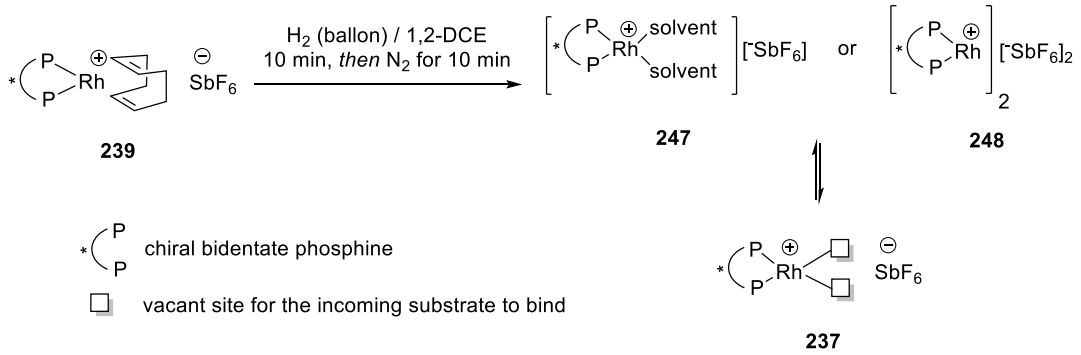

Scheme 6.1

6.2 Future Work: Double Stereodifferentiation in Enynamide Cycloisomerisation

In collaboration with Niels Marien, a visiting PhD student in the Anderson group, the synthesis of a variety of chiral enynamides to be used in examining the double stereodifferentiation of the cycloisomerisation reaction is currently underway (Scheme 6.2)

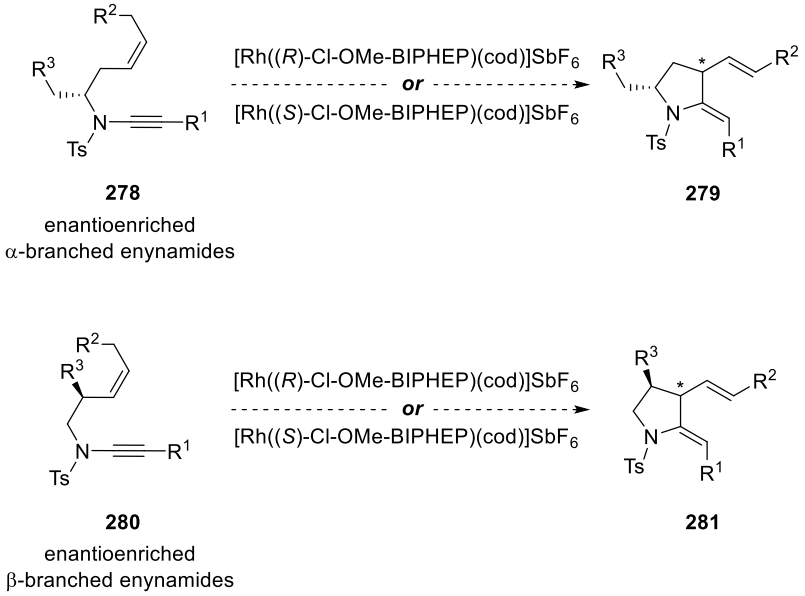

Scheme 6.2

One type of such enantioenriched enynamides is α-branched enynamides **278**, which can be synthesised from the following plan (Scheme 6.3). The route begins with sequential ring-opening of enantiopure epichlorohydrin **282** by a lithiated alkyne, followed by a Grignard reagent to afford chiral secondary alcohol **284**.[95, 96] This alkyne is partially hydrogenated with Lindlar catalyst to give *Z*-alkene **285**. The resulting alcohol will then undergo a Mitsunobu reaction with $HNTsCO_2Me$, generating **286**. The carbamate group is subsequently deprotected using a mixture of K_2CO_3 in methanol to reveal sulfonamide **287** which can be converted into the desired enynamide **278** using our ynamide synthesis methodology.[97]

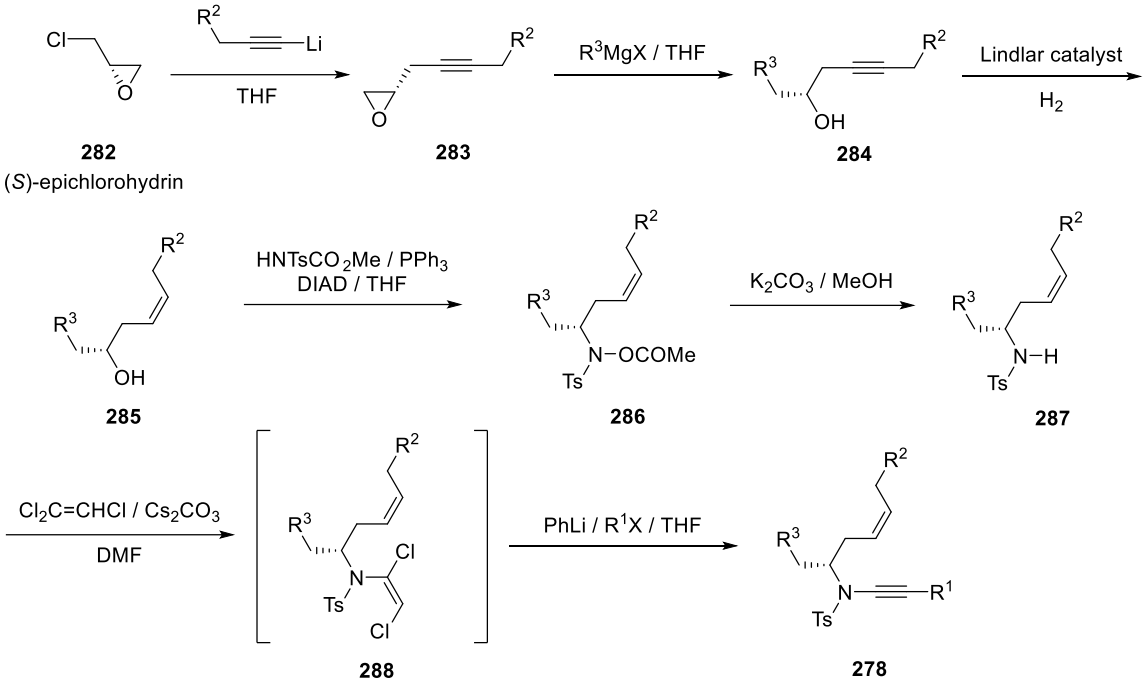

Scheme 6.3

Another class of chiral enynamides is β-branched enynamides **280**. To furnish such substrates (Scheme 6.4), the plan is to start with an asymmetric proline-catalysed aldol cyclisation between formaldehyde and aldehyde **289**.[98] The hemiacetal product **290** can then undergo Wittig olefination to deliver an enantioenriched alcohol **291**. This alcohol is subsequently reacted with $HNTsCO_2Me$ under Mitsunobu conditions to afford carbamate **292**. Carbamate deprotection and subsequent Hsung's ynamide formation will afford β-branched enynamides **280**.[99]

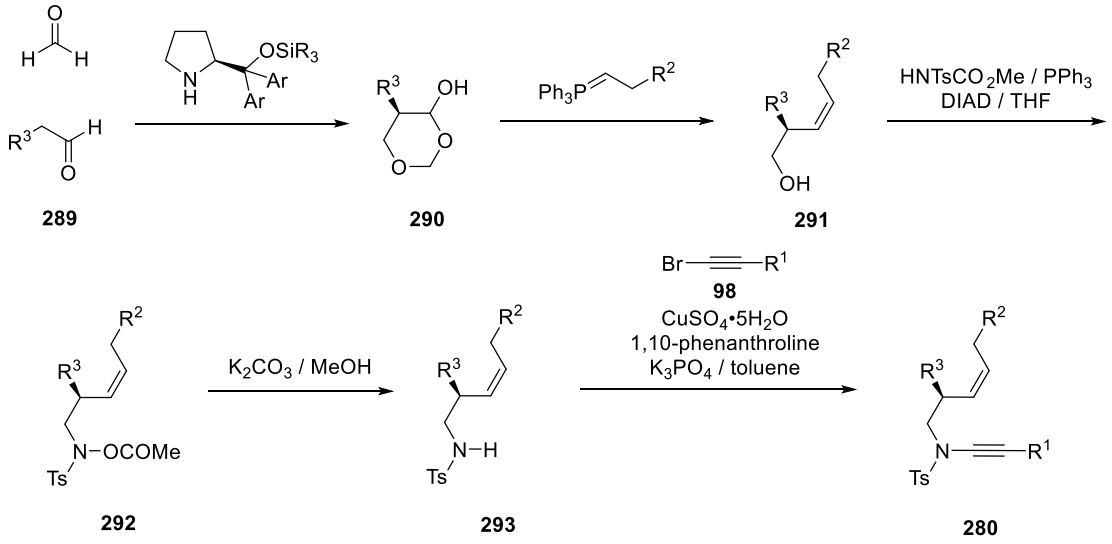

Scheme 6.4

With such chiral substrates in hand, we aim to use these single enantiomer enynamides under our rhodium catalyst conditions to investigate the impacts of the chiral catalyst system and the inherent stereochemical control of the substrate in matched and mismatched reactions. The term 'matched' implies that the stereocontrols of the catalyst and chiral starting material are reinforcing. On the other hand, 'mismatched' refers the case where the stereoinductions of the catalyst and substrate are antagonistic.

6.3 Future Work: Kinetic Resolution in Enynamide Cycloisomerisation

Instead of using single enantiomer substrates, this time racemic enynamides will be selected as substrate. These starting materials can be synthesised from racemic epichlorohydrin in the same fashion as the single enantiomer enynamides. Given the strength of the intrinsic substrate stereochemical induction, and thereby the difference between the reaction rate of the matched and mismatched reactions, we can evaluate the feasibility of kinetic resolution in the cycloisomerisation (Scheme 6.5).

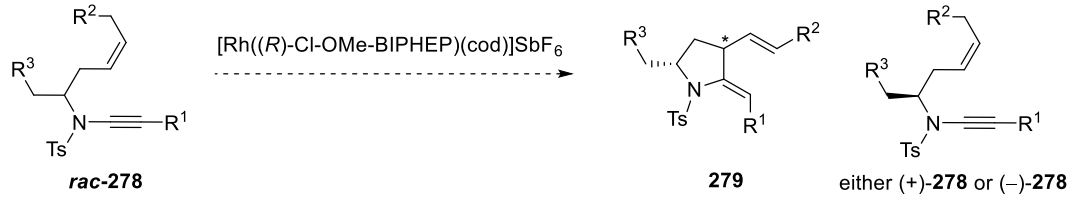

Scheme 6.5

Another scenario is if each enantiomer of the starting enynamides can undergo cycloisomerisation to deliver a different diastereomeric form of enantioenriched product; we can then examine the diastereodivergence of the cycloisomerisation (Scheme 6.6)

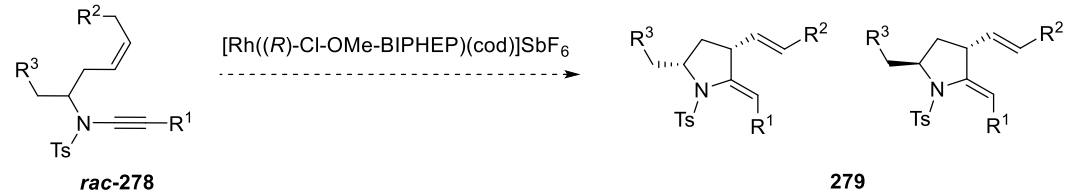

Scheme 6.6

Chapter 7: Experimental

7.1 General Experimental

NMR Spectra: ^{1}H and ^{13}C NMR spectra were recorded on Bruker AVII500 (500/125 MHz) or Bruker AV400 (400/100 MHz) spectrometers using TOPSPIN software. Proton and carbon chemical shifts (δ_H, δ_C) are quoted in ppm and referenced to tetramethylsilane with residual protonated solvent as the internal standard. Resonances are described using the following abbreviations; s (singlet), d (doublet), t (triplet), q (quartet), quin. (quintet), m (multiplet), br (broad), app (apparent), dd (doublet of doublets) *etc*. Coupling constants (*J*) are given in Hz and are rounded to the nearest 0.1 Hz. H' and H" refer to diastereotopic protons attached to the same carbon and imply no particular stereochemistry.

Mass Spectra: High resolution mass spectra were recorded by the Mass Spectrometry service of the Chemistry Research Laboratory, University of Oxford, using a Bruker Daltronics microTOF spectrometer (ESI). *m/z* values are reported in Daltons; high resolution values are calculated to four decimal places from the molecular formula, all found values being within a tolerance of 5 ppm.

Infrared Spectra: Infrared spectra were recorded on a Bruker Tensor 27 Fourier transform spectrometer, equipped with a diamond ATR module. Absorption maxima (ν_{max}) are quoted in wavenumbers (cm^{-1}).

Melting Points: Melting points were recorded on a Leica Galen III Compound Microscope and are uncorrected.

Chromatography techniques: TLC was performed on Merck DC-Alufolien 60 F_{254} 0.2 mm pre-coated plates and visualised using basic potassium permanganate, acidic vanillin or ultraviolet light. Retention factors are reported with the solvent system in parentheses. Column chromatography was performed on Merck Keiselgel 60 SiO_2 (230-400 mesh) and the solvent system used is recorded in parentheses.

Solvents were either used as commercially supplied, or purified by passage through an alumina column solvent dispensing system. Unless otherwise stated, reactions were carried out in oven-dried flasks under an atmosphere of dry argon or nitrogen.

All deuterated solvents for the NMR experiments were dried using the procedure reported by Williams *et al*.[42] The water contents in the solvents were determined using Karl-Fischer titration on a 756 KF Coulometer.

7.2 General Experimental Procedures

Procedure 1: Bromination of primary alkynes using $AgNO_3$

According to the procedure of Anderson *et al.*[20] To a suspension of alkyne (1.0 equiv.) in acetone (1 mL/mmol) was added $AgNO_3$ (2.5 mol%). The reaction mixture was stirred for 5 min and NBS (1.1 equiv.) added. The reaction mixture was stirred at room temperature for 15 h, filtered through a pad of silica (petroleum ether) and concentrated *in vacuo*.

Procedure 2: Conversion of an alcohol to a sulfonamide

According to the procedure of Anderson *et al.*[20] To a solution of alcohol (1.0 equiv.), triphenylphosphine (2.0 equiv.) and *tert*-butyl tosylcarbamate (1.3 equiv.) in THF (4 mL/mmol of alcohol) at 0 °C was added dropwise DIAD (1.5 equiv.). The reaction mixture was stirred at room temperature overnight, filtered and then concentrated *in vacuo*. The residue was then taken up in Et_2O:petroleum ether (5 mL:5 mL/mmol of alcohol), sonicated for 5 min and filtered. The filtrate was concentrated *in vacuo* to approximately 15 mL/mmol of alcohol at which point the resulting precipitation was removed by filtration before being concentrated *in vacuo* to dryness.

Procedure 3: Boc-deprotection using TFA

To a solution of carbamate (1.0 equiv.) in CH_2Cl_2 (3 mL/mmol of carbamate) was added dropwise TFA (10.0 equiv.). The reaction mixture was stirred at room temperature for 1 h, cooled to 0 °C, quenched with sat. aq. Na_2CO_3 (3 mL/mmol of carbamate) and transferred to a separating funnel. The organic layer was separated and the aqueous layer extracted with CH_2Cl_2 (2 × 2 mL/mmol of carbamate). The combined organic layers were dried ($MgSO_4$), filtered and concentrated *in vacuo*.

Procedure 4: Boc-deprotection using K_2CO_3 and MeOH

To a solution of carbamate (1.0 equiv.) in MeOH (8 mL/mmol carbamate) was added K_2CO_3 (5.0 equiv.). The reaction mixture was stirred under reflux for 5 h, allowed to cool to room temperature and concentrated *in vacuo* to approx. 5 mL. The mixture was then added to H_2O (10 mL/mmol carbamate)

and extracted with CH_2Cl_2 (3 × 10 mL/mmol carbamate). The combined organic layers were dried ($MgSO_4$), filtered and concentrated *in vacuo*.

Procedure 5: Copper(II)-catalyzed ynamide formation

According to the procedure of Hsung *et al*.[41] To a mixture of sulfonamide (1.0 equiv.), K_3PO_4 (2.0 equiv.), $CuSO_4 \cdot 5H_2O$ (0.2 equiv.) and 1,10-phenanthroline (0.4 equiv.) was added a solution of bromoalkyne (1.5 equiv.) in toluene (2 mL/mmol of sulfonamide). The reaction mixture was stirred at 70 °C for 15 h before being allowed to cool to room temperature. The reaction mixture was filtered through Celite® eluting with Et_2O, and the filtrate concentrated *in vacuo*.

Procedure 6: Palladium-catalyzed cycloisomerization of alkenyl-ynamides / enynes

According to the procedure of Anderson *et al.*[20] To a solution of ynamide / enyne (1.0 equiv.) in dry toluene (6.5 mL/mmol of ynamide) was added *N*,*N*′-bis(benzylidene)ethylenediamine (bbeda, 0.1 equiv.) and $Pd(OAc)_2$ (0.1 equiv.). The reaction mixture was stirred at the stated temperature (typically room temperature to 60 °C) for the stated time and concentrated *in vacuo*.

Procedure 7: Hydrohalogination of alkenyl-ynamides

Method 1 According to the procedure of Hsung *et al*.[77] To a solution of enynamide (1 equiv.) in wet CH_2Cl_2 (10 mL/mmol enynamide) was added $MgX_2 \cdot 6H_2O$ (X = Br or I, 1.1 equiv.). The reaction mixture was capped in a glass vial and vigorously stirred at 55 °C for 12 h. The reaction was monitored by TLC analysis. The heterogeneous mixture was washed with (2 × 10 mL/mmol enynamide) with sat. aq. $Na_2S_2O_3$ solution, dried over $MgSO_4$, and then dried *in vacuo*. The crude product was in general very pure and could be used without further purification.

Method 2 According to the procedure of Iwasawa *et al*.[76] To a solution of enynamide (1 equiv.) in anhydrous toluene (5 mL/mmol enynamide) at –78 °C was dropwise added 1 M of TMSX (X = Br or I) in dry toluene (1 equiv.) over 5 min. After 15 min stirring, H_2O (20 equiv.) was added, followed by warming to 0 °C over 50 min. The reaction mixture was then stirred for another 10 min. The reaction was quenched with sat. aq. $Na_2S_2O_3$ solution, dried over $MgSO_4$, and then dried *in vacuo*. The crude product was in general very pure and could be used without further purification.

Procedure 8: Varying water contents in deuterated solvents

To pre-dried deuterated solvent1 in a flame-dried glass vial sealed with a rubber septum was added the appropriate quantity of H_2O or D_2O *via* syringe. The vial was agitated to ensure mixing of the two liquid phases. The solution was then sampled to measure the water content using Karl-Fisher titration on a 756 KF Coulometer. Water content is reported as a mean value of triplicate measurements.

Procedure 9: NMR timecourse experiments

Spectrometer set-up: To an NMR tube was added a solution of ynamide (0.067 mmol, 1.0 equiv.) and 1,2,4,5-tetrachloronitrobenzene (internal standard) in deuterated solvent (0.4 mL, 0.167 M). This 'dummy' sample was placed in the NMR spectrometer, with a probe temperature of 308 K, for the purposes of pre-optimizing the lock and shim of the reaction sample.

Timecourse experiment: To an NMR tube containing ynamide (0.067 mmol, 1.0 equiv.), bbeda (0.0034 mmol, 0.05 equiv.) and 1,2,4,5-tetrachloronitrobenzene (internal standard), was added a solution of palladium catalyst in d_8-toluene (0.05 equiv., 0.1 mL), and the total volume adjusted to 0.4 mL (0.167 M). The reaction mixture was briefly mixed on a vortex agitator, then rapidly placed in the NMR machine (at 308K). Timecourse experiment spectra were collected at 34 s intervals (DS = 0, NS = 1, d1 = 20 s (at this relaxation time, the protons in the substrate and product had been independently confirmed to relax fully); 6 s of delay time was added before the initiation of the next acquisition to allow for automated spectrometer processes. This equates to 34 seconds between each acquisition. All experiments were run in triplicate.

The spectra were automatically phased, baseline corrected, and integrated (cross-checked against the internal standard peak) using the TOPSPIN multi_integ3 command. The integration values were plotted using Microsoft Excel as a percentage of the total starting material originally present (proportional to concentration).

Procedure 10: NMR titration experiments

$Pd_3(OAc)_5OH$ vs bbeda: To an NMR tube was added a solution of $Pd_3(OAc)_5OH$ (0.067 mmol, 1.0 equiv.) in pre-dried deuterated solvent (0.4 mL, 0.167 M). The mixture was briefly mixed on a vortex agitator, then placed in the NMR machine (at 308 K). An NMR spectrum of $Pd_3(OAc)_5OH$ was recorded (with default parameter settings: DS = 2, NS = 16, d1 = 2 s). After the spectrum had been obtained, the

tube was removed from the NMR machine, then bbeda (0.25 equiv.) was added to the tube. The reaction mixture was vigorously agitated, and subsequently resubmitted to the NMR machine to record another spectrum (with identical parameter settings). The titration was repeated until 2.0 equivalents of bbeda were added. The spectra were automatically phased, baseline corrected, and integrated using TOPSPIN software.

$Pd_3(OAc)_6$ vs bbeda: To an NMR tube was added a solution of $Pd_3(OAc)_5OH$ (0.067 mmol, 1.0 equiv.) in pre-dried deuterated solvent (0.4 mL, 0.167 M). The mixture was briefly mixed on a vortex agitator, then placed in the NMR machine (at 308 K). An NMR spectrum of $Pd_3(OAc)_5OH$ was recorded (with default parameter settings: DS = 2, NS = 16, d1 = 2 s). After the spectrum had been obtained, the tube was removed from the NMR machine, then bbeda (0.5 equiv.) was added to the tube. The reaction mixture was vigorously agitated, and subsequently resubmitted to the NMR machine to record another spectrum (with identical parameter settings). The titration was repeated until 1.5 equivalents of bbeda were added. The spectra were automatically phased, baseline corrected, and integrated using TOPSPIN software.

Procedure 11: Asymmetric rhodium-catalysed cycloisomerisation of enynamide

In a dried glass vial with a rubber septum cap, [Rh((*R*)-Cl-OMe-BIPHEP)(cod)]SbF_6 (5 mol% [Rh]) was dissolved in freshly distilled 1,2-dichloroethane (0.3 mL); the solution was hydrogenated with a hydrogen balloon for 10 min, followed by 5–10 min nitrogen sparging. A solution of substrate (0.03mmol) in dry 1,2-dichloroethane (0.2 mL) was then introduced into the solution. The resulting mixture was stirred at room temperature. Upon the completion of the reaction indicated by TLC, the reaction mixture was concentrated *in vacuo*, then directly subjected to column chromatography.

7.3 Characterisation of Compounds

7.3.1 Synthesis of cycloisomerisation substrates

1-Bromooct-1-yne, 98a

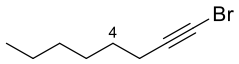

Synthesised from oct-1-yne (15.0 mL, 102 mmol) using **Procedure 2**. The resulting crude material was purified by column chromatography (petroleum ether) to give **98a** as a colourless oil (18.4 g, 97.5 mmol, 96%); $\mathbf{R}_f$ = 0.83 (1:1, petroleum ether:EtOAc); $\boldsymbol{\delta}_\mathbf{H}$ (400 MHz, $CDCl_3$) 2.19 (2H, t, *J* = 7.2 Hz, H3), 1.50 (2H, ap. quin., *J* = 7.2 Hz, H4), 1.43–1.20 (6H, m, H5–7), 0.89 (3H, t, *J* = 6.9 Hz, C*H*$_3$); $\boldsymbol{\delta}_\mathbf{C}$ (100 MHz, $CDCl_3$) 80.4, 37.4, 31.3, 28.5, 28.3, 22.5, 19.6, 14.0. Data are consistent with literature values.[100]

Methyl 3-((4-methylphenyl)sulfonamido)propanoate, 94

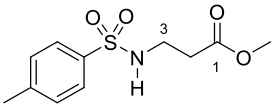

β-alanine methyl ester hydrochloride salt (500 mg, 3.58 mmol, 1.0 equiv.) was stirred in NEt_3 (0.55 mL, 3.94 mmol, 1.1 equiv.) for 1 h under a nitrogen atmosphere. To this solution was added CH_2Cl_2 (20 mL), pyridine (0.35 mL, 4.30 mmol, 1.2 equiv.) and TsCl (751 mg, 3.94 mmol, 1.1 equiv.). The reaction mixture was stirred at room temperature (monitored by TLC). Following completion, the excess solvent was removed *in vacuo*; the resulting crude material was then purified by column chromatography (20%→60% EtOAc / petroleum ether) to afford **94** (681 mg, 2.65 mmol, 74%) as a white solid; $\mathbf{R}_f$ 0.45 (3:2 petroleum ether / EtOAc); $\boldsymbol{\delta}_\mathbf{H}$ (500 MHz, $CDCl_3$) 7.75 (2H, d, *J* = 8.2 Hz, Ts*H*), 7.32 (2H, d, *J* = 8.2 Hz, Ts*H*), 5.09 (1H, t, *J* = 6.4 Hz, N*H*), 3.67 (3H, s, C*H*$_3$), 3.19 (2H, dt, *J* = 6.4 and 5.9 Hz, H3), 2.54 (2H, t, *J* = 5.9 Hz, H2), 2.43 (3H, s, C*H*$_3$Ts); $\boldsymbol{\delta}_\mathbf{C}$ (125 MHz, $CDCl_3$) 172.7, 143.7, 137.2, 130.0, 127.2, 52.2, 38.9, 34.0, 21.7. Data are consistent with literature values.[101]

_N_-(3-Hydroxypropyl-3,3-d$_2$)-4-methylbenzenesulfonamide, d$_2$-95

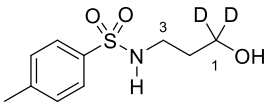

Methyl ester **94** (271 mg, 1.05 mmol, 1.0 equiv.) was dissolved in dry THF (1 mL) under an argon atmosphere, then cooled to –78 °C. This solution was transferred *via* cannula to a pre-cooled (–78 °C) suspension of $LiAlD_4$ (89 mg, 2.10 mmol, 2.0 equiv.) in dry THF (3 mL). The reaction mixture was stirred for 2 h at –78 °C under argon, then allowed to warm to –40 °C, and then quenched with sodium potassium tartrate (15 mL, sat., aq.). The resulting precipitate was removed by filtration. The filtrate was then extracted with EtOAc (3 × 10 mL). The combined organic layers were dried over $MgSO_4$, filtered, concentrated *in vacuo*, and purified by column chromatography (30%→60% EtOAc / petroleum ether) to afford d$_2$-**95** (238 mg, 1.03 mmol, 98%) as a white solid; **m.p.** 52–54 °C; $\mathbf{R_f}$ 0.18 (3:2 petroleum ether / EtOAc); $\boldsymbol{\delta_H}$ (500 MHz, $CDCl_3$) 7.75 (2H, d, *J* = 8.3 Hz, Ts*H*), 7.31 (2H, d, *J* = 8.3 Hz, Ts*H*), 5.00 (1H, t, *J* = 5.9 Hz, N*H*), 3.10 (2H, app q, *J* = 6.2 Hz, H3), 2.43 (3H, s, TsCH_3), 1.85–1.53 (1H, br s, O*H*), 1.69 (2H, t, J = 6.2 Hz, H2); $\boldsymbol{\delta_C}$ (125 MHz, $CDCl_3$) 143.6, 137.0, 130.0, 127.2, 60.7 (quin., *J* = 21.8 Hz), 41.2, 31.4, 21.7; **IR** (thin film) ν_{max}/cm^{-1} 3497, 3278, 1322, 1158; **HRMS** *m/z* (ESI+) found $[M+H]^+$ 232.09718; $C_{10}H_{14}D_2NO_3S^+$ requires 232.0976.

4-Methyl-_N_-(3-oxopropyl-3-d)benzenesulfonamide, d$_1$-96

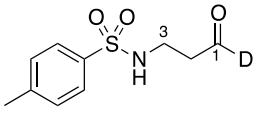

N-(3-hydroxypropyl-3,3-d$_2$)-4-methylbenzenesulfonamide d$_2$-**95** (166 mg, 0.72 mmol, 1.0 equiv.) was dissolved in CH_2Cl_2 (3.6 mL) under an argon atmosphere, then cooled to 0 °C. To the cooled solution was added Dess-Martin periodinane (458 mg, 1.08 mmol, 1.5 equiv.). The reaction mixture was then stirred for 16 h at room temperature, and subsequently filtered through a layer of silica, eluted with EtOAc (3 × 10 mL). The filtrate was concentrated *in vacuo*. This crude product was used in the next step without purification due to its instability towards storage. $\mathbf{R_f}$ 0.31 (3:2 petroleum ether / EtOAc).

_N_-(But-3-en-1-yl-3-d)-4-methylbenzenesulfonamide, d_1-97

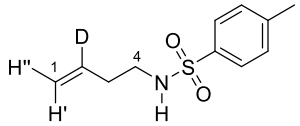

According to the procedure of Stone *et al*.[102] To a stirred suspension of methyltriphenylphosphonium bromide (247 mg, 0.69 mmol, 1.1 equiv.) in dry THF (2.4 mL), was added *t*-BuOK (1M in THF, 0.64 mL, 0.64 mmol, 1.1 equiv.). The reaction mixture was stirred for 1 h at room temperature, then cooled to 0 °C. To the cooled solution was added a solution of 4-methyl-*N*-(3-oxopropyl-3-d)benzenesulfonamide d_1-**96** (140 mg, 0.61 mmol, 1.0 equiv.) in THF (6.9 mL). The reaction mixture was then stirred for 1 h at room temperature, and subsequently quenched with NH_4Cl (10 mL, sat., aq.). The aqueous phase was extracted with Et_2O (3 × 10 mL). The combined organic layers were dried over Na_2SO_4, filtered, concentrated *in vacuo*, and purified by column chromatography (10→20% EtOAc / petroleum ether) to give d_1-**97** (133 mg, 0.59 mmol, 96%, >98% deuterium incorporation by ^{1}H NMR spectroscopy) as a pale yellow oil; $\mathbf{R}_f$ 0.61 (3:2 petroleum ether / EtOAc); $\boldsymbol{\delta}_\mathbf{H}$ (400 MHz, $CDCl_3$) 7.74 (2H, d, *J* = 8.4 Hz, Ts*H*), 7.31 (2H, d, *J* = 8.4 Hz, Ts*H*), 5.05 (1H, m, H'), 5.01 (1H, m, H''), 4.65 (1H, br s, N*H*), 3.00 (2H, app q, *J* = 6.6Hz, H4), 2.42 (3H, s, CH_3Ar), 2.19 (2H, t, *J* = 6.6 Hz, H3); $\boldsymbol{\delta}_\mathbf{C}$ (100 MHz, $CDCl_3$) 143.6, 137.0, 134.0 (t, *J* = 23.5 Hz), 129.9, 127.2, 118.1, 42.2, 33.6, 21.7; **IR** (thin film) ν_{max}/cm^{-1} 2928, 1642, 1354, 1164; **HRMS** *m/z* (ESI+) found $[M+H]^+$ 227.09610; $C_{11}H_{15}DNO_2S^+$ requires 227.0965.

_N_-(But-3-en-1-yl-3-d)-4-methyl-_N_-(oct-1-yn-1-yl)benzenesulfonamide, d_1-92

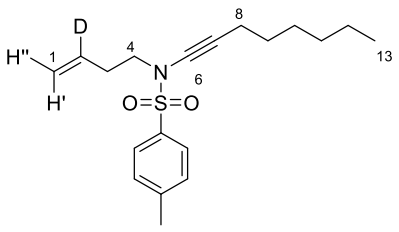

Synthesised from *N*-(but-3-en-1-yl-3-d)-4-methylbenzenesulfonamide d_1-**97** (>98% deuterium incorporation by ^{1}H NMR spectroscopy) (300 mg, 1.33 mmol) and 1-bromooct-1-yne (301 mg, 1.59 mmol) using **Procedure 5**. The resulting crude material was purified by column chromatography (petroleum ether→10% Et_2O in petroleum ether) to afford d_1-**92** (138 mg, 0.36 mmol, 83%, >98%

deuterium incorporation by ^{1}H NMR spectroscopy) as a colourless oil; $\mathbf{R_f}$ 0.69 (4:1 petroleum ether / EtOAc); $\boldsymbol{\delta_H}$ (400 MHz, $CDCl_3$) 7.77 (2H, d, *J* = 8.2 Hz, Ts*H*), 7.32 (2H, d, *J* = 8.2 Hz, Ts*H*), 5.06 (1H, br s, H'), 5.03 (1H, br s, H''), 3.32 (2H, t, *J* = 7.3 Hz, H4), 2.44 (3H, s, C*H*$_3$Ar), 2.36 (2H, t, *J* = 7.3 Hz, H3), 2.25 (2H, t, *J* = 7.0 Hz, H8), 1.45 (2H, quin, *J* = 7.1 Hz, H9), 1.38–1.24 (6H, m, H10–12), 0.88 (3H, t, *J* = 6.8 Hz, H13); $\boldsymbol{\delta_C}$ (100 MHz, $CDCl_3$) 144.2, 134.7, 133.6 (t, *J* = 23.5 Hz), 129.6, 127.6, 117.3, 72.9, 70.6, 50.8, 32.0, 31.3, 28.9, 28.4, 22.6, 21.6, 18.5, 14.0; **IR** (thin film) ν_{max}/cm^{-1} 2930, 2254, 1364, 1168; **HRMS** *m/z* (ESI+) found $[M+Na]^+$ 357.1709; $C_{19}H_{26}DNNaO_2S^+$ requires 357.1717.

***tert*-Butyl 4-nitrophenylsulfonylcarbamate, S1**

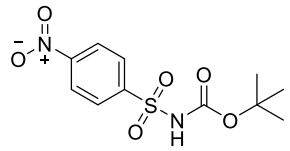

To a suspension of 4-nitrobenzenesulfonamide (10.0 g, 49.5 mmol, 1.0 equiv.) in CH_2Cl_2 (30 mL) was added triethylamine (7.6 mL, 54.4 mmol, 1.1 equiv.) and 4-dimethylaminopyridine (302 mg, 2.5 mmol, 0.05 equiv.). A solution of di-*tert*-butyl-dicarbonate (12.5 mL, 54.4 mmol, 1.1 equiv.) in CH_2Cl_2 (50 mL) was added. The reaction mixture was stirred at room temperature for 2 h and then concentrated *in vacuo*. EtOAc (100 mL) and 1M aq. HCl (80 mL) were added and the mixture separated. The organic extract was washed with H_2O (60 mL) and brine (600 mL), dried ($MgSO_4$), filtered and concentrated *in vacuo*. Trituration with hot *n*-hexane (50 mL) gave **S1** as a colourless solid (13.91 g, 46.0 mmol, 93%); **m.p.** 117–122 °C; $\mathbf{R_f}$ = 0.22 (4:1, petroleum ether:EtOAc); $\boldsymbol{\delta_H}$ (500 MHz, $CDCl_3$) 8.42–8.37 (2H, m, Ns*H*), 8.26–8.22 (2H, m, Ns*H*), 7.63 (1H, br. s, N*H*), 1.40 (9H, s, C(C*H*$_3$)$_3$); $\boldsymbol{\delta_C}$ (125 MHz, $CDCl_3$) 150.7, 148.6, 144.2, 129.7, 124.1, 85.1, 27.8. Data are consistent with literature values.[20]

***tert*-Butyl but-3-enyl(4-nitrophenylsulfonyl)carbamate. 100**

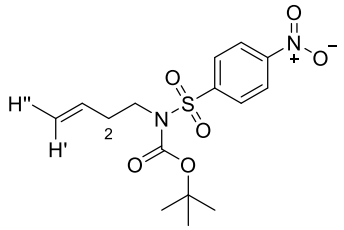

To a solution of 3-buten-1-ol **99** (1.79 mL, 20.8 mmol, 1.0 equiv.), triphenylphosphine (8.18 g, 31.2, 1.5 equiv.) and **S1** (7.55 g, 24.9 mmol, 1.2 equiv.) in THF (80 mL) at 0 °C was added dropwise DIAD (5.32 mL, 27.0 mmol, 1.3 equiv.). The reaction mixture was stirred at room temperature overnight, filtered and then concentrated *in vacuo*. The residue was then taken up in Et_2O:petroleum ether (50 mL:50 mL), sonicated for 5 min and filtered. The filtrate was concentrated *in vacuo* to approximately 15 mL/mmol of alcohol at which point the resulting precipitate was removed by filtration before being concentrated *in vacuo* to dryness. The resulting crude material was purified by column chromatography (5%→10% *t*-BuOMe in Hexanes) to give **100** as a brown solid (7.00 g, 19.6 mmol, 94%); **m.p.** 117–122 °C; $\mathbf{R_f}$ = 0.69 (4:1, Hexanes:EtOAc); $\boldsymbol{\delta_H}$ (400 MHz, $CDCl_3$) 8.38–8.33 (2H, m, Ns*H*), 8.15–8.09 (2H, m, Ns*H*), 5.80 (1H, ddt, *J* = 17.1, 10.2, 7.0 Hz, H′), 5.18–5.07 (2H, m, H''), 3.95–3.87 (H1), 2.51 (2H, ap. br. q, *J* = 7.2 Hz, H2), 1.37 (9H, s, $C(CH_3)_3$); $\boldsymbol{\delta_C}$ (100 MHz, $CDCl_3$) 150.4, 150.3, 145.8, 133.9, 129.3, 123.9, 117.9, 85.2, 46.7, 34.6, 27.9; **IR** (thin film) ν_{max}/cm^{-1} 2980, 1732, 1533, 1351, 1151; **HRMS** *m/z* (ESI+) found $[M+Na]^+$ 379.0932; $C_{15}H_{20}N_2NaO_6S^+$ requires 379.0934.

***N*-(But-3-en-1-yl)-4-nitrobenzenesulfonamide, 101**

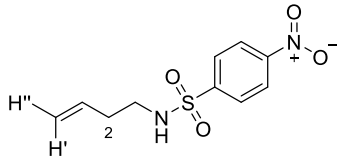

Synthesised from *tert*-butyl but-3-enyl(4-nitrophenylsulfonyl)carbamate **100** (6.00 g, 16.8 mmol) using Procedure 4 to give the title compound as an off-white solid (3.10 g, 12.1 mmol, 72%) which was used without further purification; **m.p**. 74–76 °C; $\mathbf{R_f}$ = 0.20 (4:1, hexanes:EtOAc); $\boldsymbol{\delta_H}$ (400 MHz, $CDCl_3$) 8.36 (2H, m, Ns*H*), 8.05 (2H, m, Ns*H*), 5.62 (1H, ddt, *J* = 17.1, 10.3 and 6.9 Hz, H3), 5.12–5.02 (2H, m, H' and H''), 4.81 (1H, br. t, *J* = 5.8 Hz, N*H*), 3.10 (2H, ap. q, *J* = 6.6 Hz, H1), 2.28–2.20 (2H, m, H2); $\boldsymbol{\delta_C}$ (100 MHz, $CDCl_3$) 150.1, 145.9, 133.6, 128.3, 124.4, 118.6, 42.2, 33.7; **IR** (thin film) ν_{max}/cm^{-}

[1] 3292, 3105, 1732, 1527, 1349; **HRMS** *m/z* (ESI+) found $[M+Na]^+$ 279.0414; $C_{10}H_{12}N_2NaO_4S^+$ requires 279.0410.

***N*-(But-3-en-1-yl)-4-nitro-*N*-(oct-1-yn-1-yl)benzenesulfonamide, 93**

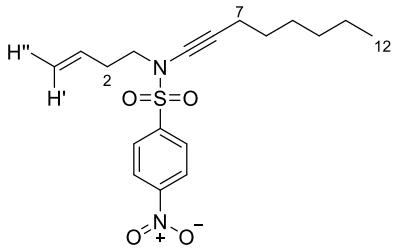

Synthesised from **101** (384 mg, 1.50 mmol) and 1-bromooct-1-yne **98a** (424 mg, 2.24 mmol) using **Procedure 5**, only the reaction mixture was heated to 105 °C for 24 h. The resulting crude material was purified by column chromatography (10% Et_2O in in petroleum ether) to give **93** as a yellow oil (412 mg, 1.13 mmol, 75%); $\mathbf{R_f}$ = 0.76 (4:1, petroleum ether:EtOAc); $\boldsymbol{\delta_H}$ (400 MHz, $CDCl_3$) 8.42–8.36 (2H, m, Ns*H*), 8.11–8.05 (2H, m, Ns*H*), 5.70 (1H, ddt, *J* = 17.1, 10.3, 6.8 Hz, H3), 5.09 (1H, ap. dq, *J* = 17.1 and 1.5 Hz, H′), 5.05 (1H, ddt, *J* = 10.3, 1.5, 1.1 Hz, H″), 3.40 (2H, t, *J* = 7.2 Hz, H1), 2.45–2.34 (2H, m, H2), 2.27 (2H, t, *J* = 7.0 Hz, H7), 1.54–1.43 (2H, m, H8), 1.40–1.21 (6H, m, H9–11), 0.89 (3H, t, *J* = 7.4 Hz, C*H*$_3$); $\boldsymbol{\delta_C}$ (125 MHz, $CDCl_3$) 150.4, 143.0, 133.3, 128.8, 124.2, 118.0, 71.7, 71.6, 51.2, 32.1, 31.3, 28.8, 28.5, 22.6, 18.4, 14.0; **IR** (thin film) ν_{max}/cm^{-1} 3105, 2930, 2859, 2255, 1607, 1531, 1402, 1372, 1174, 854, 738, 684; **HRMS** *m/z* (ESI+) found $[M+Na]^+$ 387.1336; $C_{18}H_{24}N_2NaO_4S^+$ requires 387.1349.

***tert*-Butyl but-3-en-1-yl(tosyl)carbamate, 104**

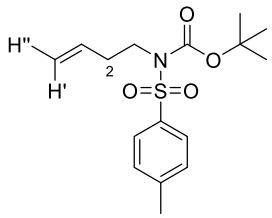

Synthesised from but-3-en-1-ol **99** (4.00 g, 55.5 mmol) using **Procedure 2**. The resulting crude material was purified by column chromatography (9:1, petroleum ether:Et_2O) to give **104** as a colourless oil (17.28 g, 53.1 mmol, 96%); $\mathbf{R_f}$ = 0.51 (4:1, petroleum ether:EtOAc); $\boldsymbol{\delta_H}$ (400 MHz, $CDCl_3$) 7.78 (2H, d, *J* = 8.2 Hz, Ts*H*), 7.29 (2H, d, *J* = 8.2 Hz, Ts*H*), 5.80 (1H, ddt, *J* = 17.2, 10.2, 6.9 Hz, H3), 5.12 (1H, dd, *J* = 17.2 and 1.5 Hz,H′), 5.07 (1H, d, *J* = 10.2 Hz, H″), 3.88 (2H, dd, *J* = 8.1 and 6.8 Hz, H1), 2.55–

2.46 (2H, m, H2), 2.43 (3H, s, ArCH_3), 1.33 (9H, s, C(CH_3)$_3$); **δ_C** (100 MHz, $CDCl_3$) 150.9, 144.0, 137.4, 134.4, 129.2, 127.8, 117.4, 84.1, 46.3, 34.5, 27.8, 21.6. Data are consistent with literature values.[103]

***N*-(But-3-en-1-yl)-4-methylbenzenesulfonamide 105**

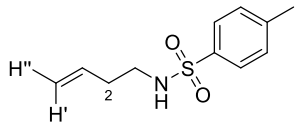

Synthesised from **104** (16.83 g, 51.7 mmol) using **Procedure 3** to give **105** as a colourless oil (11.6 g, 51.6 mmol, 99%) which was used without further purification; **R_f** = 0.33 (4:1, petroleum ether:EtOAc); **δ_H** (400 MHz, $CDCl_3$) 7.74 (2H, d, *J* = 8.2 Hz, Ts*H*), 7.29 (2H, d, *J* = 8.2 Hz, Ts*H*), 5.61 (1H, ddt, *J* = 17.0, 10.3, 6.8 Hz, H3), 5.05–4.97 (2H, m, H′ and H″), 4.84 (1H, br. t, *J* = 6.1 Hz, N*H*), 2.99 (2H, ap. q, *J* = 6.8 Hz, H1), 2.41 (3H, s, ArCH_3), 2.18 (2H, ap. q, *J* = 6.8 Hz, H2); **δ_C** (100 MHz, $CDCl_3$) 143.3, 136.8, 134.1, 129.6, 127.0, 117.9, 42.1, 33.5, 21.4. Data are consistent with literature values.[104]

***N*-(But-3-en-1-yl)-4-methyl-*N*-(oct-1-yn-1-yl)benzenesulfonamide 92**

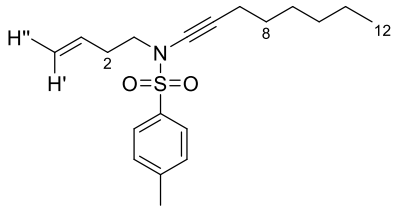

Synthesised from **105** (5.00 g, 22.2 mmol) and 1-bromooct-1-yne **98a** (5.04 g, 26.6 mmol) using **Procedure 5**. The resulting crude material was purified by column chromatography (10:1, petroleum ether:Et_2O) to give **92** as a colourless oil (7.08 g, 21.2 mmol, 96%); **R_f** = 0.51 (4:1, petroleum ether:EtOAc); **δ_H** (400 MHz, $CDCl_3$) 7.77 (2H, d, *J* = 8.2 Hz, Ts*H*), 7.32 (2H, d, *J* = 8.2 Hz, Ts*H*), 5.72 (1H, ddt, *J* = 17.2, 10.3, 6.7 Hz, H3), 5.07 (1H, dd, *J* = 17.2 and 1.5 Hz, H′), 5.03 (1H, dd, *J* = 10.3 and 1.5 Hz, H″), 3.32 (2H, t, *J* = 7.5 Hz,H1), 2.44 (3H, s, ArCH_3), 2.36 (2H, ap. q, *J* = 7.2 Hz, H2), 2.26 (2H, t, *J* = 6.9 Hz, H7), 1.51–1.42 (2H, m, H8), 1.39–1.19 (6H, m, H9–11), 0.88 (3H, t, *J* = 6.8 Hz, CH_3); **δ_C** (100 MHz, $CDCl_3$) 144.2, 134.6, 133.9, 129.5, 127.6, 117.4, 72.8, 70.5, 50.8, 32.1, 31.3, 28.9, 28.4, 22.6, 21.6, 18.4, 14.0; **IR** (thin film) ν_{max}/cm^{-1} 2930, 2253, 1364, 1170; **HRMS** *m/z* (ESI+) found $[M+Na]^+$ 356.1654; $C_{19}H_{27}NNaO_2S^+$ requires 356.1655.

4-Nitro-*N*-(3-oxopropyl)benzenesulfonamide, 96

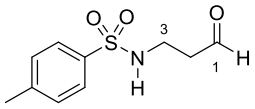

To a solution of methyl ester **104** (250 mg, 0.97 mmol, 1.0 equiv.) in dry THF (5 mL) under an argon atmosphere at –78 ºC was added DIBAL (1.9. mL, 1 M in Hexanes, 1.9 mmol, 2.0 equiv.) dropwise. The reaction mixture was stirred at –78 ºC for 5 h, quenched with sat. aq. Rochelle Salt (10 mL) and diluted with EtOAc (15 mL). The reaction mixture was left to room temperature and stirred for 1 h. The layers were separated, and the aqueous layer extracted with EtOAc (3 × 10 mL). The combined organic layers were dried ($MgSO_4$), filtered and concentrated *in vacuo*., and purified by column chromatography (5→10% EtOAc / petroleum ether) to afford **96** as a pale yellow oil (143 mg, 0.63 mmol, 65%); $\mathbf{R}_f$ = 0.51 (5:1, petroleum ether:EtOAc); $\boldsymbol{\delta}_\mathbf{H}$ (500 MHz, $CDCl_3$) 9.73 (1H, s), 7.74 (2H, d, *J* = 8.3 Hz, Ts*H*), 7.32 (2H, d, *J* = 8.2 Hz, Ts*H*), 5.25 (1H, t, *J* = 6.2 Hz, N*H*), 3.21 (2H, q, *J* = 6.1 Hz, H3), 2.75 (2H, t, *J* = 5.9 Hz, H2), 2.43 (3H, s, ArCH_3); $\boldsymbol{\delta}_\mathbf{C}$ (125 MHz, $CDCl_3$) 200.9, 143.6, 136.5, 129.7, 126.9, 43.4, 36.7, 21.5; **IR** (thin film) ν_{max}/cm^{-1} 3282, 2850, 1720, 1600, 1400, 1320, 1305, 1153, 1090, 1045, 840, 811, 705, 661; **HRMS** *m/z* (ESI+) found $[M+H]^+$ 228.0690; $C_{10}H_{14}NO_3S^+$ requires 228.0689.

***N*-(But-3-en-1-yl-4,4-d$_2$)-4-methylbenzenesulfonamide, d$_2$-110**

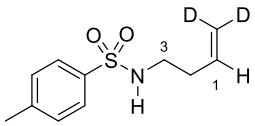

To a stirred suspension of d$_3$-methyltriphenylphosphonium bromide d$_3$-**109** (250 mg, 0.70 mmol, 1.1 equiv.) in dry THF (2.5 mL), was added *t*-BuOK (1M in THF, 0.70 mL, 0.70 mmol, 1.1 equiv.). The reaction mixture was stirred for 1 h at room temperature, then cooled to 0 °C. To the cooled solution was added a solution of 4-nitro-*N*-(3-oxopropyl)benzenesulfonamide **96** (148 mg, 0.65 mmol, 1.0 equiv.) in THF (7 mL). The reaction mixture was then stirred for 1 h at room temperature, and subsequently quenched with NH_4Cl (10 mL, sat., aq.). The aqueous phase was extracted with Et_2O (3 × 10 mL). The combined organic layers were dried over Na_2SO_4, filtered, concentrated *in vacuo*, and purified by column chromatography (10→20% EtOAc / petroleum ether) to give d$_2$-**110** (135 mg, 0.60 mmol, 92%, >98% deuterium incorporation by ^{1}H NMR spectroscopy) as a pale yellow oil; $\mathbf{R}_f$ 0.61 (3:2

petroleum ether / EtOAc); **δ_H** (400 MHz, $CDCl_3$) 7.74 (2H, d, *J* = 8.4 Hz, Ts*H*), 7.31 (2H, d, *J* = 8.4 Hz, Ts*H*), 5.62 (1H, t, *J* = 6.8 Hz, H1), 4.84 (1H, br. t, *J* = 6.1 Hz, N*H*), 2.99 (2H, ap. q, *J* = 6.8 Hz, H3), 2.41 (3H, s, ArCH_3), 2.18 (2H, ap. q, *J* = 6.8 Hz, H2); **δ_C** (100 MHz, $CDCl_3$) 143.3, 136.8, 134.1, 129.6, 127.0, 117.9 (m), 42.1, 33.5, 21.4.; **IR** (thin film) ν_{max}/cm^{-1} 2935, 1650 1350, 1162; **HRMS** *m/z* (ESI+) found $[M+H]^+$ 228.1030; $C_{11}H_{14}D_2NO_2S^+$ requires 228.1027.

***N*-(But-3-en-1-yl-4,4-d_2)-4-methyl-*N*-(oct-1-yn-1-yl)benzenesulfonamide, d_2-108**

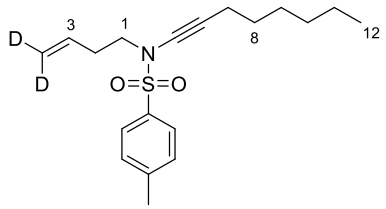

Synthesised from d_2-**110** (102 mg, 0.45 mmol) and 1-bromooct-1-yne **98a** (129 mg, 0.68 mmol) using **Procedure 5**. The resulting crude material was purified by column chromatography (10:1, petroleum ether:Et_2O) to give d_2-**108** as a colourless oil (137 mg, 0.41 mmol, 91%, >98% deuterium incorporation by ^{1}H NMR spectroscopy); **R_f** = 0.51 (4:1, petroleum ether:EtOAc); **δ_H** (400 MHz, $CDCl_3$) 7.77 (2H, d, *J* = 8.2 Hz, Ts*H*), 7.32 (2H, d, *J* = 8.2 Hz, Ts*H*), 5.72 (1H, t, *J* = 6.7 Hz, H3), 3.32 (2H, t, *J* = 7.5 Hz, H1), 2.44 (3H, s, ArCH_3), 2.36 (2H, ap. q, *J* = 7.2 Hz, H2), 2.26 (2H, t, *J* = 6.9 Hz, H7), 1.51–1.42 (2H, m, H8), 1.39–1.19 (6H, m, H9–11), 0.88 (3H, t, *J* = 6.8 Hz, CH_3); **δ_C** (100 MHz, $CDCl_3$) 144.2, 134.6, 133.9, 129.5, 127.6, 117.4 (m), 72.8, 70.5, 50.8, 32.1, 31.3, 28.9, 28.4, 22.6, 21.6, 18.4, 14.0; **IR** (thin film) ν_{max}/cm^{-1} 2933, 2253, 1365, 1173; **HRMS** *m/z* (ESI+) found $[M+H]^+$ 336.1968; $C_{19}H_{26}D_2NO_2S^+$ requires 336.1966.

Methyl-d_3 3-((4-methylphenyl)sulfonamido)propanoate-2,2-d_2, d_5-112

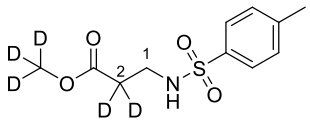

To a solution of methyl 3-(4-methylphenylsulfonamido)propanoate **104** (100 mg, 0.389 mmol, 1.0 equiv.) in d_4-MeOD (1.0 mL) was added K_2CO_3 (177 mg, 1.28 mmol, 3.3 equiv.). The reaction n mixture was stirred at room temperature for 15 h, CH_2Cl_2 (5 mL) and sat. aq. NH_4Cl (5 mL) added and the layers separated. The aqueous layer was extracted with CH_2Cl_2 (5 mL) and the combined organic layers were dried ($MgSO_4$), filtered and concentrated *in vacuo* to give d_5-**112** (91% deuterium

incorporation by ^{1}H NMR at C2) as a colourless oil (73 mg, 0.38 mmol, 71%) which was used without further purification; $\mathbf{R_f}$ = 0.34 (1:1, petroleum ether:EtOAc); $\boldsymbol{\delta_H}$ (400 MHz, $CDCl_3$) 7.73 (2H, d, *J* = 8.2 Hz, Ts*H*), 7.30 (2H, d, *J* = 8.2 Hz, Ts*H*), 3.16 (2H, s, H1), 2.41 (3H, s, ArCH_3); $\boldsymbol{\delta_C}$ (100 MHz, $CDCl_3$) 172.4, 143.5, 136.8, 129.7, 127.0, (*C*D_3O absent), 38.5, (*C*D_2CO absent), 21.5; **IR** (thin film) ν_{max}/cm^{-1} 3288, 2926, 1732, 1330, 1155; **HRMS** *m/z* (ESI+) found $[M+Na]^+$ 285.0929; $C_{11}H_{10}D_5NNaO_4S^+$ requires 285.0928.

***N*-(But-3-en-1-yl-2,2-d$_2$)-4-methylbenzenesulfonamide, d$_2$-113**

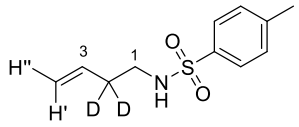

To a solution of d$_5$-**112** (91% deuterium incorporation by ^{1}H NMR) (227 mg, 0.87 mmol, 1.0 equiv.) in toluene (7 mL) at –78 ºC was added DIBAL (1.73 mL, 1 M in Hexanes, 1.73 mmol, 2.0 equiv.) dropwise. The reaction mixture was stirred at –78 ºC for 5 h, quenched with sat. aq. Rochelle Salt (10 mL) and diluted with EtOAc (15 mL). The reaction mixture was allowed to warm to room temperature and stirred for 1 h. The layers were separated and the aqueous layer extracted with EtOAc (15 mL). The combined organic layers were dried ($MgSO_4$), filtered and concentrated *in vacuo*. The residue was taken up in THF (5.0 mL), added to solution of $Cp_2TiCH_2AlCl(CH_3)_2$ (566 mg 1.99 mmol, 2.3 equiv.) in toluene (2.0 mL) at 0 °C and stirred at room temperature for 15 h. 2 M aq NaOH (0.8 mL), excess $MgSO_4$ and Et_2O (20 mL) were added, the mixture stirred at room temperature for 1 h, filtered through Celite® eluting with Et_2O and concentrated *in vacuo*. The resulting crude material was purified by column chromatography (30% Et_2O in petroleum ether) to give d$_2$-**113** (91% deuterium incorporation by ^{1}H NMR) as a colourless oil (38 mg, 0.167 mmol, 19%); $\mathbf{R_f}$ = 0.26 (4:1, petroleum ether:EtOAc); $\boldsymbol{\delta_H}$ (400 MHz, $CDCl_3$) 7.74 (2H, d, *J* = 8.3 Hz, Ts*H*), 7.30 (2H, d, *J* = 8.3 Hz, Ts*H*), 5.61 (1H, dd, *J* = 16.9 and 10.3 Hz, H3), 5.10–4.98 (2H, m, H' and H"), 4.70–4.54 (1H, br. m, N*H*), 2.99 (2H, d, *J* = 6.1 Hz, H1), 2.42 (3H, s, ArCH_3); $\boldsymbol{\delta_C}$ (100 MHz, $CDCl_3$) 143.4, 136.9, 134.0, 129.7, 127.1, 118.1, 41.9, (*C*D_2 absent), 21.5; **IR** (thin film) ν_{max}/cm^{-1} 3280, 2925, 1322, 1155; **HRMS** *m/z* (ESI+) found $[M+Na]^+$ 250.0847; $C_{11}H_{13}D_2NNaO_2S^+$ requires 250.0841.

_N_-(But-3-en-1-yl-2,2-d$_2$)-4-methyl-_N_-(oct-1-yn-1-yl)benzenesulfonamide, d$_2$-**111**

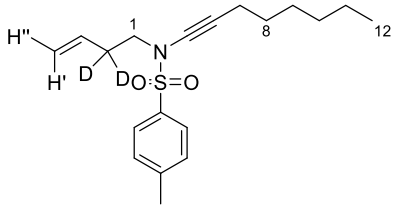

Synthesised from d$_2$-**113** (91% deuterium incorporation by $_1$H NMR) (35 mg, 0.154 mmol) and 1-bromooct-1-yne **98a** (38 mg, 0.200 mmol) using **Procedure 5**. The resulting crude material was purified by column chromatography (5% Et_2O in petroleum ether) to give d$_2$-**111** (91% deuterium incorporation by $_1$H NMR) as a colourless oil (43.5 mg, 0.130 mmol, 84%); $\mathbf{R}_f$ = 0.55 (4:1, petroleum ether:EtOAc); $\boldsymbol{\delta}_\mathbf{H}$ (400 MHz, $CDCl_3$) 7.77 (2H, d, *J* = 8.2 Hz, Ts*H*), 7.32 (2H, d, *J* = 8.2 Hz, Ts*H*), 5.71 (1H, dd, *J* = 17.1 and 10.2 Hz, H3), 5.07 (1H, dd, *J* = 17.1 and 1.8 Hz, H′), 5.03 (1H, dd, *J* = 10.2 and 1.8 Hz, H″), 3.30 (2H, s,H1), 2.44 (3H, s, ArCH_3), 2.25 (2H, t, *J* = 7.0 Hz, H7), 1.53–1.41 (2H, m, H8), 1.39–1.19 (6H, m, H9–11), 0.88 (3H, t, *J* = 7.0 Hz, CH_3); $\boldsymbol{\delta}_\mathbf{C}$ (100 MHz, $CDCl_3$) 144.2, 134.6, 133.7, 129.5, 127.6, 117.5, 72.8, 70.5, 50.6, (*C*D$_2$ absent), 31.3, 28.9, 28.4, 22.6, 21.6, 18.4, 14.0; **IR** (thin film) ν_{max}/cm^{-1} 2930, 2250, 1363, 1169; **HRMS** *m/z* (ESI+) found $[M+Na]^+$ 358.1781; $C_{19}H_{25}D_2NNaO_2S^+$ requires 358.1780.

Dimethyl 2-allyl-2-(5-((*tert*-butyldimethylsilyl)oxy)pent-2-yn-1-yl)malonate, 120

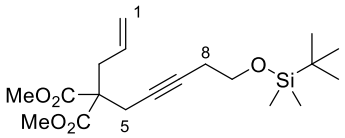

To a suspension of NaH (182 mg, 60% in mineral oil, 7.58 mmol, 1.9 equiv.) in anhydrous THF (8 mL) at 0 °C under a nitrogen atmosphere was added a solution of dimethyl 2-allylmalonate (686 mg, 3.98 mmol, 1.0 equiv.) in THF (8 mL) dropwise. The mixture was stirred for 30 min at 0 °C, then a solution of ((5-bromopent-3-yn-1-yl)oxy)(*tert*-butyl)dimethylsilane (1.05 g, 3.98 mmol, 1.0 equiv.) in THF (16 mL) was added. The mixture was allowed to warm to room temperature, and was stirred for 16 h. The reaction was quenched with H_2O (30 mL), and extracted with Et_2O (3 × 15 mL). The combined organic layers were dried ($MgSO_4$), filtered and concentrated *in vacuo*. The crude material was purified by column chromatography (0→5% EtOAc in petroleum ether) to afford **120** (1.25 g, 3.38 mmol, 85%) as

a colourless oil; $\mathbf{R_f}$ 0.29 (20:1 petroleum ether / EtOAc); $\boldsymbol{\delta_H}$ (400 MHz, $CDCl_3$) 5.67–5.57 (1H, m, H2), 5.17–5.08 (2H, m, H1), 3.71 (6H, s, 2×CO_2CH_3), 3.65 (2H, t, J = 7.2 Hz, H9), 2.78–2.74 (4 H, m, H3 and H5), 2.35–2.30 (2H, tt, J = 2.3 and 7.2 Hz, H8), 0.88 (9H, s, $SiC(CH_3)_3$), 0.05 (6H, s, 2×$SiCH_3$); $\boldsymbol{\delta_C}$ (100 MHz, $CDCl_3$) 170.6, 132.2, 119.8, 80.7, 75.6, 62.3, 57.4, 52.8, 36.8, 26.0, 23.3, 23.2, 18.5, –5.1; **IR** (thin film) ν_{max}/cm^{-1} 2940, 1738,1437,1290, 1100; **HRMS** *m/z* (ESI+) found $[M+H]^+$ 369.2097; $C_{19}H_{33}O_5Si^+$ requires 369.2092.

1-Phenylhept-3-yn-1-ol, 136

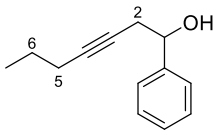

To a solution of 1-pentyne (0.41 mL, 4.16 mmol, 1.25 equiv.) in dry THF (5.0 mL) at –78 °C was added dropwise *n*–BuLi (1.6 mL, 2.5 M in hexanes, 4.00 mmol, 1.2 equiv.). The reaction mixture was allowed to warm to room temperature and dry DMSO (20 mL) was added over 5 min, followed by a solution of styrene oxide **135** (0.38 mL, 3.33 mmol, 1.0 equiv.) in dry THF (1.0 mL) dropwise. The reaction mixture was stirred at room temperature for 3 h, poured into H_2O (15 mL) and extracted with Et_2O (4 × 15 mL). The combined organic layers were washed with brine (3 × 40 mL), dried filtered and concentrated *in vacuo*. The resulting crude material was purified by column chromatography (10→15% EtOAc in petroleum ether) to give **136** as a pale yellow oil (154 mg, 1.03 mmol, 32%); $\mathbf{R_f}$ = 0.34 (4:1, petroleum ether:EtOAc); $\boldsymbol{\delta_H}$ (400 MHz, $CDCl_3$) 7.40–7.23 (5H, m, Ph*H*), 4.84–4.75 (1H, br. m, H1), 2.67–2.48 (3H, m, H2 and O*H*), 2.18–2.09 (2H, m, H5), 1.50 (2H, ap. sext, J = 7.3 Hz, H6), 0.94 (3H, t, J = 7.3 Hz, CH_3); $\boldsymbol{\delta_C}$ (100 MHz, $CDCl_3$) 142.8, 128.3, 127.7, 125.7, 83.3, 76.1, 72.6, 30.0, 22.3, 20.7, 13.4; **IR** (thin film) ν_{max}/cm^{-1} 3377, 2962; **HRMS** *m/z* (ESI+) found $[M+Na]^+$ 211.1090; $C_{13}H_{16}NaO^+$ requires 211.1093.

***tert*-Butyl (1-phenylhept-3-yn-1-yl)(tosyl)carbamate, 137**

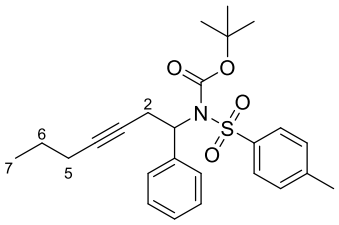

Synthesised from 1-phenylhept-3-yn-1-ol **136** (150 mg, 0.80 mmol) using **Procedure 3**. The resulting crude material was purified by column chromatography (dry loaded, 5%→10% Et_2O in petroleum ether) to give **137** as a colourless oil (253 mg, 0.57 mmol, 72%); $\mathbf{R}_f$ = 0.40 (4:1, petroleum ether:EtOAc); $\boldsymbol{\delta}_\mathbf{H}$ (500 MHz, $CDCl_3$) 7.83 (2H, d, *J* = 8.2 Hz, Ts*H*), 7.60 (2H, d, *J* = 7.6 Hz, Ph*H*), 7.35–7.30 (2H, m, m Ph*H*), 7.29–7.24 (3H, Ts*H* and Ph*H*), 5.78 (1H, ap. t, *J* = 7.9 Hz, H1), 3.25 (1H, dtt, *J* = 8.6, 8.1, 2.3 Hz, H2′), 3.13 (1H, dtt, *J* = 8.6, 7.6, 2.3 Hz, H2″), 2.43 (3H, s, ArCH_3), 2.02 (2H, ap. tq, *J* = 7.1 and 2.3 Hz, H5), 1.47–1.37 (2H, m, H6), 1.24 (9H, s, C(CH_3)$_3$), 0.90 (3H, t, *J* = 7.3 Hz, CH_3); $\boldsymbol{\delta}_\mathbf{C}$ (125 MHz, $CDCl_3$) 150.6, 143.9, 139.3, 137.3, 129.0, 128.6, 128.2, 127.4, 127.2, 84.2, 83.4, 76.6, 59.9, 27.8, 23.6, 22.2, 21.6, 20.8, 13.5; **IR** (thin film) ν_{max}/cm^{-1} 2965, 1729, 1358, 1151; **HRMS** *m/z* (ESI+) found $[M+Na]^+$ 464.1856; $C_{25}H_{31}NNaO_4S^+$ requires 464.1866.

(*Z*)-*tert*-Butyl (1-phenylhept-3-en-1-yl)(tosyl)carbamate, 138

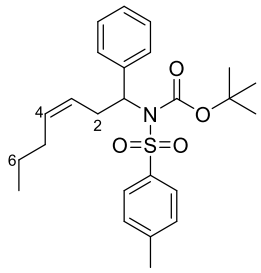

To a solution of *tert*-butyl (1-phenylhept-3-yn-1-yl)(tosyl)carbamate **137** (235 mg, 0.53 mmol, 1.0 equiv.) and quinolone (12 µL, 0.11 mmol, 0.2 equiv.) in toluene (5.0 mL) was added Pd on $CaCO_3$ (57 mg, 5 wt% Pd, 0.027 mmol, 0.05 equiv.). H_2 (balloon, 1 atm) was bubbled through the stirred reaction mixture at room temperature for 1 h. The reaction mixture was stirred for an additional 1 h, filtered through Celite® eluting with Et_2O the filtrate concentrated *in vacuo*. The resulting crude material was purified by column chromatography (15%→20% Et_2O in petroleum ether) to give **138** as a colourless oil (225 mg, 0.51 mmol, 96%); $\mathbf{R}_f$ = 0.47 (4:1, petroleum ether:EtOAc); $\boldsymbol{\delta}_\mathbf{H}$ (500 MHz, $CDCl_3$) 7.74

(2H, d, *J* = 8.5 Hz, Ts*H*), 7.44 (2H, d, *J* = 7.6 Hz, Ph*H*), 7.35–7.30 (2H, m, Ph*H*), 7.29–7.21 (3H, m, Ts*H*, Ph*H*), 5.69 (1H, dd, *J* = 8.7, 7.1 Hz, H1), 5.58–5.45 (2H, m,H3 and 4), 3.23–3.14 (1H, m, H2'), 3.05–2.97 (1H, m, H2''), 2.42 (3H, s, ArCH_3), 2.16–2.02 (2H, m, H5), 1.38 (2H, ap sextd, *J* = 7.4 and 1.6 Hz, H6), 1.20 (9H, s, C(CH_3)$_3$), 0.91 (3H, t, *J* = 7.4 Hz, CH_3); **δ_C** (125 MHz, $CDCl_3$) 150.7, 143.9, 140.0, 137.2, 132.9, 128.9, 128.6, 128.1, 127.8, 127.3, 125.9, 84.0, 60.5, 30.1, 29.6, 27.7, 22.7, 21.6, 13.8; **IR** (thin film) ν_{max}/cm^{-1} 2961, 1728, 1353, 1151; **HRMS** *m/z* (ESI+) found $[M+Na]^+$ 466.2017; $C_{25}H_{33}NNaO_4S^+$ requires 466.2023.

(*Z*)-4-Methyl-*N*-(1-phenylhept-3-en-1-yl)benzenesulfonamide, 139

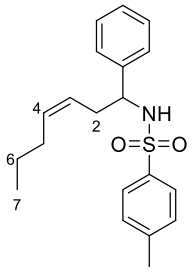

Synthesised from (Z)-*tert*-butyl (1-phenylhept-3-en-1-yl)(tosyl)carbamate **138** (205 mg, 0.47 mmol) using **Procedure 3**, only with the reaction mixture stirred, to give **139** as a colourless oil (155 mg, 0.45 mmol, 96%) which was used without further purification; **R_f** = 0.31 (4:1, petroleum ether:EtOAc); **δ_H** (500 MHz, $CDCl_3$) 7.57 (2H, d, *J* = 8.2 Hz, Ts*H*), 7.20–7.11 (5H, m, Ts*H*, Ph*H*), 7.11–7.05 (2H, m, Ph*H*), 5.47–5.39 (1H, m, H4), 5.15–5.04 (2H, m, H3, N*H*), 4.31 (1H, ap. q, *J* = 6.9 Hz, H1), 2.54–2.46 (1H, m, H2'), 2.46–2.38 (1H, m, H2''), 2.36 (3H, s, ArCH_3), 1.94–1.80 (2H, m, H5), 1.33–1.20 (2H, m, H6), 0.83 (3H, t, *J* = 7.4 Hz, CH_3); **δ_C** (125 MHz, $CDCl_3$) 143.0, 140.5, 137.4, 133.9, 129.3, 128.3, 127.3, 127.1, 126.6, 123.6, 57.7, 35.3, 29.3, 22.5, 21.4, 13.7; **IR** (thin film) ν_{max}/cm^{-1} 3275, 2959, 1324, 1159; **HRMS** *m/z* (ESI+) found $[M+Na]^+$ 366.1487; $C_{20}H_{25}NNaO_2S^+$ requires 366.1498.

(*Z*)-4-Methyl-*N*-(oct-1-yn-1-yl)-*N*-(1-phenylhept-3-en-1-yl)benzenesulfonamide, 125

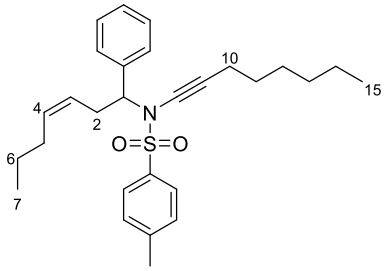

Synthesised from (*Z*)-4-methyl-*N*-(1-phenylhept-3-en-1-yl)benzenesulfonamide **139** (105 mg, 0.31 mmol) and 1-bromooct-1-yne **98a** (87 mg, 0.46 mmol) using **Procedure 5**, only the reaction mixture was heated to 105 °C for 48 h. The resulting crude material was purified by column chromatography (5%→30% Et_2O in petroleum ether) to give **125** as a colourless oil (72 mg, 0.16 mmol, 52%); $\mathbf{R_f}$ = 0.63 (4:1, petroleum ether:EtOAc); $\boldsymbol{\delta_H}$ (500 MHz, $CDCl_3$) 7.53 (2H, d, *J* = 8.2 Hz, Ts*H*), 7.30–7.24 (2H, m, Ph*H*), 7.23–7.16 (3H, m, Ph*H*), 7.12 (2H, d, *J* = 8.2 Hz, m Ts*H*), 5.40–5.31 (1H, m, H4), 5.23–5.14 (1H, m, H3), 4.89 (1H, dd, *J* = 8.5 and 7.3 Hz, H1), 2.75–2.66 (1H, m, H2'), 2.62–2.53 (1H, m, H2''), 2.36 (3H, s, ArCH_3), 2.31 (2H, t, *J* = 6.9 Hz, H10), 2.00–1.87 (2H, m, H5), 1.49 (2H, ap. quin., *J* = 7.3 Hz, H11), 1.38–1.20 (8H, m, H6, and H12–14), 0.88 (3H, t, *J* = 6.9 Hz, H15), 0.86 (3H, t, *J* = 7.4 Hz, H7); $\boldsymbol{\delta_C}$ (125 MHz, $CDCl_3$) 143.7, 139.3, 135.5, 132.7, 129.0, 128.2, 127.8, 127.7, 127.2, 124.6, 73.0, 70.9, 62.9, 31.8, 31.4, 29.5, 28.9, 28.5, 22.6, 21.5, 18.7, 14.1, 13.8; **IR** (thin film) ν_{max}/cm^{-1} 2929, 2250, 1363, 1168; **HRMS** *m/z* (ESI+) found $[M-H]^+$ 451.2549; $C_{28}H_{37}NNaO_2S^+$ requires 451.2545.

(*Z*)-4-Methyl-*N*-(oct-1-yn-1-yl)-*N*-(1-phenyloct-5-en-2-yl)benzenesulfonamide, 127

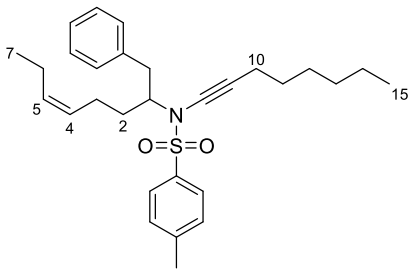

To a mixture of (*Z*)-4-methyl-*N*-(1-phenyloct-5-en-2-yl)benzenesulfonamide [kindly provided by Dr Ross P Walker] (500 mg, 1.40 mmol, 1.0 equiv.), K_2CO_3 (425 mg, 3.07 mmol, 2.2 equiv.), $CuSO_4 \cdot 5H_2O$ (140 mg, 0.56 mmol, 0.4 equiv.) and 1,10 phenanthroline (202 mg, 1.12 mmol, 0.8 equiv.) was added a solution of 1-bromooct-1-yne **98a** (529 mg, 2.80 mmol, 2.0 equiv.), in toluene (4.2 mL). The reaction mixture was stirred at 105 °C for 48 h before being allowed to cool to room temperature. The reaction

mixture was filtered through Celite® eluting with Et_2O and the filtrate concentrated *in vacuo*. The resulting crude material was purified by column chromatography (5%→10% Et2O in petroleum ether) to give **127** as a pale yellow oil (452 mg, 0.99 mmol, 71%); $\mathbf{R_f}$ = 0.55 (9:1, petroleum ether:EtOAc); $\boldsymbol{\delta_H}$ (400 MHz, $CDCl_3$) 7.51 (2H, d, *J* = 8.3 Hz, Ts*H*), 7.24–7.13 (5H, m, Ar*H*), 7.14–7.07 (2H, m, Ar*H*), 5.39–5.30 (1H, m, H5), 5.28–5.19 (1H, m, H4), 4.12 (1H, dddd, *J* = 9.5, 7.8, 6.9, 4.5 Hz, H1), 2.75 (1H, dd, *J* = 13.4 and 7.8 Hz, CH′*H*″Ph), 2.69 (1H, dd, *J* = 13.4 and 6.9 Hz, C*H*′H"Ph), 2.39 (3H, s, ArCH_3), 2.34 (2H, t, *J* = 6.8 Hz, H10), 2.11–2.00 (1H, m, H3'), 1.96 (2H, ap. quin., *J* = 7.5 Hz, H6), 1.91–1.80 (1H, m, H3"), 1.70–1.58 (1H, m, H2'), 1.56–1.45 (3H, m, H2" and H11), 1.42–1.23 (6H, m, H12–14), 0.91 (3H, t, *J* = 7.5 Hz, H7), 0.90 (3H, t, *J* = 6.8 Hz, H15); $\boldsymbol{\delta_C}$ (100 MHz, $CDCl_3$) 143.6, 138.0, 135.8, 132.4, 129.3, 128.4, 127.6, 127.4, 126.4, 72.8, 69.7, 62.0, 39.8, 32.8, 31.3, 29.0, 28.5, 23.9, 22.6, 21.5, 20.5, 18.6, 14.3, 14.1; **IR** (thin film) ν_{max}/cm^{-1} 2959, 2249, 1363, 1167; **HRMS** *m/z* (ESI+) found $[M+Na]^+$ 488.2601; $C_{29}H_{39}NNaO_2S^+$ requires 488.2594.

2-Methylpent-1-en-3-yl 2-phenylacetate, 140

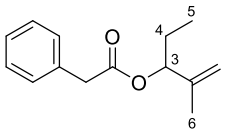

EtMgBr (24.0 mL, 3 M in Et_2O, 72 mmol, 1.2 equiv.) was added dropwise to a solution of methacryl aldehyde (4.95 mL, 60 mmol, 1.0 equiv.) in Et_2O (100 mL) at 0 °C. The reaction mixture was stirred at 0 °C for 2 h and then H_2O (30 mL) was added. The organic phase was separated, washed with H_2O (60 mL) and brine (60 mL), dried ($MgSO_4$), filtered and carefully concentrated *in vacuo* (≥ 250 mbar at 40 ºC) to give a solution of 2-methylpent-1-en-3-ol (6.67 g, 83% in Et_2O [determined by ^1H NMR spectroscopy], 55.3 mmol, 92%).

To a solution of 2-methylpent-1-en-3-ol (2.71 g, 83% in Et_2O, 22.5 mmol, 1.0 equiv.) was added CH_2Cl_2 (50 mL), the solution cooled was to 0 °C, and pyridine (2.13 mL, 27.0 mmol, 1.2 equiv.) was added followed, dropwise, by phenylacetyl chloride (3.81 mL, 24.7 mmol, 1.1 equiv.). The reaction mixture was stirred at 0 °C for 2 h and then H_2O (40 mL) was added. The organic phase was separated, washed with brine (40 mL), dried ($MgSO_4$), filtered and concentrated *in vacuo*. The resulting crude material was purified by column chromatography (19:1 hexanes/*t*-BuOMe) to give **140** (4.43 g, 20.3 mmol,

90%) as a colourless oil; $\mathbf{R_f}$ 0.70 (9:1, hexanes/EtOAc); $\boldsymbol{\delta_H}$ (400 MHz, $CDCl_3$) 7.36–7.21 (5H, m, Ph*H*), 5.10 (1H, t, *J* = 6.6 Hz, H3), 4.89–4.82 (2H, m, H1), 3.63 (2H, s, CH_2Ph), 1.71–1.49 (2H, m, H4), 1.64 (3H, s, H6), 0.82 (3H, t, *J* = 7.4 Hz, H5); $\boldsymbol{\delta_C}$ (100 MHz, $CDCl_3$) 170.8, 142.7, 134.2, 129.2, 128.5, 127.0, 112.8, 78.9, 41.7, 25.5, 18.0, 9.5; **IR** (thin film) ν_{max}/cm^{-1} 2971, 1734. **HRMS** *m/z* (ESI+) found $[M+Na]^+$ 241.1200; $C_{14}H_{18}NaO_2^+$ requires 241.1204.

(*E*)-4-Methyl-2-phenylhept-4-enoic acid, 141

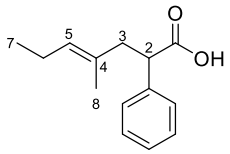

To a solution of LiHMDS (1M in toluene, 3.0 equiv.) in toluene (22 mL) at –78 ºC was added Et_3N (30 equiv.), followed by a solution of 2-methylpent-1-en-3-yl 2-phenylacetate **140** (3.93 g, 18.0 mmol, 1.0 equiv.) in toluene (45 mL). The reaction mixture was allowed to warm to room temperature overnight and was then poured into 2 M aq. NaOH (215 mL). The aqueous layer was separated, washed with *t*-BuOMe (44 mL), cooled to 0 °C, acidified with concentrated HCl and extracted with *t*-BuOMe (3 × 180 mL). These organic washings were combined, dried ($MgSO_4$), filtered and concentrated *in vacuo*. The resulting crude material was purified by column chromatography (10%→30% *t*-BuOMe in hexanes) to give **141** (2.17 g, 9.94 mmol, 55%, >20:1 *E*:*Z*) as a yellow oil; $\boldsymbol{\delta_H}$ (500 MHz, $CDCl_3$) 7.36–7.20 (5H, m, Ph*H*), 5.14 (1H, br t, *J* = 7.1 Hz, H5), 3.76 (1H, dd, *J* = 8.9 and 6.7 Hz, H2), 2.77 (1H, dd, *J* = 13.9 and 8.9 Hz, H3), 2.39 (1H, dd, *J* = 13.9 and 6.7 Hz, H3), 1.90 (2H, app quin., *J* = 7.4 Hz, H6), 1.58 (3H, s, H8), 0.81 (3H, t, *J* = 7.5 Hz, H7); $\boldsymbol{\delta_C}$ (125 MHz, $CDCl_3$) 179.4, 138.3, 130.6, 129.6, 128.6, 128.1, 127.4, 50.2, 43.1, 21.2, 15.8, 14.0; **IR** (thin film) ν_{max}/cm^{-1} 2961, 1703; **HRMS** *m/z* (ESI+) found $[M-H+2Na]^+$ 263.1014; $C_{14}H_{17}Na_2O_2^+$ requires 263.1018.

(*E*)-*tert*-Butyl (3-methyl-1-phenylhex-3-en-1-yl)carbamate, 142

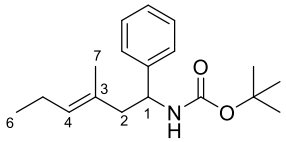

To a solution of (*E*)-4-methyl-2-phenylhept-4-enoic acid **141** (1.00 g, 4.58 mmol, 1.0 equiv.) in *t*-BuOH (6.4 mL) was added Et_3N (0.77 mL, 5.50 mmol, 1.2 equiv.) and DPPA (1.1 mL, 5.04 mmol, 1.1 equiv.). The reaction mixture was heated to 85 °C for 15 h, then cooled to room temperature and quenched with H_2O (1 mL) and $NaHCO_3$ (1 mL, sat. aq.). The *t*-BuOH was evaporated and the residue extracted with *t*-BuOMe (3 × 10 mL). The combined organic layers were washed with H_2O, dried ($MgSO_4$), filtered and concentrated *in vacuo*. The resulting crude material was purified by column chromatography (19:1, hexanes/*t*-BuOMe) to give **142** (462 mg, 1.60 mmol, 35%) as a colourless solid; **m.p.** 75–77 °C; $\mathbf{R_f}$ 0.56 (9:1 hexanes/EtOAc); $\boldsymbol{\delta_H}$ (500 MHz, $CDCl_3$) 7.34–7.18 (5H, m, Ph*H*), 5.16 (1H, br t, *J* = 6.7 Hz, H4), 4.92–4.47 (2H, br m, H1and N*H*), 2.46–2.34 (1H, m, H2), 2.34–2.20 (1H, m, H2), 1.98 (2H, app quin., *J* = 7.4 Hz, H5), 1.61 (3H, s, H7), 1.50–1.14 (9H, br m, *t*-Bu), 0.91 (3H, t, *J* = 7.5 Hz, H6); $\boldsymbol{\delta_C}$ (125 MHz, $CDCl_3$) 155.3, 143.4, 130.6, 130.5, 128.4, 126.9, 126.1, 79.3, 52.8, 47.9, 28.3, 21.2, 15.5, 14.1; **IR** (thin film) ν_{max}/cm^{-1} 3386, 2963, 1683, 1520; **HRMS** *m/z* (ESI+) found $[M+Na]^+$ 312.1937; $C_{18}H_{27}NNaO_2^+$ requires 312.1934.

(*E*)-4-Methyl-*N*-(3-methyl-1-phenylhex-3-en-1-yl)benzenesulfonamide, 143

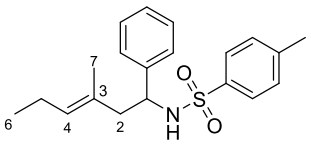

To a flask charged with (*E*)-*tert*-butyl (3-methyl-1-phenylhex-3-en-1-yl)carbamate **142** (450 mg, 1.55 mmol, 1.0 equiv.) was added 4 M HCl in dioxane (1.94 mL, 7.77 mmol, 5.0 equiv.) and the reaction mixture stirred at room temperature for 2 h, then concentrated *in vacuo*. To the residue was added CH_2Cl_2 (5 mL) and Et_3N (1.52 mL, 10.9 mmol, 7.0 equiv.) followed by *p*-toluenesulfonyl chloride (296 mg, 1.55 mmol, 1.0 equiv.) and the reaction mixture stirred at room temperature for 15 h. The reaction mixture was diluted with CH_2Cl_2 (5 mL), washed with $NaHCO_3$ (5 mL, sat. aq.) and 1 M aq. HCl (5 mL), then the organic phase was dried ($MgSO_4$), filtered and concentrated *in vacuo*. The resulting crude

material was purified by column chromatography (17:3 hexanes/*t*-BuOMe) to give **143** (441 mg, 1.28 mmol, 83%) as a pale yellow oil; $\mathbf{R_f}$ 0.29 (4:1 hexanes/EtOAc); $\boldsymbol{\delta_H}$ (500 MHz, $CDCl_3$) 7.52 (2H, d, *J* = 8.3 Hz, Ts*H*), 7.22–7.12 (7H, m, Ts*H* and Ph*H*), 5.18 (1H, br t, *J* = 6.8 Hz, H4), 4.69 (1H, br d, *J* = 3.5 Hz, N*H*), 4.27 (1H, dt, *J* = 9.5 and 4.7 Hz, H1), 2.37 (3H, s, ArCH_3), 2.30 (1H, dd, *J* = 13.8 and 4.9 Hz, H2), 2.20 (1H, dd, *J* = 13.8 and 10.1 Hz, H2), 1.96 (1H, app quin., *J* = 7.4 Hz, H5), 1.33 (3H, s, H7), 0.93 (3H, t, *J* = 7.5 Hz, H6); $\boldsymbol{\delta_C}$ (125 MHz, $CDCl_3$) 143.0, 141.4, 137.0, 132.1, 130.1, 129.2, 128.2, 127.2, 127.2, 126.6, 55.3, 48.8, 21.5, 21.2, 15.0, 14.1; **IR** (thin film) ν_{max}/cm^{-1} 3380, 2961, 1323, 1156; **HRMS** *m/z* (ESI+) found $[M+Na]^+$ 366.1501; $C_{20}H_{25}NNaO_2S^+$ requires 366.1498.

(*E*)-4-Methyl-*N*-(3-methyl-1-phenylhex-3-en-1-yl)-*N*-(oct-1-yn-1-yl)benzenesulfonamide, 131

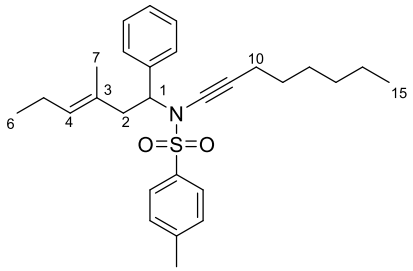

Synthesised from (*E*)-4-methyl-*N*-(3-methyl-1-phenylhex-3-en-1-yl)benzenesulfonamide **143** (100 mg, 0.29 mmol) and 1-bromooct-1-yne **98a** (110 mg, 0.58 mmol) using **Procedure 5**. The resulting crude material was purified by column chromatography (0%→5% *t*-BuOMe in hexanes) to give **131** (65 mg, 0.14 mmol, 50%) as a yellow oil; $\mathbf{R_f}$ 0.46 (9:1 hexanes / EtOAc); $\boldsymbol{\delta_H}$ (500 MHz, $CDCl_3$) 7.51 (2H, d, *J* = 8.2 Hz, Ts*H*), 7.30–7.23 (2H, m, Ph*H*), 7.21–7.14 (3H, m, Ph*H*), 7.11 (2H, d, *J* = 8.2 Hz, Ts*H*), 5.16 (1H, t, *J* = 7.1 Hz, H4), 5.08 (1H, dd, *J* = 9.0 and 6.2 Hz, H1), 2.70 (1H, dd, *J* = 13.9 and 9.1 Hz, H2), 2.43 (1H, dd, *J* = 13.9 and 6.1 Hz, H2), 2.35 (3H, s, ArCH_3), 2.32 (2H, t, *J* = 6.9 Hz, H10), 1.95–1.78 (2H, m, H5), 1.58 (3H, s, H7), 1.49 (2H, app quin., *J* = 7.2 Hz, H11), 1.40–1.20 (6H, m, H12–14), 0.89 (3H, t, *J* = 7.0 Hz, H15), 0.83 (3H, t, *J* = 7.5 Hz, H6); $\boldsymbol{\delta_C}$ (125 MHz, $CDCl_3$) 143.6, 139.6, 135.6, 131.0, 129.1, 129.0, 128.1, 127.6 (2C), 127.2, 73.2, 71.1, 61.2, 44.0, 31.4, 29.0, 28.5, 22.6, 21.5, 21.2, 18.7, 15.7, 14.1, 13.9; **IR** (thin film) ν_{max}/cm^{-1} 2928, 2254, 1363, 1167; **HRMS** *m/z* (ESI+) found $[M+H]^+$ 452.2614; $C_{28}H_{38}NO_2S^+$ requires 452.2618.

_N_-(2-(Cyclohex-1-en-1-yl)-1-phenylethyl)-4-methylbenzenesulfonamide, 146

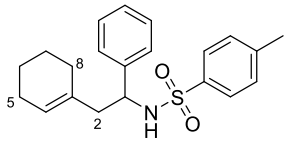

Synthesised from *tert*-butyl (2-(cyclohex-1-en-1-yl)-1-phenylethyl)(tosyl)carbamate **145** (450 mg, 0.99 mmol, 1.0 equiv.) using **Procedure 4**. The resulting crude material was purified by column chromatography (20%→30% Et_2O in petroleum ether) to give **146** (267 mg, 0.75 mmol, 76%) as a colourless solid; **m.p.** 112–114 °C; $\mathbf{R_f}$ 0.45 (7:3 petroleum ether/EtOAc); $\mathbf{\delta_H}$ (400 MHz, $CDCl_3$) 7.53 (2H, d, *J* = 8.3 Hz, Ts*H*), 7.24–7.11 (7H, m, Ts*H* and Ph*H*), 5.50–5.43 (1H, br m, H4), 4.70 (1H, br d, *J* = 3.6 Hz, N*H*), 4.25 (1H, ddd, *J* = 9.5, 5.4 and 3.6 Hz, H1), 2.37 (3H, s, ArCH_3), 2.29–2.14 (2H, m, H2), 2.04–1.88 (2H, m, H8), 1.73–1.60 (1H, m, H5), 1.59–1.38 (5H, m, H5–7); $\mathbf{\delta_C}$ (100 MHz, $CDCl_3$) 134.0, 141.5, 137.0, 133.4, 129.2, 128.2, 127.2, 127.2, 126.8, 126.5, 55.3, 47.4, 27.4, 25.2, 22.5, 22.0, 21.4; **IR** (thin film) ν_{max}/cm^{-1} 3279, 2925, 1323, 1159; **HRMS** *m/z* (ESI+) found $[M+Na]^+$ 378.1498; $C_{21}H_{25}NNaO_2S^+$ requires 378.1498.

_N_-(2-(Cyclohex-1-en-1-yl)-1-phenylethyl)-4-methyl-_N_-(oct-1-yn-1-yl)benzenesulfonamide, 133

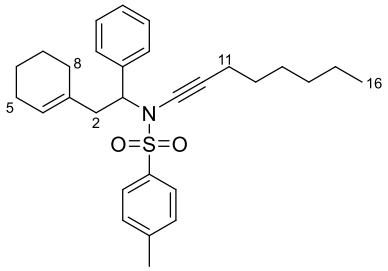

Synthesised from *N*-(2-(cyclohex-1-en-1-yl)-1-phenylethyl)-4-methylbenzenesulfonamide **146** (100 mg, 0.29 mmol) and 1-bromooct-1-yne **98a** (103 mg, 0.54 mmol) using **Procedure 5**. The resulting crude material was purified by column chromatography (17:3, petroleum ether / Et_2O) to give **133** (129 mg, 0.27 mmol, 75%) as a yellow oil; $\mathbf{R_f}$ 0.62 (4:1 hexanes/EtOAc); $\mathbf{\delta_H}$ (400 MHz, C_6D_6) 7.73 (2H, d, *J* = 8.2 Hz, Ts*H*), 7.41 (2H, d, *J* = 7.1 Hz, Ph*H*), 7.09–6.94 (3H, m, 2×Ph*H*), 6.66 (2H, d, *J* = 8.2 Hz, m Ts*H*), 5.70–5.64 (1H, br m, H4), 5.47 (1H, dd, *J* = 9.3 and 6.1 Hz, H1), 2.91 (1H, dd, *J* = 14.1 and 9.3 Hz, H2′), 2.49 (1H, dd, *J* = 14.1 and 5.8 Hz, H2″), 2.17–2.03 (1H, m, H5), 2.13 (2H, t, *J* = 6.8 Hz, H11), 1.99–1.84 (1H, m, H5), 1.81 (3H, s, ArCH_3), 1.65–1.30 (6H, m, H6, H7, H12), 1.30–1.07 (6H,

m, H13–15), 0.86 (3H, t, *J* = 7.1 Hz, H16); **δC** (100 MHz, $CDCl_3$) 143.4, 140.6, 137.0, 133.3, 129.2, 128.5, 128.2, 127.9, 127.7, 125.7, 73.4, 72.4, 61.5, 43.1, 31.7, 29.4, 28.8, 28.5, 25.7, 23.3, 23.0, 22.6, 21.1, 19.0, 14.3; **IR** (thin film) ν_{max}/cm^{-1} 2930, 2252, 1364, 1167; **HRMS** *m/z* (ESI+) found $[M+Na]^+$ 486.2441; $C_{29}H_{37}NNaO_2S^+$ requires 486.2437.

(*E*)-*N*-(Hex-3-en-1-yl-3-d)-4-methylbenzenesulfonamide, (*E*)-d$_1$-154

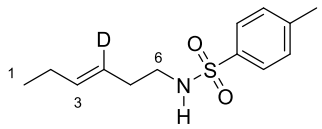

To a stirred suspension of propyltriphenylphosphonium bromide (1.29 g, 3.35 mmol, 5.1 equiv.) in dry THF (2.2 mL), was added NaHMDS (1 M in THF, 3.3 mL, 3.29 mmol, 5.0 equiv.). The reaction mixture was stirred for 1 h at 0 °C, then cooled to –78 °C. To this cooled solution was added a solution of 4-methyl-*N*-(3-oxopropyl-3-d)benzenesulfonamide d$_1$-**96** (150 g, 0.66 mmol, 1.0 equiv.) in dry THF (2.2 mL). The reaction mixture was then stirred for 2.5 h at –78 °C, and subsequently quenched with water (10 mL) and warmed to room temperature. The aqueous phase was extracted with EtOAc (3 × 10 mL). The combined organic layers were dried over $MgSO_4$, filtered, concentrated *in vacuo*, and purified by column chromatography (3:2 petroleum ether / EtOAc) to give (*E*)-d$_1$-**154** (121 mg, 0.48 mmol, 64%) as a colourless oil; **R$_f$** 0.35 (7:3 petroleum ether / EtOAc); **δH** (400 MHz, $CDCl_3$) 7.78 (2H, d, *J* = 8.2 Hz, Ts*H*), 7.34 (2H, d, *J* = 8.2 Hz, Ts*H*), 5.48 (1H, t, *J* = 6.2 Hz, H3), 5.00 (1H, t, *J* = 6.0 Hz NH), 2.98 (2H, dt, *J* = 6.1 and 6.8 Hz, H6), 2.45 (3H, s, C*H*$_3$Ar), 2.15 (2H, t, *J* = 6.8 Hz, H5), 1.98 (2H, app quin, *J* = 7.3 Hz, H2), 0.93 (3H, t, *J* = 7.6 Hz, H1); **δC** (100 MHz, $CDCl_3$) 143.3, 137.1, 135.7, 129.7, 127.2, 124.1 (t, *J* = 23.1 Hz), 42.8, 32.4, 25.5, 21.5, 13.6; **IR** (thin film) ν_{max}/cm^{-1} 3275, 2970, 2920, 1595, 1320; **HRMS** *m/z* (ESI+) found $[M+Na]^+$ 277.1088; $C_{13}H_{18}DNNaO_2S^+$ requires 277.1091.

(*E*)-*N*-(Hex-3-en-1-yl-3-d)-4-methyl-*N*-(oct-1-yn-1-yl)benzenesulfonamide, (*E*)-d$_1$-151a

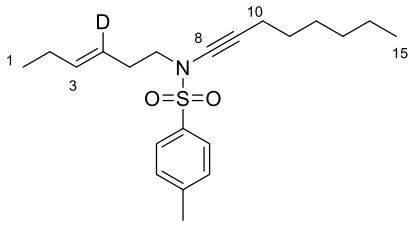

Synthesised from (*E*)-*N*-(hex-3-en-1-yl-3-d)-4-methylbenzenesulfonamide (*E*)-d$_1$-**154** (75 mg, 0.29 mmol) and 1-bromooct-1-yne **98a** (67 mg, 0.35 mmol) using **Procedure 5**. The resulting crude material was purified by column chromatography (9:1 petroleum ether / Et_2O) to afford (*E*)-d$_1$-**151a** (75 mg, 0.21 mmol, 71%) as a colourless oil; $\mathbf{R}_f$ 0.63 (4:1 petroleum ether / Et_2O); $\boldsymbol{\delta}_\mathbf{H}$ (400 MHz, $CDCl_3$) 7.77 (2H, d, *J* = 8.1 Hz, Ts*H*), 7.32 (2H, d, *J* = 8.1 Hz, Ts*H*), 5.50 (1H, m, H3), 3.28 (2H, t, *J* = 7.4 Hz, H6), 2.44 (3H, s, C*H*$_3$Ar), 2.30–2.24 (4H, m, H5 and H10), 2.04–1.93 (2H, m, H2), 1.47 (2H, quin, *J* = 7.3 Hz, H11), 1.36–1.28 (6H, m, H12–14), 0.94 (3H, t, *J* = 7.4 Hz, H1), 0.88 (3H, t, *J* = 7.0 Hz, H15); $\boldsymbol{\delta}_\mathbf{C}$ (100 MHz, $CDCl_3$) 144.3, 135.3, 135.0, 129.7, 127.8, 123.9 (t, *J* = 23.1 Hz), 73.1, 70.6, 51.5, 31.5, 31.0, 29.1, 28.6, 25.7, 22.7, 21.8, 18.6, 14.2, 13.8; **IR** (thin film) ν_{max}/cm^{-1} 2930, 2253, 1364, 1168; **HRMS** *m/z* (ESI+) found $[M+Na]^+$ 385.2027; $C_{21}H_{30}DNNaO_2S^+$ requires 385.2030.

(*Z*)-*N*-(Hex-3-en-1-yl-3-d)-4-methylbenzenesulfonamide, (*Z*)-d$_1$-154

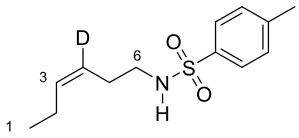

To a stirred suspension of propyltriphenylphosphonium bromide (1.29 g, 3.35 mmol, 5.1 equiv.) in THF (2.2 mL), was added KHMDS (1 M in THF, 3.3 mL, 3.29 mmol, 5.0 equiv.). The reaction mixture was stirred for 1 h at 0 °C, then cooled to –78 °C. To this cooled solution was added a solution of 4-methyl-*N*-(3-oxopropyl-3-d)benzenesulfonamide d$_1$-**96** (150 mg, 0.66 mmol, 1.0 equiv.) in THF (2.2 mL). The reaction mixture was then stirred for 2.5 h at –78 °C, and subsequently quenched with water (10 mL). The aqueous phase was extracted with EtOAc (3 × 10 mL). The combined organic layers were dried over $MgSO_4$, filtered, concentrated *in vacuo*, and purified by column chromatography (10→20%, EtOAc / petroleum ether) to give (*Z*)-d$_1$-**154** (121 mg, 0.48 mmol, 72%) as a pale yellow oil; $\mathbf{R}_f$ = 0.36 (CH_2Cl_2); $\boldsymbol{\delta}_\mathbf{H}$ (400 MHz, $CDCl_3$) 7.74 (2H, d, *J* = 8.2 Hz, Ts*H*), 7.30 (2H, d, *J* = 8.2 Hz, Ts*H*), 5.48 (1H,

t, *J* = 7.3 Hz, H3), 4.50 (1H, t, *J* = 5.9 Hz N*H*), 2.96 (2H, dt, *J* = 6.0 and 6.8 Hz, H6), 2.42 (3H, s, C*H*$_3$Ar), 2.19 (2H, t, *J* = 6.8 Hz, H5), 1.97 (2H, app quin, *J* = 7.5 Hz, H2), 0.93 (3H, t, *J* = 7.5 Hz, H1); **δ$_C$** (100 MHz, $CDCl_3$) 143.5, 137.1, 135.5, 129.9, 127.3, 123.8 (t, *J* = 23.6 Hz), 42.9, 27.4, 21.7, 20.7, 14.3; **IR** (thin film) ν_{max}/cm^{-1} 3290, 2963, 2875, 1658, 1440, 1320; **HRMS** *m/z* (ESI+) found $[M+H]^+$ 255.12718; $C_{13}H_{19}DNO_2S^+$ requires 255.1278.

(*Z*)-*N*-(Hex-3-en-1-yl-3-d)-4-methyl-*N*-(oct-1-yn-1-yl)benzenesulfonamide, (*Z*)-d$_1$-151a

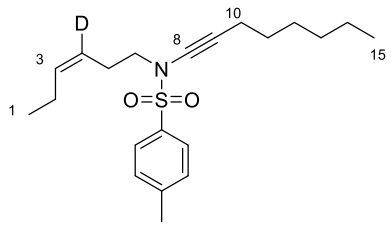

Synthesised from (*Z*)-*N*-(hex-3-en-1-yl-3-d)-4-methylbenzenesulfonamide (*Z*)-d$_1$-**154** (*Z*:*E*, 20:1; >98% deuterium incorporation by ^{1}H NMR spectroscopy) (75 mg, 0.29 mmol) and 1-bromooct-1-yne **98a** (67 mg, 0.35 mmol) using **Procedure 5**. The resulting crude material was purified by column chromatography (9:1 petroleum ether / Et_2O) to afford (*Z*)-d$_1$-**151a** (*Z*:*E*, 20:1; > 98% deuterium incorporation by ^{1}H NMR spectroscopy, 80 mg, 0.21 mmol, 76%) as a colourless oil; **R$_f$** 0.63 (4:1 petroleum ether / Et_2O); **δ$_H$** (400 MHz, $CDCl_3$) 7.77 (2H, d, *J* = 8.2 Hz, Ts*H*), 7.32 (2H, d, *J* = 8.2 Hz, Ts*H*), 5.46 (1H, t, *J* = 7.2 Hz, H3), 3.26 (2H, t, *J* = 7.3 Hz, H6), 2.43 (3H, s, C*H*$_3$Ar), 2.34 (2H, t, *J* = 7.3 Hz, H10), 2.26 (2H, t, *J* = 7.3 Hz, H5), 2.00 (2H, app quin, *J* = 7.5 Hz, H11), 1.47 (app quin, *J* = 7.5 Hz, H2), 1.38-1.24 (6H, m, H12–14), 0.94 (3H, t, *J* = 7.5 Hz, H1), 0.88 (3H, t, *J* = 6.9 Hz, H15); **δ$_C$** (100 MHz, $CDCl_3$) 144.2, 134.8, 134.6, 129.6, 127.6, 123.4 (t, *J* = 23.6 Hz), 72.9, 70.4, 51.2, 31.4, 28.9, 28.5, 25.6, 22.6, 21.6, 20.6, 18.5, 14.2, 14.0; **IR** (thin film) ν_{max}/cm^{-1} 2931, 2254, 1364, 1169; **HRMS** *m/z* (ESI+) found $[M+Na]^+$ 385.2027; $C_{21}H_{30}DNNaO_2S^+$ requires 385.2030.

tert-Butyl (_Z_)-hex-3-en-1-yl(tosyl)carbamate, (_Z_)-225

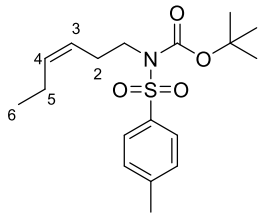

Synthesised from (*Z*)-hex-3-en-1-ol (5.00 g, 49.9 mmol) using **Procedure 2**. The resulting crude material was filtered through a silica pad (slurry packed in CH_2Cl_2) using CH_2Cl_2 (750 mL), concentrated *in vacuo* to approx. 300 mL, washed with 15% aq. H_2O_2 (600 mL), sat. aq. Na_2SO_3 (600 mL) and H_2O (500 mL). The H_2O layer was back extracted with CH_2Cl_2 (200 mL). The combined organic layers were dried ($MgSO_4$), concentrated *in vacuo* to 100 mL, filtered through a silica pad (slurry packed in CH_2Cl_2) using CH_2Cl_2 (300 mL) and then concentrated *in vacuo* to dryness to give (*Z*)-**225** as a colourless solid (15.20 g, 43.0 mmol, 68%); $\mathbf{R_f}$ = 0.41 (4:1, petroleum ether:EtOAc); $\mathbf{\delta_H}$ (400 MHz, $CDCl_3$) 7.78 (2H, d, *J* = 8.2 Hz, Ts*H*), 7.28 (2H, d, *J* = 8.2 Hz, Ts*H*), 5.55–5.46 (1H, m, H4), 5.34 (1H, dtt, *J* = 10.7, 7.5, 1.3 Hz, H3), 3.83–3.76 (2H, m, H1), 2.48 (2H, ap. q, *J* = 7.5 Hz, H2), 2.42 (3H, s, ArCH_3), 2.08 (2H, ap. quin.d, *J* = 7.5 and 1.3 Hz, H5), 1.33 (9H, s, C(CH_3)$_3$), 0.96 (3H, t, *J* = 7.5 Hz, CH3–6); $\mathbf{\delta_C}$ (100 MHz, $CDCl_3$) 150.9, 144.0, 137.5, 134.8, 129.1, 127.8, 124.0, 84.0, 46.5, 28.1, 27.8, 21.5, 20.5, 14.2. Data are consistent with literature values.[103]

(_Z_)-_N_-(Hex-3-en-1-yl)-4-methylbenzenesulfonamide, (_Z_)-153

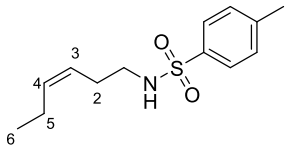

Synthesised from (Z)-*tert*-butyl hex-3-en-1-yl(tosyl)carbamate (*Z*)-**225** (7.32 g, 20.7 mmol) using **Procedure 3** to give (*Z*)-**153** as a pale yellow oil (5.14 g, 20.2 mmol, 98%) which was used without further purification; $\mathbf{R_f}$ = 0.40 (4:1, petroleum ether:EtOAc); $\mathbf{\delta_H}$ (400 MHz, $CDCl_3$) 7.74 (2H, d, *J* = 8.2 Hz, Ts*H*), 7.29 (2H, d, *J* = 8.2 Hz, Ts*H*), 5.52–5.42 (1H, m, H4), 5.14 (1H, dtt, *J* = 10.9, 7.3, 1.4 Hz, H3), 4.68 (1H, br. s, N*H*), 2.94 (2H, ap. q, *J* = 6.9 Hz, H1), 2.42 (3H, s, ArCH_3), 2.19 (2H, ap. q, *J* = 6.8 Hz, H2), 1.95 (2H, ap. quin.d, *J* = 7.5 and 1.4 Hz, H5), 0.91 (3H, t, *J* = 7.5 Hz, CH_3); $\mathbf{\delta_C}$ (100

MHz, $CDCl_3$) 143.3, 136.9, 135.3, 129.6, 127.1, 124.0, 42.7, 27.2, 21.4, 20.5, 14.1. Data are consistent with literature values.[105]

(*Z*)-*N*-(Hex-3-en-1-yl)-4-methyl-*N*-(oct-1-yn-1-yl)benzenesulfonamide, (*Z*)-151a

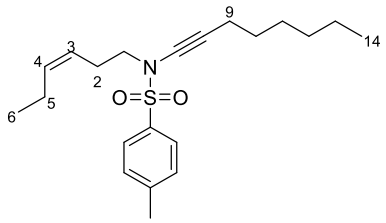

Synthesised from (Z)-*N*-(hex-3-en-1-yl)-4-methylbenzenesulfonamide (*Z*)-**225** (1.00 g, 3.95 mmol) and 1-bromooct-1-yne **98a** (896 mg, 4.74 mmol) using **Procedure 5**. The resulting crude material was purified by column chromatography (10→15% Et_2O in petroleum ether) to give (*Z*)-**151a** as a colourless oil (1.34 g, 3.71 mmol, 94%); $\mathbf{R_f}$ = 0.53 (5:1, petroleum ether:EtOAc); $\boldsymbol{\delta_H}$ (400 MHz, $CDCl_3$) 7.78 (2H, d, *J* = 8.2 Hz, Ts*H*), 7.32 (2H, d, *J* = 8.2 Hz, Ts*H*), 5.45 (1H, dtt, *J* = 10.7, 7.3, 1.4 Hz, H4), 5.27 (1H, dtt, *J* = 10.7, 7.5, 1.5 Hz, H3), 3.29–3.23 (2H, m, H1), 2.44 (3H, s, ArCH_3), 2.35 (2H, ap. q, *J* = 7.5 Hz, H2), 2.26 (2H, t, *J* = 6.9 Hz, H9), 2.01 (2H, ap. quin.d, *J* = 7.5 and 1.3 Hz, H5), 1.52–1.42 (2H, m, H10), 1.40–1.20 (6H, m, H11–13), 0.94 (3H, t, *J* = 7.6 Hz, H6), 0.88 (3H, t, *J* = 6.9 Hz, H14); $\boldsymbol{\delta_C}$ (100 MHz, $CDCl_3$) 144.2, 134.8, 129.5, 127.6, 123.7, 72.9, 70.4, 51.1, 31.3, 28.9, 28.5, 25.7, 22.6, 21.6, 20.6, 18.5, 14.2, 14.0; **IR** (thin film) ν_{max}/cm^{-1} 2933, 2254, 1365, 1169; **HRMS** *m/z* (ESI+) found $[M+Na]^+$ 384.1955; $C_{21}H_{31}NNaO_2S^+$ requires 384.1968.

_N_-((_E_)-1-Bromooct-1-en-1-yl)-_N_-((_Z_)-hex-3-en-1-yl)-4-methylbenzenesulfonamide, (_Z_)-231a

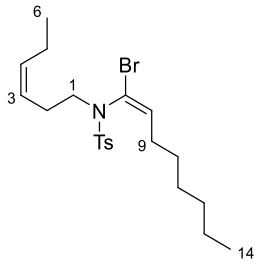

Synthesised from (*Z*)-*N*-(hex-3-en-1-yl)-4-methyl-*N*-(oct-1-yn-1-yl)benzenesulfonamide (*Z*)-**151a** (18.0 mg, 0.050 mmol) using **Procedure 7**.

Method 1

The product (*Z*)-**231a** was obtained as a colourless oil (19.2 mg, 0.045 mmol, 89%); $\mathbf{R}_f$ = 0.44 (9:1, petroleum ether:Et_2O); $\boldsymbol{\delta}_\mathbf{H}$ (400 MHz, C_6D_6) 7.83 (2H, d, *J* = 8.2 Hz, Ts*H*), 6.77 (2H, d, *J* = 8.2 Hz, Ts*H*), 6.09 (1H, t, *J* = 15.3 Hz, H8), 5.46 (1H, m, H3), 5.31 (1H, m, H4), 3.73 (1H, m, H1′), 2.95 (1H, m, H1″), 2.41 (2H, m, H2), 2.29 (2H, m, H9), 1.96 (2H, quin, J= 7.16 Hz, H5), 1.87 (3H, s, ArCH_3), 1.45–1.10 (8H, m, H10–13), 0.93–0.84 (6H, m, H6 and H14); $\boldsymbol{\delta}_\mathbf{C}$ (100 MHz, C_6D_6) 144.0, 142.7, 135.9, 135.1, 129.6, 129.0, 125.0, 118.2, 48.8, 32.0, 31.5, 31.4, 29.4, 28.8, 26.0, 23.0, 21.2, 14.3; **HRMS** *m/z* (ESI+) found $[M–H]^+$ 441.1338; $C_{21}H_{32}NO_2BrS^+$ requires 441.1337.

_N_-((_E_)-1-Bromooct-1-en-1-yl)-_N_-((_E_)-hex-3-en-1-yl)-4-methylbenzenesulfonamide, (_E_)-231a

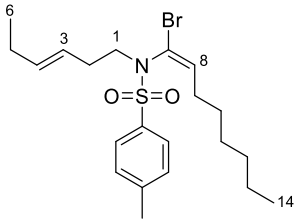

Synthesised from (*E*)-*N*-(hex-3-en-1-yl)-4-methyl-*N*-(oct-1-yn-1-yl)benzenesulfonamide (*E*)-**151a** (18.0 mg, 0.050 mmol) using **Procedure 7**.

Method 1

The product (*E*)-**231a** was obtained as a colourless oil (18.9 mg, 0.044 mmol, 87%); $\mathbf{R}_f$ = 0.43 (9:1, petroleum ether:Et_2O); $\boldsymbol{\delta}_\mathbf{H}$ (400 MHz, C_6D_6) 7.83 (2H, d, *J* = 8.2 Hz, Ts*H*), 6.77 (2H, d, *J* = 8.2 Hz, Ts*H*), 6.09 (1H, t, *J* = 15.3 Hz, H8), 5.46 (1H, m, H3), 5.31 (1H, m, H4), 3.73 (1H, m, H1′), 2.95 (1H, m, H1″), 2.28 (2H, m, H2), 2.25 (2H, m, H9), 1.90 (2H, p, J= 7.16 Hz, H5), 1.87 (3H, s, ArCH_3), 1.45–

1.10 (8H, m, H10–13), 0.93–0.84 (6H, m, H6 and H14); **δ_C** (100 MHz, C_6D_6) 144.0, 142.6, 135.9, 135.1, 129.6, 129.0, 125.0, 118.2, 48.8, 32.0, 31.5, 31.4, 29.4, 28.8, 26.0, 23.0, 21.2, 14.3, 13.8; **HRMS** *m/z* (ESI+) found $[M–H]^+$ 441.1339; $C_{21}H_{32}NO_2BrS^+$ requires 441.1337.

Method 2

The product (*E*)-**231a** was obtained as a colourless oil (21.8 mg, 0.049 mmol, 99%). Data are in accordance with those obtained from **Method 1**.

(*E*)-*N*-(1-Bromooct-1-en-1-yl)-*N*-(but-3-en-1-yl)-4-methylbenzenesulfonamide, 231c

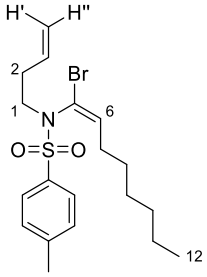

Synthesised from *N*-(but-3-en-1-yl)-4-methyl-*N*-(oct-1-yn-1-yl)benzenesulfonamide **92** (200 mg, 0.60 mmol) using **Procedure 7**.

Method 1

The product **231c** was obtained as a colourless oil (199 mg, 0.48 mmol, 80%); **R_f** = 0.42 (9:1, petroleum ether:Et_2O); **δ_H** (400 MHz, C_6D_6) 7.81 (2H, d, *J* = 8.2 Hz, Ts*H*), 6.79 (2H, d, *J* = 8.2 Hz, Ts*H*), 6.13 (1H, dt, *J* = 53.9 and 7.5 Hz, H6), 5.67 (1H, m, H3), 5.04 (2H, m, H′ and H″), 3.41 (2H, t, *J* = 6.90 Hz H1), 3.33 (2H, ap. q, *J* = 7.2 Hz, H2), 2.45–2.09 (4H, m, H7 and H8), 1.87 (3H, s, Ar-CH_3), 1.38–1.19 (6H, m, H9–11), 0.86 (3H, m, H12); **δ_c** (100 MHz, C_6D_6) 137.5, 135.9, 133.8, 129.4, 128.3, 125.9, 116.7, 111.7, 44.1, 31.9, 30.8, 29.3, 28.9, 23.7, 22.7, 21.0, 14.1; **HRMS** *m/z* (ESI+) found $[M–H]^+$ 413.1026; $C_{19}H_{29}NO_2SBr^+$ requires 413.1024

(*E*)-*N*-(But-3-en-1-yl)-*N*-(1-iodooct-1-en-1-yl)-4-methylbenzenesulfonamide, 231c′

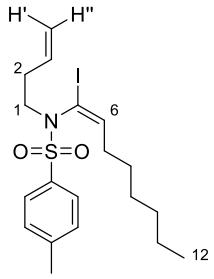

Synthesised from *N*-(but-3-en-1-yl)-4-methyl-*N*-(oct-1-yn-1-yl)benzenesulfonamide **92** (100 mg, 0.30 mmol) using **Procedure 7**.

Method 2

The product **231c′** was obtained as a pale yellow oil (135 mg, 0.29 mmol, >98%); $\mathbf{R}_f$ = 0.41 (9:1, petroleum ether:Et_2O); $\boldsymbol{\delta}_\mathbf{H}$ (400 MHz, $CDCl_3$) 7.68 (2H, d, *J* = 8.2 Hz, Ts*H*), 7.25 (2H, d, *J* = 8.2 Hz, Ts*H*), 5.87 (1H, dt, *J* = 17.2 and 6.7 Hz, H6), 5.67 (1H, m, H3), 5.04 (2H, m, H′ and H″), 3.53 (2H, t, *J* = 7.5 Hz, H1), 2.58–2.48 (2H, ap. q, *J* = 7.2 Hz, H2), 2.43 (3H, s, ArCH_3), 1.83–1.78 (2H, t, *J* = 6.9 Hz, H7), 1.63–1.54 (2H, m, H8), 1.49–1.18 (6H, m, H9–11), 0.88 (3H, t, *J* = 6.8 Hz, H12); $\boldsymbol{\delta}_\mathbf{c}$ (100 MHz, $CDCl_3$) 137.4, 135.8, 134.0, 129.4, 128.1, 120.0, 116.5, 96.1, 46.1, 30.9, 29.8, 29.3, 28.9, 25.5, 22.8, 21.3, 14.1; **HRMS** *m/z* (ESI+) found $[M–H]^+$ 460.0810; $C_{19}H_{27}INO_2S^+$ requires 460.0807.

***tert*-Butyl (*E*)-hex-3-en-1-yl(tosyl)carbamate, (*E*)-225**

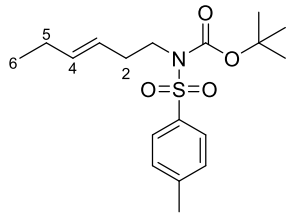

Synthesised from (*E*)-hex-3-en-1-ol (5.00 g, 49.9 mmol) using **Procedure 2**. The resulting crude material was purified by column chromatography (dry loaded, 5%→20% Et_2O in petroleum ether) to give (*E*)-**225** as a colourless solid (15.60 g, 44.1 mmol, 88%); **m.p.** 61–65 °C; $\mathbf{R}_f$ = 0.41 (4:1, petroleum ether:EtOAc); $\boldsymbol{\delta}_\mathbf{H}$ (400 MHz, $CDCl_3$) 7.79 (2H, d, *J* = 8.1 Hz, Ts*H*), 7.30 (2H, d, *J* = 8.1 Hz, m Ts*H*), 5.63–5.53 (1H, m, H4), 5.39 (1H, dtt, *J* = 15.4, 6.8, 1.3 Hz, H3), 3.88–3.80 (2H, m, H1), 2.48–2.39 (2H, m, H2), 2.44 (3H, s, ArCH_3), 2.08 (2H, ap. quin.d, *J* = 7.1, 1.3 Hz, H5), 1.34 (9H, s, $C(CH_3)_3$),

0.97 (3H, t, *J* = 7.5 Hz, H6); δ_C (100 MHz, $CDCl_3$) 150.9, 144.0, 137.6, 135.3, 129.2, 127.8, 124.5, 84.0, 46.9, 33.4, 27.9, 25.6, 21.6, 13.6. Data are consistent with literature values.[103]

(*E*)-*N*-(Hex-3-en-1-yl)-4-methylbenzenesulfonamide, (*E*)-154

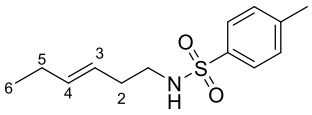

Synthesised from (*E*)-*tert*-butyl hex-3-en-1-yl(tosyl)carbamate (*E*)-**225** (15.15 g, 42.9 mmol) using **Procedure 3** to give (*E*)-**154** as a colourless oil (10.52 g, 41.5 mmol, 97%) which was used without further purification; $\mathbf{R}_f$ = 0.40 (4:1, petroleum ether:EtOAc); δ_H (400 MHz, $CDCl_3$) 7.74 (2H, d, *J* = 8.2 Hz Ts*H*), 7.29 (2H, d, *J* = 8.2 Hz, Ts*H*), 5.45 (1H, dtt, *J* = 15.3, 6.3, 1.1 Hz, H4), 5.17 (1H, dtt, *J* = 15.3, 6.8, 1.1 Hz, H3), 4.79–4.71 (1H, br. m, N*H*), 2.94 (2H, ap. q, *J* = 6.8 Hz, H1), 2.41 (3H, s, ArCH_3), 2.11 (2H, ap. qd, *J* = 6.8 and 1.1 Hz, H2), 1.94 (2H, ap qdd, *J* = 7.5, 6.3, 1.3 Hz, H5), 0.91 (3H, t, *J* = 7.5 Hz, H6); δ_C (100 MHz, $CDCl_3$) 143.2, 136.9, 135.8, 129.6, 127.0, 124.2, 42.6, 32.3, 25.4, 21.4, 13.5. Data are consistent with literature values.[105]

(Bromoethynyl)benzene, 98b

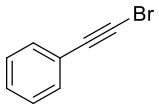

Synthesised from phenylacetylene (5.00 mL, 45.5 mmol) using **Procedure 1**. The resulting crude material was passed through a silica pad (eluting with petroleum ether) to give **98b** as a yellow oil (5.99 g, 33.1 mmol, 73%); $\mathbf{R}_f$ = 0.68 (5:1, petroleum ether:EtOAc); δ_H (400 MHz, $CDCl_3$) 7.48 (2H, dd, *J* = 7.7 and 1.9 Hz, 2×Ph*H*), 7.38–7.29 (3H, m, 3×Ph*H*); δ_C (100 MHz, $CDCl_3$) 132.0, 128.6, 128.3, 122.7, 80.0, 49.7. Data are consistent with literature values.[106]

1-(Bromoethynyl)-4-fluorobenzene, 98c

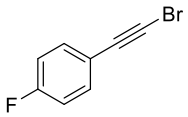

Synthesised from 1-ethynyl-4-fluorobenzene (0.24 mL, 2.08 mmol) using **Procedure 1**. The resulting crude material was passed through a silica pad (eluting with petroleum ether) to give **98c** as a pale yellow oil (250 mg, 1.26 mmol, 61%); $\mathbf{R}_f$ = 0.38 (5:1, petroleum ether:EtOAc); δ_H (500 MHz, $CDCl_3$)

7.49–7.37 (2H, m), 7.07–6.92 (2H, m); **δC** (125 MHz, $CDCl_3$) 162.8 (d, *J* = 249 Hz), 134.0 (d, *J* = 248 Hz), 118.9, (d, *J* = 3.5 Hz), 115.7, (d, *J* = 21.7 Hz), 79.0, 49.6; **δF** (470 MHz, $CDCl_3$) -115.8. Data are consistent with literature values.[107]

1-(Bromoethynyl)-4-methoxybenzene, 98d

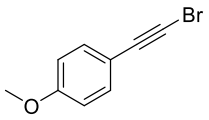

Synthesised from 1-1-ethynyl-4-methoxybenzene (0.52 mL, 4.0 mmol) using **Procedure 1**. The resulting crude material was passed through a silica pad (eluting with petroleum ether) to give **98d** as a yellow solid (0.68 g, 3.2 mmol, 80%); **m.p.** = 45–46 °C; **Rf** = 0.28 (5:1, petroleum ether:EtOAc); **δH** (500 MHz, $CDCl_3$) 7.42–7.31 (2H, m), 6.88–6.75 (2H, m), 3.81 (3H, s, OC*H*$_3$); **δC** (125 MHz, $CDCl_3$) 160.0, 133.5, 114.9, 114.0, 80.0, 55.2, 47.9. Data are consistent with literature values.[107]

(*E*)-*N*-(Hex-3-en-1-yl)-4-methyl-*N*-(oct-1-yn-1-yl)benzenesulfonamide, (*E*)-151a

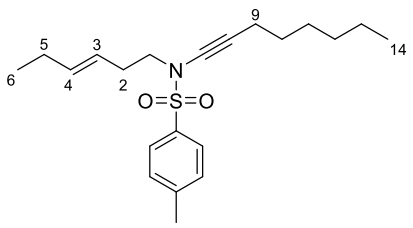

Synthesised from (*E*)-*N*-(hex-3-en-1-yl)-4-methylbenzenesulfonamide (*E*)-**154** (1.00 g, 3.95 mmol) and 1-bromooct-1-yne **98a** (896 mg, 4.74 mmol) using **Procedure 5**. The resulting crude material was purified by column chromatography (10% Et_2O in petroleum ether) to give (*E*)-**151a** as a colourless oil (1.24 g, 3.44 mmol, 87%); **R*f*** = 0.62 (5:1, petroleum ether:EtOAc); **δH** (400 MHz, $CDCl_3$) 7.77 (2H, d, *J* = 8.2 Hz, Ts*H*), 7.32 (2H, d, *J* = 8.2 Hz, Ts*H*), 5.51 (1H, dtt, *J* = 15.3, 6.3, 1.1 Hz, H4), 5.27 (1H, dtt, *J* = 15.3, 6.8, 1.4 Hz, H3), 3.30–3.24 (2H, m, H1), 2.44 (3H, s, ArC*H*$_3$), 2.33–2.25 (2H, m, H2), 2.25 (2H, t, *J* = 7.1 Hz, H9), 2.01–1.91 (2H, m, H5), 1.52–1.42 (2H, m, H10), 1.39–1.22 (6H, m, H11–13), 0.93 (3H, t, *J* = 7.5 Hz, H6), 0.88 (3H, t, *J* = 6.9 Hz, H14); **δC** (100 MHz, $CDCl_3$) 144.1, 135.2, 134.7, 129.5, 127.6, 124.0, 72.9, 70.4, 51.3, 31.3, 31.0, 28.9, 28.4, 25.5, 22.6, 21.6, 18.4, 14.0, 13.6; **IR** (thin film) ν_{max}/cm^{-1} 2930, 2253, 1364, 1168; **HRMS** *m/z* (ESI+) found $[M+Na]^+$ 384.1955; $C_{21}H_{31}NNaO_2S^+$ requires 384.1968.

(*Z*)-*N*-(Hex-3-en-1-yl)-4-methyl-*N*-(phenylethynyl)benzenesulfonamide, (*Z*)-151b

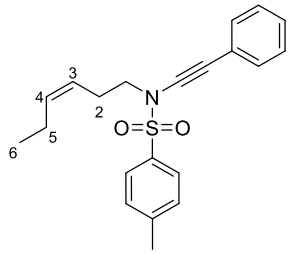

Synthesised from (*Z*)-*N*-(hex-3-en-1-yl)-4-methylbenzenesulfonamide (*Z*)-**154** (1.00 g, 3.95 mmol) and (bromoethynyl)benzene **98b** (1.07 g, 5.92 mmol) using **Procedure 5**. The resulting crude material was purified by column chromatography (10→15% Et_2O in petroleum ether) to give (*Z*)-**151b** as a yellow oil (1.03 g, 2.91 mmol, 75%); $\mathbf{R_f}$ = 0.51 (5:1, petroleum ether:EtOAc); $\mathbf{\delta_H}$ (400 MHz, $CDCl_3$) 7.84 (2H, d, *J* = 8.3 Hz, Ts*H*), 7.40–7.33 (4H, m, Ts*H* and Ph*H*), 7.33–7.26 (3H, m, Ph*H*), 5.48 (1H, dtt, *J* = 10.9, 7.3, 1.3 Hz, H4), 5.27 (1H, dtt, *J* = 10.9, 7.3, 1.5 Hz, H3), 3.42 (2H, t, *J* = 7.4 Hz, H1), 2.49–2.40 (2H, m, H2), 2.45 (3H, s, ArCH_3), 2.04 (2H, ap. quin.d, *J* = 7.4 and 1.5 Hz, H5), 0.95 (3H, t, *J* = 7.5 Hz, H6); $\mathbf{\delta_C}$ (100 MHz, $CDCl_3$) 144.6, 135.0, 134.7, 131.3, 129.7, 128.2, 127.7, 127.6, 123.5, 122.9, 82.2, 70.8, 51.3, 26.0, 21.6, 20.6, 14.2; **IR** (thin film) ν_{max}/cm^{-1} 2963, 2234, 1363, 1168; **HRMS** *m/z* (ESI+) found $[M+Na]^+$ 376.1344; $C_{21}H_{23}NNaO_2S^+$ requires 376.1342.

(*E*)-*N*-(Hex-3-en-1-yl)-4-methyl-*N*-(phenylethynyl)benzenesulfonamide, (*E*)-151b

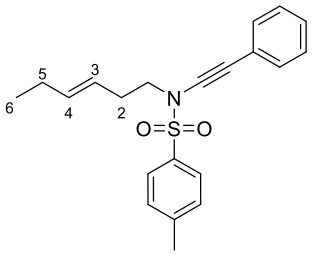

Synthesised from (*E*)-*N*-(hex-3-en-1-yl)-4-methylbenzenesulfonamide (*E*)-**154** (1.00 g, 3.95 mmol) and (bromoethynyl)benzene **98b** (1.07 g, 5.92 mmol) using **Procedure 5**. The resulting crude material was purified by column chromatography (8→10% Et_2O in petroleum ether) to give (*E*)-**151b** as a yellow oil (1.32 g, 3.73 mmol, 95%); $\mathbf{R_f}$ = 0.51 (5:1, petroleum ether:EtOAc); $\mathbf{\delta_H}$ (400 MHz, $CDCl_3$) 7.84 (2H, d, *J* = 8.3 Hz, Ts*H*), 7.40–7.33 (4H, m, Ts*H* and Ph*H*), 7.33–7.26 (3H, m, Ph*H*), 5.55 (1H, dtt, *J* = 15.3, 6.3, 1.3 Hz, H4), 5.31 (1H, dtt, *J* = 15.3, 6.8, 1.3 Hz, H3), 3.43 (2H, ap t, *J* = 7.4 Hz, H1), 2.45 (3H, s, ArCH_3), 2.38 (2H, br. ap. q, *J* = 7.1 Hz, H2), 1.97 (2H, m, H5), 0.94 (3H, t, *J* = 7.5 Hz, CH_3); $\mathbf{\delta_C}$ (100

MHz, $CDCl_3$) 144.5, 135.6, 134.7, 131.3, 129.7, 128.2, 127.7, 127.6, 123.8, 122.9, 82.3, 70.8, 51.5, 31.2, 25.6, 21.6, 13.6; **IR** (thin film) ν_{max}/cm^{-1} 2962, 2234, 1364, 1168; **HRMS** *m/z* (ESI+) found $[M+Na]^+$ 376.1331; $C_{21}H_{23}NNaO_2S^+$ requires 376.1342.

(*Z*)-*N*-((4-Fluorophenyl)ethynyl)-*N*-(hex-3-en-1-yl)-4-methylbenzenesulfonamide, (*Z*)-151c

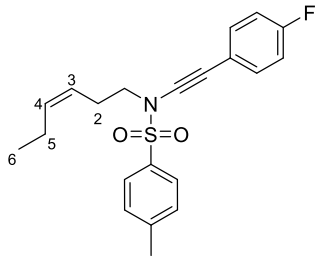

Synthesised from (*Z*)-*N*-(hex-3-en-1-yl)-4-methylbenzenesulfonamide (*Z*)-**154** (250 mg, 0.98 mmol) and 1-(bromoethynyl)-4-fluorobenzene **98c** (0.27 mg, 5.92 mmol) using **Procedure 5**. The resulting crude material was purified by column chromatography (10→20% Et_2O in petroleum ether) to give (*Z*)-**151c** as a yellow oil (228 mg, 0.62 mmol, 63%); $\mathbf{R_f}$ = 0.31 (5:2, petroleum ether:EtOAc); $\mathbf{\delta_H}$ (400 MHz, $CDCl_3$) 7.84 (2H, d, *J* = 8.3 Hz, Ts*H*), 7.40–7.33 (4H, m, Ts*H*, Ph*H*), 7.07–6.93 (2H, m, Ph*H*), 5.49 (1H, dtt, *J* = 10.9, 7.3, 1.3 Hz, H4), 5.28 (1H, dtt, *J* = 10.9, 7.3, 1.5 Hz, H3), 3.45 (2H, ap t, *J* = 7.4 Hz, H1), 2.46 (3H, s, ArCH_3), 2.44–2.40 (2H, m, H2), 2.05 (2H, ap. quin.d, *J* = 7.4 and 1.5 Hz, H5), 0.94 (3H, t, *J* = 7.5 Hz, H6); $\mathbf{\delta_C}$ (100 MHz, $CDCl_3$) 162.3 (d, *J* = 249.0 Hz), 144.3, 135.8, 134.3, 133.6 (d, *J* = 234.0 Hz), 129.5, 127.6, 123.0, 119.0 (d, *J* = 4.0 Hz), 115.6 (d, *J* = 22.0 Hz), 82.1, 70.2, 51.3, 31.1, 25.6, 21.3, 13.6; $\mathbf{\delta_F}$ (376 MHz, $CDCl_3$) -115.6; **IR** (thin film) ν_{max}/cm^{-1} 2963, 2230, 1368, 1164 1120; **HRMS** *m/z* (ESI+) found $[M+Na]^+$ 394.1250; $C_{21}H_{22}FNNaO_2S^+$ requires 394.1253.

(*Z*)-*N*-(Hex-3-en-1-yl)-*N*-((4-methoxyphenyl)ethynyl)-4-methylbenzenesulfonamide, (*Z*)-151d

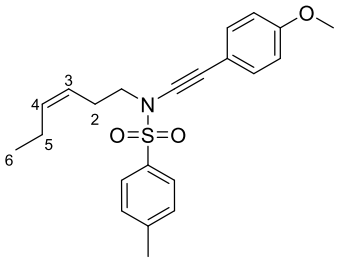

Synthesised from (*Z*)-*N*-(hex-3-en-1-yl)-4-methylbenzenesulfonamide (*Z*)-**154** (250 mg, 0.98 mmol) and 1-(bromoethynyl)-4-methoxybenzene **98d** (312 mg, 1.48 mmol) using **Procedure 1**. The resulting crude material was purified by column chromatography (10→20% Et_2O in petroleum ether) to give (*Z*)-

151d as a yellow oil (291 mg, 0.76 mmol, 78%); $\mathbf{R_f}$= 0.22 (5:2, petroleum ether:EtOAc); $\mathbf{\delta_H}$ (400 MHz, $CDCl_3$) 7.84 (2H, d, *J* = 8.3 Hz, Ts*H*), 7.35 (2H, d, *J* = 8.2 Hz, Ts*H*), 7.31 (2H, d, *J* = 8.5 Hz, Ph*H*), 6.83 (2H, d, *J* = 8.5 Hz, Ph*H*), 5.53 (1H, dtt, *J* = 15.3, 6.3, 1.3 Hz, H4), 5.30 (1H, dtt, *J* = 15.3, 6.8, 1.3 Hz, H3), 3.81 (3H, s, OCH_3), 3.40 (2H, ap t, *J* = 7.4 Hz, H1), 2.43 (3H, s, ArC*H*3), 2.36 (2H, br. ap. q, *J* = 7.1 Hz, H2), 1.97 (2H, m, H5), 0.93 (3H, t, *J* = 7.5 Hz, H6); $\mathbf{\delta_C}$ (100 MHz, $CDCl_3$) 144.8, 135.2, 134.7, 131.3, 123.0, 128.1, 127.7, 127.6, 123.8, 122.9, 81.3, 70.9, 51.5, 31.2, 25.6, 21.6, 13.6, 6.9; **IR** (thin film) ν_{max}/cm^{-1} 2968, 2231, 1370, 1170; **HRMS** *m/z* (ESI+) found $[M+Na]^+$ 406.1452; $C_{22}H_{25}NNaO_3S^+$ requires 406.1453.

(But-3-yn-1-yloxy)(*tert*-butyl)dimethylsilane, 253

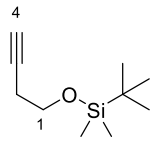

To a stirred solution of 3-butyn-1-ol **252** (14.0 g, 200 mmol, 1.0 equiv.) in dry CH_2Cl_2 (300 mL), TBSCl (45.2 g, 300 mmol, 1.5 equiv.), DMAP (1.20 g, 10 mmol, 0.05 equiv.) and Et_3N (42 mL, 300 mmol, 1.5 equiv.) was added. The reaction solution was stirred at room temperature for 8 h, and then sat. aq. NH_4Cl was added. The reaction mixture was extracted with CH_2Cl_2 (3 × 40 mL). The organic layers were combined and dried over $MgSO_4$, concentrated *in vacuo* to give **253** as a colourless oil (32.1 g, 176 mmol, 88%); $\mathbf{R_f}$= 0.83 (petroleum ether); $\mathbf{\delta_H}$ (400 MHz, $CDCl_3$) 3.74 (2H, t, *J* = 4.2 Hz, H1), 2.40 (2H, dt, *J* = 2.4 and 7.2 Hz, H2), 1.96 (1 H, t, *J* = 2.4 Hz, H4), 0.90 (9H, s, C(CH_3)$_3$), 0.06 (6H, s, 2×CH_3); $\mathbf{\delta_C}$ (100 MHz, $CDCl_3$) 81.5, 69.3, 61.7, 25.9, 22.8, 18.3, –5.3; **IR** (thin film) ν_{max}/cm^{-1} 3310, 2950, 2930, 2857, 1475, 1253, 1100, 915, 830, 771, 635. Data are consistent with literature values.[108]

***tert*-Butyldimethyl((5-phenylpent-3-yn-1-yl)oxy)silane, 254**

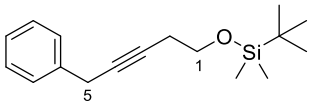

A solution of (but-3-yn-1-yloxy)(*tert*-butyl)dimethylsilane **253** (6.70 g, 24.4 mmol, 1.0 equiv.) in dry THF (50 mL) was transferred into a 250 ml flame-dried round-bottom flask. The solution was then cooled to –40 °C and 2.5 M BuLi solution in hexanes (10 mL, 25 mmol, 1.05 equiv.) was added dropwise *via* syringe. The reaction was allowed to warm up to room temperature, followed by addition

of benzyl bromide (4.18 g, 24.4 mmol, 1.0 equiv.) *via* syringe. The reaction was left stirred overnight. The reaction mixture was quenched with sat. aq. NH_4Cl (~40 mL). The mixture was extracted with EtOAc (3 × 15 mL). The organic layers were combined and dried over $MgSO_4$, concentrated *in vacuo*. The crude material was purified by column chromatography (10→30% EtOAc in petroleum ether) to give **254** as a yellow oil (3.53 g, 12.9 mmol, 53%); $\mathbf{R_f}$ = 0.62 (1:1, petroleum ether:EtOAc); $\boldsymbol{\delta_H}$ (400 MHz, $CDCl_3$) 7.35–7.21 (5H, m, Ph*H*), 3.64 (2H, t, *J* = 6.2 Hz, H1), 3.61–3.60 (2H, m, H5), 2.23–2.19 (2H, m, H2), 0.90 (9H, s, C(C*H*$_3$)$_3$), 0.06 (6H, s, 2×C*H*$_3$); $\boldsymbol{\delta_C}$ (100 MHz, $CDCl_3$) 140.5, 129.4, 128.6, 125.7, 82.3, 75.6, 61.7, 25.9, 23.9, 22.8, 18.5, –5.3. Data are consistent with literature values.[108]

(*Z*)-*tert*-Butyldimethyl((5-phenylpent-3-en-1-yl)oxy)silane, (*Z*)-255

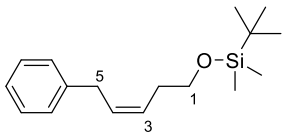

A round-bottom flask was charged with Lindlar's catalyst (500 mg) and purged with nitrogen. tert-butyldimethyl((5-phenylpent-3-yn-1-yl)oxy)silane **254** (1.14 g, 4.11 mmol, 1.0 equiv.) in MeOH (10 mL) was added followed by quinoline (35 µL, 0.27 mmol). The flask was evacuated and refilled with H_2 four times, fitted with a H_2 balloon, and stirred at room temperature under H_2 for 3 h. The reaction was filtered through a plug of silica and concentrated *in vacuo*. The crude material was purified by column chromatography (0→15% Et_2O in petroleum ether) to give (*Z*)-**255** as a pale yellow oil (1.09 g, 3.95 mmol, 97%); **Rf** = 0.62 (9:1, petroleum ether:Et_2O); $\boldsymbol{\delta_H}$ (500 MHz, $CDCl_3$) 7.26 (2H, t, *J* = 7.6 Hz, Ph*H*), 7.17 (2H, d, *J* = 7.6 Hz, Ph*H*), 7.16 (H1 t, *J* = 7.6 Hz, Ph*H*), 5.47 (1H, dt, *J* = 9.6 and 6.9 Hz, H3), 5.38 (1H, dt, *J* = 9.6 and 6.9 Hz, H4), 3.52 (2H, t, *J* =6.9 Hz, H5), 2.64 (2H, t, *J* = 6.9 Hz, H1), 2.35 (2H, q, *J* = 6.9 Hz, H2), 0.87 (9H, s, C(C*H*$_3$)$_3$), 0.02 (6H, s, 2×C*H*$_3$); $\boldsymbol{\delta_C}$ (125 MHz, $CDCl_3$) 142.0, 130.6, 128.4, 128.2, 126.4, 125.8, 62.9, 35.9, 31.1, 29.3, 18.4, −5.3. Data are consistent with literature values.[109]

(*Z*)-5-Phenylpent-3-en-1-ol, (*Z*)-256

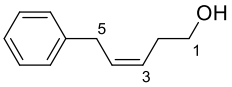

To a solution of (*Z*)-*tert*-butyldimethyl((5-phenylpent-3-en-1-yl)oxy)silane (*Z*)-**255** (1.09 g, 3.94 mmol, 1.0 equiv.) in dry THF (**7** mL) , 1 M tetrabutylammonium fluoride in THF (TBAF, 5.9 mL, 5.9 mmol, 1.5 equiv.) was added, and the mixture was stirred for 4 h at room temperature. The solvent was then concentrated *in vacuo*, and the residue was poured into water. The aqueous phase was extracted with Et_2O (3 × 15 mL). The organic extract was washed with brine, dried over Na_2SO_4 and concentrated *in vacuo*. The residue was purified by column chromatography (5→20% EtOAc in petroleum ether) to give (*Z*)-**256** as a pale yellow oil (640 mg, 3.60 mmol, 91%); $\mathbf{R}_f$ = 0.23 (7:3, petroleum ether:EtOAc); $\boldsymbol{\delta}_\mathbf{H}$ (500 MHz, $CDCl_3$) 7.28–8.31 (2H, m, Ph*H*), 7.18–7.21 (3H, m, Ph*H*), 5.74–5.79 (1H, m, H3), 5.51–5.56 (1H, m, H4), 3.71 (2H, t, *J* = 6.6 Hz, H1), 3.45 (2H, d, *J* = 7.3 Hz, H5), 2.44–2.48 (2H, m, H2), 1.44 (1H, br s, O*H*); $\boldsymbol{\delta}_\mathbf{C}$ (125 MHz, $CDCl_3$) 140.9, 131.6, 128.7, 128.5, 126.4, 126.2, 62.5, 33.8, 31.0. . Data are consistent with literature values.[110]

(*Z*)-*N*-Acetoxy-4-methyl-*N*-(5-phenylpent-3-en-1-yl)benzenesulfonamide, (*Z*)-257

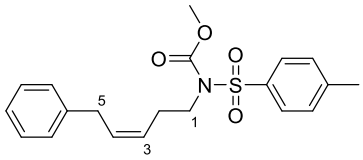

Synthesised from (*Z*)-5-phenylpent-3-en-1-ol (*Z*)-**256** (217 mg, 1.34 mmol) using **Procedure 2**. The resulting crude material was purified by column chromatography (5→20% Et_2O in petroleum ether) to give (*Z*)-**257** as a colourless oil (336 mg, 0.90 mmol, 67%); $\mathbf{R}_f$ = 0.36 (4:1, petroleum ether:Et_2O); $\boldsymbol{\delta}_\mathbf{H}$ (400 MHz, $CDCl_3$) 7.79 (2H, d, *J* = 8.1 Hz, Ts*H*), 7.37–7.23 (6H, m, Ts*H* and Ph*H*), 7.20 (1H, t, *J* = 7.3 Hz, Ph*H*), 6.46 (1H, dt, *J* = 15.9 and 7.3 Hz, H4), 6.19 (1 H, dt, *J* = 15.9 and 7.1 Hz, H3), 3.96 (2H, t, *J* = 7.3 Hz, H1), 3.65 (2H, d, *J* = 7.3 Hz, H5), 2.66 (2H, ap. q, *J* = 7.2 Hz, H2), 2.42 (3H, s, ArCH_3), 1.31 (9H, s, C(CH_3)$_3$); $\boldsymbol{\delta}_\mathbf{c}$ (100 MHz, $CDCl_3$) 150.9, 139.0, 137.4, 137.3, 132.6, 129.2, 128.5, 127.9, 127.2, 126.1, 126.0, 84.1, 46.5, 38.7, 33.8, 27.8, 21.6; **HRMS** *m/z* (ESI+) found $[M–H]^+$ 374.1428; $C_{20}H_{24}NO_2S^+$ requires 374.1426.

(*Z*)-4-Methyl-*N*-(5-phenylpent-3-en-1-yl)benzenesulfonamide, (*Z*)-258

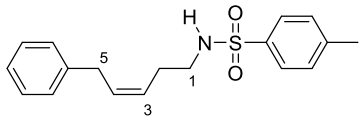

Synthesised from (*Z*)-*N*-acetoxy-4-methyl-*N*-(5-phenylpent-3-en-1-yl)benzenesulfonamide (*Z*)-**257** (300 mg, 0.80 mmol) using **Procedure 4**. The resulting crude material was purified by column chromatography (5→20% EtOAc in petroleum ether) to give (*Z*)-**258** as a colourless oil (240 mg, 0.76 mmol, 95%); $\mathbf{R}_f$ = 0.37 (4:1, petroleum ether:EtOAc); $\boldsymbol{\delta}_\mathbf{H}$ (400 MHz, $CDCl_3$) 7.74 (2H, d, *J* = 8.3 Hz, Ts*H*), 7.35–7.13 (7H, m, Ts*H* and Ph*H*), 6.49 (1H, dt, *J* = 11.6 and 7.3 Hz, H4), 5.51 (1H, dt, *J* = 11.6 and 7.1 Hz, H3), 4.73–4.56 (1H, br. m, N*H*), 3.65 (2H, d, *J* = 7.3 Hz, H5), 3.09 (2H, ap. q, *J* = 6.5 Hz, H1), 2.41 (3H, s, ArC*H*$_3$), 2.36 (2H, ap. q, *J* = 6.8 Hz, H2); $\boldsymbol{\delta}_\mathbf{c}$ (100 MHz, $CDCl_3$) 143.4, 136.9, 136.8, 133.1, 129.7, 128.5, 127.5, 127.1, 126.1, 125.5, 42.5, 38.7, 33.0, 21.5; **HRMS** *m/z* (ESI+) found $[M–H]^+$ 316.1370; $C_{18}H_{22}NO_2S^+$ requires 316.1371.

(*Z*)-4-Methyl-*N*-(oct-1-yn-1-yl)-*N*-(5-phenylpent-3-en-1-yl)benzenesulfonamide, (*Z*)-151e

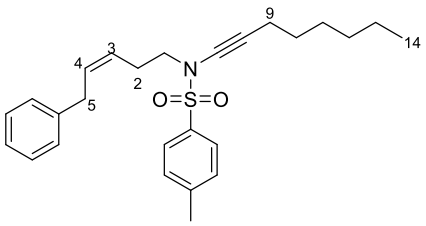

Synthesised from (*Z*)-4-methyl-*N*-(5-phenylpent-3-en-1-yl)benzenesulfonamide (*Z*)-**258** (100 mg, 0.32 mmol) and 1-bromooct-1-yne **98a** (90 mg, 0.48 mmol) using **Procedure 5**. The resulting crude material was purified by column chromatography (20% Et_2O in petroleum ether) to give (*Z*)-**151e** as a colourless oil (97.6 mg, 0.23 mmol, 72%); $\mathbf{R}_f$ = 0.27 (10:1, petroleum ether:Et_2O); $\boldsymbol{\delta}_\mathbf{H}$ (400 MHz, $CDCl_3$) 7.76 (2H, d, *J* = 8.1 Hz, Ts*H*), 7.36–7.27 (4H, m, Ts*H* and Ph*H*), 7.27–7.20 (3H, m, Ph*H*), 6.50 (1H, dt, *J* = 11.6 and 7.3 Hz, H4), 5.59 (1H, dt, *J* = 11.6 and 7.2 Hz, H3), 3.62 (2H, d, *J* = 7.3 Hz, H5), 3.38 (2H, t, *J* = 7.3 Hz, H1), 2.65 (2H, ap. q, *J* = 7.3 Hz,H2), 2.44 (3H, s, ArC*H*$_3$), 2.21 (2H, t, *J* = 6.9 Hz, H9), 1.48–1.38 (2H, m, H10), 1.37–1.18 (6H, m, H11–13), 0.88 (3H, t, *J* = 6.7 Hz, H14); $\boldsymbol{\delta}_\mathbf{C}$ (100 MHz, $CDCl_3$) 144.2, 137.0, 134.6, 131.4, 129.6, 128.6, 128.2, 127.6, 127.2, 126.8, 72.7,

70.6, 51.1, 36.4, 31.3, 28.8, 28.4, 27.1, 22.5, 21.6, 18.4, 14.0; **IR** (thin film) ν_{max}/cm^{-1} 2929, 2255, 1368, 1160; **HRMS** *m/z* (ESI+) found $[M+Na]^+$ 424.2313; $C_{26}H_{33}NNaO_2S^+$ requires 424.2310.

(*Z*)-4-Methyl-*N*-(phenylethynyl)-*N*-(5-phenylpent-3-en-1-yl)benzenesulfonamide, (*Z*)-**151f**

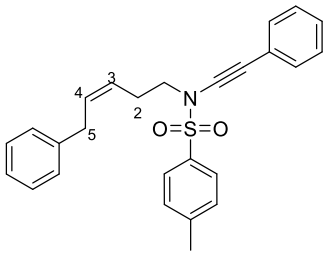

Synthesised from (*Z*)-4-methyl-*N*-(5-phenylpent-3-en-1-yl)benzenesulfonamide (*Z*)-**258** (100 mg, 0.32 mmol) and (bromoethynyl)benzene **98b** (90.5 mg, 0.50 mmol) using **Procedure 5**. The resulting crude material was purified by column chromatography (10→15% Et_2O in petroleum ether) to give (*Z*)-**151f** as a yellow oil (98.4 mg, 0.24 mmol, 74%); $\mathbf{R_f}$ = 0.23 (10:1, petroleum ether:Et_2O); $\boldsymbol{\delta_H}$ (400 MHz, $CDCl_3$) 7.76 (2H, d, *J* = 8.1 Hz, Ts*H*), 7.40–7.28 (6H, m, Ts*H* and Ph*H*), 7.27–7.16 (6H, m, Ph*H*), 6.50 (1H, dt, *J* = 11.6 and 7.3 Hz, H4), 5.59 (1H, dt, *J* = 11.6 and 7.2 Hz, H3), 3.62 (2H, d, *J* = 7.3 Hz, H5), 3.38 (2H, t, *J* = 7.3 Hz, H1), 2.65 (2H, ap. q, *J* = 7.3 Hz,H2), 2.44 (3H, s, ArC*H*$_3$); $\boldsymbol{\delta_C}$ (100 MHz, $CDCl_3$) 144.2, 137.0, 134.6, 131.4, 131.3, 129.6, 128.6, 128.2, 128.1, 127.8, 127.6, 127.2, 126.8, 122.9, 82.7, 70.6, 51.1, 36.4, 27.1, 21.6; **IR** (thin film) ν_{max}/cm^{-1} 2933, 2259, 1363, 1162; **HRMS** *m/z* (ESI+) found $[M+Na]^+$ 438.1508; $C_{26}H_{25}NNaO_2S^+$ requires 438.1504.

(*E*)-4-Iodo-3-methylbut-3-en-1-ol, (*E*)-259

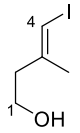

According to the procedure of Spino *et al*.[111] To a solution of 3-butyn-1-ol 4 **252** (4.52 g, 64.5 mmol, 1.0 equiv.) in CH_2Cl_2 (50 mL) at 0 °C under argon was added a solution of trimethylaluminium (2M in toluene, 10 mL, 20.0 mmol, 0.3 equiv.) and stirring was continued at the same temperature. To another flask, containing a suspension of $ZrCp_2Cl_2$ (3.77 g, 12.9 mmol, 0.20 equiv.) in CH_2Cl_2 (240 mL) at –20 °C under argon was added dropwise trimethylaluminium solution (70.5 mL, 141 mmol, 2.2 equiv.) and continued stirring for 15 min. Then H_2O (1.8 mL, 100.0 mmol, 1.55 equiv.) was added *very slowly* (Exothermic!), and the resulting yellow slurry was stirred vigorously for 30 min. The mixture of 3-

butyn-1-ol and trimethylaluminium prepared earlier was then cannulated above the slurry at –20 °C, the mixture was allowed to warm to room temperature, and stirred for 3 h. A solution of iodine (19.64 g, 77.4 mmol, 1.2 equiv.) in dry THF (130 mL) was added slowly to the above reaction mixture at –20 °C, and continued stirring at room temperature for 2.5 h. The reaction mixture was decanted into a conical flask containing sat. aq. Rochelle Salt (500 mL) at 0 °C under argon flush. (Exothermic!!) The resulting mixture was stirred for 2 h, filtered through Celite®, washed with Et_2O (100 mL). The aqueous layer was extracted with Et_2O (3 × 50 mL).and the combined organic layers were washed with sat. aq. $Na_2S_2O_3$, brine, dried over $MgSO_4$, filtered and concentrated *in vacuo*. The crude material was purified by column chromatography (10→20% EtOAc / petroleum ether) to afford (*E*)-**259** as a pale yellow oil. (10.9 g, 51.6 mmol, 80 %); $\mathbf{R_f}$ = 0.28 (1:1, petroleum ether:EtOAc); $\boldsymbol{\delta_H}$ (400 MHz, $CDCl_3$) 6.02 (1H, d, *J* = 0.9 Hz, H4), 3.72 (2H, t, *J* = 6.3 Hz, H1), 2.48 (2H, t, *J* = 6.3 Hz, H2), 1.88 (3H, d, *J* = 0.6 Hz, C*H*$_3$), 1.41 (1H, br s, O*H*); $\boldsymbol{\delta_C}$ (100 MHz, $CDCl_3$) 144.6, 76.9, 60.1, 42.3, 23.9 Data are consistent with literature values.[111]

(*E*)-*tert*-Butyl((4-iodo-3-methylbut-3-en-1-yl)oxy)dimethylsilane, (*E*)-260

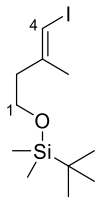

To an ice-cooled solution of (*E*)-4-iodo-3-methylbut-3-en-1-ol, (*E*)-**259** (8.3 g, 39.1 mmol, 1.0 equiv.) in CH_2Cl_2 (25 mL) were successively added Et_3N (6.5 mL, 47.0 mmol, 1.2 equiv.), a catalytic amount of DMAP (~ 10 mg.) and TBSCl (6.48 g, 43.0 mmol, 1.1 equiv.). After stirring for 1 h, the reaction mixture was poured into water. The aqueous phase was extracted with CH_2Cl_2 (3 × 25 mL). The organic extract was washed with brine, dried with Na_2SO_4 and concentrated *in vacuo*. The residue was purified by column chromatography (0→10% Et_2O / petroleum ether) to afford (*E*)-**260** as a colourless oil. (11.6 g, 35.6 mmol, 91 %); $\mathbf{R_f}$ = 0.47 (5:1, petroleum ether:EtOAc); $\boldsymbol{\delta_H}$ (400 MHz, $CDCl_3$) 5.93 (1H, s, H4), 3.68 (2H, t, *J* = 6.8 Hz, H1), 2.42 (2H, t, *J* = 6.8 Hz, H2), 1.84 (H3, s, C*H*$_3$), 0.89 (9H, s, C(C*H*$_3$)$_3$), 0.04 (6H, s, 2×C*H*$_3$) ; $\boldsymbol{\delta_C}$ (100 MHz, $CDCl_3$) 147.6, 78.9, 59.1, 45.3, 29.3, 23.9, 18.4, –5.3. Data are consistent with literature values.[111]

(*E*)-3-Methylhept-3-en-1-ol, (*E*)-261

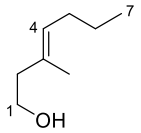

According to the procedure of Yabuta *et al*.[112] A Grignard reagent was prepared in ether from Mg (1.08 g, 45 mmol, 3.0 equiv.) and a catalytic amount of I_2 and 1-bromopropane (6.08 g, 45 mmol, 3.0 equiv.). This solution was added to a solution of (*E*)-**260** (5 g, 15 mmol, 1.0 equiv.) and $PdCl_2$(dppf) (3.68 g, 4.5 mmol, 0.3 equiv.) in dry Et_2O (100 mL) at room temperature. The reaction mixture was stirred for 12 h and then poured into water. The aqueous phase was extracted with Et_2O (3 × 20 mL), and the organic extract was dried over Na_2SO_4 and concentrated *in vacuo*. The crude residue was dissolved in dry THF (60 mL). To the solution, 1 M tetrabutylammonium fluoride (TBAF, 30 mL, 3 mmol, 0.2 equiv.) was added, and the mixture was stirred for 2 h at room temperature. The solvent was then concentrated *in vacuo*, and the residue was poured into water (80 mL). The aqueous phase was extracted with Et_2O (3 × 20 mL). The organic extract was washed with brine, dried over Na_2SO_4 and concentrated *in vacuo*. The residue was purified by column chromatography (0→10% Et_2O / petroleum ether) to afford (*E*)-**261** as a pale yellow oil. (1.44 g, 11.2 mmol, 75%); $\mathbf{R_f}$ = 0.24 (5:1, petroleum ether:EtOAc); $\boldsymbol{\delta_H}$ (400 MHz, $CDCl_3$) 5.23 (1H, t, *J* = 7.3 Hz, H4), 3.64 (2H, t, *J* = 5.8 Hz, H1), 2.26 (2H, t, *J* = 5.8 Hz, H2), 1.99 (2H, dt, *J* = 7.3 and 7.0 Hz, H5), 1.63 (3H, s, C*H*$_3$), 1.37 (2H, sext, *J* = 7.3 Hz, H6), 0.90 (3H, t, *J* = 7.3, H7); $\boldsymbol{\delta_C}$ (100 MHz, $CDCl_3$) 132.8, 122.4, 58.6, 41.5, 30.1, 23.6, 15.4, 14.9. Data are consistent with literature values.[112]

Methyl (*E*)-(3-methylhept-3-en-1-yl)(tosyl)carbamate, (*E*)-262

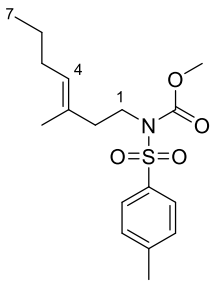

Synthesised from (*E*)-3-methylhept-3-en-1-ol (*E*)-**261** (491 mg, 3.83 mmol) using **Procedure 2**. The resulting crude material was purified by column chromatography (5→20% Et_2O in petroleum ether) to

give (*E*)-**262** as a colourless oil (818 mg, 2.41 mmol, 63%); $\mathbf{R}_f$ = 0.35 (9:1, petroleum ether:Et_2O); $\boldsymbol{\delta}_\mathbf{H}$ (400 MHz, $CDCl_3$) 7.72–7.70 (2H, m, Ts*H*), 7.33 (2H, d, *J* = 8.2 Hz, Ts*H*), 5.22 (1H, t, *J* = 7.3, Hz, H4), 3.83 (3H, s, OCH_3), 3.77 (2H, t, *J* = 6.4 Hz, H1), 2.43 (3H, s, $ArCH_3$), 2.30 (2H, ap q, *J* = 7.1 Hz, H5), 2.07–1.98 (2H, m, H2), 1.65 (3H, s, CH_3), 1.44 (2H, *m*, H6), 0.95 (3H, t, *J* = 7.6 Hz, H7); $\boldsymbol{\delta}_\mathbf{c}$ (100 MHz, $CDCl_3$) 172.4, 144.6, 134.6, 130.3, 130.0, 129.7, 127.7, 54.4, 51.9, 45.0, 23.6, 21.6, 21.2, 15.7, 14.2; **HRMS** *m/z* (ESI+) found $[M–H]^+$ 340.1580; $C_{17}H_{26}NO_4S^+$ requires 340.1583.

(*E*)-4-methyl-*N*-(3-methylhept-3-en-1-yl)benzenesulfonamide, (*E*)-263

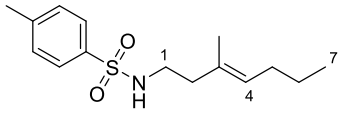

Synthesised from methyl (*E*)-(3-methylhept-3-en-1-yl)(tosyl)carbamate (*E*)-**262** (500 mg, 1.47 mmol) using **Procedure 4**. The resulting crude material was purified by column chromatography (5→20% EtOAc in petroleum ether) to give (*E*)-**263** as a colourless oil (398 mg, 1.41 mmol, 96%); $\mathbf{R}_f$ = 0.12 (5:1, petroleum ether:EtOAc); $\boldsymbol{\delta}_\mathbf{H}$ (400 MHz, $CDCl_3$) 7.72 (2H, d, *J* = 8.2 Hz, Ts*H*), 7.33 (2H, d, *J* = 8.2 Hz, Ts*H*), 5.22 (1H, t, *J* = 7.3, Hz, H4), 4.86 (1H, br s, N*H*), 3.77 (2H, t, *J* = 6.4 Hz, H1), 2.43 (3H, s, $ArCH_3$), 2.30 (2H, ap q, *J* = 7.1 Hz, H5), 2.07–1.98 (2H, m, H2), 1.65 (3H, s, CH_3), 1.42 (2H, *m*, H6), 0.93 (3H, t, *J* = 7.6 Hz, H7); $\boldsymbol{\delta}_\mathbf{c}$ (100 MHz, $CDCl_3$) 144.6, 134.6, 130.3, 130.0, 129.7, 127.7, 46.4, 40.0, 23.6, 21.6, 21.2, 15.7, 14.2; **HRMS** *m/z* (ESI+) found $[M–H]^+$ 281.1450; $C_{15}H_{23}NO_2S^+$ requires 281.1449.

(*E*)-4-Methyl-*N*-(3-methylhept-3-en-1-yl)-*N*-(oct-1-yn-1-yl)benzenesulfonamide, (*E*)-264a

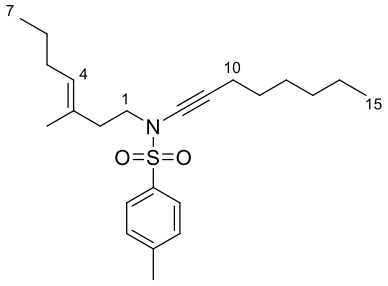

Synthesised from (*E*)-4-methyl-*N*-(3-methylhept-3-en-1-yl)benzenesulfonamide (*E*)-**263** (150 g, 0.53 mmol) and 1-bromooct-1-yne **98a** (202 mg, 1.07 mmol) using **Procedure 5**. The resulting crude material was purified by column chromatography (20% Et_2O in petroleum ether) to give (*E*)-**264a** as a colourless oil (161 mg, 0.41 mmol, 78%); $\mathbf{R}_f$ = 0.32 (9:1, petroleum ether:EtOAc); $\boldsymbol{\delta}_\mathbf{H}$ (400 MHz,

$CDCl_3$) 7.77 (2H, d, *J* = 8.2 Hz, Ts*H*), 7.32 (2H, d, *J* = 8.2 Hz, Ts*H*), 5.22 (1H, t, *J* = 7.3, Hz, H4), 3.30–3.24 (2H, m, H1), 2.44 (3H, s, ArCH_3), 2.42 (2H, ap q, *J* = 7.1 Hz, H5), 2.33–2.25 (2H, m, H2), 2.26 (2H, t, *J* = 6.9 Hz, H10), 2.01–1.98 (2H, m, H6), 1.55 (3H, s, CH_3), 1.51–1.42 (2H, m, H11), 1.39–1.19 (6H, m, H12–14), 0.90 (3H, t, *J* = 6.8 Hz, H7), 0.88 (3H, t, *J* = 6.8 Hz, H15); **δ_C** (100 MHz, $CDCl_3$) 144.6, 134.6, 130.3, 130.0, 129.7, 127.7, 54.4, 45.0, 31.3, 28.9, 28.4, 23.6, 22.6, 21.6, 21.2, 18.5, 15.7, 14.2, 14.1; **IR** (thin film) ν_{max}/cm^{-1} 2932, 2263, 1361, 1164; **HRMS** *m/z* (ESI+) found $[M+Na]^+$ 412.2285; $C_{23}H_{35}NNaO_2S^+$ requires 412.2286.

(*E*)-4-Methyl-*N*-(3-methylhept-3-en-1-yl)-*N*-(phenylethynyl)benzenesulfonamide, (*E*)-264b

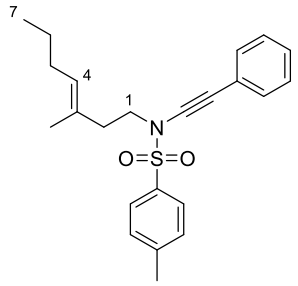

Synthesised from (*E*)-4-methyl-*N*-(3-methylhept-3-en-1-yl)benzenesulfonamide (*E*)-**263** (150 g, 0.53 mmol) and (bromoethynyl)benzene **98b** (163 mg, 0.90 mmol) using **Procedure 5**. The resulting crude material was purified by column chromatography (10→15% Et_2O in petroleum ether) to give (*E*)-**264b** as a yellow oil (172 mg, 0.45 mmol, 84%); **R_f** = 0.48 (5:1, petroleum ether:EtOAc); **δ_H** (400 MHz, $CDCl_3$) 7.77 (2H, d, *J* = 8.2 Hz, Ts*H*), 7.40–7.32 (4H, m, Ts*H* and Ph*H*), 7.30–7.26 (3H, m, Ph*H*), 5.23 (1H, t, *J* = 7.3, Hz, H4), 3.30–3.24 (2H, m, H1), 2.44 (3H, s, ArCH_3), 2.42 (2H, ap q, *J* = 7.1 Hz, H5), 2.33–2.25 (2H, m, H2), 2.01–1.98 (2H, m, H6), 1.55 (3H, s, CH_3), 0.90 (3H, t, *J* = 6.8 Hz, H7); **δ_C** (100 MHz, $CDCl_3$) 144.6, 134.6, 131.3, 130.3, 130.0, 129.7, 128.2, 127.8, 127.7, 122.8, 82.3, 70.8, 54.4, 45.0, 23.6, 21.6, 21.2, 15.7, 14.2; **IR** (thin film) ν_{max}/cm^{-1} 2933, 2257, 1363, 1160; **HRMS** *m/z* (ESI+) found $[M+Na]^+$ 404.1658; $C_{23}H_{27}NNaO_2S^+$ requires 404.1660.

(*Z*)-4-Iodo-3-methylbut-3-en-1-ol, (*Z*)-259

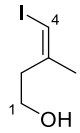

According to the procedure of Theodorakis *et al.*[113] To a solution of $ZrCp_2Cl_2$ (5.00 g, 17.1 mmol, 0.20 equiv.) in 1,2-DCE (140 mL) at 0 °C was added a solution of trimethylaluminum (2M, 107 mL, 214 mmol, 2.5 equiv.) in hexanes dropwise. A solution of but-3-yn-1-ol **252** (6.49 mL, 86 mmol, 1.0 equiv.) in 1,2-DCE (20 mL) was then added dropwise. The solution was stirred at room temperature overnight. The solution was then heated at reflux for 3 days. The reaction was then cooled to –40 °C and a solution of iodine (43.5 g, 171 mmol, 2 equiv.) in dry THF (100 mL) was added *via* cannula. The solution was stirred for 30 minutes before allowed to warm up to 0 °C. Sat. aq. K_2CO_3 was added very slowly (the solution frothed and bubbled) until eventually turning yellow with precipitate. Et_2O (250 mL) was added and the solution was filtered through Celite®. The mixture was extracted with Et_2O (200 mL) to remove all unwanted organics. H_2O (200 mL) was added to the organic phase. The aqueous layer was then extracted with Et_2O (3× 30 mL). The combined organic layers were washed once with brine, dried over $MgSO_4$ and concentrated *in vacuo*. The resulting crude material was purified by column chromatography (10→20% EtOAc in petroleum ether) to give (*Z*)-**259** as a light brown oil (10.9 g, 51.6 mmol, 60%); $\mathbf{R}_f$ = 0.31 (1:1, petroleum ether:EtOAc), $\boldsymbol{\delta}_\mathbf{H}$ (400 MHz, $CDCl_3$) 6.01 (1H, d, *J* = 1.4 Hz, H4), 3.78 (2H, t, *J* = 6.7 Hz, H1), 2.53 (2H, t, *J* = 6.7 Hz, H2), 1.94 (3H, d, *J* = 1.5 Hz, C*H*$_3$) 1.47 (1H, br s, O*H*); $\boldsymbol{\delta}_\mathbf{C}$ (100 MHz, $CDCl_3$) 144.3, 76.3, 60.1, 41.6, 23.8. Data are consistent with literature values.[113]

(*Z*)-*tert*-Butyl((4-iodo-3-methylbut-3-en-1-yl)oxy)dimethylsilane, (*Z*)-260

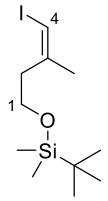

To an ice-cooled solution of (*Z*)-4-iodo-3-methylbut-3-en-1-ol, (*Z*)-**259** (8.0 g, 37.7 mmol, 1.0 equiv.) in CH_2Cl_2 (20 ml) were successively added Et_3N (6.25 mL, 45.2 mmol, 1.2 equiv.), a catalytic amount of DMAP (~ 10 mg) and TBSCl (6.25 mg, 41.5 mmol, 1.1 equiv.). After stirring for 1 h, the reaction mixture was poured into water. The aqueous phase was extracted with CH_2Cl_2 (3 × 20 mL). The organic extract was washed with brine, dried with Na_2SO_4 and concentrated *in vacuo*. The residue was purified by column chromatography (10→20% Et_2O / petroleum ether) to afford (*Z*)-**260** as a colourless oil. (11.9 g, 36.6 mmol, 97%); $\mathbf{R}_f$ = 0.52 (5:1, petroleum ether:EtOAc); $\boldsymbol{\delta}_\mathbf{H}$ (400 MHz, $CDCl_3$) 5.93 (1H, s, H4), 3.68 (2H, t, *J* = 6.4 Hz, H1), 2.41 (2H, t, *J* = 6.4 Hz, H2), 1.85 (H3, s, CH_3), 0.88 (9H, s, C(CH_3)$_3$), 0.04 (6H, s, 2×CH_3) ; $\boldsymbol{\delta}_\mathbf{C}$ (100 MHz, $CDCl_3$) 146.9, 83.9, 60.1, 45.3, 29.3, 23.9, 18.4, –5.3. Data are consistent with literature values.[112]

(*Z*)-3-Methylhept-3-en-1-ol, (*Z*)-261

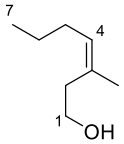

According to the procedure of Yabuta *et al*.[112] A Grignard reagent was prepared in dry Et_2O from Mg (1.08 g, 45 mmol, 3.0 equiv.) and a catalytic amount of I_2 and 1-bromopropane (6.08 g, 45 mmol, 3.0 equiv.). This solution was added to a solution of (*Z*)-**260** (5 g, 15 mmol, 1.0 equiv.) and $PdCl_2$(dppf) (3.68 g, 4.5 mmol, 0.3 equiv.) in dry Et_2O (100 mL) at room temperature. The reaction mixture was stirred for 12 h and then poured into water. The aqueous phase was extracted with Et_2O (3 × 20 mL), and the organic extract was dried over Na_2SO_4 and concentrated *in vacuo*. The crude residue was dissolved in dry THF (60 mL). To the solution, 1 M tetrabutylammonium fluoride (TBAF, 30 mL, 3 mmol, 0.2 equiv.) was added, and the mixture was stirred for 2 h at room temperature. The solvent was then concentrated *in vacuo*, and the residue was poured into water (80 mL). The aqueous phase was

extracted with Et_2O (3 × 20 mL). The organic extract was washed with brine, dried over Na_2SO_4 and concentrated *in vacuo*. The residue was purified by column chromatography (0→10% Et_2O / petroleum ether) to afford (*Z*)-**261** as a pale yellow oil. (1.57 g, 12.2 mmol, 82%); $\mathbf{R_f}$ = 0.21 (5:1, petroleum ether:EtOAc); $\boldsymbol{\delta_H}$ (400 MHz, $CDCl_3$) 5.34 (1H, t, *J* = 7.3 Hz, H4), 3.65 (2H, t, *J* = 6.3 Hz, H1), 2.30 (2H, t, *J* = 6.3 Hz, H2), 2.00 (2H, dt, *J* = 7.3 and 7.0 Hz, H5), 1.71 (3H, s, C*H*$_3$), 1.36 (2H, sext, *J* = 7.3 Hz, H6), 0.90 (3H, t, *J* = 7.3, H7); $\boldsymbol{\delta_C}$ (100 MHz, $CDCl_3$) 130.6, 121.6, 58.4, 41.3, 30.2, 23.6, 15.4, 14.9. Data are consistent with literature values.[112]

Methyl (*Z*)-(3-methylhept-3-en-1-yl)(tosyl)carbamate, (*Z*)-262

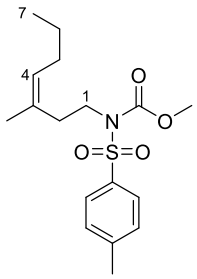

Synthesised from (*Z*)-3-methylhept-3-en-1-ol (*Z*)-**261** (490 g, 3.82 mmol) using **Procedure 2**. The resulting crude material was purified by column chromatography (5→20% Et_2O in petroleum ether) to give (*Z*)-**262** as a colourless oil (869 mg, 2.56 mmol, 67%); $\mathbf{R_f}$ = 0.38 (9:1, petroleum ether:Et_2O); $\boldsymbol{\delta_H}$ (400 MHz, $CDCl_3$) 7.72–7.70 (2H, m, Ts*H*), 7.33 (2H, d, *J* = 8.2 Hz, Ts*H*), 5.35 (1H, t, *J* = 7.3, Hz, H4), 3.82 (3H, s, OC*H*$_3$), 3.75 (2H, t, *J* = 6.4 Hz, H1), 2.46 (3H, s, ArC*H*$_3$), 2.33 (2H, ap q, *J* = 7.1 Hz, H5), 2.07–1.98 (2H, m, H2), 1.75 (3H, s, C*H*$_3$), 1.44 (2H, *m*, H6), 0.95 (3H, t, *J* = 7.6 Hz, H7); $\boldsymbol{\delta_c}$ (100 MHz, $CDCl_3$) 172.4, 144.6, 134.6, 130.3, 130.0, 129.7, 127.7, 54.6, 53.9, 42.0, 23.1, 21.5, 21.2, 15.7, 14.2; **HRMS** *m/z* (ESI+) found $[M–H]^+$ 340.1581; $C_{17}H_{26}NO_4S^+$ requires 340.1583.

(*Z*)-4-Methyl-*N*-(3-methylhept-3-en-1-yl)benzenesulfonamide, (*Z*)-263

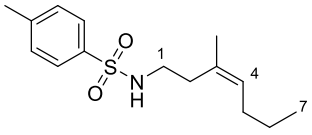

Synthesised from methyl (*Z*)-(3-methylhept-3-en-1-yl)(tosyl)carbamate (*Z*)-**262** (500 mg, 1.47 mmol) using **Procedure 4**. The resulting crude material was purified by column chromatography (5→20% EtOAc in petroleum ether) to give (*Z*)-**263** as a colourless oil (405 mg, 1.44 mmol, 98%); $\mathbf{R_f}$ = 0.15

(5:1, petroleum ether:EtOAc); δ_H (400 MHz, $CDCl_3$) 7.72 (2H, d, *J* = 8.2 Hz, Ts*H*), 7.33 (2H, d, *J* = 8.2 Hz, Ts*H*), 5.35 (1H, t, *J* = 7.3, Hz, H4), 4.63 (1H, br s, N*H*), 3.77 (2H, t, *J* = 6.4 Hz, H1), 2.43 (3H, s, ArCH_3), 2.30 (2H, ap q, *J* = 7.1 Hz, H5), 2.07–1.98 (2H, m, H2), 1.73 (3H, s, CH_3), 1.42 (2H, *m*, H6), 0.93 (3H, t, *J* = 7.6 Hz, H7); δ_c (100 MHz, $CDCl_3$) 144.6, 134.6, 130.3, 130.0, 129.7, 127.7, 46.4, 41.5, 22.8, 21.6, 21.2, 15.7, 14.2; **HRMS** *m/z* (ESI+) found $[M–H]^+$ 281.1451; $C_{15}H_{23}NO_2S^+$ requires 281.1449.

(*Z*)-4-Methyl-*N*-(3-methylhept-3-en-1-yl)-*N*-(oct-1-yn-1-yl)benzenesulfonamide, (*Z*)-264a

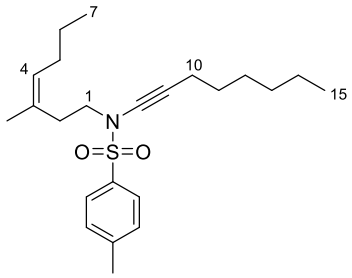

Synthesised from (*Z*)-4-methyl-*N*-(3-methylhept-3-en-1-yl)benzenesulfonamide (*Z*)-**263** (150 g, 0.53 mmol) and 1-bromooct-1-yne **98a** (202 mg, 1.07 mmol) using **Procedure 5**. The resulting crude material was purified by column chromatography (20% Et_2O in petroleum ether) to give (*Z*)-**264a** as a colourless oil (173 mg, 0.44 mmol, 83%); $\mathbf{R}_f$ = 0.33 (9:1, petroleum ether:EtOAc); δ_H (400 MHz, $CDCl_3$) 7.78 (2H, d, *J* = 8.2 Hz, Ts*H*), 7.32 (2H, d, *J* = 8.2 Hz, Ts*H*), 5.34 (1H, t, *J* = 7.3, Hz, H4), 3.30–3.24 (2H, m, H1), 2.44 (3H, s, ArCH_3), 2.42 (2H, ap q, *J* = 7.1 Hz, H5), 2.33–2.25 (2H, m, H2), 2.26 (2H, t, *J* = 6.9 Hz, H10), 2.01–1.98 (2H, m, H6), 1.55 (3H, s, CH_3), 1.51–1.42 (2H, m, H11), 1.39–1.19 (6H, m, H12–14), 0.89 (3H, t, *J* = 6.8 Hz, H7), 0.87 (3H, t, *J* = 6.8 Hz, H15); δ_C (100 MHz, $CDCl_3$) 144.6, 134.6, 130.3, 130.0, 129.7, 127.7, 54.4, 46.4, 41.3, 28.9, 28.4, 23.6, 22.6, 21.6, 21.2, 18.5, 15.7, 14.2, 14.1; **IR** (thin film) ν_{max}/cm^{-1} 2938, 2243, 1360, 1166; **HRMS** *m/z* (ESI+) found $[M+Na]^+$ 412.2285; $C_{23}H_{35}NNaO_2S^+$ requires 412.2286.

(*Z*)-4-Methyl-*N*-(3-methylhept-3-en-1-yl)-*N*-(phenylethynyl)benzenesulfonamide, (*Z*)-264b

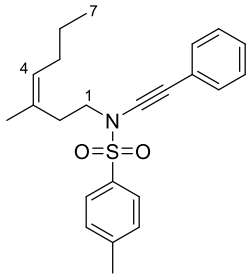

Synthesised from (*Z*)-4-methyl-*N*-(3-methylhept-3-en-1-yl)benzenesulfonamide (*Z*)-**263** (150 g, 0.53 mmol) and (bromoethynyl)benzene **98b** (164 mg, 0.91 mmol) using **Procedure 5**. The resulting crude material was purified by column chromatography (10→15% Et_2O in petroleum ether) to give (*Z*)-**264b** as a yellow oil (176 mg, 0.46 mmol, 87%); $\mathbf{R}_f$ = 0.47 (5:1, petroleum ether:EtOAc); $\boldsymbol{\delta}_\mathbf{H}$ (400 MHz, $CDCl_3$) 7.78 (2H, d, *J* = 8.2 Hz, Ts*H*), 7.40–7.32 (4H, m, Ts*H* and Ph*H*), 7.31–7.05 (3H, m, Ph*H*),5.34 (1H, t, *J* = 7.3, Hz, H4), 3.30–3.24 (2H, m, H1), 2.44 (3H, s, ArCH_3), 2.42 (2H, ap q, *J* = 7.1 Hz, H5), 2.33–2.25 (2H, m, H2), 2.01–1.98 (2H, m, H6), 1.55 (3H, s, CH_3), 0.89 (3H, t, *J* = 6.8 Hz, H7).; $\boldsymbol{\delta}_\mathbf{C}$ (100 MHz, $CDCl_3$) 144.6, 134.6, 131.3, 130.3, 130.0, 129.7, 128.2, 127.8, 127.7, 122.8, 82.3, 70.9, 46.4, 41.3, 23.6, 21.6, 21.2, 15.7, 14.2; **IR** (thin film) ν_{max}/cm^{-1} 293£, 2247, 1362, 1159; **HRMS** *m/z* (ESI+) found $[M+Na]^+$ 404.1658; $C_{23}H_{27}NNaO_2S^+$ requires 404.1660.

(*E*)-4-Methyloct-3-en-1-ol, (*E*)-266

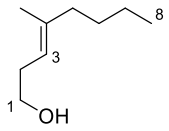

According to the procedure of Takacs *et al.*[114] 2,3-dihydrofuran **265** (3.0 g, 43 mmol, 1.8 equiv.) was dissolved in dry THF (20 mL) with subsequent cooling (–50 ºC). *t*-Butyllithium (1.7 M solution in pentanes, 16.7 mL, 28.3 mmol, 1.2 equiv.) was then added dropwise over 2 h. The mixture was allowed to slowly warm to –5 ºC, and then was cooled to –20 ºC, followed by the addition of 1-iodobutane (4.35 g, 23.7 mmol, 1.0 equiv.) over 1 h at the same temperature. The resulting mixture was allowed to warm to room temperature and stirred for 24 h. The mixture was then cooled to 0 ºC, and poured into sat. aq. NH_4Cl (100 mL) and Et_2O (100 mL). The aqueous was extracted with Et_2O (3 x 100 mL), and the combined organic layers were dried over $MgSO_4$ followed by concentration *in vacuo*. The resulting oil

(crude 2,3-dihydro-5-butylfuran) was used for the next step without purification. To a solution of $NiCl_2(PPh_3)_2$ (1.95 g, 3.0 mmol) in dry benzene (43 mL) was added methylmagnesium bromide (4.85 mL, 3 M solution in Et_2O, 14.5 mmol, 0.61 equiv.) at room temperature. After stirring for 1 h, more methylmagnesium bromide (20 mL of 3 M solution in Et_2O, 60 mmol, 2.5 equiv.) was added before the excess solvent was removed *in vacuo*. The residue was taken up in benzene (60 mL) and transferred to a three-neck round bottom flask equipped with a condenser. A solution of 2,3-dihydro-5-butylfuran in benzene (6 mL) was added and the resulting mixture was heated to reflux for 3 h. The mixture was cooled to 0 ºC and poured as a steady, slow stream into pre-cooled sat. aq. NH_4Cl (100 mL). The stirring was continued for 30 min, followed by separation of the organic layer and aqueous extract with Et_2O (3 x 100 mL). The combined organic extracts were dried over $MgSO_4$ and concentrated *in vacuo*. The resulting crude material was purified by column chromatography (15→20% EtOAc in petroleum ether) to give (*E*)-**266** as a pale yellow oil (2.43 g, 17.1 mmol, 72%); $\mathbf{R_f}$ = 0.50 (4:1, petroleum ether:EtOAc); $\boldsymbol{\delta_H}$ (400 MHz, $CDCl_3$) 5.21–5.13 (1H, m, H3), 3.63 (2H, t, *J* = 6.8 Hz, H1), 2.36–2.25 (2H, m, H2), 2.00 (2H, t, *J* = 7.2 Hz, H5), 1.66 (3H, s, C*H*$_3$), 1.46–1.33 (2H, m, H6), 1.35–1.25 (2H, m, H7), 0.91 (3H, t, *J* = 7.2 Hz, H8); $\boldsymbol{\delta_C}$ (100 MHz, $CDCl_3$) 139.2, 119.5, 62.5, 39.6, 31.5, 30.2, 22.4, 16.0, 13.9; **IR** (thin film) ν_{max}/cm^{-1} 3335, 2950, 1456, 1370, 1050; **HRMS** *m/z* (ESI+) found $[M+Na]^+$ 165.1250; $C_9H_{18}NaO^+$ requires 165.1255.

Methyl (*E*)-(4-methyloct-3-en-1-yl)(tosyl)carbamatee, (*E*)-267

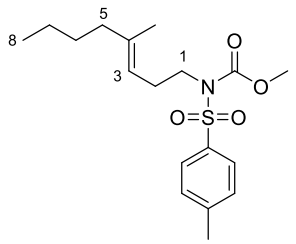

Synthesised from (*E*)-4-methyloct-3-en-1-ol (*E*)-**266** (1.00 g, 7.03 mmol) using **Procedure 2**. The resulting crude material was purified by column chromatography (5→20% Et_2O in petroleum ether) to give (*E*)-**267** as a colourless oil (1.76 g, 5.00 mmol, 71%); $\mathbf{R_f}$ = 0.56 (4:1, petroleum ether:Et_2O); $\boldsymbol{\delta_H}$ (400 MHz, $CDCl_3$) 7.77 (2H, d, *J* = 8.2 Hz, Ts*H*), 7.33 (2H, d, *J* = 8.2 Hz, Ts*H*), 5.29 (t, *J* = 5.1 Hz, H3), 3.84 (3H, s, OC*H*$_3$), 3.60 (2H, t, *J* = 7.1 Hz, H1), 2.51 (2H, ap q, *J* = 7.0 Hz, H2), 1.95 (2H, t, *J* =

7.0 Hz, H5), 1.59 (3H, s, C*H*$_3$), 1.48–1.28 (4H, m, H6 and H7), 0.92 (3H, t, *J* = 7.2 Hz, H8); **δ$_C$** (100 MHz, $CDCl_3$) 173.3, 142.7, 136.4, 136.2, 131.0, 129.3, 123.1, 53.2, 43.9, 39.9, 29.8, 26.8, 26.3, 23.4, 20.5, 14.6; **HRMS** *m/z* (ESI+) found $[M–H]^+$ 354.1740; $C_{18}H_{28}NO_4S^+$ requires 354.1739.

(*E*)-4-Methyl-*N*-(4-methyloct-3-en-1-yl)benzenesulfonamide, (*E*)-268

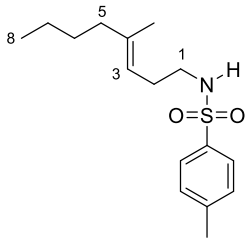

Synthesised from methyl (*E*)-(4-methyloct-3-en-1-yl)(tosyl)carbamate (*E*)-**267** (1.00 g, 2.83 mmol) using **Procedure 4**. The resulting crude material was purified by column chromatography (5→20% EtOAc in petroleum ether) to give (*E*)-**268** as a colourless oil (835 mg, 2.82 mmol, 99%); **R$_f$** = 0.21 (4:1, petroleum ether:EtOAc); **δ$_H$** (400 MHz, $CDCl_3$) 7.77 (2H, d, *J* = 8.2 Hz, Ts*H*), 7.33 (2H, d, *J* = 8.2 Hz, Ts*H*), 5.43 (t, *J* = 6.4 Hz, H3), 4.84 (1H, br s, N*H*), 3.10 (2H, t, *J* = 7.0 Hz, H1), 2.41 (2H, ap q, *J* = 6.9 Hz, H2), 2.15 (2H, t, *J* = 7.0 Hz, H5), 1.59 (3H, s, C*H*$_3$), 1.48–1.28 (4H, m, H6 and H7), 0.92 (3H, t, *J* = 7.2 Hz, H8); **δ$_C$** (100 MHz, $CDCl_3$) 142.8, 138.0, 135.6, 130.4, 127.2, 123.1, 44.6, 40.5, 29.8, 27.8, 26.0, 23.1, 21.6, 14.4; **HRMS** *m/z* (ESI+) found $[M–H]^+$ 296.1682; $C_{16}H_{26}NO_2S^+$ requires 296.1684.

(*E*)-4-Methyl-*N*-(4-methyloct-3-en-1-yl)-*N*-(oct-1-yn-1-yl)benzenesulfonamide, (*E*)-269a

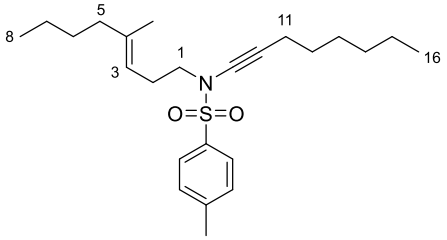

Synthesised from (*E*)-4-methyl-*N*-(4-methyloct-3-en-1-yl)benzenesulfonamide (*E*)-**268** (200 mg, 0.68 mmol) and 1-bromooct-1-yne **98a** (205 mg, 1.08 mmol) using **Procedure 5**. The resulting crude material was purified by column chromatography (20% Et_2O in petroleum ether) to give (*E*)-**269a** as a colourless oil (214 mg, 0.53 mmol, 78%); **R$_f$** = 0.39 (9:1, petroleum ether:EtOAc); **δ$_H$** (400 MHz, $CDCl_3$) 7.75 (2H, d, *J* = 8.1 Hz, Ts*H*), 7.42 (2H, d, *J* = 8.1 Hz, Ts*H*), 5.27 (1H, t, *J* = 7.0 Hz, H3), 3.34

(2H, t, *J* = 5.9 Hz, H1), 2.45 (2H, ap q, *J* = 6.0 Hz, H2), 2.43 (3H, s, ArC*H*$_3$), 2.25 (2H, t, *J* = 6.1 Hz, H11), 1.92 (2H, t, *J* = 7.0 Hz, H5), 1.59 (3H, s, C*H*$_3$), 1.55–1.37 (4H, m, H6 and H12), 1.37–1.23 (8H, m, H7 and H13–15), 0.90 (6H, m, H8 and H16); **δ$_C$** (100 MHz, $CDCl_3$) 143.9, 137.8, 129.6, 128.1, 123.3, 76.1, 58.6, 51.0, 35.5, 31.1, 29.8, 28.9, 28.5, 27.6, 26.1, 22.7, 22.4, 18.6, 16.1, 14.9, 14.0; **IR** (thin film) ν_{max}/cm^{-1} 2932, 2255, 1363, 1161; **HRMS** *m/z* (ESI+) found $[M+Na]^+$ 426.2440; $C_{24}H_{37}NNaO_2S^+$ requires 426.2443.

(*E*)-4-Methyl-*N*-(4-methyloct-3-en-1-yl)-*N*-(phenylethynyl)benzenesulfonamide, (*E*)-269b

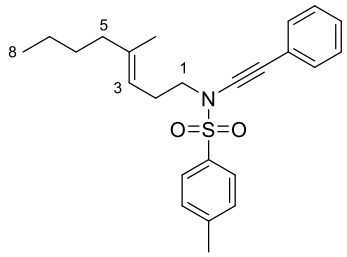

Synthesised from (*E*)-4-methyl-*N*-(4-methyloct-3-en-1-yl)benzenesulfonamide (*E*)-**268** (150 g, 0.51 mmol) and (bromoethynyl)benzene **98b** (157 mg, 0.87 mmol) using **Procedure 5**. The resulting crude material was purified by column chromatography (5→20% Et_2O in petroleum ether) to give (*E*)-**269b** as a yellow oil (163 mg, 0.41 mmol, 81%); **R$_f$** = 0.34 (5:1, petroleum ether:EtOAc); **δ$_H$** (400 MHz, $CDCl_3$) 7.75 (2H, d, *J* = 8.1 Hz, Ts*H*), 7.42–7.31 (4H, m, Ts*H* and Ph*H*), 7.30–7.22(3H, m, Ph*H*), 5.27 (1H, t, *J* = 7.0 Hz, H3), 3.34 (2H, t, *J* = 5.9 Hz, H1), 2.45 (2H, ap q, *J* = 6.0 Hz, H2), 2.43 (3H, s, ArC*H*$_3$), 2.01 (2H, t, *J* = 7.0 Hz, H5), 1.59 (3H, s, C*H*$_3$), 1.45–1.37 (2H, m, H6), 1.35–1.32 (2H, m, H7), 0.90 (3H, t, J= 7.2 Hz, H8); **δ$_C$** (100 MHz, $CDCl_3$) 144.1, 136.6, 131.1, 130.0, 129.6, 128.3, 127.1, 125.7, 123.3, 81.8, 69.0, 50.9, 39.9, 29.4, 27.6, 22.5, 21.7, 16.1, 14.3; **IR** (thin film) ν_{max}/cm^{-1} 2932, 2253, 1361, 1162; **HRMS** *m/z* (ESI+) found $[M+Na]^+$ 418.1821; $C_{24}H_{29}NNaO_2S^+$ requires 418.1817.

(*Z*)-4-Methyloct-3-en-1-ol, (*Z*)-266

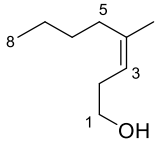

According to the procedure of Sigman *et al*.[115] $(A1Me_3)_2$ (6.3 mL, 66 mmol, 2.2 equiv.) was transferred *via* syringe into CH_2C1_2 (100 mL) contained in a three-necked round-bottom flask equipped with a gas inlet, rubber septa, and a magnetic stirring bar. The solution was cooled to 0 ºC and oct-3-yn-1-ol **270**

(3.7 mL, 30 mmol, 1.0 equiv.) was added slowly *via* syringe through a septum. The liberated methane was vented through the gas. The solution was then cooled to –78 °C, and neat $TiCl_4$ (3.6 mL, 33 mmol, 1.1 equiv.) was added dropwise to the reaction. The reaction mixture was stirred at –45 °C for 1 h, and then quenched *via* syringe addition of pre-cooled (0 °C) MeOH (30 mL). Aq. 3 N HCl sat. with NaCl (200 mL) was then added. The reaction mixture was allowed to warm to room temperature and stirred for 45 min. The combined organic layers were washed with H_2O and brine, dried over Na_2SO_4, and concentrated *in vacuo*. The residue was purified by column chromatography (5→15% EtOAc in petroleum ether) to give (*Z*)-**266** as a pale yellow oil (2.35 g, 16.5 mmol, 55%); $\mathbf{R_f}$ = 0.53 (4:1, petroleum ether:EtOAc); $\boldsymbol{\delta_H}$ (500 MHz, $CDCl_3$) 5.21–5.13 (1H, m, H3), 3.63 (2H, t, *J* = 6.8 Hz, H1), 2.36–2.25 (2H, m, H2), 2.00 (2H, t, *J* = 7.2 Hz, H5), 1.66 (3H, s, C*H*$_3$), 1.46–1.33 (2H, m, H6), 1.35–1.25 (2H, m, H7), 0.91 (3H, t, *J* = 7.2 Hz, H8); $\boldsymbol{\delta_C}$ (125 MHz, $CDCl_3$) 139.4, 120.2, 62.6, 31.6, 31.3, 30.3, 23.5, 22.7, 14.0.; **IR** (thin film) ν_{max}/cm^{-1} 3315, 2960, 2930, 2857, 14551 1381, 1050, 842; **HRMS** *m/z* (ESI+) found $[M+Na]^+$ 165.1250; $C_9H_{18}NaO^+$ requires 165.1255.

Methyl (*Z*)-(4-methyloct-3-en-1-yl)(tosyl)carbamate, (*Z*)-267

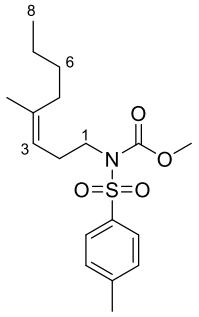

Synthesised from (*Z*)-3-methylhept-3-en-1-ol (*Z*)-**266** (1.00 g, 7.03 mmol) using **Procedure 2**. The resulting crude material was purified by column chromatography (5→20% Et_2O in petroleum ether) to give (*Z*)-**267** as a colourless oil (1.63 g, 4.64 mmol, 66%); $\mathbf{R_f}$ = 0.54 (4:1, petroleum ether:Et_2O); $\boldsymbol{\delta_H}$ (400 MHz, $CDCl_3$) 7.77 (2H, d, *J* = 8.2 Hz, Ts*H*), 7.33 (2H, d, *J* = 8.2 Hz, Ts*H*), 5.35 (t, *J* = 6.2 Hz, H3), 3.84 (3H, s, OC*H*$_3$), 3.77 (2H, t, *J* = 7.1 Hz, H1), 2.41 (2H, ap q, *J* = 7.0 Hz, H2), 1.95 (2H, t, *J* = 7.0 Hz, H5), 1.59 (3H, s, C*H*$_3$), 1.48–1.28 (4H, m, H6 and H7), 0.92 (3H, t, *J* = 7.2 Hz, H8); $\boldsymbol{\delta_c}$ (100 MHz, $CDCl_3$) 173.3, 142.8, 136.8, 136.1, 130.8, 129.3, 123.0, 53.2, 43.9, 37.5, 29.8, 26.8, 26.4, 23.4, 20.5, 14.6; **HRMS** *m/z* (ESI+) found $[M–H]^+$ 354.1741; $C_{18}H_{28}NO_4S^+$ requires 354.1739.

(*Z*)-4-Methyl-*N*-(4-methyloct-3-en-1-yl)benzenesulfonamide, (*Z*)-268

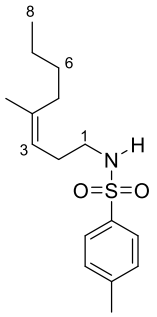

Synthesised from methyl (*Z*)-(4-methyloct-3-en-1-yl)(tosyl)carbamate (*Z*)-**267** (1.00 g, 2.83 mmol) using **Procedure 4**. The resulting crude material was purified by column chromatography (5→20% EtOAc in petroleum ether) to give (*Z*)-**268** as a colourless oil (833 mg, 2.81 mmol, 98%); $\mathbf{R}_f$ = 0.25 (4:1, petroleum ether:EtOAc); $\boldsymbol{\delta}_\mathbf{H}$ (400 MHz, $CDCl_3$) 7.77 (2H, d, *J* = 8.2 Hz, Ts*H*), 7.33 (2H, d, *J* = 8.2 Hz, Ts*H*), 5.28 (t, *J* = 6.8 Hz, H3), 4.84 (1H, br s, N*H*), 3.60 (2H, t, *J* = 7.0 Hz, H1), 3.21 (2H, ap q, *J* = 6.9 Hz, H2), 2.15 (2H, t, *J* = 7.0 Hz, H5), 1.59 (3H, s, CH_3), 1.48–1.28 (4H, m, H6 and H7), 0.92 (3H, t, *J* = 7.2 Hz, H8); $\boldsymbol{\delta}_\mathbf{c}$ (100 MHz, $CDCl_3$) 142.8, 137.9, 135.6, 130.1, 127.2, 123.1, 44.6, 37.5, 29.8, 27.7, 26.0, 23.1, 21.6, 14.3; **HRMS** *m/z* (ESI+) found $[M–H]^+$ 296.1682; $C_{16}H_{26}NO_2S^+$ requires 296.1684.

(*Z*)-4-Methyl-*N*-(4-methyloct-3-en-1-yl)-*N*-(oct-1-yn-1-yl)benzenesulfonamide, (*Z*)-269a

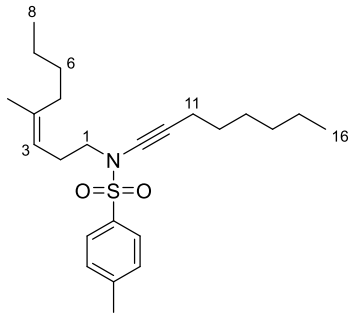

Synthesised from (*Z*)-4-methyl-*N*-(3-methylhept-3-en-1-yl)benzenesulfonamide (*Z*)-**268** (200 mg, 0.68 mmol) and 1-bromooct-1-yne **98a** (206 mg, 1.09 mmol) using **Procedure 5**. The resulting crude material was purified by column chromatography (20% Et_2O in petroleum ether) to give (*Z*)-**269a** as a colourless oil (206 mg, 0.51 mmol, 75%); $\mathbf{R}_f$ = 0.37 (9:1, petroleum ether:EtOAc); $\boldsymbol{\delta}_\mathbf{H}$ (400 MHz, $CDCl_3$) 7.77 (2H, d, *J* = 8.1 Hz, Ts*H*), 7.42 (2H, d, *J* = 8.1 Hz, Ts*H*), 5.37 (1H, t, *J* = 6.4 Hz, H3), 3.34 (2H, t, *J* = 5.9 Hz, H1), 2.45 (2H, ap q, *J* = 6.0 Hz, H2), 2.43 (3H, s, ArCH_3), 2.25 (2H, t, *J* = 6.1 Hz,

H11), 1.92 (2H, t, *J* = 7.0 Hz, H5), 1.64 (3H, s, C*H*$_3$), 1.55–1.37 (4H, m, H6 and H12), 1.37–1.23 (8H, m, H7 and H13–15), 0.95–0.84 (6H, m, H8 and H16); **δ$_C$** (100 MHz, $CDCl_3$) 144.1, 136.8, 129.6, 128.1, 123.3, 76.1, 58.6, 51.0, 35.5, 31.1, 29.8, 28.9, 28.5, 26.6, 26.1, 22.3, 22.1, 21.6, 18.5, 14.9, 14.1; **IR** (thin film) ν_{max}/cm^{-1} 2931, 2252, 1367, 1161; **HRMS** *m/z* (ESI+) found $[M+Na]^+$ 426.2441; $C_{24}H_{37}NNaO_2S^+$ requires 426.2443.

(*Z*)-4-Methyl-*N*-(4-methyloct-3-en-1-yl)-*N*-(phenylethynyl)benzenesulfonamide, (*Z*)-269b

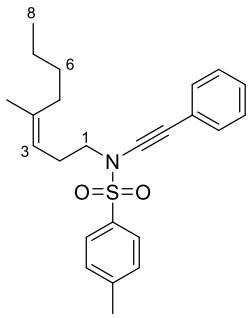

Synthesised from (*Z*)-4-methyl-*N*-(3-methylhept-3-en-1-yl)benzenesulfonamide (*Z*)-**268** (150 g, 0.51 mmol) and (bromoethynyl)benzene **98b** (160 mg, 0.89 mmol) using **Procedure 5**. The resulting crude material was purified by column chromatography (10→15% Et_2O in petroleum ether) to give (*Z*)-**269b** as a yellow oil (165 mg, 0.42 mmol, 82%); **R$_f$** = 0.35 (5:1, petroleum ether:EtOAc); **δ$_H$** (400 MHz, $CDCl_3$) 7.7 (2H, d, *J* = 8.1 Hz, Ts*H*), 7.42–7.31 (4H, m, Ts*H* and Ph*H*), 7.30–7.22(3H, m, Ph*H*), 5.35 (1H, t, *J* = 6.5 Hz, H3), 3.34 (2H, t, *J* = 5.9 Hz, H1), 2.45 (2H, ap q, *J* = 6.0 Hz, H2), 2.42 (3H, s, ArC*H*$_3$), 2.01 (2H, t, *J* = 7.0 Hz, H5), 1.59 (3H, s, C*H*$_3$), 1.45–1.37 (2H, m, H6), 1.35–1.32 (2H, m, H7), 0.90 (3H, t, J= 7.2 Hz, H8); **δ$_C$** (100 MHz, $CDCl_3$) 144.2, 136.8, 131.0, 129.9, 129.5, 128.3, 127.1, 125.7, 123.3, 81.8, 69.0, 50.9, 36.9, 29.4, 26.6, 26.1, 22.5, 20.1, 14.3; **IR** (thin film) ν_{max}/cm^{-1} 2936, 2242, 1359, 1163; **HRMS** *m/z* (ESI+) found $[M+Na]^+$ 418.1821; $C_{24}H_{29}NNaO_2S^+$ requires 418.1817.

2-(Cyclohex-1-en-1-yl)ethan-1-ol, 272

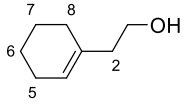

To a suspension of $LiAlH_4$ (183 mg, 4.82 mmol, 1.5 equiv.) in dry THF (4 mL) at 0 °C was added a solution of 2-(cyclohex-1-en-1-yl)acetic acid **271** (450 mg, 3.21 mmol, 1.0 equiv.) in dry THF (4 mL). The reaction mixture was stirred at room temperature for 5 h. The solution was cooled to 0 °C, H_2O (1

mL/g $LiAlH_4$) added dropwise, followed by 4M aq. NaOH (1 mL/g $LiAlH_4$), further H_2O (3 mL/g $LiALH_4$) and then excess $MgSO_4$. The reaction mixture was stirred at room temperature for 1 h, filtered through Celite® eluting with Et_2O and concentrated *in vacuo*. The resulting crude material was purified by column chromatography (20→30% EtOAc in petroleum ether) to give **272** as a colourless oil (138 mg, 1.15 mmol, 36%); $\mathbf{R_f}$ = 0.38 (7:3, petroleum ether:EtOAc); $\boldsymbol{\delta_H}$ (400 MHz, $CDCl_3$) 5.49 (1H, br. s, H4), 3.66 (2H, t, *J* = 6.3 Hz, H1), 2.21 (2H, t, *J* = 6.3 Hz, H2), 2.07–1.88 (4H, m, H5 and H8), 1.70–1.49 (4H, m, H6 and H7); $\boldsymbol{\delta_C}$ (100 MHz, $CDCl_3$) 134.0, 124.1, 60.1, 41.0, 27.9, 25.2, 22.8, 22.3. Data are consistent with literature values.[116]

***tert*-Butyl (2-(cyclohex-1-en-1-yl)ethyl)(tosyl)carbamate, 273**

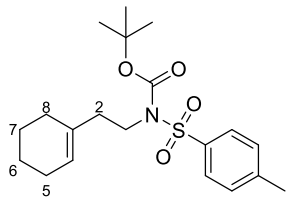

Synthesised from 2-(cyclohex-1-en-1-yl)ethanol **272** (100 mg, 0.79 mmol) using **Procedure 2**. The resulting crude material was purified by column chromatography (dry loaded, 10% Et_2O in petroleum ether) to give **273** as a colourless oil (221 mg, 0.58 mmol, 74%); $\mathbf{R_f}$ = 0.61 (4:1, petroleum ether:EtOAc); $\boldsymbol{\delta_H}$ (500 MHz, $CDCl_3$) 7.78 (2H, d, *J* = 8.3 Hz, Ts*H*), 7.29 (2H, d, *J* = 8.3 Hz, Ts*H*), 5.50 (1H, br. s, H4), 3.91–3.84 (2H, m, H1), 2.43 (3H, s, ArCH_3), 2.35 (2H, t, *J* = 7.6 Hz, H2), 2.04–1.95 (4H, m, H5 and H8), 1.66–1.51 (4H, m, H6 and H7), 1.33 (9H, s, $C(CH_3)_3$); $\boldsymbol{\delta_C}$ (125 MHz, $CDCl_3$) 150.9, 143.9, 137.7, 134.2, 129.2, 127.8, 123.9, 83.9, 46.1, 38.5, 28.2, 27.9, 25.3, 22.9, 22.5, 21.6; **IR** (thin film) ν_{max}/cm^{-1} 2929, 1727, 1356, 1155; **HRMS** *m/z* (ESI+) found $[M+Na]^+$ 402.1701; $C_{20}H_{29}NNaO_4S^+$ requires 402.1710.

***N*-(2-(Cyclohex-1-en-1-yl)ethyl)-4-methylbenzenesulfonamide, 274**

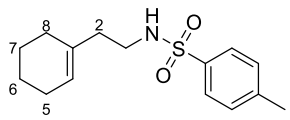

Synthesised from *tert*-butyl (2-(cyclohex-1-en-1-yl)ethyl)(tosyl)carbamate **273** (200 mg, 0.53 mmol) using **Procedure 3** to give **274** as a colourless oil (141 mg, 0.50 mmol, 95%) which was used without further purification; $\mathbf{R_f}$ = 0.45 (4:1, petroleum ether:EtOAc); $\boldsymbol{\delta_H}$ (400 MHz, $CDCl_3$) 7.74 (2H, d, *J* =

8.1 Hz, Ts*H*), 7.31 (2H, d, *J* = 8.1 Hz, Ts*H*), 5.38 (1H, br. s, H4), 4.35–4.25 (1H, br. m, N*H*), 3.00 (2H, ap. q, *J* = 6.4 Hz, H1), 2.43 (3H, s, ArCH_3), 2.05 (2H, t, *J* = 6.4 Hz, H2), 2.01–1.91 (2H, br. m, H5), 1.74–1.66 (2H, br. m, H8), 1.59–1.44 (4H, m, H6 and H7); δ_C (100 MHz, $CDCl_3$) 143.3, 136.7, 133.4, 129.6, 127.1, 124.8, 40.4, 37.3, 27.4, 25.1, 22.6, 22.1, 21.5. Data are consistent with literature values.[20]

***N*-(2-(Cyclohex-1-en-1-yl)ethyl)-4-methyl-*N*-(oct-1-yn-1-yl)benzenesulfonamide, 275a**

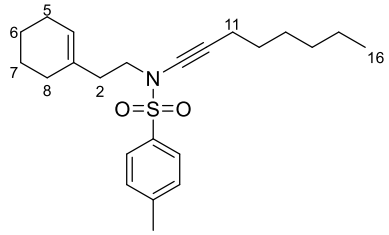

Synthesised from *N*-(2-(cyclohex-1-en-1-yl)ethyl)-4-methylbenzenesulfonamide **274** (120 mg, 0.43 mmol) and 1-bromooct-1-yne **98a** (97 mg, 0.52 mmol) using **Procedure 5**. The resulting crude material was purified by column chromatography (0→5% Et_2O in petroleum ether) to give **275a** as a pale yellow oil (138 mg, 0.36 mmol, 83%); $\mathbf{R_f}$ = 0.72 (4:1, petroleum ether:EtOAc); δ_H (500 MHz, $CDCl_3$) 7.78 (2H, d, *J* = 8.2 Hz, Ts*H*), 7.32 (2H, d, *J* = 8.2 Hz, Ts*H*), 5.45–5.40 (1H, br. m, H4), 3.36–3.29 (2H, m, H1), 2.44 (3H, s, ArCH_3), 2.29–2.18 (4H, m, H11 and H2), 1.99–1.93 (2H, m, H5), 1.93–1.86 (2H, m, H8), 1.64–1.41 (6H, m, H7, H6 and H12), 1.39–1.19 (6H, m, H13–15), 0.89 (3H, t, *J* = 7.1 Hz, CH_3); δ_C (125 MHz, $CDCl_3$) 144.1, 134.9, 133.6, 129.5, 127.8, 123.9, 73.0, 70.3, 50.2, 36.2, 31.3, 28.9, 28.4, 28.2, 25.2, 22.8, 22.6, 22.2, 21.6, 18.5, 14.1; **IR** (thin film) ν_{max}/cm^{-1} 2928, 2252, 1364, 1169; **HRMS** *m/z* (ESI+) found $[M+Na]^+$ 410.2109; $C_{23}H_{33}NNaO_2S^+$ requires 410.2124.

***N*-(2-(Cyclohex-1-en-1-yl)ethyl)-4-methyl-*N*-(phenylethynyl)benzenesulfonamide, 275b**

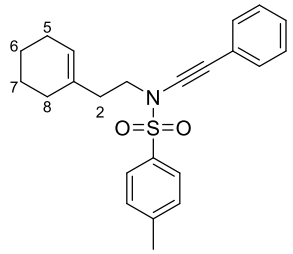

Synthesised from *N*-(2-(cyclohex-1-en-1-yl)ethyl)-4-methylbenzenesulfonamide **274** (100 mg, 0.36 mmol) and (bromoethynyl)benzene **98b** (104 mg, 0.57mmol) using **Procedure 5**. The resulting crude material was purified by column chromatography (0→5% Et_2O in petroleum ether) to give **275b** as a

pale yellow oil (88.8 mg, 0.23 mmol, 65%); $\mathbf{R_f}$ = 0.72 (4:1, petroleum ether:EtOAc); $\boldsymbol{\delta_H}$ (500 MHz, $CDCl_3$) 7.78 (2H, d, *J* = 8.2 Hz, Ts*H*), 7.40–7.32 (4H, m, Ts*H* and Ph*H*), 7.30–7.26 (3H, m, Ph*H*), 5.45–5.40 (1H, br. m, H4), 3.36–3.29 (2H, m, H1), 2.44 (3H, s, ArCH_3), 2.23 (2H, t, *J* = 7.3 Hz, H2), 1.99–1.93 (2H, m, H5), 1.93–1.86 (2H, m, H8), 1.54–1.37 (4H, m, H7 and H6); $\boldsymbol{\delta_C}$ (125 MHz, $CDCl_3$) 144.1, 134.9, 133.6, 131.3, 129.5, 128.2, 127.8, 127.7, 123.9, 122.8, 73.0, 70.3, 50.2, 36.2, 28.2, 25.2, 22.8, 22.2, 21.6; **IR** (thin film) ν_{max}/cm^{-1} 2933, 2251, 1367, 1164; **HRMS** *m/z* (ESI+) found $[M+Na]^+$ 402.1507; $C_{23}H_{25}NNaO_2S^+$ requires 402.1504.

7.3.2 Ligands / Catalysts / Pre-catalysts

_N,N'_-(Ethane-1,2-diyl)bis(1-phenylmethanimine), bbeda

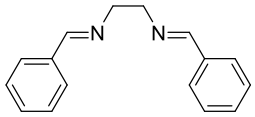

According to the procedure of Fontecave *et al*.[117] To a stirred solution of benzaldehyde (3.05 mL, 30.0 mmol, 2.0 equiv.) in MeOH (40 mL) was added ethylenediamine (1.0 mL, 15.0 mmol, 1.0 equiv.) dropwise. The reaction mixture was stirred at room temperature for 1 h and then concentrated *in vacuo* to give **bbeda** as a colourless solid (3.32 g, 126 mmol, 84%) which was used without further purification; **m.p.** 43-46 °C; $\mathbf{R_f}$ = 0.27 (5:1, petroleum ether:EtOAc); $\boldsymbol{\delta_H}$ (400 MHz, $CDCl_3$) 8.29 (2H, s, C*H*=N), 7.73–7.67 (4H, m, *o*-Ph*H*), 7.43–7.35 (6H, m, *m*-Ph*H*, *p*-Ph*H*), 2.17 (4H, s, CH_2); $\boldsymbol{\delta_C}$ (100 MHz, $CDCl_3$) 162.6, 136.1, 130.6, 128.5, 128.0, 61.6. Data are consistent with literature values.[117]

2,2'-(Ethane-1,2-diyl-d_4) bis(isoindoline-1,3-dione), d_4-118

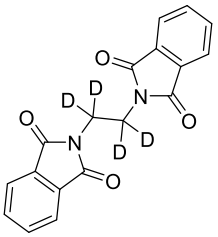

According to the procedure of Bonnesen *et al.*[46] Potassium phthalimide (4.25 g, 22.0 mol, 2.2 equiv.) was added to a solution of d_4-1,2-dibromoethane (2.00 g, 10.4 mol, 1.0 equiv.) in dry DMF (30 mL). The mixture was stirred at 95 °C overnight, then cooled to room temperature. Water (50 mL) was added

to form a white precipitate, which was stirred for another 30 min. The solid was collected by filtration, and washed with water (3 × 20 mL), then dried under vacuum to afford d_4-**118** (3.14 g, 9.7 mol, 93%) as a white solid; **m.p.** 235-236 °C; δ_H (400 MHz, $CDCl_3$) 7.79–7.76 (4H, m, Ar*H*), 7.70–7.67 (4H, m, Ar*H*); δ_C (100 MHz, $CDCl_3$) 168.4, 134.2, 132.2, 123.5, 36.6 (t, J = 22.9 Hz). Data are consistent with literature values.[46]

Ethane-d_4-1,2-diamine dihydrogen chloride, d_4-119

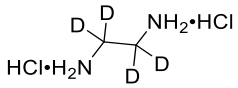

Diphthalimide d_4-**118** (2.00 g, 6.17 mmol, 1.0 equiv.) was dissolved in methanol (12 mL), then heated to reflux. Hydrazine monohydrate (680 mg, 13.6 mmol, 2.2 equiv.) was added to the solution. The solution was refluxed overnight, during which time a white precipitate formed. The mixture was allowed to cool to room temperature, and the precipitate was filtered off and washed with methanol (3 × 10 mL). The combined filtrate was acidified to pH 2 using 6 M hydrochloric acid, resulting in a formation of white precipitate. The solid was collected by filtration, then dried under vacuum to afford d_4-**119** (735 mg, 5.36 mmol, 87%) as a white crystalline powder.

(1*E*,1′*E*)-*N*,*N*′-(Ethane-1,2-diyl-d_4)bis(1-phenylmethanimine), d_4-bbeda

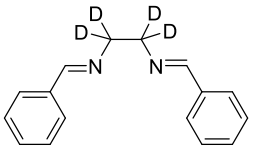

To a stirred solution of benzaldehyde (637 mL, 6.01 mmol, 2.0 equiv.) in MeOH (30 mL) was added ethane-d_4-1,2-diamine dihydrogen chloride d_4-**119** (700 mg, 3.0 mmol, 1.0 equiv.) dropwise. A solution of 5% NaOH (40 mL, aq.) was subsequently added to the stirred solution. The reaction mixture was stirred at room temperature for 3 h, and then extracted with CH_2Cl_2 (3 × 10 mL). The combined organic layers were dried over $MgSO_4$, filtered and concentrated *in vacuo*. The resulting crude material was washed with 1:3 toluene / petroleum ether, to give **d_4-bbeda** (1.00 g, 2.25 mmol, 75%) as a white crystalline powder; **m.p.** 49 °C; δ_H (400 MHz, $CDCl_3$) 8.29 (2H, s, C*H*=N), 7.71–7.68 (4H, m, Ph*H*), 7.41–7.37 (6H, m, Ph*H*); δ_C (100 MHz, $CDCl_3$) 162.9, 136.3, 130.8, 128.7, 128.3, 61.6 (weak m); **IR**

(thin film) ν_{max}/cm^{-1} 2845, 2199, 2079, 1640, 1370, 1156; **HRMS** *m/z* (ESI+) found $[M+H]^+$ 241.16345; $C_{16}H_{13}D_4N_2^+$ requires 241.1643.

Trimeric palladium acetate, $Pd_3(OAc)_6$ (as also known as palladium acetate)

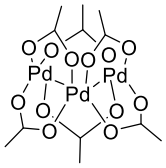

According to the procedure of Colacot *et al*.[49] A round-bottom flask equipped with a magnetic stirrer bar was charged with $Pd_3(OPiv)_6$ (247 mg, 0.80 mmol) and acetic acid (0.93 mL, 16.2 mmol). The flask was heated to 100 ºC and stirred for 5 hours. The reaction mixture was then cooled to room temperature and filtered under gravity, followed by dying *in vacuo* to afford the tiled product as a brick red solid (155 mg, 0.69 mmol, 86%); δ_H (400 MHz, C_6D_6) 1.76 (18H, s). Data are consistent with literature values.[49]

[$Pd_3(\mu^2$-OH)$(OAc)_5$], 107a

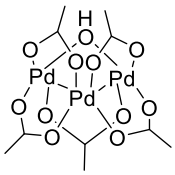

According to the procedure of Bedford *et al*.[43] A solution of $Pd(OAc)_2$ (50 mg, 0.0743 mmol, 1.0 equiv.) and H_2O (40 µL, 2.29 mmol, 30 equiv.) were stirred in acetone (5 mL) for 30 min. Nitrogen gas was bubbled through the solution, while *n*-hexane was slowly added to maintain the total volume of solution for 10 min, resulting in a formation of brown precipitate. The solid was then washed with *n*-hexane (2 × 5 mL) and dried *in vacuo* to obtain **107a** (48 mg, 0.0428 mmol, 86%) as a brown powder; δ_H (400 MHz, $CDCl_3$) 2.03 (6H, s, C*H*$_3$), 1.97 (3H, s, C*H*$_3$), 1.89 (6H, s, C*H*$_3$), –1.04 (1H, br s, O*H*); δ_C (100 MHz, $CDCl_3$) 190.1, 189.7, 186.1, 23.4, 22.7, 22.1. Data are consistent with literature values.[43]

[Pd(*R*)-BINAP](dba), 229

According to the procedure of Buchwald *et al*.[118] A solution of $Pd_2(dba)_3$ (72 mg, 0.08 mmol, 1.0 equiv.) and (*R*)-BINAP (100 mg, 0.16 mmol, 2.0 equiv.) in benzene (5 mL) was stirred at room temperature for 3 h. The resulting orange solution was filtered through Celite® and concentrated *in vacuo* to give an oily residue that was dissolved in dry Et_2O (5 mL). The precipitate that formed overnight was collected,

washed with dry Et_2O, and dried in vacuo to afford **229** (110 mg, 70%) as an orange solid: δ_H (400 MHz, $CDCl_3$) 7.83 (t, *J* = 8.3 Hz), 7.70 (br), 7.56 (br), 7.50 (m), 7.38 (t, *J* = 8.5 Hz), 7.20 (q, *J* = 7.6 Hz), 7.10 (m), 7.0–6.7 (br, m), 6.61 (t, *J* = 7.4 Hz), 6.46 (t, *J* = 6.8 Hz), 6.31 (t, *J* = 6.8 Hz); δ_P $\{^1H\}$(120 MHz, $CDCl_3$) 25.8, 24.6; **IR** (thin film) ν_{max}/cm^{-1} 3041, 1645, 1585, 1501, 1472,1430, 1330, 1210, 1095, 741, 690. Data are consistent with literature values.[118]

***N*,*N'*-((1*R*,2*R*)-cyclohexane-1,2-diyl)bis(1-phenylmethanimine), 227**

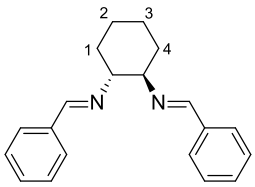

To a vigorously stirred mixture of (1*R*,2*R*)-*trans*-cyclohexane-1,2-diammonium *L*-Tartrate (1.00 g, 3.78 mmol, 1.0 equiv.), K_2CO_3 (1.04 g, 7.56 mmol, 2.0 equiv.) and H_2O (5 mL) was added EtOH (20 mL). The mixture was heated to reflux and a solution of benzaldehyde (0.77 mL, 7.56 mmol, 2.0 equiv.) in EtOH (8 mL) added over 10 mins. The reaction mixture was heated under reflux for 2 h, allowed to cool to room temperature, concentrated *in vacuo* and the residue diluted with H_2O. The resulting mixture was stirred at 0 ºC for 1 h and the precipitate was filtered to give the crude imine. The residue was dissolved in CH_2Cl_2 (15 mL), washed with H_2O (2 × 10 mL) and brine (10 mL), dried ($NaSO_4$), filtered and concentrated *in vacuo* to give **227** as a colourless solid (1.030 g, 3.55 mmol, 94%); **m.p.** 61–65 °C; $\mathbf{R}_f$ = 0.41 (4:1, petroleum ether:EtOAc); δ_H (400 MHz, $CDCl_3$) 8.21 (2H, s, =C*H*Ph), 7.63–7.53 (4H, m, Ph*H*), 7.36–7.27 (6H, m, Ph*H*), 3.48–3.36 (2H, m, C*H*-N), 1.95 1.72 (6H, m, H1',H1", H4', H4" H2', H3"), 1.58–1.41 (2H, m, H2" and H3'); δ_C (100 MHz, $CDCl_3$) 161.0, 136.4 , 130.2, 128.4, 127.9, 73.8, 33.0, 24.5. Data are consistent with literature values.[119]

[Rh((*R*)-Cl-OMe-biphep)(cod)]SbF$_6$, 239a

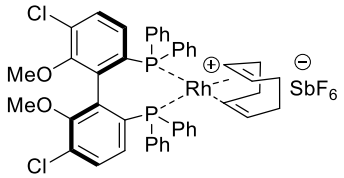

[Rh(cod)$_2$]SbF$_6$ (10 mg, 0.018 mmol, 1.0 equiv.) and (*R*)-Cl-OMe-BIPHEP (11.7 mg, 0.018 mmol, 1.0 equiv.) were dissolved in anhydrous CH_2Cl_2 (0.5 mL), and stirred at room temperature for 1 h. The solvent was removed *in vacuo* to afford a bright orange solid. The crude solid was purified by recrystallisation (vapour diffusion of *n*-pentane), the product **239a** was obtained as a bright orange crystal (14.3 mg, 0.013 mmol, 72%); δ_H (400 MHz, $CDCl_3$) 7.76 (4H, m, Ar*H*), 7.60–7.14 (20H, m, Ph*H*), 4.50 (2H, m, =C*H*), 4.69 (2H, m, =C*H*), 3.50 (2H, m, OCH_3), 2.68 (2H, m, OCH_3), 2.44 (2H, m, CH_2), 2.22 (2H, m, CH_2), 2.06 (2H, m, CH_2); δ_P {^{1}H}(162 MHz, $CDCl_3$) 24.7 (d, J = 146.1 Hz, P–Rh). This rhodium complex was also characterised by X-ray crystallography (*see* X-Ray Crystallographic Data section).

7.3.3 Palladium-catalysed cycloisomerisation products

(Z)-2-Heptylidene-3-methylene-1-tosylpyrrolidine, 102

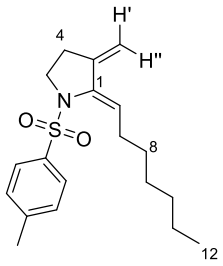

Synthesised from *N*-(but-3-en-1-yl)-4-methyl-*N*-(oct-1-yn-1-yl)benzenesulfonamide **92** (50 mg, 0.150 mmol) using **Procedure 6**, with the reaction mixture stirred for 10 min. The resulting crude material was purified by column chromatography (10% Et_2O in petroleum ether) to give **102** as a pale yellow oil (41 mg, 0.123 mmol, 82%); $\mathbf{R}_f$ = 0.49 (5:1, petroleum ether:EtOAc); δ_H (500 MHz, $CDCl_3$) 7.68 (2H, d, J = 8.2 Hz, Ts*H*), 7.23 (2H, d, J = 8.2 Hz, Ts*H*), 5.87 (1H, t, J = 7.4 Hz, H4), 5.20 (1H, t, J = 2.3 Hz, H'), 4.64 (1H, t, J = 2.3 Hz, H''), 3.53 (2H, t, J = 7.4 Hz, H3), 2.53 (2H, q, J = 7.6 Hz, H7), 2.42 (2H, s, ArCH_3), 1.83 (2H, tt, J = 7.4 and 2.3 Hz, H4), 1.48–1.23 (8H, m, H8–11), 0.89 (3H, t, J =

6.9 Hz, C*H*$_3$); **δ$_C$** (125 MHz, $CDCl_3$) 143.8, 143.2, 136.5. 136.0, 129.5, 127.7, 122.1, 103.5, 48.5, 31.7, 29.7, 29.5, 29.1, 29.0, 22.7, 21.6, 14.1. Data are consistent with literature values.[20]

(*Z*)-2-(Heptylidene-1-d)-3-methylene-1-tosylpyrrolidine, d$_1$-92

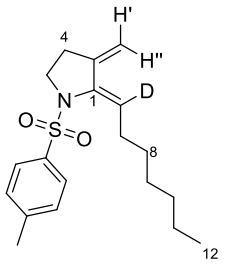

Synthesised from *N*-(but-3-en-1-yl)-4-methyl-*N*-(oct-1-yn-1-yl)benzenesulfonamide d$_1$-**92** (1.00 g, 3.00 mmol), d$_4$-bbeda (7.1 mg, 0.030 mmol) and $Pd(OAc)_2$ (6.7 mg, 0.030 mmol) using **Procedure 6**. The reaction mixture was stirred at 60 °C for 2.5 h, and then concentrated *in vacuo*. The resulting crude material was purified by column chromatography (10% EtOAc in petroleum ether) to give d$_1$-**102** (830 mg, 2.49 mmol, 83%) as a colourless oil; **R$_f$** 0.49 (5:1 petroleum ether / EtOAc); **δ$_H$** (500 MHz, $CDCl_3$) 7.68 (2H, d, *J* = 8.2 Hz, Ts*H*), 7.23 (2H, d, *J* = 8.2 Hz, Ts*H*), 5.21 (1H, t, *J* = 2.3 Hz, H'), 4.64 (1H, t, *J* = 2.3 Hz, H"), 3.53 (2H, t, *J* = 7.4 Hz, H5), 2.53 (2H, t, *J* = 7.4 Hz, H7), 2.41 (3H, s, ArC*H*$_3$), 1.83 (2H, tt, *J* = 2.1 and 7.4 Hz, H4), 1.44–1.24 (8H, m, H8-H11), 0.89 (3H, t, *J* = 6.8 Hz, H12); **δ$_C$** (125 MHz, $CDCl_3$) 143.9, 143.4, 136.6, 136.1, 129.7, 127.9, 122.3 (t, *J* = 23.8 Hz), 103.7, 48.9, 31.9, 29.9, 29.7, 29.3, 29.2, 22.8, 21.8, 14.3; **IR** (thin film) ν_{max}/cm^{-1} 2925, 1166, 1091, 801, 415; **HRMS** *m/z* (ESI+) found $[M+Na]^+$ 357.1719; $C_{19}H_{26}DNNaO_2S^+$ requires 357.1723.

(*Z*)-2-Heptylidene-3-methylene-1-(4-nitrophenylsulfonyl)pyrrolidine, 103

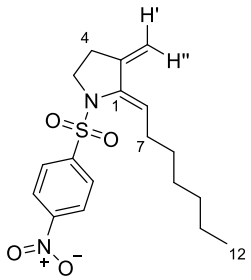

Synthesised from *N*-(but-3-en-1-yl)-4-nitro-*N*-(oct-1-yn-1-yl)benzenesulfonamide **93** (50 mg, 0.137 mmol) using **Procedure 6** (0.333 M; 2.5 mol% cat.), with the reaction mixture stirred for 20 mins. The resulting crude material was purified by column chromatography (10→15% Et_2O in petroleum ether) to give **103** as a pale yellow oil (42 mg, 0.115 mmol, 84%); **R$_f$** = 0.28 (9:1, petroleum ether:EtOAc); **δ$_H$**

(500 MHz, $CDCl_3$) 8.33–8.26 (2H, m, Ns*H*), 8.02–7.96 (2H, m, Ns*H*), 5.92 (1H, t, *J* = 7.4 Hz, H6), 5.23 (1H, t, *J* = 2.4 Hz, H'), 4.67 (1H, t, *J* = 2.0 Hz, H''), 3.61 (2H, t, *J* = 7.4 Hz, H3), 2.52 (2H, ap. q, *J* = 7.5 Hz, H7), 1.94–1.85 (2H, m, H4), 1.51–1.41 (2H, m, H8), 1.40–1.24 (6H, m, H9–11), 0.89 (3H, t, *J* = 7.4 Hz, C*H*$_3$); **δ$_C$** (125 MHz, $CDCl_3$) 150.3, 144.5, 142.0, 135.7, 129.0, 124.0, 123.2, 104.7, 48.6, 31.7, 29.7, 29.4, 29.1, 28.8, 22.6, 14.1; **IR** (thin film) ν_{max}/cm^{-1} 2926, 1531, 1349, 1170; **HRMS** *m/z* (ESI+) found $[M+Na]^+$ 387.1340; $C_{18}H_{24}N_2NaO_4^+S$ requires 387.1349.#

(*Z*)-2-Heptylidene-3-(methylene-d$_2$)-1-tosylpyrrolidine, d$_2$-113

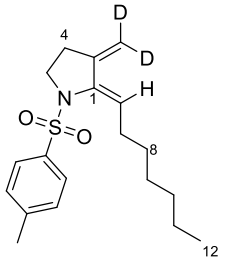

Synthesised from *N*-(but-3-en-1-yl-4,4-d$_2$)-4-methyl-*N*-(oct-1-yn-1-yl)benzenesulfonamide, d$_2$-**111** (15 mg, 0.045 mmol) using **Procedure 6**, with the reaction mixture stirred for 10 min. The resulting crude material was purified by column chromatography (10% Et_2O in petroleum ether) to give d$_2$-**113** as a colourless oil (13 mg, 0.040 mmol, 89%, >98% deuterium incorporation); **R$_f$** = 0.49 (5:1, petroleum ether:EtOAc); **δ$_H$** (500 MHz, $CDCl_3$) 7.68 (2H, d, *J* = 8.2 Hz, Ts*H*), 7.23 (2H, d, *J* = 8.2 Hz, Ts*H*), 5.87 (1H, t, *J* = 7.4 Hz, H4), 3.53 (2H, t, *J* = 7.4 Hz, H3), 2.53 (2H, q, *J* = 7.6 Hz, H7), 2.42 (2H, s, ArC*H*$_3$), 1.83 (2H, tt, *J* = 7.4 and 2.3 Hz, H4), 1.48–1.23 (8H, m, H8–11), 0.89 (3H, t, *J* = 6.9 Hz, C*H*$_3$); **δ$_C$** (125 MHz, $CDCl_3$) 143.8, 143.2, 136.5. 136.0, 129.5, 127.7, 122.1, 103.5 (m), 48.5, 31.7, 29.7, 29.5, 29.1, 29.0, 22.7, 21.6, 14.1; **HRMS** *m/z* (ESI+) found $[M+Na]^+$ 358.4919; $C_{19}H_2D_2NNaO_2S^+$ requires 358.4920.

Dimethyl (*E*)-3-(3-((*tert*-butyldimethylsilyl)oxy)propylidene-1-d)-4-methylenecyclopentane-1,1-dicarboxylate, 121/d$_1$-121

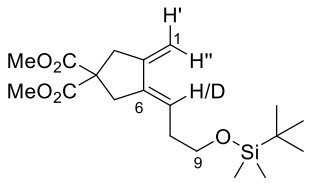

Synthesised from dimethyl 2-allyl-2-(5-((*tert*-butyldimethylsilyl)oxy)pent-2-yn-1-yl)malonate **120** (50 mg, 0.136 mmol, 1.0 equiv.), **d$_4$-bbeda** (1.62 mg, 0.007 mmol, 0.05 equiv.) and $Pd(OAc)_2$ (1.52 mg, 0.007 mmol, 0.05 equiv.) using **Procedure 6**. The reaction mixture was stirred at 60 °C for 31 h, and then concentrated *in vacuo*. The resulting crude material was purified by column chromatography (10% EtOAc in petroleum ether) to give d$_1$-**121** (43.6 mg, 0.118 mmol, 87%, 15% deuterium incorporation by ^{1}H NMR spectroscopy) as a colourless oil. Data for deuterated compound d$_1$-**121**; **R$_f$** 0.44 (7:3 petroleum ether / EtOAc); **δ$_H$** (400 MHz, $CDCl_3$) 5.26–5.25 (1H, m, H'), 4.84 (1H, ap. s, H''), 3.73 (6H, s, 2×CO_2CH_3), 3.65 (2H, t, *J* = 6.8 Hz, H9), 3.01–3.00 (4 H, m, H3 and H5), 2.32 (2H, q, *J* = 6.8 Hz, H8), 0.89 (9H, s, $SiC(CH_3)_3$), 0.05 (6H, s, 2×$SiCH_3$); **δ$_C$** (100 MHz, $CDCl_3$) 172.0, 145.2, 137.8, 118.8 (t, *J* = 19.5 Hz), 103.4, 62.6, 57.8, 53.0, 41.7, 38.0, 33.5, 26.1, 18.6, –5.1; **IR** (thin film) ν_{max}/cm^{-1} 2954, 1737,1434,1288, 1095; **HRMS** *m/z* (ESI+) found $[M+H]^+$ 370.2153; $C_{19}H_{32}DO_5Si^+$ requires 370.2160.

(3*RS*,5*RS*,*Z*)-3-((*E*)-But-1-en-1-yl)-2-heptylidene-5-phenyl-1-tosylpyrrolidine, 126

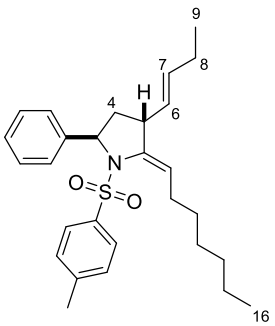

Synthesised from (*Z*)-4-methyl-*N*-(oct-1-yn-1-yl)-*N*-(1-phenylhept-3-en-1-yl)benzenesulfonamide **125** (20 mg, 0.044 mmol) using **Procedure 8**, only with the reaction mixture stirred at room temperature for 3 h. The resulting crude material was purified by column chromatography (5→10% Et_2O in petroleum ether) to give **126** as a colourless oil (17.4 mg, 0.040 mmol, 87%); **R$_f$** = 0.47 (4:1, petroleum ether:EtOAc); **δ$_H$** (500 MHz, $CDCl_3$) 7.69 (2H, d, *J* = 8.2 Hz, Ts*H*), 7.32–7.19 (7H, m, Ts*H* and Ph*H*),

5.34 (1H, dt, *J* = 15.0 and 6.2 Hz, H7), 5.17 (1H, dd, *J* = 7.6 and 3.8 Hz, H3), 5.13 (1H, ddd, *J* = 9.4, 4.8, 1.0 Hz, H10), 4.63 (1H, ddt, *J* = 15.0, 8.4, 1.5 Hz, H6), 3.02 (1H, ap. br. q, *J* = 7.7 Hz, H5), 2.61–2.51 (1H, m, H11'), 2.49–2.38 (1H, m, H11''), 2.42 (3H, s, ArCH_3), 1.92–1.82 (3H, m, H4', H8' and H8''), 1.52–1.44 (2H, m, H4'' and H12'), 1.39–1.22 (7H, m, H12'' and H13–15), 0.90 (3H, t, *J* = 7.4 Hz, H9), 0.89 (3H, t, *J* = 6.9 Hz, H16); **δ_C** (125 MHz, $CDCl_3$) 143.7, 141.7, 139.5, 136.3, 132.8, 129.7, 129.4, 128.4, 128.0, 127.1, 125.9, 122.0, 64.5, 46.6, 38.0, 31.8, 29.9, 29.8, 29.1, 25.3, 22.7, 21.5, 14.1, 13.5; **IR** (thin film) ν_{max}/cm^{-1} 2926, 1357, 1167; **HRMS** *m/z* (ESI+) found $[M+Na]^+$ 474.2421; $C_{28}H_{37}NNaO_2S^+$ requires 474.2437.

(3*R*,5*R*,*Z*)-2-Heptylidene-3-methyl-5-phenyl-3-((*E*)-prop-1-en-1-yl)-1-tosylpyrrolidine, 132

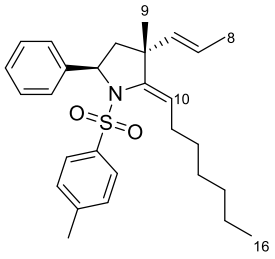

Synthesised from (*E*)-4-methyl-*N*-(3-methyl-1-phenylhex-3-en-1-yl)-*N*-(oct-1-yn-1-yl)benzenesulfonamide **131** (34 mg, 0.075 mmol) using **Procedure 8** (0.167 M; 10 mol% cat.), with the reaction mixture stirred for 30 min at 60 °C. The resulting crude material was purified by column chromatography (9:1 hexanes / *t*-BuOMe) to give **132** (28.5 mg, 0.063 mmol, 84%) as a pale yellow oil; **R_f** 0.31 (10:1 hexanes / EtOAc); **δ_H** (500 MHz, $CDCl_3$) 7.44 (2H, d, *J* = 8.2 Hz, Ts*H*), 7.31–7.18 (5H, m, Ph*H*), 7.10 (2H, d, *J* = 8.2 Hz, Ts*H*), 5.46 (1H, dq, *J* = 15.4 and 6.4 Hz, H7), 5.08–5.01 (1H, m, H6), 5.01–4.94 (2H, m, H5 and H10), 2.39–2.32 (2H, m, H11), 2.35 (3H, s, ArCH_3), 2.28 (1H, dd, *J* = 12.5 and 7.4 Hz, H4), 1.58 (1H, dd, *J* = 12.5 and 8.9 Hz, H4), 1.55–1.45 (4H, m, H8 and H12), 1.42–1.20 (7H, m, H12 and H13–15), 1.10 (3H, s, H9), 0.89 (3H, t, *J* = 6.8 Hz, H16); **δ_C** (125 MHz, $CDCl_3$) 144.5, 143.2, 143.1, 136.8, 135.0, 128.9, 128.4, 128.0, 127.2, 126.4, 123.2, 116.9, 62.9, 47.5, 47.1, 31.7, 29.8, 29.4, 29.0, 25.6, 22.7, 21.4, 18.0, 14.1; **IR** (thin film) ν_{max}/cm^{-1} 2925, 1347, 1166; **HRMS** *m/z* (ESI+) found $[M+H]^+$452.2623; $C_{28}H_{38}NO_2S^+$ requires 452.2618.

Conformational Analysis

Assignment of stereochemistry of **132** is based on interpretation of 1D ^{1}H NMR nOe data (C_6D_6). Enhancements are seen between protons on the alpha face of the molecule (as depicted below) between the alkene sidechain (H6), the benzylic proton (H5), and H4α. Complementary enhancements are seen between the methyl group and H4β, and from the Ph (*ortho*-protons) to H4β.

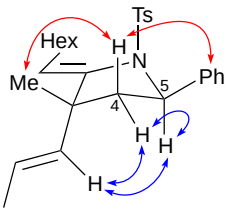

(3*RS*,5*RS*,*Z*)-1-Heptylidene-3-phenyl-2-tosyl-2-azaspiro[4.5]dec-6-ene, 134

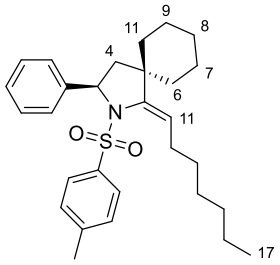

Synthesised from *N*-(2-(cyclohex-1-en-1-yl)-1-phenylethyl)-4-methyl-*N*-(oct-1-yn-1-yl)benzenesulfonamide **133** (35 mg, 0.075 mmol) using **Procedure 8** (0.167 M; 5 mol% cat.), with the reaction mixture stirred at 60 °C for 30 min. The resulting crude material was purified by column chromatography (5⟶10% Et_2O in petroleum ether) to give **134** (≥ 98:2 d.r., 27.5 mg, 0.059 mmol, 78%) as a pale yellow oil; $\mathbf{R}_f$ 0.65 (4:1 hexanes/EtOAc); $\boldsymbol{\delta}_\mathbf{H}$ (500 MHz, C_6D_6) 7.70 (2H, d, *J* = 8.1 Hz, Ts*H*), 7.28 (2H, d, *J* = 7.3 Hz, Ph*H*), 7.12 (2H, app t, *J* = 7.6 Hz, Ph*H*), 7.06–7.00 (1H, m, Ph*H*), 6.68 (2H, d, *J* = 8.1 Hz, Ts*H*), 5.62 (1H, br d, *J* = 10.0 Hz, H6), 5.48 (1H, dt, *J* = 10.0 and 3.6 Hz, H7), 5.42 (1H, dd, *J* = 6.1 and 7.9 Hz, H3), 5.22 (1H, dd, *J* = 9.0 and 4.9 Hz, H11), 2.78–2.61 (2H, m, H12), 2.00 (1H, dd, *J* = 12.4 and 7.9 Hz, H4), 1.82 (3H, s, ArCH_3), 1.82–1.67 (2H, m, H8), 1.62 (1H, dd, *J* = 12.4 and 6.1 Hz, H4), 1.61–1.53 (2H, m, H10 and H13), 1.50–1.40 (2H, m, H9 and H13), 1.40–1.20 (8H, m, H14–16, H9 and H10), 0.88 (3H, t, *J* = 6.9 Hz, H17); $\boldsymbol{\delta}_\mathbf{C}$ (125 MHz, C_6D_6) 145.5, 143.5, 143.1, 138.3, 132.3, 129.3, 128.7, (*o*-TsH obscured by solvent peak), 127.3, 126.6, 125.9, 118.6, 63.1, 47.9, 47.2,

35.2, 32.2, 30.5, 30.3, 29.6, 25.1, 23.1, 21.1, 20.6, 14.4; **IR** (thin film) ν_{max}/cm^{-1} 2927, 1361, 1167; **HRMS** *m/z* (ESI+) found $[M+Na]^+$ 486.2444; $C_{29}H_{37}NNaO_2S^+$ requires 486.2437.

Conformational Analysis: Assignment of stereochemistry of **134** is based on interpretation of 1D ^1H NMR nOe data ($CDCl_3$). Enhancements are seen between protons on the alpha face of the molecule (as depicted below) between the alkene moiety of the cyclohexenyl substituent (H6), the benzylic proton (H3), and H4α. Complementary enhancement is seen between CH_2-10 and H4β, as well as between the Ph (*ortho*-protons) and H4β.

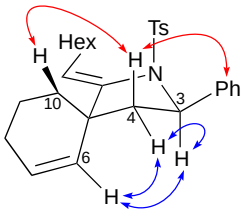

(*Z*)-2-(Heptylidene-1-d)-3-((*E*)-prop-1-en-1-yl)-1-tosylpyrrolidine, d_1-153a

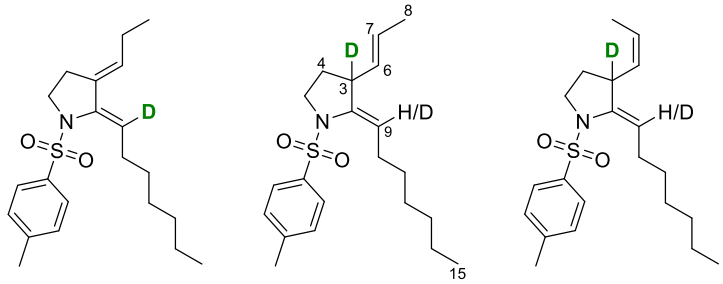

d_1-**152a**		(*E*)-d_1-**153a**		(*Z*)-d_1-**153a**
11	:	87	:	2

Synthesised from (*E*)-*N*-(hex-3-en-1-yl-3-d)-4-methyl-*N*-(oct-1-yn-1-yl)benzenesulfonamide, (*E*)-d_1-**151a**, (20 mg, 0.055 mmol, 1.0 equiv.) using **Procedure 6**. The crude material was passed through a silica plug with Et_2O as eluent, and then concentrated *in vacuo* to give an inseparable mixture of **152a**, (*E*)-d_1-**153a** and (*Z*)-d_1-**153a** (11:87:2) as a pale yellow oil (16.8 mg). NOTE: Up to 11% deuterium incorporation at the enamide proton is expected across these products, arising from 11% formation of 4b. For clarity, products (*E*)-d_1-**153a** and (*Z*)-d_1-**153a** are represented as singly-deuterated compounds. Data are reported for the major isomer ((*E*)-d_1-**153a**); δ_H (500 MHz, $CDCl_3$) 7.69 (2H, d, J = 8.1 Hz, Ts*H*), 7.28 (2H, d, *J* = 8.1 Hz, Ts*H*), 5.27 (1H, dq, J = 15.1 and 6.5 Hz, H7), 4.99 (1H, m, H6), 3.54 (1H, ddd, *J* = 11.4, 8.6 and 3.0 Hz, H5'), 3.38 (ddd, *J* = 11.4, 9.2 and 7.9 Hz, H5''), 2.50 (2H, m, H10),

2.43 (3H, s, C*H*$_3$Ar), 2.24 (1H, m, H3), 1.71–1.65 (1H, m, H4'), 1.61 (3H, dd, *J* = 6.6 and 1.6 Hz, H8), 1.45–1.24 (9H, m, H4" and H11–14), 0.88 (3H, t, *J* = 6.9 Hz, H15). **δ$_C$** (125 MHz, $CDCl_3$) 143.8, 140.1, 134.9, 130.5, 129.6, 128.0, 127.7, 121.4 (t, J = 19.2 Hz), 49.3, 45.8, 31.9, 30.0, 29.5, 29.3, 29.2, 22.9, 21.8, 18.0, 14.3.

(*Z*)-2-Heptylidene-3-((*E*)-prop-1-en-1-yl)-1-tosylpyrrolidine-3-d, d$_1$-153a

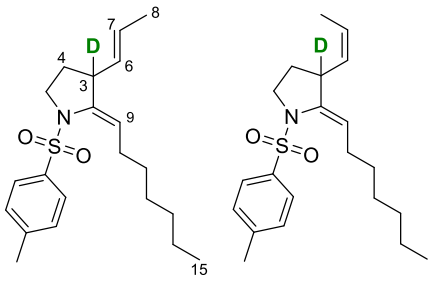

Synthesised from (*Z*)-*N*-(hex-3-en-1-yl-3-d)-4-methyl-*N*-(oct-1-yn-1-yl)benzenesulfonamide, (Z)-d$_1$-**151a**, (20 mg, 0.055 mmol, 1.0 equiv.), $Pd(OAc)_2$ (0.6 mg, 0.0028 mmol, 0.05 equiv.), and bbeda (0.7 mg, 0.0028 mmol, 0.05 equiv.) using **Procedure 6**. The resulting crude material was passed through a silica plug with Et_2O as eluent, and then concentrated *in vacuo* to afford an inseparable mixture of (*E*)-d$_1$-**153a** and (*Z*)-d$_1$-**153a** (86:16) as a pale yellow oil (18.5 mg). Data reported for the major isomer: **δ$_H$** (500 MHz, $CDCl_3$) 7.69 (2H, d, *J* = 8.1 Hz, Ts*H*), 7.28 (2H, d, *J* = 8.1 Hz, Ts*H*), 5.27 (1H, dq, *J* = 15.1 and 6.5 Hz, H7), 5.00–4.92 (2H, m, H6 and H9), 3.54 (1H, ddd, *J* = 11.4, 8.6 and 3.0 Hz, H5'), 3.38 (ddd, *J* = 11.4, 9.2 and 7.9 Hz, H5"), 2.43 (3H, s, C*H*$_3$Ar), 2.40 (2H, m, H10), 1.69 (1H, dt, *J* = 7.4 and 2.4 Hz, H4'), 1.62 (3H, dd, *J* = 6.6 and 1.6 Hz, H8), 1.45–1.24 (9H, m, H4" and H11–14), 0.88 (3H, t, *J* = 6.9 Hz, H15). **δ$_C$** (125 MHz, $CDCl_3$) 143.8, 140.1, 135.0, 130.6, 129.6, 128.0, 127.7, 121.4, 49.3, 45.6 (t, *J* = 21.7 Hz), 31.9, 30.0, 29.5, 29.2, 29.0, 22.8, 21.8, 18.0, 14.3.

7.3.4 Rhodium-catalysed cycloisomerisation products

(–)-(*Z*)-2-Heptylidene-3-((*E*)-prop-1-en-1-yl)-1-tosylpyrrolidine, (*E*)-153a

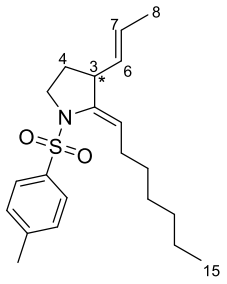

Synthesised from (*Z*)-*N*-(hex-3-en-1-yl)-4-methyl-*N*-(oct-1-yn-1-yl)benzenesulfonamide (*Z*)-**151a** (20 mg, 0.055 mmol) using **Procedure 11**, with the reaction mixture stirred at room temperature for 5 min. The resulting crude material was purified by column chromatography (10% Et_2O in petroleum ether) to give (*E*)-**153a** as a colourless oil (19.8 mg, 0.054 mmol, 98%); $[\boldsymbol{\alpha}]_{\boldsymbol{D}}^{\mathbf{25}}$ –67.3 (c = 1.0, $CHCl_3$); 97% *ee* (CHIRALPAK IC, 40% IPA/hexane, 0.3 mL/min, t_R major – 18.26 min, minor – 19.87 min); $\mathbf{R}_f$ = 0.62 (4:1, petroleum ether:EtOAc); $\boldsymbol{\delta}_\mathbf{H}$ (500 MHz, $CDCl_3$) 7.69 (2H d, *J* = 8.1 Hz, Ts*H*), 7.28 (2H, d, *J* = 8.1 Hz, Ts*H*), 5.27 (1H, dq, *J* = 15.1, 6.5 Hz, H7), 5.02–4.92 (2H, m, H6 and H9), 3.54 (1H, ddd, *J* = 11.4, 8.6, 3.0 Hz,H3'), 3.38 (1H, ddd, *J* = 11.4, 9.2, 7.9 Hz, H3''), 2.49–2.34 (2H, m, H10), 2.43 (3H, s, ArCH_3), 2.24 (1H, br. ap. q, *J* = 8.5 Hz, H3), 1.69 (1H, dddd, *J* = 12.0, 8.0, 7.9, 3.0 Hz, H4'), 1.62 (3H, dd, *J* = 6.6, 1.6 Hz, H8), 1.45–1.24 (9H, m, H4'' and H11–14), 0.88 (3H, t, *J* = 6.9 Hz, H15); $\boldsymbol{\delta}_\mathbf{C}$ (125 MHz, $CDCl_3$) 143.6, 139.9, 134.8, 130.4, 129.4, 127.8, 127.5, 121.2, 49.1, 45.6, 31.7, 29.8, 29.3, 29.0, 29.0, 22.7, 21.6, 17.8, 14.1; **IR** (thin film) ν_{max}/cm^{-1} 2923, 1355, 1165; **HRMS** *m/z* (ESI+) found $[M+Na]^+$ 384.1964; $C_{21}H_{31}NNaO_2S^+$ requires 384.1968.

(–)-2-((*Z*)-Henzylidene)-3-((*E*)-prop-1-en-1-yl)-1-tosylpyrrolidine, (*E*)-153b

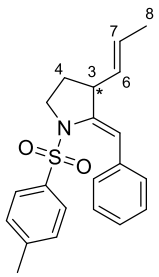

Synthesised from (*Z*)-*N*-(hex-3-en-1-yl)-4-methyl-*N*-(phenylethynyl)benzenesulfonamide (*Z*)-**151b** (10 mg, 0.028 mmol) using **Procedure 11**, with the reaction mixture stirred for 10 min. The resulting crude

material was purified by column chromatography (25% Et_2O in petroleum ether) to give (*E*)-**153b** as a pale yellow oil (9.4 mg, 0.026 mmol, 93%); $[\boldsymbol{\alpha}]_{\boldsymbol{D}}^{\mathbf{25}}$ –38.1 (c = 1.0, $CHCl_3$); 96% *ee* (CHIRALPAK IC, 40% IPA/hexane, 0.3 mL/min, t_R major – 20.56 min, minor – 22.84 min); $\mathbf{R}_f$ = 0.32 (5:1, petroleum ether:EtOAc); $\boldsymbol{\delta}_\mathbf{H}$ (500 MHz, $CDCl_3$) 7.66 (2H, d, *J* = 8.5 Hz, Ts*H*), 7.62 (2H, d, *J* = 7.6 Hz, Ph*H*), 7.32–7.24 (4H, m, Ts*H* and Ph*H*), 7.18 (1H, br. t, *J* = 7.4 Hz, Ph*H*), 5.93 (1H, d, *J* = 1.9 Hz, =C*H*Ph), 5.40 (1H, dq, *J* = 15.1 and 6.3 Hz, H7), 5.10 (1H, ddd, *J* = 15.1, 8.3, 1.6 Hz, H6), 3.69 (1H, ddd, *J* = 11.4, 8.7, 3.2 Hz, H3′), 3.52 (1H, ddd, *J* = 11.4, 9.1, 7.6 Hz, H3″), 2.52 (1H, dddd, *J* = 10.5, 8.3, 8.0, 1.9 Hz, H3), 2.43 (3H, s, ArCH_3), 1.80 (1H, dddd, *J* = 12.0, 8.0, 7.6, 3.2 Hz, H4'), 1.68 (3H, dd, *J* = 6.3 and 1.6 Hz, CH_3), 1.42 (1H, dddd, *J* = 12.0, 10.5, 9.1, 8.7 Hz, H4"); $\boldsymbol{\delta}_\mathbf{C}$ (125 MHz, $CDCl_3$) 143.9, 141.0, 136.5, 134.5, 130.1, 129.4, 128.8, 128.3, 128.0, 127.7, 126.7, 118.5, 49.1, 46.7, 28.9, 21.6, 17.9; **IR** (thin film) ν_{max}/cm^{-1} 2968, 1358, 1164; **HRMS** *m/z* (ESI+) found $[M+Na]^+$ 376.1343; $C_{21}H_{23}NNaO_2S^+$ requires 376.1342.

(–)-2-((*Z*)-4-Fluorobenzylidene)-3-((*E*)-prop-1-en-1-yl)-1-tosylpyrrolidine, (*E*)-**153c**

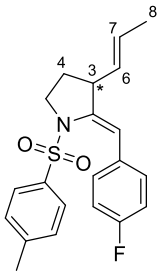

Synthesised from (*Z*)-*N*-((4-fluorophenyl)ethynyl)-*N*-(hex-3-en-1-yl)-4-methylbenzenesulfonamide (*Z*)-**151c** (10 mg, 0.027 mmol) using **Procedure 11**, with the reaction mixture stirred for 30 min. The resulting crude material was purified by column chromatography (25% Et_2O in petroleum ether) to give (*E*)-**153c** as a pale yellow oil (9.5 mg, 0.026 mmol, 95%); $[\boldsymbol{\alpha}]_{\boldsymbol{D}}^{\mathbf{25}}$ –23.5 (c = 1.0, $CHCl_3$); 94% *ee* (CHIRALPAK IC, 40% IPA/hexane, 0.3 mL/min, t_R major – 20.48 min, minor – 22.35 min); $\mathbf{R}_f$ = 0.28 (5:1, petroleum ether:EtOAc); $\boldsymbol{\delta}_\mathbf{H}$ (500 MHz, $CDCl_3$) 7.77 (2H, d, *J* = 8.5 Hz, Ts*H*), 7.61 (2H, d, *J* = 7.6 Hz, Ph*H*), 7.32–7.24 (4H, m, Ts*H* and Ph*H*), 5.97 (1H, d, *J* = 1.9 Hz, =C*H*Ph), 5.40 (1H, dq, *J* = 15.1 and 6.3 Hz, H7), 5.10 (1H, ddd, *J* = 15.1, 8.3, 1.6 Hz, H6), 3.69 (1H, ddd, *J* = 11.4, 8.7, 3.2 Hz, H3′), 3.52 (1H, ddd, *J* = 11.4, 9.1, 7.6 Hz, H3″), 2.52 (1H, dddd, *J* = 10.5, 8.3, 8.0, 1.9 Hz, H3), 2.43 (3H, s, ArCH_3), 1.80 (1H, dddd, *J* = 12.0, 8.0, 7.6, 3.2 Hz, H4'), 1.68 (3H, dd, *J* = 6.3 and 1.6 Hz, CH_3),

1.42 (1H, dddd, *J* = 12.0, 10.5, 9.1, 8.7 Hz, H4"); **δC** (125 MHz, $CDCl_3$) 160.1 (d, J = 249.0 Hz), 146.3, 143.8, 136.0, 133.6 (d, J = 234.0 Hz), 129.8, 129.7, 129.6, 129.5, 128.3, 128.0, 127.4, 115.1 (d, J = 22.0 Hz), 49.7, 47.3, 32.6, 21.7, 17.8; **δF** (470 MHz, $CDCl_3$) –116.3; **IR** (thin film) ν_{max}/cm^{-1} 3067, 2920, 1594, 1503, 1357, 1225, 1162; **HRMS** *m/z* (ESI+) found $[M+Na]^+$ 394.1250; $C_{21}H_{22F}NNaO_2S^+$ requires 394.1253.

(–)-2-((*Z*)-4-Methoxybenzylidene)-3-((*E*)-prop-1-en-1-yl)-1-tosylpyrrolidine, (*E*)-153d

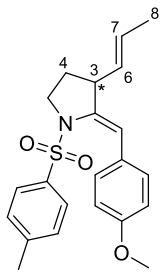

Synthesised from (*Z*)-*N*-(hex-3-en-1-yl)-*N*-((4-methoxyphenyl)ethynyl)-4-methylbenzenesulfonamide (*Z*)-**151d** (10 mg, 0.026 mmol) using **Procedure 11**, with the reaction mixture stirred for 5 min. The resulting crude material was purified by column chromatography (25% Et_2O in petroleum ether) to give (*E*)-**153d** as a pale yellow oil (8.7 mg, 0.023 mmol, 87%); $[\boldsymbol{\alpha}]_{\boldsymbol{D}}^{\mathbf{25}}$ –53.5 (c = 1.0, $CHCl_3$); 95% *ee* (CHIRALPAK IC, 40% IPA/hexane, 0.3 mL/min, t_R major – 26.81 min, minor – 28.02 min); $\mathbf{R}_f$ = 0.22 (5:1, petroleum ether:EtOAc); **δH** (500 MHz, $CDCl_3$) 7.77 (2H, d, *J* = 8.5 Hz, Ts*H*), 7.43 (2H, d, *J* = 7.6 Hz, Ph*H*), 7.32–7.21 (4H, m, Ts*H* and Ph*H*), 5.37 (1H, d, *J* = 1.5 Hz, =C*H*Ph), 5.40 (1H, dq, *J* = 15.1 and 6.3 Hz, H7), 5.10 (1H, ddd, *J* = 15.1, 8.3, 1.6 Hz, H6), 3.69 (1H, ddd, *J* = 11.4, 8.7, 3.2 Hz, H3′), 3.57 (3H, s, OCH_3), 3.52 (1H, ddd, *J* = 11.4, 9.1, 7.6 Hz, H3″), 2.52 (1H, dddd, *J* = 10.5, 8.3, 8.0, 1.9 Hz, H3), 2.43 (3H, s, ArCH_3), 1.80 (1H, dddd, *J* = 12.0, 8.0, 7.6, 3.2 Hz, H4'), 1.68 (3H, dd, *J* = 6.3 and 1.6 Hz, CH_3), 1.42 (1H, dddd, *J* = 12.0, 10.5, 9.1, 8.7 Hz, H4"); **δC** (125 MHz, $CDCl_3$) 161.0, 146.1, 143.8, 136.1, 130.1, 129.8, 129.7, 129.2, 128.2, 128.0, 127.4, 113.3, 55.4, 49.7, 47.0, 32.7, 21.6, 17.6; **IR** (thin film) ν_{max}/cm^{-1} 3012, 2950, 2835, 1609, 1513, 1352, 1242, 1161; **HRMS** *m/z* (ESI+) found $[M+Na]^+$ 406.1451; $C_{22}H_{25}NNaO_3S^+$ requires 406.1453.

(–)-(*Z*)-2-Heptylidene-3-((*E*)-styryl)-1-tosylpyrrolidine, (*E*)-153e

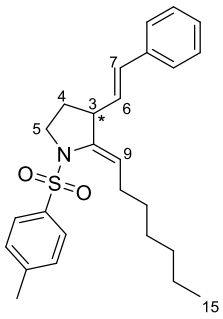

Synthesised from (*Z*)-4-methyl-*N*-(oct-1-yn-1-yl)-*N*-(5-phenylpent-3-en-1-yl)benzenesulfonamide (*Z*)-**151e** (10 mg, 0.024 mmol) using **Procedure 11**, with the reaction mixture stirred at room temperature for 30 min. The resulting crude material was purified by column chromatography (20% Et_2O in petroleum ether) to give (*E*)-**153e** as a colourless oil (9.1 mg, 0.022 mmol, 93%); $[\boldsymbol{\alpha}]_{\boldsymbol{D}}^{\mathbf{25}}$ –125.5 (c = 1.0, $CHCl_3$); 93% *ee* (CHIRALPAK IC, 40% IPA/hexane, 0.3 mL/min, t_R major – 19.18 min, minor – 21.43 min); $\mathbf{R}_f$ = 0.50 (4:1, petroleum ether:EtOAc); $\boldsymbol{\delta}_\mathbf{H}$ (500 MHz, $CDCl_3$) 7.78 (2H d, *J* = 8.1 Hz, Ts*H*), 7.43–7.25 (6H, m, Ts*H* and Ph*H*), 7.22–7.19(1H, m, Ph*H*), 6.40–6.27 (2H, m, H6 and H7), 5.02 (1H, dt, *J* = 6.9 and 1.8 Hz, H9), 3.54 (1H, ddd, *J* = 11.4, 8.6, 3.0 Hz,H5'), 3.38 (1H, ddd, *J* = 11.4, 9.2, 7.9 Hz, H5"), 2.49–2.34 (2H, m, H10), 2.43 (3H, s, ArCH_3), 2.24 (1H, br. ap. q, *J* = 8.5 Hz, H3), 1.69 (1H, dddd, *J* = 12.0, 8.0, 7.9, 3.0 Hz, H4'), 1.62 (3H, dd, *J* = 6.6, 1.6 Hz, H8), 1.45–1.24 (9H, m, H4" and H11–14), 0.88 (3H, t, *J* = 6.9 Hz, H15); $\boldsymbol{\delta}_\mathbf{C}$ (125 MHz, $CDCl_3$) 143.7, 140.2, 137.3, 136.0, 130.7, 129.7, 129.4, 128.6, 128.3, 128.2, 126.1, 117.7, 48.5, 47.4, 32.8, 31.7, 28.90, 28.4, 25.3, 22.7, 21.5, 14.1; **IR** (thin film) ν_{max}/cm^{-1} 2934, 2257, 1358, 1167; **HRMS** *m/z* (ESI+) found $[M+Na]^+$ 424.2313; $C_{26}H_{33}NNaO_2S^+$ requires 424.2310.

(–)-2-((*Z*)-Benzylidene)-3-((*E*)-prop-1-en-1-yl)-1-tosylpyrrolidine, (*E*)-153f

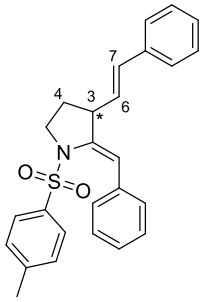

Synthesised from (*Z*)-4-methyl-*N*-(phenylethynyl)-*N*-(5-phenylpent-3-en-1-yl)benzenesulfonamide (*Z*)-**151f** (10 mg, 0.024 mmol) using **Procedure 11**, with the reaction mixture stirred for 45 min. The resulting crude material was purified by column chromatography (25% Et_2O in petroleum ether) to give (*E*)-**153f** as a pale yellow oil (8.4 mg, 0.020 mmol, 83%); $[\boldsymbol{\alpha}]_{\boldsymbol{D}}^{\mathbf{25}}$ –83.5 (c = 1.0, $CHCl_3$); 94% *ee* (CHIRALPAK IC, 40% IPA/hexane, 0.3 mL/min, t_R major – 19.76 min, minor – 21.43 min); $\mathbf{R}_f$ = 0.41 (5:1, petroleum ether:EtOAc); $\boldsymbol{\delta}_\mathbf{H}$ (500 MHz, $CDCl_3$) 7.78 (2H, d, *J* = 8.5 Hz, Ts*H*), 7.35–7.18 (12H, m, Ts*H* and Ph*H*), 5.93 (1H, d, *J* = 1.9 Hz, =C*H*Ph), 5.40 (1H, dq, *J* = 15.1 and 6.3 Hz, H7), 5.10 (1H, ddd, *J* = 15.1, 8.3, 1.6 Hz, H6), 3.69 (1H, ddd, *J* = 11.4, 8.7, 3.2 Hz, H5′), 3.52 (1H, ddd, *J* = 11.4, 9.1, 7.6 Hz, H5″), 2.52 (1H, dddd, *J* = 10.5, 8.3, 8.0, 1.9 Hz, H3), 2.43 (3H, s, ArCH_3), 1.80 (1H, dddd, *J* = 12.0, 8.0, 7.6, 3.2 Hz, H4'), 1.68 (3H, dd, *J* = 6.3 and 1.6 Hz, CH_3), 1.42 (1H, dddd, *J* = 12.0, 10.5, 9.1, 8.7 Hz, H4"); $\boldsymbol{\delta}_\mathbf{C}$ (125 MHz, $CDCl_3$) 146.1, 144.1, 136.8, 136.0, 134.4, 131.0, 129.8, 129.5, 129.0, 128.6, 128.4, 128.2, 128.1, 128.0, 127.72, 126.5, 50.7, 47.2, 32.4, 21.5; **IR** (thin film) ν_{max}/cm^{-1} 2938, 2254, 1350, 1159; **HRMS** *m/z* (ESI+) found $[M+Na]^+$ 438.1508; $C_{26}H_{25}NNaO_2S^+$ requires 438.1504.

(–)-(*Z*)-3-((*E*)-But-1-en-1-yl)-2-heptylidene-3-methyl-1-tosylpyrrolidine, (*E*)-276a

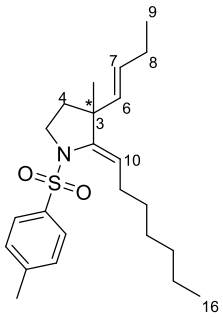

Synthesised from (*Z*)-4-methyl-*N*-(3-methylhept-3-en-1-yl)-*N*-(oct-1-yn-1-yl)benzenesulfonamide (*Z*)-**264a** (10 mg, 0.025 mmol) using **Procedure 11**, with the reaction mixture stirred for 80 min. The resulting crude material was purified by column chromatography (25% Et_2O in petroleum ether) to give (*E*)-**276a** as a pale yellow oil (6.2 mg, 0.015 mmol, 61%); $[\boldsymbol{\alpha}]_{\boldsymbol{D}}^{\mathbf{25}}$ –53.5 (c = 1.0, $CHCl_3$); 94% *ee* (CHIRALPAK IC, 40% IPA/hexane, 0.3 mL/min, t_R major – 16.26 min, minor – 18.19 min); $\mathbf{R}_f$ = 0.53 (5:1, petroleum ether:EtOAc); $\boldsymbol{\delta}_\mathbf{H}$ (500 MHz, $CDCl_3$) 7.70 (2H d, *J* = 8.1 Hz, Ts*H*), 7.28 (2H, d, *J* = 8.1 Hz, Ts*H*), 5.27 (1H, dt, *J* = 15.1, 6.5 Hz, H7), 5.02–4.92 (2H, m, H6 and H10), 3.54 (1H, ddd, *J* = 11.4, 8.6, 3.0 Hz,H5'), 3.38 (1H, ddd, *J* = 11.4, 9.2, 7.9 Hz, H5''), 2.49–2.34 (2H, m, H11), 2.43 (3H, s, ArCH_3), 1.99 (2H, m, H8), 1.69 (1H, ddd, *J* = 12.0, 7.9, 3.0 Hz, H4'), , 1.45–1.24 (9H, m, H4'' and H12–15), 1.18 (3H, s, CH_3), 0.95 (3H, t, *J* = 7.0, H9), 0.88 (3H, t, *J* = 6.9 Hz, H16); $\boldsymbol{\delta}_\mathbf{C}$ (125 MHz, $CDCl_3$) 146.0, 143.8, 136.6, 135.8, 135.9, 129.8, 128.3, 111.3, 53.7, 46.8, 40.3, 31.2, 28.9, 28.1, 26.3, 26.2, 25.3, 22.5, 21.7, 14.1, 13.9; **IR** (thin film) ν_{max}/cm^{-1} 2924, 1357, 1163; **HRMS** *m/z* (ESI+) found $[M+Na]^+$ 412.2285; $C_{23}H_{35}NNaO_2S^+$ requires 412.2286.

(–)-2-((*Z*)-Benzylidene)-3-((*E*)-but-1-en-1-yl)-3-methyl-1-tosylpyrrolidine, (*E*)-276b

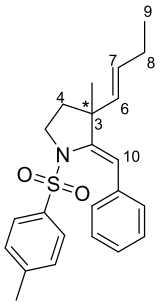

Synthesised from (*Z*)-4-methyl-*N*-(3-methylhept-3-en-1-yl)-*N*-(phenylethynyl)benzenesulfonamide (*Z*)-**264b** (10 mg, 0.026 mmol) using **Procedure 11**, with the reaction mixture stirred for 105 min. The resulting crude material was purified by column chromatography (25% Et_2O in petroleum ether) to give (*E*)-**276b** as a pale yellow oil (5.2 mg, 0.014 mmol, 52%); $[\boldsymbol{\alpha}]_{\boldsymbol{D}}^{\mathbf{25}}$ –31.7 (c = 1.0, $CHCl_3$); 92% *ee* (CHIRALPAK IC, 40% IPA/hexane, 0.3 mL/min, t_R major – 23.41 min, minor – 24.77 min); $\mathbf{R}_f$ = 0.33 (5:1, petroleum ether:EtOAc); $\boldsymbol{\delta}_{\mathbf{H}}$ (500 MHz, $CDCl_3$) 7.70 (2H d, *J* = 8.1 Hz, Ts*H*), 7.43–7.16 (4H, m, Ts*H* and Ph*H*), 7.03 (1H, m, Ph*H*), 5.27 (1H, dt, *J* = 15.1, 6.5 Hz, H7), 5.02–4.92 (2H, m, H6 and H10), 3.54 (1H, ddd, *J* = 11.4, 8.6, 3.0 Hz,H5'), 3.38 (1H, ddd, *J* = 11.4, 9.2, 7.9 Hz, H5''), 2.43 (3H, s, ArCH_3), 1.99 (2H, m, H8), 1.69 (1H, ddd, *J* = 12.0, 8.0, 3.0 Hz, H4'), , 1.45–1.24 (1H, m, H4'') 1.18 (3H, s, CH_3), 0.95 (3H, t, *J* = 7.0, H9); $\boldsymbol{\delta}_{\mathbf{C}}$ (125 MHz, $CDCl_3$) 148.4, 143.8, 136.7, 135.9, 135.6, 132.1, 130.1, 129.1, 128.4, 128.1, 127.8, 126.1, 54.5, 43.9, 40.4, 26.1, 25.4, 21.3, 14.3; **IR** (thin film) ν_{max}/cm^{-1} 2963, 1352, 1162; **HRMS** *m/z* (ESI+) found $[M+Na]^+$ 404.1658; $C_{23}H_{27}NNaO_2S^+$ requires 404.1660.

(–)-(*Z*)-2-Heptylidene-3-((*E*)-pent-2-en-2-yl)-1-tosylpyrrolidine, (*E*)-**276c**

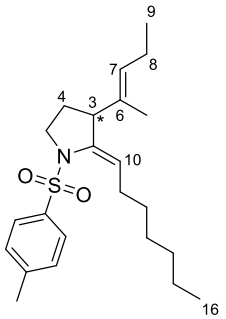

Synthesised from (*Z*)-4-methyl-*N*-(4-methyloct-3-en-1-yl)-*N*-(oct-1-yn-1-yl)benzenesulfonamide (*Z*)-**269a** (10 mg, 0.025 mmol) using **Procedure 11**, with the reaction mixture stirred at room temperature for 45 min. The resulting crude material was purified by column chromatography (10% Et_2O in

petroleum ether) to give (*E*)-**276c** as a colourless oil (9.4 mg, 0.024 mmol, 95%); $[\alpha]_D^{25}$ –63.5 (c = 1.0, $CHCl_3$); 93% *ee* (CHIRALPAK IC, 40% IPA/hexane, 0.3 mL/min, t_R major – 18.86 min, minor – 21.25 min); $\mathbf{R}_f$ = 0.54 (4:1, petroleum ether:EtOAc); $\boldsymbol{\delta}_\mathbf{H}$ (500 MHz, $CDCl_3$) 7.70 (2H d, *J* = 8.1 Hz, Ts*H*), 7.28 (2H, d, *J* = 8.1 Hz, Ts*H*), 5.27 (1H, t, *J* = 7.0 Hz, H7), 5.05 (1H, m, H10), 3.54 (1H, ddd, *J* = 11.4, 8.6, 3.0 Hz,H5'), 3.38 (1H, ddd, *J* = 11.4, 9.2, 7.9 Hz, H5"), 2.49–2.34 (2H, m, H11), 2.43 (3H, s, ArCH_3), 2.24 (1H, br. t, *J* = 8.5 Hz, H3), 1.69 (1H, dddd, *J* = 12.0, 8.0, 3.0 Hz, H4'), 1.62 (3H, d9, *J* = 6.6, 1.6 Hz, H8), 1.57 (3H, s, CH_3), 1.45–1.24 (9H, m, H4" and H12–15), 0.90 (3H, t, *J* = 7.0 Hz, H9), 0.88 (3H, t, *J* = 6.9 Hz, H16); $\boldsymbol{\delta}_\mathbf{C}$ (125 MHz, $CDCl_3$) 143.5, 140.0, 136.1, 132.7, 133.0, 129.8, 127.3, 113.1, 51.3, 47.8, 32.4, 31.8, 28.9, 28.1, 25.6, 22.6, 21.3, 20.4, 16.0, 14.2, 14.0; **IR** (thin film) ν_{max}/cm^{-1} 2930, 1345, 1164; **HRMS** *m/z* (ESI+) found $[M+Na]^+$ 426.2441; $C_{24}H_{37}NNaO_2S^+$ requires 426.2443.

(–)-2-((*Z*)-Benzylidene)-3-((*E*)-pent-2-en-2-yl)-1-tosylpyrrolidine, (*E*)-276d

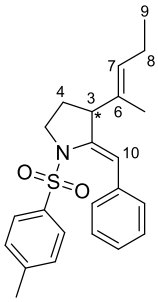

Synthesised from (*Z*)-4-methyl-*N*-(4-methyloct-3-en-1-yl)-*N*-(phenylethynyl)benzenesulfonamide (*Z*)-**269b** (10 mg, 0.025 mmol) using **Procedure 11**, with the reaction mixture stirred for 55 min. The resulting crude material was purified by column chromatography (25% Et_2O in petroleum ether) to give (*E*)-**276d** as a pale yellow oil (9.4 mg, 0.023 mmol, 92%); $[\alpha]_D^{25}$ –23.5 (c = 1.0, $CHCl_3$); 94% *ee* (CHIRALPAK IC, 40% IPA/hexane, 0.3 mL/min, t_R major – 24.86 min, minor – 25.71 min); $\mathbf{R}_f$ = 0.33 (5:1, petroleum ether:EtOAc); $\boldsymbol{\delta}_\mathbf{H}$ (500 MHz, $CDCl_3$) 7.70 (2H d, *J* = 8.1 Hz, Ts*H*), 7.40–7.28 (4H, m, Ts*H* and Ph*H*), 7.15(1H, m, Ph*H*), 5.27 (1H, t, *J* = 7.0 Hz, H7), 5.05 (1H, m, H10), 3.54 (1H, ddd, *J* = 11.4, 8.6, 3.0 Hz,H5'), 3.38 (1H, ddd, *J* = 11.4, 9.2, 7.9 Hz, H5"), 2.43 (3H, s, ArCH_3), 2.25 (1H, br. t, *J* = 8.5 Hz, H3), 1.69 (1H, dddd, *J* = 11.9, 7.9, 8.0, 3.0 Hz, H4'), 1.62 (3H, dq, *J* = 6.6, 1.6 Hz, H8), 1.57 (3H, s, CH_3), 1.45–1.24 (1H, dddd, *J* = 12.0, 7.9, 8.0, 2.8 Hz, H4"), 0.90 (3H, t, *J* = 7.0 Hz, H9); $\boldsymbol{\delta}_\mathbf{C}$ (125 MHz, $CDCl_3$) 144.2, 143.0, 136.1, 135.1, 132.8, 132.7, 132.4, 129.9, 129.2, 128.5, 128.3, 128.0,

54.3, 48.1, 32.3, 21.6, 21.3, 16.1, 14.1; **IR** (thin film) ν_{max}/cm^{-1} 2927, 1355, 1164; **HRMS** *m/z* (ESI+) found $[M+Na]^+$ 418.1821; $C_{24}H_{29}NNaO_2S^+$ requires 418.1817.

7.4 X-Ray Crystallographic Data[1]

Low temperature[120] single crystal X-ray diffraction data were collected using I19-1 at the Diamond Light Source[121] at 100 K. Data were reduced using CrysAlisPro. All structures were solved ab initio using SuperFlip[123] and the structures were refined using CRYSTALS.[124]

Structure DIA0293 (**239a**) contained large solvent accessible voids comprising weak, diffuse electron density. The discrete Fourier transforms of the void regions were treated as contributions to the A and B parts of the calculated structure factors using PLATON/SQUEEZE[125] integrated within the CRYSTALS software.

Table 7.1 Summary of X-ray crystallographic data

Compound Number	**239a (DIA0293)**
Moiety Formula	$RhSbF_6Cl_2O_2P_2C_{46}H_{64}$
CCDC	n/a
Space Group	P 6_5
a [Å]	11.45500(10)
b [Å]	11.45500(10)
c [Å]	57.6292(5)
α [°]	90
β [°]	90
γ [°]	120
V [$Å^3$]	6548.82(12)
Z	6
T [K]	100
Total Reflections	133295
R_{int}	0.1128
Reflections, Restraints, Parameters (I>-3.0/ σ (I))	21721, 1, 542
Min. and Max. Residual Density, [$eÅ^{-3}$]	-1.69, 1.77
R_1 (I>2σ(I))	0.0453
wR_2	0.1065

[1] The X-ray data were collected and processed by Steven J. Mansfield.

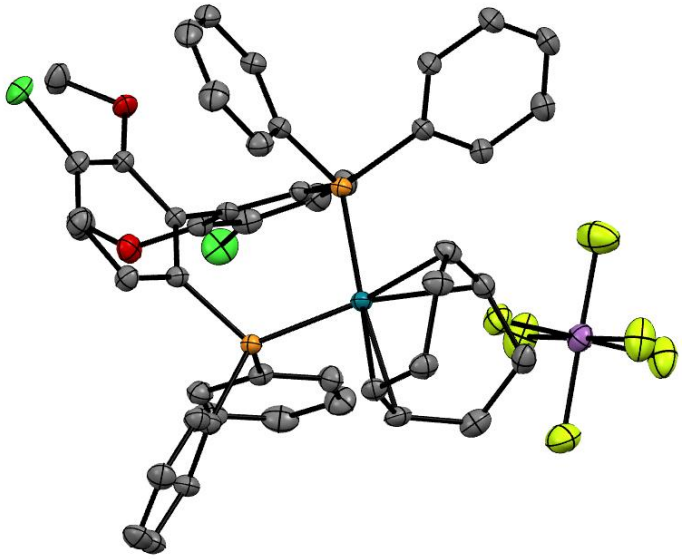

Figure 7.1: Solid state structure of **239a**. Displacement ellipsoid plots are drawn at 50% probability. Hydrogen atoms are omitted for clarity.

Chapter 8: References

1. K. Alder, F. Pascher and A. Schmitz, *Ber. Dtsch. Chem. Ges. B*, **1943**, *76*, 27–53.

2. V. Michelet, P. Y. Toullec, and J. P. Genêt, *Angew. Chem. Int. Ed.* **2008**, *47*, 4268–4315.

3. S. I. Lee and N. Chatani, *Chem. Commun.* **2009**, 371–384.

4. A. Marinetti, H. Jullien, and A. Voituriez, *Chem. Soc. Rev.* **2012**, *41*, 4884–4908.

5. W. Oppolzer and V. Snieckus, *Angew. Chem. Int. Ed. Engl.* **1978**, *17*, 476–486.

6. B. M. Trost and M. Lautens, *J. Am. Chem. Soc.* **1985**, *107*, 1781–1783.

7. I. D. G. Watson and F. D. Toste, *Chem. Sci.* **2012**, *3*, 2899–2919.

8. G. C. Lloyd-Jones, *Org. Biomol. Chem.* **2003**, *1*, 215–236.

9. B. M. Trost, M. Lautens, C. Chan, D. J. Jebaratnam, and T. Mueller, *J. Am. Chem. Soc*. **1991**, *113*, 636–644.

10. B. M. Trost, G. J. Tanoury, M. Lautens, C. Chan, and D. T. MacPherson, J . Am. Chem. Soc. **1994**, *116*, 4255–4267.

11. B. M. Trost and G. J. Tanoury, *J. Am. Chem. Soc.*, 1987, **109**, 4753–4755.

12. Trost, B. M. *Chem. Eur. J.* **1998**, *4*, 2405–2412.

13. C. Amatore, A. Jutand, G. Meyer, I. Carelli, and I. Chiarotto, *Eur. J. Inorg. Chem.* **2000**, 1855–1859.

14. B. M. Trost, D. C. Lee and F. Rise, *Tetrahedron Lett.* **1989**, *30*, 651–654.

15. B. M. Trost, D. L. Romero and F. Rise, *J. Am. Chem. Soc.* **1994**, *116*, 4268–4278.

16. B. M. Trost and Y. Shi, *J. Am. Chem. Soc.* **1993**, *115*, 9421–9438.

17. M. Hatano, M. Terada and K. Mikami, *Angew. Chem. Int., Ed.* **2001**, *40*, 249–253.

18. K. Mikami and M. Hatano, *Proc. Natl. Acad. Sci.* **2004**, *101*, 5767–5769.

19. B. M. Trost, E. M. Ferreira and A. C. Gutierrez, *J. Am. Chem. Soc.* **2008**, *130*, 16176–16177.

20. P. R. Walker, C. D. Campbell, A. Suleman, G. Carr and E. A. Anderson, *Angew. Chem. Int. Ed.* **2013**, *52*, 9139–9143.

21. M. Nishida, N. Adachi, K. Onozuka, H. Matsumura and M. Mori, *J. Org. Chem.* **1998**, *63*, 9158–9159.

22. M. Mori, Y. Kozawa, M. Nishida, M. Kanamaru, K. Onozuka and M. Takimoto, *Org. Lett.* **2000**, *2*, 3245–3247.

23. B. M. Trost and F. D. Toste, *J. Am. Chem. Soc.* **1999**, *121*, 9728–9729.

24. B. M. Trost and F. D. Toste, *J. Am. Chem. Soc.* **2000**, *122*, 714–715.

25. B. M. Trost and F. D. Toste, *J. Am. Chem. Soc.* **2002**, *124*, 5025–5036.

26 B. M. Trost and F. D. Toste, *Tetrahedron Lett.* **1999**, *40*, 7739–7743.

27. J. Le Paih, D. C. Rodriguez, S. Derien and P. H. Dixneuf, *Synlett*, **2000**, *1*, 95–97.

28. B. M. Trost, J. P. Surivet, and F. D. Toste, *J. Am. Chem. Soc.* **2004**, *126*, 15592–15602.

29. B. M. Trost, E. M. Ferreira, and A. C. Gutierrez, *J. Am. Chem. Soc.* **2008**, *130*, 16176–16177.

30. K. Takamoto, S. Ohno, N. Hyogo, H. Fujioka, and M. Arisawa, *J. Org. Chem.* **2017**, *82*, 8733−8742.

31. R. Dorel and A. M. Echavarren, *Chem. Rev.* **2015**, *115*, 9028−9072

32. E. Jiménez-Núñez and A. M. Echavarren, *Chem. Rev.* **2008**, *108*, 3326–3350.

33. C. Ferrer, M. Raducan, C. Nevado, C. K. Claverie and A. M. Echavarren, *Tetrahedron* **2007**, *63*, 6306−6316.

34. C. Nieto-Oberhuber, M. P. Muñoz, S. López, E. Jiménez-Núñez, C. Nevado, E. Herrero-Gómez, M. Raducan, and A. M. Echavarren, *Chem. Eur. J.* **2006**, *12*, 1677−1693. (corrigendum: *Chem. Eur. J.* **2008**, *14*, 5096).

35. R. Grigg, P. Stevenson and T. Worakun, *Tetrahedron*, **1988**, *44*, 4967−4972.

36. B. M. Trost and J. M. Tour, *J. Am. Chem. Soc.* **1987**, *109*, 5268−5270.

37. P. Cao, B. Wang and X. M. Zhang, *J. Am. Chem. Soc*. **2000**, *122*, 6490−6491.

38. F. A. Hicks, N. M. Kablaoui and S. L. Buchwald, *J. Am. Chem. Soc.* **1996**, *118*, 9450−9451.

39. B. M. Trost and S. F. Chen, S. F., *J. Am. Chem. Soc.* **1986**, *108*, 6053−6054.

40. B. M. Trost and D. C. Lee, *J. Org. Chem.* **1989**, *54*, 2271−2274.

41. Y. Zhang, R. P. Hsung, M. R. Tracey, K. C. M. Kurtz, and E. L. Vera, *Org. Lett.* **2004**, *6*, 1151–1154.

42. D. B. G. Williams and M. Lawton, *J. Org. Chem.* **2010**, *75*, 8351–8354.

43. R. B. Bedford, J. G. Bowen, R. B. Davidson, M. F. Haddow, A. E. Seymour-Julen, H. A. Sparkes and R. L. Webster, *Angew. Chem. Int. Ed.* **2015**, *54*, 6591–6594.

44. B. M. Trost, C. D. Haffner, D. J. Jebaratnam, M. J. Krische and A. P. Thomas, *J. Am. Chem. Soc.* **1999**, *121*, 6183−6192.

45. M. Miyashita, M. Sasaki, I. Hattori, M. Sakai and K. Tanino, *Science* **2004**, 305, 495−499.

46. J. Yang, K. Hong and P. V. Bonne, *J. Label Compd. Radiopharm*. **2012**, *55* 463–466.

47. V. I. Bakhmutov, J. F. Berry, F. A. Cotton, S. Ibragimov and C. A. Murillo, *Dalton Trans.* **2005**, 1989−1992.

48. S. E. Bajwa, T. E. Storr, L. E. Hatcher, T. J. Williams, C. G. Baumann, A. C. Whitwood, D. R. Allan, S. J. Teat, P. R. Raithby and I. J. S. Fairlamb, *Chem. Sci.* **2012**, *3*, 1656–1661.

49. W. A. Carole, J. Bradley, M. Sarwar and T. J. Colacot, *Org. Lett.* **2015**, *17*, 5472−5475.

50. V. Chintalapudi, E. A. Galvin, R. L. Greenaway and E. A. Anderson, *Chem. Comm*. **2016**, *52*, 693–696.

51. M. J. Hilton, L. P. Xu, P. O. Norrby, Y. D. Wu, O. Wiest and M. S. Sigman, *J. Org. Chem*. **2014**, *79*, 11841−11850.

52. M. Gómez-Gallego and M. A. Sierra, *Chem. Rev.* **2011**, *111*, 4857−4963.

53. M. R. Netherton and G. C. Fu, *Angew. Chem., Int. Ed.* **2002**, *41*, 3910−3912.

54. R. A. M. O'Ferrall, *J. Chem. Soc. B* **1970**, 785−790.

55. J. Louie, F. Paul and J. F. Hartwig, *Organometallics* **1996**, *15*, 2794−2805.

56. For reviews on enantioselective cycloisomerisations, *see*: I. J. S. Fairlamb, *Angew. Chem. Int. Ed.* **2004**, *43*, 1048–1052; I. D. G. Watson, F. D. Toste, *Chem. Sci.* **2012**, *3*, 2899–2919.

57. B. M. Trost and B. A. Czeskis, *Tetrahedron Lett*. **1994**, *35*, 211–214.

58. A. Goeke, R. Kuwano, Y. Ito, and M.Sawamura, *Angew. Chem. Int. Ed.* **1996**, *35*, 662–663.

59. M. Hatano and K. Mikami, *J. Am. Chem. Soc.* **2003**, *125*, 4704–4705.

60. H. Imase, T. Suda, Y. Shibata, K. Noguchi, M. Hirano and K. Tanaka, *Org. Lett.* **2009**, *11*, 1805–1808.

61. N. Kadoya, M. Murai, M. Ishiguro, J. Uenishi, and M. Uemura, *Tetrahedron Lett*. **2013**, *54*, 512–514.

62. X. Quan, J. Liu, W. Rabten, S. Diomedi, T. Singh, and P. G. Andersson, *Eur. J. Org. Chem.* **2016**, 3427–3433.

63. A. Lei, M. He, S. Wu, and X. Zhang, *Angew. Chem. Int. Ed*. **2002**, *41*, 3457–3460.

64. A. Lei, J. P. Waldkirch, M. He, and X. Zhang. *Angew. Chem. Int. Ed*. **2002**, *41*, 4526–4529.

65. A. Lei, M. He, and X. Zhang, *J. Am. Chem. Soc*. **2002**, *124*, 8198–8199.

66. A. Lei, M. He, and X. Zhang *J. Am. Chem. Soc.* **2003**, *125*, 11472–11473.

67. N. Körber, F. Rominger, and T. J. J. Müller, *Adv. Synth. Catal.* **2009**, *351*, 2921–2935.

68. K. C. Nicolaou, A. Li, S. P. Ellery, and D. J. Edmonds, *Angew. Chem. Int. Ed*. **2009**, *48*, 6293–6295; and K. C. Nicolaou, A. Li, D. J. Edmonds, G. S. Tria, and S. P. Ellery, *J. Am. Chem. Soc.* **2009**, *131*, 16905–16918.

69. T. Nishimura, Y. Maeda, and T. Hayashi, *Org. Lett*. **2011**, *13*, 3674–3677.

70. T. Nishimura, Y. Takiguchi, Y. Maeda, and T. Hayashi, *Adv. Synth. Catal.* **2013**, *355*, 1374–1382.

71. K. Masutomi, K. Noguchi, and K. Tanaka, *J. Am. Chem. Soc*. **2014**, *136*, 7627–7630.

72. X. Deng, S. Ni, Z. Han, Y. Guan, H. Lv, L. Dang, and X. Zhang, *Angew. Chem. Int. Ed*. **2016**, *55*, 6295–6299.

73. L. Charruault, V. Michelet, R. Taras, S. Gladiali and J. Genêt, *Chem. Commun*. **2004**, 850–851.

74. M. P. Muñoz, J. Adrio, J. C. Carretero, and A. M. Echavarren, *Organometallics*. **2005**, *24*, 1293–1300.

75. T. Shibata, Y. Kobayashi, S. Maekawa, N. Toshida, and K. Takagi, *Tetrahedron*. **2005**, *61*, 9018–9024.

76. For reviews on applications of cycloisomerisations, *see*: C. I. Stathakis, P. L. Gkizisa, and A. L. Zografos*, Nat. Prod. Rep.*, **2016**, *33*,1093–1117; Y. Hu, M. Bai, Y. Yanga, and Q. Zhou, *Org. Chem. Front.*, **2017**, *Advance Article.*

77. J. P. Wolfe and S. L. Buchwald, *J. Org. Chem*. **2000**, *65*, 1144–1157.

76. J. A. Mulder, K. C. M. Kurtz, R. P. Hsung, H. Coverdale, M. O. Frederick, L. Shen, and C. A. Zificsak, *Org. Lett.* **2003**, *5* 1547–1550.

77. A. H. Sato, K. Ohashi, and T. Iwasawa, *Tetrahedron Lett.* **2013**, *54*, 1309–1311.

78. A. B. Dounay and L. E. Overman, *Chem. Rev.* **2003**, *103*, 2945–2964.

79. For reviews, *see*: I. J. S. Fairlamb, *Angew. Chem. Int. Ed.* **2004**, *43*, 1048–1052; and W. Chen and M. Xu, *Org. Biomol. Chem.* **2017**, *15*, 1029–1050.

80. R. N. Straker, Q. Peng, A. Mekareeya, R.S. Paton, and E. A. Anderson, *Nat. Commun*. **2016**, *7*, 1–9.

81. A. Lei, M. He, S. Wu, and X. Zhang, *Angew. Chem. Int. Ed*. **2002**, *41*, 3457–3460.

82. K. C. Nicolaou, A. Li, S. P. Ellery, and D. J. Edmonds, *Angew. Chem. Int. Ed*. **2009**, *48*, 6293–6295; and K. C. Nicolaou, A. Li, D. J. Edmonds, G. S. Tria, and S. P. Ellery, *J. Am. Chem. Soc.* **2009**, *131*, 16905–16918.

83. R. N. Straker, *Higher-Order Cycloisomerisations of Enynamides*, DPhil Thesis, University of Oxford, **2016**.

84. A. Lei, J. P. Waldkirch, M. He, and X. Zhang. *Angew. Chem. Int. Ed*. **2002**, *41*, 4526–4529.

85. I. D. Gridnev, N. Higashi, K. Asakura, and T. Imamoto, *J. Am. Chem. Soc.* **2000**, *122*, 7183–7194; and I. D. Gridnev and T. Imamoto, *Acc. Chem. Res.* **2004**, *37*, 633–644.

86. A. Preetz, C. Fischer, C. Kohrt, H. Drexler, W. Baumann, and D. Heller, *Organometallics*, **2011**, *30*, 5155–5159.

87. C. L. Rand, D. E. Van Horn, M. W. Moore, and E. A. Negishi, *J. Org. Chem.* **1981**, *46*, 4093–4096.

88. A. Yajima, M. Yamamoto, T. Nukada, and G. Yabuta, *Biosci. Biotechnol. Biochem.* **2007**, *71*, 2720–2724.

89. S. Ma and E. A. Negishi, *J. Org. Chem.* **1997**, *62*, 784–785.

90. S. M. Smith and J. M. Takacs, *J. Am. Chem. Soc.* **2010**, *132*, 1740–1741.

91. J. C. Ewing, G. S. Ferguson, D. W. Moore, F. W. Schultz, D. W. Thompson, *J. Org. Chem.* **1985**, *50*, 2124–2128.

92 A. Mekareeya, P. R. Walker, A. Couce-Rios, C.D. Campbell, A. Steven, R. S. Paton, and E. A. Anderson *J. Am. Chem. Soc.* **2017**, *139*. 10104–10114.

93. a) I. D. Gridnev, and T. Imamoto. *Acc. Chem. Res.* **2004**, *37*, 633–644.

b) I. D. Gridnev, N. Higashi, K. Asakura, and T. Imamoto. *J. Am. Chem. Soc*. **2000**, *122*, 7183–7194.

94. A. Preetz, C. Fischer, C. Kohrt, H. Drexler, W. Baumann, and D. Heller. *Organometallics*. **2011**, *30*, 5155–5159.

95. C. Aquino, S. N. Greszler, and G. C. Micalizio. *Org. Lett*. **2016**, *18*, 2624–2627.

96. H. Lee, V. Sampath, and Y Yoon. *Synlett*. **2009**, *2*, 249–252.

97. S. J. Mansfield, C. D. Campbell, M. W. Jones, and E. A. Anderson, *Chem. Commun*. **2015**, *51*, 3316.

98. R. K. Boeckman Jr., K. F. Biegasiewicz, D. J. Tusch, and J. R. Miller. *J. Org. Chem.* **2015**, *80*, 4030–4045.

99. 41. Y. Zhang, R. P. Hsung, M. R. Tracey, K. C. M. Kurtz, and E. L. Vera, *Org. Lett*. **2004**, *6*, 1151–1154.

100. Fukudome, Y.; Naito, H.; Hata, T.; Urabe, H. *J. Am. Chem. Soc.* **2008**, *130*, 1820–1821.

101. Pak, C. S.; Kim, T. H.; Ha, S. J. *J. Org. Chem.* **1998**, *63*, 10006–10010.

102. Cho, Y.-J.; Kim, H.-Y.; Huang, H.; Slutsky, A.; Minko, I. G.; Wang, H.; Nechev, L. V.; Kozekov, I. D.; Kozekova, A.; Tamura, P.; Jacob, J.; Voehler, M.; Harris, T. M.; Lloyd, R. S.; Rizzo, C. J.; Stone, M. P. *J. Am. Chem. Soc.* **2005**, *127*, 17686–17696.

103. Ito, H.; Omodera, K.; Takigawa, Y.; Taguchi, T. *Org. Lett.* **2002**, *4*, 1499–1501.

104. Tsui, G. C.; Menard, F.; Lautens, M. *Org. Lett.* **2010**, *12*, 2456–2459.

105. Jones, A. D.; Knight, D. W.; Hibbs, D. E. *J. Chem. Soc., Perkin Trans. 1* **2001**, 1182–1203.

106. Usanov, D. L.; Yamamoto, H. *J. Am. Chem. Soc.* **2011**, *133*, 1286–1289.

107. S. K. Moodapelly, G. V. M. Sharma and V. R. Doddi, *Adv. Synth. Catal.* **2017**, *359*,1535–1540.

108. C. Blons, M. S. T. Morin, T. E. Schmid, T. Vives, S. Colombel-Rouen, O. Basl, T. Reynaldo, C. L. Covington, S. Halbert, S. N. Cuskelly, P. V. Bernhardt, C. M. Williams, J. Crassous, P. L. Polavarapu, C. Crevisy, H. Gerard and M. Mauduit, *Chem. Eur. J*. **2017**, *23*, 7515–7525.

109. M. Shimogaki, M. Fujita and T Sugimura, *Angew. Chem. Int. Ed.* **2016**, *55*, 15797–15801.

110. C. L. Joe, T. P. Blaisdell, A. F. Geoghan and K. L. Tan, *J. Am. Chem. Soc.* **2014**, *136*, 8556–8559.

111. M. Gund, M. Déry, V. Amzallag and Claude Spino, *Org. Lett.* **2016**, *18*, 4280–4283.

112. A. Yajima, M. Yamamoto, T. Nukada and G. Yabuta, *Biosci. Biotechnol. Biochem.* **2007**, *71*, 2720–2724.

113. A. Saitman, P. Rulliere, S. D. E. Sullivan, and E. A. Theodorakis, *Org. Lett*. **2011**, *13*, 5854–5857.

114. S. M. Smith and J. M. Takacs, *J. Am. Chem. Soc*. **2010**, *132*, 1740–1741.

115. T.-S. Mei, H. H. Patel and M. S. Sigman, *Nature*, **2014**, *508*, 340–344.

116. Kamata, K.; Hirano, T.; Kuzuya, S.; Mizuno, N. *J. Am. Chem. Soc*. **2009**, *131*, 6997–7004.

117. Ménage, S.; Galey, J.-B.; Dumats, J.; Hussler, G.; Seité, M.; Luneau, I. G.; Chottard, G.; Fontecave, M. *J. Am. Chem. Soc.* **1998**, *120*, 13370–13382.

118. J. P. Wolfe and S. L. Buchwald, *J. Org. Chem.* **2000**, *65*, 1144–1157.

119. Jones, M. D.; Mahon, M. F., J. *Organomet. Chem.* **2008**, *693*, 2377–2382.

120. J. Cosier & A. M. Glazer, *J. Appl. Cryst.*, **1986**, *19*, 105–107.

121. H. Nowell, S. A. Barnett, K. E. Christensen, S. J. Teat and D. R. Allan, *J. Synch. Rad.*, **2012**, *19*, 435–441.

122. L. Palatinus and G. Chapuis, *J. Appl. Cryst.* **2007**, *40*, 786–790.

123. a) P. W. Betteridge, J. R. Carruthers, R. I. Cooper, K. Prout, & D. J. Watkin, *J. Appl. Cryst*. **2003**, *36*, 1487; b) R. I. Cooper, A. L. Thompson and D. J. Watkin, *J. Appl. Cryst.* **2010**, *43*, 1100–1107.

124. a) Spek, A., *J. Appl. Cryst*. **2003**, *36*, 7–13; b) van der Sluis, P.; A. L. *Spek, Acta Cryst.* **1990**, *A46*, 194–201.

Chapter 9: Appendix

9.1 Publications during DPhil research

1. Computational ligand design in enantio- and diastereoselective ynamide [5+2] cycloisomerization

R. N. Straker, Q. Peng, A. Mekareeya, R. S. Paton and E. A. Anderson, *Nat. Commun*. **2016**, *7*, 1–9.

2. Mechanistic Study of Arylsilane Oxidation through ^{19}F NMR Spectroscopy

E. J. Rayment, A. Mekareeya, N. Summerhill and E. A. Anderson, *J. Am. Chem. Soc*. **2017**, *139*, 6138–6145.

3. Mechanistic Insight into Palladium-Catalyzed Cycloisomerization: A Combined Experimental and Theoretical Study

A. Mekareeya, P. R. Walker, A. Couce-Rios, C. D. Campbell, A. Steven, R. S. Paton and E. A. Anderson, *J. Am. Chem. Soc.* **2017**, *139*. 10104–10114.

4. Copper-Catalyzed Synthesis and Applications of Yndiamides

S. J. Mansfield, K. E. Christensen, A. L. Thompson, K. Ma, M. W. Jones, A. Mekareeya and E. A. Anderson, *Angew. Chem. Int. Ed.* **2017**, *56*, 1–7.

nature COMMUNICATIONS

ARTICLE

Received 10 Sep 2015 | Accepted 3 Nov 2015 | Published 5 Jan 2016

DOI: 10.1038/ncomms10109 OPEN

Computational ligand design in enantio- and diastereoselective ynamide [5 + 2] cycloisomerization

R.N. Straker[1], Q. Peng[1], A. Mekareeya[1], R.S. Paton[1] & E.A. Anderson[1]

Transition metals can catalyse the stereoselective synthesis of cyclic organic molecules in a highly atom-efficient process called cycloisomerization. Many diastereoselective (substrate stereocontrol), and enantioselective (catalyst stereocontrol) cycloisomerizations have been developed. However, asymmetric cycloisomerizations where a chiral catalyst specifies the stereochemical outcome of the cyclization of a single enantiomer substrate—regardless of its inherent preference—are unknown. Here we show how a combined theoretical and experimental approach enables the design of a highly reactive rhodium catalyst for the stereoselective cycloisomerization of ynamide-vinylcyclopropanes to [5.3.0]-azabicycles. We first establish highly diastereoselective cycloisomerizations using an achiral catalyst, and then explore phosphoramidite-complexed rhodium catalysts in the enantioselective variant, where theoretical investigations uncover an unexpected reaction pathway in which the electronic structure of the phosphoramidite dramatically influences reaction rate and enantioselectivity. A marked enhancement of both is observed using the optimal theory-designed ligand, which enables double stereodifferentiating cycloisomerizations in both matched and mismatched catalyst–substrate settings.

[1] Chemistry Research Laboratory, University of Oxford, 12 Mansfield Road, Oxford OX1 3TA, UK. Correspondence and requests for materials should be addressed to E.A.A. (email: edward.anderson@chem.ox.ac.uk) or to R.S.P. (email: robert.paton@chem.ox.ac.uk) or to Q.P. (email: qian.peng@chem.ox.ac.uk).

Demand for higher efficiency, economy and selectivity in the synthesis of novel molecular scaffolds drives organic chemistry[1,2]. In this context, cycloisomerizations represent ideal methods for the formation of cyclic organic molecules, as they can fulfil all of these criteria. Despite much research into transition metal-catalysed cycloisomerization[3,4], and reports where high enantioselectivity is achieved for the cyclization of prochiral substrates to enantioenriched products[5,6], this important field of synthetic methodology has neglected the development of enantiospecific diastereoselective transformations, where single enantiomer starting materials are subjected to asymmetric cycloisomerization to give specific diastereomer products (that is, double stereodifferentiation, where catalyst and substrate stereocontrol compete)[7–10]. In an age where absolute control of molecular substitution and stereochemistry is paramount for applications, the realization of such processes would represent a major advance in the sustainable synthesis of precision-manufactured target molecules.

Here we describe rationally designed cycloisomerization catalysts that address these challenges. The reaction selected for this study was the [5+2] cycloisomerization of ynamide-vinylcyclopropanes to [5.3.0] azabicycles (**1**→**2**, **3**, Fig. 1). Although [5+2] processes have a rich history in the field of alkyne-vinylcyclopropanes[11–22], the development of this process using ynamides—or indeed any asymmetric cycloisomerization of ynamide-tethered enynes—has not been explored either experimentally or theoretically[23–27]. More generally, we question whether a catalyst system optimized to achieve an enantioselective cyclization (**1**→**2**, Fig. 1b) can translate to a double stereodifferentiating setting (**1**→**3** or ***epi*-3**, Fig. 1c), particularly should the catalyst be required to overcome powerful substrate stereocontrol. Intrinsic to these studies is a combined theoretical and experimental approach to optimize catalyst design[28–30], which in the event reveals an unexpected mechanistic pathway for rhodium-catalysed [5+2] carbocyclizations (Fig. 1a). This work demonstrates the powerful role of density functional level of theory (DFT) computations in understanding asymmetric catalysis, leading to quantitative computational-led design of new, highly selective ligands.

Results

Substrate synthesis and reaction optimization. A selection of ynamide cycloisomerization substrates **1** were readily accessed from allylic esters **4** (Fig. 2) by an Ireland-Claisen/Curtius rearrangement/ynamide formation sequence. Substituents could be introduced at one or both of the carbon atoms on the ene-ynamide backbone, and by incorporating an enzymatic resolution into this synthesis, enantioenriched ynamides could be prepared. Ynamide formation (**6**→**1**) was achieved using copper-catalysed coupling of the sulfonamide with a bromoalkyne[32], or via formation of an intermediate dichloroenamide[33]. Initial screening of ruthenium[14] and rhodium[20,34] catalyst systems (Table 1) revealed that only the latter afforded high yields of azabicycle **7a** from ynamide **1a**; using [Rh(cod)naphthalene]SbF_6 (5 mol%) as the catalyst[35,36], the cycloisomerization could be effected within 3 h at room temperature, giving **7a** in 91% yield (Entry 6).

Substrate scope. A variety of ynamides **1a–s** were now examined in the cycloisomerization using these optimized conditions (Fig. 3). Aryl-substituted ynamides **1b–d** reacted with high efficiency, and revealed a clear electronic effect on the reaction rate, with electron-deficient ynamides **1b** and **1c** showing reduced reaction times. Alkyl-substituted ynamides **1e–g** also displayed enhanced reactivity compared with phenyl ynamide **1a**, affording the corresponding [5.3.0]-azabicycles **7e–g** in excellent yields within 15 min at ambient temperature. Similar efficient reactivity was observed for the cyclization of the heteroaryl-substituted ynamides **1h** and **1i** to the indolyl- and pyrrolyl-substituted products **7h** and **7i**. The mild conditions of the reaction are emphasized by the cyclization of the aniline-derived ynamide **1j**, which led to tricycle **7j** in 74% yield—notably, this 1,4-diene did not undergo *in situ* isomerization to the indole.

Of clear interest was the level of substrate stereocontrol that might be achieved using ynamides **1l–s**. Excellent levels of substrate stereoinduction were observed, with products **7l–s** afforded in high yield and as single diastereomers for substrates featuring an allylic stereocenter; and, for **7s**, as a single regioisomer as well as diastereoisomer[14]. Cyclization of substrates containing homoallylic stereocenters proved less selective; however, good stereoselectivity ($dr = 12{:}1$) could be achieved using $[Rh(cod)Cl]_2$. These collected results are significant in the wider context of [5+2] cycloisomerization, where high levels of substrate stereocontrol have previously been generally interpreted to arise from an 'inside alkoxy effect' from oxygen-bearing stereocenters allylic to the vinylcyclopropane[37,38]. In this work, it is apparent that such stereoelectronic effects are not a prerequisite for high stereoselectivity.

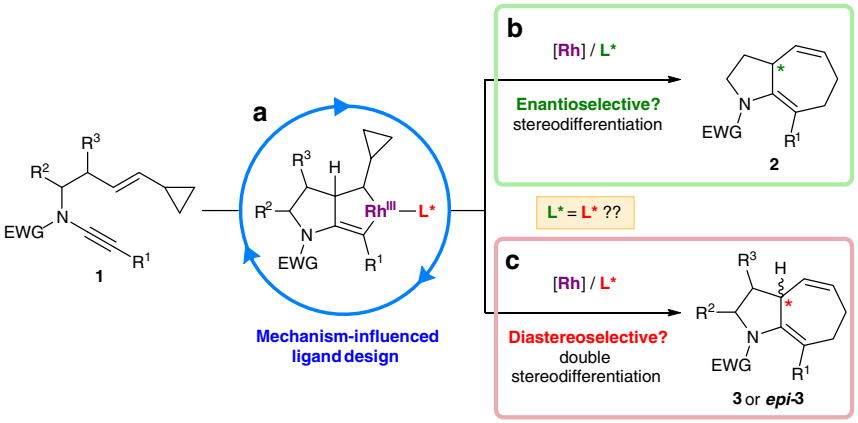

Figure 1 | A reaction blueprint for enantioselective and/or double stereodifferentiating diastereoselective ynamide-vinylcyclopropane cycloisomerization. (**a**) We show that mechanistic calculations are crucial in the design of an enantioselective cycloisomerization catalyst. (**b**) Enantioselective higher order ynamide cycloisomerization is realized. (**c**) Despite high levels of substrate stereocontrol, the computationally designed catalyst is able to define product stereochemistry.

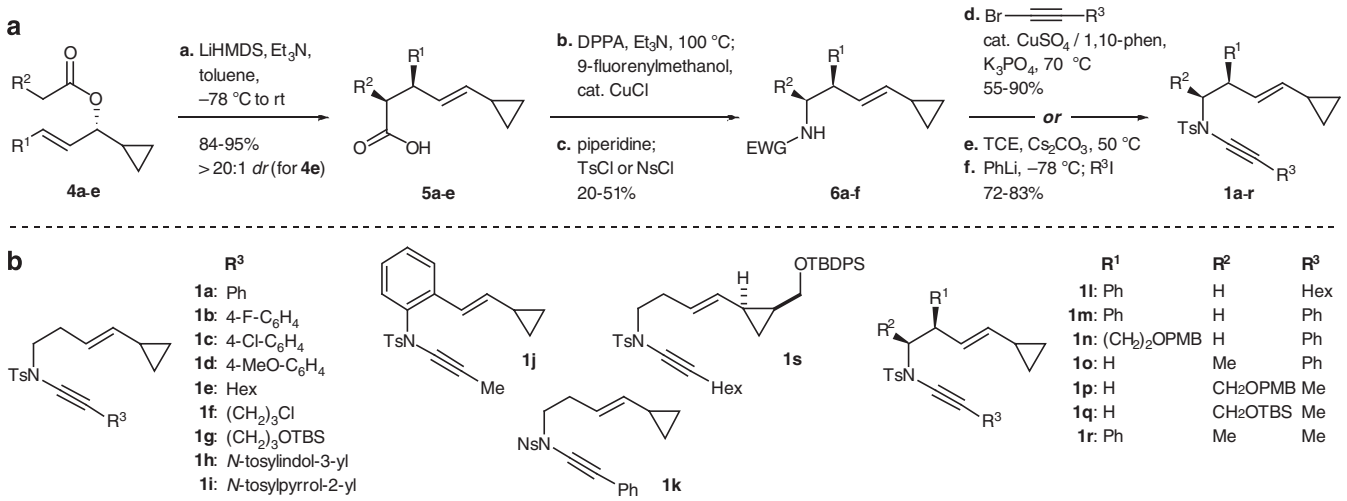

Figure 2 | Synthesis of ynamide-vinylcyclopropanes 1. (**a**) The synthetic route employed uses an Ireland-Claisen rearrangement of esters **4a–e** to construct the vinylcyclopropane and install up to two backbone substituents; subsequent Curtius rearrangement / sulfonylation converts the carboxylic acids **5** to sulfonamides **6**; ynamide formation is then achieved using copper-catalysed coupling with a bromoalkyne or, for hindered or aniline-derived ynamides, a two step route via a dichloroenamide. For the preparation of enantioenriched esters **4b**, **4d** and **4e**, and ynamides **1q** and **1s**, see Supplementary Fig. 4. (**b**) Ynamide-vinylcyclopropanes prepared using this strategy.

Table 1 | Optimization of the [5 + 2] cycloisomerization reaction.

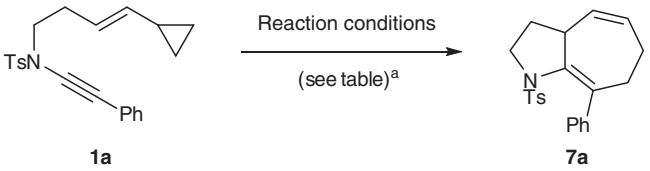

Entry	Catalyst (mol%)	Solvent	Temp. (°C)	Time (h)	Yield (%)
1	$[CpRu(MeCN)_3]PF_6$ (10)	acetone	50	20	– [b]
2	$[RhCl(cod)]_2$ (10)	toluene	110	20	– [b]
3	$RhCl(PPh_3)_3$ (10)	toluene	110	1	72
4	$[(C_{10}H_8)Rh(cod)]SbF_6$ (10)	1,2-dichloroethane	rt	1.5	92
5	$[(C_{10}H_8)Rh(cod)]SbF_6$ (10)	CH_2Cl_2	rt	1.5	94
6	$[(C_{10}H_8)Rh(cod)]SbF_6$ (5)	CH_2Cl_2	rt	3	91

[a]Reactions performed at 0.1 M substrate in the solvent stated. [b]Reaction gave a complex mixture of products.

Enantioselective cycloisomerization. In targeting an asymmetric version of the cyclization, we were mindful of the excellent asymmetric [5 + 2] Rh-catalysed cycloisomerization of alkyne-vinylcyclopropanes described by Shintani *et al.*[39,40], which employed the versatile phosphoramidite ligand **L1** (Fig. 4a)[41]. A preliminary screen of a range of phosphoramidite ligands **L1**–**L4** revealed that **L1** indeed seemed optimal for the enantioselective cycloisomerization of ynamide-vinylcyclopropane **1a**, delivering product (–)-**7a** in excellent yield and enantioselectivity (96%, 98% *ee*) after just 15 min at room temperature (see Supplementary Information for assignment of absolute stereochemistry). However, forays with other substrates suggested that this ligand might not meet our expectations in more challenging settings, and we realized that any further advance would require a combined theoretical and experimental design approach.

To this end, we conducted a computational exploration of the reaction pathway, which began with investigation of the empirical model adopted by Shintani *et al.* to explain the enantioselectivity of vinylcyclopropane-alkyne cycloisomerization. This model (Fig. 4b) is based on an X-ray crystal structure of [Rh(**L1**) norbornadiene]BF_4 reported by Mezetti (**8**) (ref. 42), which reveals an η^2-complexation of one of the α-methylbenzylamine arenes to the rhodium cation—the phosphoramidite thus acting as a bidentate ligand. The Shintani–Hayashi model docks the vinylcyclopropane-alkyne onto this ligated rhodium framework as in structure **9**, such that the alkyne coordinates *trans* to the phosphorous atom of the phosphoramidite ligand, and the vinylcyclopropane coordinates *trans* to the η^2-complexed arene, with an orientation that minimizes steric interactions between the cyclopropane ring and naphthyl group.

Computational study and ligand optimization. Computation, particularly at the DFT level, has emerged as a powerful tool for assessing the feasibility of mechanistic steps involved in catalysis[43]. Our theoretical work first explored eight possibilities for the binding of ynamide-vinylcyclopropane **1a** to the [Rh(**L1**)]

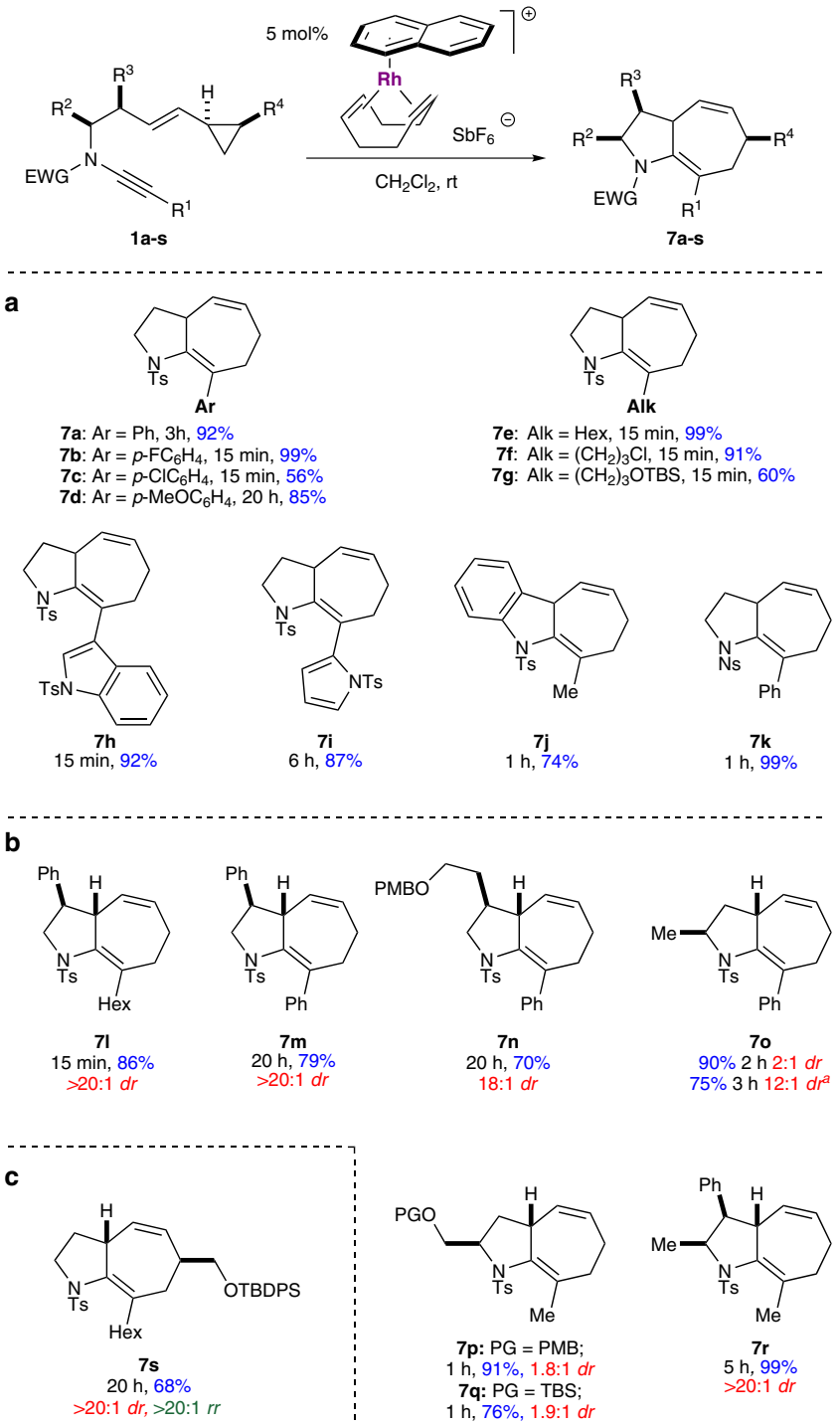

Figure 3 | Rhodium-catalysed ynamide [5 + 2] cycloisomerization. (**a**) Ynamide substituent scope. (**b**) Diastereoselective cycloisomerization proceeds with high levels of substrate stereoinduction. (**c**) High regioselectivity and diastereoselectivity is observed with a substituted cyclopropane. [a]Reaction performed using $[Rh(cod)Cl]_2$ (10 mol%), toluene, 110 °C.

cation (Table 2). In contrast to the Shintani–Hayashi model, this suggested that the lowest energy complex of [Rh(**L1**)**1a**] positions the ynamide proximal to the naphthyl ring and *trans*- to the arene ligand, and the vinylcyclopropane *trans*- to the phosphorous atom (**10**, Fig. 5, P-*trans*-ene/Up). The next lowest energy structure maintains this positional selectivity of substrate binding, but inverts its orientation (that is, P-*trans*-ene/Down). Next, calculations were carried out to explore the two widely accepted mechanisms for [5 + 2] cycloisomerization, which initiate either with an oxidative addition into the vinylcyclopropane, followed by alkyne insertion into the resultant σ/π-allyl rhodium(III) complex **11** to give eight-membered rhodacycle **12** (vinylcyclopropane pathway), or via oxidative cycloaddition of Rh(I) with the alkyne and alkene to give rhodacyclopentene **13**, followed by ring expansion into the cyclopropane to give the same intermediate **12** (metallacyclopentene pathway). Where investigations by Yu, Houk and Wender on Rh-catalysed [5 + 2] cycloisomerizations suggest that oxidative addition into the vinylcyclopropane is the first step on the catalytic pathway[17,21], our DFT calculations

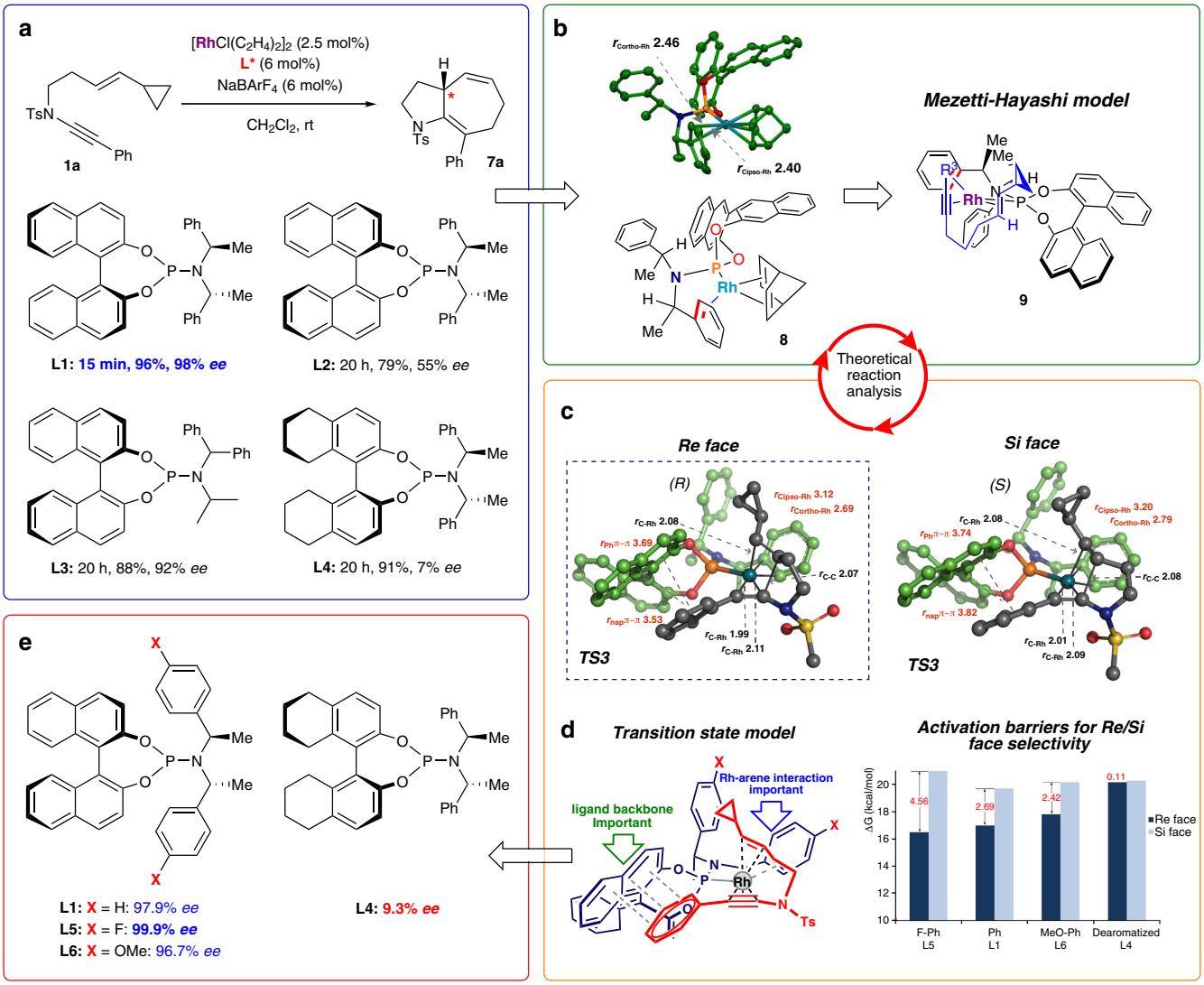

Figure 4 | Exploration of asymmetric ynamide [5 + 2] cycloisomerization inspires a computation-guided ligand design. (**a**) A selection of phosphoramidite ligands screened reveals a strong dependence of enantioselectivity and reaction rate on amine and BINOL components' structure and chirality, with **L1** giving superior results. (**b**) The Shintani–Hayashi model for enantioselectivity is based on a crystal structure of [**L1** Rh(norbornadiene)]$^+$. (**c**) Our calculations (Fig. 5) support an alternative mode of binding of the ynamide, and an alternative reaction pathway that initiates with rhodacyclopentene formation. *Re* face binding of the vinylcyclopropane is favoured, with calculated structures, and activation barriers (kcal mol^{-1})/selectivities depicted (distances in Å). (**d**) A transition state model is shown that identifies key ligand design parameters. (**e**) Variation of the electronic character of the η^2-bound arene of the phosphoramidite leads to predicted enantioselectivies for **L5** (*p*-F) and **L6** (*p*-OMe), and an excellent correlation of experiment and theory for **L1** and **L4**.

(Fig. 5) suggest that oxidative coupling of the alkene-ynamide to form metallacyclopentene **13** appears to be the preferred reaction pathway for an ynamide-vinylcyclopropane to give **12**, followed by ring expansion of the cyclopropane. Notably, this mechanism has also been calculated to be the preferred pathway in ruthenium-catalysed [5 + 2] cycloisomerization[17]. The preference for this pathway over vinylcyclopropane oxidative addition is in the range of 4–12 kcal mol^{-1}, depending on the orientation with which **1a** binds to the [Rh(**L1**)] cation; notably, the transition states for both pathways favour *Re*-face binding of the alkene in a P-*trans*-ene/Down orientation. This sequence of steps is favoured in this intramolecular reaction due to additional stabilization of the forming Rh(III) intermediate in the oxidative coupling step by the electron-rich ynamide. The free energy profile for the catalytic cycle is exergonic by more than 40 kcal mol^{-1}, and product inhibition is predicted to be minimal, since the reactant preferentially binds to the catalyst by 6.2 kcal mol^{-1}; taken together with a turnover and selectivity determining barrier of 17.0 kcal mol^{-1} for the metallacyclopentene pathway, our computations are consistent with the short reaction times observed at room temperature for the conversion of **1a**–**7a** using **L1**.

The lowest energy transition state for the oxidative coupling of this metallacyclopentene pathway (TS3) is illustrated in Fig. 4c. This transition state leads to a calculated enantioselectivity for cyclization with ligand **L1** of 97.9% *ee* ($\Delta\Delta G^{\ddagger}_{Re/Si} = -2.69$ kcal mol^{-1}), which is in excellent agreement with the experimental value (*R*, 98% *ee*). The calculated enantioselectivity for phosphoramidite **L4** (9.3% *ee*, $\Delta\Delta G^{\ddagger}_{Re/Si} = -0.11$ kcal mol^{-1}) also correlates well with the poor selectivity we had already observed experimentally with this ligand (7% *ee*), supporting the mechanistic model, and implying that the naphthyl ring plays a crucial role—likely related (for aryl ynamides) to a stabilizing dispersive ($\pi - \pi$) interaction between

Table 2 | Eight possible orientations of enynamide docking onto the L1-Rh cation are explored.

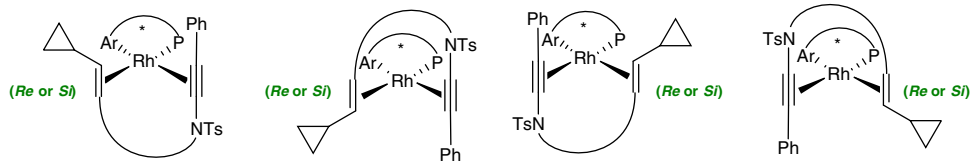

Orientation 1: P *trans* to **ene** Backbone of substrate **Down** to Ar-Rh-P

Orientation 2: P *trans* to **ene** Backbone of substrate **Up** to Ar-Rh-P

Orientation 3: P *trans* to **yne** Backbone of substrate **Down** to Ar-Rh-P

Orientation 4: P *trans* to **yne** Backbone of substrate **Up** to Ar-Rh-P

Orientation	Metallacyclopentene Pathway		Vinylcyclopropane pathway	
	***Re*-selectivity (*R*)**	***Si*-selectivity (*S*)**	***Re*-selectivity (*R*)**	***Si*-selectivity (*S*)**
1	18.7	31.3	23.0	22.0
2	**17.0**	19.7	21.9	24.8
3	23.6	23.9	29.3	24.5
4	23.2	30.7	35.3	41.7

Transition state energies (SMD-ωB97XD/6-311+G(d,p)/Lanl2TZ//ωB97XD/6-31G(d)/Lanl2DZ Gibbs free energies, shown in kcal mol^{-1}) associated with each mode of binding are tabulated.

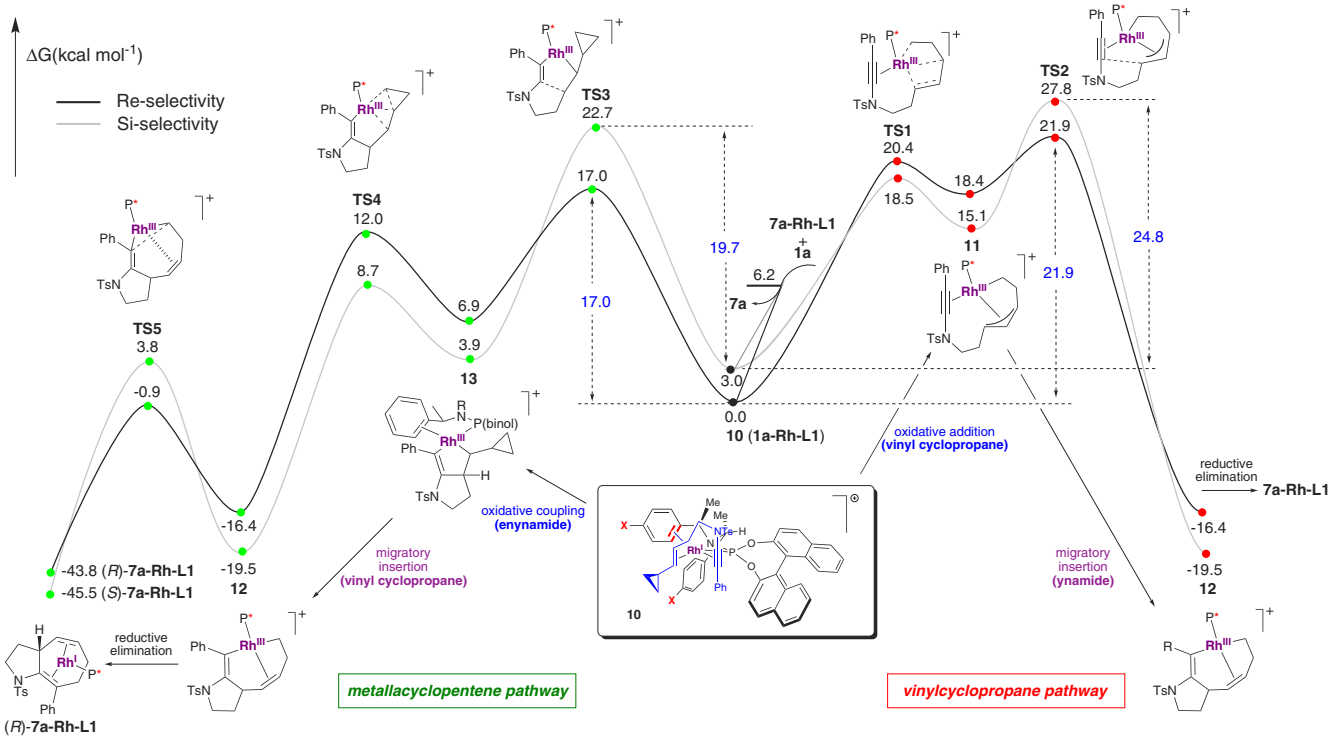

Figure 5 | Theoretical reaction analysis. Complex **10** (*Re* face binding) is found to be the lowest energy ground state for ynamide complexation, and transition state for oxidative coupling (metallacyclopentene pathway, see Table 2). The calculated energy profiles of the cycloisomerization for Re-face (black, bold) and Si-face (grey) substrate association via pathways initiating with metallacyclopentene formation (left), or vinylcyclopropane insertion (right) are illustrated; the former is favoured. SMD-ωB97XD/6-311+G(d,p)/Lanl2TZ//ωB97XD/6-31G(d)/Lanl2DZ Gibbs free energies are shown in kcal mol^{-1}.

the ynamide substituent and the naphthyl group in TS3. Although partial saturation of the naphthyl backbone (that is, in **L4**) leads to higher activation barriers, it is notable that the erosion of enantioselectivity for this ligand results from a greater increase (by 2.58 kcal mol^{-1}) to the activation barrier for *Re*-face addition compared with *Si*-face addition; this supports the existence, and importance, of stabilizing non-bonding (dispersion) interactions because of the aromatic backbone of **L1** in favouring the major enantiomer. Alkyl substituents are expected to experience similar attractive non-bonding interactions (CH–π); these interactions are further evident from an analysis of the computed non-covalent interaction index (Supplementary Fig. 68).

The oxidative coupling (TS3) is the rate-limiting and enantioselectivity determining step in this rhodacyclopentene mechanism. As observed in the Mezetti norbornene crystal structure (Fig. 4b)[42], one of the ligand benzylamine groups acts as 2π-electron donor (2.6–2.7 Å) in these transition states.

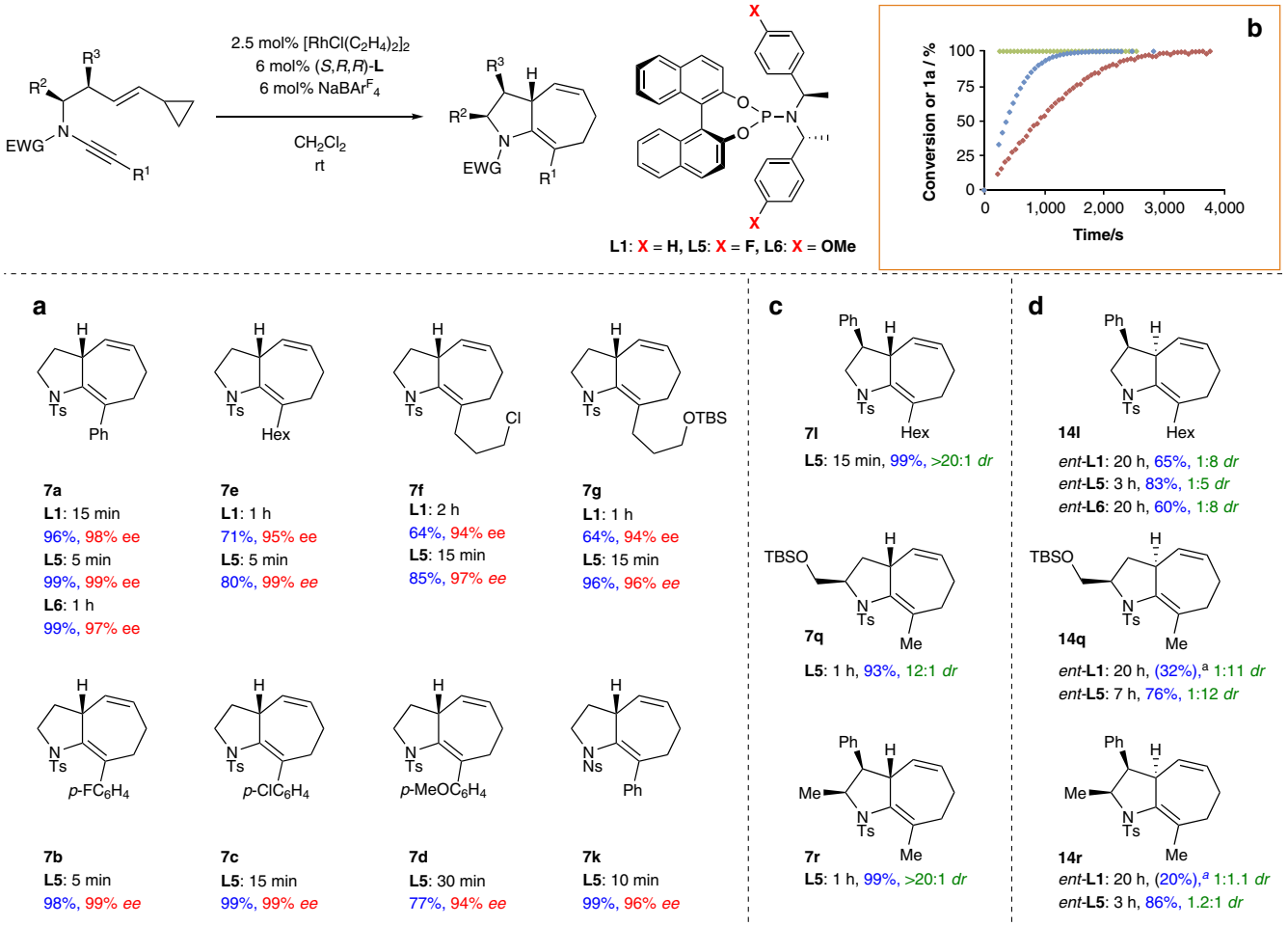

Figure 6 | Enantioselective and double stereodifferentiating, ynamide [5 + 2] cycloisomerizations. (**a**) Enantioselective cyclization is tested against a range of ynamide-vinylcyclopropanes, showing an excellent correlation of computation and experiment for the theory-designed ligands **L5** and **L6**. The synthesis of **7e** was performed on 1 mmol scale (1.25 mol% catalyst). (**b**) ^{1}H NMR spectroscopic monitoring of reaction progress emphasizes the rate enhancement between ligands **L6**, **L1** and **L5**, also predicted theoretically. (**c**) Matched double stereodifferentiating cycloisomerizations proceed with high selectivity and rate. (**d**) Mismatched double stereodifferentiating cycloisomerizations proceed successfully under catalyst stereocontrol using the enantiomers of ligands **L1**, **L5** and **L6** (that is, (*R,S,S*)-**L** stereochemistry); the major diastereomer is shown. The [a] signifies reaction conversion, as judged by ^{1}H NMR spectroscopic analysis.

We hypothesized that variation of the electronic character of this η^2-complexed arene could dramatically influence both the rate, and selectivity, of the reaction. Calculations on the effect of electronically-biasing methoxy and fluoro groups at the *para* position of these arenes suggested that decreasing the electron density on the arene (*p*-F, **L5**, Fig. 4d,e) would lead to an increase in reaction rate ($\Delta\Delta G^{\ddagger}_{\mathbf{L5/L1}} = -0.47$ kcal mol^{-1}) and enantioselectivity ($\Delta\Delta G^{\ddagger}_{\mathrm{Re/Si}} = -4.56$ kcal mol^{-1}, 99.9% *ee*), while an electron-donating substituent (*p*-MeO, **L6**) would have the opposite effect ($\Delta\Delta G^{\ddagger}_{\mathbf{L6/L1}} = +0.76$ kcal mol^{-1}, $\Delta\Delta G^{\ddagger}_{\mathrm{Re/Si}} = -2.42$ kcal mol^{-1}, 96.7% *ee*). This computed trend in reactivity and enantioselectivity, namely **L5** > **L1** > **L6**, results from a weakened metal-arene interaction in the TS leading to the major enantiomer, which is compensated for through stronger coordination of the alkynyl and alkenyl groups (see Supplementary Information for further details and discussion). These ligand structural modifications also modulate the Lewis basicity at phosphorus, however preferential stabilization of the major enantiomeric pathway confirms that the predominant effect is not inductive in nature, but rather depends on through-space interactions involving the Rh-coordinating aryl group.

Substrate scope in the asymmetric cycloisomerization. While phosphoramidite **L6** is known, (ref. 44) **L5** is not, but could be readily synthesized using standard methods[45]. Both were evaluated in the enantioselective cyclization alongside **L1** (Fig. 6a). To our delight, experiment correlated well with the predicted outcomes of these cyclizations; the *p*-fluorobenzyl ligand **L5** indeed showed a dramatic enhancement of rate and selectivity in the cyclization of **1a** compared with the parent ligand **L1**, affording **7a** in under 5 min with 99% *ee* (calc. 99.9% *ee*), while the *p*-methoxybenzyl ligand **L6** exhibited a much reduced rate of reaction, and also lower enantioselectivity (1 h, 97% *ee*, calc. 96.7% *ee*). The cyclization of alkyl-substituted ynamides **1e–g** to give enantioenriched azabicycles **7e–g** also showed a rate and selectivity enhancement between **L1** and **L5**. The potent reactivity of the latter ligand was extended to a variety of aryl-substituted ynamides, where the marked rate difference between electron-poor (**1b**) and electron-rich (**1d**) ynamides supports the hypothesis that the ynamide is intimately involved in the rate-determining step (that is, a metallacyclopentene pathway). In all cases using ligand **L5**, these reactions proceeded in under 30 min with excellent levels of enantioselectivity (94–99% *ee*); furthermore, the synthesis of **7e**

could be achieved on a 1 mmol scale in less than 5 min with 1.25 mol% catalyst loading. Monitoring of reaction conversion by ^{1}H NMR spectroscopy (in $CDCl_3$, Fig. 6b) emphasizes the dramatic rate difference between these three ligands, with the reaction using **L5** complete in under 4 min, compared with the slower cyclizations with **L1** and **L6** (addition of the catalyst solution to the substrate followed by NMR spectroscopic analysis necessitated a four minute delay between reaction initiation and acquisition of the first NMR spectrum. The reaction catalysed by [L5Rh] was complete by this time).

Finally, the performance of these ligands was tested against the challenge of cyclizations that proceed with high levels of substrate stereocontrol, to address the question of how a high enantioselectivity-inducing catalyst would cope with mismatched substrate-catalyst diastereoselective cycloisomerization scenarios. Three substrates were chosen for this challenge: ynamides **1l**, **1q** and **1r**, which gave >20:1, 1.8:1 and >20:1 *dr*, respectively when cyclized using [Rh(cod)naphthalene]SbF_6 (Fig. 3). As expected, these single enantiomer substrates cyclized rapidly, and with high efficiency and selectivity, with the matched substrate-catalyst combination (that is, (*S,R,R*)-**L5**, Fig. 6c). To our delight, we found that cycloisomerization of substrate **1l** using the enantiomeric catalyst system ((*R,S,S*)-**L1**) successfully overturned this powerful substrate stereoselectivity, giving **14l** in up to 1:8 *dr*. Interestingly, it was ligand **L1**—and not **L5**—which performed optimally in this challenging situation, albeit requiring an extended reaction time. In the case of **1q**, the catalyst (with either **L1** or **L5**) was able to achieve an equivalent (reversed) level of selectivity to that achieved in the matched sense—in this instance, a modest level of inherent substrate stereocontrol being completely overturned. Finally, the most challenging setting of the reinforcing substituents in **1r** proved a hurdle that could also be partly overcome, again demonstrating significant catalyst influence.

These observations may suggest that tighter substrate-Rh complexation in the case of **L5** (a consequence of a slightly weaker ligand-metal interaction observed in our calculations (see Supplementary Information for details), which improves rate and enantioselectivity), enhances unfavourable (that is, mismatched) steric effects in a double stereodifferentiating setting such that it effectively increases the stereocontrolling influence of the substrate relative to that of the ligand. The most reactive/selective catalysts for enantioselective cyclizations could thus suffer from higher than expected transition state energies in diastereoselective cyclizations, where such steric effects are enhanced compared with 'less enantioselective' catalysts (looser substrate binding); and that different considerations are therefore needed in the development of double stereodifferentiating reactions, with more 'promiscuous' catalysts potentially giving superior selectivity.

Discussion

In summary, the first example of an enantioselective ynamide-tethered cycloisomerization has been achieved, with a series of highly enantio- and diastereoselective cyclizations giving a range of substituted/enantioenriched [5.3.0] azabicycles. Theoretical reaction analysis crucially influenced ligand design, leading to a catalyst system that displayed enhanced rate and enantioselectivity in the cycloisomerization. The demonstration of the first successful examples of enantiospecific diastereoselective transition metal-catalysed cycloisomerizations in a significantly mismatched substrate-catalyst environment illustrates that cycloisomerization can assemble functionalized ring systems with tuneable selectivity. These studies set the stage for the development of further computationally guided catalyst systems.

Methods

Racemic [5 + 2] cycloisomerization. To an oven-dried vial containing the ynamide vinylcyclopropane (1.0 equiv.) under Ar was added a solution of [($C_{10}H_8$)Rh(cod)]SbF_6 (5 mol%) in degassed CH_2Cl_2 (10 ml mmol^{-1} of ynamide). The reaction mixture was stirred at room temperature under Ar until consumption of the ynamide was observed by thin layer chromatography (see Fig. 3 for reaction times). The reaction mixture was then concentrated, and the resulting material was purified by flash chromatography (SiO_2, petroleum ether/ethyl acetate eluent) (Fig. 3).

Asymmetric [5 + 2] cycloisomerization. A solution of [$RhCl(C_2H_4)_2$]$_2$ (2.5 mol%), $NaBAr^F_4$ (6 mol%) and phosphoramidite ligand (6 mol%) in degassed CH_2Cl_2 (10 ml mmol^{-1} of ynamide) was stirred for 20 min under Ar. The solution was filtered (through a PTFE filter-tipped syringe) into an oven-dried vial containing ynamide vinylcyclopropane (1.0 equiv.) under Ar. The reaction mixture was stirred at room temperature under Ar until consumption of the ynamide was observed by thin layer chromatography (see Fig. 6 for reaction times). The reaction mixture was then concentrated, and the resulting material was purified by flash chromatography (SiO_2, petroleum ether/ethyl acetate eluent) (Fig. 6).

Computational methods. Molecular geometries were fully optimized at the DFT theory level in Gaussian 09 (rev. D.01), using the dispersion-corrected ω-B97XD functional[46] without symmetry constraints. The effective core potentials (ECPs) of Hay and Wadt[47] with a double-ζ basis set (LanL2DZ) were used for Rh, S and P, and the 6-31G(d) basis set was used for H, C, N and O(BS1). The energies were further estimated using a larger basis set (6-311 + G (d, p) basis set for H, C, N, O, S and P) and triple-ζ basis set (LanL2TZ)[48] for Rh (BS2) by single-point calculations, in implicit solvent CH_2Cl_2 treated with the SMD universal solvation models[49]. The structures of the ynamide substrate and a series of phosphoramidite ligands were computed in full, while the toluenesulfonamide *p*-tolyl group was modelled as a methyl group in the interests of computational tractability. See Supplementary Methods for further details.

References

1. Newhouse, T., Baran, P. S. & Hoffmann, R. W. The economies of synthesis. *Chem. Soc. Rev.* **38,** 3010–3021 (2009).
2. Trost, B. M. The atom economy–a search for synthetic efficiency. *Science* **254,** 1471–1477 (1991).
3. Michelet, V., Toullec, P. Y. & Genet, J. P. Cycloisomerization of 1,n-enynes: challenging metal-catalyzed rearrangements and mechanistic insights. *Angew. Chem. Int. Ed.* **47,** 4268–4315 (2008).
4. Inglesby, P. A. & Evans, P. A. Stereoselective transition metal-catalysed higher-order carbocyclisation reactions. *Chem. Soc. Rev.* **39,** 2791–2805 (2010).
5. Marinetti, A., Jullien, H. & Voituriez, A. Enantioselective, transition metal catalyzed cycloisomerizations. *Chem. Soc. Rev.* **41,** 4884–4908 (2012).
6. Watson, I. D. G. & Toste, F. D. Catalytic enantioselective carbon-carbon bond formation using cycloisomerization reactions. *Chem. Sci.* **3,** 2899–2919 (2012).
7. Feducia, J. A., Campbell, A. N., Doherty, M. Q. & Gagné, M. R. Modular catalysts for diene cycloisomerization: Rapid and enantioselective variants for bicyclopropane synthesis. *J. Am. Chem. Soc.* **128,** 13290–13297 (2006).
8. Ham, Y. J. *et al.* Rhodium-catalyzed reductive cyclization of 1,6-enynes and stereoselective synthesis of the putative structure of lucentamycin A and its stereoisomers. *Tetrahedron* **68,** 1918–1925 (2012).
9. Lei, A., He, M. & Zhang, X. Rh-catalyzed kinetic resolution of enynes and highly enantioselective formation of 4-alkenyl-2,3-disubstituted tetrahydrofurans. *J. Am. Chem. Soc.* **125,** 11472–11473 (2003).
10. Trost, B. M., Ryan, M. C., Rao, M. & Markovic, T. Z. Construction of enantioenriched [3.1.0] bicycles via a ruthenium-catalyzed asymmetric redox bicycloisomerization reaction. *J. Am. Chem. Soc.* **136,** 17422–17425 (2014).
11. Wender, P. A., Takahashi, H. & Witulski, B. Transition metal catalyzed [5 + 2] cycloadditions of vinylcyclopropanes and alkynes: a homolog of the Diels-Alder reaction for the synthesis of seven-membered rings. *J. Am. Chem. Soc.* **117,** 4720–4721 (1995).
12. Wender, P. A. *et al.* Transition metal-catalyzed [5 + 2] cycloadditions with substituted cyclopropanes: first studies of regio- and stereoselectivity. *J. Am. Chem. Soc.* **121,** 10442–10443 (1999).
13. Trost, B. M., Toste, F. D. & Shen, H. Ruthenium-catalyzed intramolecular [5 + 2] cycloadditions. *J. Am. Chem. Soc.* **122,** 2379–2380 (2000).
14. Trost, B. M. *et al.* Syntheses of seven-membered rings: ruthenium-catalyzed intramolecular [5 + 2] cycloadditions. *Chem. Eur. J.* **11,** 2577–2590 (2005).
15. Pellissier, H. Recent developments in the [5 + 2] cycloaddition. *Adv. Synth. Catal.* **353,** 189–218 (2011).
16. Ylijoki, K. E. O. & Stryker, J. M. [5 + 2] Cycloaddition reactions in organic and natural product synthesis. *Chem. Rev.* **113,** 2244–2266 (2013).
17. Mustard, T. J. L., Wender, P. A. & Cheong, P. H.-Y. Catalytic efficiency is a function of how rhodium(I) (5 + 2) catalysts accommodate a conserved

substrate transition state geometry: induced fit model for explaining transition metal catalysis. *ACS Catal.* **5,** 1758–1763 (2015).
18. Hong, X., Trost, B. M. & Houk, K. N. Mechanism and origins of selectivity in Ru(II)-catalyzed intramolecular (5 + 2) cycloadditions and ene reactions of vinylcyclopropanes and alkynes from density functional theory. *J. Am. Chem. Soc.* **135,** 6588–6600 (2013).
19. Xu, X. *et al.* Ligand effects on rates and regioselectivities of Rh(I)-catalyzed (5 + 2) cycloadditions: a computational study of cyclooctadiene and dinaphthocyclooctatetraene as ligands. *J. Am. Chem. Soc.* **134,** 11012–11025 (2012).
20. Liu, P. *et al.* Electronic and steric control of regioselectivities in Rh(I)-catalyzed (5 + 2) cycloadditions: experiment and theory. *J. Am. Chem. Soc.* **132,** 10127–10135 (2010; .
21. Liu, P., Cheong, P. H.-Y., Yu, Z.-X., Wender, P. A. & Houk, K. N. Substituent effects, reactant preorganization, and ligand exchange control the reactivity in RhI-catalyzed (5 + 2) cycloadditions between vinylcyclopropanes and alkynes. *Angew. Chem. Int. Ed.* **47,** 3939–3941 (2008).
22. Yu, Z.-X., Wender, P. A. & Houk, K. N. On the Mechanism of $[Rh(CO)_2Cl]_2$-Catalyzed Intermolecular (5 + 2) Reactions between Vinylcyclopropanes and Alkynes. *J. Am. Chem. Soc.* **126,** 9154–9155 (2004).
23. Walker, P. R., Campbell, C. D., Suleman, A., Carr, G. & Anderson, E. A. Palladium- and ruthenium-catalyzed cycloisomerization of enynamides and enynhydrazides: A rapid approach to diverse azacyclic frameworks. *Angew. Chem. Int. Ed.* **52,** 9139–9143 (2013).
24. Couty, S., Meyer, C. & Cossy, J. Diastereoselective gold-catalyzed cycloisomerizations of ene-ynamides. *Angew. Chem. Int. Ed.* **45,** 6726–6730 (2006).
25. Witulski, B. & Alayrac, C. A highly efficient and flexible synthesis of substituted carbazoles by rhodium-catalyzed inter- and intramolecular alkyne cyclotrimerizations. *Angew. Chem. Int. Ed.* **41,** 3281–3284 (2002).
26. Wang, X.-N. *et al.* Ynamides in ring forming transformations. *Acc. Chem. Res.* **47,** 560–578 (2014).
27. Nishimura, T., Takiguchi, Y., Maeda, Y. & Hayashi, T. Rhodium-catalyzed asymmetric cycloisomerization of 1,6-ene-ynamides. *Adv. Synth. Catal.* **355,** 1374–1382 (2013).
28. Tsang, A. S. K., Sanhueza, I. A. & Schoenebeck, F. Combining experimental and computational studies to understand and predict reactivities of relevance to homogeneous catalysis. *Chem. Eur. J.* **20,** 16432–16441 (2014).
29. Nielsen, M. C., Bonney, K. J. & Schoenebeck, F. Computational ligand design for the reductive elimination of $ArCF_3$ from a small bite angle PdII complex: remarkable effect of a perfluoroalkyl phosphine. *Angew. Chem. Int. Ed.* **53,** 5903–5906 (2014).
30. Sperger, T., Sanhueza, I. A., Kalvet, I. & Schoenebeck, F. Computational studies of synthetically relevant homogeneous organometallic catalysis involving Ni, Pd, Ir, and Rh: An overview of commonly employed DFT methods and mechanistic insights. *Chem. Rev* **115,** 9532–9586 (2015).
31. Kocienski, P. J., Christopher, J. A., Bell, R. & Otto, B. Nucleophilic addition of α-metallated carbamates to planar chiral cationic η^3-allylmolybdenum complexes: a stereochemical study. *Synthesis* 75–84 (2005).
32. Zhang, X. *et al.* Copper(II)-catalyzed amidations of alkynyl bromides as a general synthesis of ynamides and Z-enamides. An intramolecular amidation for the synthesis of macrocyclic ynamides. *J. Org. Chem.* **71,** 4170–4177 (2006).
33. Mansfield, S. J., Campbell, C. D., Jones, M. W. & Anderson, E. A. A robust and modular synthesis of ynamides. *Chem. Commun.* **51,** 3316–3319 (2015).
34. Saito, A., Ono, T. & Hanzawa, Y. Cationic Rh(I) catalyst in fluorinated alcohol: mild intramolecular cycloaddition reactions of ester-tethered unsaturated compounds. *J. Org. Chem.* **71,** 6437–6443 (2006).
35. Wender, P. A. & Williams, T. J. $[(arene)Rh(cod)]^+$ Complexes as catalysts for [5 + 2] cycloaddition reactions. *Angew. Chem. Int. Ed.* **41,** 4550–4553 (2002).
36. Wender, P. A. *et al.* Structural complexity through multicomponent cycloaddition cascades enabled by dual-purpose, reactivity regenerating 1,2,3-triene equivalents. *Nat. Chem* **6,** 448–452 (2014).
37. Trost, B. M., Shen, H. C., Schulz, T., Koradin, C. & Schirok, H. On the diastereoselectivity of Ru-catalyzed [5 + 2] cycloadditions. *Org. Lett.* **5,** 4149–4151 (2003).
38. Trost, B. M., Waser, J. & Meyer, A. Total synthesis of (−)-pseudolaric acid B. *J. Am. Chem. Soc.* **130,** 16424–16434 (2008).
39. Shintani, R., Nakatsu, H., Takatsu, K. & Hayashi, T. Rhodium-catalyzed asymmetric [5 + 2] cycloaddition of alkyne-vinylcyclopropanes. *Chem. Eur. J.* **15,** 8692–8694 (2009).
40. Wender, P. A. *et al.* Asymmetric catalysis of the [5 + 2] cycloaddition reaction of vinylcyclopropanes and π-systems. *J. Am. Chem. Soc.* **128,** 6302–6303 (2006).
41. Teichert, J. F. & Feringa, B. L. Phosphoramidites: Privileged ligands in asymmetric catalysis. *Angew. Chem. Int. Ed.* **49,** 2486–2528 (2010).
42. Mikhel, I. S. *et al.* A chiral phosphoramidite beyond monodentate coordination: Secondary pi-interactions turn a dangling aryl into a two-, four-, or six-electron donor in d(6) and d(8) complexes. *Organometallics* **27,** 2937–2948 (2008).
43. Cheng, G.-J., Zhang, X., Chung, L. W., Xu, L. & Wu, Y.-D. Computational organic chemistry: bridging theory and experiment in establishing the mechanisms of chemical reactions. *J. Am. Chem. Soc.* **137,** 1706–1725 (2015).
44. Polet, D. & Alexakis, A. Kinetic study of various phosphoramidite ligands in the iridium-catalyzed allylic substitution. *Org. Lett.* **7,** 1621–1624 (2005).
45. Roth, P. M. C., Sidera, M., Maksymowicz, R. M. & Fletcher, S. P. Copper-catalyzed asymmetric conjugate addition of alkylzirconium reagents to cyclic enones to form quaternary centers. *Nat. Protoc.* **9,** 104–111 (2014).
46. Chai, J. D. & Head-Gordon, M. Long-range corrected hybrid density functionals with damped atom-atom dispersion corrections. *Phys. Chem. Chem. Phys.* **10,** 6615–6620 (2008).
47. Wadt, W. R. & Hay, P. J. *Ab initio* effective core potentials for molecular calculations. Potentials for main group elements Na to Bi. *J. Chem. Phys.* **82,** 284–298 (1985).
48. Roy, L. E., Hay, P. J. & Martin, R. L. Revised basis sets for the LANL effective core potentials. *J. Chem. Theory Comput.* **4,** 1029–1031 (2008).
49. Marenich, A. V., Cramer, C. J. & Truhlar, D. G. Universal solvation model based on solute electron density and on a continuum model of the solvent defined by the bulk dielectric constant and atomic surface tensions. .*J. Phys. Chem. B* **113,** 6378–6396 (2009).

Acknowledgements

E.A.A. and R.N.S. thank the EPSRC (EP/K005391/1, EP/H025839/1 and a studentship to R.N.S. (EP/K503113/1)) for support. R.S.P. thanks the Chemical Structure Association Trust, and Q.P. thanks the European Community (FP7-PEOPLE-2012-IIF under grant agreement 330364) for support. We acknowledge the use of the EPSRC UK National Service for Computational Chemistry Software (CHEM773) in carrying out this work. A.M. thanks the Royal Thai Government and the DPST project for a studentship.

Author contributions

E.A.A. and R.N.S. conceived of the synthetic methodology. R.N.S. carried out the experimental work, with the aid of A.M. Q.P. and R.S.P. carried out the theoretical calculations. R.N.S., E.A.A., Q.P. and R.S.P. analysed the collected results. E.A.A., R.N.S., Q.P. and R.S.P. wrote the manuscript.

Additional information

Supplementary Information accompanies this paper at http://www.nature.com/naturecommunications

Competing financial interests: The authors declare no competing financial interests.

Reprints and permission information is available online at http://npg.nature.com/reprintsandpermissions/

How to cite this article: Straker, R. N. *et al.* Computational ligand design in enantio- and diastereoselective ynamide [5 + 2] cycloisomerization. *Nat. Commun.* 7:10109 doi: 10.1038/ncomms10109 (2016).

This work is licensed under a Creative Commons Attribution 4.0 International License. The images or other third party material in this article are included in the article's Creative Commons license, unless indicated otherwise in the credit line; if the material is not included under the Creative Commons license, users will need to obtain permission from the license holder to reproduce the material. To view a copy of this license, visit http://creativecommons.org/licenses/by/4.0/

This is an open access article published under a Creative Commons Attribution (CC-BY) License, which permits unrestricted use, distribution and reproduction in any medium, provided the author and source are cited.

JACS
JOURNAL OF THE AMERICAN CHEMICAL SOCIETY
Article
pubs.acs.org/JACS

Mechanistic Study of Arylsilane Oxidation through ^{19}F NMR Spectroscopy

Elizabeth J. Rayment,[†] Aroonroj Mekareeya,[†] Nick Summerhill,[‡,§] and Edward A. Anderson*[,†]

[†]Chemistry Research Laboratory, University of Oxford, 12 Mansfield Road, Oxford, OX1 3TA, United Kingdom
[‡]Worldwide Medicinal Chemistry, Pfizer, Sandwich, Kent CT13 9NJ, United Kingdom

Supporting Information

ABSTRACT: The mechanism of the oxidation of arylsilanes to phenols has been investigated using ^{19}F NMR spectroscopy. The formation of silanols in these reactions results from a rapid background equilibrium between silanol and alkoxysilane; the relative rates of reaction of these species was evaluated by modeling of concentration profiles obtained through ^{19}F NMR spectroscopic reaction monitoring. Combining these results with a study of initial rates of phenol formation, and of substituent electronic effects, a mechanistic picture involving rapid and reversible formation of a pentavalent peroxide ate complex, prior to rate-limiting aryl migration, has evolved.

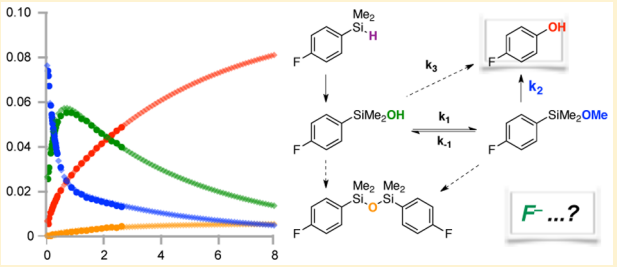

INTRODUCTION

Arylsilanes are highly versatile intermediates in organic synthesis, with a number of methods having recently been disclosed for both their preparation[1] and transformations.[2] Among these, the oxidation of arylsilanes to phenols is relatively underexploited compared to the equivalent conversion of alkyl and alkenylsilanes into aliphatic alcohols and ketones, respectively,[3,4] and has only recently been developed as an efficient and general methodology.[5,6] Despite the demonstrated synthetic utility of this oxidation,[5g,7] mechanistic explorations of this phenol synthesis are limited to a study of arylfluorosilane oxidation by Tamao and co-workers,[3h] and theoretical investigations on the oxidation of alkylfluorosilanes,[8] and alkylalkoxysilanes (and mixed alkoxyfluorosilane derivatives)[9] by Mader and Norrby. Here we describe an experimental study of the mechanism of the H_2O_2-mediated oxidation of arylalkoxysilanes, a reaction that proceeds in the presence or absence[3g,5a,10] of fluoride. In addition to shedding new light on the dynamic behavior of alkoxysilanes, this work explores the effects of low concentrations of fluoride ion on the oxidation, which can be rationalized by consideration of the relative reactivity of different organosilane intermediates.

The Tamao group's seminal mechanistic studies on the hydrogen peroxide-mediated oxidation of fluorosilanes (and their corresponding fluoride ate complexes) led to their proposal (Scheme 1a) of a rate-limiting addition of hydrogen peroxide or hydroperoxide anion, under neutral or basic conditions respectively, to pentacoordinate ate complex **1** (formed by rapid and reversible addition of fluoride ion to **2**).[3h] This peroxide association step was proposed to be rate-limiting, as the reaction was found to be first order with respect to H_2O_2. Each pathway leads to a hexacoordinate species (**3** or **4**), and then to pentacoordinate aryloxysilane **5** via aryl migration; a concerted peroxide association/migration was not excluded. Tamao found that aryl groups migrate in preference to alkyl

Scheme 1. Mechanistic Paradigms in the Tamao Oxidation, and Previous Work from Our Group

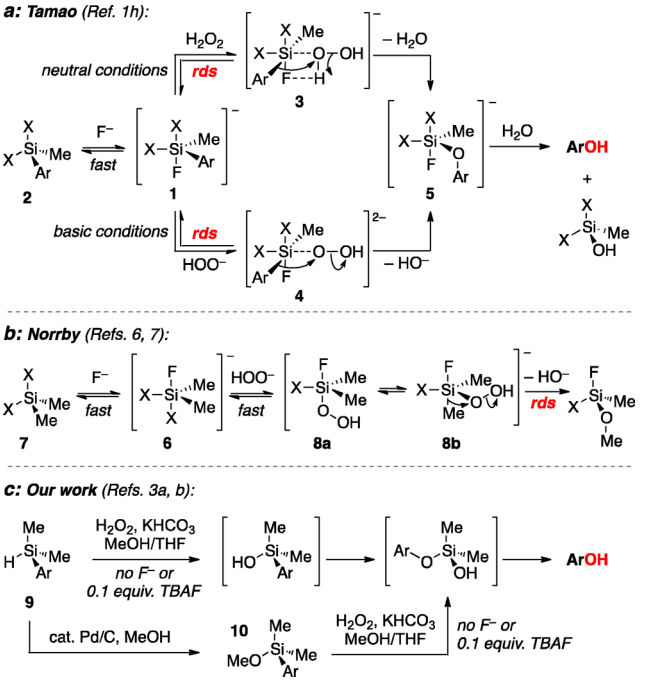

Received: January 11, 2017
Published: April 19, 2017

© 2017 American Chemical Society

DOI: 10.1021/jacs.7b00357
J. Am. Chem. Soc. 2017, 139, 6138–6145

groups,[11] and proposed that the addition of fluoride ion is necessary for the oxidation to proceed.

Mader and Norrby subsequently calculated (Scheme 1b) that anionic substitution of anionic pentavalent silicates (e.g., **6**) is rapid,[12] and that hydroperoxide anion is more likely to attack pentacoordinate silicon (**6**) than the neutral species (**7**).[8,9] They also proposed that addition of fluoride ions is not essential for the oxidation to proceed, but increases the rate of hydroperoxide attack at silicon via formation of a greater proportion of pentavalent trifluorosiliconate species, which are more reactive toward substitution of F^- by HOO^- than neutral tetravalent difluorosilanes. Importantly, these authors concluded that alkyl migration from conformer **8b**, and not peroxide ion attack to generate hexacoordinate species such as **3** or **4**, is the rate-limiting step. Our own experimental work (Scheme 1c)[5a] had shown that the oxidation of arylhydrosilanes **9**,[5d] and arylalkoxysilanes **10**, proceeds under fluoride-promoted or fluoride-free conditions, thus supporting the notion that fluoride ion is a nonessential (but generally beneficial) component of the reaction.

Several points arise from this previous work. First, there is a general acceptance that stoichiometric amounts of fluoride are required for successful oxidation (albeit that fluoride ion may not be coordinated to silicon in the migration step itself), and that fluoride is sequestered in the course of the reaction by liberated silanes. Second, the peroxide-mediated oxidation of silanes featuring only one, or even no electronegative substituents, has not been studied from a mechanistic perspective. Third, no experimental correlation of Mader and Norrby's calculations on alkoxysilane oxidation has been achieved. Finally, the observation of silanols and disiloxanes, as intermediates or byproducts, has not been considered in detail. In this work, we disclose investigations of arylsilane oxidation which unite the various experimental and computational studies in the field, and provide a comprehensive picture of the equilibria that are at play during oxidation, as well as the influence of fluoride.

RESULTS AND DISCUSSION

In earlier work,[5a,b] we had found that the addition of a fluoride source was not essential to achieve full conversion of arylsilanes to phenols, but that even substoichiometric amounts increase the overall efficiency of oxidation. This observation is mirrored in studies by Phillips and co-workers on the deprotection of silyl ethers using catalytic amounts of TBAF (0.1 equiv),[13] which also demonstrate that fluoride ion can be recycled from fluorosilane byproducts (that fluorosilanes are formed irreversibly is an understandable assumption based on the strength of the Si–F bond, ~135 kcal mol^{-1}).[14] Phillips found the deprotection of arylsilyl ethers to be especially rapid, underlining that these ethers are particularly susceptible to nucleophilic attack, and thus potentially more amenable to fluoride recycling as is also required in a fluoride-catalyzed oxidation manifold.[15] Both our group and the Phillips group found the predominant fate of the organosilane to be the formation of a silanol (rather than fluorosilane, alkoxysilane, or disiloxane), again supporting the release of fluoride at some point after silyl ether cleavage.[5a] With these observations in mind, we set out to study the processes at play during the oxidation of arylhydrosilanes and arylalkoxysilanes, under fluoride-free and fluoride-catalyzed reaction conditions.

Oxidation of Arylhydrosilanes in THF/MeOH. We began this work by examining the oxidation of arylhydrosilanes ($ArMe_2SiH$), substrates which do not contain an electronegative substituent as has previously been thought to be crucial for Tamao oxidation. The conversion of 4-(dimethylsilyl)benzonitrile **9a**, a substrate we had found to be among the more reactive toward oxidation, was monitored by ^1H NMR spectroscopy (Figure 1). To reproduce "standard"

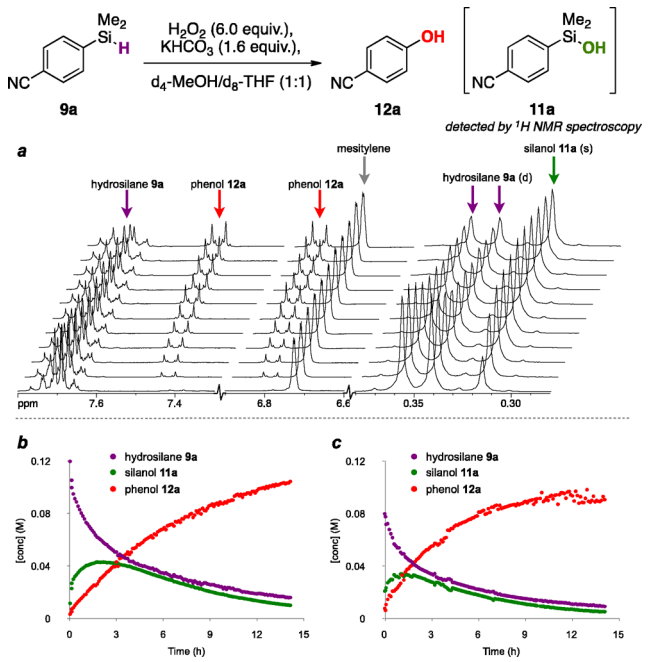

Figure 1. ^1H NMR spectroscopic reaction profiles of the oxidation of hydrosilane **9a** to phenol **12a**. (a) Reaction evolution as monitored by ^1H NMR spectroscopy. (b) Depiction of variation of concentration of **9a**, **12a**, and silanol **11a** with time. (c) Oxidation of a 4:1 mixture of hydrosilane **9a** and authentic silanol **11a**. Reactions run in 1:1 d_4-MeOH/d_8-THF (1:1, 0.3 M) at 298 K.

Tamao oxidation conditions, this experiment was performed in a mixed deuterated solvent system of d_4-MeOD/d_8-THF (1:1), with 6.0 equiv H_2O_2 (30% aq.) and 1.6 equiv $KHCO_3$. Although monitoring of the reaction was complicated by a broad water peak at 3.5–5.5 ppm, two regions of the spectrum proved informative (Figure 1a): the aromatic region (>6.5 ppm), where oxidation is characterized by an upfield shift of the aromatic protons; and the silane region (<0.5 ppm), where the silane substituents are characterized by their multiplicity (the methyl signals appear as a doublet in the hydrosilane, but as a singlet in compounds that do not contain Si–H). The profile of this reaction is shown in Figure 1b. This revealed a smooth consumption of hydrosilane **9a**, and the formation of a nonoxidized arylsilane species assigned as silanol **11a**,[16] which was converted to phenol **12a** as the reaction proceeded. The identity of **11a** was confirmed through independent synthesis,[17,18] and submission of a mixture of authentic **11a** and hydrosilane **9a** to the oxidation. Identical chemical shifts and a similar reaction profile were observed for this mixture as had been seen in the first oxidation, which confirmed the identity of **11a** in the mixed NMR solvent system.

We questioned whether the silanol observed in this oxidation was a necessary intermediate, or if direct hydrosilane oxidation could compete. Due to the limitations of observing the oxidation by ^1H NMR spectroscopy, we turned to *p*-fluorodimethylsilane (**9b**, Figure 2), which enabled reaction

DOI: 10.1021/jacs.7b00357
J. Am. Chem. Soc. 2017, 139, 6138–6145

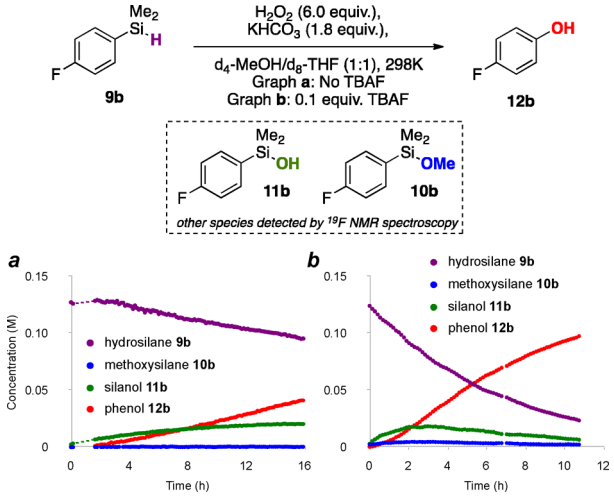

Figure 2. ^{1}H NMR spectroscopic reaction profiling of the oxidation of hydrosilane **9b** to phenol **12b**. (a) Reaction run in the absence of fluoride. (b) Reaction run in the presence of 0.1 equiv TBAF. Reactions run in 1:1 d_4-MeOH/d_8-THF (1:1, 0.3 M) at 298 K.

monitoring by ^{19}F NMR spectroscopy. **9b** is significantly less reactive than benzonitrilesilane **9a**, but nonetheless revealed a similar trend of reactivity (Graph a), and allowed us to observe subtle details of the early phase of the oxidation, where a significant lag in the production of phenol was apparent until appreciable quantities of silanol had formed.[18] This supports the intermediacy of the silanol in the oxidation, rather than a direct oxidation of the hydrosilane (i.e., migration of H is favored over Ar in the initial oxidation).

Interestingly, small amounts of methoxysilane **10b** were observed throughout the reaction. As expected, the equivalent oxidation of **9b** under fluoride-promoted conditions proceeded more rapidly (0.1 equiv TBAF, Graph b), although a delay in the production of phenol was again observed, with silanol **11b** being produced alongside small amounts of methoxysilane **10b** throughout the reaction.[19] This suggests that an equivalent (but accelerated) reaction pathway operates in the presence of fluoride.

Oxidation of Silanols and Methoxysilanes in THF/MeOH. Although silanols were clearly intermediates in the oxidation of arylhydrosilanes under either fluoride-free or fluoride-promoted conditions, their reactivity relative to methoxysilanes, and the importance of exchange between these two species, was as yet unclear. To probe this, the fluoride-free oxidations of (4-fluorophenyl)dimethylsilanol **11b** and (4-fluorophenyl) methoxydimethylsilane **10b** were studied (Figure 3). We immediately noticed that oxidation of silanol **11b** (Figure 3a) proceeded at a much reduced rate compared to methoxysilane **10b** (Figure 3b), and that the latter oxidation featured significant quantities of silanol. Oxidation of **10b** under fluoride-promoted conditions (0.1 equiv TBAF, Figure 3c) proceeded at an overall rate broadly similar to that of the fluoride-free reaction. However, the composition of the various reaction intermediates was rather different, with silanol **11b** produced to a much greater extent, in addition to small amounts of a further silicon-containing species which was identified as disiloxane **13b**.[18]

While both the methoxysilane and silanol could potentially serve as substrates for oxidation, it was not clear whether both indeed did, given that these two components likely exist in equilibrium. To study this, methoxysilane **10b** was subjected to

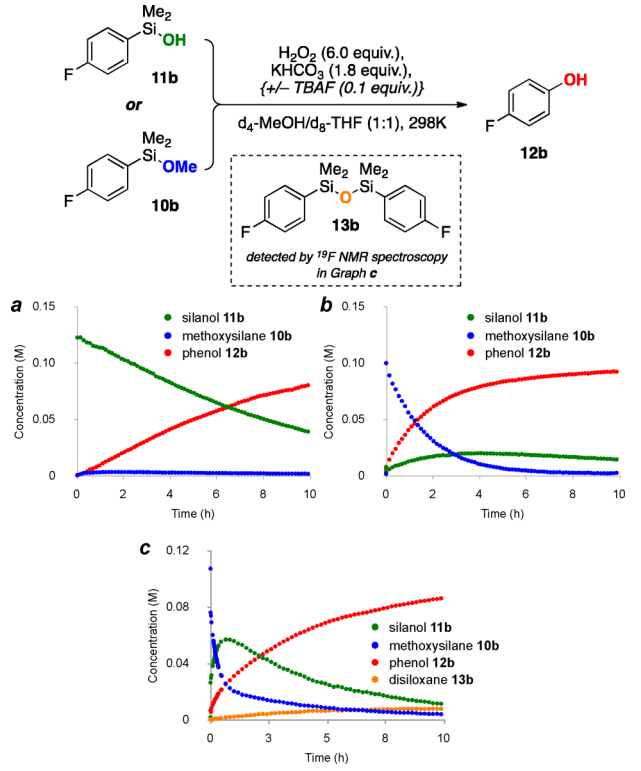

Figure 3. ^{1}H NMR spectroscopic reaction profiling in the oxidation of silanol **11b** and methoxysilane **10b** to phenol **12b**. Reactions run in d_4-MeOH/d_8-THF (1:1, 0.1 M) at 298 K. (a) Fluoride-free oxidation of silanol **11b**. (b) Fluoride-free oxidation of methoxysilane **10b**. (c) Fluoride-promoted (0.1 equiv. TBAF) oxidation of methoxysilane **10b**.

basic conditions ($KHCO_3$) in deuterated THF/MeOH (1:1, plus a volume of water equivalent to that of the 30% aq. H_2O_2 used in the oxidations), in the presence and absence of TBAF. Under fluoride- and peroxide-free conditions (Figure 4, Graph

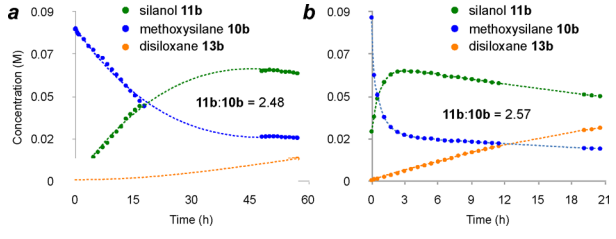

Figure 4. ^{1}H NMR spectroscopic profiling of the equilibria between methoxysilane **10b** and silanol **11b**. (a) Fluoride-free equilibrium. (b) Fluoride-promoted equilibrium (0.1 equiv TBAF). Reactions run in d_4-MeOH/d_8-THF (1:1, 0.1 M substrate) at 298 K.

a), an equilibrium between **10b** and **11b** was established over ~48 h, which stabilized with an equilibrium constant of K_{eq} = 2.48 (in favor of silanol **11b**). The addition of TBAF greatly increased the rate at which equilibrium was reached, but not its position (Graph b, ~3 h, K_{eq} = 2.57; see the Supporting Information (SI) for further details on this equilibrium and the negligible effect of fluoride ion concentration). In both experiments, significant amounts of disiloxane **13b** were formed at the expense of the equilibrium mixture of silanol and methoxysilane; this side-reaction, which is to the detriment of oxidation,[20] was clearly promoted by fluoride. Under "true" oxidation conditions, the rate of equilibration could also be

DOI: 10.1021/jacs.7b00357
J. Am. Chem. Soc. 2017, 139, 6138–6145

affected by the nucleophilic hydroperoxide anion, particularly in the case of fluoride-free Graph 4a.

This suggested that under both sets of oxidation conditions, a dynamic equilibrium between the silanol and methoxysilane operates alongside the oxidation of either or both species, which is consistent with the exchange of ligands between different ate complexes. To elucidate the relative rates of these various processes, we modeled the timecourse kinetic data of the oxidation of methoxysilane **10b** in THF/MeOH using Berkeley Madonna software, based on the reaction scheme in Figure 5a. Graph b illustrates the experimental and modeled

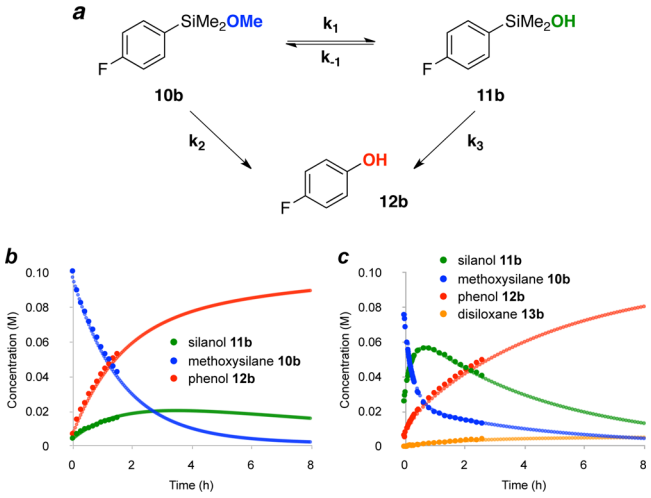

Figure 5. Modeling of kinetic data for oxidations of methoxysilane **10b**, as shown in Figure 3, using Berkeley Madonna. The model is based on experimental data up to 50% conversion (data points shown). (a) Modeled reaction pathways; (b) model for fluoride-free oxidation. (c) model for fluoride-promoted oxidation (0.1 equiv TBAF). Values are normalized relative to k_3. Experimental data obtained at 0.1 M substrate, 0.6 M H_2O_2, 1.8 equiv $KHCO_3$ in d_4-MeOH/d_8-THF (1:1). Relative rate coefficients were obtained by best fit of parameters to the reaction profile a.

data for the fluoride-free oxidation of **10b**, and Graph c illustrates the data for fluoride-promoted oxidation.[21] Best-fit correlations of the experimental data with the illustrated reaction scheme were obtained, which led to the relative rate coefficients depicted in the Table (Figure 5).[22]

The modeling led to an excellent fit between experiment and theory, suggesting that the reaction scheme adopted is a valid depiction of the processes at play during the oxidation. Both models correlate with the equilibrium constants obtained experimentally ($K_{eq} \approx 2.5$, c.f. Figure 4), and give a qualitative indication that the rate of methoxysilane oxidation is around 10-fold that of silanol oxidation (i.e., $k_2 \gg k_3$). This may reflect the propensity of the silanol to form hydrogen bonds with methanol (Si–O–H···O(H)Me), which could increase electron density at the silicon atom and therefore deactivate it toward attack by hydroperoxide anion.[23] In the absence of TBAF, the rate of methoxysilane oxidation appears significantly faster than substitution at silicon by water/hydroxide ($k_2 \gg k_1 > k_{-1}$). Although hydroperoxide presumably serves as a highly competent nucleophile for ate complex formation (as evidenced by the more rapid interconversion of methoxysilane and silanol in its presence compared to the peroxide-free equilibrium experiment in Figure 4a), the peroxide ate complex formed from the methoxysilane seems more prone to undergo (unimolecular) oxidation than (bimolecular) substitution. Equilibrium between methoxysilane and silanol is not reached until ~5 h reaction time (Figure 3b), such that a greater proportion of more reactive methoxysilane is present in the reaction before this time point. However, in the presence of TBAF (Figure 3c), the rate of substitution at silicon (i.e., the interconversion of methoxysilane and silanol) is increased to such an extent that it now outpaces the rate of oxidation ($k_1 > k_{-1} > k_2$). This seems reasonable, in that the interconversion of the methoxysilane and silanol would benefit significantly from fluoride (c.f. Figure 4b), and the rapid establishment of this equilibrium is to the detriment of methoxysilane oxidation.[8,9] The culmination of these effects is that fluoride-free and fluoride-promoted methoxysilane oxidations proceed at similar overall rates, but by different compositions of intermediates.

Attempts to fit reaction parameters to the slower oxidation of the silanol (i.e., Figure 3a) proved more challenging: although these oxidations gave reproducible *trends* in 1:1 THF/MeOH, they did not afford reproducible relative rates of reaction, which prevented reliable parameter fitting. The reactions were found to be highly susceptible to agitation, with a momentary effervescence being observed which coincided with a marked "spike" (increase) in the rate of reaction. We surmised that this corresponded to release of carbon dioxide (from $KHCO_3$/H_2CO_3 decomposition), the evolution of which would have a dramatic effect on the acid–base equilibria of the reaction system and therefore presumably on the concentration of peroxide (or other) anions. This could be circumvented to an extent by purging the reaction mixture with argon, which displaced solubilized CO_2. However, the most significant improvement was gained through the use of methanol alone as solvent, which now gave reproducible kinetic profiles.[24]

The oxidations of the methoxysilane **10b** and silanol **11b** were monitored under these modified conditions (Figure 6), and the profiles modeled using Berkeley Madonna.[21] Considering the fluoride-free oxidations of **10b** (Graph a) and **11b** (Graph b), it was immediately apparent that the rate of nucleophilic substitution at silicon was significantly enhanced in pure MeOH compared to MeOH/THF mixtures:[25] after initial rapid equilibration of silanol and methoxysilane (perhaps promoted by the higher solubility of $KHCO_3$ in MeOH), the two reaction profiles were very similar. Due to the high reproducibility of the reactions,[24] we were able to fit *identical* rate coefficients to the oxidation of both the silanol and methoxysilane, indicating that these oxidations operate under a Curtin–Hammett situation where rapid interconversion of **10b** and **11b** precedes rate-limiting oxidation—in other words, near identical reaction pathways operate from both arylsilanol and arylmethoxysilane substrates. The oxidation rate coefficients evaluated in the modeling suggest that although the silanol predominates at equilibrium, the vast majority of oxidation proceeds via the methoxysilane (i.e., $k_1 > k_{-1} \gg k_2 \gg k_3$).

The reaction profile of the fluoride-catalyzed oxidation of methoxysilane **10b** (0.1 equiv TBAF, Graph c) also revealed broadly similar kinetics, with a rapid equilibrium of methoxysilane and silanol compared to methoxysilane oxidation. TBAF might be expected to further enhance the rate of methoxysilane–silanol exchange, but no accompanying acceleration of oxidation was apparent. The reason for this was soon to become clear.

Influence of Reagent Concentration on Initial Rate of Reaction. The influence of the concentration of the various reagents was evaluated by measurement of initial rates of

DOI: 10.1021/jacs.7b00357
J. Am. Chem. Soc. 2017, 139, 6138–6145

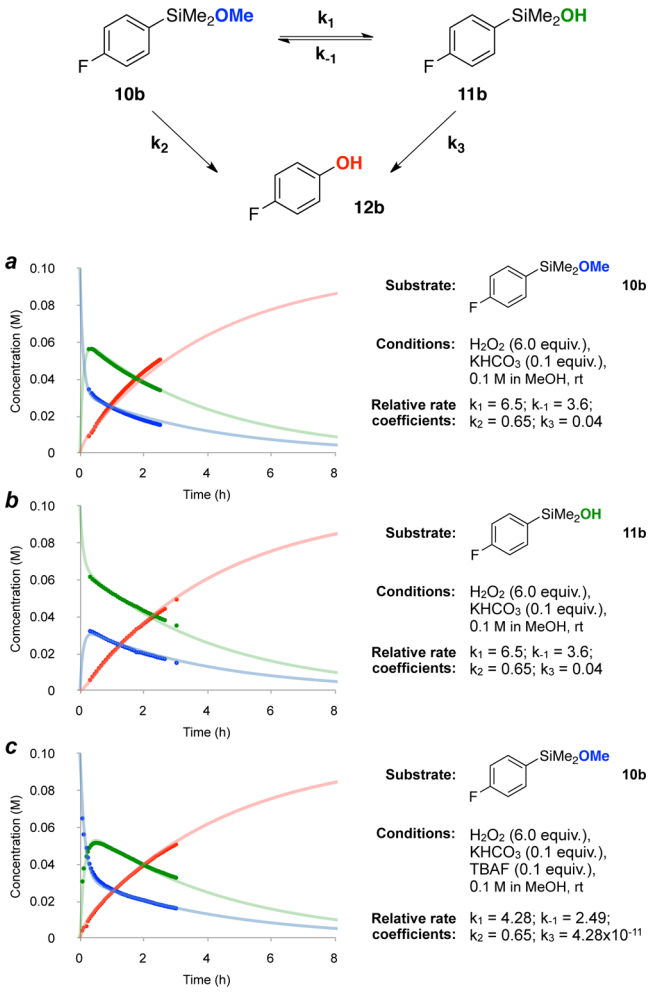

Figure 6. ^{19}F NMR spectroscopic observation, and modeled reaction parameters, for oxidations in MeOH. (a) Fluoride-free oxidation of methoxysilane **10b**; (b) fluoride-free oxidation of silanol **11b**; and (c) fluoride-promoted oxidation of **10b**. Experimental data obtained under the conditions indicated in d_4-MeOH. Relative rate coefficients were obtained by best fit of parameters to the illustrated reaction profiles.

phenol formation in MeOH (Figure 7, experiments run in triplicate for each data point). Graph a shows the variation in initial rate of phenol formation with hydrogen peroxide concentration. As expected, the reaction shows a linear relationship to $[H_2O_2]$, but at higher concentrations a plateau effect is seen. We propose that this arises from the limiting concentration of $KHCO_3$ present in the reaction, which in turn limits the maximum concentration of active hydroperoxide anion. Similar results were obtained when the concentration of $KHCO_3$ was varied (Graph b): an increase in rate can again be seen with increasing concentration of base, with plateauing observed as the reaction mixture approaches a limit of base solubility at 0.3 equiv. $KHCO_3$ (i.e., 0.03 M).

The effect of TBAF concentration was next examined. Here we were surprised to observe an overall *inhibitory* effect of fluoride in the initial rate profiles (Graph c). Fluoride ions increase the rate of nucleophilic substitution around tetravalent silicon by increasing the electrophilicity of the silicon center in a pentavalent silicon-fluoride ate complex, where negative charge is dispersed onto the electronegative apical ligands; nucleophilic attack at pentavalent silicon can be up to 150 times faster than at tetravalent silicon.[12b,26] However, in the oxidation

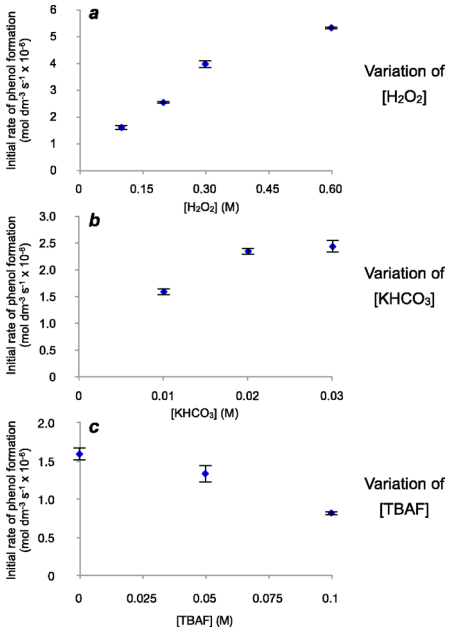

Figure 7. Order of reaction for the oxidation of methoxysilane **10b** with respect to reagents. Reactions run 0.1 M in substrate, in MeOH. Variation of concentration of (a) H_2O_2 (0.1 equiv TBAF, 0.1 equiv $KHCO_3$); (b) $KHCO_3$ (0.1 equiv TBAF, 6.0 equiv H_2O_2); (c) TBAF (0.1 equiv $KHCO_3$, 6.0 equiv H_2O_2). Data points represent the mean rate coefficient of three reactions. Error bars indicate one standard deviation from the mean. See the SI for raw data sets.

reaction, we suggest that this effect is offset by an increased rate of interconversion of the various tetracoordinate and pentacoordinate silicon species, including the possibility that fluoride could retard the overall rate of oxidation by competitive displacement of hydroperoxide from preoxidation ate complexes, thereby decreasing the overall rate of reaction. Finally, the effect of water present in the reaction was examined, as this would likely also affect the concentration of the two silane species, and hence the rate of oxidation. Figure 8 illustrates the influence of water on the methoxysilane−silanol equilibrium constant. Not only is there a clear correlation between K_{obs} and the concentration of water, but also with the nature of the cosolvent, with a higher proportion of silanol being observed in THF/MeOH mixtures (Series A) compared

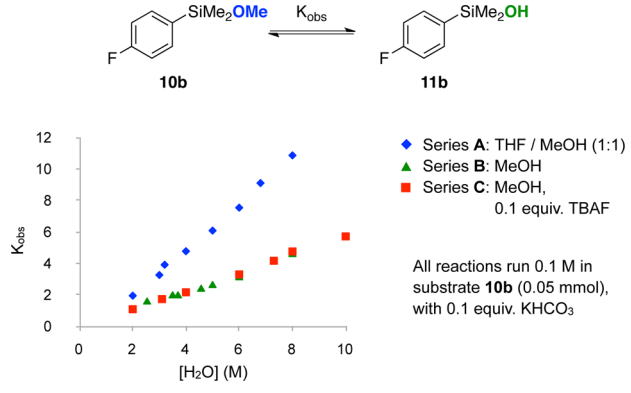

Figure 8. Effect of water on the methoxysilane/silanol equilibrium. All experiments employed 0.05 mmol **10b** and 0.1 equiv $KHCO_3$. Series A: THF/MeOH (1:1). Series B: MeOH. Series C: MeOH, 1 equiv TBAF.

DOI: 10.1021/jacs.7b00357
J. Am. Chem. Soc. 2017, 139, 6138−6145

to MeOH alone (Series B, C). It is again notable in the latter solvent that fluoride does not affect the position of equilibrium. These results suggest that increasing amounts of water are likely to inhibit oxidation, albeit the inorganic base will be better solubilized.

Aryldimethylfluorosilane Intermediacy. The importance of fluoride ions in silicon chemistry merited a search for fluorosilane intermediates, which we expected would likely be present during the oxidation. To study this, we prepared the *p*-fluorophenyl dimethylfluorosilane (4-$FC_6H_4SiMe_2F$), and recorded its ^{19}F NMR spectrum, which showed two signals at −113.5 (C−F) and −165.1 (Si−F)[27] ppm (in MeOH, Figure 9a).[28] Close inspection of the reaction profiles of the oxidation

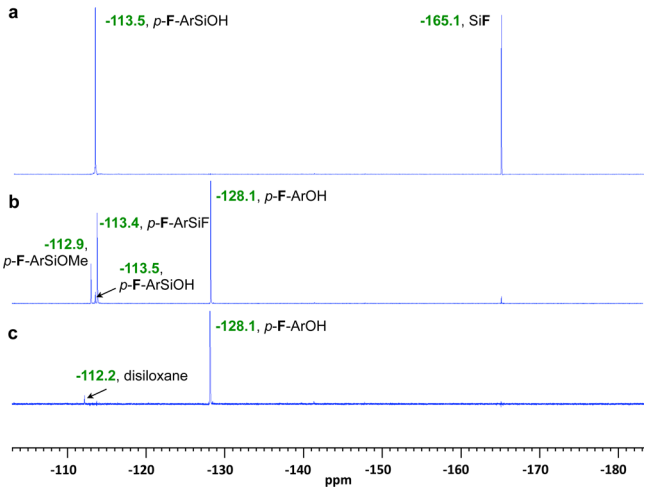

Figure 9. ^{19}F NMR spectra of 4-$FC_6H_4SiMe_2F$, and oxidation of **10b**, in MeOH. (a) Authentic sample of fluorosilane. (b) Oxidation of **10b** after 4 h reaction time. (c) Spectrum of reaction mixture of oxidation of **10b** at completion (36 h), showing consumption of the fluorosilane.

of methoxysilane **10b** in MeOH, using 0.1 equiv TBAF and 3 or 6 equiv of H_2O_2, revealed a small amount of this fluorosilane to be rapidly formed in these reactions (Figure 9b, 6 equiv H_2O_2). The proportion of fluorosilane observed was inversely proportional to the concentration of H_2O_2, and the fluorosilane peak completely disappeared in the reaction using 6 equiv of H_2O_2 once this reaction reached completion (Figure 9c).[29] These observations substantiate the notion that fluorosilane formation is indeed influential on reaction progress, and that fluoride ion can be recycled from silane intermediates.

Charge Development in the Rate-Limiting Step. The experimental data obtained supports a rapid exchange of electronegative ligands around silicon (methoxide, hydroxide, hydroperoxide, and fluoride) as a prelude to a slower, rate-determining migration. In methanol, the rate of ligand exchange approaches a Curtin−Hammett situation, with the majority of the oxidation proceeding via the less abundant, but far more reactive methoxysilane. Given its greater intrinsic nucleophilicity, the reaction of tetravalent silicon with hydroperoxide anion itself is likely to be significantly faster than methoxide or hydroxide.

To further investigate this, we compared the relative rates of oxidation of a variety of para-substituted arylmethoxysilanes, which would enable the construction of linear free-energy relationship (LFER) plots and evaluation of associated reaction parameters. The relative rates of oxidation of these arylmethoxysilanes were measured by reaction of an equimolar mixture of two silanes in the presence of 6 equiv H_2O_2. Five arylsilanes were investigated (*p*-OMe, Me, F, Br, CN), each run in competition with the *p*-F arylsilane. In each case, the proportion of products was measured by ^1H NMR spectroscopic monitoring of the reaction (experiments run in triplicate, ratios, which were consistent, were taken up to ∼50% conversion). To compare solvent effects, each set of experiments was performed in THF/MeOH (1:1), and MeOH.

The resultant LFER plots are depicted in Figure 10. Graph a shows the Hammett plot in 1:1 THF/MeOH, and Graph b the

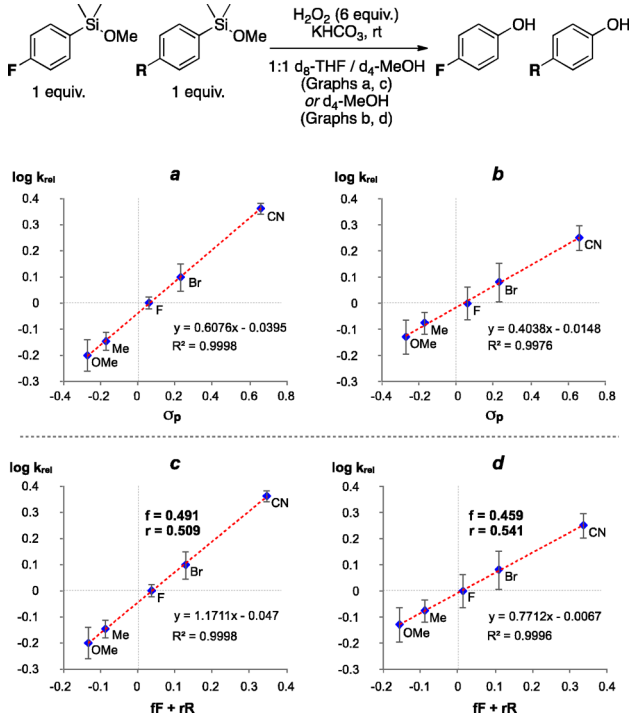

Figure 10. LFER plots for the oxidations of *p*-substituted $ArSiMe_2OMe$. (a) Hammett plot in 1:1 d_8-THF/d_4-MeOH; (b) Hammett plot in d_4-MeOH; (c) Swain−Lupton plot in 1:1 d_8-THF/d_4-MeOH; (d) Swain−Lupton plot in d_4-MeOH. All reactions run with 1.0 equiv each of two arylsilanes, 6 equiv H_2O_2, 16 h, rt, with (a) 0.5 equiv. $KHCO_3$, 0.1 M in THF/MeOH (1:1); (b) 0.5 equiv. $KHCO_3$, 0.1 M MeOH, reaction progress monitored by ^1H NMR spectroscopy. All reactions run in competition with 4-$FC_6H_4SiMe_2OMe$. k_{rel} = [*p*-XC_6H_4OH]/[*p*-FC_6H_4OH], as determined by ^1H NMR spectroscopic analysis of each reaction. Error bars show one standard deviation from the mean.

Hammett plot in MeOH, which pleasingly show an excellent straight line fit, with reaction constants of ρ = +0.60 and ρ = +0.45 for Graphs a and b, respectively. Mindful that mesomeric effects might play a limited role during a rate-limiting migration step, we also explored Swain−Lupton plots of these data;[30] Graph c shows the Swain−Lupton plot in 1:1 THF/MeOH (ρ_{SL} = 1.17), and Graph d in MeOH (ρ_{SL} = 0.77). Of great intrigue is the balance of Swain−Lupton sensitivity factors *f* (field/inductive) and *r* (resonance), which were obtained using Dual Obligation Vector Evaluation (DOVE) as reported by Swain et al.[30] In MeOH/THF, *f* = 0.491, *r* = 0.509; while in MeOH, *f* = 0.459, *r* = 0.541. These values show that mesomeric and inductive effects play an equal role in the rate-determining step of the oxidation.

Despite a significant change in the rates of nucleophilic substitution at silicon when the solvent system is changed from

DOI: 10.1021/jacs.7b00357
J. Am. Chem. Soc. 2017, 139, 6138−6145

THF/MeOH to pure MeOH (Compare Figures 4 and 6, respectively), the somewhat similar ρ values observed for these two reactions under both Hammett and Swain−Lupton analyses further argues against nucleophilic attack of hydrogen peroxide at silicon being rate-determining, albeit H_2O_2 concentration clearly has a rate-influencing effect. These values are, nonetheless, indicative of modest negative charge development in the transition state of the rate-limiting step, which may reflect a positioning of the migrating group in the (charge dense) apical position around pentacoordinate silicon prior to/during the migration step itself. The balance of inductive and mesomeric effects is harder to interpret, as these could affect both migration, or HOO^- coordination to the silane, but provide an additional interesting insight into the electronic characteristics of the RDS. The effect of the solvent on the extent of negative charge development adjacent to the arene in the RDS may reflect a change in the position of the transition state. For instance, it seems reasonable to suppose that O−O bond breaking may be more advanced in MeOH due to better solvation of the hydroxide leaving group.

Finally, we note that these reaction constants are similar in magnitude to the results of an intramolecular competition study of aryl migration conducted by the Tamao group (Scheme 2, eq 1), which was attributed to electronic effects on aryl migration alone,[3h] but lower than a related intermolecular competition (eq 2) which Tamao concluded implied a rate-limiting attack of peroxide at silicon.[31]

Scheme 2. Summary of Results of Linear Free Energy Relationship Experiments

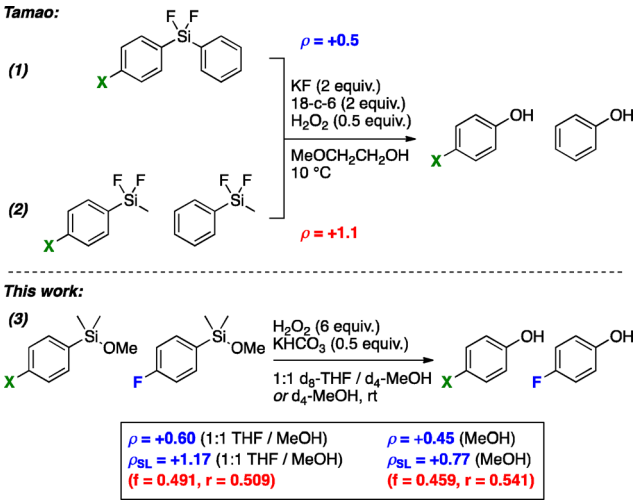

CONCLUSIONS

By observing the oxidation of arylsilanes using ^{19}F NMR spectroscopy, the major reaction components of the oxidation have been identified and the reaction profiles characterized. A significant formation of silanol during the oxidations was revealed, as well as a sensitivity of the oxidation to solvent effects. The rapid rate of nucleophilic substitution at silicon in MeOH compared to THF/MeOH, but the similarity between the LFER reaction parameters for the oxidation in MeOH and THF/MeOH mixtures, indicates that hydrogen peroxide coordination is *not* a rate-limiting process. Instead, aryl migration is proposed to be the rate limiting step, supporting the conclusions of previous theoretical work. The results of these studies offer new insight into organosilane reactivity for the design of silicon-based organic reactions.

ASSOCIATED CONTENT

Supporting Information

The Supporting Information is available free of charge on the ACS Publications website at DOI: 10.1021/jacs.7b00357.

Experimental procedures and data sets for NMR timecourse experiments. Characterization data and copies of NMR spectra for reaction intermediates (PDF)

AUTHOR INFORMATION

Corresponding Author

*edward.anderson@chem.ox.ac.uk.

ORCID

Edward A. Anderson: 0000-0002-4149-0494

Present Address

§Quotient Bioresearch, The Old Glassworks, Nettlefold Road, Cardiff, CF24 5JQ, U.K.

Notes

The authors declare no competing financial interest.

ACKNOWLEDGMENTS

E.J.R. thanks Pfizer (U.K.) for a CASE studentship award. A.M. thanks the Royal Thai Government and the DPST project for a studentship. E.A.A. thanks the EPSRC for an Advanced Research Fellowship (EP/E055273/1), and for additional funding (EP/M019195/1). We thank Dr. John M. Brown for insightful discussions on kinetic data.

REFERENCES

(1) (a) Su, B.; Zhou, T.-G.; Li, X.-W.; Shao, X.-R.; Xu, P.-L.; Wu, W.-L.; Hartwig, J. F.; Shi, Z.-J. *Angew. Chem., Int. Ed.* **2017**, *56*, 1092−1096. (b) Hua, Y.; Asgari, P.; Avullala, T.; Jeon, J. *J. Am. Chem. Soc.* **2016**, *138*, 7982−7991. (c) Ma, Y.; Wang, B.; Zhang, L.; Hou, Z. *J. Am. Chem. Soc.* **2016**, *138*, 3663−3666. (d) Yin, Q.; Klare, H. F. T.; Oestreich, M. *Angew. Chem., Int. Ed.* **2016**, *55*, 3204−3207. (e) Lee, K.-s.; Katsoulis, D.; Choi, J. *ACS Catal.* **2016**, *6*, 1493−1496. (f) Toutov, A. A.; Liu, W.-B.; Betz, K. N.; Fedorov, A.; Stoltz, B. M.; Grubbs, R. H. *Nature* **2015**, *518*, 80−84. (g) Wübbolt, S.; Oestreich, M. *Angew. Chem., Int. Ed.* **2015**, *54*, 15876−15879. (h) Toutov, A. A.; Liu, W.-B.; Betz, K. N.; Stoltz, B. M.; Grubbs, R. H. *Nat. Protoc.* **2015**, *10*, 1897−1903. (i) Cheng, C.; Hartwig, J. F. *J. Am. Chem. Soc.* **2015**, *137*, 592−595. (j) Cheng, C.; Hartwig, J. F. *Science* **2014**, *343*, 853. (k) Cheng, C.; Hartwig, J. F. *Chem. Rev.* **2015**, *115*, 8946−8975.

(2) (a) Bähr, S.; Oestreich, M. *Angew. Chem., Int. Ed.* **2017**, *56*, 52−59. (b) Corrie, T. J. A.; Ball, L. T.; Russell, C. A.; Lloyd-Jones, G. C. *J. Am. Chem. Soc.* **2017**, *139*, 245−254. (c) Komiyama, T.; Minami, Y.; Hiyama, T. *ACS Catal.* **2017**, *7*, 631−651. (d) Morstein, J.; Hou, H.; Cheng, C.; Hartwig, J. F. *Angew. Chem., Int. Ed.* **2016**, *55*, 8054−8057. (e) Komiyama, T.; Minami, Y.; Hiyama, T. *Angew. Chem., Int. Ed.* **2016**, *55*, 15787−15791. (f) Morstein, J.; Kalkman, E. D.; Cheng, C.; Hartwig, J. F. *Org. Lett.* **2016**, *18*, 5244−5247. (g) Shi, W.-J.; Zhao, H.-W.; Wang, Y.; Cao, Z.-C.; Zhang, L.-S.; Yu, D.-G.; Shi, Z.-J. *Adv. Synth. Catal.* **2016**, *358*, 2410−2416. (h) Omann, L.; Oestreich, M. *Angew. Chem., Int. Ed.* **2015**, *54*, 10276−10279. (i) Ball, L. T.; Lloyd-Jones, G. C.; Russell, C. A. *Science* **2012**, *337*, 1644.

(3) (a) Tamao, K.; Kakui, T.; Akita, M.; Iwahara, T.; Kanatani, R.; Yoshida, J.; Kumada, M. *Tetrahedron* **1983**, *39*, 983−990. (b) Tamao, K.; Akita, M.; Kumada, M. *J. Organomet. Chem.* **1983**, *254*, 13−22. (c) Tamao, K.; Ishida, N.; Tanaka, T.; Kumada, M. *Organometallics* **1983**, *2*, 1694−1696. (d) Tamao, K.; Ishida, N.; Kumada, M. *J. Org.*

DOI: 10.1021/jacs.7b00357
J. Am. Chem. Soc. 2017, 139, 6138−6145

Chem. **1983**, *48*, 2120−2122. (e) Tamao, K.; Ishida, N. *J. Organomet. Chem.* **1984**, *269*, c37−c39. (f) Tamao, K.; Kumada, M.; Maeda, K. *Tetrahedron Lett.* **1984**, *25*, 321−324. (g) Sato, K.; Kira, M.; Sakurai, H. *Tetrahedron Lett.* **1989**, *30*, 4375−4378. (h) Tamao, K.; Hayashi, T.; Ito, Y. *Frontiers of Organosilicon Chemistry*; The Royal Society of Chemistry: Cambridge, 1991. (i) Tamao, K. *Proc. Jpn. Acad., Ser. B* **2008**, *84*, 123−133. (j) Jones, G. R.; Landais, Y. *Tetrahedron* **1996**, *52*, 7599−7662. (k) Fleming, I. *Chemtracts: Org. Chem.* **1996**, 1−64.

(4) (a) For the related Fleming oxidation, see: Fleming, I.; Henning, R.; Parker, D. C.; Plaut, H. E.; Sanderson, P. E. J. *J. Chem. Soc., Perkin Trans. 1* **1995**, 317−337. (b) Fleming, I.; Henning, R.; Plaut, H. *J. Chem. Soc., Chem. Commun.* **1984**, 29−31.

(5) (a) Rayment, E. J.; Summerhill, N.; Anderson, E. A. *J. Org. Chem.* **2012**, *77*, 7052−7060. (b) Bracegirdle, S.; Anderson, E. A. *Chem. Commun.* **2010**, *46*, 3454−3456. (c) Sarkar, D.; Gevorgyan, V. *Chem. - Eur. J.* **2016**, *22*, 11201−11204. (d) Cho, S. H.; Hartwig, J. F. *J. Am. Chem. Soc.* **2013**, *135*, 8157−8160. (e) Simmons, E. M.; Hartwig, J. F. *J. Am. Chem. Soc.* **2010**, *132*, 17092−17095. (f) Cordonnier, M.-C. A.; Kan, S. B. J.; Gockel, B.; Goh, S. S.; Anderson, E. A. *Org. Chem. Front.* **2014**, *1*, 661−673. (g) Ihara, H.; Suginome, M. *J. Am. Chem. Soc.* **2009**, *131*, 7502−7503. (h) Tlais, S. F.; Lam, H.; House, S. E.; Dudley, G. B. *J. Org. Chem.* **2009**, *74*, 1876−1885. (i) Lam, H.; House, S. E.; Dudley, G. B. *Tetrahedron Lett.* **2005**, *46*, 3283−3285. (j) For Tamao conditions see: Sunderhaus, J. D.; Lam, H.; Dudley, G. B. *Org. Lett.* **2003**, *5*, 4571−4573.

(6) For the palladium-catalyzed conversion of aryltrimethylsilanes to phenolic acetates, see: Gondo, K.; Oyamada, J.; Kitamura, T. *Org. Lett.* **2015**, *17*, 4778−4781.

(7) (a) Goh, S. S.; Chaubet, G.; Gockel, B.; Cordonnier, M.-C. A.; Baars, H.; Phillips, A. W.; Anderson, E. A. *Angew. Chem., Int. Ed.* **2015**, *54*, 12618−12621. (b) Goh, S. S.; Baars, H.; Gockel, B.; Anderson, E. A. *Org. Lett.* **2012**, *14*, 6278−6281. (c) Tun, M. K. M.; Wustmann, D.-J.; Herzon, S. B. *Chem. Sci.* **2011**, *2*, 2251−2253. (d) Cordonnier, M.-C. A.; Kan, S. B. J.; Anderson, E. A. *Chem. Commun.* **2008**, 5818−5820.

(8) Mader, M. M.; Norrby, P.-O. *J. Am. Chem. Soc.* **2001**, *123*, 1970−1976.

(9) Mader, M. M.; Norrby, P.-O. *Chem. - Eur. J.* **2002**, *8*, 5043−5048.

(10) For examples of the oxidation of arylfluorosilanes without additional fluroide promoter, see: Brough, P. A.; Fisher, S.; Zhao, B.; Thomas, R. C.; Snieckus, V. *Tetrahedron Lett.* **1996**, *37*, 2915−2918.

(11) For earlier work on migratory aptitude, see: Buncel, E.; Davies, A. G. *J. Chem. Soc.* **1958**, 1550−1556.

(12) (a) Deiters, J. A.; Holmes, R. R. *J. Am. Chem. Soc.* **1990**, *112*, 7197−7202. (b) Brefort, J. L.; Corriu, R. J. P.; Guerin, C.; Henner, B. J. L.; Wong Chi Man, W. W. C. *Organometallics* **1990**, *9*, 2080−2085. (c) Holmes, R. R. *Chem. Rev.* **1990**, *90*, 17−31. (d) Bassindale, A. R.; Parker, D. J.; Taylor, P. G.; Turtle, R. *Z. Anorg. Allg. Chem.* **2009**, *635*, 1288−1294.

(13) DiLauro, A. M.; Seo, W.; Phillips, S. T. *J. Org. Chem.* **2011**, *76*, 7352−7358.

(14) For the related observation of the conversion of fluorosilanes to silanols and methoxysilanes, see: Knölker, H.-J.; Wanzl, G. *Synlett* **1995**, *1995*, 378−382.

(15) The heightened reactivity of aryloxysilyl ethers over alkoxysilyl ethers towards basic hydrolysis has also been noted by Corriu, see: Corriu, R. J. P.; Guerin, C.; Henner, B. J. L.; Wang, Q. *Organometallics* **1991**, *10*, 3200−3205.

(16) For a review on the generation of silanols from hydrosilanes, see: Jeon, M.; Han, J.; Park, J. *ACS Catal.* **2012**, *2*, 1539−1549.

(17) Lee, M.; Ko, S.; Chang, S. *J. Am. Chem. Soc.* **2000**, *122*, 12011−12012.

(18) See the SI for details of the identification of various key reaction intermediates through comparison with authentic materials.

(19) We suggest that the lack of an observable lag in product formation from the *p*-CN hydrosilane (Figure 1) is due to a much higher rate of silanol-methoxysilane equilibration, and methoxysilane oxidation, which masks the expected lag.

(20) Aryldisiloxanes are poor substrates for oxidation, see ref 5a.

(21) Modelling is based on the first 50% conversion, with the concentration of H_2O_2 assumed constant. See the SI for details.

(22) Relative rate coefficients have been normalized with respect to silanol oxidation (k_{rel} = 1 s^{-1}). Relative second order rate coefficients for the formation of the disiloxane **13b** were also modeled. The relative rate coefficient for formation of **13b** from **10b** and **11b** was k_3 = 20.2 s^{-1} mol^{-1} dm^3. The relative rate coefficient for the formation of **13b** from two molecules of **11b** was 4.1 × 10^{-7} s^{-1} mol^{-1} dm^3. The concentration of H_2O_2 is assumed constant in these calculations.

(23) The extreme of this interaction in a basic medium would be deprotonation of the silanol; however, the presence of silanolate ions was not detected spectroscopically.

(24) These experiments were run in triplicate. See the SI for reaction profiles, which gave identical rate data. For example, the oxidation of the methoxysilane under fluoride-free conditions in d_4-MeOD using a standardized degassing procedure gave three initial rate coefficients of 5.316 × 10^{-6}, 5.322 × 10^{-6} and 5.312 × 10^{-6} mol dm^{-3} s^{-1}, with r^2 values of 0.92, 0.99, and 0.99 respectively; %RSD (relative standard deviation) = 0.082.

(25) For this reason, reactions in MeOH were run at increased dilution (0.1M). See the SI for details of the optimization of conditions, and consistency of kinetic data.

(26) Corriu, R. J. P.; Guerin, C.; Henner, B. J. L.; Wong Chi Man, W. W. C. *Organometallics* **1988**, *7*, 237−238.

(27) Kunai, A.; Sakurai, T.; Toyoda, E.; Ishikawa, M. *Organometallics* **1996**, *15*, 2478−2482.

(28) The Si−F ^{19}F NMR peak at −165.1 ppm is masked when using hexafluorobenzene as internal standard. These NMR spectra are run in the absence of this internal standard.

(29) Reaction using 3 equiv of H_2O_2 did not reach completion after 24 h, and fluorosilane remained after this time. We note that the fluorosilane could arise from a number of reaction pathways, including breakdown of fluoride-peroxide ate complexes.

(30) We thank a reviewer for the helpful suggestion to analyze the LFER data using the Swain−Lupton method. See: Swain, C. G.; Unger, S. H.; Rosenquist, N. R.; Swain, M. S. *J. Am. Chem. Soc.* **1983**, *105*, 492−502.

(31) We suggest that the reduced susceptibility of the diarylsilane to electronic effects could reflect the difference in reactivity effects for this substrate class, as opposed to an arylmethylsilane.

DOI: 10.1021/jacs.7b00357
J. Am. Chem. Soc. 2017, 139, 6138−6145

This is an open access article published under a Creative Commons Attribution (CC-BY) License, which permits unrestricted use, distribution and reproduction in any medium, provided the author and source are cited.

JACS
JOURNAL OF THE AMERICAN CHEMICAL SOCIETY
Article
pubs.acs.org/JACS

Mechanistic Insight into Palladium-Catalyzed Cycloisomerization: A Combined Experimental and Theoretical Study

Aroonroj Mekareeya,[†] P. Ross Walker,[†] Almudena Couce-Rios,[‡] Craig D. Campbell,[†] Alan Steven,[§] Robert S. Paton,*[,†] and Edward A. Anderson*[,†]

[†]Chemistry Research Laboratory, University of Oxford, 12 Mansfield Road, Oxford OX1 3TA, U.K.
[‡]Departament de Química, Universitat Autònoma de Barcelona, 08193 Cerdanyola del Vallès, Spain
[§]AstraZeneca Pharmaceutical Techology and Development, Charter Way, Macclesfield, Cheshire SK10 2NA, U.K.

Supporting Information

ABSTRACT: The cycloisomerization of enynes catalyzed by $Pd(OAc)_2$ and bis-benzylidene ethylenediamine (bbeda) is a landmark methodology in transition-metal-catalyzed cycloisomerization. However, the mechanistic pathway by which this reaction proceeds has remained unclear for several decades. Here we describe mechanistic investigations into this reaction using enynamides, which deliver azacycles with high regio- and stereocontrol. Extensive ^1H NMR spectroscopic studies and isotope effects support a palladium(II) hydride-mediated pathway and reveal crucial roles of bbeda, water, and the precise nature of the $Pd(OAc)_2$ pre-catalyst. Computational studies support these mechanistic findings and lead to a clear picture of the origins of the high stereocontrol that can be achieved in this transformation, as well as suggesting a novel mechanism by which hydrometalation proceeds.

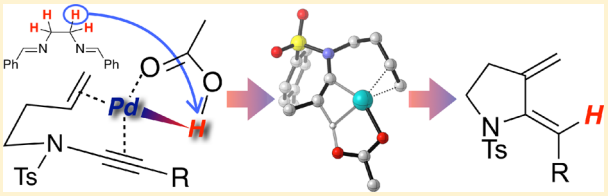

INTRODUCTION

Transition-metal-catalyzed cycloisomerizations are among the most atom-efficient methods to access organic ring systems.[1] The appeal of these skeletal reorganizations lies in both the importance of ring synthesis in organic chemistry and the diversity of products that can arise from a single substrate, depending on the mechanistic pathway taken.[1a,b,2] Among the many transition metals that have been used for enyne cycloisomerization, palladium catalysts have seen widespread use, with extensive work from Trost and co-workers demonstrating the versatility of this metal in three particularly robust catalyst systems (Scheme 1, eq 1):[3] $Pd(OAc)_2$/triarylphosphine,[4] $Pd(OAc)_2$/bis-benzylidene ethylenediamine (bbeda),[4d,e,5] and $Pd_2dba_3{\cdot}CHCl_3$/AcOH (with or without phosphine ligand or bbeda).[6] Since these pioneering studies, palladium-catalyzed cycloisomerization has been widely exploited in methodology[3] and synthesis contexts.[4b,5b,7] Our group has shown that $Pd(OAc)_2$/bbeda is particularly effective in catalyzing the cycloisomerization of enynamides to pyrrolidine and piperidine enamides (Scheme 1, eq 2),[8] useful heterocycles that can undergo a variety of further ring-forming transformations.[9]

Scheme 1. Palladium-Catalyzed Cycloisomerization of Enynes and Enynamides

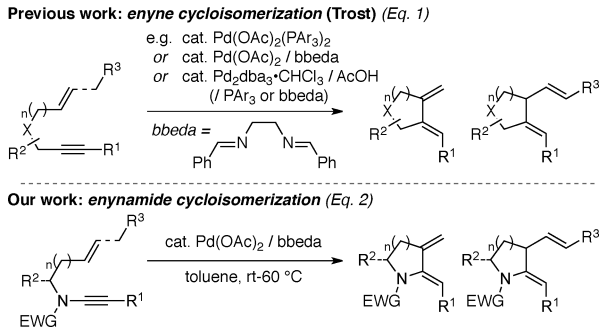

Despite this rich history, the mechanism by which the $Pd(OAc)_2$/bbeda catalyst system operates is far from clear. Under Pd_2dba_3 catalysis, it is widely accepted that reaction of Pd(0) with acetic acid generates a palladium(II) hydride species (Scheme 2, Path A), which effects cycloisomerization by alkyne hydropalladation (**1** → **2**), alkene carbopalladation (**3**), and β-hydride elimination. This latter process, which regenerates palladium(II) hydride, can give rise to three isomeric products: a 1,3-diene and (*E*)- or (*Z*)-1,4-dienes (**4**–**6**, respectively), depending on the hydrogen atom involved. In contrast, it is not apparent that this mechanism also operates for $Pd(OAc)_2$/bbeda, not least as there is no obvious pathway for the generation of palladium(II) hydride from these components. This in part likely contributed to early proposals[4d,e,5] that this catalyst instead effects cycloisomerization by a Pd(II) → Pd(IV) oxidative coupling to form an intermediate palladacyclopentene **7** (Path B),[4d,5c,10] followed by β-hydride elimination (**8**) and then reductive elimination—a route believed to

Received: May 26, 2017
Published: July 12, 2017

© 2017 American Chemical Society

DOI: 10.1021/jacs.7b05436
J. Am. Chem. Soc. 2017, 139, 10104–10114

Scheme 2. Mechanistic Dichotomy for Pd-Catalyzed Enyne Cycloisomerization

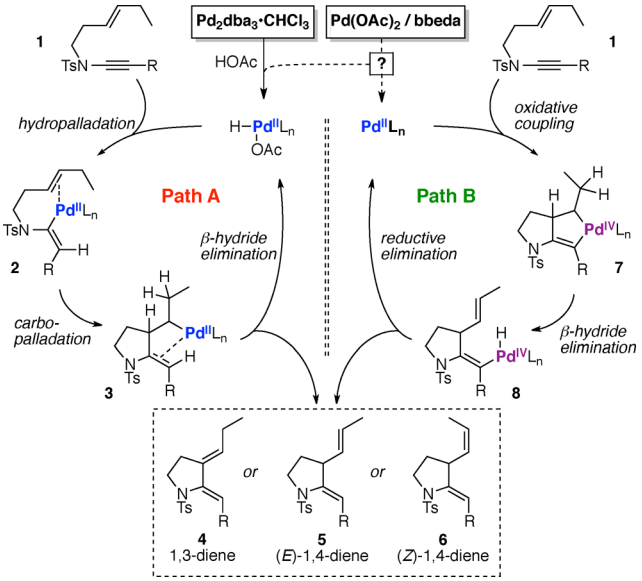

Scheme 3. Regio- and Stereoselectivity in the Cyclization of Mono- and 1,2-Disubstituted Enynamides

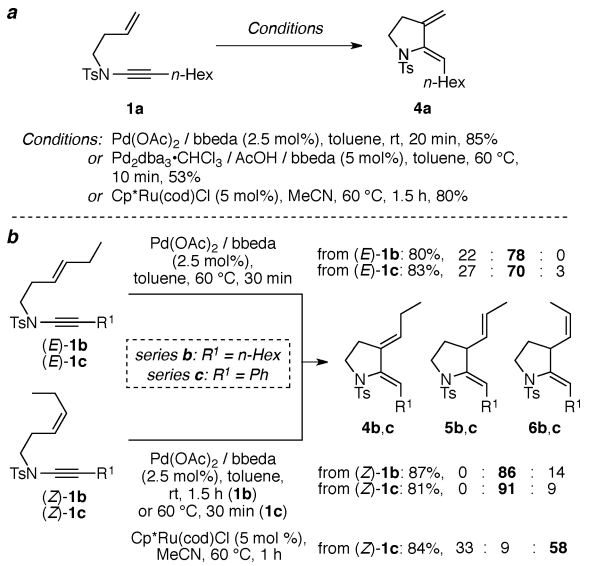

operate for other transition metals such as ruthenium and rhodium.[1g,6f] However, despite the proposal of Pd(IV) palladacycles in other palladium-catalyzed processes,[11] no direct evidence for palladacyclopentenes has been reported. Other support for this pathway includes high selectivity for β-hydride elimination "away" from the newly formed ring (leading to a 1,4-diene), which would be favored on geometric grounds as the C−Pd and bridgehead C−H bonds cannot easily adopt a *syn*-coplanar orientation in palladacycle **7**, and also through the observation of different product distributions between the various palladium catalyst systems.[3a,6e] In light of this continuing uncertainty, both mechanistic explanations have been routinely adopted.[12]

On the basis of our own experimental observations,[8] we questioned whether enynamide cyclizations could offer new insight into this mechanistic puzzle, and a deeper understanding of the high stereoselectivity that can be achieved in the cyclizations. We report here studies that offer compelling evidence for palladium(II) hydride intermediacy in enynamide cycloisomerization under $Pd(OAc)_2$/bbeda catalysis, including the discovery of significant kinetic isotope effects, the influence of water and the nature of the precatalyst on the reaction pathway, and three distinct processes that depend on bbeda. Alongside this, theoretical analysis of the reaction mechanism rationalizes reaction stereoselectivity, and leads to the proposal of a new mechanism for hydropalladation.

RESULTS AND DISCUSSION

Reaction Optimization and Regio-/Stereoselectivity Observations. A screen of palladium-catalyzed enyne cycloisomerization conditions[4−6] had revealed that cyclization of enynamide **1a** to amidodiene **4a** (Scheme 3a) could best be effected using Pd(II) precatalysts, with $Pd(OAc)_2$/bbeda offering superior reactivity.[8,13] Pd_2dba_3·$CHCl_3$/AcOH systems gave poor conversion unless employed in combination with bbeda, which effected rapid conversion of **1a** to **4a**, albeit at higher temperature. Cyclization of enynamide **1a** under Ru catalysis (5 mol% Cp*Ru(cod)Cl in MeCN)[14] provided a useful reference point of a reaction widely recognized to proceed through a metallacycle intermediate.[1g,6f]

Under the $Pd(OAc)_2$/bbeda catalytic manifold, we found that the cycloisomerization of 1,2-disubstituted alkenes occurs with high stereo- and regioselectivity: enynamides (*E*)-**1b**/**c** gave predominantly the (*E*)-1,4-dienes **5b** and **5c**, with minor amounts of 1,3-diene and only traces of (*Z*)-1,4-diene, while reaction of enynamides (*Z*)-**1b**/**c** also afforded **5b** and **5c** as the major products, but now with minor amounts of (*Z*)-1,4-diene and only traces of 1,3-diene.[15] The equivalent cyclization of (*Z*)-**1c** under ruthenium catalysis led to a contrasting product ratio, with (*Z*)-1,4-diene **6c** being the major product. As this latter cyclization likely proceeds through a ruthenacycle intermediate,[16] this differing selectivity already seemed suggestive of distinct mechanistic pathways.

We also observed very high levels of substrate stereocontrol in cycloisomerizations that generate new stereocenters (Table 1). Entry 1 shows the influence of a substituent adjacent to the ynamide nitrogen atom, which gave a single regio- and stereoisomer of pyrrolidine enamide **5d**. The formation of trisubstituted piperidine enamide **5e** (Entry 2) proceeded with equivalent stereoselectivity, but reduced regioselectivity, with small amounts of 1,3- and 1,5-diene produced alongside the (*E*)-1,4-diene **5e**. The formation of a 1,5-diene may reflect a reversible β-hydride elimination in the final step of the catalytic pathway, as is often seen in Heck reactions. A disubstituted enynamide tether also led to exceptional stereocontrol in the formation of tetrasubstituted pyrrolidine **5f** (Entry 3).[17] Entries 4 and 5 depict cyclizations that generate quaternary stereocenters with remarkable stereocontrol, with pyrrolidines **5g** and **5h** formed as single isomers. The exquisite stereoselectivity imparted in these cyclizations can be rationalized by a theoretical analysis of the reaction pathway (see below), in which the irreversible cyclization step operates with very high levels of stereocontrol.

Deuterium Crossover Experiments/^{1}H NMR Spectroscopic Reaction Profiling. Deuterium crossover experiments could offer insight as to whether an inter- or intramolecular hydride transfer takes place; the former would suggest involvement of a discrete palladium hydride species, while the

DOI: 10.1021/jacs.7b05436
J. Am. Chem. Soc. 2017, 139, 10104−10114

Table 1. Diastereoselective Cycloisomerizations of Enynamides with Substituted Tethers[a]

Entry	Substrate	Product(s)	Yield (%)[b]	Ratio / comments
1	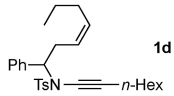 1d	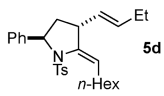 5d	87	single isomer
2	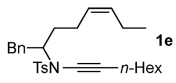 1e	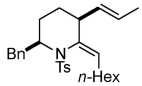 5e	86	9:77:14[c]
3	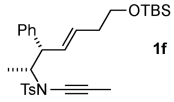 1f	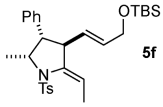 5f	95	single isomer
4	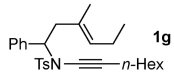 1g	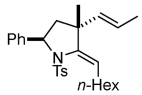 5g	84	single isomer
5	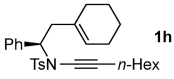 1h	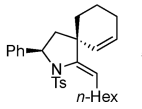 5h	78	single isomer

[a]Reaction conditions: 5 mol% $Pd(OAc)_2$, 5 mol% bbeda, toluene (0.167 M), 60 °C, 30 min; entry 2 reaction time = 90 min. [b]Isolated yield. [c]Ratio of 1,3-:1,4-:1,5-dienes as determined by ^{1}H NMR spectroscopic analysis of the crude reaction mixture.

latter would be more consistent with a metallacycle pathway. To explore this, deuterated toluenesulfonyl enynamide **D-1a** (>98% D)[18] and non-deuterated *p*-nitrobenzenesulfonyl enynamide **1i** were reacted in a 1:1 ratio using each of the catalyst systems (Scheme 4). With Pd_2dba_3·$CHCl_3$/AcOH/bbeda,

Scheme 4. Deuterium Crossover Experiments

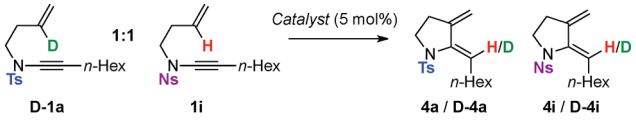

Catalyst system	Conversion (%)	%D	%D
Pd_2dba_3·$CHCl_3$ / AcOH / bbeda	55	42	44
Cp*Ru(cod)Cl, d_3-MeCN, 60 °C	78	83	0
$Pd(OAc)_2$ / bbeda	100	43	44

complete crossover of the deuterium label was observed. In contrast, under ruthenium catalysis, no crossover occurred and **D-4a** was isolated with 83% D incorporation (supporting an intramolecular hydride transfer pathway). Finally, products **4a** and **4i** arising from the equivalent $Pd(OAc)_2$/bbeda experiment also featured nearly equivalent amounts of deuterium incorporation (43 and 44% respectively), thus supporting intermolecular transfer of hydride via a discrete Pd−H/D intermediate under both palladium-catalyzed reaction conditions.

To compare the three reaction manifolds in more detail, we next monitored the cyclizations of **1a** using ^{1}H NMR spectroscopy. Under Pd_2dba_3·$CHCl_3$/AcOH/bbeda or Cp*Ru(cod)Cl catalysis (Figure 1, graphs a and b), immediate conversion of starting material to product was observed, sugggesting that a catalytically competent species is present, or rapidly formed, at the start of the reaction.[19] In the case of Pd_2dba_3·$CHCl_3$, this is presumably a palladium(II) hydride

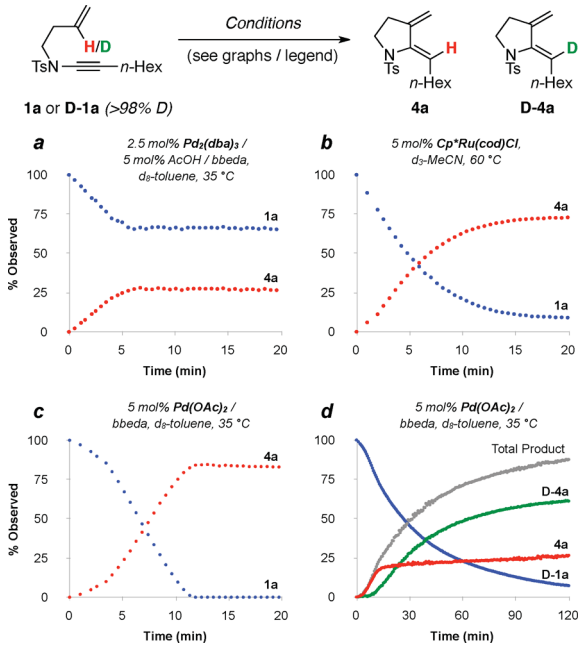

Figure 1. ^{1}H NMR spectroscopic profiles of reaction of enynamide **1a**, and deuterated enynamide **D-1a**. Graphs a−c show the conversion of **1a** (blue) to **4a** (red); reaction conditions are indicated. Graph d shows the conversion of **D-1a** (blue) to **4a** (red) and **D-4a** (green); total product formation is shown in gray.[21]

species, formed through oxidative addition of Pd(0) with acetic acid;[3b,6,20] whereas the ruthenium-catalyzed reaction likely only requires ligand exchange of cyclooctadiene and the substrate in the $Cp^*Ru(I)(L)_2$ complex. A marked difference in reaction profile was observed with $Pd(OAc)_2$/bbeda (graph c): despite this being a superior catalyst system (compared to the other catalysts) in terms of conversion and scope, this reaction exhibited a distinct induction period that presumably relates to the generation of an active catalyst species from $Pd(OAc)_2$. The conversion of **D-1a** to the deuterated product **D-4a** was also monitored (graph d): this reaction required a much extended reaction time to reach full conversion compared with non-deuterated**1a**, revealing significant deuterium isotope effects (*vide infra*). Of greater intrigue was the observation that the *extent* of product deuteration changed during the reaction. At early stages, *only* protiated product was produced (red curve), whereas at later stages, the deuterated product was formed almost exclusively (green curve)—in this case leading to a drop of deuterium incorporation from 100% D in the starting material **D-1a**, to ∼70% in the product **D-4a**.

This result led us to speculate that water has a crucial impact on reaction progress and product formation, with deuterium loss arising from an exchange process with water present in the NMR reaction solvent. We therefore set about comparing the reaction profiles of **1a** and **D-1a** using d_8-toluene containing varying concentrations of water (determined by Karl Fischer titration); the results of these collected experiments are illustrated in Figure 2. Non-deuterated **1a** was first tested using pre-dried d_8-toluene as solvent (dried for several days over 4 Å molecular sieves, 3 ppm H_2O).[22] We found that a somewhat extended reaction time was required to reach completion (Figure 2, graph HA) compared to the reaction using "bottle" d_8-toluene (82 ppm of H_2O, graph HB), indicating a beneficial effect of water on reaction rate. This trend extended to water-saturated d_8-toluene (480 ppm, graph

DOI: 10.1021/jacs.7b05436
J. Am. Chem. Soc. 2017, 139, 10104−10114

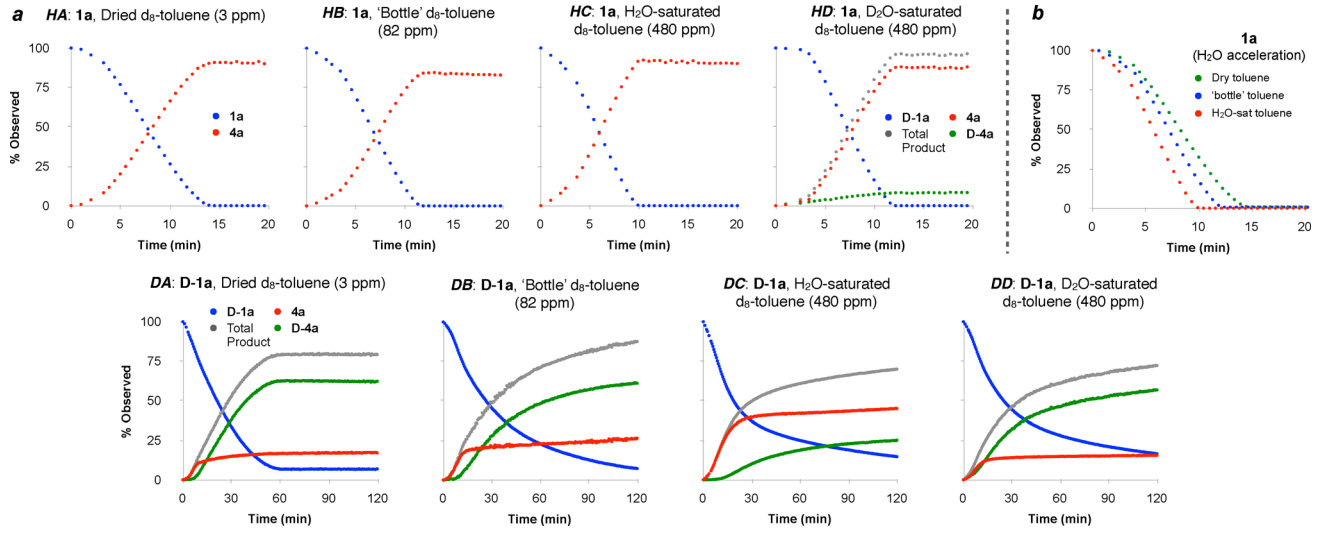

Figure 2. (a) ^{1}H NMR spectroscopic reaction profiles of **1a** (graphs HA–HD) and **D-1a** (graphs DA–DD) using dry, bottle, and H_2O- or D_2O-saturated d_8-toluene as reaction solvent. Graphs HA–HD show the conversion of **1a** (blue) to **4a** (red) and **D-4a** (green). Graphs DA–DD shows the conversion of **D-1a** (blue) to **4a** (red) and **D-4a** (green); total product formation is shown in gray. (b) Comparison of increasing water content on reaction of enynamide **1a**.[21] All reactions run at 35 °C, 0.167 M in substrate, using 5 mol% $Pd(OAc)_2$/bbeda.

HC), where a further acceleration was observed; a summary of this effect is illustrated in Figure 2b. Interestingly, running the reaction in d_8-toluene saturated with D_2O led to the incorporation of a small amount of deuterium into the product (graph HD), thus confirming that adventitious water can indeed serve as a source of "hydride". The equivalent reactions of the deuterated substrate **D-1a** (graphs DA-DD) showed that as the water (H_2O) content of the reaction solvent increases, so does the proportion of protiated product **4a** (red curves in graphs DA-DC), which is consistently and exclusively produced at the start of all reactions. Notably, around 15% of protiated product was produced in both reactions DA and DD, despite the use of 100% deuterated substrate and a reaction medium devoid of H_2O. This observation was later to be rationalized through discovery of the pathway for reaction initiation.[23]

The Role of Water. We hypothesized that water could accelerate the reaction through involvement in the initiation process. Bedford et al.[24] recently characterized the influence of water on $Pd(OAc)_2$, which in organic solutions exists as a trimeric complex $[Pd_3(OAc)_6]$, a structure with D_{3h} symmetry featuring bridging acetate ligands.[25] In the presence of water, this trimer is in equilibrium with the $[Pd_3(OAc)_5OH]$ (Figure 3a), in which one of the bridging acetate ligands has been replaced by a bridging hydroxide ion.[24] In increasingly water-rich environments, a greater proportion of this complex is formed, and we questioned whether this could act as a more reactive pre-catalyst. To test this, $[Pd_3(OAc)_5OH]$ was prepared as reported by Bedford.[24] Reaction of **1a** with $[Pd_3(OAc)_5OH]$/bbeda in pre-dried d_8-toluene indeed showed a reduced induction period (Figure 3a, red curve), compared to $[Pd_3(OAc)_6]$/bbeda in H_2O-saturated d_8-toluene (blue curve), suggesting that hydrolysis of $[Pd_3(OAc)_6]$ is an important process in reaction initiation. Interestingly, the post-initiation rate of these reactions was similar, which may imply that a common catalytic species forms from both pre-catalysts.

The Role of bbeda. Although $Pd(OAc)_2$-catalyzed cycloisomerizations can operate in the absence of bbeda, reactions in which it is present reach completion more rapidly. ^{1}H NMR spectroscopic reaction profiles for the cycloisomerization of **1a** showed that bbeda-free reactions fail to reach completion after >3 h (Figure 4, red curve), compared to ~15 min in its presence (blue curve). The appearance of these reactions also differs markedly: in the absence of bbeda, black particulates develop over time, as opposed to a consistent yellow color (and

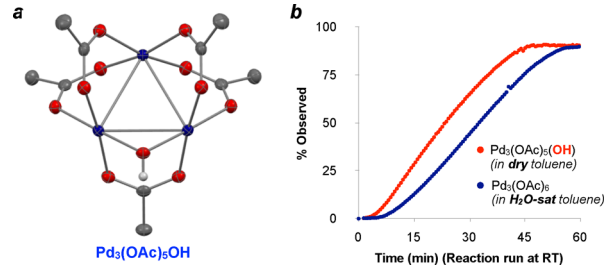

Figure 3. Effects of water on the cycloisomerization of **1a** to **4a** (product formation shown). (a) Structure of $[Pd_3(OAc)_5OH]$.[25b] (b) $[Pd_3(OAc)_5OH]$/bbeda in dried d_8-toluene (red) and $[Pd_3(OAc)_6]$/bbeda in H_2O-saturated d_8-toluene (blue). Reactions carried out with 5 mol% [Pd]/bbeda at room temperature.

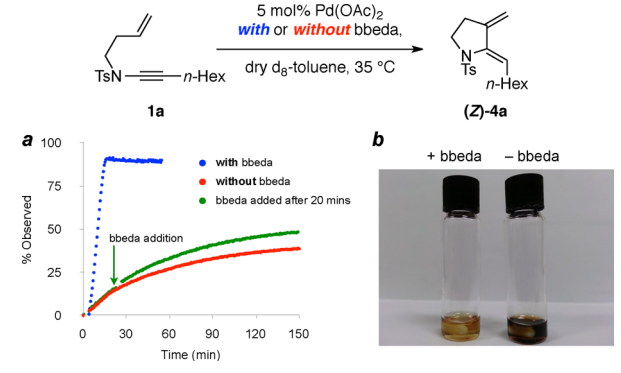

Figure 4. Influence of bbeda on the cycloisomerization of **1a**. (a) Reaction profile in the presence (blue) and absence (red) of bbeda; and a delayed bbeda addition (green). (b) Visual comparison of bbeda-promoted and bbeda-free reactions.

DOI: 10.1021/jacs.7b05436
J. Am. Chem. Soc. 2017, 139, 10104–10114

little or no particulate formation) in reactions containing the imine. Possible roles of bbeda include that of a ligand which accelerates the catalytic cycle,[7f] or a stabilizing component for off-cycle palladium species. Interestingly, addition of bbeda after 20 min reaction time to a bbeda-free reaction did not lead to a marked acceleration (Figure 4, green curve) but did result in a somewhat higher rate of reaction being sustained compared to the bbeda-free reaction. Although these two reactions may well operate by different pathways, this could indicate that bbeda inhibits catalyst aggregation.

From these experiments, it also seemed possible that bbeda might also be involved in precatalyst deaggregation and/or reaction initiation. To explore this, we titrated solutions of $[Pd_3(OAc)_5(OH)]$ and $[Pd_3(OAc)_6]$ in anhydrous d_8-toluene with bbeda (Figure 5). A dramatic effect was seen on addition

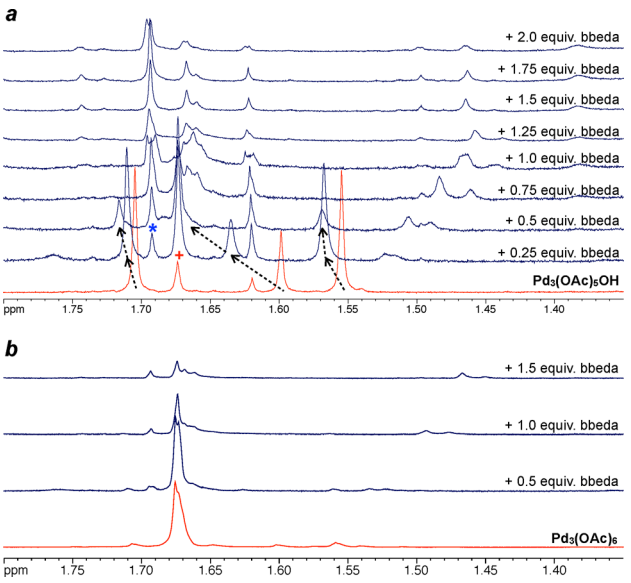

Figure 5. Effect of bbeda on (a) $[Pd_3(OAc)_5OH]$ and (b) $[Pd_3(OAc)_6]$. Titrations performed in dry d_8-toluene at room temperature.

of even 0.25 equiv of bbeda to $[Pd_3(OAc)_5(OH)]$ (titration a): the ^{1}H NMR signals corresponding to this complex at δ_H 1.70, 1.60, and 1.55 ppm shifted downfield (dashed arrows), and a significant new signal appeared at 1.69 ppm (*). The proportion of $[Pd_3(OAc)_6]$ (+, 1.67 ppm) appeared to increase; with addition of further bbeda, this peak was consumed. Under these conditions, it thus seems that these two complexes are in facile equilibrium, and that $[Pd_3(OAc)_5(OH)]$ is converted by bbeda to an unidentified species, which we suggest to be a deaggregated complex. In contrast, a solution of pure $[Pd_3(OAc)_6]$ was barely affected by bbeda until 1.0−1.5 equiv of ligand was added (titration b). The greater susceptibility of $[Pd_3(OAc)_5(OH)]$ to the action of bbeda may explain the decreased induction period observed when using this complex, or $[Pd_3(OAc)_6]$ in water-rich reactions (see Figure 3); however, the dramatically enhanced rate of reactions run in the presence of bbeda (Figure 4) yet remained unexplained.

Initiation Pathway. Although we had now identified a number of different factors that influenced the rate of initiation, the *source* of the putative palladium(II) hydride remained a mystery, particularly given the consistent low levels of protiated product observed under anhydrous/protium-free reactions of **D-1a** (graphs DA and DD, Figure 2). The reactions of a number of other substrates deuterated at various positions did not lead to any deuteration of the enamide alkene, suggesting the substrate is not the origin of hydride. This left bbeda itself—and a key observation of the production of small amounts of benzaldehyde at early stages of our NMR experiments.[26] This aldehyde could arise from Lewis acid (i.e., Pd(II)) promoted hydrolysis of bbeda by water in the reaction solvent, a process that would release a primary amine (**9**, Figure 6a), which could then undergo β-hydride elimination

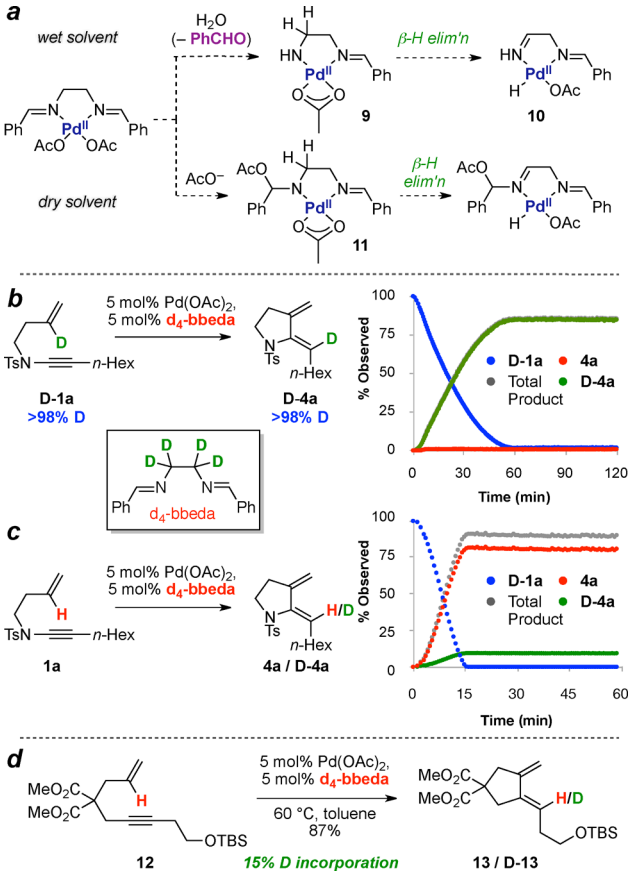

Figure 6. Bbeda as a source of hydride. (a) Proposed mechanism for the formation of Pd(II)−H from bbeda. (b) Use of d_4-bbeda leads to complete deuteration of **D-4a** from **D-1a**. (c) Use of d_4-bbeda leads to partial deuteration of **4a** from **1a**.[21] (d) Use of d_4-bbeda with enyne **12** also leads to partial deuteration of **13**.

to generate palladium(II) hydride. Tautomerization of the resulting imine **10** to the corresponding enamine could then release further hydrogen atoms. For water-free reactions (where only traces of benzaldehyde were observed), nucleophilic activation via addition of acetate to Pd(II)-complexed bbeda could lead to an aminal (**11**) that could also be susceptible to β-hydride elimination.

To test this, d_4-bbeda was prepared by reaction of d_4-ethylenediamine with benzaldehyde.[18] To our delight, cycloisomerization of **D-1a** in dry toluene using d_4-bbeda afforded **D-4a** with >98% deuteration (Figure 6b), thus supporting the proposal that *bbeda itself is the source of hydride* in the initiation pathway, and explaining the formation of protiated product in experiments using **D-4a** and h_4-bbeda. Furthermore, reaction of the protiated substrate **1a** in dry toluene with d_4-bbeda (5 mol %) led to a low level of product deuteration (15%),[27]

DOI: 10.1021/jacs.7b05436
J. Am. Chem. Soc. 2017, 139, 10104−10114

reinforcing this hypothesis (Figure 6c). Equally importantly, we also observed deuterium incorporation (15%) using enyne **12** (87% yield), thus supporting this process as a general mechanism for initiation of enyne cycloisomerization using $Pd(OAc)_2$/bbeda (Figure 6d).

Batch Dependency. During these investigations, we also uncovered a critical dependence of the stereochemical outcome of the reaction on the batch of $Pd(OAc)_2$ employed as catalyst. This discovery was made through the chance purchase of $Pd(OAc)_2$ from a different supplier, which led to an unexpected ratio of enamide alkene geometries ((*Z*):(*E*)-**4a** = 80:20), rather than the typical ratio of ~97:3. Screening of further samples of $Pd(OAc)_2$ gave variable results, the most extreme being a *reversal* of stereoselectivity to 40:60 in favor of the (*E*)-isomer. This batch-dependency was soon explained upon acquisition of ^{1}H NMR spectra of the various catalysts: while our original bottle of $Pd(OAc)_2$ exhibited a ^{1}H NMR spectrum (in $CDCl_3$) characteristic of pure $Pd(OAc)_2$ (Figure 7, batch 1,

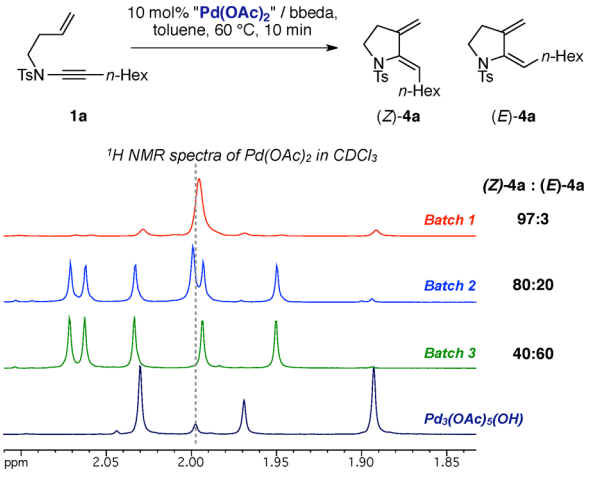

Figure 7. ^{1}H NMR spectra ($CDCl_3$) of batches of $Pd(OAc)_2$, and batch-dependent product ratios for cycloisomerization of **1a**.

a singlet corresponding to the D_{3h}-symmetric $[Pd_3(OAc)_6]$ trimer, minor peaks arise from $[Pd_3(OAc)_5OH]$),[25a] other samples showed increasing amounts of an impurity (batches 2 and 3), with the worst product ratio arising from samples *devoid* of $[Pd_3(OAc)_6]$. This latter batch in fact consisted solely of $[Pd_3(OAc)_5(NO_2)]$, an impurity common in $Pd(OAc)_2$ that arises from its method of production, as previously characterized by Cotton and Murillo.[25a,28] The ability of this "impurity" to mediate palladium-catalyzed reactions has been documented, albeit in many cases its presence does not affect the reaction outcome;[29] the observation of such a significant overturning of product selection is, to our knowledge, unprecedented. The synthesis of pure $Pd(OAc)_2$ from $Pd(NO_3)_2$ and NaOAc as reported by Stolyarov and co-workers[28] offers a convenient solution to this problem, and delivers palladium(II) acetate of purity equivalent to the original supply; ^{1}H NMR spectroscopic analysis of subsequent commercial batches of $Pd(OAc)_2$ gave reassurance that these would behave as expected. Interestingly, monitoring of the reaction of **1a** with $[Pd_3(OAc)_5(NO_2)]$/bbeda (Figure 8) revealed that reactions with this catalyst proceeded at a somewhat lower rate than pure $Pd(OAc)_2$/bbeda, and that the isomeric ratio of enamide products remained consistent throughout the reaction. Submission of pure (*Z*)-**4a** to this

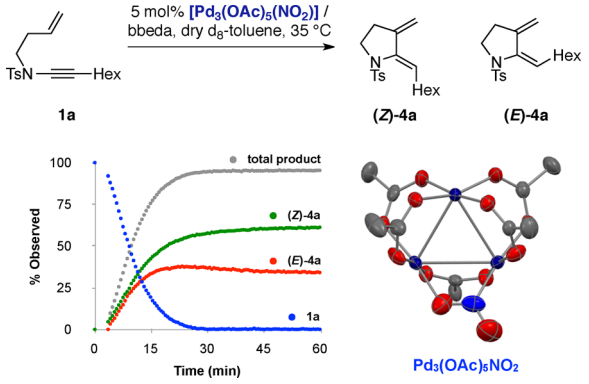

Figure 8. ^{1}H NMR spectroscopic reaction profile for conversion of **1a** to (*Z*)-**4a** and (*E*)-**4a** catalyzed by $[Pd_3(OAc)_5)(NO_2)]$/bbeda, in pre-dried d_8-toluene at 35 °C, and X-ray crystal structure of $Pd_3(OAc)_5NO_2$.[25a]

catalyst did not result in alkene isomerization, suggesting that the two isomers arise during the cycloisomerization as a consequence of a divergent reaction mechanism, rather than through product isomerization. While the mechanistic origin of this isomer mixture remains unknown, recent studies on alkyne semireduction using $Pd(PEt_3)_4$ and formic acid suggest that isomerization of alkenylpalladium complexes formed through hydropalladation can be facile.[30]

Computational Analysis of the Reaction Pathway. With significant experiemental evidence for the intermediacy of palladium(II) hydride species in hand, we set out to explore the reaction pathway from a theoretical perspective to establish whether a hydropalladation reaction mechanism would prove energetically feasible. In addition, we hoped to rationalize the stereoselectivity of the reaction, and to gain insight into the observed kinetic isotope effects.[31] Density functional theory (DFT) and local coupled cluster calculations were performed with *Gaussian09* rev D.01 and with Orca v4.[32] The meta-generalized gradient approximation (meta-GGA) TPSS exchange-correlation functional[33] was used for all geometry optimizations[34] with density fitting for Coulomb integrals (RI-J), a fine integration grid and the Karlsruhe def2-TZVP basis set for all elements.[35] A quasi-harmonic approximation[36] was used in which the treatment of vibrational entropies switches from a rigid-rotor harmonic oscillator to a free rotor at frequencies below 100 cm^{-1}, implemented in Python.[37] Dispersion effects were included by a Becke–Johnson damped D3-correction[38] and solvation effects by an SMD description of toluene.[39] Single point energy calculations were also performed with hybrid meta-GGA functionals (M06 and PW6B95-D3), and with the DLPNO-CCSD(T) local coupled cluster method for comparison.[40] The energy profile is qualitatively consistent across the different methods, and the RMSD between between TPSS-D3 and DLPNO-CCSD(T) energies over the entire catalytic cycle is only 2.9 kcal/mol. Computed diastereoselectivities are consistent within 1 kcal mol^{-1} across different levels (see the Supporting Information (SI) for full details). The putative catalytic cycle, involving hydropalladation, migratory insertion and β-hydride elimination steps, was obtained with a monomeric Pd-catalyst[41] with a single acetate ligand, using model system **1j** (Figure 9), which closely resembles substrate **1a** with the alkyne substituent (*n*-Hex in **1a**) represented by a methyl group.

Hydropalladation occurs from the Pd(0) acetic acid complex **A**. The expected palladium(II) hydride complex was found to

DOI: 10.1021/jacs.7b05436
J. Am. Chem. Soc. 2017, 139, 10104–10114

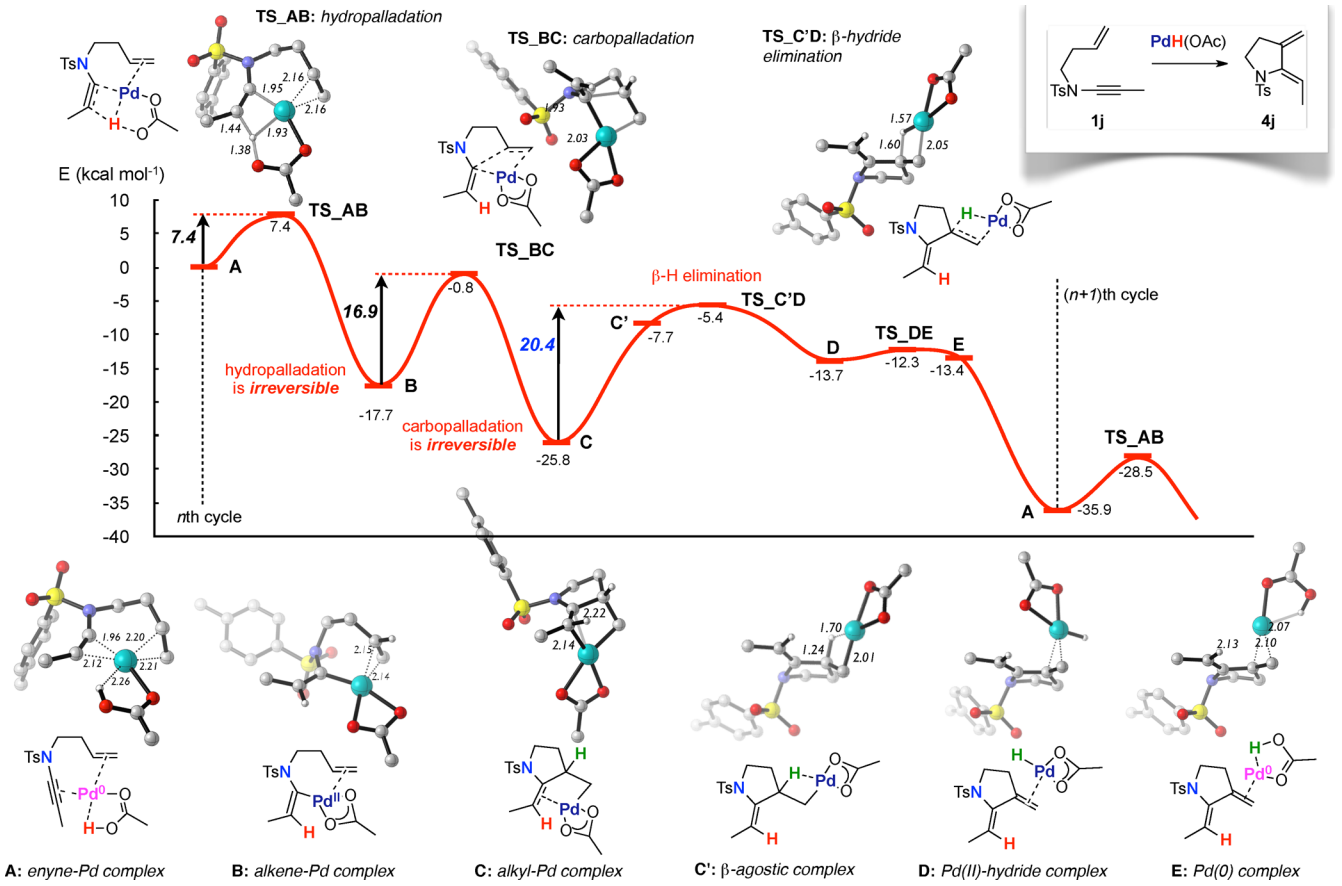

Figure 9. SMD-TPSS-D3/def2-TZVP//TPSS/def2-TZVP energy profile for the catalytic cycle of the cycloisomerization.

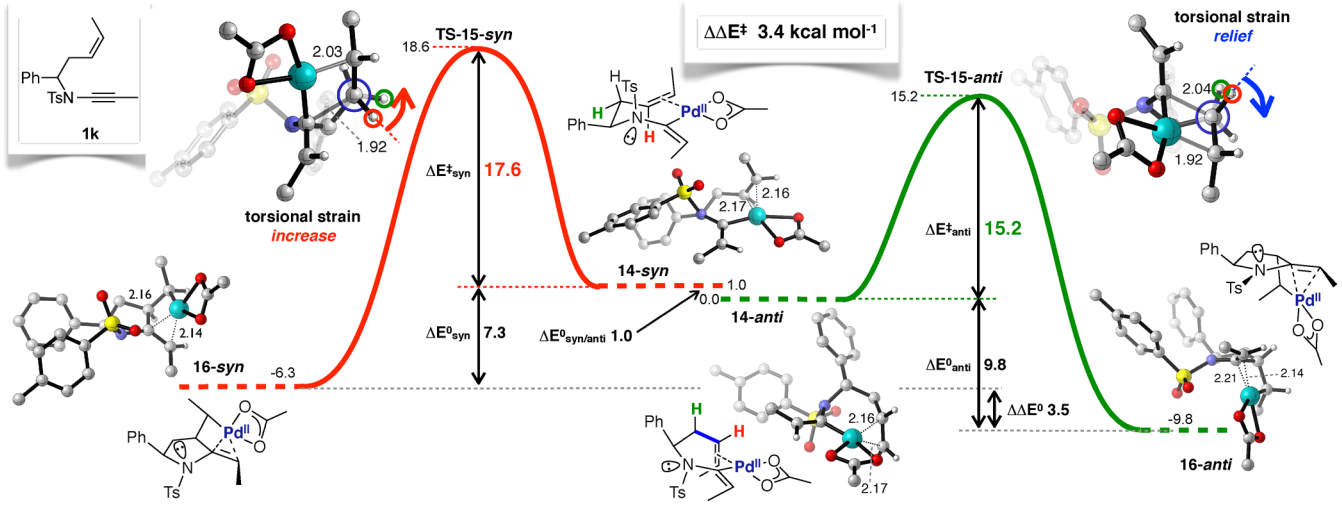

Figure 10. DFT calculations rationalize the stereochemical outcome of the *anti*-diastereoselective cycloisomerization of enynamide **1k**.

be significantly less stable at all levels of theory, by 21.4−33.1 kcal mol^{-1}.[42] As hydropalladation takes place to give **B**, transfer of the hydrogen atom to the β-carbon of the ynamide is facilitated by an agostic interaction with the metal (**TS_AB**, $\Delta G^{\ddagger}$ = 7.4 kcal mol^{-1}), suggesting that a discrete palladium(II) hydride is not formed, or is not located as an energy minimum on the potential energy surface; in effect, oxidative addition to Pd(0) by acetic acid, and hydropalladation, take place as a single concerted process from the favored substrate-bound Pd(0)(HOAc) complex. As well as representing a new pathway for alkyne hydrometalation, complex **A** also accounts for the facile exchange of H/D with water in the reaction solvent (and with hydrolyzed bbeda) which can thus be mediated by acetic acid rather than requiring a specific isotope exchange process at the metal. It also accounts for the difficulty in detecting elusive palladium(II) hydride species by ^{1}H NMR spectroscopy, and is consistent with the notion that oxidative addition of Pd(0) into acetic acid is rapid and reversible.[20b] Subsequent to this irreversible hydrometalation to give **B**, the metal then effects carbopalladation of the alkene (**TS_BC**, $\Delta G^{\ddagger}$ = 16.9 kcal

DOI: 10.1021/jacs.7b05436
J. Am. Chem. Soc. 2017, 139, 10104−10114

mol^{-1}), leading to an alkylpalladium species **C** that remains complexed to the enamide alkene. Carbopalladation is also irreversible at all levels of theory considered, and is followed by rate-limiting β-hydride elimination (**TS_C′D**, $\Delta G^{\ddagger}$ = 20.4 kcal mol^{-1}), a process that first requires endothermic enamide decomplexation and C−C bond rotation in order to position the C−Pd bond *syn*-coplanar with the C−H bond (**C** → **C′**). The degree of reversibility of β-hydride elimination is challenging to assess, as it depends on the kinetics of product dissociation from the resultant (alkene)Pd(H)(OAc) complex (**D** or **E**), and complexation with the next molecule of substrate. This is in part likely to be product dependent, as only in certain cases is alkene isomerization observed in the product. Formation of product-bound Pd(0)(HOAc) complex **E** from **D** is facile, with a barrier of 2.1 kcal/mol. This is true across all levels of theory, where the barrier for this step ranges from 1.7−4.2 kcal/mol. In **TS_DE** the κ^2-acetate rotates out of the plane to adopt a κ^1-coordination mode bound *cis* to the hydride (see the SI for full details).

The calculated energy profile of **1j** is consistent with room temperature reactivity:[43] the energetic span of the computed catalytic cycle (20.4 kcal mol^{-1}) is commensurate with a $t_{1/2}$ of 3 min. To compute the KIEs we applied the Bigeleisen−Mayer equation with a parabolic tunneling correction based on scaled TPSS/def2-TZVP harmonic frequencies at 35 °C.[44] Our calculations predict a primary KIE for β-hydride elimination of 2.225,[45] an inverse secondary KIE of 0.916 for carbopalladation, and a primary KIE for alkyne hydropalladation of 4.689 (12.671 with a parabolic tunneling correction). The latter value may reflect the trifurcated nature of bonding to the hydrogen atom in the hydropalladation transition state **TS_AB**.[46]

The stereoselectivity of the cyclization of enynamide **1e** (see Table 1, entry 1) was next modeled using substrate **1k** (Figure 10). The carbopalladation substrate derived from **1k** exists in two energetically similar conformations: **14-*anti*** and **14-*syn***, the diastereomeric transition states from which (**TS-15-*anti*** and **TS-15-*syn***) lead to products ***anti*-16** (the observed outcome) and ***syn*-16** respectively. A free energy difference between these transition states of $\Delta\Delta G^{\ddagger}$ = 3.4 kcal mol^{-1} corresponds to a calculated diastereoselectivity of >180:1,[47] which is consistent with the observed reaction outcome. The energy difference between these transition states (consistent with M06 and DLPNO-CCSD(T), as discussed in the SI) can be rationalized by changes in torsional strain upon carbopalladation of the alkene by the alkenylpalladium complex: in the case of transition state **TS-15-*anti***, this strain is relieved as carbopalladation proceeds (from the eclipsed C−H bonds to red and green hydrogens in **14-*anti***). For the alternative transition state **TS-15-*syn***, eclipsing interactions increase during this step (from the staggered C−H bonds to red and green hydrogens in **14-*syn***).[48]

Experimental Observations on Isotope Effects.[49] The data collected in the time course experiments indicate the influence of several isotope effects, resulting in marked differences in reaction rate and isotope incorporation as the reaction proceeds. We now turned to correlation of our computational work with these experimental observations, in particular the KIE for the rate-determining β-hydride elimination. This was achieved by comparison of the product distribution from disubstituted alkene (*E*)-**1b** with that of its deuterated equivalent (*E*)-**D-1b** (Scheme 5, >98% D, *E*:*Z* > 20:1), where β-deuteride elimination is required for the latter to generate 1,3-diene products. The ratio of 1,3:1,4-dienes (**4b**: **D-5b**/**D-6b**, as determined by integration of appropriate peaks in the ^{1}H NMR spectrum)[50] was found to be 8.09, compared to a ratio of 3.54 for (*E*)-**1b**, which gives an experimental KIE for β-hydride elimination of 2.29. This value is consistent with other reports on β-hydride elimination from alkylpalladium complexes, and with the computed value (2.07 at 60 °C; 2.23 at 35 °C for model substrate **1j**).[45,49,51]

Scheme 5. Primary KIE for β-Hydride Elimination

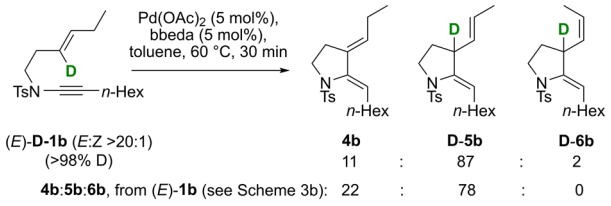

While the isotope effect associated with β-hydride elimination is consistent with computation and with literature values, the overall difference in reaction rate between substrates **1a** and **D-1a** at typical catalyst loadings of 5 mol% is not explained by β-hydride elimination alone. Although negligible KIEs would be expected from the hydropalladation and carbopalladation steps, it seemed possible that off-cycle equilibrium processes might be affected by the difference in activation energies between hydro- and deuteriopalladation. The path from product decomplexation to substrate association (and subsequent irreversible hydropalladation) could involve complexation of palladium by bbeda, or its hydrolysis product, or catalyst re-aggregation (to dimeric or trimeric complexes). These processes would be expected to depend on catalyst concentration,[52] with hydropalladation perturbing the equilibria by effectively sequestering monomeric "active" Pd(0)(AcOH).

This indeed turned out to be the case. The relative rates of reaction of substrates **1a** and **D-1a** were compared at various catalyst concentrations (by observation of the post-induction regions of reactions such as HA and DA, see Figure 2, once the production of protiated product has plateaued in reactions involving **D-1a**). The rates of cyclization of each substrate were measured at five different catalyst loadings (0.5, 1, 2.5, 5, and 10 mol%, Figure 11a), with each experiment run in triplicate. The rate constants for both substrates, and their associated errors (one standard deviation) are shown in the table in Figure 11. Plateau effects were observed for both substrates at higher catalyst concentrations:[52] for **1a**, this occurs at or above 5 mol %, while for **D-1a**, at or above 2.5 mol%. We speculate this may be related to the difference in energy barriers for hydro- vs deuteriopalladation, which in the latter case could increase the extent of off-cycle catalyst sequestration, compared to substrate complexation and entry to the catalytic cycle. The dominance of hydropalladation at early reaction stages using **D-1a** adds support to the influence of this step on entry to the catalytic cycle. In addition, this data allowed us to determine the order of reaction with respect to the metal catalyst. A plot of ln(k_{obs}) against ln([Pd(OAc)$_2$]) showed a linear relationship (Figure 11b), supporting the proposal of a monomeric palladium species as the active catalyst.[53]

Alongside this, we were intrigued to observe that the rate of cycloisomerization of (*Z*)-**D-1b** exceeded that of (*Z*)-**1b**

DOI: 10.1021/jacs.7b05436
J. Am. Chem. Soc. 2017, 139, 10104−10114

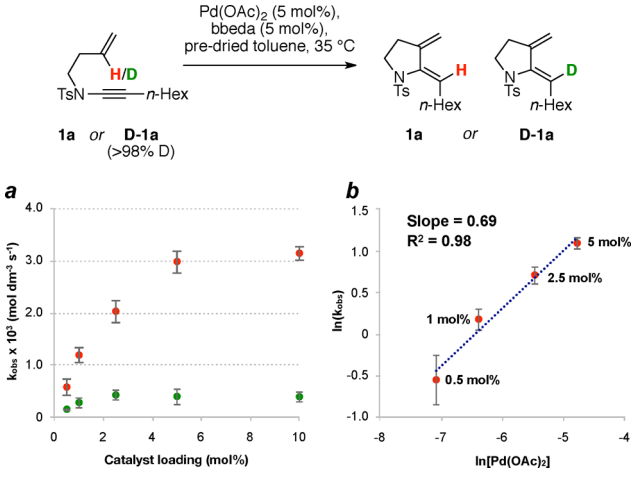

Figure 11. Dependence of reaction rate on catalyst concentration. k_H and k_D are given in units of 10^3 mol dm^{-3} s^{-1}. Errors of one standard deviation are shown. (a) k_H(obs) and k_D(obs) at different catalyst concentrations; table shows values and ratios of observed rate constants. (b) Plot of ln(k_H(obs)) against ln[Pd(OAc)$_2$] shows first-order dependence with respect to the catalyst. See the SI for further details.

(Figure 12); comparison of the steady-state regions of these reactions (6−11 min) gave a gradient ratio of 0.87 (±0.01).

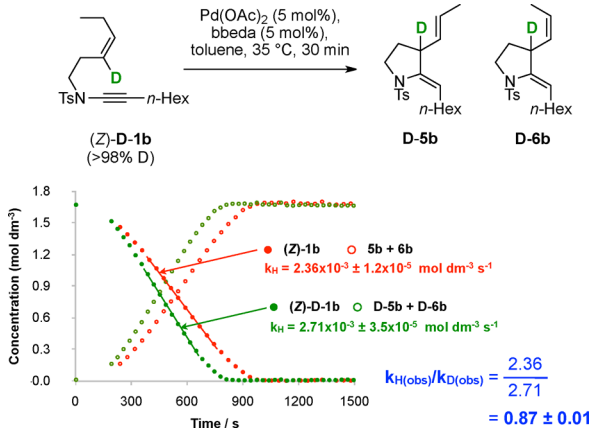

Figure 12. Isotope effect from alkene deuteration.[21]

The reason for this secondary KIE is not clear: with the theoretical pathway indicating carbopalladation to be non-rate-determining, we suggest that this effect could relate to differences between the two isotopes in agostic interactions, or hyperconjugation effects during the enamide decomplexation/β-hydride elimination steps, or during product decomplexation.

DISCUSSION

The above experimental and theoretical studies provide strong support for a hydropalladation mechanism for Pd(OAc)$_2$/bbeda-catalyzed enynamide cycloisomerization. A full outline of the proposed reaction pathway is illustrated in Scheme 6. Reaction initiation entails a number of processes, commencing with a water-promoted Pd$_3$(OAc)$_6$ equilibrium with [Pd$_3$(OAc)$_5$(OH)], the latter of which undergoes bbeda-assisted deaggregation, presumably to give a monomeric [(bbeda)Pd(OAc)$_2$] complex. Partial hydrolysis of this complex

Scheme 6. Pd-Catalyzed Cycloisomerization: Overview

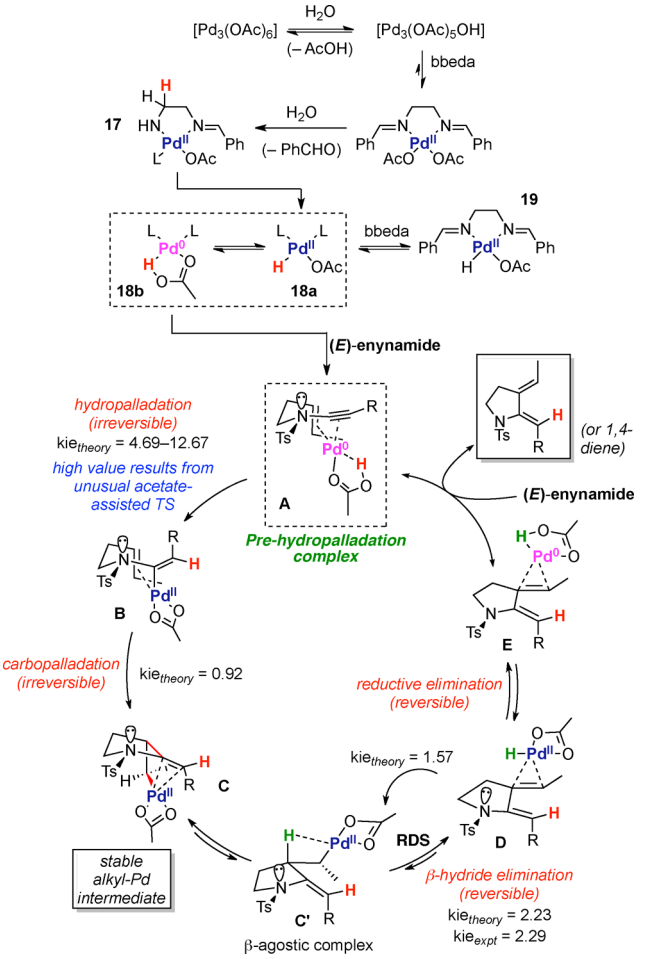

liberates benzaldehyde and amine complex **17**, which undergoes β-hydride elimination to form Pd(II)−H complex **18a** (this process could also be promoted by addition of acetate, see Scheme 6a). Throughout the reaction, additional bbeda (or the derived amine ligand) could stabilize off cycle Pd(II) species (**19**), thereby prolonging catalyst lifetime. The resultant L$_2$Pd(II)H(OAc) complex **18a** is in equilibrium with L$_2$Pd(0)-(κ^2-HOAc) **18b**, with the latter form predicted computationally to be favored on binding the enynamide substrate (**A**), and required for hydropalladation.[54] Notably, acetic acid complex **18b** also explains the facile exchange of H/D with water. The substrate-complexed Pd(0) catalyst (**A**) then effects an irreversible "oxidative hydropalladation" of the alkyne component (to give **B**), followed by irreversible carbopalladation with a pseudo-axially oriented alkene group. The resulting alkylpalladium(II) species (**C**) offers a possible resting state of the catalyst; further reaction requires an endergonic decomplexation of the enamide from the metal, C−C bond rotation, and agostic coordination of the bridgehead hydrogen atom (**C′**). β-Hydride elimination then proceeds rapidly and potentially reversibly, delivering a Pd(II)H(OAc)(alkene) complex (**D**) that is in equilibrium with Pd(0)(AcOH) (**E**). Finally, we note that although original proposals for different reaction pathways using Pd(II) or Pd(0) precatalysts were based on observed differences in reaction outcomes or product distributions, we suggest that these may relate more to the influence of the specific ligand environment around the metal center, rather than the cycloisomerization pathway itself.

DOI: 10.1021/jacs.7b05436
J. Am. Chem. Soc. 2017, 139, 10104−10114

CONCLUSION

Palladium-catalyzed enyne cycloisomerization is a fundamentally important reaction manifold in this field of ring synthesis. Despite the utility of the $Pd(OAc)_2$/bbeda catalyst system, mechanistic understanding has remained elusive. Through extensive NMR studies with deuterated substrates, we have uncovered the crucial influences of water, the precatalyst, and the ligand itself in this reaction. Our demonstration that bbeda itself serves as a source of Pd(II)−H, combined with theoretical analysis of the reaction pathway correlated with experimental isotope effects, offers a new level of understanding of this classic cyclization process, and offers enhanced understanding for the design of applications of this chemistry in stereoselective synthesis.

ASSOCIATED CONTENT

Supporting Information

The Supporting Information is available free of charge on the ACS Publications website at DOI: 10.1021/jacs.7b05436.

Experimental details of NMR time course experiments, characterization of novel compounds, ^1H and ^{13}C NMR spectra, and additional experimental details (PDF)

AUTHOR INFORMATION

Corresponding Authors

*robert.paton@chem.ox.ac.uk

*edward.anderson@chem.ox.ac.uk

ORCID

Alan Steven: 0000-0002-0134-0918

Robert S. Paton: 0000-0002-0104-4166

Edward A. Anderson: 0000-0002-4149-0494

Notes

The authors declare no competing financial interest.

ACKNOWLEDGMENTS

This paper is dedicated to Prof. Barry Trost on the occasion of his 75th birthday. E.A.A. thanks the EPSRC (EP/K005391/1, EP/H025839/1) for support. R.S.P. thanks the Chemical Structure Association Trust. We acknowledge the use of the EPSRC UK National Service for Computational Chemistry Software (CHEM773) in carrying out this work. A.M. thanks the Royal Thai Government and the DPST project for a studentship. A.C.-R. is grateful to the Spanish MINECO for an FPI fellowship. We also thank Dr. John M. Brown for valuable discussions on isotope effects.

REFERENCES

(1) (a) Michelet, V.; Toullec, P. Y.; Genet, J. P. *Angew. Chem., Int. Ed.* **2008**, *47*, 4268−4315. (b) Lee, S. I.; Chatani, N. *Chem. Commun.* **2009**, 371−384. (c) Marinetti, A.; Jullien, H.; Voituriez, A. *Chem. Soc. Rev.* **2012**, *41*, 4884−4908. (d) Watson, I. D. G.; Toste, F. D. *Chem. Sci.* **2012**, *3*, 2899−2919. (e) Dorel, R.; Echavarren, A. M. *Chem. Rev.* **2015**, *115*, 9028. (f) Furstner, A. *Chem. Soc. Rev.* **2009**, *38*, 3208−3221. (g) Trost, B. M.; Frederiksen, M. U.; Rudd, M. T. *Angew. Chem., Int. Ed.* **2005**, *44*, 6630−6666. (h) Zhang, L.; Sun, J.; Kozmin, S. A. *Adv. Synth. Catal.* **2006**, *348*, 2271−2296. (i) Jiménez-Núñez, E.; Echavarren, A. M. *Chem. Rev.* **2008**, *108*, 3326−3350. (j) Yamamoto, Y. *Chem. Rev.* **2012**, *112*, 4736−4769. (k) Aubert, C.; Buisine, O.; Malacria, M. *Chem. Rev.* **2002**, *102*, 813−834.

(2) (a) Lloyd-Jones, G. C. *Org. Biomol. Chem.* **2003**, *1*, 215−236. (b) Nieto-Oberhuber, C.; López, S.; Jiménez-Núñez, E.; Echavarren, A. M. *Chem. - Eur. J.* **2006**, *12*, 5916−5923.

(3) (a) Trost, B. M. *Acc. Chem. Res.* **1990**, *23*, 34−42. (b) Trost, B. M. *Chem. - Eur. J.* **1998**, *4*, 2405−2412.

(4) (a) Trost, B. M.; Lautens, M. *J. Am. Chem. Soc.* **1985**, *107*, 1781−1783. (b) Trost, B. M.; Chung, J. Y. L. *J. Am. Chem. Soc.* **1985**, *107*, 4586−4588. (c) Trost, B. M.; Lautens, M. *Tetrahedron Lett.* **1985**, *26*, 4887−4890. (d) Trost, B. M.; Lautens, M.; Chan, C.; Jebaratnam, D. J.; Mueller, T. *J. Am. Chem. Soc.* **1991**, *113*, 636−644. (e) Trost, B. M.; Chen, S. F. *J. Am. Chem. Soc.* **1986**, *108*, 6053−6054.

(5) (a) Trost, B. M.; Jebaratnam, D. J. *Tetrahedron Lett.* **1987**, *28*, 1611−1613. (b) Trost, B. M.; Hipskind, P. A.; Chung, J. Y. L.; Chan, C. *Angew. Chem., Int. Ed. Engl.* **1989**, *28*, 1502−1504. (c) Trost, B. M.; Tanoury, G. J.; Lautens, M.; Chan, C.; Macpherson, D. T. *J. Am. Chem. Soc.* **1994**, *116*, 4255−4267.

(6) (a) Trost, B. M.; Lee, D. C.; Rise, F. *Tetrahedron Lett.* **1989**, *30*, 651−654. (b) Trost, B. M.; Lee, D. C. *J. Org. Chem.* **1989**, *54*, 2271−2274. (c) Trost, B. M.; Shi, Y. *J. Am. Chem. Soc.* **1993**, *115*, 9421−9438. (d) Trost, B. M.; Shi, Y. *J. Am. Chem. Soc.* **1993**, *115*, 12491−12509. (e) Trost, B. M.; Romero, D. L.; Rise, F. *J. Am. Chem. Soc.* **1994**, *116*, 4268−4278. (f) Trost, B. M.; Gutierrez, A. C.; Ferreira, E. M. *J. Am. Chem. Soc.* **2010**, *132*, 9206−9218.

(7) (a) Peixoto, P. A.; Severin, R.; Tseng, C.-C.; Chen, D. Y. K. *Angew. Chem., Int. Ed.* **2011**, *50*, 3013−3016. (b) Trost, B. M.; Krische, M. J. *J. Am. Chem. Soc.* **1996**, *118*, 233−234. (c) Zilke, L.; Hall, D. G. *Eur. J. Org. Chem.* **2012**, *2012*, 4153−4163. (d) Pichlmair, S.; de Lera Ruiz, M.; Basu, K.; Paquette, L. A. *Tetrahedron* **2006**, *62*, 5178−5194. (e) Trost, B. M.; Corte, J. R.; Gudiksen, M. S. *Angew. Chem., Int. Ed.* **1999**, *38*, 3662−3664. (f) Trost, B. M.; Haffner, C. D.; Jebaratnam, D. J.; Krische, M. J.; Thomas, A. P. *J. Am. Chem. Soc.* **1999**, *121*, 6183−6192. (g) Trost, B. M.; Li, Y. *J. Am. Chem. Soc.* **1996**, *118*, 6625−6633. (h) Trost, B. M.; Dong, L.; Schroeder, G. M. *J. Am. Chem. Soc.* **2005**, *127*, 10259−10268. (i) Yamada, H.; Aoyagi, S.; Kibayashi, C. *J. Am. Chem. Soc.* **1996**, *118*, 1054−1059. (j) Yanagita, Y.; Suto, T.; Matsuo, N.; Kurosu, Y.; Sato, T.; Chida, N. *Org. Lett.* **2015**, *17*, 1946−1949.

(8) Walker, P. R.; Campbell, C. D.; Suleman, A.; Carr, G.; Anderson, E. A. *Angew. Chem., Int. Ed.* **2013**, *52*, 9139−9143.

(9) (a) For related Diels−Alder reactions of exocyclic 2-amidodienes, see: Campbell, C. D.; Greenaway, R. L.; Holton, O. T.; Walker, P. R.; Chapman, H. A.; Russell, C. A.; Carr, G.; Thomson, A. L.; Anderson, E. A. *Chem. - Eur. J.* **2015**, *21*, 12627−12639. (b) Straker, R. N.; Peng, Q.; Mekareeya, A.; Paton, R. S.; Anderson, E. A. *Nat. Commun.* **2016**, *7*, 10109.

(10) (a) See also: Trost, B. M.; Tanoury, G. J. *J. Am. Chem. Soc.* **1987**, *109*, 4753−4755. (b) Trost, B. M.; Tanoury, G. J. *J. Am. Chem. Soc.* **1988**, *110*, 1636−1638. (c) Trost, B. M.; Yanai, M.; Hoogsteen, K. *J. Am. Chem. Soc.* **1993**, *115*, 5294−5295.

(11) (a) Xu, L.-M.; Li, B.-J.; Yang, Z.; Shi, Z.-J. *Chem. Soc. Rev.* **2010**, *39*, 712−733. (b) Malacria, M.; Maestri, G. *J. Org. Chem.* **2013**, *78*, 1323−1328. (c) Catellani, M.; Motti, E.; Della Ca', N. *Acc. Chem. Res.* **2008**, *41*, 1512−1522. (d) Maestri, G.; Motti, E.; Della Ca', N.; Malacria, M.; Derat, E.; Catellani, M. *J. Am. Chem. Soc.* **2011**, *133*, 8574−8585. (e) Sehnal, P.; Taylor, R. J. K.; Fairlamb, I. J. S. *Chem. Rev.* **2010**, *110*, 824−889.

(12) Yamada, H.; Aoyagi, S.; Kibayashi, C. *Tetrahedron Lett.* **1996**, *37*, 8787−8790.

(13) See the SI for full details of reaction optimization.

(14) (a) Le Paih, J.; Rodriguez, D. C.; Derien, S.; Dixneuf, P. H. *Synlett* **2000**, 95−97. (b) Kaminsky, L.; Clark, D. A. *Org. Lett.* **2014**, *16*, 5450−5453.

(15) The cycloisomerization of (*Z*)-**1b,c** would likely afford the (*Z,Z*)-diene diastereomer of **4b,c**; related stereoselectivity is seen in the cycloisomerization of styrenyl enynamides; see ref 8.

(16) 6,4-Fused ring systems are formed using homologated enynamides, rather than 1,3-dienes, which is consistent with a ruthenacycle pathway. See ref 8 for further details.

(17) Chintalapudi, V.; Galvin, E. A.; Greenaway, R. L.; Anderson, E. A. *Chem. Commun.* **2016**, *52*, 693−696.

(18) See the SI for synthetic details. All deuterated compounds are fully deuterated as judged at the limits of accuracy of ^1H NMR spectroscopic analysis, and as such are reported as >98% D.

DOI: 10.1021/jacs.7b05436
J. Am. Chem. Soc. 2017, 139, 10104−10114

(19) Reactions catalyzed by $Pd_2dba_3{\cdot}CHCl_3$/AcOH/bbeda proved capricious, particularly when run as NMR experiments, and often failed to reach completion for enynamide substrates.
(20) (a) Grushin, V. V. *Chem. Rev.* **1996**, *96*, 2011−2034. (b) Amatore, C.; Jutand, A.; Meyer, G.; Carelli, I.; Chiarotto, I. *Eur. J. Inorg. Chem.* **2000**, *2000*, 1855−1859.
(21) Experiments were run at 0.167 M, 35 °C using 5 mol% Pd catalyst/ligand, with 1,2,4,5-tetrachloro-3-nitrobenzene as internal standard, in triplicate. See the SI for full details of NMR time course experiments.
(22) Williams, D. B. G.; Lawton, M. *J. Org. Chem.* **2010**, *75*, 8351−8354.
(23) In contrast to **1a**, the reactions of **D-1a** appear to show a retardation effect as the concentration of water increases. This may reflect an off-cycle complexation of water to the metal, which is discussed in further detail in the SI.
(24) Bedford, R. B.; Bowen, J. G.; Davidson, R. B.; Haddow, M. F.; Seymour-Julen, A. E.; Sparkes, H. A.; Webster, R. L. *Angew. Chem., Int. Ed.* **2015**, *54*, 6591−6594.
(25) (a) Bakhmutov, V. I.; Berry, J. F.; Cotton, F. A.; Ibragimov, S.; Murillo, C. A. *Dalton Trans.* **2005**, 1989−1992. (b) Nosova, V. M.; Ustynyuk, Y. A.; Bruk, L. G.; Temkin, O. N.; Kisin, A. V.; Storozhenko, P. A. *Inorg. Chem.* **2011**, *50*, 9300−9310.
(26) This was confirmed by ^{1}H NMR spectroscopy through addition of benzaldehyde to reaction samples in d_8-toluene.
(27) We suggest that 15% product deuteration arises from the release of additional deuterium through imine/enamine tautomerization of **10**.
(28) Stolyarov, I. P.; Demina, L. I.; Cherkashina, N. V. *Russ. J. Inorg. Chem.* **2011**, *56*, 1532−1537.
(29) (a) Fairlamb, I. J. S. *Angew. Chem., Int. Ed.* **2015**, *54*, 10415−10427. (b) For a subsequent analysis of this problem, see: Bajwa, S. E.; Storr, T. E.; Hatcher, L. E.; Williams, T. J.; Baumann, C. G.; Whitwood, A. C.; Allan, D. R.; Teat, S. J.; Raithby, P. R.; Fairlamb, I. J. S. *Chem. Sci.* **2012**, *3*, 1656−1661. (c) Carole, W. A.; Bradley, J.; Sarwar, M.; Colacot, T. J. *Org. Lett.* **2015**, *17*, 5472−5475.
(30) Shen, R.; Chen, T.; Zhao, Y.; Qiu, R.; Zhou, Y.; Yin, S.; Wang, X.; Goto, M.; Han, L.-B. *J. Am. Chem. Soc.* **2011**, *133*, 17037−17044.
(31) (a) For calculations on intermolecular ene−yne coupling, see: Henriksen, S. T.; Tanner, D.; Skrydstrup, T.; Norrby, P.-O. *Chem. - Eur. J.* **2010**, *16*, 9494−9501. (b) For calculations on Pd-catalyzed 1,6-enyne cycloisomerization, see: Nelson, B.; Herres-Pawlis, S.; Hiller, W.; Preut, H.; Strohmann, C.; Hiersemann, M. *J. Org. Chem.* **2012**, *77*, 4980−4995. (c) See also: Goj, L. A.; Widenhoefer, R. A. *J. Am. Chem. Soc.* **2001**, *123*, 11133−11147.
(32) (a) Frisch, M. J.; et al. *Gaussian 09*, Revision D.01; Gaussian, Inc.: Wallingford, CT, 2009. (b) Neese, F. *WIREs Comput. Mol. Sci.* **2012**, *2*, 73−78.
(33) Tao, J.; Perdew, J. P.; Staroverov, V. N.; Scuseria, G. E. *Phys. Rev. Lett.* **2003**, *91*, 146401.
(34) (a) TPSS is superior to GGA functionals in structure optimizations of transition metal complexes. See: Rydberg, P.; Olsen, L. *J. Phys. Chem. A* **2009**, *113*, 11949−11953. (b) Minenkov, Y.; Singstad, A.; Occhipinti, G.; Jensen, V. R. *Dalton Trans.* **2012**, *41*, 5526−5541. (c) Steinmetz, M.; Ueda, K.; Grimme, S.; Yamaguchi, J.; Kirchberg, S.; Itami, K.; Studer, A. *Chem. - Asian J.* **2012**, *7*, 1256−1260. (d) Semakul, N.; Jackson, K. E.; Paton, R. S.; Rovis, T. *Chem. Sci.* **2017**, *8*, 1015−1020.
(35) (a) Schäfer, A.; Horn, H.; Ahlrichs, R. *J. Chem. Phys.* **1992**, *97*, 2571−2577. (b) Schäfer, A.; Huber, C.; Ahlrichs, R. *J. Chem. Phys.* **1994**, *100*, 5829−5835.
(36) Grimme, S. *Chem. - Eur. J.* **2012**, *18*, 9955−9964.
(37) Funes-Ardois, I.; Paton, R. S. *GoodVibes* v1.0.1, 2016; http://doi.org/10.5281/zenodo.60811.
(38) (a) Grimme, S.; Antony, J.; Ehrlich, S.; Krieg, H. *J. Chem. Phys.* **2010**, *132*, 154104. (b) Grimme, S.; Ehrlich, S.; Goerigk, L. *J. Comput. Chem.* **2011**, *32*, 1456−1465. (c) Johnson, E. R.; Becke, A. D. *J. Chem. Phys.* **2006**, *124*, 174104.
(39) Marenich, A. V.; Cramer, C. J.; Truhlar, D. G. *J. Phys. Chem. B* **2009**, *113*, 6378−6396.
(40) (a) Zhao, Y.; Truhlar, D. G. *Theor. Chem. Acc.* **2008**, *120*, 215−241. (b) Zhao, Y.; Truhlar, D. G. *J. Phys. Chem. A* **2005**, *109*, 5656−5667. (c) Riplinger, C.; Sandhoefer, B.; Hansen, A.; Neese, F. *J. Chem. Phys.* **2013**, *139*, 134101.
(41) (a) Paton, R. S.; Brown, J. M. *Angew. Chem., Int. Ed.* **2012**, *51*, 10448−10450. (b) Sanhueza, I. A.; Wagner, A. M.; Sanford, M. S.; Schoenebeck, F. *Chem. Sci.* **2013**, *4*, 2767. Further evidence for a monomeric palladium species was gained through determination of the order of reaction with respect to the catalyst, as shown in Figure 11.
(42) The reactivity of a cationic bbeda-Pd(II)H catalyst was also computed; see the SI for details.
(43) The energy and Gibbs energy profiles are very similar since the change in entropy along the intramolecular reaction coordinate is small: Peng, Q.; Paton, R. S. *Acc. Chem. Res.* **2016**, *49*, 1042−1051.
(44) (a) Rzepa, H. S. *KINISOT*, 2015; http://doi.org/10.5281/zenodo.19272. (b) Paton, R. S. *Kinisot.py*, 2016; http://doi.org/10.5281/zenodo.60082.
(45) For a calculation of the KIE (2.66) for β-hydride elimination in palladium-catalyzed chain-walking, see: Hilton, M. J.; Xu, L.-P.; Norrby, P.-O.; Wu, Y.-D.; Wiest, O.; Sigman, M. S. *J. Org. Chem.* **2014**, *79*, 11841−11850.
(46) (a) Measurement of a KIE for hydropalladation of an alkyne, directed by a pyridylphosphine ligand, has been reported. This high value was ascribed to an alternative mechanism involving intramolecular protonation of an alkyne-Pd(II) complex. See: Scrivanti, A.; Beghetto, V.; Campagna, E.; Zanato, M.; Matteoli, U. *Organometallics* **1998**, *17*, 630−635. (b) For KIE measurement in allene hydropalladation, see: Zhu, C.; Yang, B.; Qiu, Y.; Bäckvall, J.-E. *Chem. - Eur. J.* **2016**, *22*, 2939−2943.
(47) Irreversible C−C bond formation ensures carbopalladation is diastereodetermining and product selectivity may be computed applying TST assuming Curtin−Hammett-type behavior. See: Peng, Q.; Duarte, F.; Paton, R. S. *Chem. Soc. Rev.* **2016**, *45*, 6093−6107.
(48) See the SI for rationalization of the stereoselective cycloisomerizations of **1h** and of an (*E*)-enynamide.
(49) Gómez-Gallego, M.; Sierra, M. A. *Chem. Rev.* **2011**, *111*, 4857−4963.
(50) Up to 11% deuterium incorporation at the enamide proton is expected across these products, arising from 11% formation of **4b**. For clarity, products **D-5b** and **D-6b** are represented as singly deuterated compounds.
(51) (a) Netherton, M. R.; Fu, G. C. *Angew. Chem., Int. Ed.* **2002**, *41*, 3910−3912. (b) O'Ferrall, R. A. M. *J. Chem. Soc. B* **1970**, 785−790. (c) For a cautionary note, see: Lloyd-Jones, G. C.; Slatford, P. A. *J. Am. Chem. Soc.* **2004**, *126*, 2690−2691. (d) Bissember, A. C.; Levina, A.; Fu, G. C. *J. Am. Chem. Soc.* **2012**, *134*, 14232−14237. (e) Ogawa, R.; Shigemori, Y.; Uehara, K.; Sano, J.; Nakajima, T.; Shimizu, I. *Chem. Lett.* **2007**, *36*, 1338−1339.
(52) The reduction in turnover frequency with increasing catalyst loading provides support for off-pathway oligomerization. See: Rosner, T.; Le Bars, J.; Pfaltz, A.; Blackmond, D. G. *J. Am. Chem. Soc.* **2001**, *123*, 1848−1855.
(53) Louie, J.; Paul, F.; Hartwig, J. F. *Organometallics* **1996**, *15*, 2794−2805.
(54) We believe that bidentate coordination of the substrate to the metal is required, as only 1,6- and 1,7-enynamides undergo successful cycloisomerization. This alkene-coordination effect was also noted by Trost; see ref 5c.

DOI: 10.1021/jacs.7b05436
J. Am. Chem. Soc. 2017, 139, 10104−10114

Synthetic Methods

International Edition: DOI: 10.1002/anie.201706915
German Edition: DOI: 10.1002/ange.201706915

Copper-Catalyzed Synthesis and Applications of Yndiamides

*Steven J. Mansfield, Kirsten E. Christensen, Amber L. Thompson, Kai Ma, Michael W. Jones, Aroonroj Mekareeya, and Edward A. Anderson**

Abstract: *The first synthetic route to yndiamides, a novel class of double aza-substituted alkyne, has been established by the copper(I)-catalyzed cross-coupling of 1,1-dibromoenamides with nitrogen nucleophiles. The utility of these compounds is demonstrated in a range of transition-metal-catalyzed and acid-catalyzed transformations to afford a wide variety of 1,2-diamide functionalized products.*

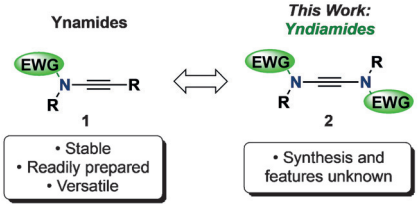

Figure 1. Comparison between ynamides and yndiamides. EWG = electron-withdrawing group.

Ynamides (**1**, Figure 1) are extremely versatile building blocks in organic synthesis.[1] Their rich chemistry can in part be attributed to the conjugation and polarization effects afforded by the amide group, which leads to heightened reactivity and regioselectivity in their reactions. In contrast, the synthesis and chemistry of yndiamides (**2**), acetylenes that feature two amido substituents, is unknown.[2] This class of alkyne would be of considerable interest as a synthetic building block—as well as introducing an additional nitrogen substituent, yndiamides could exhibit distinct reactivity compared to ynamides. Herein, we report the first method for the preparation of yndiamides, and an exploration of their unique reactivity, which reveals them to be valuable components in azacycle synthesis.

Exploration of potential yndiamide precursors revealed the copper-catalyzed coupling of 1,1-dibromoenamide **3a**[3] with sulfonamide **4a** to be most promising (Table 1).[4] Although the conditions developed for dibromoalkene–amide coupling (CuI, dmeda, Cs_2CO_3)[5] led mainly to decomposition of **3a** (entry 1), conditions more usually applied to bromoalkynes ($CuSO_4$·5 H_2O, 1,10-phenanthroline, K_3PO_4)[6] delivered appreciable amounts of yndiamide **2a**, along with the byproduct bromoketene aminal **5a** (entries 2 and 3). In the absence of the copper salt, **5a** was formed almost exclusively (entry 4), suggesting its origin to be independent of yndiamide formation. The use of CuI led to similar results (entry 5),[7] however, the formation of **5a** could be reduced by using a lower loading of Cs_2CO_3 (entry 6), with THF being superior to solvents such as toluene, acetonitrile, or DMF. The choice of 1,10-phenanthroline as a ligand was crucial, with other imine-based ligands proving ineffective (entries 7 and 8). Lowering the reaction temperature to 60 °C dramatically improved the proportion of yndiamide formed, with **2a** isolated in 83 % yield (entry 9).

Table 1: Selected optimization of yndiamide formation.

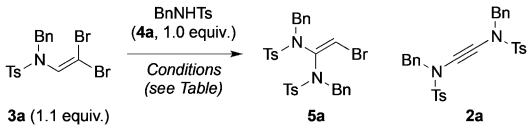

Entry	[Cu]/L (equiv)	Base (equiv)	*T* [°C]	Solvent	**3a**:**4a**:**5a**:**2a**[a]
1	CuI (0.12)/dmeda (0.18)	Cs_2CO_3 (4.0)	60	dioxane	0:90:10:0
			60	DMF	0:78:15:7
2	$CuSO_4$·5 H_2O (0.2)/1,10-phen (0.4)	K_3PO_4 (2.5)	110	PhMe	11:10:20:59
			85		10:10:10:70
3	$CuSO_4$·5 H_2O (0.2)/1,10-phen (0.4)	K_3PO_4 (4.0)	85[b]	THF	13:11:10:66
4	–	Cs_2CO_3 (4.0)	85	THF	0:0:94(**92**):6
5	CuI (0.2)/1,10-phen (0.4)	Cs_2CO_3 (4.0)	85	THF	3:0:33:64
6	CuI (0.2)/1,10-phen (0.4)	Cs_2CO_3 (2.5)	85	THF	2:2:21:75
7	CuI (0.2)/bipy (0.4)	Cs_2CO_3 (2.5)	85	THF	9:11:73:7
8	CuI (0.2)/terpy (0.4)	Cs_2CO_3 (2.5)	85	THF	6:8:80:6
9	CuI (0.2)/1,10-phen (0.4)	Cs_2CO_3 (2.5)	60	THF	9:0:2:89(**83**)

[a] Ratios were determined by ^{1}H NMR spectroscopic analysis of the crude reaction mixture after 18 h. Isolated yields in parentheses. [b] Sealed tube. Ts = 4-Me$C_6H_4SO_2$; dmeda = *N*,*N*′-dimethylethylenediamine; DMF = *N*,*N*′-dimethylformamide; 1,10-phen = 1,10-phenanthroline; THF = tetrahydrofuran; bipy = 2,2′-bipyridine; terpy = 2,2′:6′,2″-terpyridine.

A variety of amide nucleophiles **4** were screened using the optimized conditions described above. Sulfonamides and phosphoramidates[8] underwent smooth coupling with **3a**, giving yndiamides **2b**–**s** in high yields (Figure 2a).[9] A wide

[*] S. J. Mansfield, Dr. K. E. Christensen, Dr. A. L. Thompson, K. Ma, Dr. M. W. Jones, A. Mekareeya, Prof. E. A. Anderson
Chemistry Research Laboratory
12 Mansfield Road, Oxford,
OX1 3TA (UK)
E-mail: edward.anderson@chem.ox.ac.uk
Supporting information and the ORCID identification number(s) for the author(s) of this article can be found under: https://doi.org/10.1002/anie.201706915.

 © 2017 Wiley-VCH Verlag GmbH & Co. KGaA, Weinheim

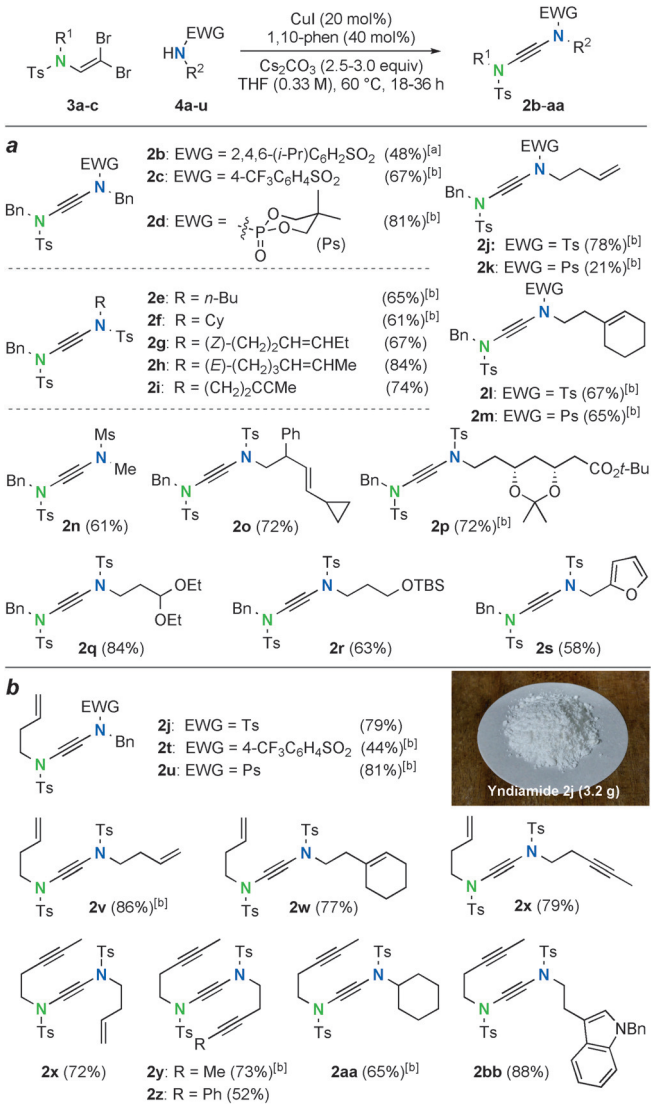

Figure 2. Yndiamide synthesis. a) Amide scope (**4**). b) Dibromoenamide scope (**3**). Isolated yields are given. [a] Bromoketene aminal **5b** (see the Supporting Information) was also produced in this reaction (28% yield); [b] X-ray crystallographic data has been obtained for this compound.[9,10] Bn = benzyl; Cy = cyclohexyl; Ms = $MeSO_2$; Ps = $Me_2C(CH_2O)_2PO$; TBS = $tBuMe_2Si$.

range of functionality was tolerated on the amide, including alkenes and alkynes (**2g–m**, **2o**), esters (**2p**), acetals (**2p**, **2q**), silyl ethers (**2r**), and heterocycles (**2s**). Evaluation of dibromoenamide scope (Figure 2b) showed that sulfonamide-based enamides were required for effective coupling, with amides or carbamates proving to be unreactive.[9] The sidechain of the sulfonamide was readily varied, leading to a selection of difunctionalized yndiamides (**2j**, **2t–bb**). The flexibility of this approach to unsymmetrical yndiamides is emphasized by compounds **2j** and **2x**, which could be produced from either of their respective sulfonamide/enamide partners in comparable yields (**2j**: 78/79%; **2x**: 72/79%). Efficiency was maintained on larger scales, with >3 g of yndiamide **2j** prepared by using 10 mmol (5 g) of **3a** (61%). The yndiamides were found to be bench-stable compounds

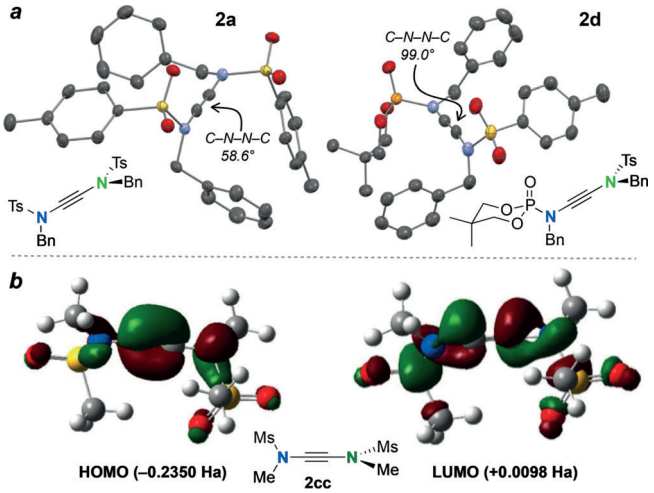

Figure 3. a) Solid-state structures[10] of **2a** and **2d**. Displacement ellipsoid plots are drawn at 50% probability. Hydrogen atoms are omitted for clarity. b) HOMO and LUMO shapes for yndiamide **2cc** (B3LYP/6-31G(d,p)).[9]

(see inset in Figure 2b) that can be routinely purified by silica-gel chromatography.

Single-crystal X-ray analysis[10] revealed that yndiamides possess highly twisted conformations,[11] with C-N-N-C dihedral angles generally between 60–100° (Figure 3).[9] The amide substituents adopt near trigonal planar arrangements, and alkyne bond lengths were found to range from 1.17–1.19 Å ("typical" alkyne ≈ 1.20 Å). This behavior was also manifested in solution, with ^{1}H NMR spectra of **2o** and **2p** showing the diastereotopic nature of the benzylic protons, despite being rather remote from the stereocenter(s), thus implying restricted rotation of the axially chiral yndiamide. This conformational effect was found to derive from stereoelectronic factors: DFT calculations (B3LYP/6-31G(d,p))[9] showed partial conjugation of the lone pairs of both nitrogen atoms with each of the alkyne π-systems (to different extents, according to the dihedral angles between the N lone pair and the C p-orbitals). This results in two near-degenerate alkyne-centered HOMOs for the yndiamide, compared to HOMOs of rather different energy for an ynamide. Interestingly, the LUMO of the yndiamide also extends across the whole N-C-C-N structure, encompassing both N-S σ* orbitals, and is thus lower in energy compared to that of an ynamide.

Yndiamides proved to be excellent substrates for a variety of transformations. Palladium-catalyzed cycloisomerizations using $Pd(OAc)_2$/*N*,*N*'-bis(benzylidene)ethylene diamine (bbeda; Table 2, entries 1–6)[12] proceeded at reduced rates compared to those of the equivalent ynamides,[12a,b] but afforded 1,3-diene **6a** and various 1,4-dienes, including spirocycle **6d**, in good yields (72–79%, entries 1–4).[13] High levels of substrate stereocontrol were observed in the reaction of vinylcyclopropane **2o**, which gave triene **6e** as a single diastereomer at the newly formed stereocenter (66%, entry 5). In contrast to ynamides, bbeda was an essential component in these cyclizations; in its absence, the reaction of **2j** resulted in the surprising formation of imine **6f** (63%, entry 6) following initial rapid formation of diene **6a**. It is

 © 2017 Wiley-VCH Verlag GmbH & Co. KGaA, Weinheim

Table 2: Transition-metal-catalyzed and acid-catalyzed reactions of enyndiamides.

Entry	Substrate	Conditions (t)[a]	Product		Yield [%][b]
1	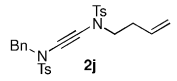 **2j**	**A** (40 min)	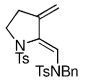	**6a**	73
2	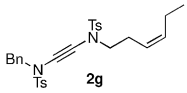 **2g**	**A** (25 min)	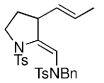	(*E*)-**6b**	79[c]
3	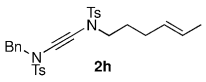 **2h**	**A** (90 min)	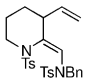	**6c**	72[d]
4	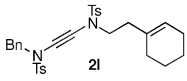 **2l**	**A** (30 min)	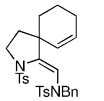	**6d**	73[e]
5	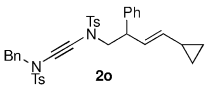 **2o**	**A** (60 min)	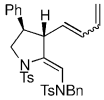	**6e**	66[f]
6	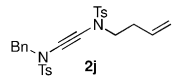 **2j**	**B** (35 min)	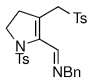	**6f**	63[g]
7	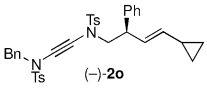 (−)-**2o**	**C** (16 h)	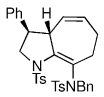	**7**	58
8	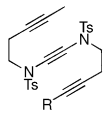 **2y**: R = Me **2z**: R = Ph	**D** (2 h)	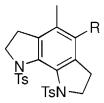	**8a**: R = Me **8b**: R = Ph	96
9		**D** (8 h)			91
10	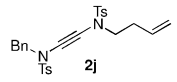 **2j**	**E** (5 h)	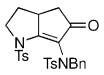	**9**	88
11		**F** (8 h)	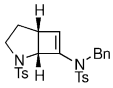	**10**	51
12	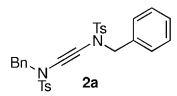 **2a**	**G** (10 min)	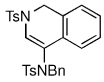	**11**	78
13		**H** (10 min)	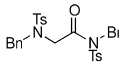	**12**	86
14	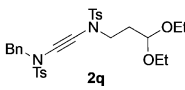 **2q**	**I** (24 h)	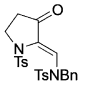	**13**	63

[a] Conditions **A**: $Pd(OAc)_2$/*N*,*N*′-bis(benzylidene)ethylene diamine (bbeda) (10 mol%), PhMe, 60°C; **B**: $Pd(OAc)_2$ (10 mol%), PhMe, 60°C; **C**: $[(C_{10}H_8)Rh(cod)]SbF_6$ (5 mol%), 1,2-dichloroethane, 80°C; **D**: $RhCl(PPh_3)_3$ (10 mol%), PhMe, 50°C; **E**: $Co_2(CO)_8$ (1.1 equiv), PhMe, 110°C; **F**: $AuCl(PPh_3)$/$AgSbF_6$ (30 mol%), CH_2Cl_2; **G**: TfOH (2.0 equiv), CH_2Cl_2, −60°C; **H**: CF_3CO_2H (2.0 equiv), silica gel, CH_2Cl_2, 0°C; **I**: HCl (1.8 equiv), dioxane, $CHCl_3$; [b] Isolated yields; [c] 81:15:4 (*E*)-**6c**:(*Z*)-**6c**:1,5-diene; [d] 85:15 **6d**:1,3-diene; [e] 85:15 **6e**:1,5-diene; [f] 57:43 (*Z*)-**6f**:(*E*)-**6f**; [g] NMR yield; cod = cycloocta-1,5-diene, Tf = CF_3SO_2.

possible that bbeda suppresses further reaction of **6a** by promoting decomplexation of palladium from the product.

Rh-catalyzed [5+2] cycloisomerization of vinylcyclopropane yndiamide (−)-**2o** yielded a single diastereomer of the 5,7-fused bicycle **7** (entry 7),[14] again requiring more forcing conditions compared to the equivalent ynamides. However, cyclization of triynes **2y** and **2z** by using Wilkinson's catalyst[15] proceeded more rapidly than with the related ynamides, giving pyrroloindolines **8a** and **8b** in excellent yields (96 and 91%, respectively, entries 8 and 9).[16] The Pauson–Khand reaction of **2j** afforded the amidocyclopentenone **9** (88%, entry 10), whereas Au-catalyzed cyclization led to cyclobutenamide **10** (entry 11), an outcome that is again distinct from that of the equivalent ynamide chemistry, which affords ring-opened products.[17]

Yndiamide activation could also be achieved by using Brønsted acids. Treatment of **2a** with triflic acid gave dihydroisoquinoline **11** (78%, entry 12), whereas the use of trifluoroacetic acid led to amide **12** (via the enol trifluoroacetate, entry 13). These reactions reveal the potent reactivity of yndiamides towards Brønsted acids, and in the former case represent the first test of 5- versus 6-membered ring formation in keteniminium ion cyclizations.[18] Finally, reaction of **2q** with HCl resulted in smooth conversion to enone **13** (entry 14), presumably by means of 1,5-hydride transfer onto an intermediate keteniminium ion.[11,19]

Further transformations of dienamide **6a** (Scheme 1) underline the utility of yndiamides. Diels–Alder reactions with *N*-phenylmaleimide, dimethylacetylene dicarboxylate, and 4-phenyl-1,2,4-triazoline-3,5-dione (PTAD) afforded cycloadducts **14a–c** in high yields (65–85%). Dihydropyran **14d** was formed as a single regio- and diastereoisomer through the Lewis acid catalyzed reaction of **6a** with 4-bromobenzaldehyde, a result that shows the powerful electron-donating effect of the exocyclic enamide compared to the pyrrolidine nitrogen atom.[20] Similarly, acidic hydrolysis afforded enal **15** exclusively. Oxidation of **6a** with 1.5 equivalents of 3-chloroperoxybenzoic acid (*m*-CPBA) gave dihydrofuran **16**, which underwent

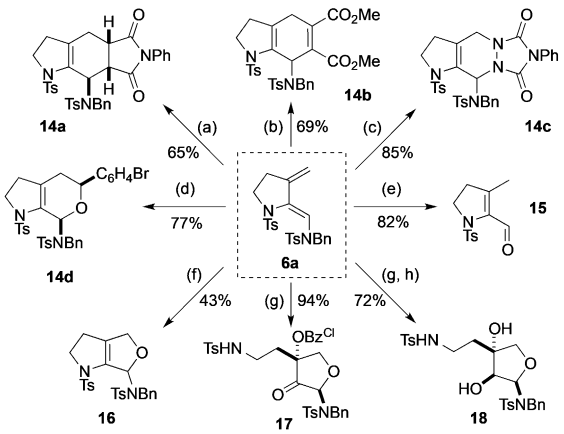

Scheme 1. Conditions: a) *N*-phenylmaleimide (1.0 equiv), PhMe, 60°C; b) $MeO_2CC{\equiv}CCO_2Me$ (1.0 equiv), PhMe, 60°C; c) PTAD (1.0 equiv), PhMe, RT; d) 4-BrC_6H_4CHO (1.1 equiv), $BF_3{\cdot}OEt_2$ (0.5 equiv), CH_2Cl_2, −78°C; e) CF_3CO_2H (2.0 equiv), CH_2Cl_2, −60°C; f) *m*-CPBA (1.5 equiv), CH_2Cl_2, −78°C; g) *m*-CPBA (5.0 equiv), CH_2Cl_2, −78°C; h) $NaBH_4$ (5.0 equiv), MeOH/CH_2Cl_2, RT, then 15% NaOH (aq), RT. Bz^{Cl} = 3-ClC_6H_4CO.

 © 2017 Wiley-VCH Verlag GmbH & Co. KGaA, Weinheim

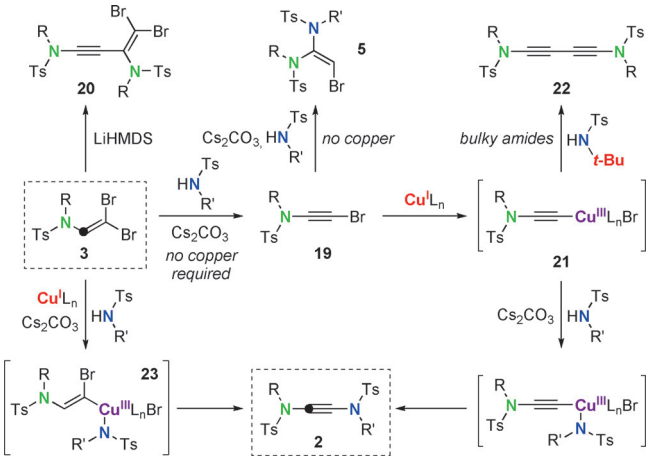

Scheme 2. Possible mechanisms for yndiamide formation.

further oxidation using excess *m*-CPBA to give keto-ester **17** (94%). Reduction/hydrolysis of **17** led to a single diastereomer of the unusual, highly functionalized aminosugar **18** (72%).

In considering possible mechanisms for yndiamide formation, bromoynamide **19** (Scheme 2) is an attractive intermediate. This intermediate is also the likely source of bromoketene aminal **5** (the near exclusive product in the absence of copper catalyst), and could arise from elimination of HBr by the amide anion. Efforts to prepare **19** by using lithium hexamethyldisilazide (LiHMDS) led only to isolation of the formal bromoynamide dimer **20**.[9] Attempted conversion of the ketene aminal **5** to the yndiamide failed under a variety of conditions, likely ruling out a vinylidene carbene rearrangement pathway (also supported by a ^{13}C labelling experiment as shown in Scheme 2, in which a single labelled yndiamide was formed).[9] If the bromoynamide is indeed a reaction intermediate, formation of a copper acetylide, such as **21**, could offer a feasible route for C–N bond formation. Circumstantial evidence for the formation of **21** was found in the isolation of byproduct diyndiamide **22** in reactions with hindered amide coupling partners. Alternative routes, such as amido-cupration of **19** followed by β-elimination of bromide, or direct amination of the dibromoenamide (**23**) followed by elimination of HBr, cannot be ruled out at this stage.

In conclusion, we report the first route to yndiamides—novel, bench-stable alkyne derivatives that are readily prepared from simple precursors. Yndiamides are highly versatile, and provide access to a range of nitrogen-substituted frameworks by using transition-metal-catalyzed or acid-catalyzed processes. Yndiamides have a unique reactivity profile, which both mirrors and contrasts that of ynamides, suggesting significant potential for future applications.

Acknowledgements

SJM is supported by the EPSRC Centre for Doctoral Training in Synthesis for Biology and Medicine (EP/L015838/1). EAA thanks the EPSRC (EP/M019195/1). AM thanks the Royal Thai Government and the DPST project for a studentship. We thank Diamond Light Source for beamtime on I19-1 (MT13639), and Niels Marien for assistance with DFT calculations.

Conflict of interest

The authors declare no conflict of interest.

Keywords: copper catalysis · cycloisomerization · heterocycles · ynamides · yndiamides

How to cite: *Angew. Chem. Int. Ed.* **2017**, *56*, 14428–14432
Angew. Chem. **2017**, *129*, 14620–14624

[1] a) A. Siva Reddy, K. C. Kumara Swamy, *Angew. Chem. Int. Ed.* **2017**, *56*, 6984; *Angew. Chem.* **2017**, *129*, 7088; b) B. Zhou, L. Li, X.-Q. Zhu, J.-Z. Yan, Y.-L. Guo, L.-W. Ye, *Angew. Chem. Int. Ed.* **2017**, *56*, 4015; *Angew. Chem.* **2017**, *129*, 4073; c) D. V. Patil, S. W. Kim, Q. H. Nguyen, H. Kim, S. Wang, T. Hoang, S. Shin, *Angew. Chem. Int. Ed.* **2017**, *56*, 3670; *Angew. Chem.* **2017**, *129*, 3724; d) W.-B. Shen, X.-Y. Xiao, Q. Sun, B. Zhou, X.-Q. Zhu, J.-Z. Yan, X. Lu, L.-W. Ye, *Angew. Chem. Int. Ed.* **2017**, *56*, 605; *Angew. Chem.* **2017**, *129*, 620; e) Z. Nairoukh, G. G. K. S. N. Kumar, Y. Minko, I. Marek, *Chem. Sci.* **2017**, *8*, 627; f) T. Wang, T. R. Hoye, *J. Am. Chem. Soc.* **2016**, *138*, 13870; g) L. Hu, S. Xu, Z. Zhao, Y. Yang, Z. Peng, M. Yang, C. Wang, J. Zhao, *J. Am. Chem. Soc.* **2016**, *138*, 13135; h) L.-G. Xie, S. Shaaban, X. Chen, N. Maulide, *Angew. Chem. Int. Ed.* **2016**, *55*, 12864; *Angew. Chem.* **2016**, *128*, 13056; i) V. Tona, S. A. Ruider, M. Berger, S. Shaaban, M. Padmanaban, L.-G. Xie, L. Gonzalez, N. Maulide, *Chem. Sci.* **2016**, *7*, 6032; j) C. F. Heinrich, I. Fabre, L. Miesch, *Angew. Chem. Int. Ed.* **2016**, *55*, 5170; *Angew. Chem.* **2016**, *128*, 5256; k) L.-G. Xie, S. Niyomchon, A. J. Mota, L. González, N. Maulide, *Nat. Commun.* **2016**, *7*, 10914; l) M. Lecomte, G. Evano, *Angew. Chem. Int. Ed.* **2016**, *55*, 4547; *Angew. Chem.* **2016**, *128*, 4623; m) Reviews: X.-N. Wang, H.-S. Yeom, L.-C. Fang, S. He, Z.-X. Ma, B. L. Kedrowski, R. P. Hsung, *Acc. Chem. Res.* **2014**, *47*, 560; n) Y. Zhang, K. A. DeKorver, H. Y. Li, A. G. Lohse, R. Hayashi, Z. J. Lu, R. P. Hsung, *Chem. Rev.* **2010**, *110*, 5064; o) G. Evano, A. Coste, K. Jouvin, *Angew. Chem. Int. Ed.* **2010**, *49*, 2840; *Angew. Chem.* **2010**, *122*, 2902.

[2] a) Analogous yndiamines (diaminoacetylenes) are known, but are highly reactive and moisture sensitive. For pioneering work, see: H. G. Viehe, M. Reinstein, *Angew. Chem. Int. Ed.* **1964**, *3*, 506–506; *Angew. Chem.* **1964**, *76*, 537; b) S. Y. Delavarenne, H. G. Viehe, *Chem. Ber.* **1970**, *103*, 1198; c) S. Y. Delavarenne, H. G. Viehe, *Chem. Ber.* **1970**, *103*, 1209; d) A. R. Petrov, C. G. Daniliuc, P. G. Jones, M. Tamm, *Chem. Eur. J.* **2010**, *16*, 11804.

[3] a) D. Brückner, *Tetrahedron* **2006**, *62*, 3809; b) For related work from our group using dichloroenamides, see: S. J. Mansfield, C. D. Campbell, M. W. Jones, E. A. Anderson, *Chem. Commun.* **2015**, *51*, 3316.

[4] Other substrates, such as terminal ynamides or chloroynamides, proved to be ineffective. See the Supporting Information for full details.

[5] A. Coste, G. Karthikeyan, F. Couty, G. Evano, *Angew. Chem. Int. Ed.* **2009**, *48*, 4381; *Angew. Chem.* **2009**, *121*, 4445.

[6] a) Y. Zhang, R. P. Hsung, M. R. Tracey, K. C. M. Kurtz, E. L. Vera, *Org. Lett.* **2004**, *6*, 1151; b) X. Zhang, Y. Zhang, J. Huang, R. P. Hsung, K. C. M. Kurtz, J. Oppenheimer, M. E. Petersen, I. K. Sagamanova, L. Shen, M. R. Tracey, *J. Org. Chem.* **2006**, *71*, 4170.

[7] Y. Yang, X. Zhang, Y. Liang, *Tetrahedron Lett.* **2012**, *53*, 6557.

 © 2017 Wiley-VCH Verlag GmbH & Co. KGaA, Weinheim

[8] a) K. A. DeKorver, M. C. Walton, T. D. North, R. P. Hsung, *Org. Lett.* **2011**, *13*, 4862; b) K. A. DeKorver, X.-N. Wang, M. C. Walton, R. P. Hsung, *Org. Lett.* **2012**, *14*, 1768; c) X.-N. Wang, G. N. Winston-McPherson, M. C. Walton, Y. Zhang, R. P. Hsung, K. A. DeKorver, *J. Org. Chem.* **2013**, *78*, 6233.

[9] See the Supporting Information for full details.

[10] Low-temperature single-crystal diffraction data were collected by using a Nonius Kappa CCD or a (Rigaku) Oxford Diffraction SuperNova A diffractometer. Raw frame data were collected and reduced by using DENZO-SMN [Z. Otwinowski, W. Minor, *Methods Enzymol.* **1997**, *276*, 307] or CrysAlisPro, solved by using SuperFlip [L. Palatinus, G. Chapuis, *J. Appl. Crystallogr.* **2007**, *40*, 786] or SIR92, and refined by using CRYSTALS [P. W. Betteridge, J. R. Carruthers, R. I. Cooper, K. Prout, D. J. Watkin, *J. Appl. Crystallogr.* **2003**, *36*, 1487; R. I. Cooper, A. L. Thompson, D. J. Watkin, *J. Appl. Crystallogr.* **2010**, *43*, 1100]. Data for very small crystals were collected by using I19-1 at Diamond Light Source [H. Nowell, S. A. Barnett, K. E. Christensen, S. J. Teat, D. R. Allan, *J. Synchrotron Radiat.* **2012**, *19*, 435]; see the Supporting Information (CIF). CCDC 1022576, 1022577, 1022578 and 1571980 – 1572017 contain the supplementary crystallographic data for this paper. These data can be obtained free of charge from The Cambridge Crystallographic Data Centre.

[11] S. Ohashi, S. Inagaki, *Tetrahedron* **2001**, *57*, 5361.

[12] a) A. Mekareeya, P. R. Walker, A. Couce-Rios, C. D. Campbell, A. Steven, R. S. Paton, E. A. Anderson, *J. Am. Chem. Soc.* **2017**, *139*, 10104; b) P. R. Walker, C. D. Campbell, A. Suleman, G. Carr, E. A. Anderson, *Angew. Chem. Int. Ed.* **2013**, *52*, 9139; *Angew. Chem.* **2013**, *125*, 9309; c) B. M. Trost, G. J. Tanoury, M. Lautens, C. Chan, D. T. Macpherson, *J. Am. Chem. Soc.* **1994**, *116*, 4255.

[13] 1,3- and 1,5-dienes were observed as minor products in Table 2, entries 2–4, which is consistent with related ynamide processes, see Ref. [11a].

[14] a) R. N. Straker, Q. Peng, A. Mekareeya, R. S. Paton, E. A. Anderson, *Nat. Commun.* **2016**, *7*, 10109; b) P. A. Wender, T. J. Williams, *Angew. Chem. Int. Ed.* **2002**, *41*, 4550; *Angew. Chem.* **2002**, *114*, 4732.

[15] a) B. Witulski, T. Stengel, *Angew. Chem. Int. Ed.* **1999**, *38*, 2426; *Angew. Chem.* **1999**, *111*, 2521; b) B. Witulski, C. Alayrac, *Angew. Chem. Int. Ed.* **2002**, *41*, 3281; *Angew. Chem.* **2002**, *114*, 3415; c) M. R. Tracey, J. Oppenheimer, R. P. Hsung, *J. Org. Chem.* **2006**, *71*, 8629.

[16] For [2+2+2] ynamide cyclotrimerization applied to the related herbindole natural products, see: N. Saito, T. Ichimaru, Y. Sato, *Org. Lett.* **2012**, *14*, 1914.

[17] S. Couty, C. Meyer, J. Cossy, *Angew. Chem. Int. Ed.* **2006**, *45*, 6726; *Angew. Chem.* **2006**, *118*, 6878.

[18] Y. Zhang, R. P. Hsung, X. Zhang, J. Huang, B. W. Slafer, A. Davis, *Org. Lett.* **2005**, *7*, 1047.

[19] a) C. Theunissen, B. Metayer, M. Lecomte, N. Henry, H.-C. Chan, G. Compain, P. Gerard, C. Bachmann, N. Mokhtari, J. Marrot, A. Martin-Mingot, S. Thibaudeau, G. Evano, *Org. Biomol. Chem.* **2017**, *15*, 4399; b) G. Evano, M. Lecomte, P. Thilmany, C. Theunissen, *Synthesis* **2017**, *49*, 3183; c) C. Madelaine, V. Valerio, N. Maulide, *Chem. Asian J.* **2011**, *6*, 2224.

[20] a) For Diels – Alder reactions of related exocyclic 2-amidodienes, see: C. D. Campbell, R. L. Greenaway, O. T. Holton, P. R. Walker, H. A. Chapman, C. A. Russell, G. Carr, A. L. Thomson, E. A. Anderson, *Chem. Eur. J.* **2015**, *21*, 12627; b) R. L. Greenaway, C. D. Campbell, H. A. Chapman, E. A. Anderson, *Adv. Synth. Catal.* **2012**, *354*, 3187.

Manuscript received: July 7, 2017
Revised manuscript received: August 11, 2017
Accepted manuscript online: September 5, 2017
Version of record online: October 13, 2017

 © 2017 Wiley-VCH Verlag GmbH & Co. KGaA, Weinheim